Lucio Olivetti
Luigi Grazioli
Editors

Imaging of Urogenital Diseases

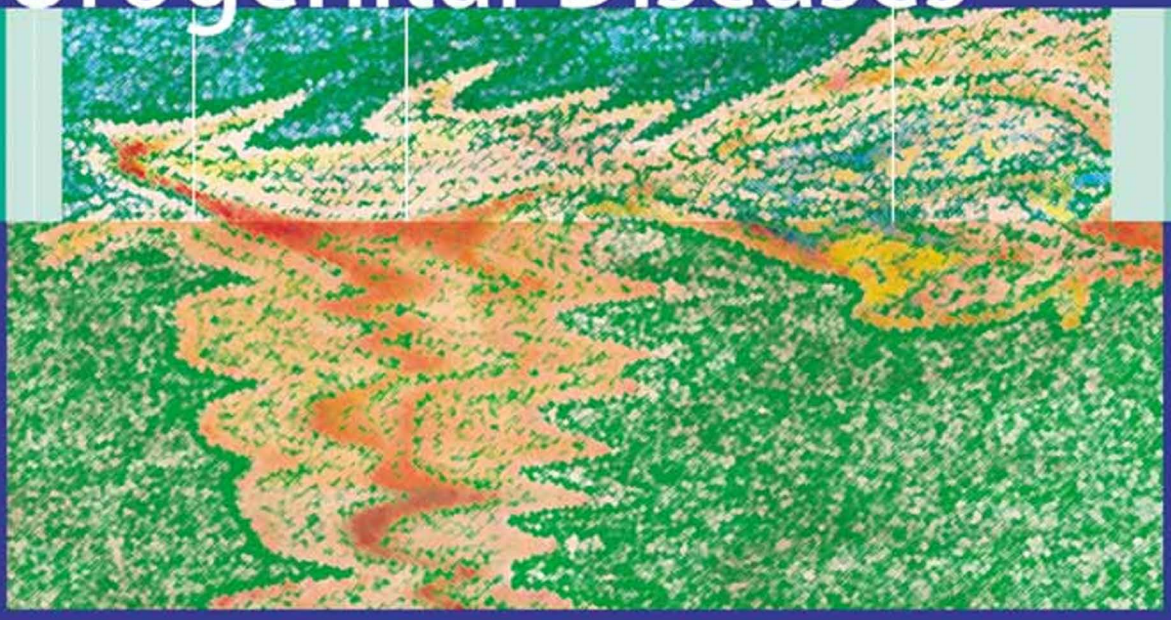

A Color Atlas

Foreword by
Roberto Pozzi Mucelli

Springer

Lucio Olivetti • Luigi Grazioli
Editors

Imaging of Urogenital Diseases

A Color Atlas

Springer

Editors

Lucio Olivetti
Department of Diagnostic Imaging
Istituti Ospitalieri di Cremona
Cremona, Italy

Luigi Grazioli
First Department of Radiology
A. O. Spedali Civili
Brescia, Italy

Originally published as:
Diagnostica per immagini dell'apparato urogenitale
Lucio Olivetti, Luigi Grazioli

Translation: Alexander Cormack, Trieste, Italy

Anatomical drawings by Annalisa Caporali
Istituti Ospitalieri di Cremona, Italy

Library of Congress Control Number: 2009920944

ISBN 978-88-470-1343-8 Springer Milan Berlin Heidelberg New York
e-ISBN 978-88-470-1344-5

Springer is a part of Springer Science+Business Media
springer.com

Typesetting: Compostudio, Cernusco s/N (Milan), Italy
Printing and binding: Printer Trento S.r.l., Trento, Italy

Printed in Italy
Springer-Verlag Italia S.r.l., Via Decembrio 28, I-20137 Milan, Italy

To my daughter Elena
L.O.

… forever your splendor…
L.G.

Foreword

This work presents the entire urogenital system in a methodical and thorough fashion. It is a highly topical book given that the progress achieved by diagnostic imaging in this body system has profoundly changed our way of operating and examining urogenital disease.

The most evident example of this change in diagnostic imaging is intravenous urography. Until a few years ago this technique was considered the reference examination for many renal and urinary tract diseases, whereas today it has largely been replaced by ultrasonography, CT urography and MR urography.

This is not to suggest that urography has completely disappeared from the radiologic scene, because its imaging characteristics can be transferred to CT urography and MR urography. It is however clear that the CT and MR studies are able to provide – in a single examination – information regarding the renal parenchyma and the collecting system, the adjacent organs and structures, and functional and vascular characteristics, all of which cannot be captured in a simple urographic examination.

This change has come about not only in intravenous urography, but also in other forms of imaging of the urinary tract, such as antegrade and retrograde pyelography, which today is limited to only a few and principally interventional or intraoperative applications. However, the most important change in the imaging of the urogenital system, as with other organs and systems, is the broadening of the diagnostic imaging spectrum. Today the radiologist is involved on a number of fronts, from diagnosis – intended as the identification of a lesion, its characterization and, in the case of oncologic disease, its staging – to prognosis and follow-up. Added to these are functional evaluations such as can be obtained with Doppler ultrasonography, spectroscopy and dynamic studies with contrast media.

In this work Olivetti and Grazioli manage to provide thorough and up-dated information on all of these aspects, with a highly topical and modern interpretation of contemporary radiology of the urogenital system.

The book is divided into nine sections, beginning with the anatomy of the urinary tract which is accompanied by excellent illustrations, some of which can be found in the later chapters. The presentation of normal anatomy is followed by radiologic anatomy, which includes urography, angiography, standard ultrasonography, color Doppler and contrast enhanced ultrasonography, computed tomography complete with CT urography, magnetic resonance with MR angiography and MR urography. This is followed by chapters on the normal human anatomy and radiologic anatomy of the male and female reproductive systems which, are organized in the same way as the previous chapters.

The following sections deal with clinical features and imaging of the various organs and systems. Particularly worthwhile in terms of content and images are the sections dedicated to malformations, lithiasis, and renal and urinary tract neoplasms. In the oncologic setting special attention is paid to the problems associated with tumor recurrences in the male and female reproductive systems. Similarly interesting and

topical is the section on female pelvic floor dysfunction and its evaluation with new technologies. The last section deals with interventional radiology in its various forms and includes chapters on biopsies, the treatment of varicocele, drainage and embolization.

My sincere congratulations go to Olivetti and Grazioli for this fine book which clearly reflects not only their professionalism, but also their passion and enthusiasm for our discipline.

Verona, February 2009

Prof. Roberto Pozzi Mucelli
Radiology Section
University of Verona

Preface

Like every book worth its salt, *Imaging of Urogenital Diseases: A Color Atlas* has the obligation of a preface. This was the warm suggestion of the publisher and so it was decided.

After a year of solid commitment, L.O. and L.G. face this final task with relief, a task which is the most demanding and thankless of the entire book. It forces them to justify (first and foremost to themselves) the reasons which prompted them to write a medicine book, and especially on a topic like the urogenital system, which is not nearly as popular as, for example, the thorax or liver.

On the back cover the reader will probably have discovered that this book aims to fill a gap in medical publishing by presenting in a single volume the state of the art in clinical practice and diagnostic imaging of a disease spectrum of undisputed incidence and social importance and therefore of great interest. At least that is how it seems to the two editors. During their undergraduate studies one dreamt of becoming a gynecologist, the other a urologist. Both ended up radiologists, with some regrets… financial regrets first and foremost.

Perhaps this is one of their primary motivations: the aspiration, having passed fifty years of age (even though L.G. obstinately points out that he falls short of that mark by a few months), to regain possession by an alternative route of a specialization they wanted to practice when they were (somewhat) younger. Added to this is a touch of narcissism, a bit of boredom with the daily clinical routine (with no intention of belittling its importance) and the presumption of being able to write something different, or at least the same things in a different way, by exploiting their experience and extensive image bank (only a portion of which is reproduced here) acquired throughout their lengthy activity, and recently reorganized for conferences and courses held in Cremona and Brescia.

Looking back over the drafts, L.O. and L.G. believe they are offering the reader (but the reader will be the final judge) a splendid work. To be honest, they could have done better (one always can) if more time had been available and not stolen from their respective families, to whom this book is also dedicated.

In the certainty, as is always the case, that no-one will read this preface (the book, hopefully, will be read by many), L.O. and L.G. bid their volume farewell and wish it luck.

> "To diagnose the presence of a bladder stone, Rolando advises: *the doctor should seat the patient on his own lap. With the left hand, introduce two fingers into the patient's anus. Then with the right fist strongly compress the bladder region. If you feel a hard mass, it is a stone. If you feel a fleshy mass, then this is obstructing urination.* Avicenna advises palpating the anus of a virgin, the vulva of a deflowered woman".
> (Penso G., 1991, *La medicina medioevale*, p. 296)

Have we written something new and more up-to-date?
L.O. and L.G. look at each other, smile and nod with satisfaction.

Cremona and Brescia, February 2009 *Lucio Olivetti and Luigi Grazioli*

Note for the Reader

The topics covered are classified according to the colored box surrounding the page number, as follows:


Anatomy

Clinical Medicine


Imaging


Interventional Radiology

Contents

Part IV
Disease of the Male Reproductive System

Part V
Oncologic Recurrences of the Male Reproductive System

Part VI
Female Pelvic Floor

Part VII
Disease of the Female Reproductive System

Part VIII
Oncologic Recurrences of the Female Reproductive System

Part IX
Interventional Radiology

Contributors

Alessandro Antonelli
Department of Urology
University of Brescia
A. O. Spedali Civili
Brescia, Italy

Evangelos Apostolopoulos
First Department of Radiology
A. O. Spedali Civili
Brescia, Italy

Maria Pia Bondioni
Department of Radiology
University of Brescia
A. O. Spedali Civili
Brescia, Italy

Enrico Capaccio
Department of Surgery and Integrated Morphologies
University of Genoa
San Martino Hospital
Genoa, Italy

Luisa Carrara
Department of Gynaecology and Obstetrics
University of Brescia
A. O. Spedali Civili
Brescia, Italy

Giuseppe Maria Ciravolo
Department of Gynaecology and Obstetrics
University of Brescia
A. O. Spedali Civili
Brescia, Italy

Gian Paolo Cornalba
Department of Radiology
University of Milan
San Paolo Hospital
Milan, Italy

Sergio Cosciani Cunico
Department of Urology
University of Brescia
A. O. Spedali Civili
Brescia, Italy

Maria Assunta Cova
Department of Radiology
University of Trieste
Cattinara Hospital
Trieste, Italy

Alberto Cozzoli
Department of Urology
University of Brescia
A. O. Spedali Civili
Brescia, Italy

Lorenzo E. Derchi
Department of Surgery and Integrated Morphologies
University of Genoa
San Martino Hospital
Genoa, Italy

Fabio Franco
First Department of Radiology
A. O. Spedali Civili
Brescia, Italy

Barbara Frittoli
First Department of Radiology
A. O. Spedali Civili
Brescia, Italy

Adelinda Frugoni
Department of Gynaecology and Obstetrics
University of Brescia
A. O. Spedali Civili
Brescia, Italy

Sebastiana Gambarini
First Department of Radiology
A. O. Spedali Civili
Brescia, Italy

Daniela Gatti
Department of Gynaecology and Obstetrics
University of Brescia
A. O. Spedali Civili
Brescia, Italy

Giuseppe Giordano
Department of Radiology
University of Milan
San Paolo Hospital
Milan, Italy

Luigi Grazioli
First Department of Radiology
A. O. Spedali Civili
Brescia, Italy

Alessandro Guarise
Department of Radiology
San Bassiano Hospital
Bassano del Grappa (VI), Italy

Giovanni Marchetti
Department of Pathology
Istituti Ospitalieri di Cremona
Cremona, Italy

Paola Martingano
Department of Radiology
University of Trieste
Trieste, Italy

Gian Carlo Mazza
Department of Radiology
Istituti Ospitalieri di Cremona
Cremona, Italy

Katiuscia Menni
Department of Radiology
Fondazione Poliambulanza
Istituto Ospedaliero
Brescia, Italy

Susanna Milianti
Department of Pediatric Surgery
University of Brescia
A. O. Spedali Civili
Brescia, Italy

Gianfranco Minini
Department of Urogynaecology
A. O. Spedali Civili
Brescia, Italy

Giuseppe Mirabella
Department of Urology
University of Brescia
A. O. Spedali Civili
Brescia, Italy

Sara Mombelloni
First Department of Radiology
A. O. Spedali Civili
Brescia, Italy

Giovanni Morana
Department of Radiology
Santa Maria dei Battuti Hospital
Treviso, Italy

Alessandra Moroni
Department of Urology
University of Brescia
A. O. Spedali Civili
Brescia, Italy

Franco Odicino
Department of Gynaecology and Obstetrics
University of Brescia
A. O. Spedali Civili
Brescia, Italy

Lucio Olivetti
Department of Diagnostic Imaging
Istituti Ospitalieri di Cremona
Cremona, Italy

Brunella Pasinetti
Department of Gynaecology and Obstetrics
University of Brescia
A. O. Spedali Civili
Brescia, Italy

Sergio Pecorelli
Department of Gynaecology and Obstetrics
University of Brescia
A. O. Spedali Civili
Brescia, Italy

Andrea Podestà
Department of Surgery and Integrated
Morphologies
University of Genoa
San Martino Hospital
Genoa, Italy

Federico Quaglia
Department of Gynaecology and Obstetrics
University of Brescia
A. O. Spedali Civili
Brescia, Italy

Fabio Rampinelli
Department of Gynaecology and Obstetrics
University of Brescia
A. O. Spedali Civili
Brescia, Italy

Alessandra Ranza
First Department of Radiology
A. O. Spedali Civili
Brescia, Italy

Enrico Sartori
Department of Gynaecology and Obstetrics
University of Brescia
A. O. Spedali Civili
Brescia, Italy

Mauro Scanzi
Department of Urology
University of Brescia
A. O. Spedali Civili
Brescia, Italy

Claudio Simeone
Department of Urology
University of Brescia
A. O. Spedali Civili
Brescia, Italy

Fulvio Stacul
Department of Radiology
University of Trieste
Cattinara Hospital
Trieste, Italy

Claudia Stanga
First Department of Radiology
A. O. Spedali Civili
Brescia, Italy

Giancarlo Tisi
Department of Gynaecology and Obstetrics
University of Brescia
A. O. Spedali Civili
Brescia, Italy

Davide Turilli
Department of Radiology
Fondazione Poliambulanza
Istituto Ospedaliero
Brescia, Italy

Giuseppe Voltini
Department of Radiology
Istituti Ospitalieri di Cremona
Cremona, Italy

Silvia Zanelli
Department of Urogynaecology
A. O. Spedali Civili
Brescia, Italy

Danilo Zani
Department of Urology
University of Brescia
A. O. Spedali Civili
Brescia, Italy

Tiziano Zanotelli
Department of Urology
University of Brescia
A. O. Spedali Civili
Brescia, Italy

Narciso Zappa
First Department of Radiology
A. O. Spedali Civili
Brescia, Italy

Part I
Anatomy

Urinary System: Normal Gross and Microscopic Anatomy

1

L. Olivetti, G. Marchetti

The urogenital system can be divided into two functionally different units, the urinary system and the reproductive system, which are nonetheless closely related in terms not only of anatomy but also of embryology. In fact both develop from the same primitive cell mass, the intermediate mesoderm situated along the posterior wall of the abdominal cavity, and the excretory ducts of both systems initially have a common outlet, the cloaca. Despite their close relationship, it would appear opportune to treat them separately.

Embryology

During gestation three partly overlapping but different systems are formed in a distinct craniocaudal and temporal sequence: the pronephros, the mesonephros and lastly the metanephros or definitive kidney (6th week of gestation). Initially situated at the lumbosacral transition, the metanephros later migrates cranially in relation to the development of the organ, especially with the rapid increase in the length of the vertebral column.

Once the definitive kidney has been formed the ureteric bud of the mesonephric duct and the metanephrogenic blastema cooperate. The former gives rise to the ureter, the pelvis, the calices and the collecting duct system, while the latter develops into the renal tubules, and then the nephrons.

During the 4th and up to the 7th week of gestation the terminal portion of the posterior intestine, the cloaca, is subdivided by a septum forming the anorectal canal (posterior) and the primitive urogenital sinus (anterior). The primitive urogenital sinus later subdivides into a larger upper portion, the future urinary bladder, and a smaller lower portion, the definitive urogenital sinus. In males the latter in turn develops into a small pelvic portion forming the inferior part of the prostatic urethra, and a longer phallic component which later gives rise to the spongy urethra. In females the inferior portion of the primitive urogenital sinus gives rise to a small portion of the urethra, the inferior fifth of the vagina and the vestibule.

Sandler TW (2009) Langman's medical embriology. 11th edn. Wolters Kluwer, Lippincott Williams & Wilkins, Baltimore

Normal Anatomy

Kidney

The kidney lies retroperitoneally at the level of T12 to L3 vertebrae, is connected to the perirenal fascia by collagen bundles and surrounded by perirenal fat. It measures around 12 cm in bipolar diameter, 6 cm in width and 2.5 cm in thickness. In males it

L. Olivetti, L. Grazioli (eds.), *Imaging of Urogenital Diseases*,

weighs 125–170 g and in females 115–155 g. It is subdivided into 8–10 lobes, each of which is composed of around 1 cm-thick overlying cortex and a renal pyramid, the apex of which (papilla) opens into a minor calix. The lobulations, which are particularly appreciable in neonates, disappear from the surface of the kidney in adulthood, but clearly remain as internal subdivisions. The renal columns of Bertin are the extension of the cortical tissue between the medullary pyramids (**Figs. 1.1, 1.2**). The renal capsule is covered by fat, which is in turn surrounded by a condensation of retroperitoneal connective tissue, the perirenal fascia of Geruta.

The external surface is covered with a capsule composed of two layers. The internal

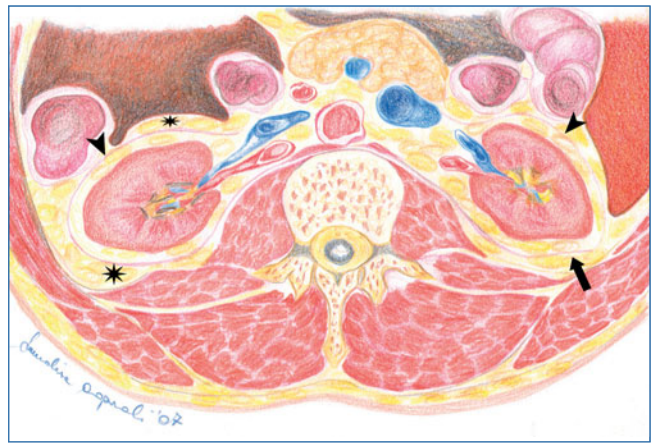

Fig. 1.1. Anatomic diagram of an axial plane passing through the renal hilum. The figure shows the position of the kidney in the perirenal space bounded by the anterior (*arrowheads*) and posterior (*arrow*) perirenal fascia. The anterior and posterior pararenal spaces are also shown (*asterisks*)

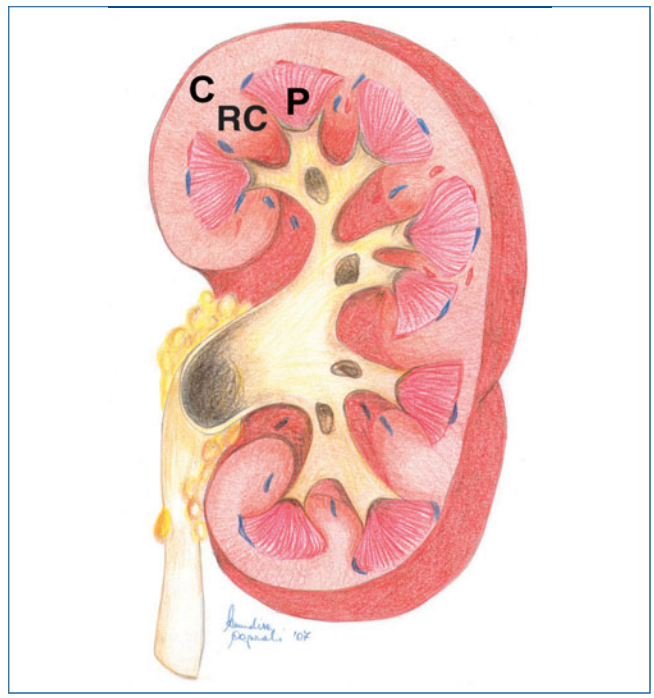

Fig. 1.2. Coronal anatomic diagram of the right kidney. The figure shows the cortex (*C*), the renal columns (*RC*) and the pyramids (*P*) with the minor calices opening at the apex of the latter

fibroblastic layer cannot easily be dissected from the underlying nephrons, whereas the outer, thicker, collagenous layer can more readily be stripped, as may occur in closed abdominal trauma.

An important component, but one which is rarely emphasized as a pathway of tumor spread, is the renal sinus. Located on the medial aspect of the kidney it contains the renal calices, a variable portion of the pelvis, the major vessels and the nerves, the latter composed of adrenergic fibers arising from the celiac plexus. These anatomic structures are surrounded by abundant richly vascularized connective tissue which is continuous with the perirenal fat and not separated from it by a capsule, in contrast to the convex lateral margin.

The calices are divided into major and minor. Each minor calix is indented by a renal papilla, which in number are the same as or less than the number of renal pyramids, since two or three papillae may be fused together (in which cases the papilla forms the common apex of more than one pyramid). The major calices (superior, middle and inferior) are formed by the merging of the minor calices, and in turn merge in the pelvis. There are notable interindividual variations in the morphology of the calices and the pelvis, the two opposite extremes being the ampullary and ramified types.

Vascularization is typically provided by a renal vein and a renal artery, which arborizes in the renal sinus supplying the parenchyma in such a way that each nephron (each kidney contains 1–2 million nephrons) is a self-contained functioning unit with its own blood supply and filtration system.

The lymphatic vessels, which are numerous in the renal cortex, are absent in the medulla. Drainage occurs via the renal sinus and from here to the lymph nodes adjacent to the aorta and the inferior vena cava.

In **microscopic anatomy** the kidney is a compound tubular gland. The functional unit, the nephron, is undoubtedly the most complex secretory unit of the human body. It is a long epithelial tubule which begins with the renal glomerulus and, after a convoluted course in the cortex and the medulla, terminates by emptying into the collecting duct system. Histologically, a normal kidney is therefore composed of glomeruli, tubules, interstitium and vessels.

The basic filtration unit of the kidney – the glomerulus – is regularly spherical in shape with a diameter varying from 150 to 200 micron. It is surrounded by a capsule (Bowman's capsule) composed of a urinary pole, with the proximal convoluted tubule, and a vascular pole, with the afferent arteriole and efferent arteriole (**Fig. 1.3**). The afferent arteriole branches to form the glomerular capillary network, like a mush-

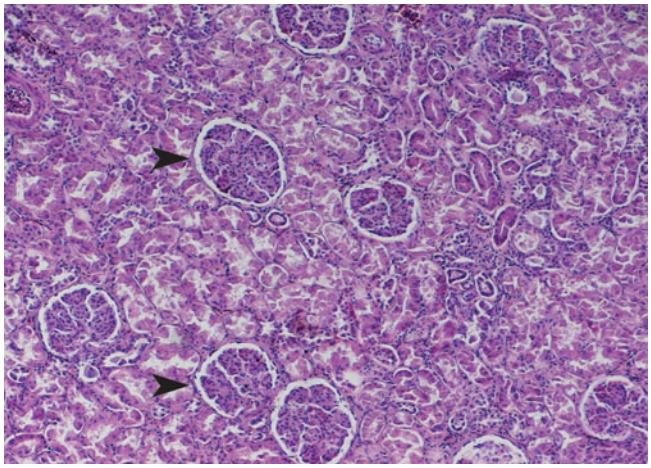

Fig. 1.3. Photomicrograph of renal cortex. Numerous glomeruli (*arrowheads*) are clearly visible. Hematoxylin-eosin stain, x 200

room projecting into the lumen of the glomerular capsule. The capillary network is made up of interstitial mesangium and endothelial and epithelial cells organized around a basement membrane known as the basal lamina.

The glomerular filtrate collected in the capsule is sent to the renal tubule. This is made up of the proximal convoluted tubule followed by the loop of Henle, which consists of a thin descending limb and a thick ascending limb running parallel to each other and joined by a sharp-angled apex. The glomerular filtrate continues along a tortuous course, which, despite being shorter than the proximal tract, is justifiably known as the distal convoluted tubule. The filtrate then reaches the collecting ducts. These unite to form the papillary duct there are 20-25 of these, which each open into the peak of one of the renal papillae.

Ureter

In the normal adult the ureter measures around 30 cm in length and 5 mm in diameter. It lies retroperitoneally and runs inferomedially such that it inserts into the urinary bladder several centimeters from the controlateral ureter (**Fig. 1.4**).

The ureter can be divided into three segments: abdominal, pelvic and intramural. The middle segment has anatomic relations which are obviously different in males and females. In females it lies continuously with the uterine artery, which renders the ureter vulnerable to injury (risk of ligation) during surgical procedures on the

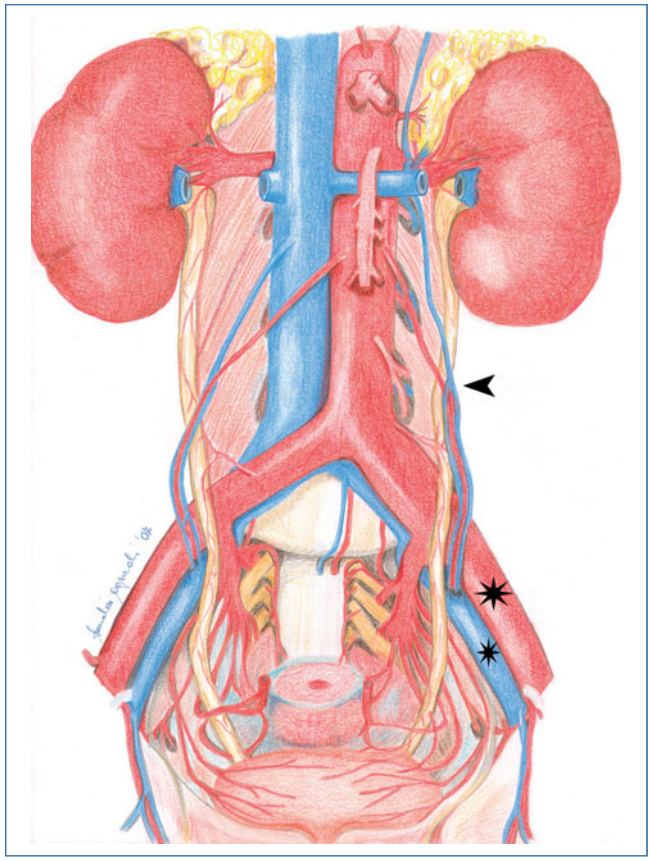

Fig. 1.4. Coronal anatomic diagram of the lumbar and pelvic course of the ureters. The figure shows their relations with the iliac (*asterisks*) and gonadic vessels (*arrowheads*)

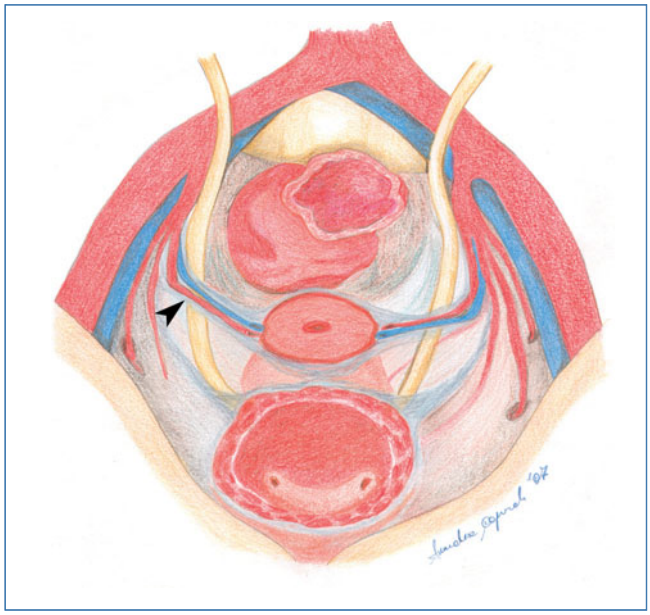

Fig. 1.5. Coronal anatomic diagram of the pelvic course of the ureters. The figure shows the ureters crossing the uterine vessels (*arrowhead*)

reproductive organs (Fig. 1.5). The 1.5 cm – long intramural tract has an identical site and course in both sexes. It runs obliquely through the wall of the urinary bladder, crossing its various layers anteroinferiorly up to the mucosa raised in a fold – which is visible in the lumen of the urinary bladder.

The ureter is also characterized by two physiologic constrictions (isthmuses), the first shortly after its origin at around 7 cm from the renal hilum and the second situated where it crosses the pelvic brim.

The **microscopic anatomy** of the ureter reveals the typical stratification of hollow organs. It is composed of a mucous layer, a submucous coat and a muscular wall, which in turn is covered by fibrous adrentia. In contrast to the urinary bladder, the ureteral mucosa is normally arranged in folds from which rounded aggregates of cells may be avalsed into urinary specimens during ureteroscopy (these papillary clusters may the cause of diagnostic confusion in the differential cytologic evaluation of low-grade urothelial tumors).

Urinary Bladder

The urinary bladder is situated extraperitoneally. An understanding of urinary bladder disease requires an anatomic description of the trigone of the bladder, a triangular region whose anterior apex is represented by the internal urethral orifice and whose posterior base is formed by the two ureteric orifices. The latter have a major oblique axis converging towards the medial line and are characterized by the presence of a posterior fold which, as the bladder fills, presses the walls of the ureters, thus partially acting like a valve (Fig. 1.6). Posterior to the trigone the interureteric ridge, which is formed by the submucosal oblique intramural course of the ureters, delimits the bladder bed. In elderly males this may be lower than the trigone. This position is accentuated in prostatic hypertrophy, where the urethral orifice is not the lowest point of the bladder, thus leading to incomplete emptying.

The relations of the bladder with the reproductive organs are anatomically important.

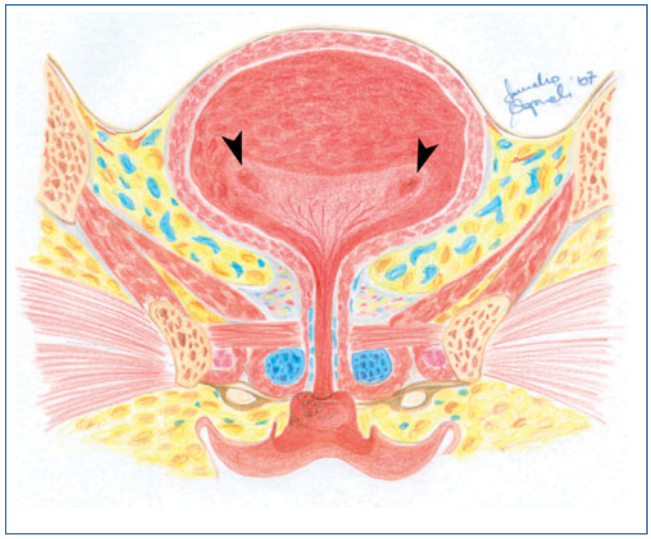

Fig. 1.6. Coronal anatomic diagram of the urinary bladder in a female subject. The figure shows the ureteric orifices (*arrowheads*) and the relations between the urethra and the urogenital diaphragm

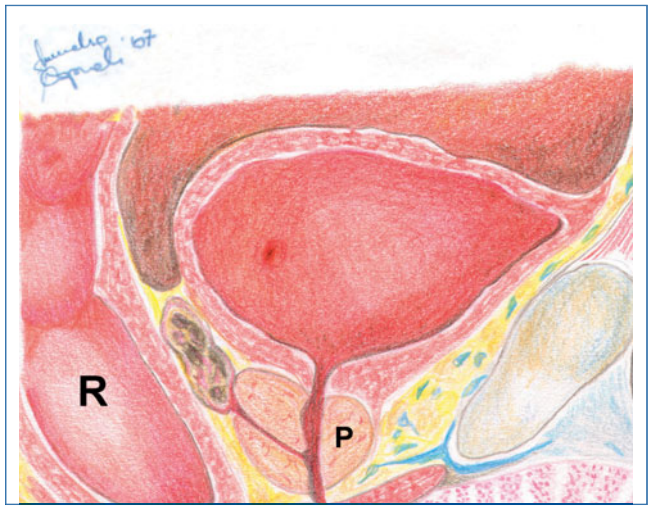

Fig. 1.7. Sagittal anatomic diagram of the pelvis in a male subject. The figure shows the anatomic relations of the urinary bladder with the prostate (*P*), the seminal vesicles and the rectum (*R*)

In males the bladder is related to the prostate, the seminal vesicles and the distal segments of both ductus deferens, through which the fundus, when distended, comes into contact with the rectum (Fig. 1.7). In females the bladder is closely related to the uterus which rests on the apex of the bladder. The serous peritoneum covers the superior surface of the bladder and is reflected on the anterior surface of the uterus. There is therefore a peritoneal space between the two organs, such that the uterus may be easily raised from its contact with the bladder. The fundus of the bladder is continuously related with the cervix up to the level of the fundus of the vagina. These structures separate the bladder from the rectouterine pouch and the rectum, which therefore is not in contact with the bladder (Fig. 1.8).

The bladder wall, the thickness of which varies from 3-4 mm when distended to 10–15 mm when empty, consists of a mucosa (transitional epithelial tissue), submu-

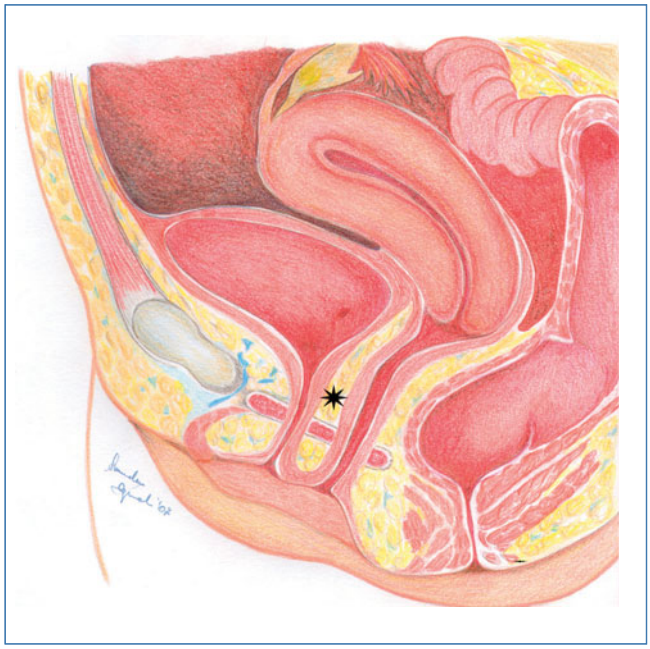

Fig. 1.8. Sagittal anatomic diagram of the pelvis in a female subject. The figure shows the anatomic relations of the urinary bladder with the vagina and the uterus. The *asterisk* indicates the vesicovaginal septum

cosa, muscolaris propria and adventia. The muscular coat is particularly developed and forms the detrusor muscle of the bladder. This is made up of three ill-defined layers which are not of uniform thickness. At the level of the trigone the musculature is thicker and has different characteristics to the other regions (the bundles are more compact and barely separated by connective tissue) such that it has been identified as a distinct structure known as the trigonal muscle.

Urethra

In the adult male the urethra is a muscular tube with an average length of 18–20 cm. Only in its proximal segment does it exclusively convey urine (urinary urethra, which corresponds to the entire female urethra). Distally, from the seminal colliculus (or verumontanum), i.e. the opening of the ejaculatory ducts to the urinary meatus, the urethra also conveys sperm (common urethra). In relation to the adjacent organs, the urethra is subdivided into three segments: prostatic, 3–3.5 cm in length; membranous, 1–1.5 cm in length, which includes the urogenital diaphragm; and spongy, 13–15 cm in length, which is contained in the corpus spongiosum and in turn is divided into bulbous and pendulous urethra (**Fig. 1.9**).

The female urethra (**Figs. 1.6, 1.8**) is a tubular structure 4–5 cm in length, arising from the urinary bladder, which opens into the anterior part of the vestibule of the vagina. The narrow lumen at its extremity, where it measures 7 mm, can easily be dilated allowing a surgeon to introduce instruments as large as 2 cm in diameter.

Microscopically, in the adult male the mucosa of the prostatic and membranous parts of the urethra is essentially composed of transitional epithelium, although there are also areas of prostatic epithelium. In the spongy part, the layer consists of pseudostratified or squamous epithelial tissue.

The submucous coat contains the bulbourethral and periurethral glands. Moving distally along its course the urethra is surrounded by the musculature of the bladder

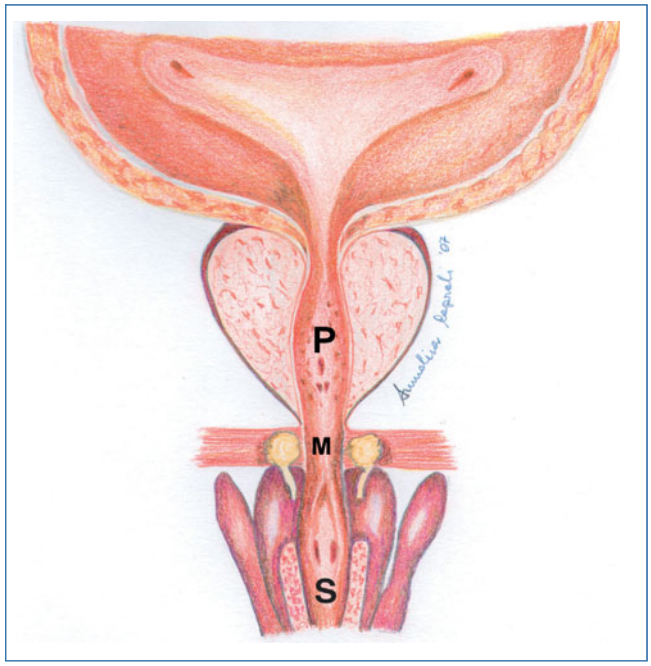

Fig. 1.9. Coronal anatomic diagram of the male urethra. The figure depicts the prostatic (*P*), membranous (*M*) and spongy (bulbous portion) (*S*) parts

neck, the prostate, the urogenital diaphragm (external sphincter), and lastly the corpus spongiosum of the penis.

The female urethra is composed of three layers: mucous, submucous and muscular. The mucosa consists of the transitional epithelium of the urinary tract in its superior part and pavement epithelium similar to that of the vestibule of the vagina in its inferior part. It rests on a supporting layer of loose connective tissue abundant with elastic fibers. The mucosa contains small mucous-secreting acinar glands similar to the glands of the male urethra. The submucous layer is made up of connective tissue vascularized by a fine plexus of thin-walled veins. The muscular layer consists of an internal layer of smooth muscle (longitudinally and circularly arranged muscle fibers) and an external sleeve of striated muscle (external sphincter) which from the perineal trigone that surrounds the urethra immediately below the urinary bladder.

Agur AMR, Dalley AF (2005) Atlas of anatomy. 11th edn. Lippincott Williams & Wilkins, Baltimore

Martini F, Timmons MJ, Tallitsch RB (2008) Human Anatomy. 6th edn. Benjamin-Cummings Publishing Company, San Francisco

Murphy WM, Grignon DJ, Perlman EJ (2004) Tumors of the kidney, bladder, and related urinary structures. American Registry of Pathology, Washington DC

Sandler TW (2009) Langman's medical embriology. 11th edn. Wolters Kluwer, Lippincott Williams & Wilkins, Baltimore

Urinary System: Normal Radiologic Anatomy

2

L. Olivetti, L. Grazioli, G. Voltini

Radiographic Anatomy

Under normal conditions plain film radiography of the urinary system only provides information regarding the level of the kidney areas, since the perirenal fat, particularly in obese subjects, provides natural contrast to the kidneys. The examination can determine the site, dimensions, shape and contours, parameters which are susceptible to slight interindividual variation.

The right kidney is generally located in a position slightly lower than the left kidney. In the radiograph with the patient supine the upper pole is located at the 12th thoracic vertebra, whereas the lower pole, with slight variations in different cases and on the two sides, extends to the level of the 3rd–4th lumbar transverse process. The normal mobility of the kidneys in the craniocaudal direction is limited. In the supine position with normal respiration it is around 2–3 cm and can reach 5–10 cm with a deep breath. In the upright position the kidney descends about one vertebral level. In the lateral view, the kidney overlies the vertebral column, which may lead to the erroneous attribution of renal calcifications (calculi) to the vertebral column.

The long axis of the kidneys runs in a dorsolumbar, craniocaudal and mediolateral direction, which is why in supine position AP views it appears shorter than it really is. Average values measured radiologically are about 12.5–13 cm in male adults and 12–12.5 cm in females, with a cross-sectional diameter between 5.5 and 6.5 cm.

The shape has been likened to a bean with the medial border immediately beside and parallel to the psoas muscle. The contours are smooth, and any modifications are due to the relations with the spleen and especially the liver, in which case the upper pole appears smaller and the lower pole more squat.

In plain film radiographs the ureters are not visible, whereas the urinary bladder, if distended with urine, appears as a slightly radiopaque rounded shadow with no intrinsic clinical value.

The injection of water-soluble iodinated contrast medium allows functional information at the level of the kidneys to be obtained and especially enables the morphologic appearance of the urinary tract to be evaluated.

Under normal conditions, the ultrafast injection of contrast medium during a urographic examination produces a nephrographic effect (following the accumulation in the renal tubules of contrast medium filtered through the glomeruli and concentrated in the tubules themselves) within 30–60 s and is sufficient for 10–15 min, thus enabling detailed study of the renal parenchyma. The opaque urine appears after 2–3 min, with no substantial differences between the two sides. At 5 min the renal cavities are well opacified. Maximum intensity is achieved at about 15 min and is maintained for up to 40–45 min, after which it progressively decreases and then disappears completely.

The nephrographic effect, i.e. the parenchymal opacification of the kidney, is better able to define the morphologic features already described in the plain film examination.

L. Olivetti, L. Grazioli (eds.), *Imaging of Urogenital Diseases*,

In the excretory phase the urinary tract can be evaluated. Even though the collecting systems are subject to slight morphologic variation, the prevailing anatomic profile can nonetheless be described. The kidney can be seen as made up of many simple kidneys, each of which corresponds to a renal pyramid, the apex of which (papilla) opens into a minor calix (the number of calices, therefore, depends on the number of papillae, which can, however, be less than the number of renal pyramids since 2–3 papillae may empty into a single calix). The fornix, i.e. the part of the calix which surrounds the papilla, is more or less crescent shaped in relation to the extent to which the calix projects around the pyramid, and thus may have a circular appearance with an indentation in the center corresponding to the papilla. The major calices, formed by the merging of the minor calices, are generally three in number (superior, middle and inferior) and merge in the renal pelvis, which can be bifurcated, trifurcated or ampullary in appearance. In an AP view with the patient supine, the renal pelvis (the major axis of which is oblique lateromedially and posteranteriorly) is generally located at the level of the 1st lumbar transverse process, whereas the pyeloureteric junction, situated posteriorly, is located at the level of the 2nd lumbar transverse process. In the lateral view the renal pelvis projects onto the lumbar vertebral column. In the event of a pyelotomy, the position of the pelvis in relation to the renal parenchyma can be determined thanks to a line which ideally joins the base of the superior and inferior calices and in relation to which the pelvis is either lateral (and therefore intrarenal) or medial (and therefore extrarenal). The renal pelvis has a capacity of 6–8 mL, but in ascending pyelography there may be the onset of pain indicating overdistension after the injection of 2–5 mL (**Fig. 2.1**).

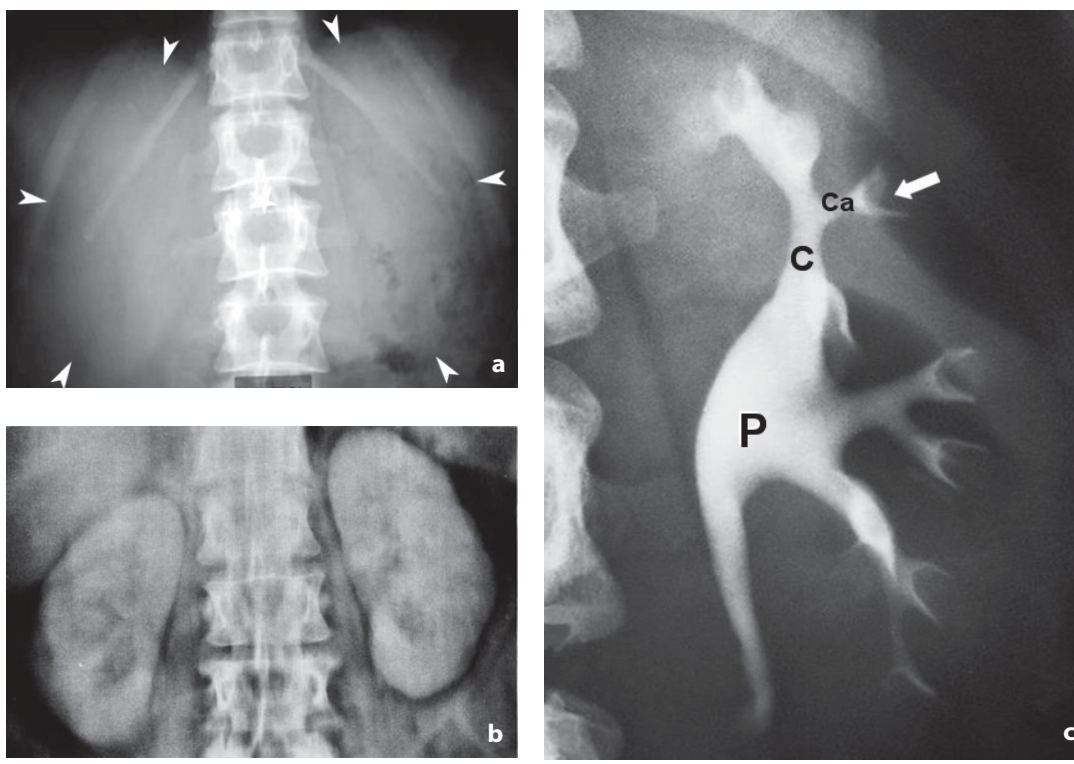

Fig. 2.1a-c. Urography. Kidney. **a** Plain film radiography. The kidneys (*arrowheads*) can be identified thanks to the natural contrast provided by the perirenal fat. **b** Nephrographic phase. The uniform enhancement provided by the contrast medium displays the morphology of the kidney. **c** Excretory phase. Detailed visualization of the pyelocaliceal cavities. The arrow indicates the papilla. *C*, major calix; *Ca*, minor calix; *P*, pelvis

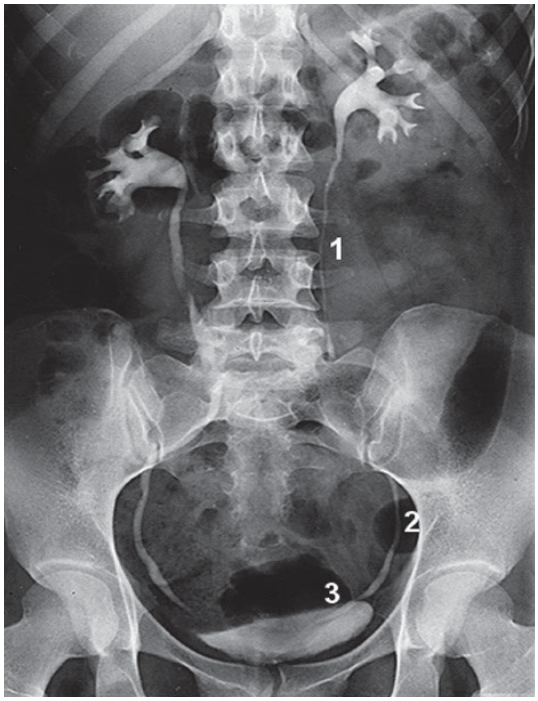

Fig. 2.2. Urography. The image shows the three segments of the ureter: lumbar (*1*), pelvic (*2*) and intramural (*3*). The bladder is in the filling phase

With an average diameter of 3–5 mm the ureters overlie the psoas muscle running alongside the transverse processes of the lumbar vertebrae. Passing over the pelvic brim they run posteroinferiorly on the lateral walls of the pelvis. They then curve anteromedially and insert into the urinary bladder. The can be divided into three parts (lumbar, pelvic and intramural) with three physiologic constrictions: the first (isthmus) at the pyeloureteric junction, the second where it crosses the iliac vessels, i.e. at the level of the innominate line (border between the lumbar and pelvic parts), and the third where it enters the urinary bladder (**Fig. 2.2**).

The appearance of the urinary bladder depends largely on the degree of filling. In the initial phase, in the AP view, it has the shape of a more-or-less deflated vessel. As it distends, the superior concavity is gradually reduced until it disappears completely. In the middle filling phase it takes on the appearance characteristic in males and females. In the former it is rounded, whereas in the latter it is oval shaped, with the transverse diameter being prevalent and the superior border tending to flatten, which in the elderly woman appears sunken in the middle due to the extrinsic impression of the uterus (the bladder in the child often has a tapered appearance). As it fills, the urinary bladder distends eccentrically: since the urethral orifice and the bladder bed are fixed, expansion occurs prevalently in the superior, posterior and lateral directions (**Fig. 2.3**). Emptying begins with contraction of the detrusor muscle and relaxation of the perineum. At this point the bladder changes shape as it moves downwards and slightly backwards.

The male urethra, which can be visualized during voiding cystourethrography (**Fig. 2.4**) or better still with retrograde urethrography (**Fig. 2.5**), is around 16–20 cm in length with a varying diameter in the three parts: prostatic (where the stricture of the seminal colliculus is evident), membranous (the most fixed and slender part), and spongy, which can be further subdivided into bulbous and pendulous. Within the corpus spongiosum the urethra presents two distensions: the first prior to the root of the penis (intrabulbar fossa) and the second corresponding to the navicular fossa. Along its course it presents a double curve: the proximal subpubic curve (from the

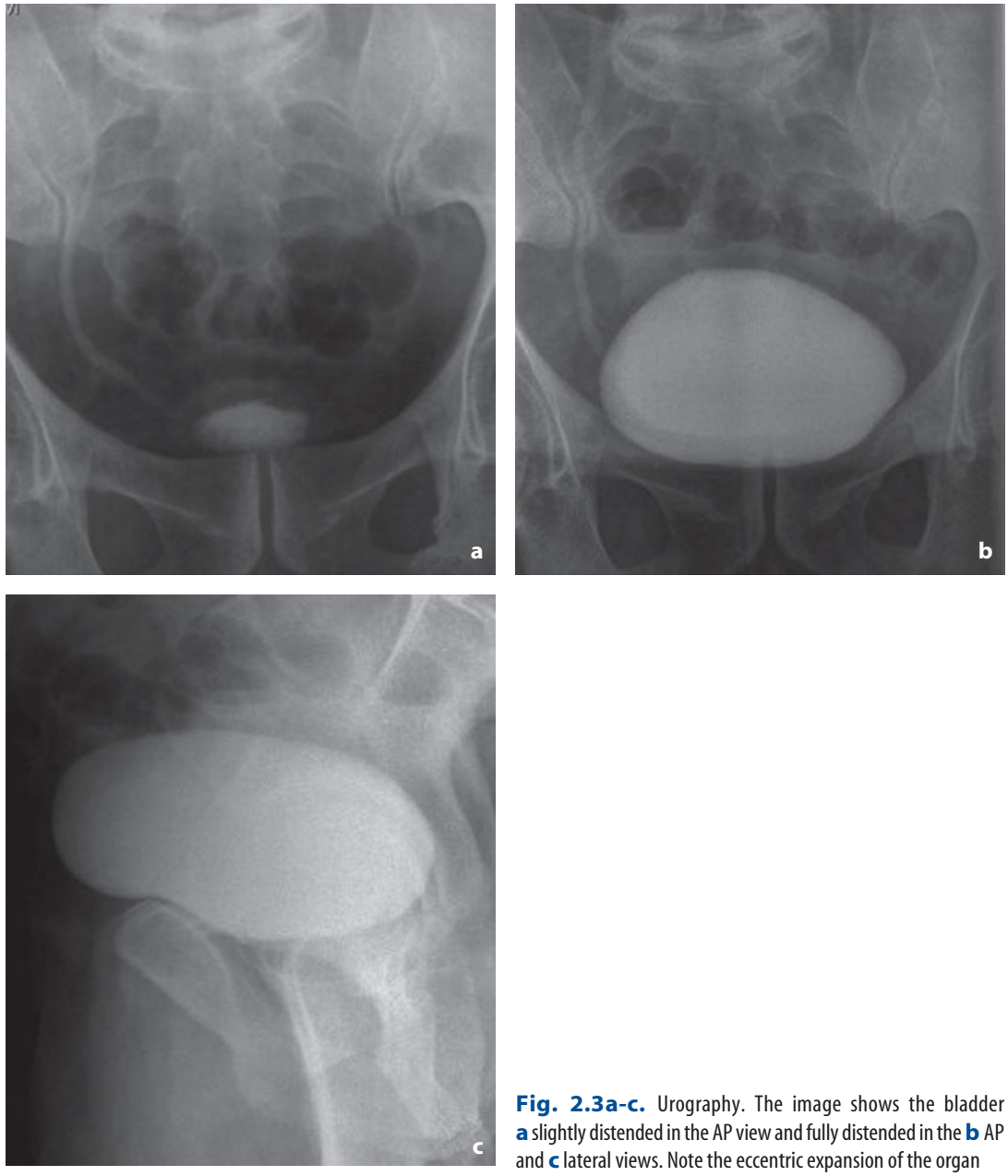

Fig. 2.3a-c. Urography. The image shows the bladder **a** slightly distended in the AP view and fully distended in the **b** AP and **c** lateral views. Note the eccentric expansion of the organ

internal urethral orifice to the urogenital diaphragm) is concave forwards and upwards, while the second prepubic curve is concave downwards and backwards and of practically no importance.

The female urethra has an average length of 4 cm and corresponds to the membranous and prostatic parts of the male urethra. Its course runs downwards and forwards.

Witten DM, Utz DC, Myers Gm (1998) Emmett's Clinical Urography. WB Saunders Co., Philadelphia

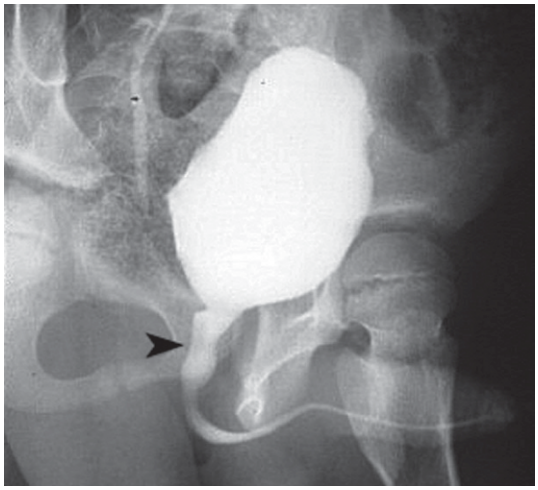

Fig. 2.4. Voiding cystourethrography. The male urethra is visualized during voiding with excellent enhancement of the prostatic segment (*arrowhead*)

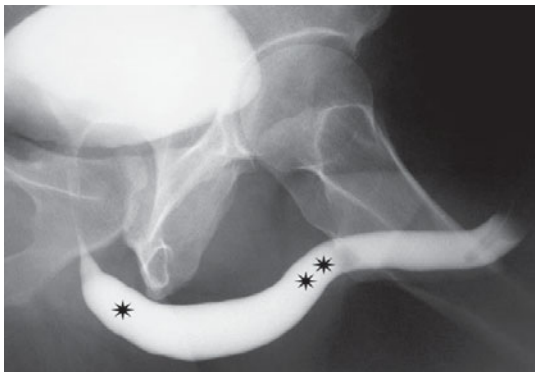

Fig. 2.5. Retrograde urethrography. This technique provides a more detailed visualization of the bulbar (*asterisk*) and cavernous (*asterisks*) segments of the male urethra. The prostatic segment is less well defined

Angiographic Anatomy of the Kidney

The kidney is a highly vascularized organ. Knowledge of the normal vascular anatomy is fundamental for an understanding of the vascular expression of kidney diseases, both parenchymal and, more specifically, vascular.

The normal renal arteries arise at the level of the intervertebral disc between L1 and L2 vertebrae or at the level of the inferior part of L1, since the right vessel usually has a higher origin than the contralateral vessel and slightly greater length, due to the left paramedial position of the aorta. In angiography the diameter ranges from 5 to 7 mm. Between 15% and 20% of subjects present supernumerary renal arteries which are more common on the left side and arise from the abdominal aorta, or less commonly from adjacent arteries. These accessory vessels may enter the kidney through the hilum or any part of the renal surface. Each artery divides close to the hilum into two main branches – ventral and dorsal – which supply the anterior and posterior interpolar part of the kidney, respectively. The main arteries in turn divide into segmental arteries that are end arteries. Each segmental artery is distributed to its own well-defined segment which cannot be supplied by preexisting collateral vessels (**Fig. 2.6**).

Due to the rotation of the kidney on its longitudinal axis, the urographic and angiographic AP view commonly used tends to depict the lateral border as a part of the ventral surface of the organ. Therefore, the peripheral branches of the dorsal artery terminate more medially than those of the ventral artery. As a result, in the analysis of

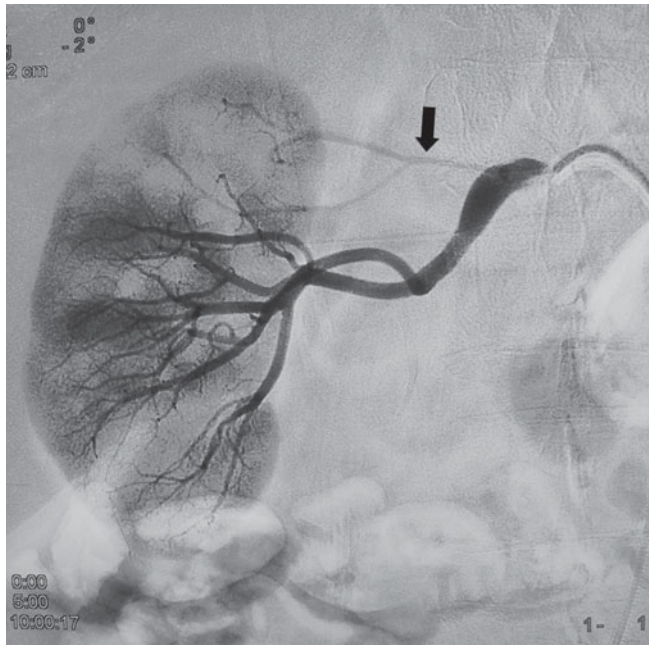

Fig. 2.6. Angiography. Femoral approach. Selective catheterization of the right renal artery. The image precisely depicts the main ventral and dorsal arteries and the segmental branches. The *arrow* indicates an upper polar artery

a renal arteriogram, an artery whose branches reach the lateral margin of the kidney may be erroneously identified as a ventral artery.

At the level of the renal sinus, the branches of the ventral artery never cross over each other, and the same is true for the dorsal artery. In contrast, overlapping of the two arteries is characteristic in the renal sinus. Therefore, if an arteriogram fails to show the two vessels crossing each other, two conclusions can be drawn: involuntary selective injection of the dorsal or ventral artery (the latter is usually more robust and continuous with the renal artery) or occlusion of the nonvizualized branch.

On the basis of the vasculature, four segments can be identified: (1) upper polar, supplied in 50% of cases by both the ventral and dorsal arteries, in 20% by only the dorsal, in 10% by only the ventral, and in the remaining 20% of cases by segmental branches arising from the renal artery prior to its subdivision; (2) anterior intermedial, supplied by the ventral artery; (3) posterior intermedial, supplied by the dorsal artery; and (4) lower polar, supplied in 60% of cases only by the ventral artery, in 20% of cases prevalently by the same vessel and in the remaining 20% of cases by the dorsal artery in the posterior part and the ventral artery in the anterior part.

Saadoon K (1991) Atlas of normal and variant angiographic anatomy. WB Saunders Co., Philadelphia, pp 387–428

Ultrasonographic Anatomy

Unlike computed tomography, ultrasonography (US) is unable to visualize the connective fascia surrounding the anatomic site of the kidney for several reasons. These include slight difference in acoustic impedance between connective tissue and retroperitoneal fat, the absence of sufficient adipose tissue in thin subjects in whom

high-frequency transducers could be used, and at the other extreme the abundance of adipose tissue in larger patients in whom the use of high-resolution transducers becomes impossible. Nonetheless, US is able to define a number of normal parameters. In particular, in axial and sagittal scans on the right side it can be used to identify: (a) a single hyperechoic interface (more characteristic in thin subjects) consisting of the peritoneum, the pararenal fat and the anterior perirenal fascia, the anterior perirenal fat and the renal capsule; (b) a hyperechoic dual interface (the anterior layer being the peritoneum and the posterior the renal capsule), separated by a more-or-less thick hypoechoic layer composed of pararenal and anterior perirenal fat.

The relations with the adjacent organs are described with appropriate scans: posterior oblique longitudinal scan (POLS) for the suprarenal gland, which on the right side can be better evaluated with an anterior axial scan (AAS); anterior longitudinal scan (ALS) and lateral longitudinal scan (LLS) together with POLS for the liver; LLS and POLS for the spleen; posterior longitudinal scan (PLS) to study the relations between the tail of the pancreas and the anterior polar surface of the left kidney. PLS is able to precisely define the relations between the left kidney and the aorta and the relations between the right kidney and the inferior vena cava (the latter can also be evaluated with AAS).

Thanks to its multiplanar characteristics, which are superior to other imaging modalities, US is able to precisely evaluate the real volume of the kidney. In the adult the average diameter is 10.3 cm on the right and 10.4 cm on the left (SD 0.88), dimensions which on average are 30% less than those measured radiologically.

US morphology clearly varies according to the scan used. If the kidney is normally positioned, the ALS and PLS performed along the greater long axis do not cross the hilum and the kidney appears ellipsoid in shape, with a continuous parenchymal ring whose anterior margin appears more convex and posterior margin more rectilinear (**Fig. 2.7a**). In LLS, the shape is closer to that seen in radiographic AP views, with the lateral margin convex and the medial margin rectilinear or slightly concave. In POLS the ultrasound beam passes through the renal hilum: the parenchymal ring at the hilum appears discontinuous with evidence of superior and inferior tubules, while the lateroposterior margin is clearly convex (**Fig. 2.7b**). In AS, the renal parenchyma is visualized as a complete ring interrupted only at the level of the hilum, which appears bounded by the anterior and posterior lips (**Fig. 2.7c**).

Between the peripheral hyperechogenicity of the capsule and the central hyperechogenicity of the sinus is the renal parenchyma, with echogenicity lower than the liver and the spleen. Externally the morphology is that described above regarding the kidney in general, whereas internally it is characterized by the presence of the pyramids and the septa or renal columns. The latter are usually best visualized in young subjects and in scans which do not cross the more central part of the sinus.

In the parenchyma, US can distinguish the cortex, which is weakly more reflective, and the medulla, which is anechoic. These features are best appreciated in the right kidney (ALS), and especially in young subjects. In the child, where the echogenicity is generally greater than in the adult, the two parenchymal components are always identifiable. The arch-shaped vessels appear as hyperechoic spots between the cortex and the base of the pyramids.

Under normal conditions hypertrophy of the renal columns can be visualized at the level of the middle third of the kidney with an echogenicity similar to the remaining parenchyma which extends into the renal sinus, at times dividing it into two halves, the inferior half of which is generally prevalent (this condition is associated with a duplex collecting system). Depending on the scan plane, mid-renal columnar hypertrophy can produce hypoechoic pseudonodular images, giving the echogenicity of the renal sinus the appearance of a pseudotumor. The correct identification of this condition is based on the recognition of the normal parenchyma and especially the two pyramids which define the columnar hypertrophy.

Other anatomic variations which may be commonly encountered are fetal lobula-

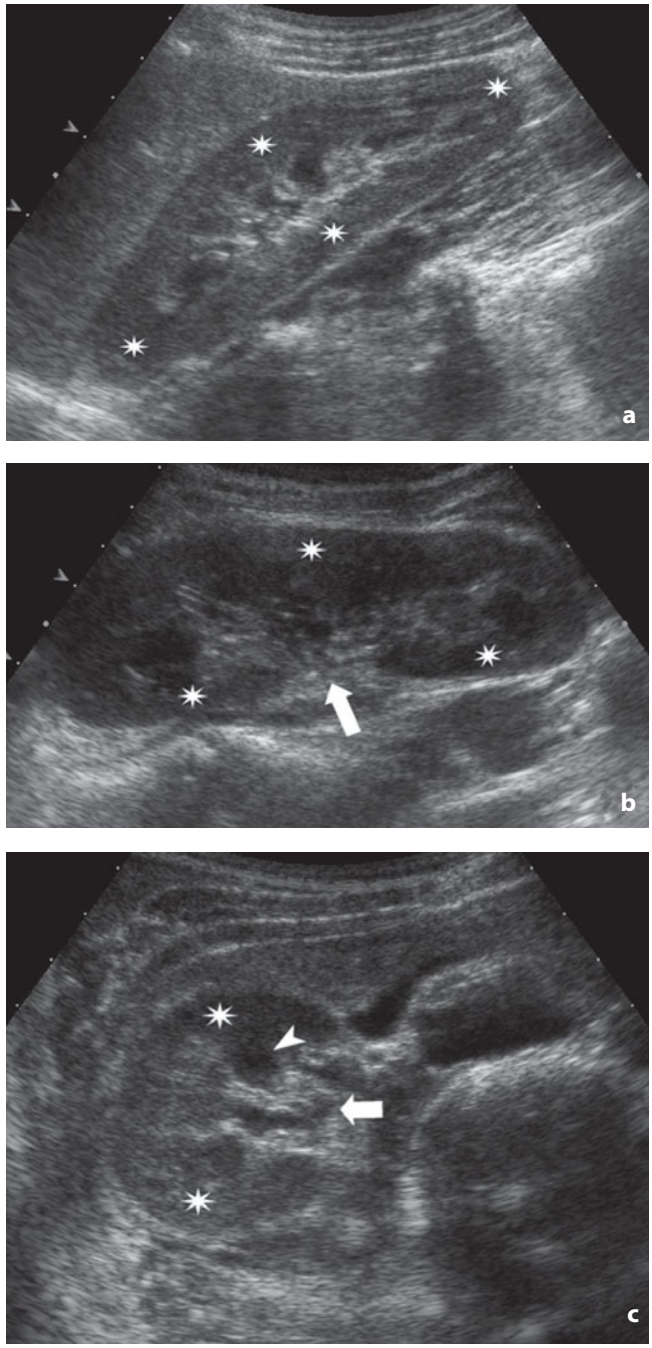

Fig. 2.7a-c. Ultrasonography. Kidney. **a** Anterior longitudinal scan. The cortical ring (*asterisks*) appears continuous. **b** Posterior oblique longitudinal scan. The cortical ring (*asterisks*) appears interrupted at the level of the renal hilum (*arrow*). **c** Anterior axial scan. The kidney is cut along the short axis. The sonogram shows the cortex (*asterisks*), the pyramids (*arrowheads*) and the renal sinus (*arrow*)

tions and notches, the parahilar line and the hyperechoic triangle, hypertrophy of the tubules and lips, and the dromedary hump kidney.

The renal sinus is a hyperechoic structure between the pelvis and the renal parenchyma. Its morphology, which is conditioned by the parenchyma, varies

according to the US approach adopted, being ovular in LS, horseshoe-shaped at the level of the hilum in AAS and circular above and below it. In neonates and children the sinus is less reflective due to the lack of fibrous tissue. In relation to its greater compliance in these subjects, dilatation of the urinary tract is easier to identify, even in the presence of only slight distension of the bladder. In contrast, under normal conditions in adults the groups of calices whose lumens are closed cannot be identified in the central echoes of the renal sinus. However, the intrarenal collecting system can become visible in adults, at least as branching anechoic structures, in the presence of certain physiologic conditions which lead to water overload or stasis due to overdistension of the urinary bladder.

One anatomic variant that is more common in the elderly patient is lipomatosis, which is defined as an increase in the dimensions of the renal sinus, whose hyperechoic structure expands peripherally at the expense of the parenchyma. With regard to the hypoechoic pattern fat can display in the human body, some investigators have conceded that lumps of lipomatosis can also be present in hypo-anechoic (i.e. non-cystic) areas within the renal sinus. In fact, in adults and the elderly lymphatic cysts of unknown pathogenesis commonly occur in the sinus, varying in number, dimension and structure (not completely anechoic), which can lead to clinical suspicion of lipomatosis. A comparison with CT and sonographically guided percutaneous interventional procedures has clarified the real cystic nature in such cases.

In the event of extrarenal development, the pelvis can be identified in the sinus or at the hilum posterior to the vessels. In some physiologic conditions or anatomic variants the lumen of the pelvis is no longer virtual.

The renal vessels can be identified in AAS, although this is not always possible on the left side due to disturbances caused by gastrointestinal gas.

Color Doppler and power Doppler help in the identification of the renal vessels and enable the identification of the interlobular vessels, the arched-shaped vessels and part of the interlobular circulation (**Fig. 2.8**).

The Doppler trace of the renal arteries in normal conditions is that typical of low-resistance peripheral arteries supplying parenchyma, being characterized by a prominent systolic peak and a well-represented diastolic curve. Beneath the systolic peak is a window in which no Doppler signal can be detected, since flow is laminar. Nonetheless, even in normal conditions this window can in part be occupied, both by turbulence created by the near right angle of the origin of the renal artery from the aorta and by the reduced diameter of the vessel which influences the placement of the sample volume near to the wall where flow is nonuniform. The peak systolic velocity is usually less than 100 cm/s, but in some subjects, particularly the young, greater velocities can be detected even in the absence of stenosis (**Fig. 2.9a**).

Even within the parenchyma the vessels are visible in both systole and diastole. This indicates that the flow towards the parenchyma is continuous and low resistance, which is confirmed by the spectral analysis where the end-diastolic velocity is equal to one-half/one-third of the systolic peak (**Fig. 2.9b**). The normal arterial renal resistance index is below 0.7 with bilateral values differing by no greater than 0.1

The right renal vein has a short straight course from the renal hilum to the inferior vena cava and is ventral to the corresponding artery. The left renal vein is longer and runs anterior to the corresponding artery and in most cases passes anterior to the aorta, between the aorta and the superior mesenteric artery. Prior to emptying into the inferior vena cava it is related for a short section with the right renal artery which runs posteriorly. On two-dimensional US, the renal veins appear more-or-less distended, partly in relation to respiratory dynamics, and the vessel walls present pulsed motion transmitted by the adjacent arteries. The Doppler study shows continuous intraluminal flow which may be pulsed. Cardiac pulsatility and respiratory phasicity are more evident near to the outflow into the inferior vena cava.

The recent diffusion of second-generation US contrast media has made possible the evaluation of parenchymal enhancement in a manner similar to CT and MR (**Fig. 2.10**).

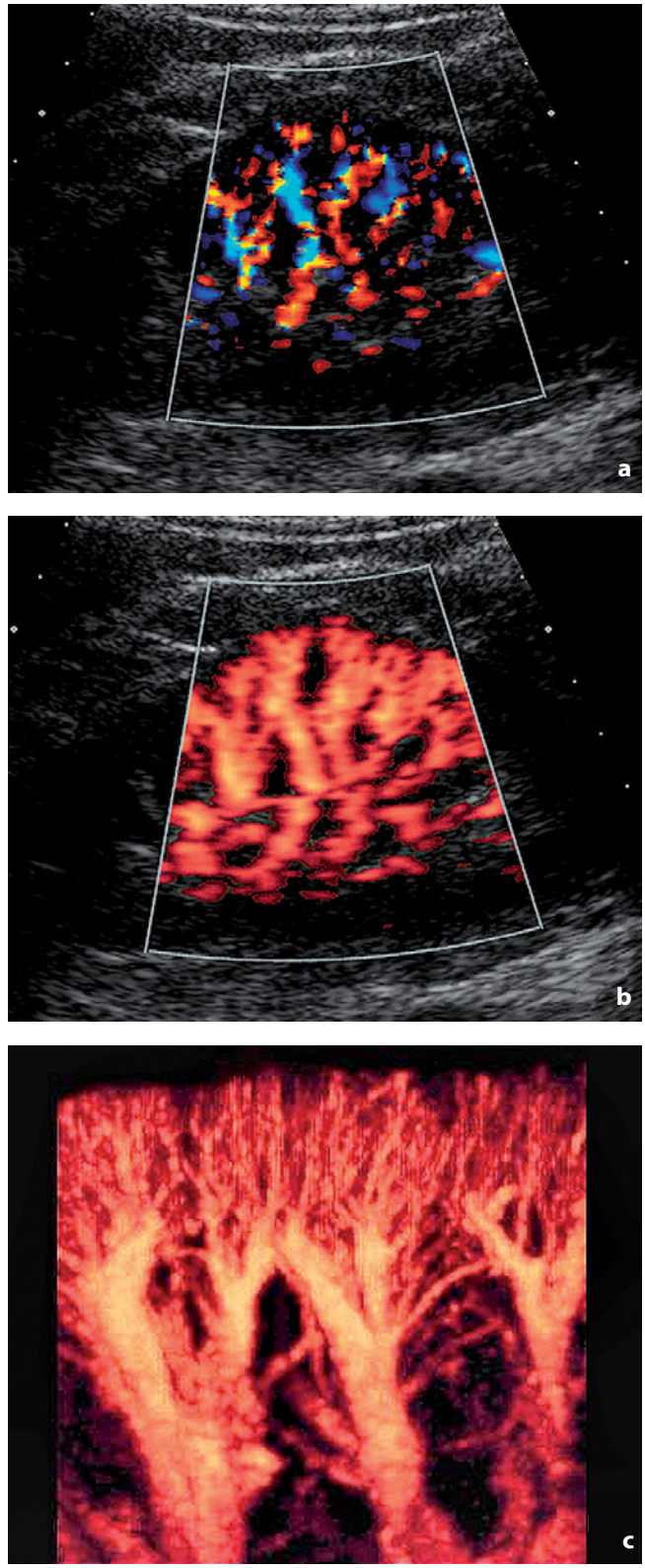

Fig. 2.8a-c. Color Doppler and power Doppler. Kidney. **a** Color Doppler and **b** power Doppler images show the intrarenal vascular flow. **c** Power Doppler can also provide a three-dimensional view of the parenchymal vasculature

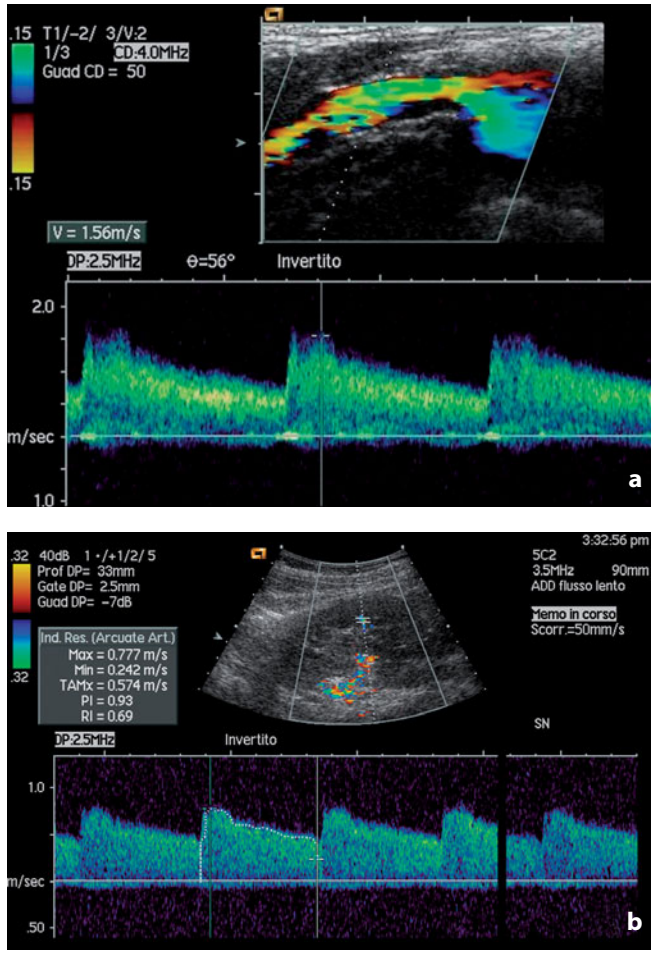

Fig. 2.9a,b. Doppler trace. Renal artery, young male subject. **a** The image shows the systolic and diastolic components of flow. **b** Intraparenchymal vessels. The resistance index (0.69) is the range of normal

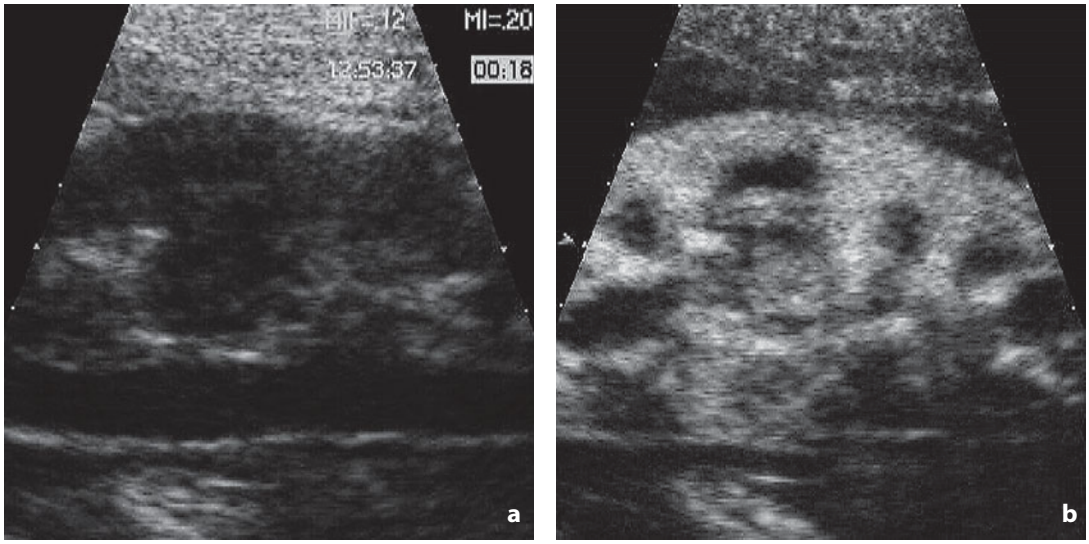

Fig. 2.10a,b. Ultrasonography, dynamic study with contrast medium. **a** Baseline sonogram. **b** Arterial or corticomedullary phase. The typical intravascular distribution of the microbubbles of US contrast medium provides information on the vascularization of different parenchymal components. Since the blood supply is greater to the cortex than the medulla, the intense enhancement facilitates their differentiation

In normal conditions the ureters cannot be assessed with US.

The urinary bladder can be correctly evaluated when distended. Its shape and size evidently varies in relation to the degree of filling. When adequately filled, it has an anechoic appearance which is ovoid in longitudinal scans and quadrangular in transverse scans. Scans can identify the base (neck and trigone), dome and the posterior and lateral walls, the thickness of which with the organ distended should not exceed 5 mm in normal adults and is generally 2–2.5 mm in children (**Fig. 2.11**). The walls are echoic and with a high-frequency transducer three layers can be identified: a hyperechoic external layer corresponding to the adventitia and the interface between the bladder wall and the surrounding adipose tissue, a hypoechoic middle layer corresponding to the muscular coat, and a hyperechoic internal layer corresponding to the submucosa and mucosa (**Fig. 2.12**).

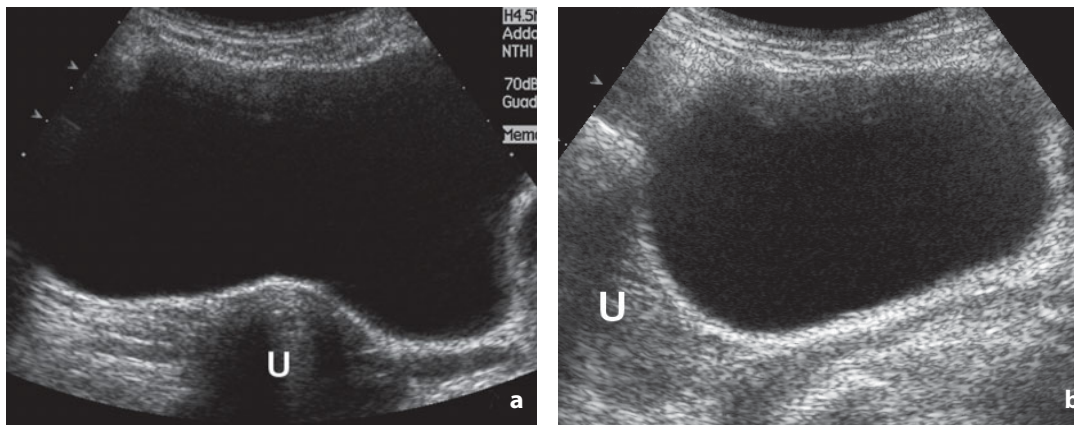

Fig. 2.11a,b. Ultrasonography. Urinary bladder. **a** Anteroposterior scan. **b** Lateral scan. In normal conditions the bladder appears with thin regular walls and a perfectly anechoic lumen. *U*, uterus

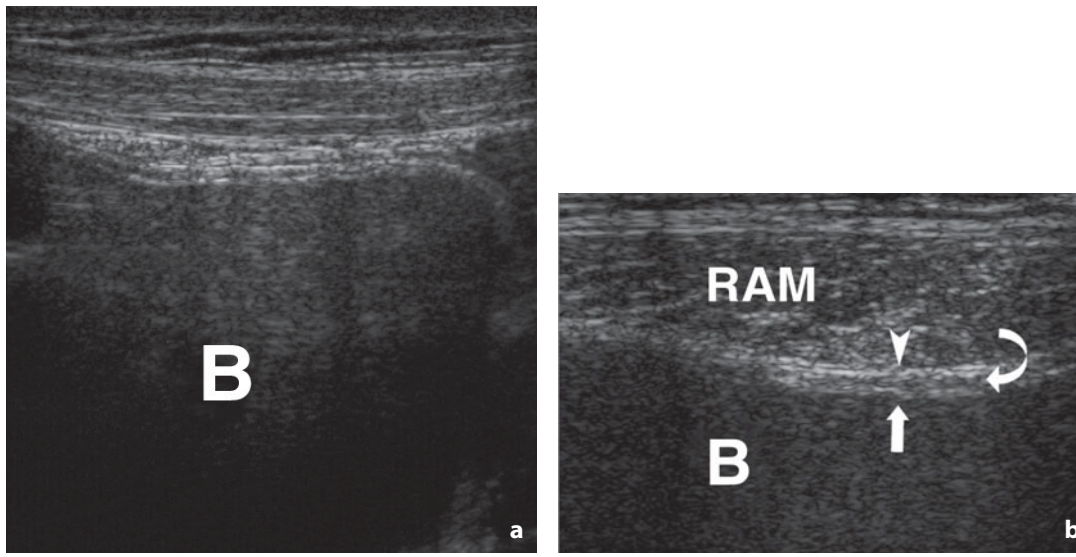

Fig. 2.12a,b. Ultrasonography. Urinary bladder. With the use of a high-frequency transducer the different layers making up the bladder wall can be distinguished, particularly in the detailed image (**b**): external, hyperechoic, corresponding to the adventitia and the surrounding adipose tissue (*arrowhead*); middle, hypoechoic, corresponding to the muscle coat (*curved arrow*); internal, hyperechoic, corresponding to the submucosa and mucosa (*arrow*). *RAM*, rectus abdominis muscle; *B*, urinary bladder

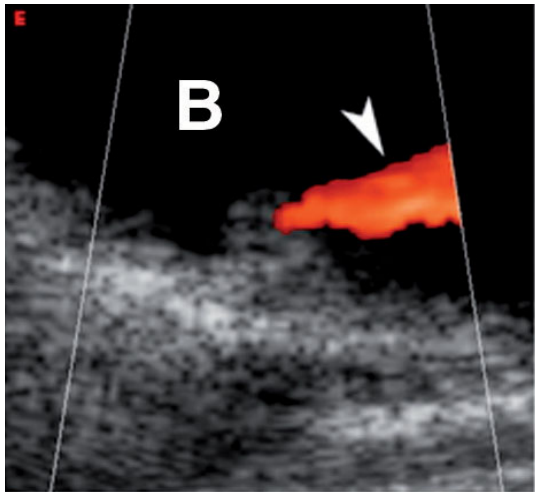

Fig. 2.13. Ultrasonography. With the use of the color module a jet from the urethral meatus can be identified (*arrowhead*). *B*, urinary bladder

A typical feature at the level of the trigone and best viewed with color Doppler is ureteric jet, i.e. the intermittent flow of urine from the ureteric orifice into the bladder. The turbulence created by the ejection of urine from the meatus appears as a jet with intravesical color and length between 3 and 5 cm. In normal conditions the jet is not simultaneous on both sides and appears with an intermittent frequency varying from 5 to 30 s (**Fig. 2.13**).

Rumack CM, Wilson SR, Charboneau JW (2004) Diagnostic ultrasound. 3rd edn. Mosly, St Louis

Sethi D (2005) Ultrasound anatomy & normal appearance: a pratical aproach. Aushan, Tumbridge Wells, Kent

Weil FS, Bihr E, Rohmer P et al (eds) (1987) Renal sonography. Springer-Verlag, Berlin

Computed Tomography Anatomy

Computed tomography (CT) is the best diagnostic imaging modality and is able to define the anatomic position of the kidneys in the retroperitoneal space, which is commonly divided into three compartments: anterior pararenal, perirenal and posterior pararenal (**Fig. 2.14**).

The anterior pararenal space, which unlike the other compartments contains a limited adipose component, and is situated between the posterior parietal peritoneum and the anterior portion of the renal fascia. It contains the pancreas, the duodenum, the ascending colon and the descending colon. Centrally it is continuous with the root of the mesentery and the mesocolon. It terminates inferiorly at the height of the iliac crest, where it communicates with the inferior retroperitoneal space (extraperitoneal space).

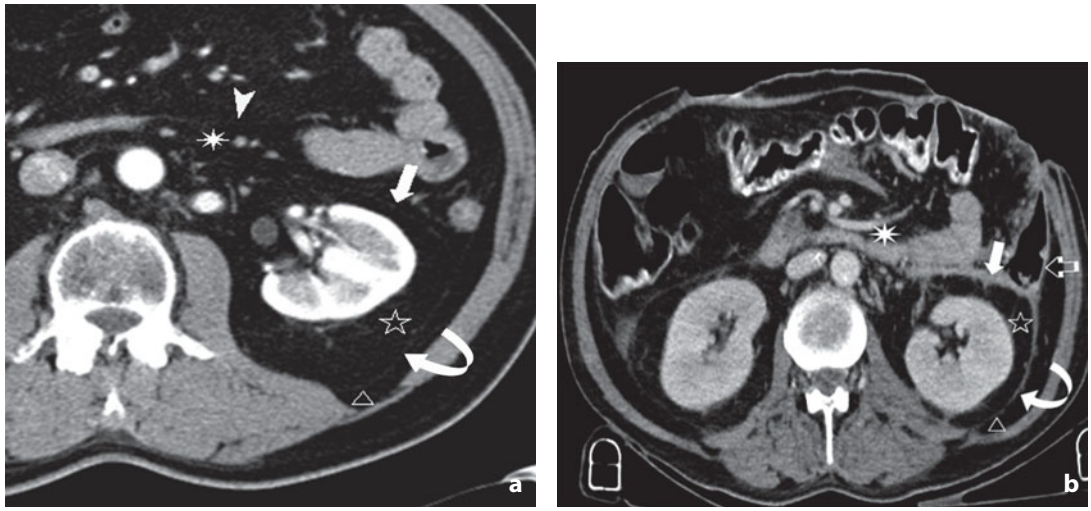

Fig. 2.14a,b. Computed tomography. Axial scan. Perirenal and pararenal spaces. **a** The anterior pararenal space (*asterisk*) is bounded by the posterior parietal peritoneum (*arrowhead*) and the anterior perirenal fascia (*arrow*). The perirenal space (star) is bounded by the anterior perirenal fascia and the posterior perirenal fascia (*curved arrow*). The posterior pararenal space (*triangle*) is bounded by the posterior perirenal fascia and the transverse fascia, which covers the psoas and quadratus lumborum muscles, and is only visible in its lateral portion. **b** The spaces are better defined when the fasciae are thickened. The unfilled arrow indicates the lateroconal fascia

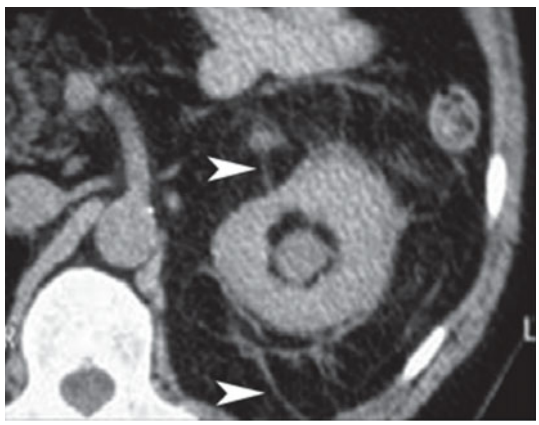

Fig. 2.15. Computed tomography. Axial scan. Perirenal space. In this post-pyelonephritis patient bridging septa are visible connecting the capsule and the fascia (*arrowheads*)

The perirenal space is bounded by the anterior and posterior renal fascia, which blend laterally to form the lateroconal fascia. It contains the suprarenal gland, the kidney and the renal adipose body. It may be divided into compartments by bridging fibrous septa attached only to the renal capsule, connecting the renal capsule and the pararenal fascia, or connecting the anterior and posterior renal fascia (**Fig. 2.15**).

The posterior pararenal space is bounded by the posterior and transverse renal fascia. Medially it is bounded by the margin of the psoas muscle and is open laterally towards the flank and inferiorly towards the pelvis. Unlike the two preceding spaces it only contains fat. In thin subjects its visualization may prove difficult.

Coronal reconstructions provide the best visualization of the compartments, particularly in the upper polar and lower polar regions (**Fig. 2.16**).

The perirenal fat of the renal sinus enables clear definition of the parenchymal margins of the kidney, which in nonenhanced images shows uniform structure with attenuation values between 35 and 55 HU in relation to the hematocrit and degree of

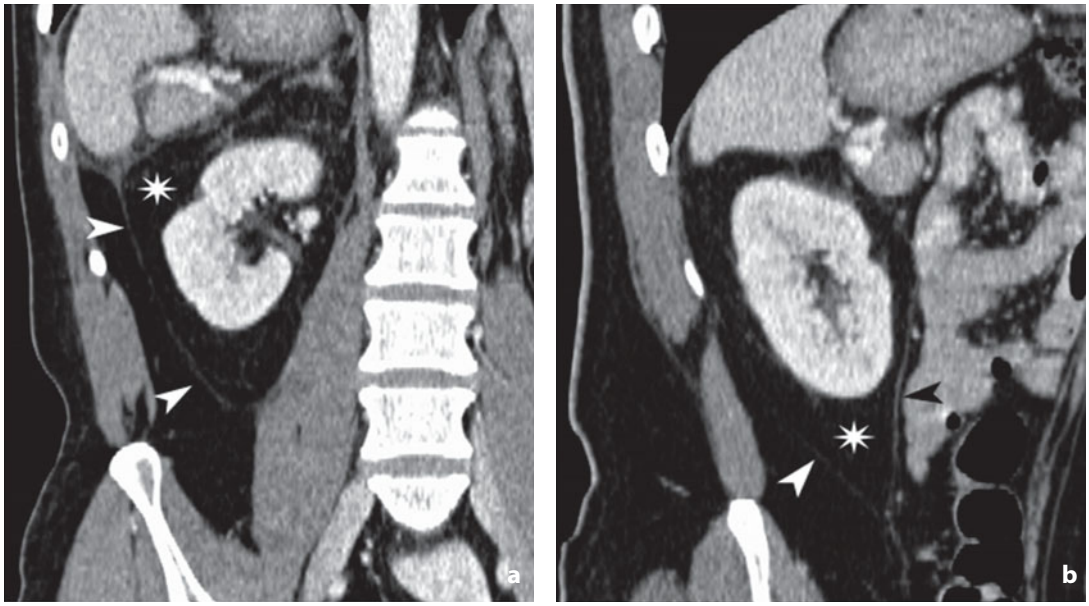

Fig. 2.16a,b. Computed tomography. Coronal reconstructions. Kidney area. The renal fascia (*arrowheads*) are visible as hyperattenuating thin lines. The asterisk indicates the perirenal space

hydration of the subject. Focal areas of increased attenuation (60–70 HU) due to reduced hydration and an increase in the concentration of urinary solutes may be observed at the level of the papillary apices.

Renal enhancement is evaluated during a dynamic study after the injection of 100 mL of contrast medium, generally at an injection rate of 3 mL/s. Three phases can be identified: corticomedullary (at 25–70 s), during which the renal cortex displays enhancement (with peaks = 120 HU) much greater than that of the slower medulla, thus enabling their differentiation; nephrographic (at 80–180 s), during which the renal parenchyma becomes uniform; and excretory (>180 s), during which the collecting systems are opacified (**Fig. 2.17**).

CT and MR are the best techniques for confirming and documenting the presence of anatomic variants such as mid-renal hypertrophy, malrotation, horseshoe kidney and ectopia. The course of the nondilated ureter can be visualized with certainty after contrast enhancement.

The ureter may originate from the renal pelvis at the level of L2 and run across the surface of the psoas muscle, accompanied by the gonadic vessels which it later crosses at the level of the pelvic entrance. In males, at a site shortly before the meatus, it is located between the bladder and the seminal vesicles, whereas in females the ureter runs 1.5–2 cm laterally to the cervix and is crossed by the uterine vessels.

The size, shape and thickness of the bladder walls vary according to the degree of distension. In axial images the dome and fundus are poorly defined due to partial volume effect, which can be avoided with thinner sections. The position of the ureteric orifices is usually difficult to define, but their localization can be aided by the identification of ureteric jet, described above. CT is unable to differentiate the different layers of the wall (**Fig. 2.18**).

High-definition three-dimensional CT reconstructions are able to visualize the cavities of the collecting system with a definition very similar to urography. They can also be used for a highly detailed anatomic study of the renal arteries (**Figs. 2.19, 2.20**).

Schild HH, Schweden FJ, Lang E (eds) (1992) Computed tomography in urology. Georg Thieme Verlag, Stuttgart-New York

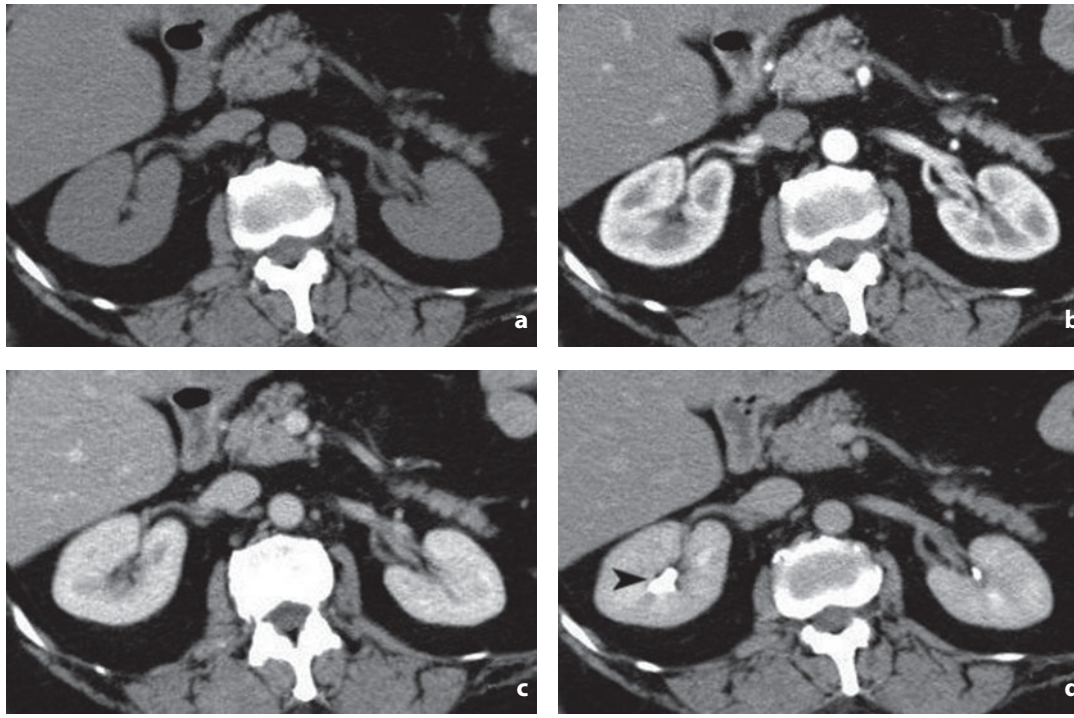

Fig. 2.17a-d. Computed tomography. Multiphase dynamic study. Kidney. **a** Baseline image. The cortex and medulla cannot be differentiated. **b** Arterial or corticomedullary phase. Greater enhancement of the cortex than the medulla. **c** Venous or nephrographic phase. Uniform hyperattenuation of the renal parenchyma. **d** Excretory phase. Enhancement of the pyelocaliceal cavity (*arrowhead*)

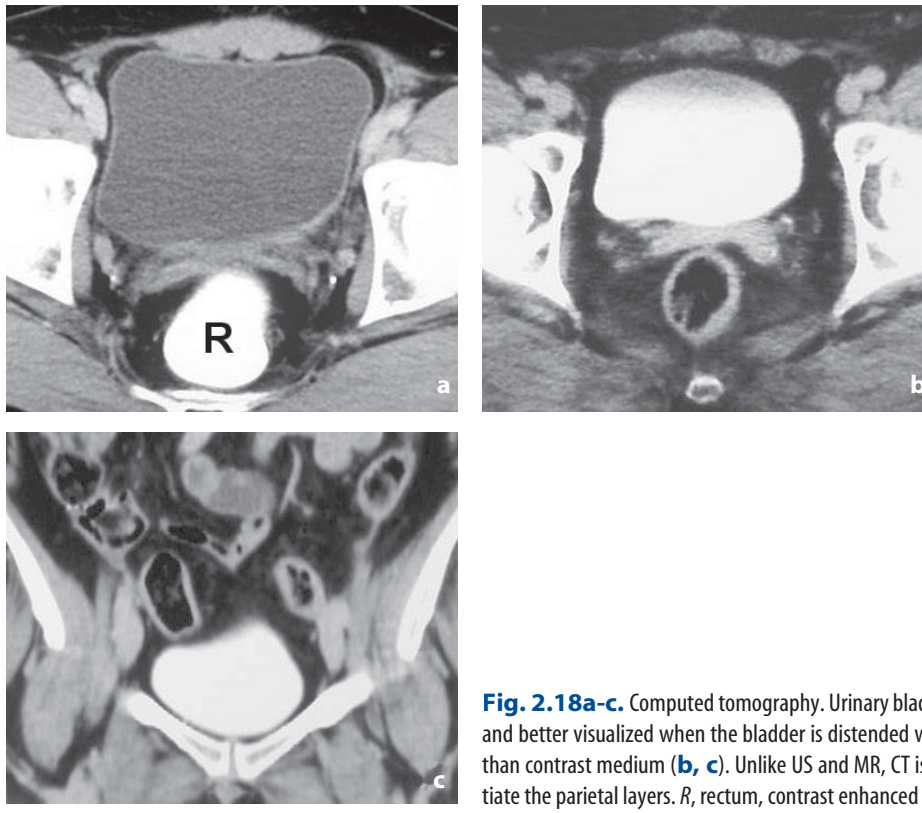

Fig. 2.18a-c. Computed tomography. Urinary bladder. The wall is thin and better visualized when the bladder is distended with urine (**a**) rather than contrast medium (**b, c**). Unlike US and MR, CT is unable to differentiate the parietal layers. *R*, rectum, contrast enhanced

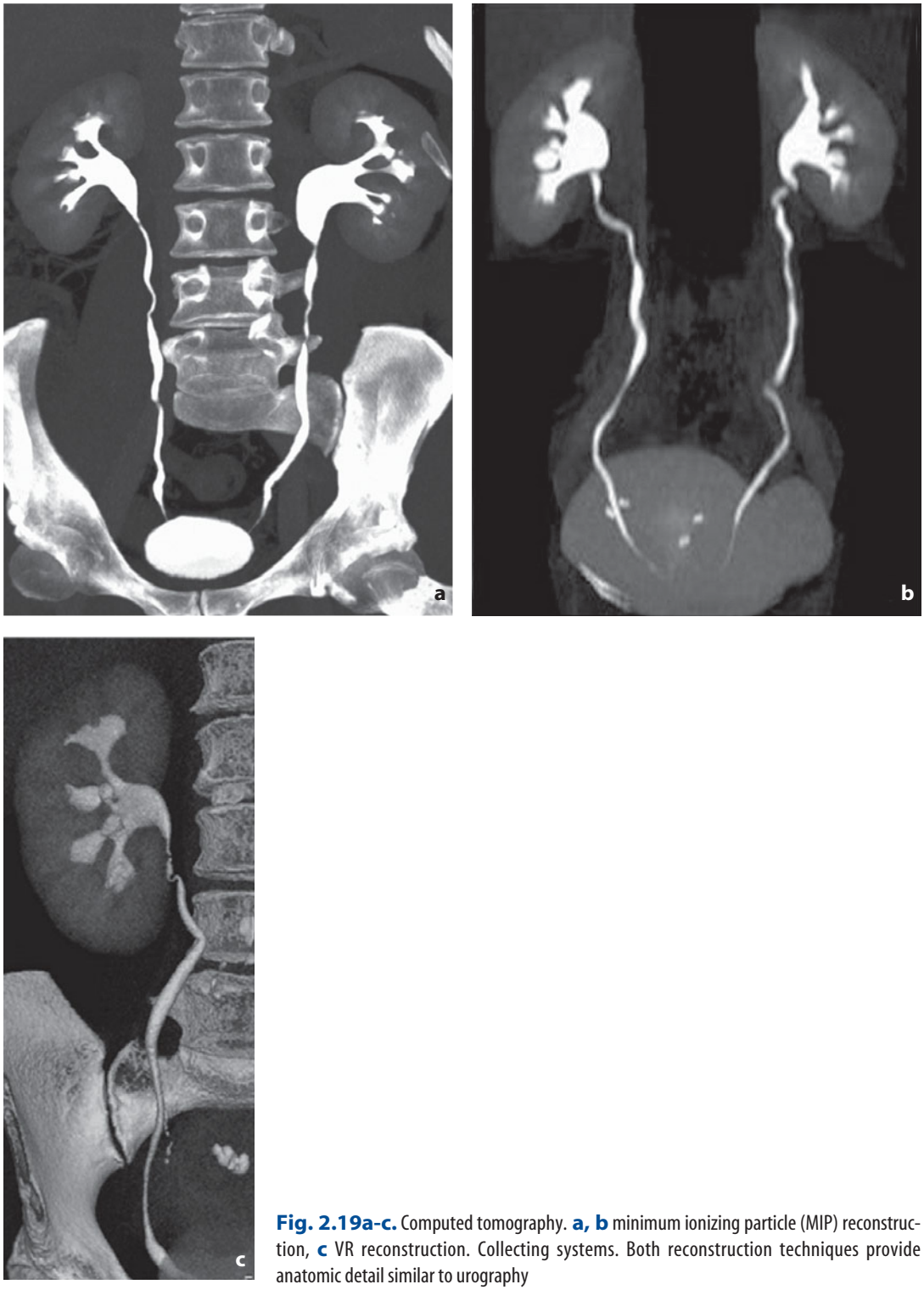

Fig. 2.19a-c. Computed tomography. **a, b** minimum ionizing particle (MIP) reconstruction, **c** VR reconstruction. Collecting systems. Both reconstruction techniques provide anatomic detail similar to urography

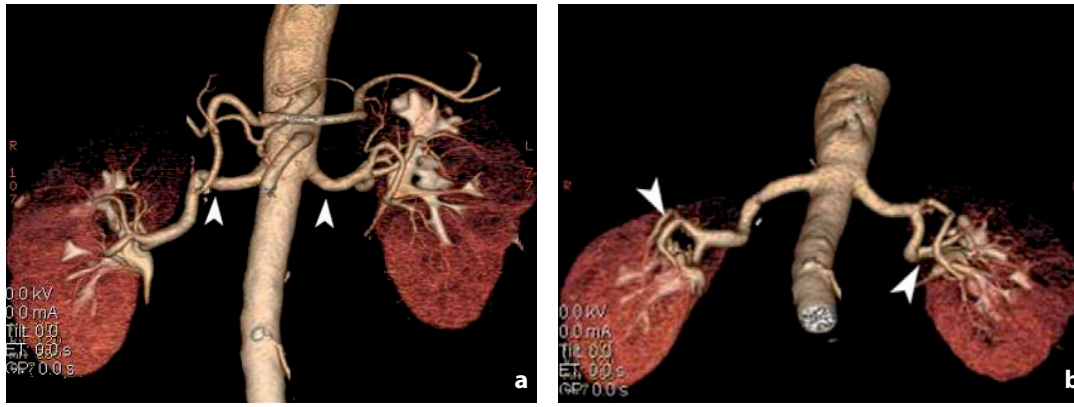

Fig. 2.20a,b. Computed tomography. VR reconstructions of the aorta and renal arteries. **a** The *arrowheads* indicate the renal arteries, which are visualized right up to their hilar subdivision (**b**)

Magnetic Resonance Anatomy

The magnetic resonance (MR) appearance of the kidneys depends on the degree of hydration and the type of sequence used. Generally, in T1-weighted images the renal parenchyma can be clearly distinguished in the cortex (higher signal intensity) and medulla. In T2-weighted images the differentiation is not as good and the cortex appears slightly less intense than the medulla (**Fig. 2.21**). A line of low signal intensity can often be observed at the interface between parenchyma and perirenal fat. This should not be confused with the capsule, as this appearance arises from a chemical shift artifact along the phase encoding axis.

As described above, renal enhancement can be observed in a dynamic study after the injection of paramagnetic contrast medium usually with a concentration of 0.1 mmol/kg and an injection speed of 2 mL/s. The medium is readily filtered in the glomerules and is not secreted or reabsorbed by the epithelial cells of the tubules. Its concentration at the level of the kidneys, therefore, is directly correlated with perfusion and glomerular filtrate. The paramagnetic contrast medium has the property of modifying relaxation times, and with the low doses generally used causes a shortening of tissue T1, thus increasing the tissue signal (obviously in T1-weighted sequences). In normal subjects three enhancement phases can be identified: corticomedullary (at 25–70 s), during which the renal cortex displays enhancement much greater than that of the slower medulla, thus enabling their differentiation; nephrographic (at 80–180 s), during which the renal parenchyma becomes uniform and the corticomedullary differentiation can no longer be appreciated; and excretory (>180 s), during which the collecting systems are opacified (**Fig. 2.22**).

The use of organ-specific contrast media can provide both morphologic and functional information (**Fig. 2.23**).

In nonenhanced images the pyelocaliceal cavities generally cannot be visualized unless distended. Urine has an elevated T1 and T2 relaxation time and therefore has low signal intensity in T1-weighted images and high signal intensity in T2.

In nonenhanced images the vessels, and especially the veins, can be easily identified as tubular structures without intraluminal signal intensity due to the flow which causes dephasing of the protons in the blood. Their visualization is clearly improved in MR angiography sequences obtained with time-of-flight, phase contrast, or, better still, with the administration of paramagnetic contrast medium (contrast-enhanced MRA) (**Figs. 2.24, 2.25**).

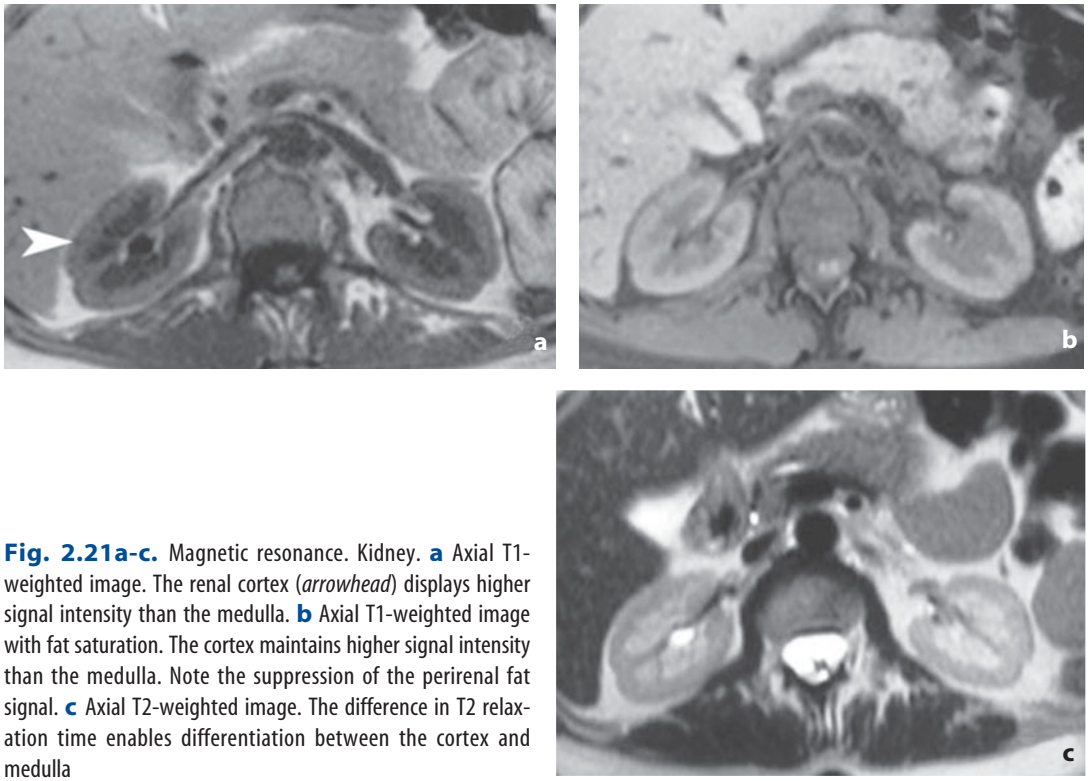

Fig. 2.21a-c. Magnetic resonance. Kidney. **a** Axial T1-weighted image. The renal cortex (*arrowhead*) displays higher signal intensity than the medulla. **b** Axial T1-weighted image with fat saturation. The cortex maintains higher signal intensity than the medulla. Note the suppression of the perirenal fat signal. **c** Axial T2-weighted image. The difference in T2 relaxation time enables differentiation between the cortex and medulla

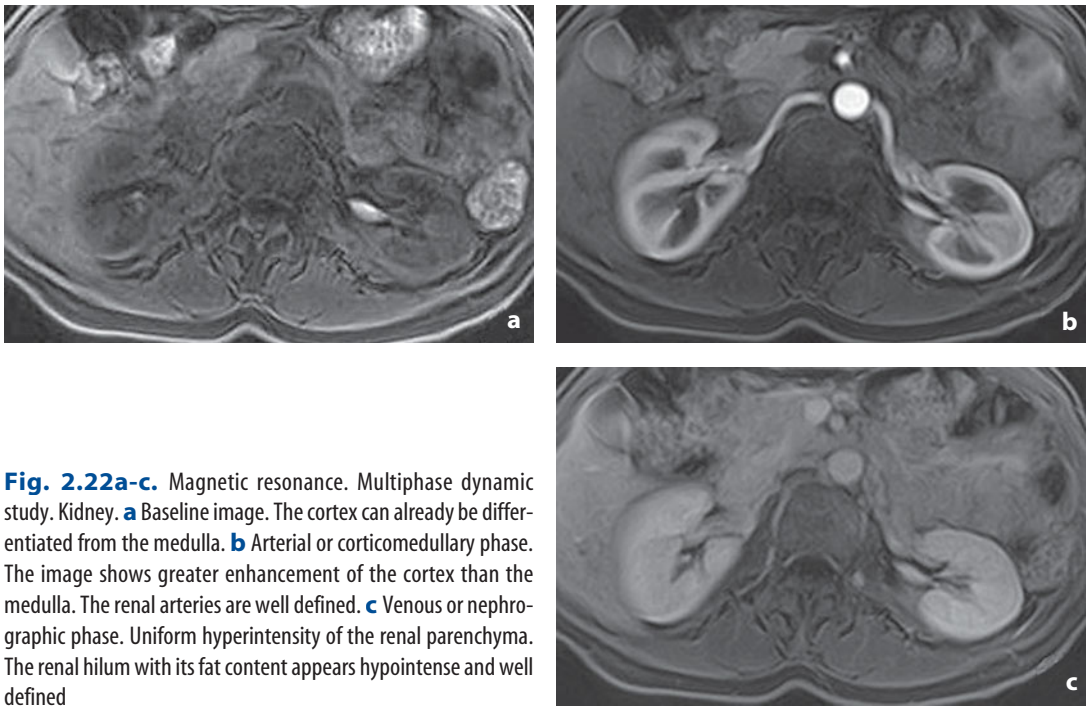

Fig. 2.22a-c. Magnetic resonance. Multiphase dynamic study. Kidney. **a** Baseline image. The cortex can already be differentiated from the medulla. **b** Arterial or corticomedullary phase. The image shows greater enhancement of the cortex than the medulla. The renal arteries are well defined. **c** Venous or nephrographic phase. Uniform hyperintensity of the renal parenchyma. The renal hilum with its fat content appears hypointense and well defined

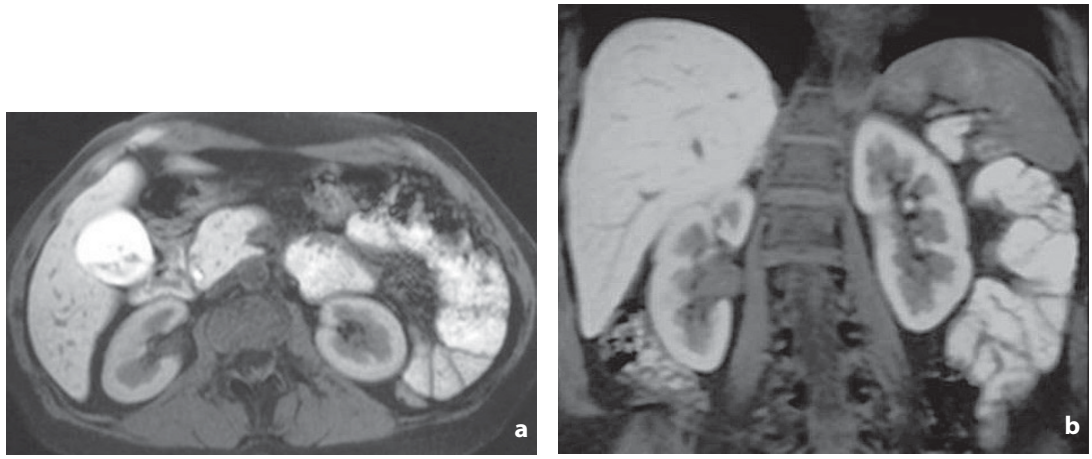

Fig. 2.23a,b. Magnetic resonance. Axial (**a**) and coronal (**b**) images. Kidney. The same subject as in Figure 2.20. After injection and uptake by the glomerules of organ-specific contrast medium (Mn-DPDP) uniform enhancement of the cortex can be appreciated. Note the enhancement also of the suprarenal glands, the liver and the pancreas

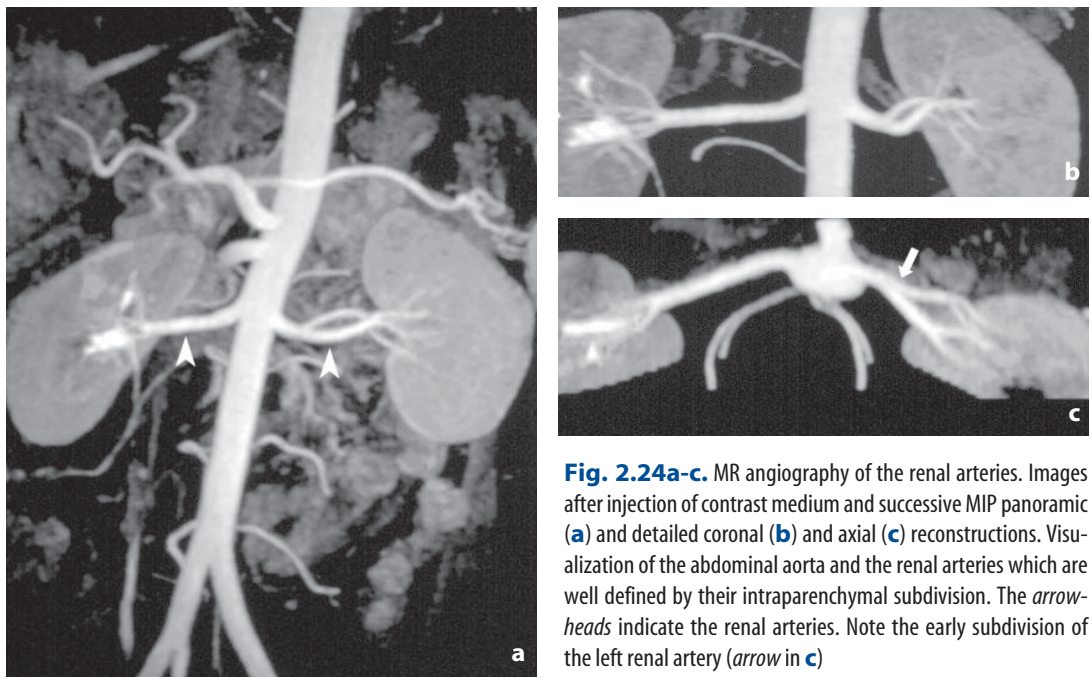

Fig. 2.24a-c. MR angiography of the renal arteries. Images after injection of contrast medium and successive MIP panoramic (**a**) and detailed coronal (**b**) and axial (**c**) reconstructions. Visualization of the abdominal aorta and the renal arteries which are well defined by their intraparenchymal subdivision. The *arrowheads* indicate the renal arteries. Note the early subdivision of the left renal artery (*arrow* in **c**)

Perirenal fat has a higher signal intensity that renal parenchyma in T1-weighted images, whereas it appears slightly hypointense in T2. The renal fascia appears as a thin line of low signal intensity in both T1 and T2. Its identification is facilitated by the elevated signal intensity of the perirenal and pararenal spaces.

In normal conditions the thin-diameter ureter is not easily identifiable along its entire course in the absence of paramagnetic contrast medium, with or without the association of diuretics (Fig. 2.26). However, MR images can provide excellent visualization of the collecting system and the urinary bladder when distended with urine.

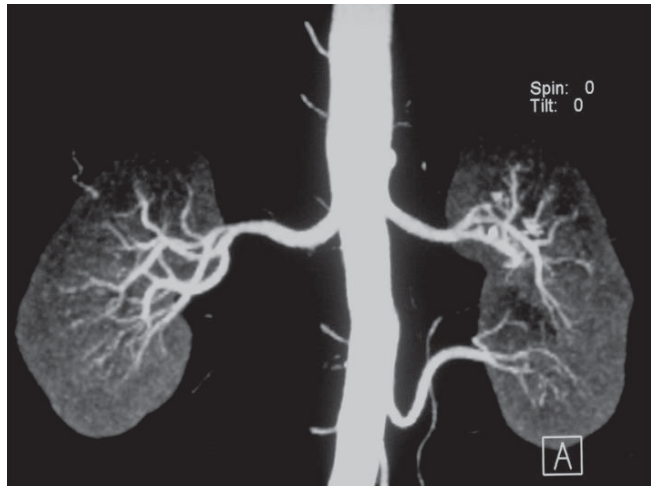

Fig. 2.25. MR angiography of the renal arteries. Coronal image after injection of contrast material and successive MIP reconstruction. Dual left renal artery

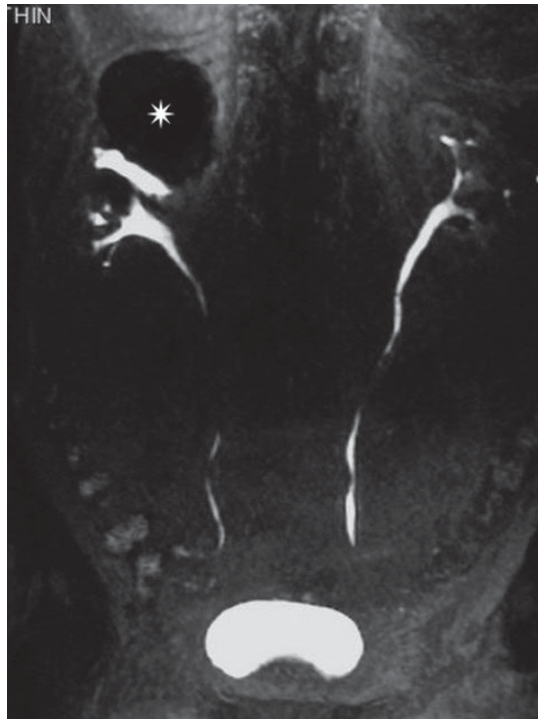

Fig. 2.26. MR urography. MIP reconstruction of the collecting systems visualized after the injection of contrast medium. A cortical cyst (*asterisk*) is present at the upper pole of the right kidney

The muscular layer and the lamina propria cannot be distinguished. Unlike in T1 (where the signal intensity is similar), in images weighted in proton density and T2 the mucosa and the lamina propria in some cases can be differentiated from the muscle coat given their elevated signal intensity. The muscular layer has intermediate signal intensity in T1, similar to that of skeletal muscle, and low signal in T2-weighted images. The adventitia is too low to be visualized (**Figs. 2.27, 2.28**).

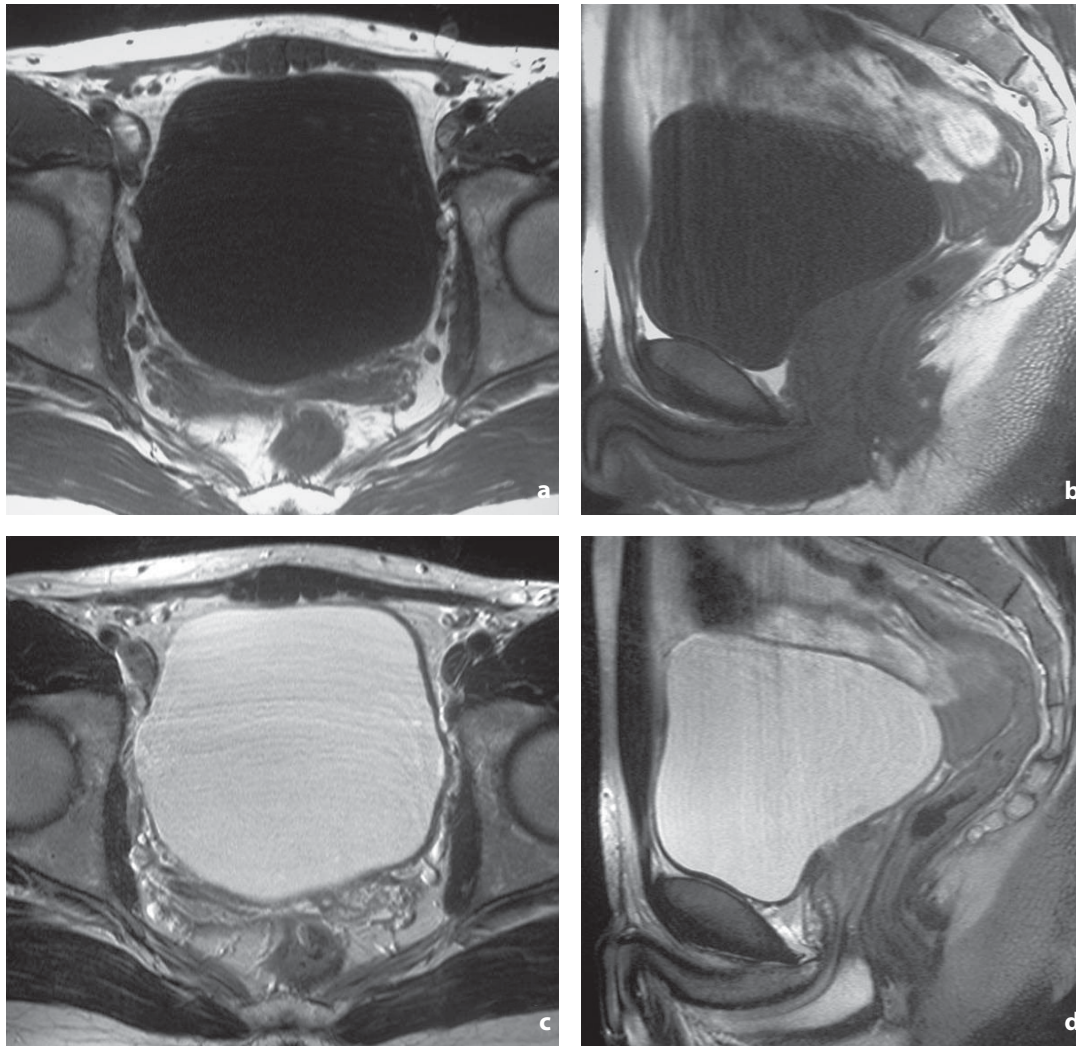

Fig. 2.27a-d. Magnetic resonance. Urinary bladder. Axial (**a**) and sagittal (**b**) T1-weighted images. The signal of the wall is of middle intensity, while the urine is hypointense. Axial (**c**) and coronal (**d**) T2-weighted images. The urine has a hyperintense signal

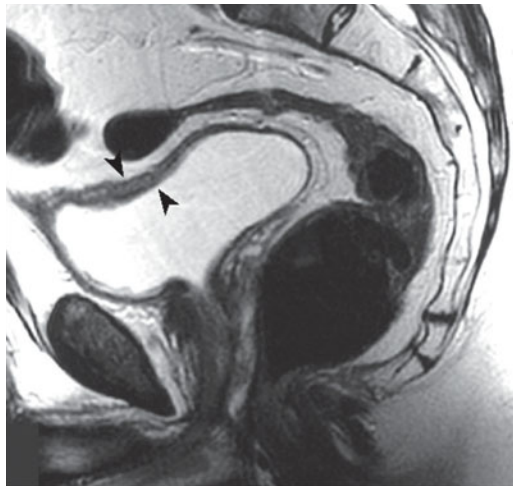

Fig. 2.28. Magnetic resonance. Urinary bladder. Axial T2-weighted image. The different layers making up the bladder wall can be distinguished (*arrowheads*)

In the early-phase dynamic images (45–100 s) acquired with the injection of paramagnetic contrast medium, the enhanced lamina propria can be distinguished from the muscle coat, which remains hypointense. In the late-phase sequences the enhancement of the mucosa and lamina propria decreases, while the enhancement of the muscle coat increases thus the two layers can no longer be differentiated.

Luboldt W, Krestin GP (2000) Kidneys. In: Heuck A, Reiser M (eds) Abdominal pelvic MRI. Springer-Verlag, Berlin, pp 149-166

Martin DR, Brown MA, Semelka RC (2005) Primer on MR imaging of the abdomen and pelvis. Wiley & Sons, Hoboken, New Yersey

Male Reproductive System: Normal Gross and Microscopic Anatomy

3

L. Grazioli, E. Apostolopoulos, N. Zappa

The male reproductive system consists of the gonads (testes or testicles), the duct system (epididymis, ductus deferens and ejaculatory duct), accessory glands (seminal vesicles, prostate and bulbourethral glands) and external genital organs (scrotum and penis).

Embryology

Although the sex of the embryo is genetically determined at the moment of fertilization, the gonads acquire their characteristic male or female morphology only in the seventh week of gestation.

The gonads initially appear as two longitudinal elevations, the gonadal or genital ridges, originating from the proliferation of celomic epithelium. No germ cells are present in the gonadal ridges until the sixth week of gestation. Shortly before and during their arrival, the celomic epithelium actively proliferates, penetrating the underlying mesenchyme to form a number of irregular cords called the primitive sex cords.

These cords remain connected to the surface epithelium both in males and females. At this stage the gonads are identical in males and females and are therefore called indifferent gonads.

If the embryo is genetically male, the primordial germ cells present XY sex chromosomes. Under the influence of chromosome Y, which encodes testes determining factor, the sex cords continue to proliferate between the seventh and eighth week of gestation, penetrating into the medulla of the gonad to form the testicular or medullary cords. These are composed of primordial germ cells and Sertoli's supporting cells and develop from the surface epithelium of the gonads. Through the testicular hilum the cords are interrupted, forming a network of fine cellular filaments which will later give rise to the tubules of the rete testis. In the advanced stage of development the testicular cords lose contact with the surface epithelium and become separated from it by a thin layer of fibrous connective tissue known as the tunica albuginea.

The interstitial Leydig cells develop from the mesenchyme of the gonadal ridge. Located between the testicular cords, these cells begin developing immediately following the differentiation of the cords. By the eighth week of gestation the Leydig cells begin to produce testosterone. The testicles then become able to influence the sexual differentiation of the genital ducts and the external genitalia. The cords remain solid until puberty, when they form lumens, becoming the convoluted seminiferous tubules.

The testicles initially develop in the lumbar region, in a laterovertebral position. From the third month of gestation they begin their descent towards the future scrotum, which is normally reached at the end of pregnancy. This migration is made possible by the caudal genital ligament and the gubernaculums testis.

The embryos of both sexes initially have two pairs of genital ducts: the mesonephric (Wolffian) ducts and the paramesonephric (Müllerian) ducts. The differentiation of

L. Olivetti, L. Grazioli (eds.), *Imaging of Urogenital Diseases*,

the conduits and the external genital organs occurs under the influence of hormones. The Sertoli cells produce a nonsteroid substance – anti-Müllerian hormone, also known as Müllerian inhibiting substance – which promotes the atrophy of the paramesonephric ducts. The Leydig cells secrete testosterone which stimulates the development of the mesonephric ducts.

As the testicles increase in volume the mesonephros undergoes atrophy, with only a few tubules from its caudal portion remaining by the eighth week. The remaining tubules shorten, lose contact with their glomeruli, fuse with the ductules of the rete testis forming the efferent tubules which connect the rete testis to the mesonephric duct. In male embryos the mesonephric duct remains, being transformed into the epididymis and the ductus deferens.

Shortly before they open into the urogenital sinus, each mesonephric duct, which have now become ductus deferens, gives off a diverticulum which further develops to become the seminal vesicle. The short tract of the distal duct to the seminal vesicle takes the name of ejaculatory duct and opens onto the posterior face of the urogenital sinus. During the third month a cluster of epithelial outgrowths derived from the epithelium lining the posterior wall of the sinus develop in the mesenchyme surrounding the ejaculatory ducts, giving rise to the prostate.

The paramesonephric ducts fully atrophy in the male, with the exception of vestigial remnants near the testis – the appendix testis.

During the third gestational week mesenchymal cells developed from the primordial germ cells migrate around the cloacal membrane causing the formation of a pair of slightly elevated folds (the cloacal folds), which inferior to the cloacal membrane join to form the genital tubercle.

The development of the external genitals is influenced by the secretion of androgens from the fetal testicles and is characterized by a rapid lengthening of the genital tubercle which forms the penis.

The genital swellings are initially situated in the inguinal region. As they develop they move caudally, with each swelling becoming a half of the scrotum separated from the other by the scrotal septum.

Sandler TW (2009) Langman's medical embriology. 11th edn. Wolters Kluwer, Lippincott Williams & Wilkins, Baltimore

Normal Anatomy

Testicles

The testicles or testes have the dual function of producing germ cells (spermatozoa) and secreting male sex hormones.

The testicle is a symmetrical ovoid organ, slightly flattened transversally, which is situated below the penis and contained in a cutaneous sac (scrotum) suspended at the inferior end of the spermatic cord (**Fig. 3.1**).

The two testicles are separated from each other by the scrotal septum. In the adult they measure 4×3×2.5 cm and weigh 20-30 g (including the epididymis). The inferior testicular pole is attached to the base of the scrotum by a fibromuscular cord (the scrotal ligament). The external surface of the testis is almost completely enveloped by a dual-layered serous sac, the tunica vaginalis, which is composed of peritoneal tissue. The parietal and visceral layers of the tunica vaginalis are fused at the level of the posterior testicular margin. The virtual space between the two contains a small amount of serous liquid (**Fig. 3.2**).

The testicle is covered by a highly resistant fibrous fascia known as the tunica albuginea. At its posterior border it is reflected to form the hilum or mediastinum testis which contains the rete testis. Numerous fibrous septa arise from the deep fascia of

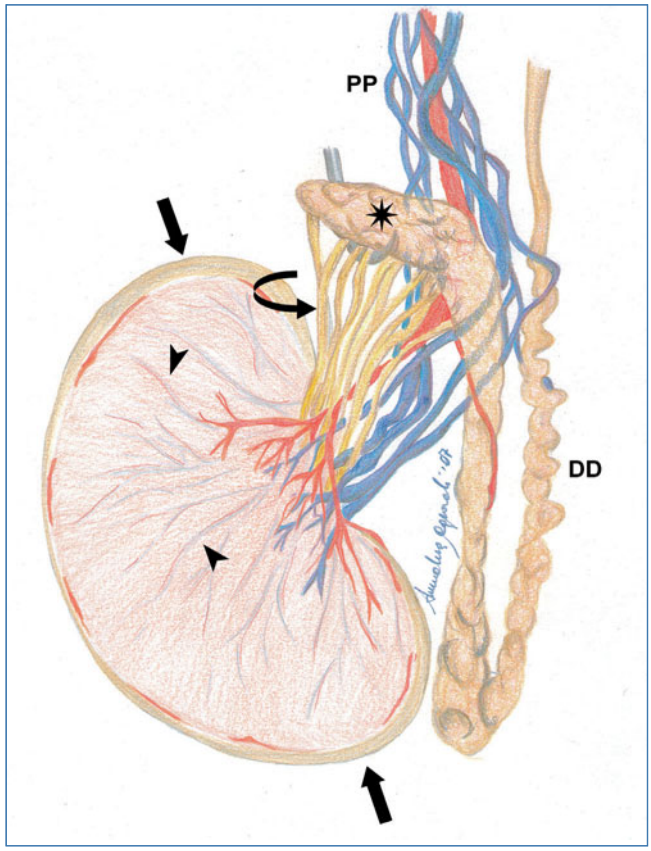

Fig. 3.1. Anatomic diagram of the testicle, epididymis, ductus deferens and pampiniform plexus. The sagittal section shows the tunica albuginea (*arrows*) and the septa (*arrowheads*), between which lie the seminiferous tubules which converge towards the mediastinum testis. At this level the efferent ductules are recognizable (*curved arrow*); these drain into the head of epididymis (*asterisk*). *DD*, ductus deferens; *PP*, pampiniform plexus

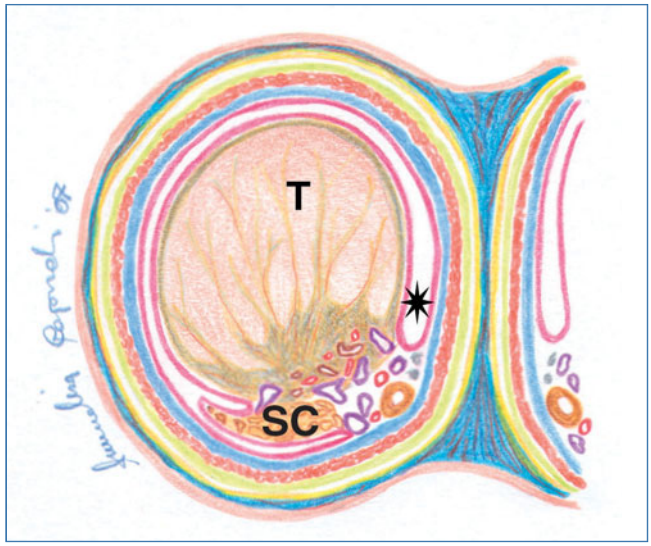

Fig. 3.2. Anatomic diagram of the right scrotum. Axial section. Superficial to deep the figure shows the external spermatic fascia in green, the cremaster muscle in red, the internal spermatic fascia in blue and the parietal and visceral layers of the tunica vaginalis in pink. The *asterisk* indicates the processus vaginalis. *T*, testicle; *SC,* spermatic cord

the tunica albuginea and run radially through the testicle to reach the mediastinum testis, thus dividing the testicular parenchyma in around 250-300 lobules. These are pyramidal in shape with the base abutting the tunica albuginea and the apex at the mediastinum testis.

Each lobule contains between 1 and 4 seminiferous tubules, each of which is 30-180 cm in length. These tubules have an extremely tortuous course, converging towards the mediastinum to form a single straight tubule which leads to the rete testis.

Vascularization of the testes is provided by the testicular arteries, which arise from the aorta slightly below the renal arteries.

The veins of the testicle and the epididymis join at the level of the posterior border to form larger anastomizing vessels with a tortuous course (pampiniform plexus) which ascend to become part of the spermatic cord. The latter gives rise to the testicular vein which empties on the right into the inferior vena cava and on the left into the left renal artery.

The lymphatic drainage of the testis follows the reverse course of the testicular artery, terminating in the pre- and para-aortic lymph nodes.

Microscopically, the wall of the seminiferous tubules consists of a lamina propria and a multilayered germinal epithelium. In the midst of the germinal epithelium, sperm cells and supporting (Sertoli) cells can be identified. Leydig interstitial cells, which have an endocrine function, are found in the connective tissue between the seminiferous tubules (**Fig. 3.3**).

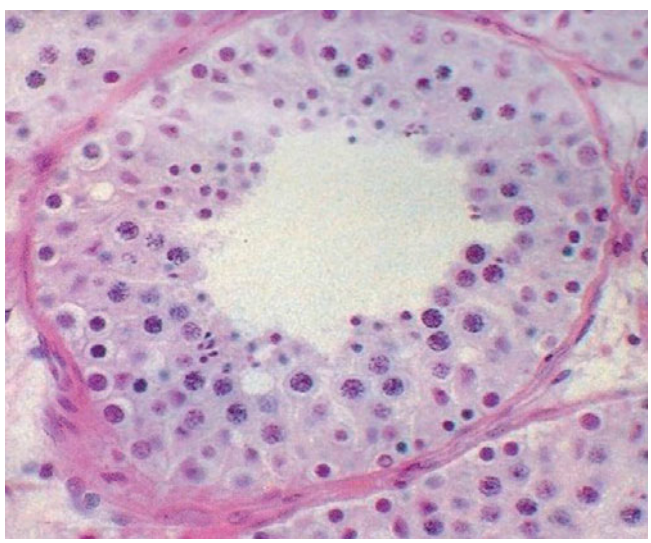

Fig. 3.3. Photomicrograph of a seminiferous tubule. The germ cells can be identified lining the wall of the tubule

Pathway of Sperm

The pathway of sperm begins in the testicle with the straight tubules and the rete testis and continues with the epididymis, ductus deferens, the ejaculatory duct and the urethra.

The rete testis gives rise to 10-15 efferent ductules. These emerge from the posterosuperior surface of the testis and form the head of the epididymis. The epididymis has the function of collecting the spermatozoa and facilitating their maturation. Each epididymis has the shape of a large comma situated on the posterosuperior surface of the testis. They can be divided into an enlarged end, the head (related to the testicle superiorly), an intermediate part, the body, and an inferior end, the tail, which continues in the ductus deferens.

At the level of the head of the epididymis, the merging of the efferent ducts gives rise to a single conduit (duct of epididymis), which has an extremely tortuous course.

The tail of the epididymis is followed by the ductus deferens, which is roughly cylindrical in shape with a diameter of 2-3 cm and a length of 40 cm. Four segments of the ductus deferens can be identified: testicular, spermatic cord, inguinal and abdominal-pelvic. The testicular part lies against the posterior face of the tail and body of epididymis. At the level of the transition between the body and head of epididymis, the ductus deferens leaves the latter to ascend vertically, becoming part of the spermatic cord (**Fig. 3.1**).

In addition to the ductus deferens, which is situated posteriorly, the spermatic cord contains the external spermatic artery (or cremasteric artery), the testicular veins (pampiniform plexus), lymph vessels, nerves, processus vaginalis and internal cremaster muscle.

Still contained within the spermatic cord, the ductus deferens (inguinal segment) passes through the inguinal canal. At the level of the internal abdominal orifice it leaves the other elements of the spermatic cord, and, running along the extraperitoneal pelvic space (abdominal-pelvic segment), it reaches the posterior surface of the urinary bladder. It passes above and medially to the ureter to then head inferomedially towards the base of the prostate and converges with the contralateral ductus. At that level it joins with the ipsilateral seminal vesicle and gives rise to the ejaculatory duct.

The ejaculatory ducts are 2-2.5 cm in length and run for most of their course through the prostate gland. They open through two small orifices at the level of posterior wall of the prostatic urethra, at the site of a longitudinal elevation known as the seminal colliculus or verumontanum.

The male urethra has a length of 18-20 cm. Only in its initial part does it exclusively transport urine, whereas from the opening of the ejaculatory ducts to the urethral meatus it also transports sperm. The urethra can be divided into a prostatic part (around 3 cm in length), a membranous part (around 1.5 cm in length) situated within the urogenital diaphragm, and a spongy part, which is the longest section (13-15 cm) and is contained in the sleeve-like corpus spongiosum. The spongy urethra can be divided into a bulbous segment, a penile segment and the navicular fossa, and opens onto the external urethral meatus.

Up to the level of the glans penis the urethra is lined by transition epithelium which is then substituted by squamous epithelium. The walls of the organ are abundant with urethral (Littré) glands.

Situated within the urogenital diaphragm are the bulbourethral glands (or Cowper's glands), whose ducts open into the initial part of the spongy urethra (**Fig. 3.4**).

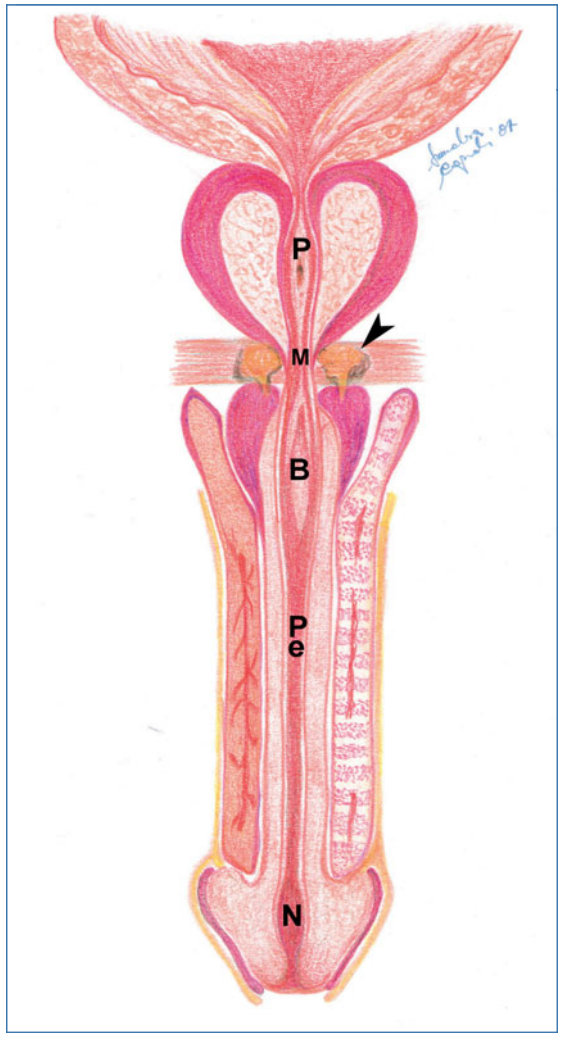

Fig. 3.4. Anatomic diagram of the male urethra. Coronal section. The various parts of the urethra are shown. The *arrowhead* indicates the bulbourethral gland. *P*, prostatic; *M*, membranous; *B*, bulbar; *Pe*, penile; *N*, navicular fossa

Seminal Vesicles

The seminal vesicles are a pair of small symmetrical glands which are poorly developed in the child and atrophied in the elderly. In the adult their longest axis, directed downwards, forwards and medially, measures 5-8 cm. They are situated in the pelvis between the fundus of the urinary bladder and the rectum and related to the prostate posterosuperiorly. Each seminal vesicle merges at an acute angle with its respective ductus deferens to form the ejaculatory ducts (Fig. 3.5).

Histologically they consist of a tubule with an irregular diameter which curls up on itself several times throughout its course. A saccular gland, its duct at the inferior end, joins the ipsilateral ductus deferens. Its wall is made up of a fibrous capsule and a mucous coat composed of pseudostratified epithelium.

Lazo DL (2004) Fundamentals of sectional anatomy: an imaging approach. Thomson Delmar Learning, pp 216-218

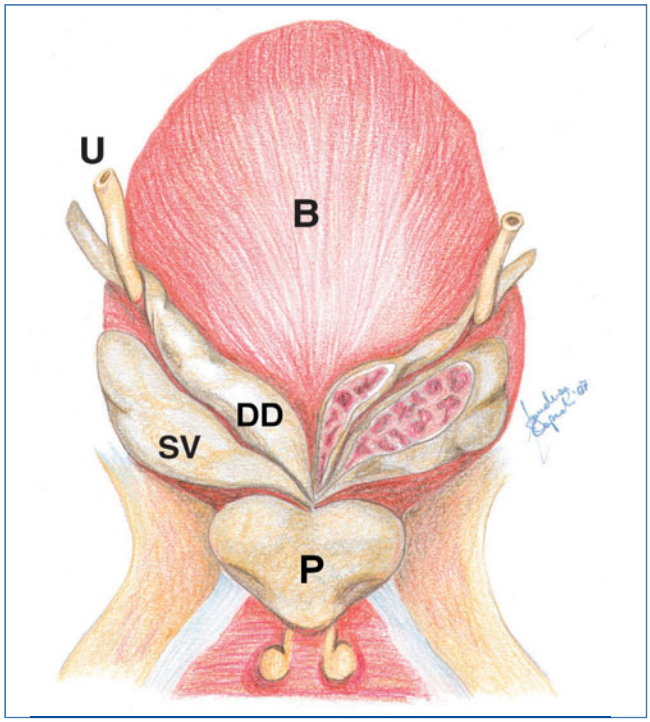

Fig. 3.5. Anatomic diagram of the distal ductus deferens, the seminal vesicles and the prostate. Posterior view, which shows the anatomic relations between the ductus deferens (*DD*), prostate (*P*), ureter (*U*), urinary bladder (*B*) and seminal vesicles (*SV*)

Prostate

The prostate is a single glandular organ situated medially in the pelvis (peritoneal pelvic space) between the fundus of the urinary bladder and the urogenital diaphragm, behind the pubic symphysis and in front of the ampulla of the rectum, between the medial fasciae of the two levator ani muscles. The prostate is the size and shape of a walnut, with an apex pointing down and forwards, and a base turned upwards and backwards (**Figs. 3.6, 3.7**).

Grayish-reddish in color with a hard elastic consistency, the prostate appears very small in the child and only begins to grow at puberty: towards 20-25 years of age it reaches an average of 3 cm in height, 4 cm in width (corresponding to the base) and 2.5 cm in thickness. At this age it usually weighs 20 g.

The prostate is surrounded by a sheath of muscle fibers and collagen which form the prostatic capsule (**Fig. 3.8**). Anteriorly it is connected to the pubic symphysis by two bands of connective tissue, known as puboprostatic ligaments. Posteriorly it is separated from the rectum by the rectovesical septum.

The seminal vesicles are related to the gland posterosuperiorly, between the fundus of the urinary bladder and the rectum. Inferiorly the prostatic apex is related to the perineal membrane.

Passing through the prostate, from above to below, is the first portion of the urethra (prostatic urethra), into which the prostate empties its secretion during ejaculation. An angle of 145° halfway between the base and the apex of the prostate, it divides the urethra into proximal and distal segments of approximately the same length but with

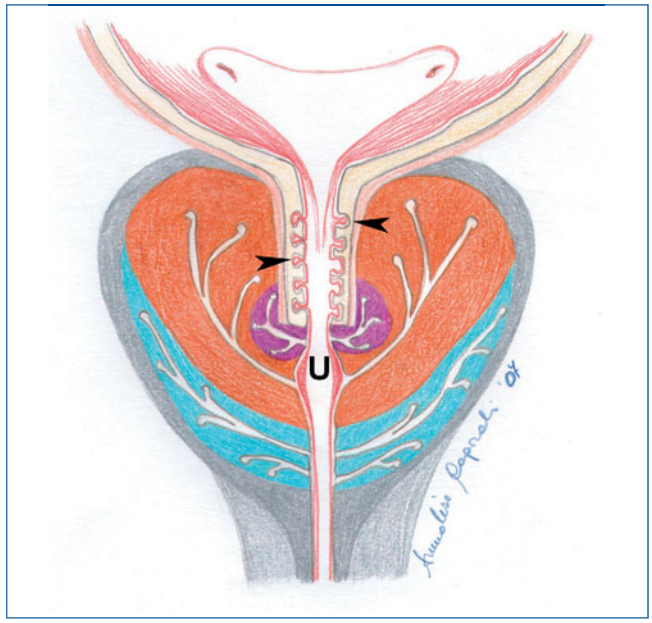

Fig. 3.6. Diagram of the zonal anatomy of the prostate. The coronal section illustrates the peripheral zone (*blue*), the central zone (*brown*), and the transition zone (*purple*). The *arrowheads* indicate the peri-urethral glands. *U*, urethra

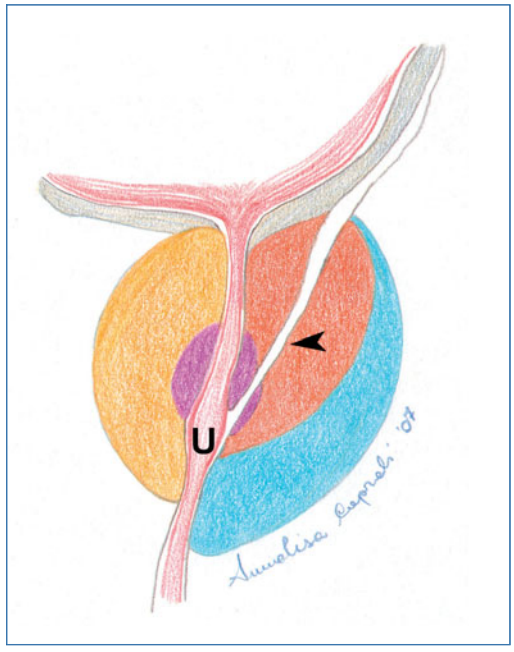

Fig. 3.7. Diagram of the zonal anatomy of the prostate. The sagittal section illustrates the peripheral zone (*blue*), the central zone (*brown*), the transition zone (*purple*) and the anterior fibromuscular zone (*yellow*). The *arrowhead* indicates the ejaculatory duct. *U*, urethra

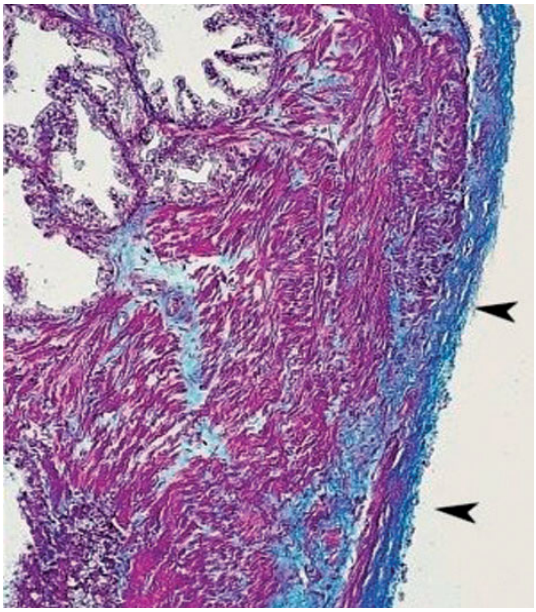

Fig. 3.8. Photomicrograph of the prostatic capsule. On the inner side the prostatic capsule is poorly defined, consisting of smooth muscle fibers running transversely which intertwine with peri-acinar smooth muscle fibers. Collagen fibers are constantly present and appear compact in a thin membrane comprising the outer limit of the capsule (*arrowheads*)

markedly different anatomic relations. The first sphincter formed by a cylinder of smooth muscle fibers surrounds the proximal segment of the urethra between the base of the seminal colliculus and the neck of the bladder (preprostatic sphincter). It is likely that the only function of this sphincter is to prevent the retrograde flow of semen during ejaculation. The seminal colliculus is situated in the distal segment. This is covered with a second semicylindrical sphincter of striated muscle fibers which is continuous with the external striated sphincter beyond the apex of the gland.

Also passing through the prostate, obliquely in the posterosuperior wall, are the ejaculatory ducts.

The prostate can be divided into four lobes on the basis of their different relations with the urethra and the ejaculatory ducts: anterior, median and two lateral lobes. The two lateral lobes (right and left) are larger and extend posteriorly to a frontal plane passing through the ejaculatory ducts.

The anatomic subdivision proposed by McNeal takes into consideration the heterogeneous composition of the prostate, which in addition to the glandular regions includes purely muscular and fibromuscular regions. Each glandular region drains into a specific urethral segment and also differs histologically from the others.

On the basis of the McNeal classification the urethra roughly divides the prostate into an anterior (or ventral fibromuscular) part and a posterior (or dorsal glandular) part.

The ventral fibromuscular connective tissue is mainly composed of smooth muscle which is continuous with the fibers of the detrusor of the anterior bladder wall. In fact these fibers extend distally from the neck of the bladder and are arranged laterally, covering the entire anterior and anterolateral surface of the prostate. The thickness of the muscular tissue increases distally up to the seminal colliculus, where its mass is further augmented by a fibrous component. Caudal to the seminal colliculus the muscle tissue becomes increasingly thinner towards the prostatic apex.

The dorsal glandular portion can in turn be subdivided into an external and internal region. The former includes the central and peripheral zone, which account for approximately 25% and 70% of the volume of the prostate, respectively, and are clearly distinct from each other both macroscopically and microscopically, especially in the normal prostate of young subjects. The central zone surrounds the proximal

segment of the urethra and the entire course of the ejaculatory ducts posterosuperiorly, such that the orifices of the latter are surrounded by those of the ducts of the central zone on the rounded apex of the seminal colliculus. The peripheral zone surrounds both the central zone and the distal segment of the urethra. Its main ducts open in a double lateral line in the distal segment of the prostatic urethra, separately from those of the central zone.

The internal region includes the peri-urethral zone (less than 1% of the prostate) and the transition zone (around 5% in the young adult). The transition zone is made up of two small lobules immediately lateral to the preprostatic sphincter. The ducts open along the proximal continuation of the lateral double line formed by the orifices of the ducts of the peripheral zone.

The peri-urethral glands are contained in the connective tissue immediately adjacent to the proximal urethra. The ducts open into the proximal urethral segment in a double lateral line, thus further representing the proximal continuation of the ductal systems of the peripheral and transition zones (**Fig. 3.6**).

The zone classification is important for the distribution of prostate cancers: 70–80% of adenocarcinomas originate in the peripheral zone, whereas only 20-30% develop in the transition and central zones. The transition zone, which is refractory to the development of cancer, is the site of benign prostatic hyperplasia.

Prostatic vascularization is mainly provided by the inferior vesical arteries. The periprostatic venous plexus surrounds the gland and drains into the internal iliac veins and the presacral venous plexus. Anteriorly numerous small veins compose the Santorini plexus.

The lymphatic vessels chiefly drain into the obturator, the internal and external iliac, and the common and presacral lymph nodes.

Microscopically, the prostate consists of a complex of 30-50 branched tubuloalveolar serous glands which open some 15-40 excretory ducts into the prostatic urethra. The epithelium lining the excretory ducts is initially stratified cylindrical, which tends to become simple cylindrical epithelium in the smaller ducts. The cylindrical cells are of variable height and contain numerous secretory granules in their apex.

The branching ducts of the central zone form acini with irregular borders partially subdivided by an intricate system of intraluminal ridges, whereas the acini of the peripheral zone are uniformly small and rounded with smooth walls (**Fig. 3.9**).

The glandular tissue of the transition and peri-urethral zones is histologically identical to that of the peripheral zone.

McNeal JE (1968) Regional morphology and pathology of the prostate. Am J Clin Pathol 49:347-357

McNeal JE (1972) The prostate and prostatic urethra: a morphological synthesis. J Urol 107:1008-1016

McNeal JE (1978) Origin and evolution of benign prostatic enlargement. Invest Urol 15:340-345

McNeal JE (1981) The zonal anatomy of the prostate. Prostate 2:35-49

McNeal JE (1981) Normal and pathological anatomy of prostate. Urology 17:11-16

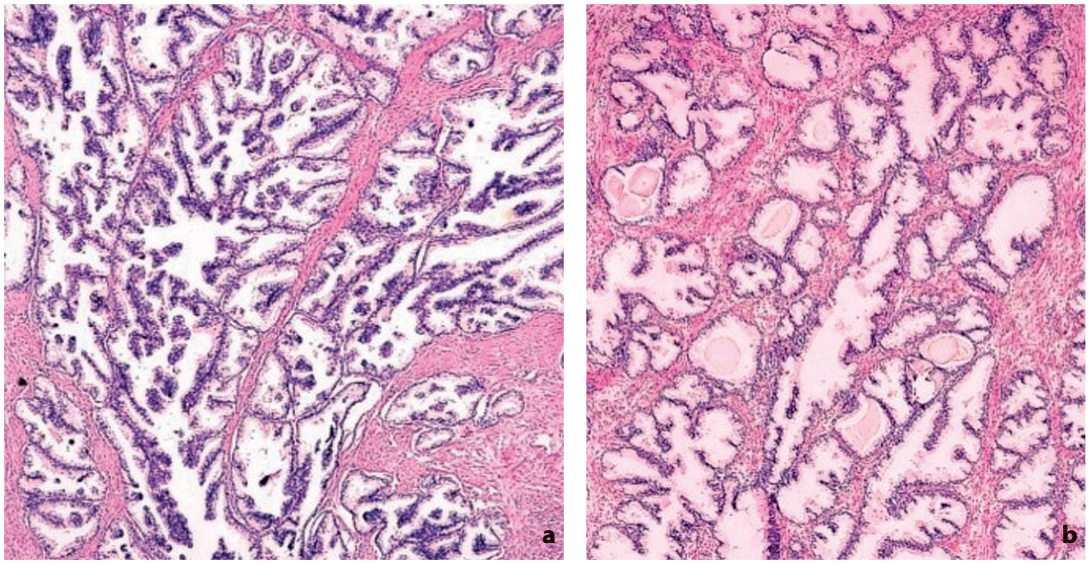

Fig. 3.9a,b. Photomicrograph of the prostate. **a** Ducts and acini of the central zone. **b** Ducts and acini of the peripheral zone

Penis

The penis is the male organ of copulation, which it achieves by its erectile ability. It is made up of three elongated formations: the two corpora cavernosa and the corpus spongiosum, which contains the urethra. The penis also consists of a fixed part or root, a mobile part or body and an enlarged extremity known as the glans penis (Fig. 3.10).

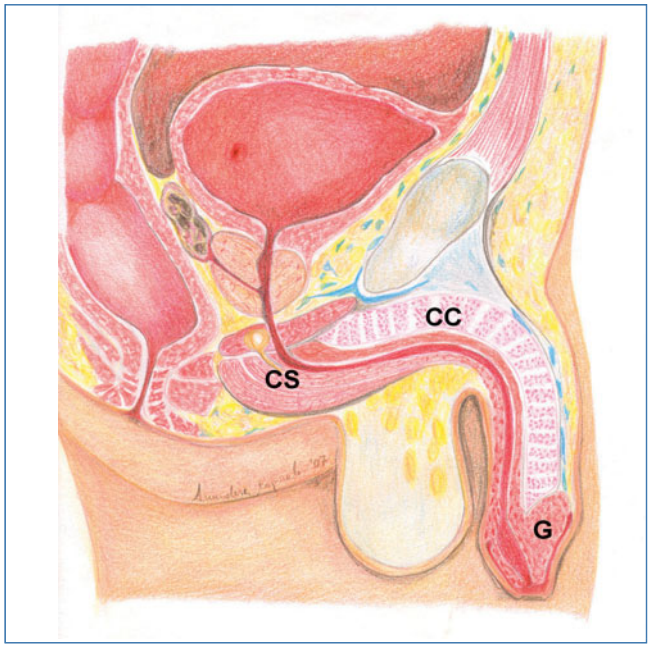

Fig. 3.10. Anatomic diagram of the penis. Sagittal section. The figure shows the fixed part, the mobile part and the glans penis. *CC*, corpus cavernosum; *CS*, corpus spongiosum; *G*, glans penis

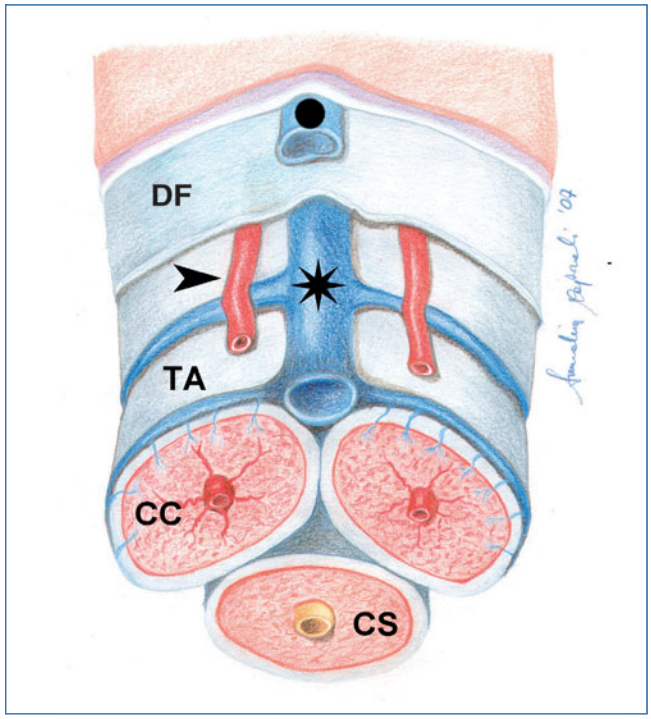

Fig. 3.11. Anatomic diagram of the penis. Transverse section. The *arrowhead* indicates the dorsal artery, the *asterisk* the deep dorsal vein and the dot the superficial dorsal vein. *CC*, corpus cavernosum; *CS*, corpus spongiosum of the urethra; *DF*, deep fascia; *TA*, tunica albuginea

The root is located deep within the anterior perineum. The proximal portions of the two corpora cavernosa are attached to the ischial tuberosity and surrounded by the ischiocavernous muscles, while the corpus spongiosum is attached to the inferior part of the urogenital diaphragm and covered by the bulbospongiosus muscle. Distally the two corpora cavernosa converge forming the pendulous part which, in the flaccid state, forms an angle of 60° with the root. The corpus spongiosum of the urethra is located in a depression between the ventral surfaces of the two corpora cavernosa. Distally the corpus spongiosum expands abruptly to form the glans penis.

The corpora cavernosa of the penis and the corpus spongiosum of the urethra are composed of a fibrous outer covering, the tunica albuginea, and cavernous (or erectile) tissue. All three corpora are surrounded by a series of sheaths, which from the outermost to the innermost are the skin, loose connective tissue and deep fascia (**Fig. 3.11**).

The vasculature of the penis and the urethra is chiefly provided by the dorsal artery which arises from the internal pudendal artery, the terminal branch of the internal iliac artery.

Tanagho E, McAninch JW (2007) Smith's general urology. McGrow-Hill, pp 1-30

Walsh PC, Retik AB, Darracott Vaughan E et al (2002) Campbell's urology. WB Saunders Co., Philadelphia, pp 7-23

Male Reproductive System: Normal Radiologic Anatomy

4

L. Grazioli, L. Olivetti, N. Zappa, E. Apostolopoulos

Ultrasonographic Anatomy

Scrotum and Testicles

B-mode ultrasonography (US) of the scrotum and its contents is done with a linear transducer which should have a scan surface of at least 5 cm to be able to perform precise measurements of the testicular volume. The frequency used should not be lower than 7.5 MHz. The examination begins with the patient in the supine position being asked to hold the end of the penis upwards. It may then be useful to perform the examination with the patient in the upright position to better visualize the venous plexuses.

The normal anatomy of the scrotum is given by a three-layered US image: hyperechoic external layer, hypoechoic middle layer and hyperechoic internal layer.

Under normal conditions, the tunica vaginalis cannot be visualized. Only in the presence of hydrocele does it become possible to identify the two layers of the tunica vaginalis propria, both of which are hyperechoic.

The US study of the testicle (located in the scrotum and not able to be moved into the inguinal canal with the external pressure of the transducer) should be performed with axial and longitudinal scans. The testis has an elongated ovoid appearance with two fasciae (medial and lateral), two borders (anterior and posterior) and two poles (upper and lower). The greater and slightly oblique sagittal axis is between 44 and 58 mm. The laterolateral diameter is 18-24 mm, while the anteroposterior diameter measures 30-36 mm. The testicular volume, which is calculated using the elissoid formula, is normally 17±5.5 cm^3 on the right and 17±5.8 cm^3 on the left.

The parenchymal structure is characterized by fine, dense and uniformly distributed echoes. They have a low-level pattern in the prepubescent period which becomes mid-level in the adult, similar to that of the thyroid (**Fig. 4.1**). An irregular and nonuniform pattern should always be considered pathologic and is significantly correlated with reduced testicular function. The very thin tunica albuginea is difficult to distinguish in the absence of hydrocele. It can be recognized by a thin hypoechoic line underlying the visceral layer of the tunica vaginalis propria. In contrast, the mediastinum testis can almost always be visualized as a hyperechoic ovular or triangular image in axial scans and as densely hyperechoic streaks in the sagittal plane (**Fig. 4.2**). The rete testis is not visible if it is not dilated. The vessels can be distinguished as thin hypoechoic streaks distributed obliquely from the anterior to the posterior border. In the presence of hydrocele at the upper testicular pole, a small pedunculated body less than 6 mm in size is often identifiable projecting into the processus vaginalis: this is the appendix testis and is usually isoechoic to the testicle.

Study with **color Doppler** is able to evaluate the testicular vessels. The testicular artery is the main vessel and it runs across the posteromedial surface of the testicle towards the lower pole. From here it ascends anteriorly towards the upper pole, penetrates the tunica albuginea and subdivides, forming a network of vessels below the

L. Olivetti, L. Grazioli (eds.), *Imaging of Urogenital Diseases*,

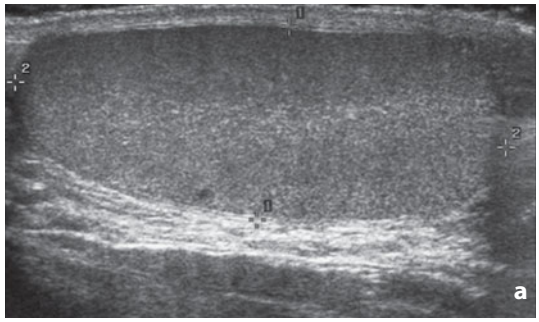

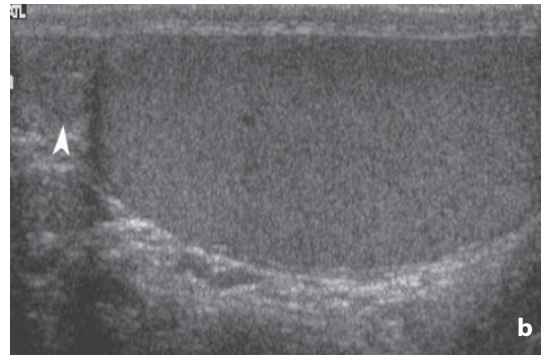

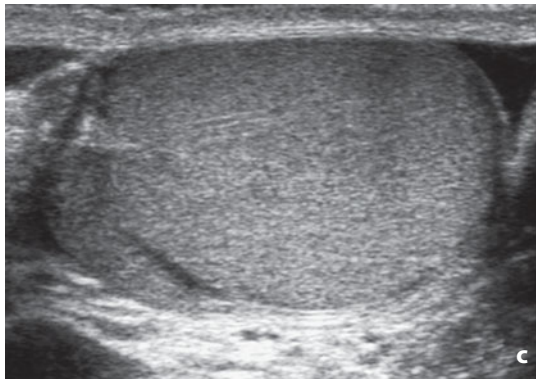

Fig. 4.1a-c. Ultrasonography. Testicle. **a,b** Longitudinal scans. **c** Transverse scan. In the normal testicle the structure is uniform. In image **b**, the head of the epididymis (*arrowhead*) is visible at the upper pole

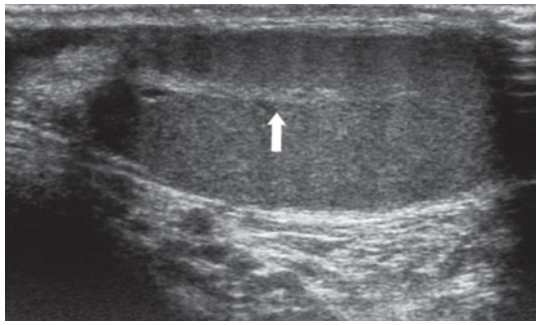

Fig. 4.2. Ultrasonography. Mediastinum testis. The *arrow* indicates a hyperechoic band crossing the testicle, corresponding to the mediastinum testis

t unica albuginea known as capsular vessels. These give rise to the centripetal branches which run towards the mediastinum (**Figs. 4.3, 4.4**).

After the injection of US contrast medium, the testicular parenchyma appears uniformly hyperechoic. Indications for the use of contrast medium are limited essentially to differentiation of focal lesions with altered enhancement (inflammation or tumors) from those with no enhancement (hematomas, trauma).

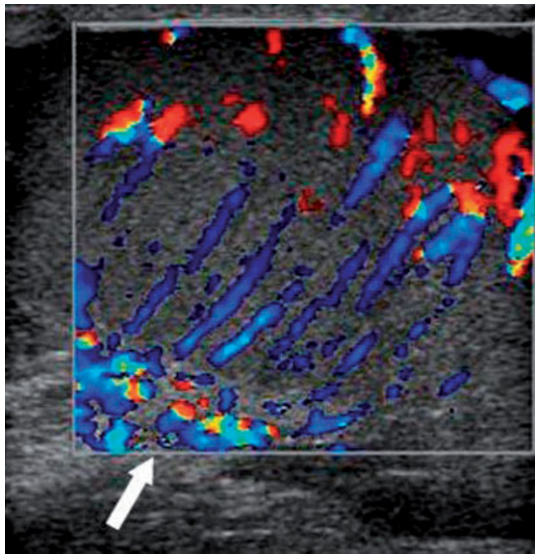

Fig. 4.3. Color Doppler. The image shows the rich vasculature of the testicle with fan-shaped distribution. The *arrow* indicates the mediastinum testis

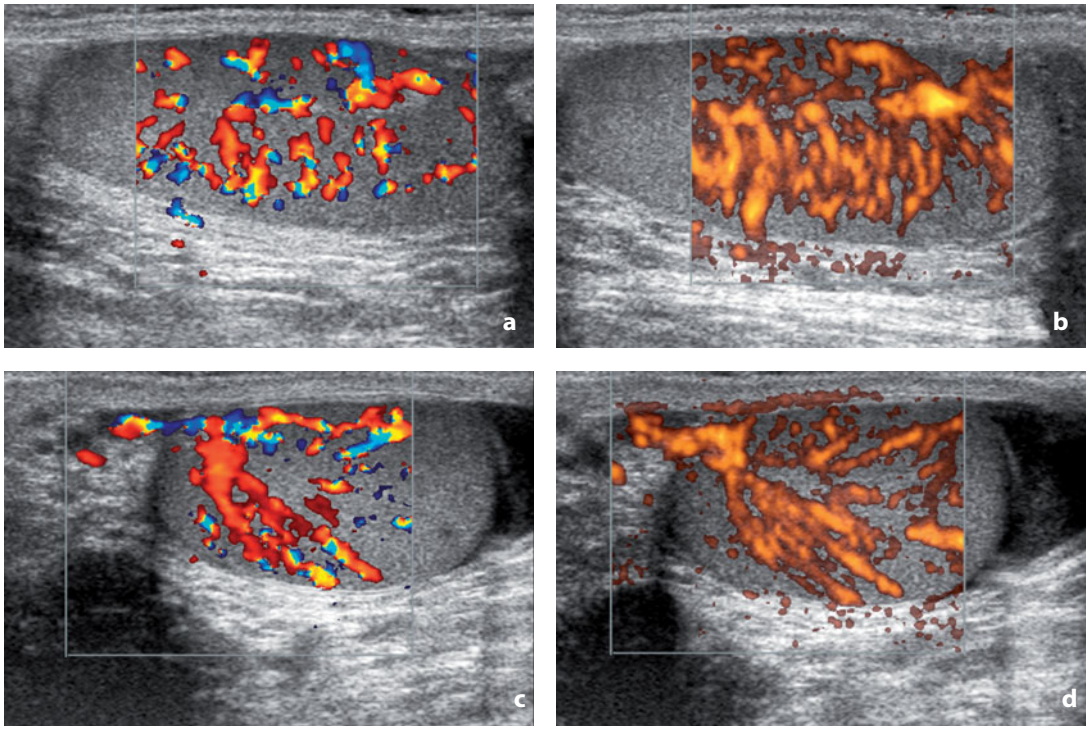

Fig. 4.4a-d. Color and power Doppler. Vasculature of the normal testicle. **a,b** Longitudinal scans. **c,d** Transverse scans. The images afford a comparison of color Doppler (**a,c**) and power Doppler (**b,d**)

Epididymis, Ductus Deferens and Spermatic Cord

The head of the epididymis is the portion that can best be evaluated with US. Located above the upper pole of the testis it is well contrasted by the liquid contained in the potential cavity of the processus vaginalis. Its structure is similar to that of the testis, from which it is well separated by a thin hypoechoic fissure. In the craniocaudal

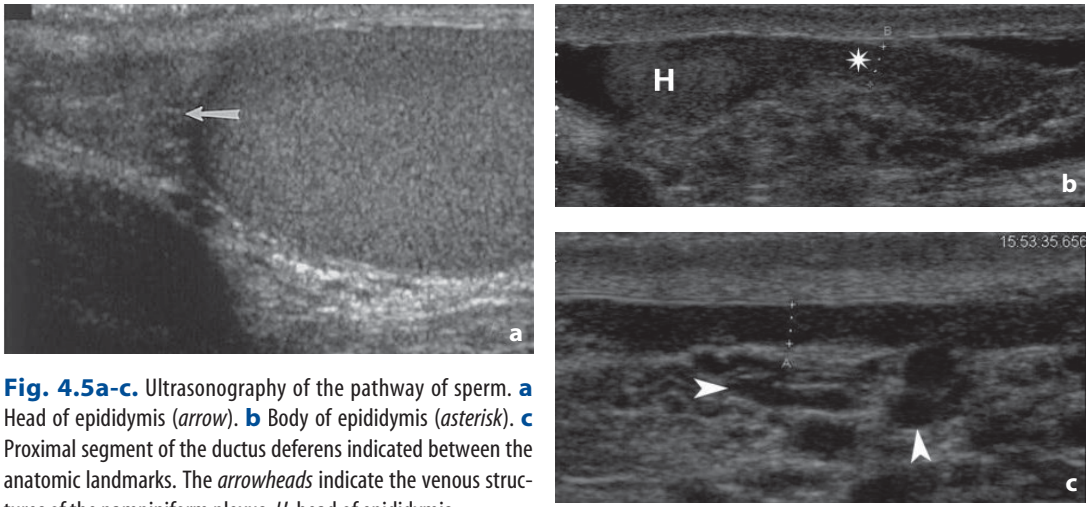

Fig. 4.5a-c. Ultrasonography of the pathway of sperm. **a** Head of epididymis (*arrow*). **b** Body of epididymis (*asterisk*). **c** Proximal segment of the ductus deferens indicated between the anatomic landmarks. The *arrowheads* indicate the venous structures of the pampiniform plexus. *H*, head of epididymis

direction it usually measures no more than 12 mm. The head of the epididymis can give rise to a small, generally isoechoic appendix with a possible cystic appearance.

The body of the epididymis is thin (maximum thickness around 3 mm) in relation to the testis posteriorly, from which it is separated by a thin hyperechoic line (sinus of epididymis). The body, however, may be situated laterally to the testis. In longitudinal scans it appears as a tubular structure which follows the convex profile of the testicle, in comparison to which it is only slightly less reflective. In axial scans the body of the epididymis appears as a thin ellipsoidal formation beside the mediastinum. The tails of the epididymis and ductus deferens are markedly hypoechoic in comparison with the remaining portions. The ductus deferens is situated in the posterior compartment of the spermatic cord and has a curved course as it runs towards the inguinal canal (**Fig. 4.5**).

The spermatic cord is well visualized in axial scans, situated above the upper testicular pole. The anterior compartment, containing the testicular artery and the pampiniform plexus, and the posterior compartment, containing the ductus deferens, the artery and the deferential venous plexus, can be readily differentiated.

Color Doppler study of the spermatic cord is able to detect blood flow in both arterial and venous vessels. Pulsed Doppler can be used to detect two different types of arterial flow: low-resistance flow typical of parenchymal organs, which is indicative of the testicular artery, and high-resistance flow attributable to the deferential artery situated posterior to the testicular artery (**Fig. 4.6**).

Cochlin DL, Dubbins PA, Goldberg BB et al (1994) Urogenital ultrasound: a test atlas. Martin Dunitz, London, pp 197-202

Vallone G, Rea G (2002) Scroto. In: Bazzocchi M (ed) Ecografia. Idelson Gnocchi, Naples, pp 1057-1087

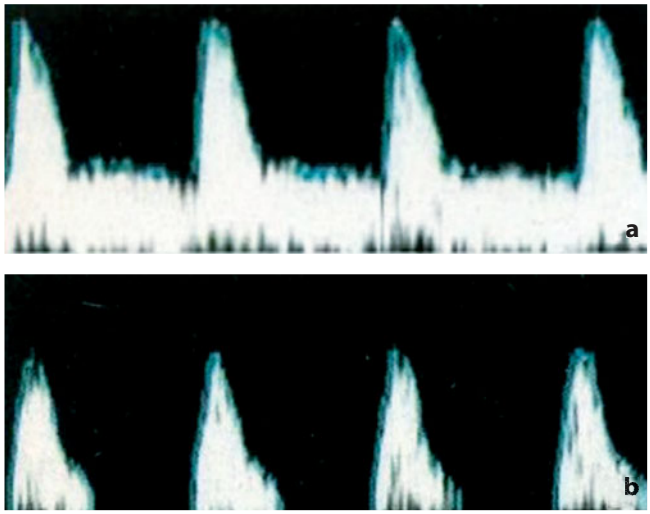

Fig. 4.6a,b. Doppler traces. **a** The image shows the normal trace of a testicular artery. The diastolic component is clearly visible, a typical finding in low-resistance vessels. **b** In the trace of the deferential artery the diastolic component is clearly absent

Prostate

US, whether **suprapubic** or **transrectal** (TRUS), is the imaging modality of choice for the study of the prostate. The examination, which should also be performed for a panoramic visualization of the urinary system, generally begins with the patient supine and the examination of the kidneys, ureters, urinary bladder, seminal vesicles and prostate gland in that order.

The suprapubic examination can identify intravesical prostatic protrusions and alterations of the wall (diverticuli) and contents (calculi) of the urinary bladder. Lastly, it can be used in the post-voiding phase to provide a relatively good estimation of residual urinary volume.

TRUS (performed in patients in the gynecologic position, or more simply lying on their side with their knees bent) is unable to correctly define the relations of the base of the prostate with the seminal vesicles and the fundus of the bladder. However, thanks to the minimal distance between the transducer and the gland it can better define the volume, morphology and structural appearance of the prostate, with immediate detection of asymmetries, particularly of the peripheral portion. End-fire transducers have in fact replaced biplane probes and are able to acquire both axial and sagittal images of the prostate. The former are obtained by withdrawing the transducer from the fundus of the bladder to the apex of the prostate, the latter by rotating the transducer laterally with respect to the median plane (**Fig. 4.7**).

In US study of the prostate the urethra and the ejaculatory ducts are taken as anatomic landmarks. The structural reference pattern is provided by the isoechoic prostatic glandular tissue (**Fig. 4.8**).

The seminal vesicles can be easily visualized by inferiorly and laterally orienting the transducer in the hyperechoic space between the rectum and the bladder. They appear as club-shaped structures with finely irregular borders, the echogenicity of which is only slightly nonuniform, a little lower than that of the prostate. Their thickness normally varies between 7 and 12 mm. Measurements above 14 mm are considered abnormal and suggestive of ectasia of the vesicle (**Fig. 4.9**).

The terminal, dilated part of the ductus deferens consists of the ampulla. Generally, its thickness does not exceed 8-10 mm, and its structure is similar to the seminal vesicles.

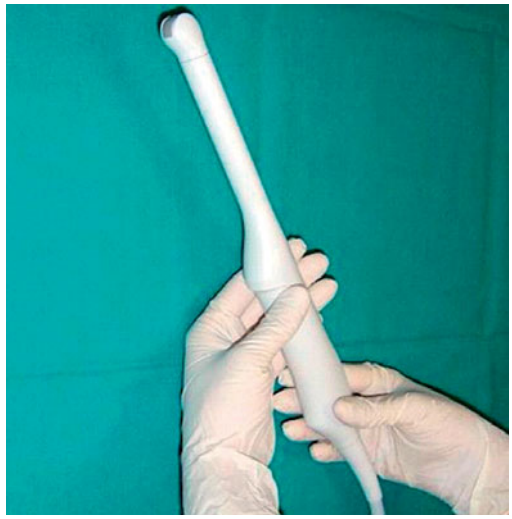

Fig. 4.7. End-fire transducer

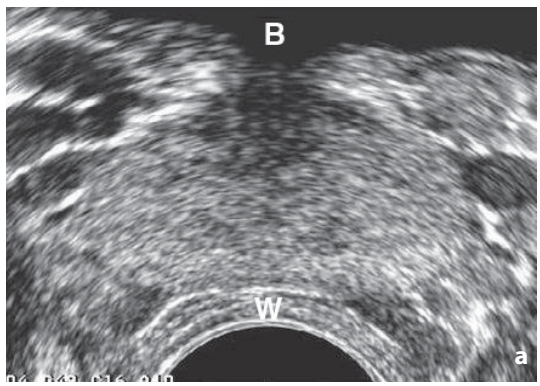

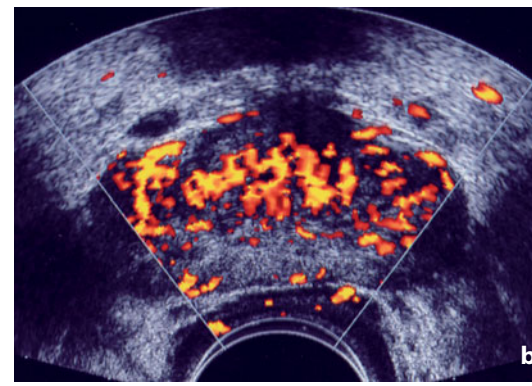

Fig. 4.8a,b. Ultrasonography. Normal prostate in a young adult. Axial scan. **a** The glandular structure is uniform, with no clear distinction between the central and peripheral portions. **b** Depiction of normal vasculature at power Doppler. *B*, urinary bladder; *W*, wall of the ampulla of the rectum

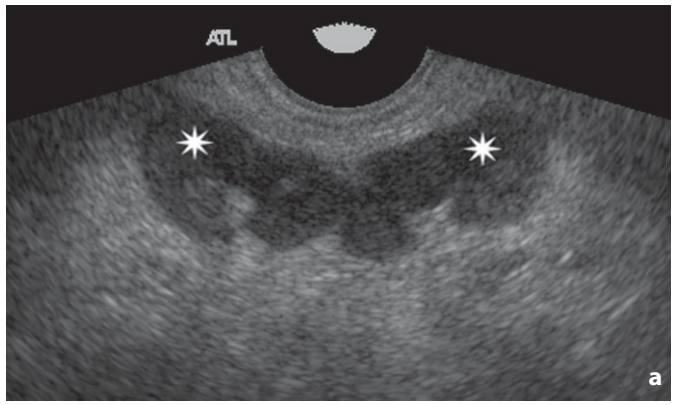

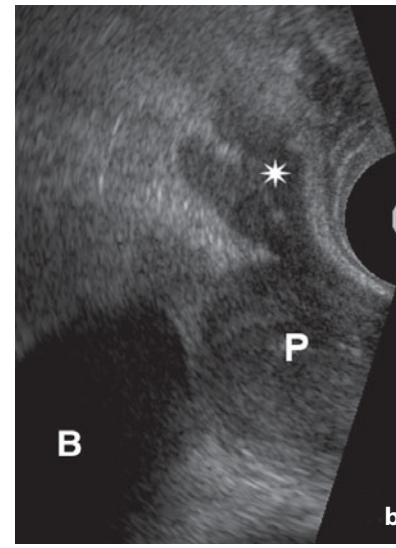

Fig. 4.9a,b. Ultrasonography. Seminal vesicles. Transrectal approach. **a** Axial scan. **b** Sagittal scan. The two vesicles (*asterisks*) appear hyperechoic with a multilobulated appearance. *P*, prostate; *B*, urinary bladder

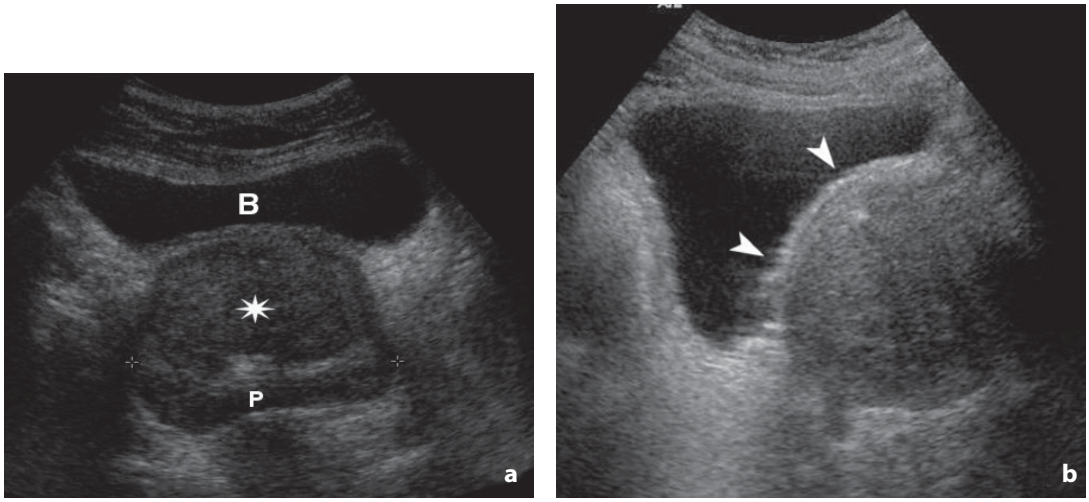

Fig. 4.10a,b. Ultrasonography. Prostate. Suprapubic approach, axial (**a**) and sagittal (**b**) scans. The prostate is clearly enlarged due to the presence of an adenoma (*asterisk*) constricting the peripheral zone (*P*). Note the impression on the fundus of the urinary bladder (*arrowheads*). *B*, urinary bladder

If not dilated by obstruction, the ejaculatory ducts are difficult to define with US. In the sagittal plane they appear as thin hypoechoic lines that are convex posteriorly. In the axial plane they are more easily identified in relation to the base of the prostate as two small contiguous holes.

The normal prostate is always well defined thanks to the contrast provided by the hyperechogenicity of the periglandular adipose tissue. Interindividual morphology is quite variable in the median sagittal plane, whereas it appears more constant in the axial plane.

The prostatic capsule, which consists of a thin layer of fibrous tissue surrounding the gland inferiorly, laterally and posteriorly, cannot be identified with US. The borders of the gland, however, can always be well defined by the intensely hyperechoic periprostatic adipose tissue. The structure of the prostate in the young is usually uniform and mid reflective. Under normal conditions the dilated glandular lumens cannot be identified. Small dispersed echoic spots are relatively common and are of no pathologic significance.

In the elderly patient, the development of benign prostatic hyperplasia produces a mid to low echogenicity in the central part of the gland where the adenoma develops. In addition, parenchymal calcifications in the form of disseminated microlithiasis, or single/multiple calculi are more common in elderly subjects (**Figs. 4.10, 4.11**).

The volume of the prostate is usually calculated using the formula for the volume of an ellipsoid, (A×B×C)×0.523, even though a more precise formula appears to be (A×B×C)×0.7. Thickness and width are evaluated at the point of maximum expansion of the mid-glandular portion in the axial plane. The length is measured between the fundus of the bladder and the proximal portion of the striatal sphincter, on the median line of sagittal scans.

Color and **power Doppler** demonstrate that in the normal prostate the flow signal is generally low or poorly represented. Increased vascularization is evident in inflamed or neoplastic tissue, whereas a reduction in flow is present in fibrous, ischemic or infarcted areas. Color and power Doppler, however, are unable to study small, newly formed vessels (**Fig. 4.12**).

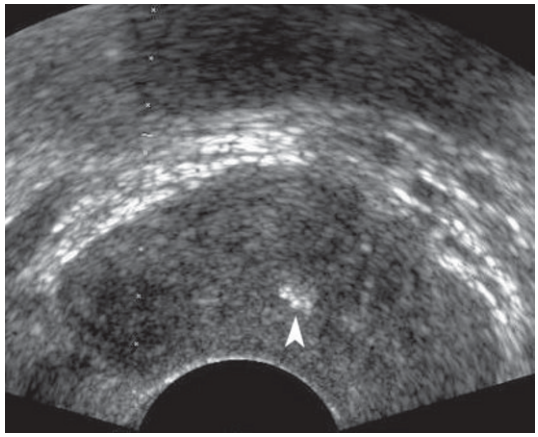

Fig. 4.11. Ultrasonography. Prostate. Transrectal approach. Calcifications (*arrowhead*) are evident in the central portion of the gland

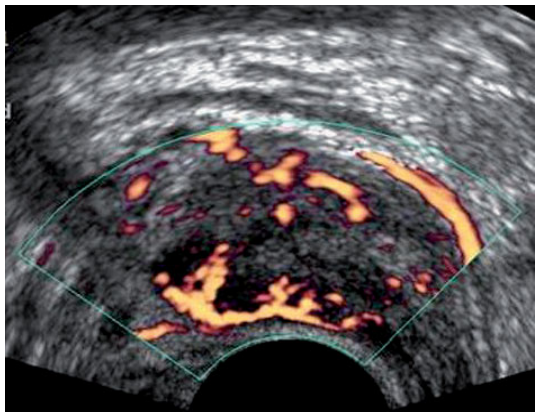

Fig. 4.12. Power Doppler. Prostate. Transrectal approach, axial scan. The image depicts the vasculature of the gland, which is more evident peripherally

Sonographic contrast media appear to be able to overcome this limitation, thanks to the ability of the microbubbles to document even very small vessels.

The examination technique involves the acquisition of baseline scans with and without power and color Doppler. These are followed by injection of the contrast medium. The infusion of first-generation molecules is slow, whereas with second-generation molecules rapid administration is preferable. During the injection the operator should continue the US observation to evaluate the precise moment of arrival of the contrast medium (**Fig. 4.13**).

The use of sonographic contrast media in the study of the prostate is aimed mainly at the characterization of focal lesions, especially for differentiation between prostatic carcinoma and aspecific granulomatous prostatitis.

Hanno PM, Malkowicz SB, Wein AL (2001) Clinical manual of urology. Mc Grow-Hill, USA, pp 437-471

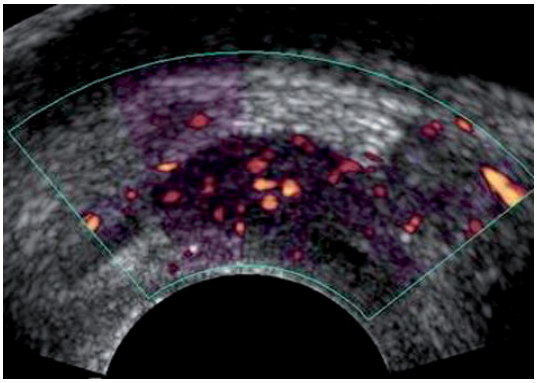

Fig. 4.13. Ultrasonography with contrast medium and color Doppler. Transrectal approach, axial scan. The color effect has been strengthened in the central part of the gland

Penis

The corpora cavernosa and corpus spongiosum of the penis can be well defined on US. In the flaccid state the tissue layers surrounding the corpora cavernosa are only partially identifiable (they can be best visualized during an erection). Skin, subcutaneous tissue and dartos cannot always be readily separated. An extremely thin hyperechoic line identifies the interface formed by the deep fascia of the penis. Immediately deep to it lies an echogenic layer composed of vascular connective tissue superficial to the tunica albuginea, in which the circumflex veins and the neurovascular bundle run dorsally.

In axial scans the tunica albuginea appears as a uniformly thick hypoechoic fascia surrounding the corpora cavernosa. The normal structure of the latter has relatively uniform intermediate echogenicity. During erection the tunica albuginea thins, while the vascular spaces in the corpora cavernosa dilate. The cavernosal arteries appear as two thin hyperechoic paraseptal lines in sagittal scans (**Fig. 4.14**).

Dynamic color Doppler enables simple and noninvasive simultaneous evaluation of the conditions of the erectile tissue, the state of the vessels and flow characteristics. The technique is mainly used in the characterization of organic impotence, the most common form of which is vasculogenic. The examination should be performed in a private setting, preferably with only the operator present in the examination room. In the supine position the patient is requested to hold the distal end of the penis upwards. The study begins with evaluation of the outer layers and erectile tissue, with the penis in the flaccid state in order to rule out lesions to these structures. After this preliminary phase pharmacologic stimulation is begun with the intracavernous injection of 10 μg of PGE1, followed by a short massage aimed at facilitating the distribution of the agent. In the following 5 min color Doppler is used to observe the dilatation of the cavernosal arteries and evaluate the symmetry of their diameters and flow. The diameter is measured in longitudinal scans and varies in erection from 0.2 to 1.3 mm (mean 0.7 mm). After the morphologic evaluation, flow velocity is measured at different times during the process of erection. In the flaccid state the systolic velocity rarely exceeds 15 cm/s and diastolic flow is often absent. In the initial phase of erection there is an increase in both systolic (≥30 cm/s) and diastolic (~10 cm/s) flow velocity. With the progressive increase in intracavitary pressure of the corpora cavernosa, diastolic flow decreases to the point of stopping altogether, and in some cases it can reverse. The phase of maximum rigidity is characterized by a progressive reduction in the systolic velocity as well. When the intracavernous pressure reaches 90-110 mmHg (equal to the mean systemic pressure), complete halting of flow occurs. The peak systolic value of 30 mmHg has been selected as the cutoff for differentiating normal cavernosal arteries from those with severe lesions (**Fig. 4.15**).

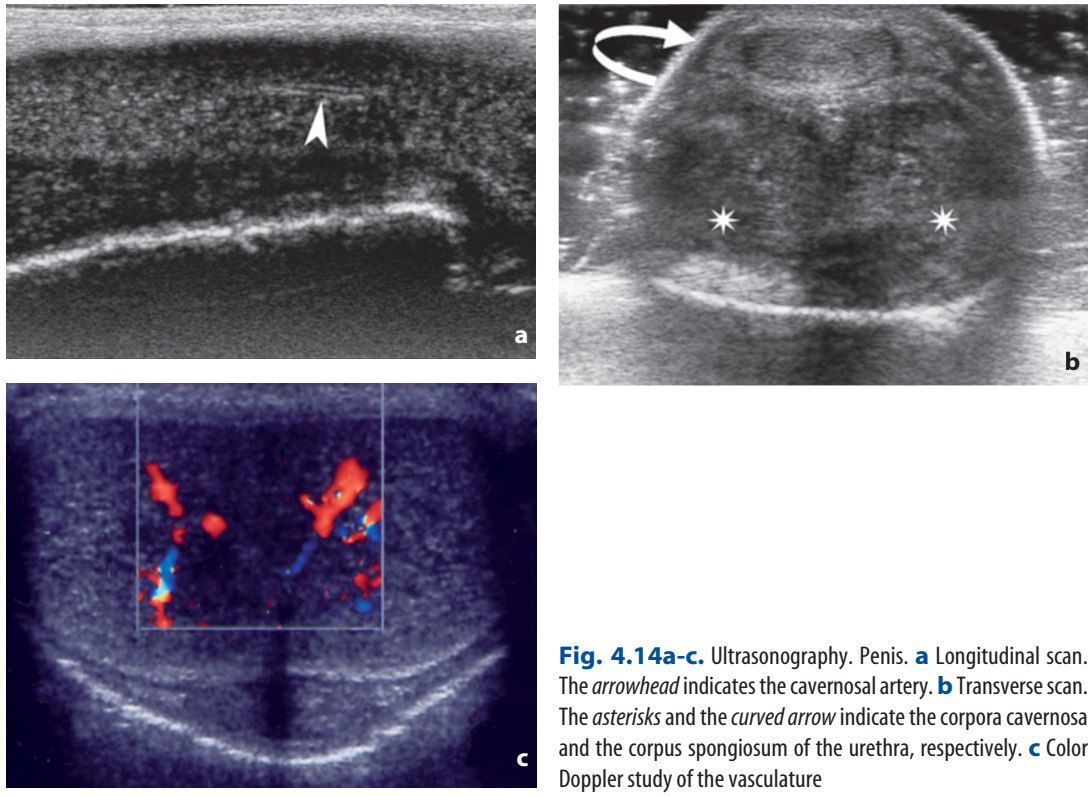

Fig. 4.14a-c. Ultrasonography. Penis. **a** Longitudinal scan. The *arrowhead* indicates the cavernosal artery. **b** Transverse scan. The *asterisks* and the *curved arrow* indicate the corpora cavernosa and the corpus spongiosum of the urethra, respectively. **c** Color Doppler study of the vasculature

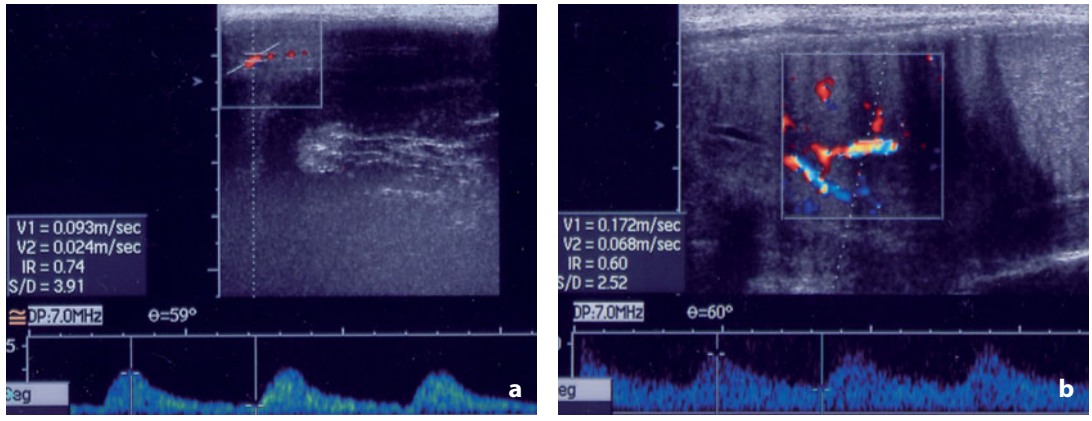

Fig. 4.15a,b. Ultrasonography. Penis. Dynamic study. **a** Longitudinal scan of the flaccid penis with Doppler sampling of the cavernosal artery. **b** Longitudinal scan of the erect penis after intracavernous injection of prostaglandin. Note the increase (in this case less than normal) of both systolic and diastolic flow

Cochlin DL, Dubbins PA, Goldberg BB et al (1994) Urogenital ultrasound: a test atlas. Martin Dunitz, London, pp 197-202

Pavlica P, Barozzi L (2002) Pene. In: Bazocchi M (ed) Ecografia. Idelson Gnocchi, Napoli, pp 1013-1053

Computed Tomography Anatomy

Scrotum and Testicles

For reasons of radioprotection **computed tomography** (CT) is not indicated for the study of these organs

Prostate and Seminal Vesicles

The role of CT is significantly limited by its poor ability to differentiate the zone anatomy of the prostate, which in the absence of contrast media is characterized by uniform density (40-65 HU), similar to that of skeletal muscle. Only after injecting contrast medium can the peripheral zone be identified, which appears relatively hypoattenuating with respect to the other zones (**Fig. 4.16**). The lateral border of the gland is usually hidden by the contiguous bundles of the levator ani muscles, although it can be partially studied using the thin slice technique. The surface towards the urinary bladder runs almost horizontally or rises slightly inferiorly with the subject in the dorsal position. Due to partial volume effects, CT is unable to visualize slight irregularities in the bladder wall and/or the prostate borders. These can in part be visualized in coronal and sagittal reconstructions.

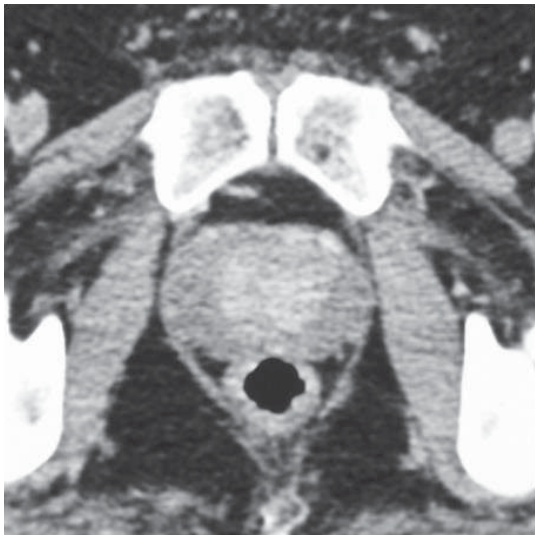

Fig. 4.16. Computed tomography. Prostate in a young adult. Axial contrast-enhanced scan. The peripheral zone is identifiable as hypoattenuating in comparison to the central part of the gland

Magnetic Resonance Anatomy

Scrotum and Testicles

Although it does not have the limitations imposed by ionizing radiation, **magnetic resonance** (MR) is little used in the study of the scrotum and the testicles, which can be adequately studied on US.

The testicles display intermediate uniform signal intensity in T1-weighted images and elevated signal intensity in T2-weighted sequences, which are mainly used in the imaging of the scrotum to obtain contrast between the testes and the adjacent structures. In T2-weighted images the mediastinum testis can be identified as a thin hypointense band with respect to the adjacent testicular parenchyma. The tunica albuginea

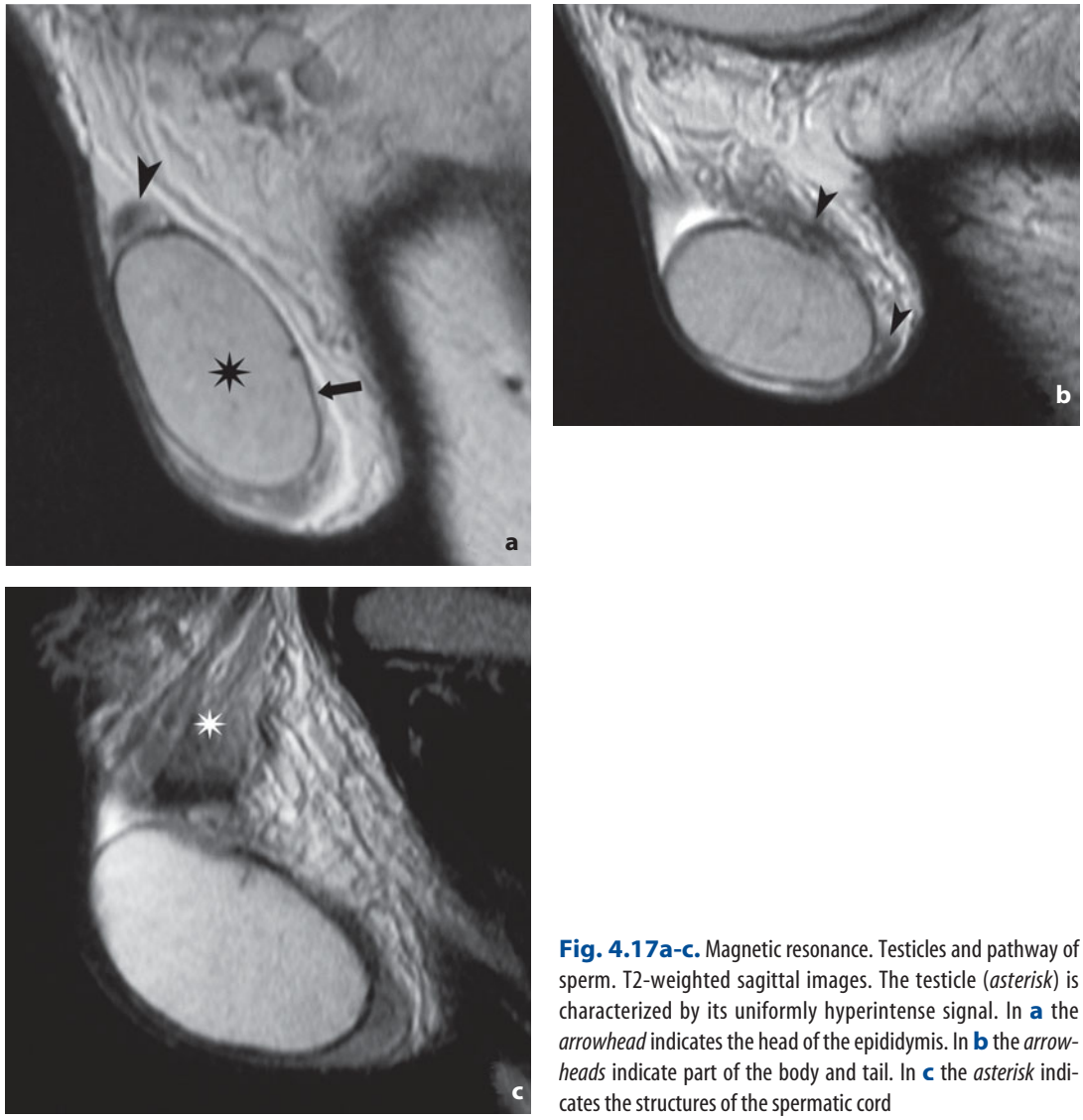

Fig. 4.17a-c. Magnetic resonance. Testicles and pathway of sperm. T2-weighted sagittal images. The testicle (*asterisk*) is characterized by its uniformly hyperintense signal. In **a** the *arrowhead* indicates the head of the epididymis. In **b** the *arrowheads* indicate part of the body and tail. In **c** the *asterisk* indicates the structures of the spermatic cord

surrounding each testicle is hypointense both in T1 and T2. The epididymis and spermatic cord in T1 have the same intensity as the testicle, whereas they appear slightly hypointense in T2 (Fig. 4.17).

Thurnher S, Hricak H, Carroll PR et al (1998) Imaging the testis: comparison between MR imaging and US. Radiology 167:631-636

Prostate and Seminal Vesicles

With respect to US and CT, MR has the advantage of better contrast resolution, which enables differentiation of the zones of the prostate and evaluation of the relations of the gland with the surrounding pelvic structures. In addition, the periprostatic adipose tissue acts as an excellent natural contrast; consequently the cleavage planes with the bladder, rectum, and the musculoskeletal and vascular structures are clearly visualized.

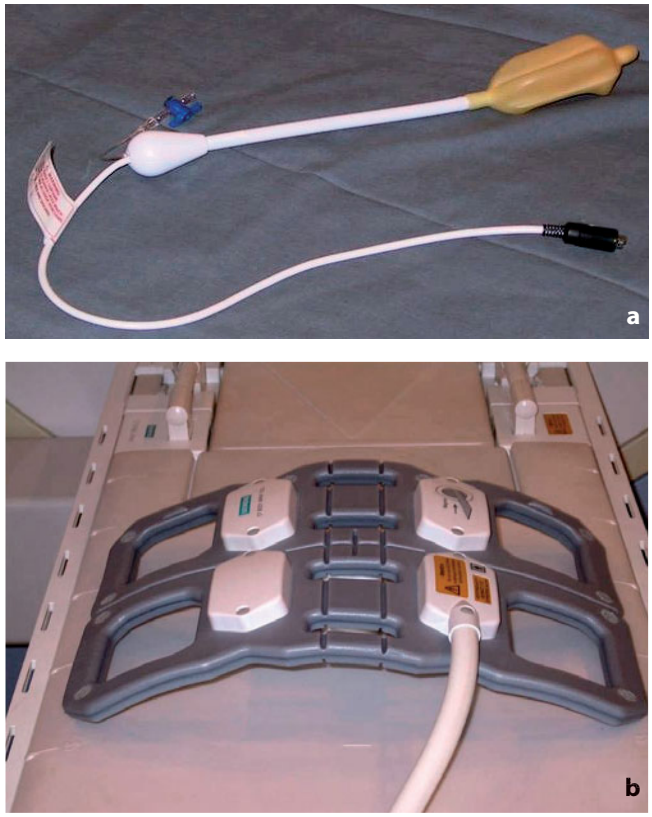

Fig. 4.18a,b. a Intracavitary coil. **b** Multichannel phased array coil

Technological progress, which has witnessed body coils being replaced by surface phased array and intracavitary coils, has led to considerable improvement in spatial resolution and signal-to-noise ratio. It should nonetheless be borne in mind that even intracavitary coils have some drawbacks which can negatively influence image quality. These include artifacts caused by peristaltic motion and excessive signal near to the coil itself. A good diagnostic result can be achieved even with a 0.5 T scanner, although image quality is markedly improved with 1.5-3.0 T devices.

An optimal study of the prostate requires the use of both an intracavitary and a surface phased array coil. If the instrumentation does not allow for this combination then the best choice is the intracavitary coil (Fig. 4.18). After an initial rectal exploration and appropriate rotation, given that it has an anterior and posterior side, the coil is inserted into the ampulla of the rectum until its most caudal portion is at the level of the anal sphincter. Around 40 mL of air is then insufflated to maintain it in this position.

The standard examination is performed with T2-weighted acquisitions in the axial, coronal and sagittal planes, followed by T1-weighted axial images. The axial sequences should be slanted perpendicularly to the longitudinal axis of the prostate, and include the seminal vesicles and the entire gland from the base to the apex. The coronal sequences should be slanted according to an axis parallel to the longitudinal axis of the prostate. The coronal and sagittal images provide good visualization of the relations between the prostate and the seminal vesicles, and the fundus of the urinary bladder and the rectum.

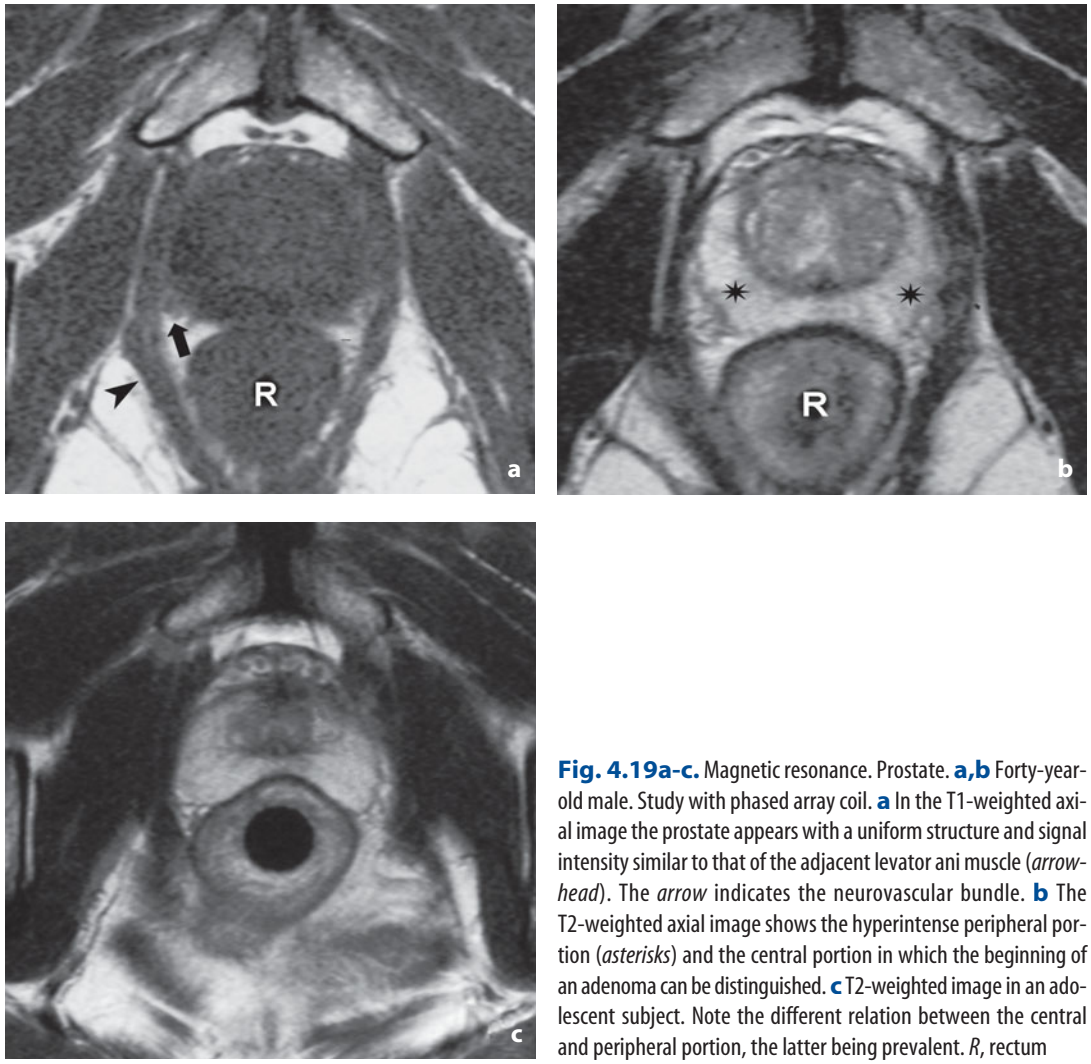

Fig. 4.19a-c. Magnetic resonance. Prostate. **a,b** Forty-year-old male. Study with phased array coil. **a** In the T1-weighted axial image the prostate appears with a uniform structure and signal intensity similar to that of the adjacent levator ani muscle (*arrowhead*). The *arrow* indicates the neurovascular bundle. **b** The T2-weighted axial image shows the hyperintense peripheral portion (*asterisks*) and the central portion in which the beginning of an adenoma can be distinguished. **c** T2-weighted image in an adolescent subject. Note the different relation between the central and peripheral portion, the latter being prevalent. *R*, rectum

In T1-weighted sequences the prostate appears with a uniformly isointense signal which is similar to that of skeletal muscle, although the zonal anatomy of the gland cannot be identified (**Fig. 4.19a**). In the axial images the neurovascular bundle is well visualized, appearing as a rounded hypointense structure which is less evident at the apex of the prostate.

In T2-weighted images the peripheral zone of the gland can readily be distinguished from central zone. The former is hyperintense due to the presence of abundant glandular tissue, whereas the latter appears hypointense due to the greater presence of connective tissue and the less abundant glandular component (**Figs. 4.19b-c, 4.20**). In the elderly patient affected by benign prostatic hyperplasia, the origin of which is mainly in the periurethral zone, the adenoma can be easily distinguished from the peripheral portion of the gland (**Fig. 4.21**).

The normal prostate gland is surrounded by a thin hypointense ring indicating the capsule, the thickness of which appears greater than is anatomically the case (chemical shift phenomenon).

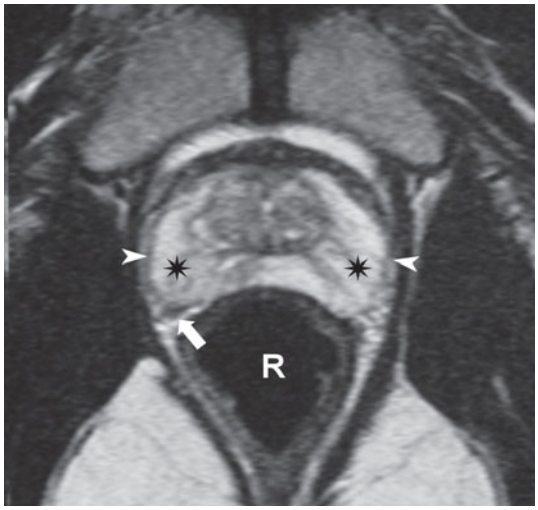

Fig. 4.20. Magnetic resonance. Prostate. Young adult male. Study performed with intracavitary coil. T2-weighted axial image. The intracavitary coil provides greater spatial and contrast resolution than the phased array coil. The *asterisks* indicate the peripheral zone bounded by the capsule (*arrowheads*). The *arrow* indicates the vascular nerve bundle. *R*, rectum

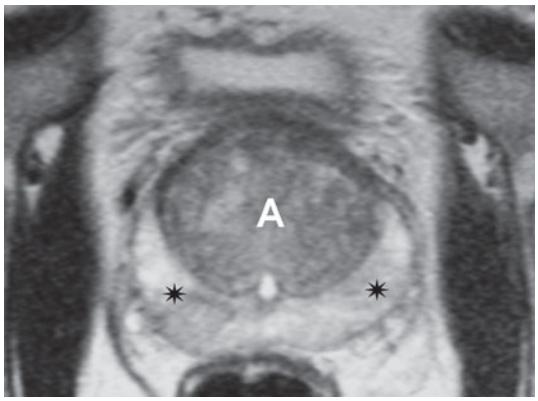

Fig. 4.21. Magnetic resonance. Prostate. Elderly male. Study performed with intracavitary coil. T2-weighted axial sequence. In the centre of the gland an adenoma can be identified (*A*). The *asterisks* indicate the peripheral zone

The seminal vesicles, which are studied together with the prostate, have a clearly hyperintense signal under normal conditions in T2-weighted sequences due to their elevated water content, whereas the walls appear as thin hypointense septa. In T1-weighted sequences the signal is uniformly intermediate-low (**Fig. 4.22**).

The pampiniform plexus has a high signal intensity due to low-velocity intraluminal flow.

Coakley FV, Hricak H (2000) Radiological anatomy of the prostate gland: a clinical approach. Radiol Clin North Am 38:15-30

Kurhanewicz J, Vigneron DB, Males RG et al (2000) The prostate: MR imaging and spectroscopy. Radiol Clin North Am 38:115-138

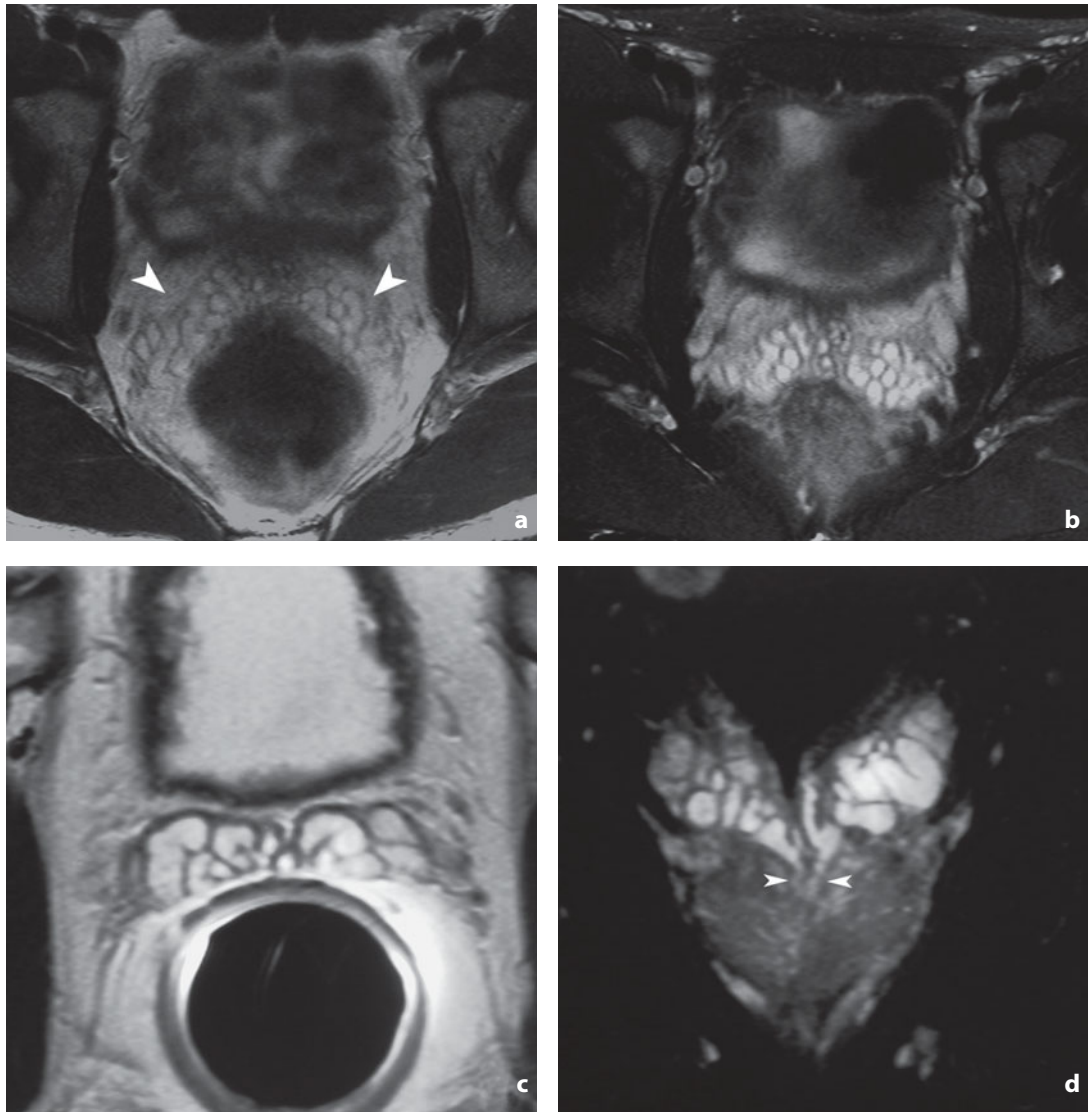

Fig. 4.22a-d. Magnetic resonance. Seminal vesicles. **a,b** Adolescent subject. T2-weighted image without (**a**) and with (**b**) fat signal suppression. Typical honeycomb appearance of the vesicles (*arrowheads*). **c,d** Adult. T2-weighted axial (**c**) and coronal (**d**) images. The latter clearly depicts the ejaculatory ducts (*arrowheads*)

Penis

MR is able to provide multiplanar images visualizing the various anatomic components of the penis. The use of surface coils, positioned 2-3 cm from the penis, is technically the best solution, even though a common body coil can be used. The patient is positioned supine, with the penis fixed to the anterior pelvic wall by sticking plaster, to avoid motion during the examination.

Axial images provide a good depiction of the root and mobile portion of the penis. In the sagittal plane the bulb of the penis and the relations with the musculature of the perineum are better visualized. The coronal plane in turn offers the advantage of a panoramic view.

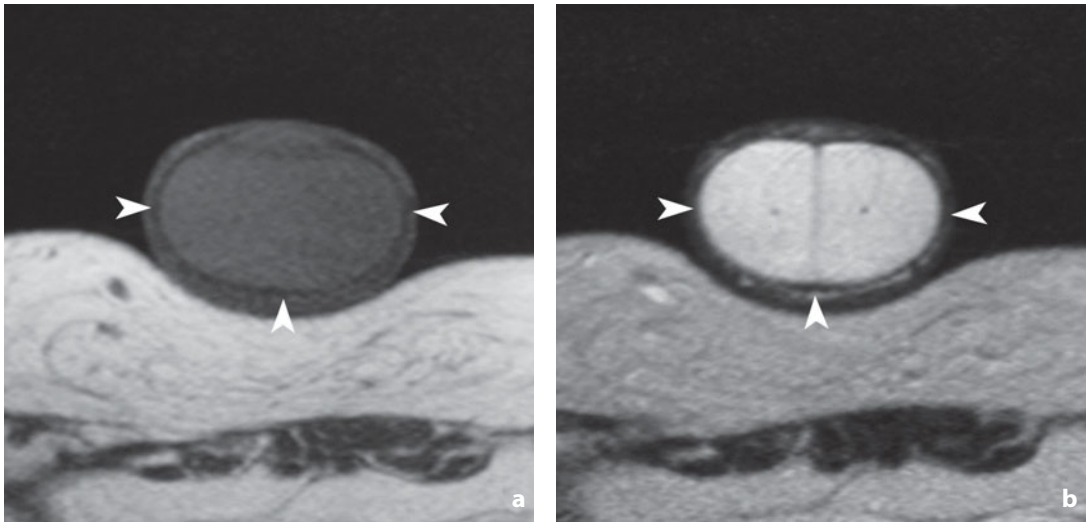

Fig. 4.23a,b. Magnetic resonance. Penis. Axial images. The signal of the corpora cavernosa is uniform. Medially intense in T1 (**a**), it appears hyperintense in T2 (**b**). The tunica albuginea (*arrowheads*) is hypointense in all sequences

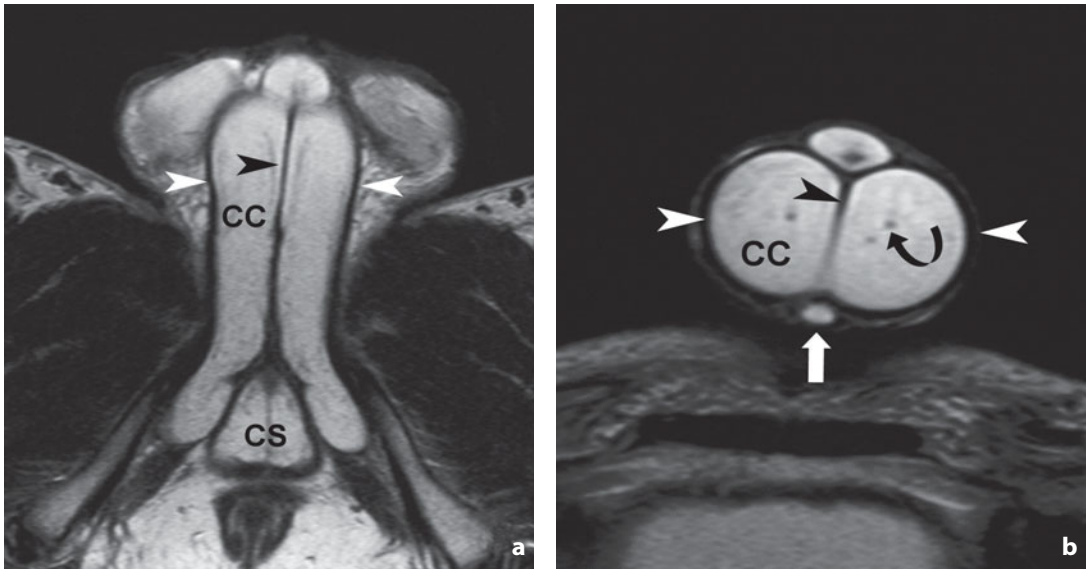

Fig. 4.24a,b. Magnetic resonance. Penis. Axial T2-weighted scans, acquired after pharmacologic stimulation at the level of the root (**a**) and the shaft (**b**). The *arrowheads* indicate the tunica albuginea and the intercavernosal septum, the *arrow* indicates the dorsal vein, and the *curved arrow* indicates the cavernosal artery. *CC*, corpora cavernosa, *CS*, corpus spongiosum

Both T1- and T2-weighted images are used. The former highlight the contrast between the adipose tissue and the other anatomic structures of the penis. The latter, on the other hand, separate the corpora cavernosa and the corpus spongiosum (hyperintense) from the tunica albuginea (hypointense) (**Fig. 4.23**).

While not indispensable, the induction of tumescence or erection via pharmacologic stimulation with prostaglandin is advisable, since it provides 100% increase in diagnostic information (**Figs. 4.24, 4.25**). In T2-weighted sequences the corpora cavernosa have a higher signal intensity, which is moreover variable in relation to the

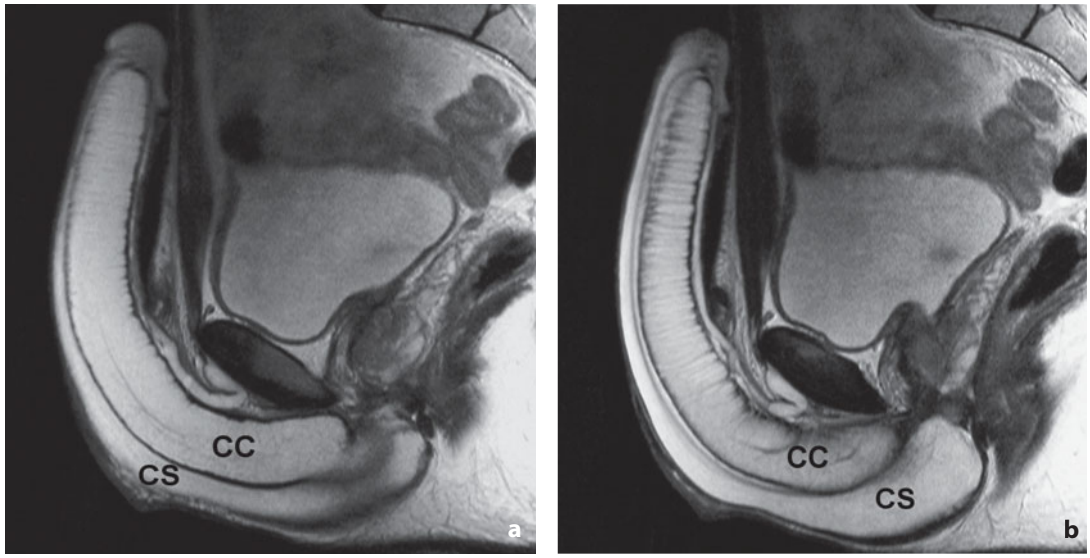

Fig. 4.25a,b. Magnetic resonance. Penis. T2-weighted sagittal images acquired with pharmacologic stimulation. *CC*, corpora cavernosa; *CS*, corpus spongiosum

degree of tumescence of the penis. The glans penis and the crura are isointense with respect to the erectile tissue of the corpora cavernosa. The cavernosal arteries are readily identifiable as hypointense linear images, as are the intercavernosal septa which also appear isointense. In the coronal plane the arteries appear as markedly hypointense rounded formations surrounded by the hyperintensity of the cavernosal tissue. The deep fascia of the penis are normally hypointense in T2 and can be distinguished from the tunica albuginea, despite being closely related to it during erection. On the dorsal surface, between the tunica albuginea and the deep fascia of the penis, the deep dorsal vein, the two dorsal arteries and often other venous vessels can be clearly visualized. The suspensory ligament is readily identifiable in sagittal scans as a hypointense structure inserted at the pubic symphysis and the dorsal face of the penis.

Pretorius ES, Siegelbaum ES, Ramchandani P et al (2001) MR imaging of the penis. RadioGraphics 21:S283-S298

Female Reproductive System: Normal Gross and Microscopic Anatomy

5

L. Olivetti, G.C. Mazza, S. Mombelloni

The female reproductive system, in addition to the embryonic rests, consists of the reproductive organs contained and fixed by a system of suspensory ligaments and aponeurotic supporting muscles.

Embryology

The development of the female reproductive system is closely related to the development of the urinary system.

The early development of the gonads, both female and male, takes place towards the 4th week of gestation in the form of a projection from the genital ridge, composed of a thickening of celomic epithelium. However, up to the 6th week of gestation the gonads remain undifferentiated and the mesonephric and paramesonephric ducts coexist. At the 6th-7th week the male genes located on the Y chromosome or the female genes located on the X chromosome encode for the production of inducers which begin the differentiation of the primitive gonads into testicles or ovaries, respectively. In particular, a sequential development occurs in the female gonads of two types of cords: medullary and cortical. The latter give rise to the germ cells which will become definitive follicles.

During their development the female gonads also undergo a change of site (descent of the ovaries), albeit to a lesser extent than the male gonads. By the third month of gestation the ovaries have arrived in the lumbar region of the greater pelvis, and later, during the first year, they reach their final destination in the pelvic cavity.

In females the paramesonephric ducts form the uterine tubes, the uterus and the superior part of the vagina, whereas the mesonephric ducts atrophy. For this to happen, the presence of the ovary is not required, in that there is a spontaneous tendency towards feminization. In contrast, in males the testicles secrete an inhibitory substance which opposes the spontaneous tendency towards feminization and causes atrophy of the paramesonephric ducts and formation of the ductus deferens, the seminal vesicles and the mesonephric ducts.

Between the 8th and 12th weeks of gestation the external genitals are defined. The genital portion of the urogenital sinus gives rise to the inferior third of the vagina and the vestibule, into which the vagina proper and the urethra open. Also in this case there is a spontaneous tendency towards feminization. In the male the testicles produce testosterone, which leads to differentiation towards being male.

In the following weeks up to birth the production of hormones continues, but at a decreasing rate. Afterwards the gonads begin a period of quiescence, to then become active again at puberty, with the awakening of specific sexual neurosecretion.

Sandler TW (2009) Langman's medical embriology. 11th edn. Wolters Kluwer, Lippincott Williams & Wilkins, Baltimore

L. Olivetti, L. Grazioli (eds.), *Imaging of Urogenital Diseases*,

Ovaries

The female gonads are a pair of symmetrical organs which produce egg cells and female hormones (estrogen, progesterone and a small amount of androgen).

Located on the posterior surface of the broad ligament and the lateral wall of the lesser pelvis, the ovary in the nulliparous subject occupies the ovarian fossa, bounded posteriorly by the uterus and the iliac vessels, whereas in the pluriparous subject it tends to prolapse inferiorly towards the rectouterine pouch.

The postpubertal ovary is almond/shaped and measures 2-4 cm in length and 1.5-3 cm in width, with a thickness of around 1 cm. These measurements vary during the menstrual cycle, in the first trimester of gestation (presence of true corpus luteum) and after menopause (ovarian atrophy).

The ovaries have a superior or tubal pole, an inferior or uterine pole, and mesovarian and free borders. The uterine pole is attached to the ovarian ligament which is inserted into the body of the uterus posterior to the intramural segment of the uterine tube. Laterally the suspensory ligament anchors the ovary to the pelvic wall and conveys the vessels, nerves and efferent and afferent lymphatic vessels. The ovary is also anchored by the mesovarium, a short peritoneal ligament which detaches from the broad ligament and the tubo-ovarian ligament which connects the superior pole of the ovary to the infundibulum of the uterine tube (**Fig. 5.1**).

The main blood supply is provided by the ovarian artery (branch of the aorta) contained in the suspensory ligament. A second source is provided by the ovarian branch of the uterine artery, which follows the uterine ligament and sends branches through the mesovarium which anastomose with those of the ovarian artery. The venous network forms a rich pampiniform plexus at the level of the ovarian hilum. The veins arising from the plexus merge to form the ovarian vein, which initially runs inside the suspensory ligament and then empties into the renal vein on the left and the inferior vena cava on the right.

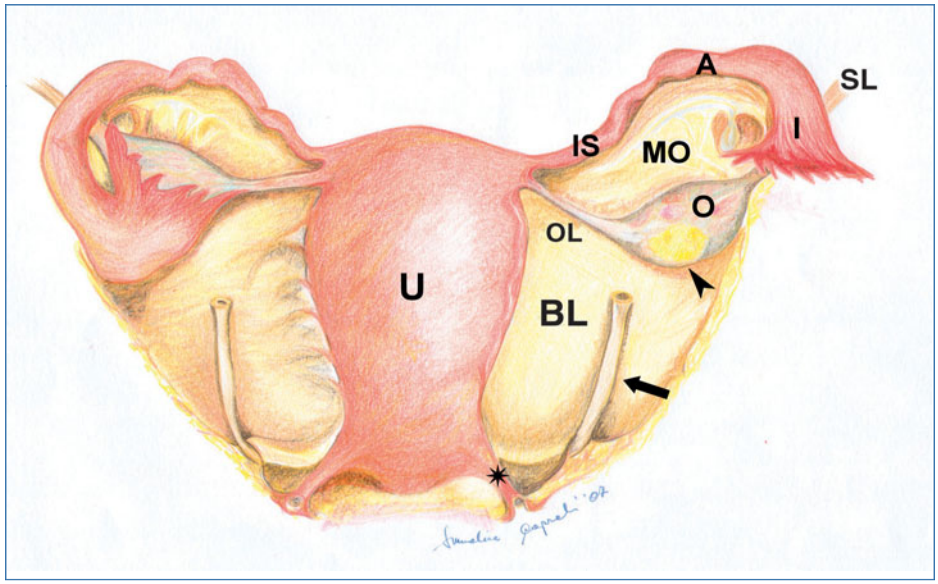

Fig. 5.1. Anatomic diagram of the female reproductive system. The *arrowhead* indicates a luteal body, the *arrow* a ureter and the *asterisk* a uterosacral ligament. *A*, ampulla; *BL*, broad ligament; *I*, infundibulum; *IS*, isthmus; *MO*, mesovarium; *O*, ovary; *OL*, ovarian ligament; *SL*, suspensory ligament of ovary; *U*, uterus

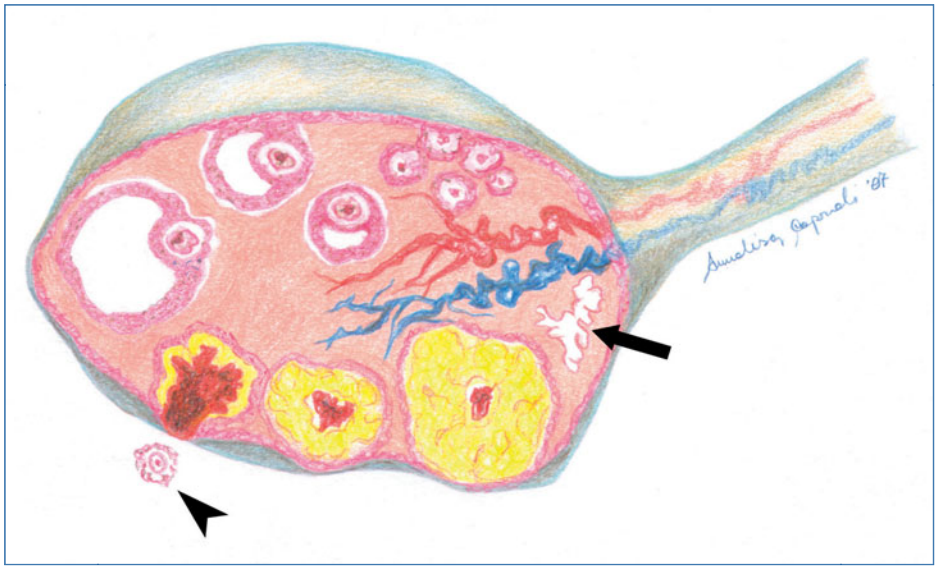

Fig. 5.2. Anatomic diagram of the developmental stages from ovarian follicle to luteal body. Counterclockwise from left: primordial and primary follicles, maturing follicles, ruptured follicle (or hemorrhagic body), luteal bodies, initial and mature, corpus albicans (*arrow*). The *arrowhead* indicates a released egg

The lymphatic vessels of the ovaries are abundant and drain into the preaortic and para-aortic lymph nodes.

Innervation of the ovary is provided by the nerve branches which accompany the arterial vessels, comprising the ovarian plexus and thus representing an extension of the celiac and renal plexuses.

Microscopically, the ovarian parenchyma is composed of hilum, a medulla and a cortex. The hilum is the point where the mesovarium is inserted and the ovarian vessels and nerves penetrate the ovary. The medulla is the central portion of the ovary which is continuous with the hilar region and contains loose connective tissue, large blood vessels, lymphatic vessels and nerves. The cortex is the functional layer of the ovary where the primordial and developing follicles are found and where in the fertile woman the luteal bodies and their regressed form (corpora albicantia) are located, the latter being none other than fibrous scars on the cortical surface of the ovary (**Fig. 5.2**).

The ovary is covered, from deep to superficial, by three thin layers: (1) the albuginea, composed of connective tissue; (2) germinal epithelium, composed of modified cubical peritoneal cells; (3) peritoneum (the only extraperitoneal portion is formed by the hilum).

Uterine Tubes

Together with the ovaries the uterine tubes (**Fig. 5.1**) may be considered annexes of the uterus. They are paired muscular-membranous conduits which create a communication between the uterine and peritoneal cavities. They are indispensable for the capture of the egg cells after ovulation and their transport towards the uterus, for the migration of spermatozoa and their capacitation, for fertilization and conveying the embryo towards the uterus and for the early phase of its development.

Each tube is located in the superior wing of the broad ligament, lateral to the uterus, anterior to the ovary and posterior to the round ligament. They originate from the uterine horns, running obliquely superiorly, laterally and posteriorly towards the

pelvic wall. Nonetheless, their position is dynamic, at times being located in the ovarian fossa, at others in the rectouterine pouch.

Their length on average is 12-18 cm and the diameter of the tube varies from 0.5 to 1.0 mm at the level of insertion into the uterus, to 8-15 mm at the distal end.

Anchorage of the uterine tubes is provided by continuity with the uterus and the tubo-ovarian ligament, which connects the distal part of the tube to the superior pole of the ovary. The tubes can, however, become fixed in an anomalous position due to adherences produced by genital or perigenital disease.

Each uterine tube is divided into four parts:

- the uterine part (length 1-2.5 cm), the intramural segment which passes through the myometrium and communicates with the uterine cavity by the uterine opening of the uterine tube;
- the isthmus (length 2-3 cm), an almost straight segment which follows the uterine segment and emerges from the uterine horn;
- the ampulla (length 6-8 cm), a segment with alternating dilatations and constriction in the lumen;
- the infundibulum (length 1-2 cm), the most lateral, funnel-shaped segment, which terminates in finger-like processes called fimbriae at the opening forming a communication between the peritoneal cavity and the tubal lumen (abdominal opening of the uterine tube).

The vasculature of the uterine tubes consists of the tubal branches arising as anastomosing terminal branches of the uterine and ovarian arteries. Similarly, venous drainage is to the uterine and ovarian veins.

Microscopically, from deep to superficial, the tubal wall consists of a mucous coat and a muscular layer connected with the serous peritoneal lining by an underlying layer of loose connective tissue. The epithelial lining of the mucosa, which lies on a pavement of lamina propria, rises in folds and is composed of ciliated cells, secreting cells and club cells in varying proportions in relation to the phase of the menstrual cycle.

Uterus

The uterus is a hollow muscular organ situated in the pelvic cavity posterior to the urinary bladder and anterior to the rectum. It is conical in shape with the base upwards and the trunk forming the apex pointing downwards. Its average dimensions in a nulliparous woman are 6.5 cm in length, 4 cm in breadth and 2 cm in depth. These measurements and the weight of the uterus are slightly greater in women with prior pregnancies. The capacity of the uterine cavity is around 4 cm^3 in the nulliparous and 5-6 cm^3 in the pluriparous woman.

The uterus is divisible in to three anatomically and functionally separate parts: the body, isthmus and cervix. The body is the superior part of the organ and has a flat or slightly convex anteroinferior surface, a convex posterosuperior surface and two rounded lateral borders. The highly convex superior border corresponds to the part of the uterus that projects beyond a plane through the point of entrance of the uterine tubes and takes the name of fundus. The isthmus is a slight constriction between the body and the cervix and has an anatomic-functional role only during labor. The cervix comprises the inferior part of the uterus that protrudes into the vagina. It can be divided into a supravaginal part and a rounded vaginal part, whose distal end communicates with the vagina via the external uterine os (**Fig. 5.3**).

The uterine cavity is flattened from the front to the back and is divided by the isthmus into two parts: the cavity of the body, triangular in shape and virtual, and the cavity of the cervix, spindle shaped and real.

This uterus is a relatively mobile organ. Normally it is located in an anteverted and anteflexed position. Indeed its axis forms an angle of 90° with the axis of the vagina

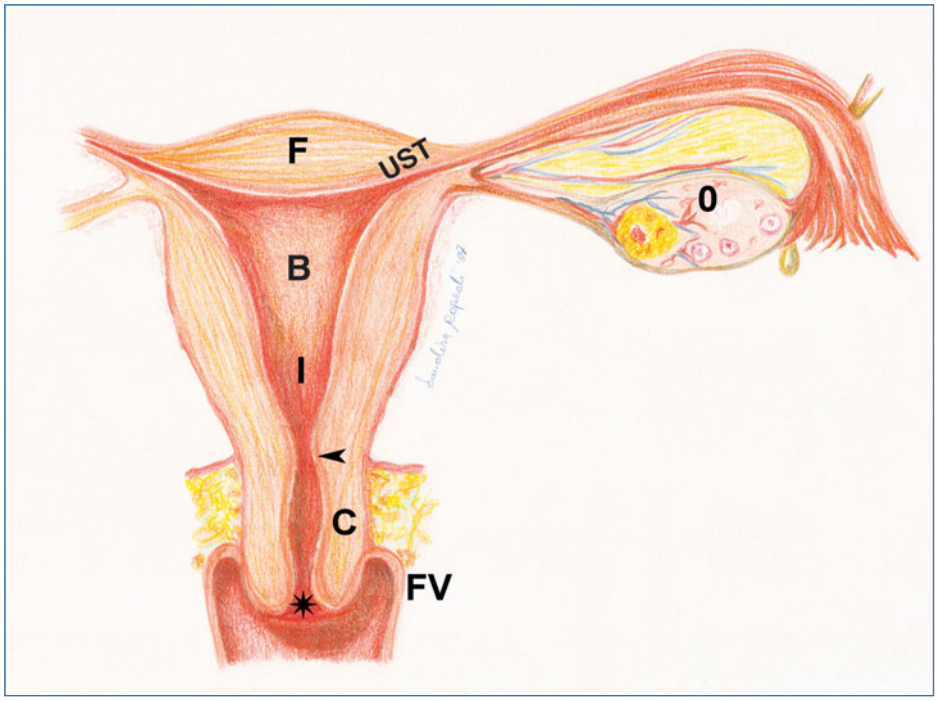

Fig. 5.3. Anatomic diagram of the uterus. Coronal section. The *arrowhead* indicates the internal uterine os, the *asterisk* the external uterine os. *B*, body; *C*, cervix; *F*, fundus; *FV*, fornix vaginalis; *I*, isthmus; *O*, ovary; *UST*, uterine segment of tube

(angle of anteversion). The axis of the cervix forms an angle of 120-170° with the axis of the body (angle of anteflexion).

This position is maintained by a complex system of connections which is schematically composed of supports, suspensory ligaments and directional structures. The principal supports are the pelvic fascia and the urinary bladder. The suspensory structures, in contrast, consist of the uterosacral ligaments posteriorly, the vesicouterine ligament anteriorly and the transverse cervical ligaments laterally. The latter are formed by a thickening of the subperitoneal connective tissue and run at the base of the broad ligaments, forming a robust transverse band of tissue which connects the supravaginal cervix and the vagina with the lateral wall of the pelvis.

The directional system is instead responsible for maintaining uterine anteversion (round ligaments) and limiting lateroversion (broad ligaments). The round ligaments are two fibromuscular bands, accompanied by vessels, which extend from the openings of the uterine tubes to the labia majora and the pubis passing through the inguinal canal. The broad ligaments consist of a double layer of peritoneum and connect both sides of the uterine body to the lateral wall of the pelvis.

The uterus may at times be found in an anomalous position (retroversion, lateroversion, etc.) due to congenital or acquired causes, generally inflammatory in nature.

The uterus is an organ covered by peritoneum. The parietal peritoneum, in fact, descends from the anterior wall of the abdomen, is reflected onto the urinary bladder, covering it in part, and returns to the anterior wall of the uterus. After having covered the uterine fundus, it descends over the posterior surface of the uterus, also covering a part of the posterior vaginal wall, and is reflected again to cover the rectum, thus forming the rectouterine pouch. Laterally the anterior and posterior parietal peritoneum join to form the broad ligaments.

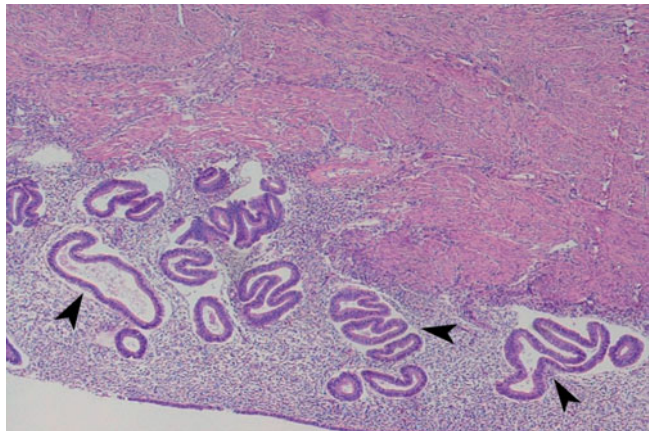

Fig. 5.4. Photomicrograph of the uterine wall. At the bottom the endometrial epithelial lining with the presence of glandular structures (*arrowheads*), at the top the muscular wall (myometrium)

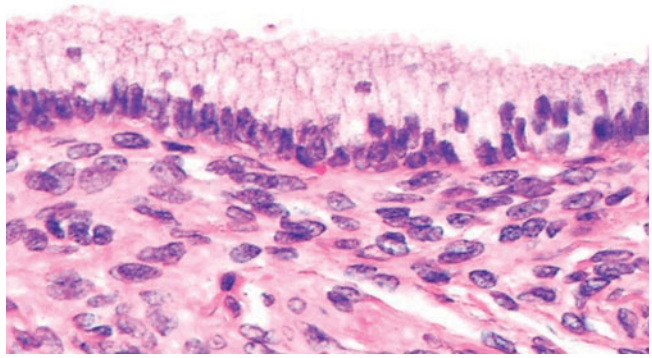

Fig. 5.5. Photomicrograph of endocervical epithelium. A single layer of cylindrical epithelium with pseudoglandular appearance

The uterus is served by three arteries: the uterine, the ovarian arteries and the artery of the round ligament.

The uterine wall structurally consists of three layers: mucous (endometrium), muscular (myometrium) and serous (perimetrium).

Microscopically, the endometrium displays different morphologic characteristics at the level of the body and the uterine cervix. In the body the endometrium is composed of prismatic epithelium which also covers the numerous simple tubular uterine glands contained in the stroma (Fig. 5.4). In contrast, the endometrium of the cervix (endocervical epithelium) is composed of a single layer of cylindrical cells which secrete mucus and have a pseudoglandular appearance (Fig. 5.5).

Externally the vaginal part of the uterus is covered by stratified pavement epithelium (exocervical epithelium) similar to that of the vagina, with no glandular structures (Fig. 5.6). The transition between endo- and exocervical epithelium is marked and may be the origin of malignant tumors.

During a normal menstrual cycle the uterine mucus undergoes morphologic and structural changes which occur almost exclusively in the superficial functional layer of the endometrium, whereas the underlying basal layer contains the glands which set in motion the endometrial regeneration at the beginning of each cycle.

The myometrium is composed of bundles of smooth muscle cells, which, based on

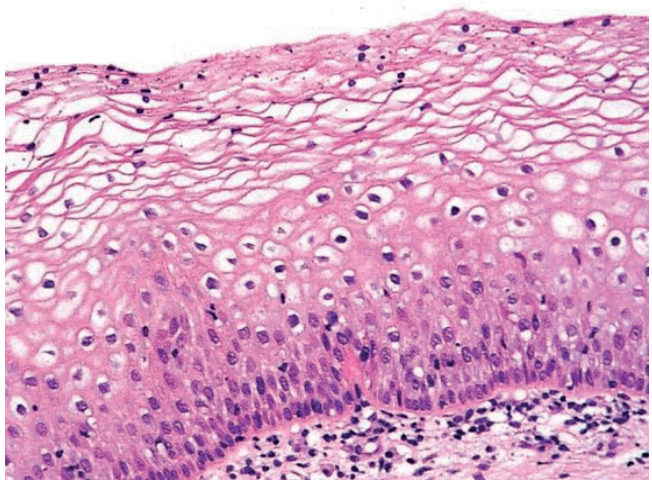

Fig. 5.6. Photomicrograph of exocervical epithelium. Keratinized stratified pavement epithelium similar to that lining the vagina

their course, divide it into three layers: external (subserous), intermediate and internal. At the level of the uterine cervix the muscular coat is less developed, with a greater presence of connective tissue rich with elastic fibers.

The perimetrium is the external layer consisting of serous peritoneum.

Vagina

The vagina is a muscular-membranous conduit around 8 cm in length which extends from the uterus to the vulva. Running obliquely downwards and forwards it is located partly in the pelvis and partly in the perineum. The superior end surrounds the uterine cervix between the inferior third and the middle, thus forming a recess called the vaginal fornix which is usually described as having four segments: anterior, posterior, right lateral and left lateral.

The anterior wall of the vagina is related to the urinary bladder from which it is separated by relatively loose connective tissue, the vesicovaginal septum, and to the urethra via a dense fibrous urethrovaginal septum. The posterior wall, at the level of the fornix, is related to the rectouterine pouch, while caudally it is closely related to the rectum from which it is separated by the rectovaginal fascia. The lateral walls of the pelvic segment above the levator ani muscle correspond to the broad ligament.

The vagina is supplied on each side, superior to inferior, by branches deriving from the uterine artery, the vaginal artery (branch of the iliac) and the middle rectal artery.

The external and internal iliac lymph nodes drain the lymphatic vessels of the superior part of the vagina, the internal iliac lymph nodes drain the middle part, while the superficial inguinal lymph nodes drain the inferior part.

Microscopically, the wall of the vagina (3-4 mm thick) from deep to superficial is composed of three layers: mucous, muscular and adventitial. The mucous layer extends superiorly from the mucosa of the external uterine os and consists of a lining of stratified pavement epithelium and a lamina propria.

Vulva

The vulva is made up of the female external genitalia. Bounded by the medial aspects of the thighs, the vulva extends anteroposteriorly immediately below the pubic symphysis up to around 3 cm in front of the anus. It includes the mons pubis, labia majora, labia minora, vestibule, clitoris and greater vestibular glands.

The arterial vasculature consists of the external, superior and inferior pudendal arteries (branches of the femoral) and the internal pudendal artery (branch of the internal iliac).

The lymph nodes which drain the rich network of the lymphatic vessels of the vulva are the superficial inguinal, deep inguinal (clitoris) and iliac (Bartolino glands).

Agur AMR, Dalley AF (2005) Atlas of anatomy. 11th edn. Lippincott Williams & Wilkins, Baltimore

Martini F, Timmous MJ, Tallitsch RB (2008) Human Anatomy. 6th edn. Benjamin-Cummings Publishing Company, San Francisco

Female Reproductive System: Normal Radiologic Anatomy

6

L. Olivetti, L. Grazioli, G.C. Mazza

Radiologic Anatomy

Hysterosalpingography is the reference radiologic technique for evaluation of the patency of the uterine tubes. It also enables morphologic study of the uterine cavity. It is generally performed as an outpatient procedure with no need for special preparation by the patient. Indications for the examination include infertility and recurrent miscarriage, fistulae of the genital system, congenital uterine anomalies (unicornuate, bicornuate, septate, didelphic, hypoplastic uterus), acquired uterine anomalies (submucous myomas, endometrial polyps, intracavitary synechia) and suspected alterations of the uterine tubes (proximal or distal occlusions, tuberculosis, peritubal adherences). Contraindications include metrorrhagia, acute and subacute inflammation of the pelvic cavity, allergies to contrast media, and of course pregnancy.

The examination is preferably performed between the 8th and 12th day of the menstrual cycle, or at any rate after the cessation of menstrual flow and prior to ovulation. In this time window pregnancy is unlikely and the endometrium is thin, which facilitates interpretation of the radiologic images. The subject is placed in the gynecologic position on the radiologic table equipped with an image intensifier connected to a monitor. The procedure involves the use of atraumatic catheters, uterine injector (connected to a manometer to monitor injection pressure, which should not exceed 250-300 mmHg) and nonionic iodinated contrast medium (10-20 mL).

The study involves a precontrast enhancement examination obtained after inserting the catheter into the internal uterine os. The contrast medium is then slowly injected and several images are acquired under fluoroscopic monitoring during progressive enhancement of the uterus and uterine tubes. The first image is acquired during the beginning of uterine filling, the second when the uterus is completely distended, the third during the enhancement of the uterine tubes and a final image when the contrast material is leaking into the peritoneal cavity (**Fig. 6.1**).

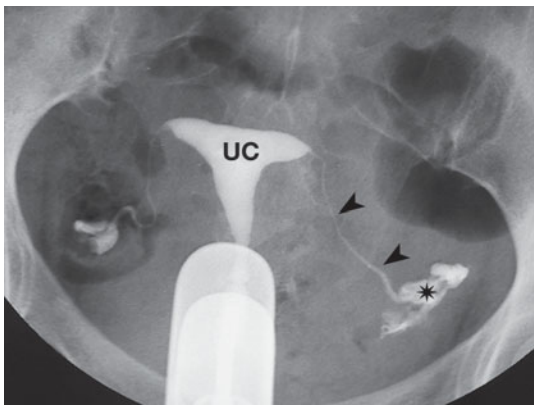

Fig. 6.1. Hysterosalpingography. The uterine tubes (*arrowheads*) appear regular in diameter and course. The normal patency is documented by the leakage of contrast medium into the peritoneal cavity (*asterisk*). *UC*, uterine cavity

L. Olivetti, L. Grazioli (eds.), *Imaging of Urogenital Diseases*,

The complications associated with the procedure include bleeding and infection. Some patients may report pelvic discomfort following catheter placement, which may be intense to the point of interrupting the examination. Rare complications include vasovagal reactions, and even less frequently adverse reactions to the contrast medium.

At hysterosalpingography the uterus normally appears in a medial position and conical in shape with the apex inverted. The uterine tubes are visualized with two segments: a thin medial segment corresponding to interstitial and isthmian parts, and a lateral tortuous segment due to the ampullary part.

Simpson WL Jr, Beitia LG, Mester F (2006) Hysterosalpingography: a reemerging study. RadioGraphics 26:419-431

Ultrasonographic Anatomy

It should be stated at the outset that the morphology and dimensions of the female reproductive organs vary with age.

At birth the uterus is relatively large and has a configuration similar to that of the adult, since during pregnancy it experiences the hormonal stimulation of the maternal estrogen. In the absence of this effect, the uterus decreases in size (around 2-3 cm in length, and 0.5-1 cm in breadth). It remains this size until puberty, when its volume increases and it takes on the pear shape typical in the adult. In the postnatal period it appears uniformly enlarged, while in menopause it undergoes progressive atrophy.

The ovaries are difficult to identify in the early years of life in that they are yet to complete their descent into the pelvis. Their growth is long and progressive, and at puberty they may appear already developed as in the adult. In fact they may even be larger in the adolescent. After menopause they undergo progressive atrophy.

In the following section the description refers to a woman of fertile age, unless otherwise stated.

The ultrasonographic (US) examination of the female pelvis can be performed transabdominally (TA) with a 3.5-5 MHz sector or convex transducer, or transvaginally (TV) with a 5-7 MHz transducer. In special cases, such as the study of the cervix or the vaginal vault, a transrectal (TR) approach may be used.

The TA examination offers a wider field of view, but requires a certain level of filling of the urinary bladder so as to shift the intestinal loops upwards and the uterus posteriorly, which is normally anteverted and anteflexed. In this way the abdominal wall, a number of pelvic muscles, the pelvic vessels, the ureters, the urinary bladder, the uterus, the vagina, the ovaries and the intestinal loops will all be identifiable.

Located in the ovarian fossa, the ovaries are identifiable laterally at the uterine fundus, medial to the external iliac arteries and the levator ani muscle, and anterior to the internal iliac arteries and the ureters. The pulsation of the internal iliac or uterine arteries ensures their identification. The position of the ovaries is not always symmetrical and generally the left ovary is more difficult to visualize with the TA approach due to the interposition of the sigmoid colon. In prepubertal and postmenopausal individuals they may be difficult to identify due to their reduced dimensions.

The ovarian structure displays a central echogenic stromal part and a peripheral cortical part, at the level of which the follicles are visible (anechoic images of around 3-4 mm).

In individuals of fertile age the ovary is almond shaped (length 25-35 mm, breadth 20-25 mm, anteroposterior diameter 12-20 mm), with echogenicity slightly higher than the myometrium and the internal obturator muscle. It appears covered by a thin hyperechoic layer which corresponds to the germinal epithelium and the tunica albuginea.

The size and shape vary during the menstrual cycle in relation to the presence of one or more developing follicles or the luteal body.

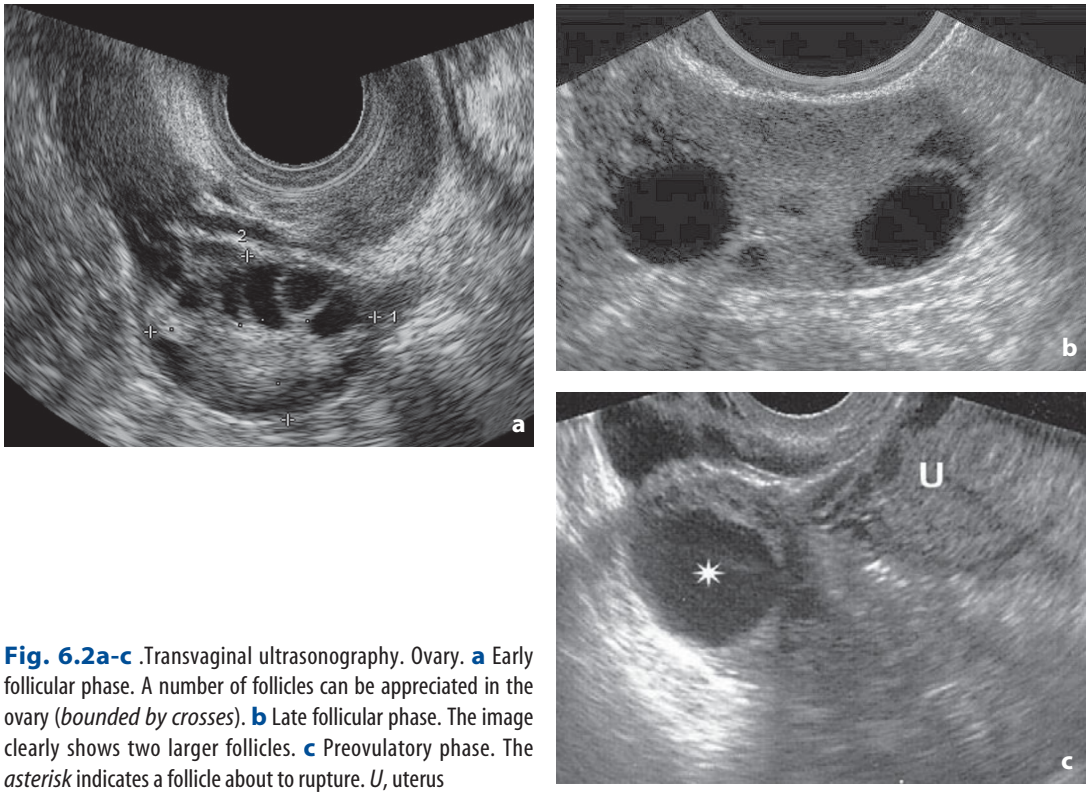

Fig. 6.2a-c .Transvaginal ultrasonography. Ovary. **a** Early follicular phase. A number of follicles can be appreciated in the ovary (*bounded by crosses*). **b** Late follicular phase. The image clearly shows two larger follicles. **c** Preovulatory phase. The *asterisk* indicates a follicle about to rupture. *U*, uterus

In the first five days of the menstrual cycle the average diameter of the follicle is 3-5 mm. These follicles, known as antral follicles, vary in number. They decrease with age and are a marker for premature menopause. In IVF centers the antral follicle count is important for predicting the type of ovarian response to gonadotropin stimulation. From the 6th to 8th day the follicle, which reaches the maximum diameter of 20 mm in the follicular phase, is defined the dominant follicle (Fig. 6.2). The dominant follicle is characterized by the presence of granulosa cells, which appear as hyperechoic in the lumen of the cystic component. With ovulation, the follicle decreases in size and becomes hyperechoic due to the increase in the thickness of the wall. The echogenicity of the luteal body increases due to the continued proliferation of granulosa cells.

The uterine tubes are not appreciable in normal conditions. With transverse scans they may be identified in the proximal tract as a continuation of the uterine body. With the TV approach the tubal isthmus can be recognized, appearing as a cylindrical shape with a diameter of 2-3 mm. The distal tract of the tube is not visible unless there is the presence of hydrosalpinx or peritoneal effusion.

The TVUS study of the uterus begins with longitudinal, median and paramedian pelvic scans which make possible the calculation of the longitudinal and anteroposterior diameters of the uterine fundus. These are followed by oblique transverse scans (Fig. 6.3).

The uterus is situated in a median position in the pelvis, between the posterior wall of the urinary bladder and the anterior wall of the rectum, and its borders are sharp and regular.

In longitudinal scans the uterus is shaped like an inverted cone. The superior 2/3 correspond to the body and the inferior 1/3 to the cervix. The isthmus is barely identifiable. In transverse scans the body is ovoid in shape with a transverse long axis, while the isthmus and cervix are rounded.

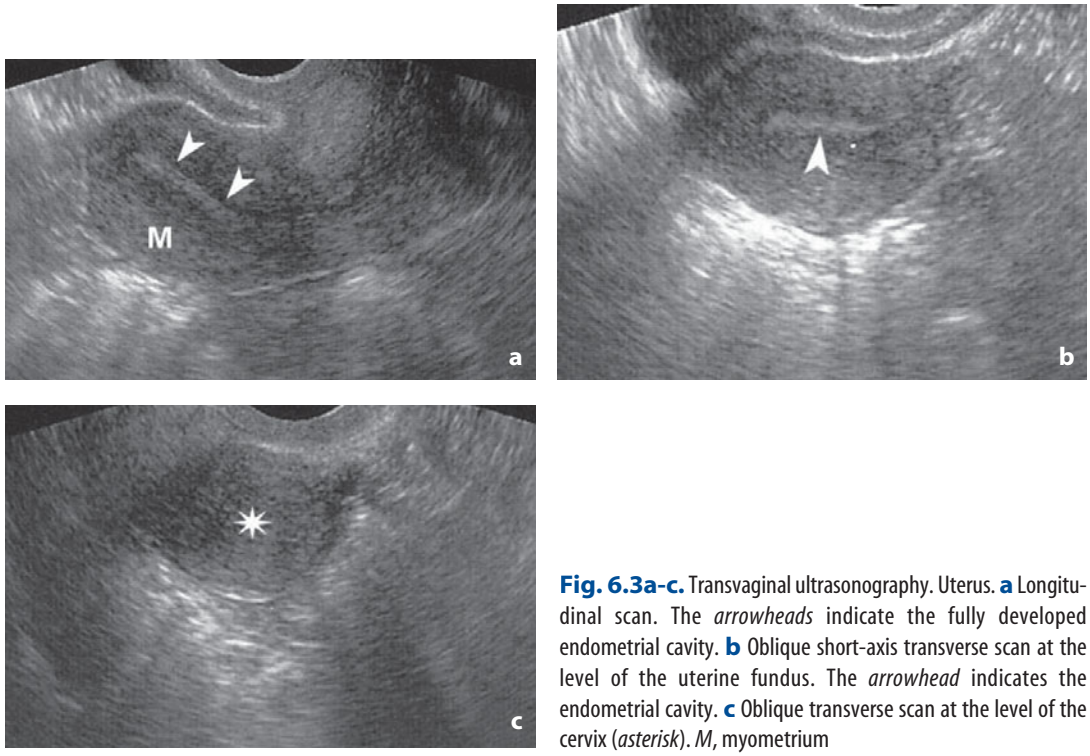

Fig. 6.3a-c. Transvaginal ultrasonography. Uterus. **a** Longitudinal scan. The *arrowheads* indicate the fully developed endometrial cavity. **b** Oblique short-axis transverse scan at the level of the uterine fundus. The *arrowhead* indicates the endometrial cavity. **c** Oblique transverse scan at the level of the cervix (*asterisk*). *M*, myometrium

The dimensions of the uterus are variable. In general it measures 7 cm from the top of the fundus to the cervix, 5 cm transversally and 4 cm anteroposteriorly. With either the TV or TA approach, under normal conditions with the urinary bladder relatively empty, the axis of the uterine body forms an "angle of flexion" of around 150° with the axis of the cervix, known as physiologic anteflexion of the uterus. Similarly, the longitudinal axis of the uterus forms an angle of around 60° with the axis of the vagina, known as physiologic anteversion. The structure of the myometrium is uniform, with an intermediate-low signal similar to that of muscular tissue, which is constant throughout the menstrual cycle. In particularly thin women, the arcuate vessels can be visualized at the level of the anterior myometrium and appear as pulsating anechoic tubular or ovoid structures.

The virtual uterine cavity can be recognized as a central line with variable echogenicity in the different phases of the menstrual cycle. During menstruation the endometrium is extremely thin, in that it is composed of only the basal layer. It appears as a thin hyperechoic line, which is really due to the interface between the anterior and posterior walls of the uterus. Under the stimulation of estrogen during the follicular phase this central interface becomes bordered by an initially thin hypoechoic layer which progressively thickens. The hypoechoic layer, which represents the endometrium proper, is marked by a weakly echoic line indicating the endometrial-myometrial interface and the basal layer of the endometrium. Externally to this line is a hypoechoic halo representing the vasculature. In the late follicular and periovulation phase the thickness of the endometrium is generally 8-11 mm[1].

Immediately after ovulation the endometrium becomes progressively hyperechoic due to increased reflectivity produced by accumulation of mucus and secretions

[1] The thickness of the endometrium can be calculated both globally (myometrial-endometrial interface from one part to the other) or by measuring each individual layer. The method used should be clearly stated. The values reported here refer to the global measurement from one myometrial-endometrial interface to the other

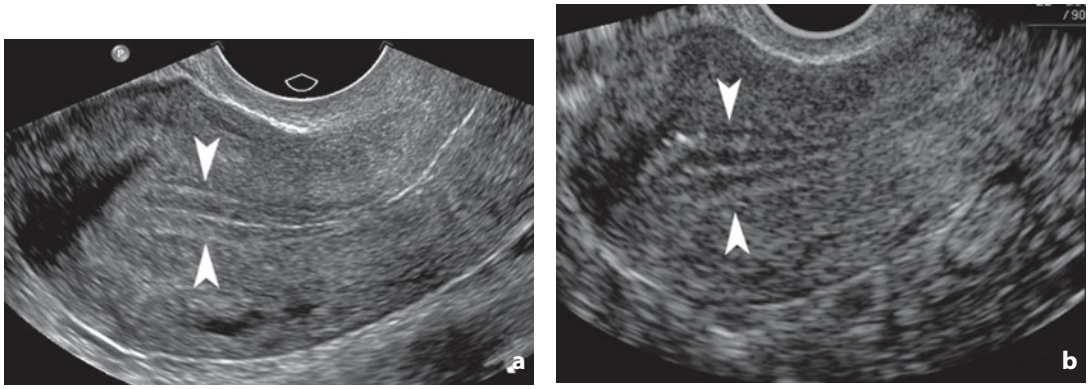

Fig. 6.4a, b. Transvaginal ultrasonography. Uterus. Longitudinal scans. Examples of follicular phase. The images show the trilaminar appearance of the endometrium between the *arrowheads*

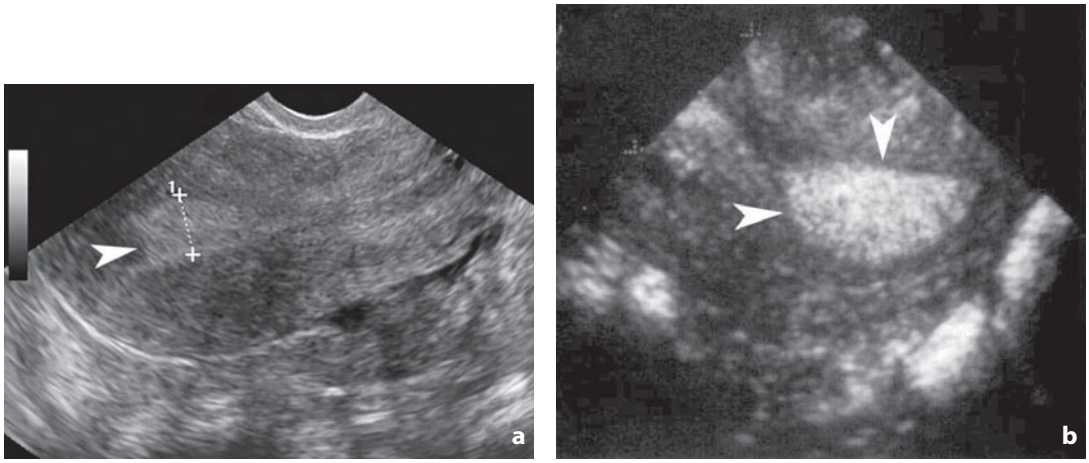

Fig. 6.5a,b. Transvaginal ultrasonography. **a** Longitudinal and **b** transverse scans. Uterus. Luteal phase. The endometrial cavity (*arrowheads*) appears broadened and hyperechoic

(Fig. 6.4). During the luteal phase it may reach up to 14-16 mm in thickness. They hyperechogenicity continues to increase due to stromal edema and the presence of glands increasingly rich in glycogen and mucous secretions (Fig. 6.5).

The postmenopausal evaluation needs to bear in mind the clinical history of the patient and especially whether she is undergoing hormone replacement therapy (HRT). The endometrium (if not completely atrophied, and therefore not visible) appears thin, uniform and hyperechoic (Fig. 6.6). In general, a thickness less than 5 mm without focal thickening rules out the presence of significant disease and is compatible with atrophy. The endometrium of a patient undergoing HRT may appear slightly thickened. The examination, therefore, should be performed either at the beginning or the end of a treatment cycle when the thickness of the endometrium is minimal and any pathologic thickening is therefore more evident.

The presence of a layer of liquid in the uterine cavity of elderly patients is not necessarily a pathologic finding, in that it is probably due to the collection of mucous secretions.

In longitudinal scans performed during ovulation, the canal of the cervix appears as a small hyperechoic line which broadens due to the glandular mucous secretion, which is why this portion of the cervix has a higher echogenicity (Fig. 6.7). The walls of the cervix may be the site of Naboth cysts, i.e. small mucous cysts due to the obliteration of the excretory ducts of the glands. They appear as anechoic rounded formations with a diameter which varies from a few millimeters to 2-3 cm, and are of no pathologic significance.

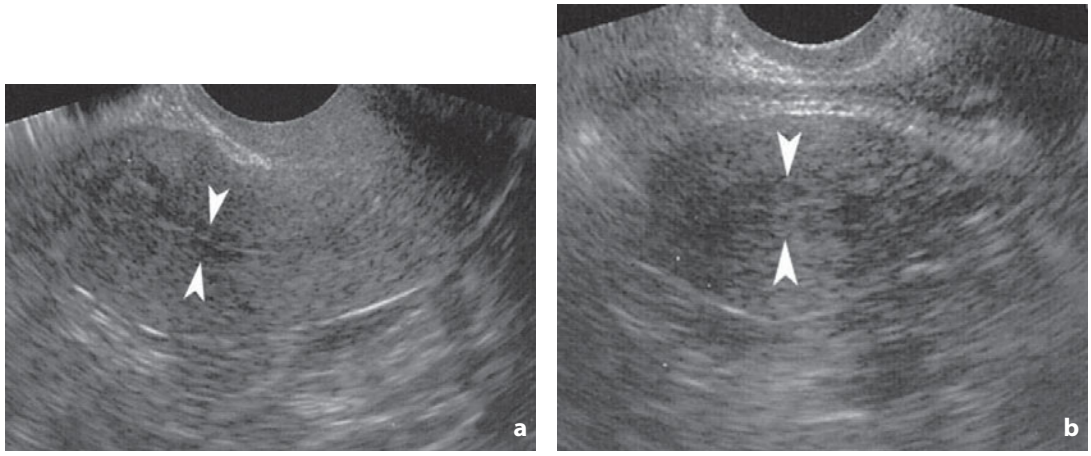

Fig. 6.6a,b. Transvaginal ultrasonography. **a** Longitudinal and **b** transverse scans. Postmenopausal uterus. The *arrowheads* indicate the thinned, hyperechoic endometrial cavity

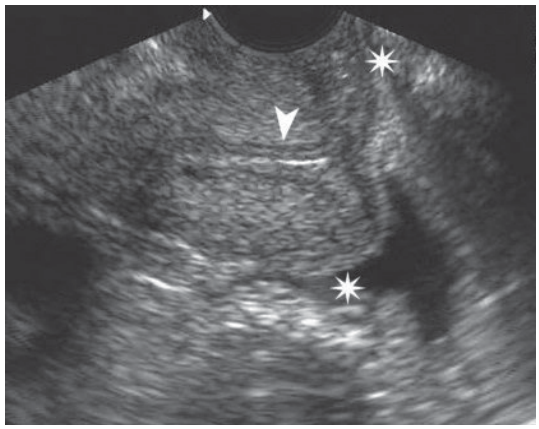

Fig. 6.7. Transvaginal ultrasonography. Longitudinal scan. Uterine cervix. The *arrowhead* indicates the hyperechoic cervical canal. The *asterisks* are positioned at the level of the vaginal fornices

The vaginal portion of the cervical canal can be studied well with TV ultrasonography, making possible the evaluation of the borders and adipose cleavage planes with respect to the bladder, anteriorly, and the rectum, posteriorly.

The TV approach also enables study of the rectouterine pouch, the most sloping portion of the peritoneal cavity, in which in normal conditions (during the menstrual and periovulatory phase) a thin layer of liquid is normally appreciable.

Visualized with a suprapubic transducer, the vagina has a length varying from 7 to 10 cm. It appears as a thin, flat structure with a thickness of less than 1 cm and a trilinear appearance produced by the coinciding walls (moderately echoreflective) and the central interface (hyperechoic). The lumen is recognizable when it contains menstrual blood. In transverse scans the posterior fornix can be identified as a crescent-shaped anechoic layer.

The **color Doppler examination** completes the US study and is able to obtain information about the vasculature of the ovaries and the uterus (**Figs. 6.8, 6.9**). The vasculature of the ovaries can be identified well with color Doppler. There are two afferent vessels: the ovarian artery (which arises directly from the aorta) and the ovarian branch of the uterine artery. The study can visualize small arterioles in the stroma and the Doppler trace shows intermediate resistance vessels without early diastolic notching. The flow pattern is related to the various phases of the menstrual cycle, and therefore undergoes changes in the postmenopausal period when the ovaries decrease in size and the echogenicity increases in relation to the increase in the fibrous component.

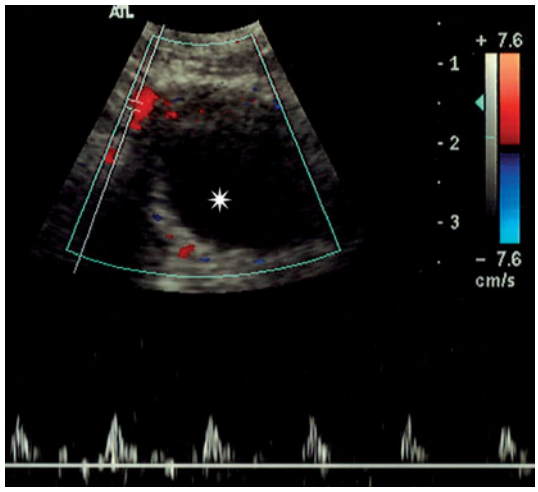

Fig. 6.8. Transvaginal ultrasonography. Flow pattern trace of the right ovarian artery of a woman of fertile age. The *asterisk* indicates a follicle in the preovulatory phase

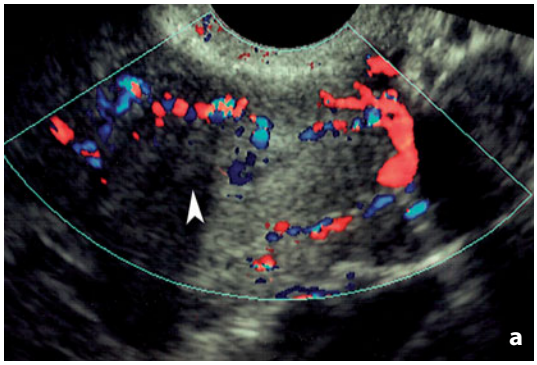

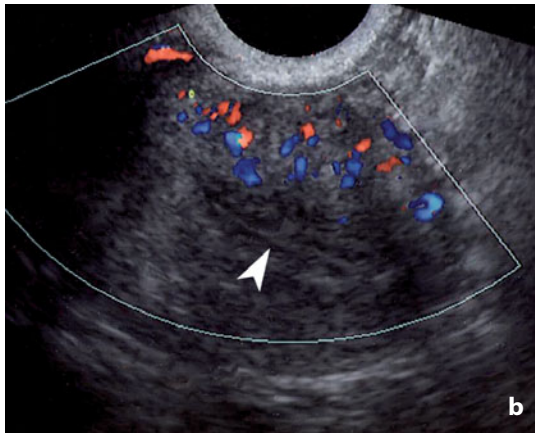

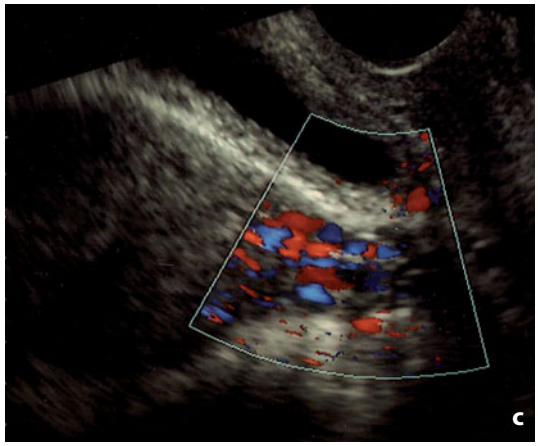

Fig. 6.9a-c. Transvaginal ultrasonography. Color Doppler. Woman of fertile age, follicular phase of the menstrual cycle. Normal vasculature of the uterine fundus (**a**, axial scan), the uterine body (**b**, longitudinal scan) and uterine cervix (**c**, longitudinal scan). The *arrowhead* indicates the uterine cavity

The two uterine arteries are visible in the parametrium at the level of the transition between the uterine body and cervix and are connected via the arcuate artery which runs in the most superficial layer of the myometrium. The flow pattern of the uterine artery depends on the uterine trophism. The blood supply is clearly greater during menstruation: during the follicular phase the trace is similar to that of the internal iliac artery. With the periovulatory decrease in estrogen there is a concomitant reduction

in perfusion. Diastolic flow increases in the second luteal phase of the cycle. In the postmenopausal period the diastole disappears from the trace.

Callen P (2007) Ultrasonography in obstetrics and ginecology. Elsevier Saunders, Philadelphia

Derchi LE, Serafini G, Gandolfo N et al (2001) Ultrasound in gynecology. Eur Radiol 11:2137-2155

Laing FC, Brown DL, Di Salvo DN (2001) Gynecologic ultrasound. Radiol Clin North Am 39:523-540

Anatomy in Computed Tomography

CT examination of the pelvis is rarely performed for purely gynecologic indications since it is poorly suited to studying the endometrium in detail and the changes it undergoes during the menstrual cycle. It can, however, correctly visualize the pelvic bones and the psoas, iliac, internal obturator and pyriform muscles, the levator ani muscle and the muscles of the pelvic floor. CT is also the best technique for identifying pathologic calcifications, as can be found in uterine fibromyomas and at the level of the lymph nodes. Like MR and US, CT is useful for establishing the relations of the pelvic organs.

The examination is best performed with the urinary bladder moderately distended, thus rendering the axis of the uterine body vertical and removing the bowel loops from the lesser pelvis. It may also be useful to introduce around 100 mL of contrast medium, diluted at 5-10%, into the rectum.

The CT examination involves acquisition of noncontrast-enhanced images, which are indispensable in the diagnosis of acute hemorrhage, and a study during the administration of nonionic iodinated intravenous contrast medium (300-350 mgI/mL; 120-130 mL; injection speed 2 mL/s). Arterial-phase acquisitions are generally not requested, whereas the venous phase is important (around 70 s after injection of the contrast medium). A late-phase scan (after 3-5 min) may be useful for the evaluation of possible pathologic involvement of the bladder wall or the distal ureteric tract.

The ovaries are usually well visualized and are located in the ovarian fossa, anterior to the ureters and posterolateral to the uterus. The anatomic landmark for visualization of the ovary is the tubal angle of the uterus (**Fig. 6.10**).

The dimensions of the follicles vary with the phases of the menstrual cycle. The maximum diameter, which is measured shortly before ovulation, may reach and exceed 2 cm.

On CT the uterus, covered with peritoneum which is continuous over the urinary vault and which posteriorly ascends the anterior wall of the rectum to form the rectovesical pouch, appears as a triangular or oval parenchymal structure related to the bladder posterosuperiorly. The uterine body is usually triangular in shape, while the uterine cervix is more cylindrical. Nonetheless, uterine morphology at CT is variable, depending on the scan plane, the spatial orientation of the organ itself and, of course, the planes used in the multiplanar reconstructions (MPR). Similarly, the dimensions and position of the uterus vary in that they are influenced by a variety of factors, including age and hormonal state. In baseline conditions the endometrial secretions produce a central and elongated area of hypoattenuation. During the menstrual cycle, variations in the endometrial and myometrial thicknesses can be observed. In general the cervix appears of uniform density, often slightly hypoattenuating with respect to the remainder of the uterus, and rounded in appearance when the section is perpendicular to its long axis (**Fig. 6.11**).

In a woman of fertile age the uterine body has variable dimensions from 5 to 8 cm. The cervix normally measures no more than 3 cm in axial scans.

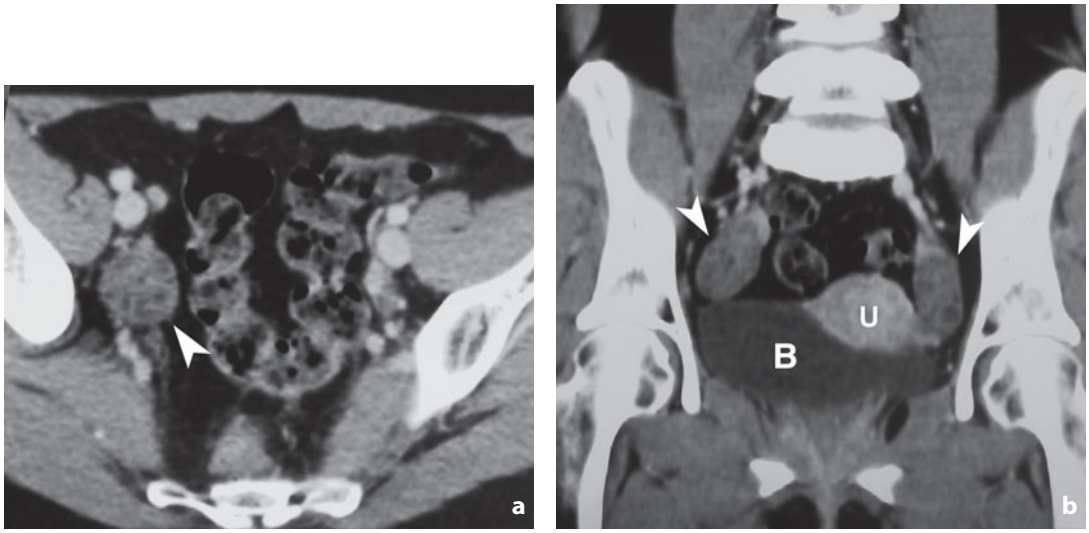

Fig. 6.10a,b. Computed tomography. Normal anatomy of the ovary. **a** Axial scan. Several small follicles are identifiable in the right ovary (*arrowhead*). **b** Coronal reconstruction. Both of the ovaries are appreciable (*arrowheads*) with several follicles. *B*, urinary bladder; *U*, uterus

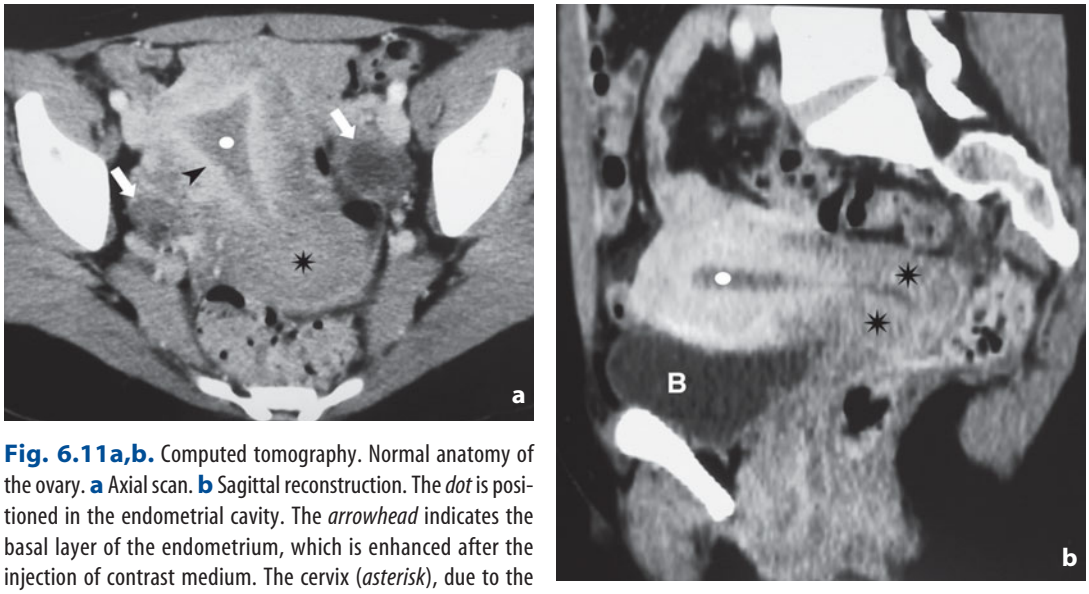

Fig. 6.11a,b. Computed tomography. Normal anatomy of the ovary. **a** Axial scan. **b** Sagittal reconstruction. The *dot* is positioned in the endometrial cavity. The *arrowhead* indicates the basal layer of the endometrium, which is enhanced after the injection of contrast medium. The cervix (*asterisk*), due to the greater stromal component, appears hypoattenuating in comparison to the myometrium of the uterine body and fundus. The *arrows* indicate the ovaries. *B*, urinary bladder

On CT images the vagina is characterized by a density similar to that of the surrounding soft tissue and appears as a flattened transverse structure which widens at the level of the fornices situated lateral to the cervix. The virtual vaginal lumen cannot be clearly identified. It is best visualized with the insertion of a tampon (**Fig. 6.12**).

The layer of connective tissue underlying the peritoneum, which is continuous with the base of the broad ligament and surrounds the supravaginal part of the cervix, comprises the parametrium. The distal pelvic tract of the ureter can be identified running some 2 cm lateral to the uterine cervix.

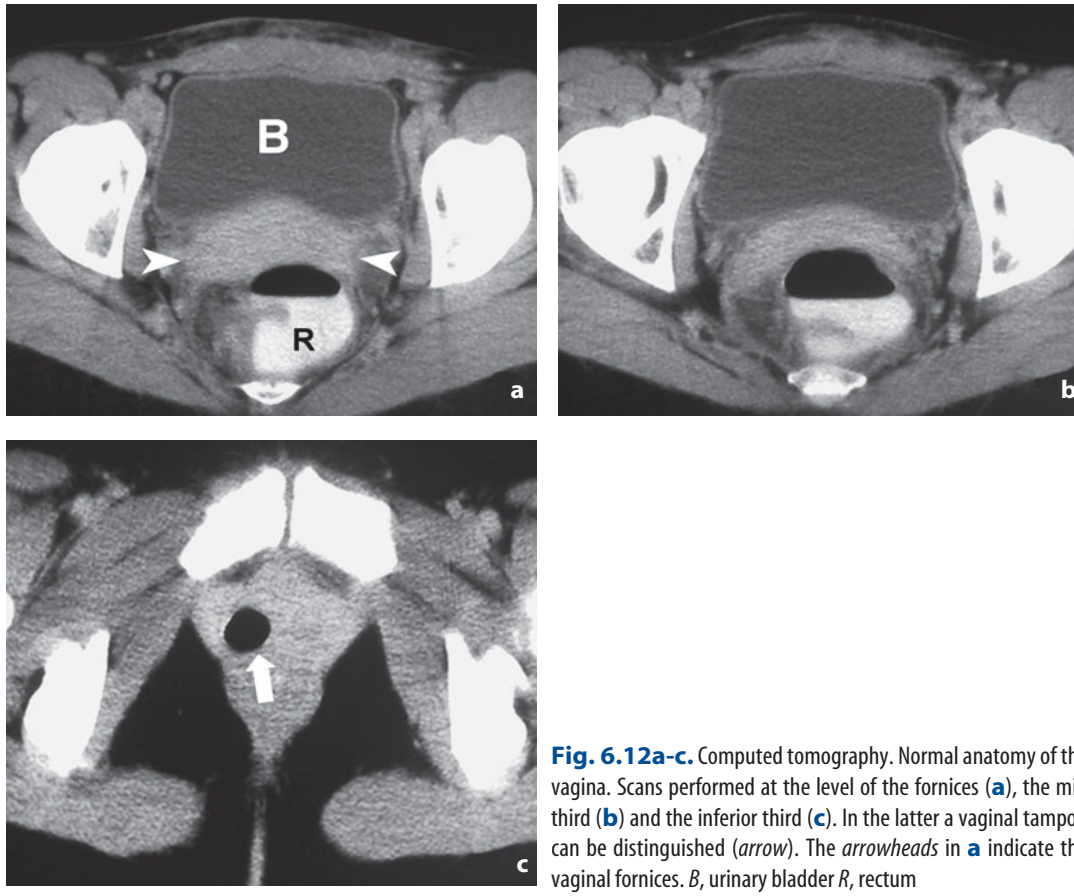

Fig. 6.12a-c. Computed tomography. Normal anatomy of the vagina. Scans performed at the level of the fornices (**a**), the mid third (**b**) and the inferior third (**c**). In the latter a vaginal tampon can be distinguished (*arrow*). The *arrowheads* in **a** indicate the vaginal fornices. *B*, urinary bladder *R*, rectum

Structures which can be visualized on CT include the uterine ligaments, especially when they are thickened after radiotherapy. The round ligament has a ribbon-like appearance, and the broad ligament is readily identifiable due to the structures it contains or which surround it. The cardinal ligament, in contrast, is not always visible along its entire course, which from the cervix and the superior part of the vagina, reaches the fascia of the internal obturator muscle.

The injection of contrast medium enables identification of the uterovaginal vascular plexus. The two ovarian arteries can be distinguished only during the arterial phase. The ovarian vein can be visualized, especially postnatally or if ectasic, at the level of the psoas muscle, lateral to the ureter.

Klüner C, Hamm B (2007) Normal imaging findings of the uterus. In: Hamm B, Forstner R (eds) MRI and CT of the female pelvis. Springer-Verlag, Berlin

Anatomy in Magnetic Resonance

Magnetic resonance (MR) has taken on a pre-eminent role in the diagnostic imaging of the female pelvis. The technique provides excellent visualization of the female genital organs, and thanks to its panoramic views also enables a complete examination of the pelvic region and its structures (lymph nodes, bone and muscles of the pelvic wall). It has high contrast resolution, and with the recent introduction of phased array coils high spatial resolution as well.

In MR the ovaries are better visualized in the coronal plane, on the posterior surface of the broad ligament and inferolateral to the tubes. They present the characteristic

almond shape with variable dimensions in relation to age and the phase of the menstrual cycle. The volume is around 6-8 cm^3 in woman of fertile age, during which they can be identified in almost 90% of cases. In woman of prepubertal and postmenopausal age the ovaries cannot be easily identified given their reduced volume and absence of follicles.

In those of fertile age the T1-weighted signal of the ovaries is low-intermediate, generally uniform and similar to that of the bowel loops and the myometrium. They may present small focal images of higher or lower signal indicating hemorrhagic luteal bodies or cystic follicles, respectively. In T2-weighted sequences the zonal anatomy of the ovaries can be identified. In the fibromuscular ovarian stroma (intermediate-low signal) a superficial cortical zone rich in stromal cells can be appreciated, with denser connective tissue and limited extracellular matrix producing a relatively hypointense signal, as well as a medullary zone with a relatively higher signal in relation to the lower density of the medullary connective tissue.

In the postmenopausal period the contrast between the cortical and medullary zones is evident and the signal is more uniformly hypointense.

The ovarian follicles are recognizable in the superficial cortex and the subcortical zone in T2-weighted images, appearing as small, rounded, hyperintense formations possibly surrounded by a thin hypointense rim. As noted above, the follicles enable the immediate identification of the ovaries in MR images, appearing more evident if the sequences are acquired with phased array coils. The dimensions of the follicles are considered normal when their diameter is less than 25 mm (**Fig. 6.13**). In their cystic form the luteal body appears hypointense in T1-weighted images and hyperintense in

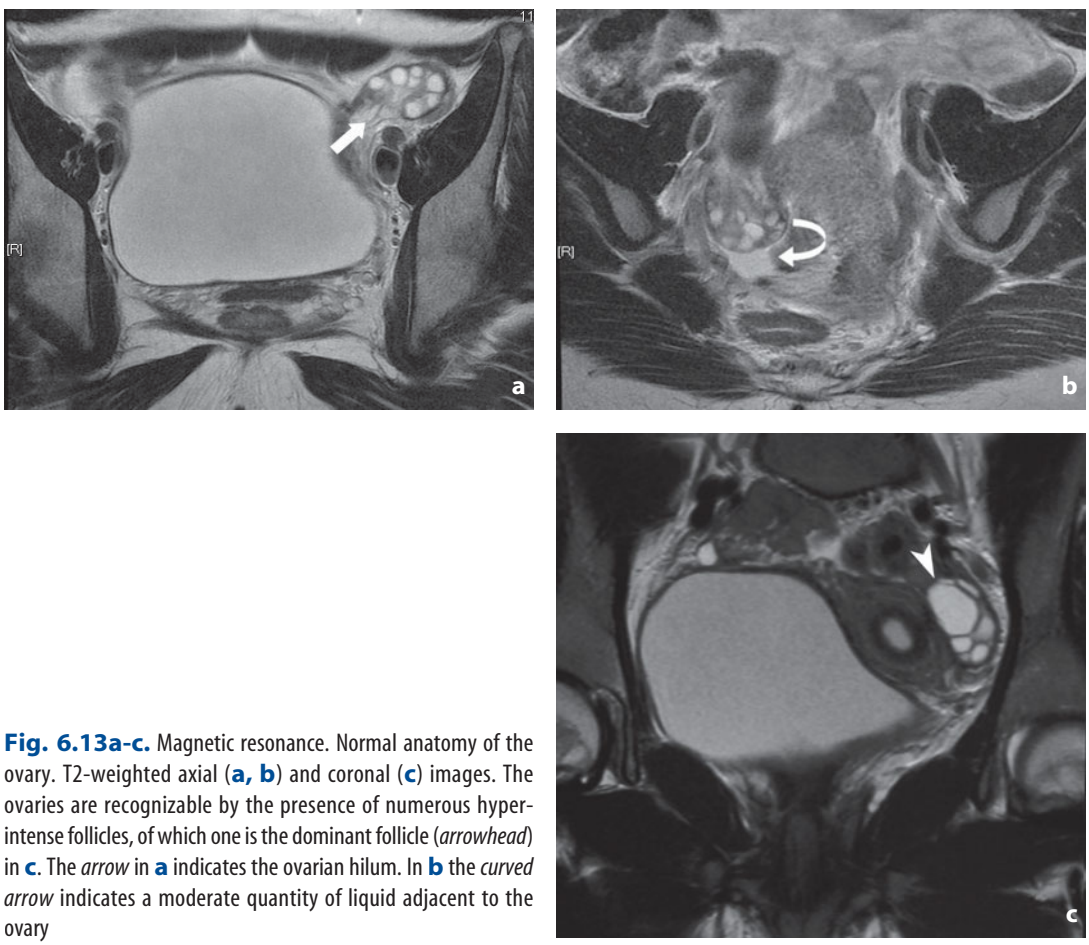

Fig. 6.13a-c. Magnetic resonance. Normal anatomy of the ovary. T2-weighted axial (**a, b**) and coronal (**c**) images. The ovaries are recognizable by the presence of numerous hyperintense follicles, of which one is the dominant follicle (*arrowhead*) in **c**. The *arrow* in **a** indicates the ovarian hilum. In **b** the *curved arrow* indicates a moderate quantity of liquid adjacent to the ovary

T2-weighted images. It appears bounded by a rim (due to a deposit of hemosiderin) which is hypointense in T1 and hyperintense in T2 and enhances after contrast medium administration.

After the administration of paramagnetic contrast medium an increase in signal occurs only in the stromal part of the ovary. Occasionally, in relation to angiogenesis, there may be a focal strengthening of the signal around a follicle or in a luteal body. In woman of fertile age, the enhancement of the ovary is however less intense than that of the myometrium, whereas it becomes similar to that of the latter in post-menopausal women.

The broad ligament is the only support structure recognizable, having a hypointense signal in the coronal or parasagittal plane. The other structures are only recognizable in the presence of ascites.

The tubes are appreciable in the coronal plane, appearing as elongated formations arising from the uterine body and extending laterally towards the pelvic wall. They present low or intermediate signal intensity.

The MR study of the uterus does not require any special preliminary preparation. However, performing the examination with the urinary bladder moderately distended is preferable. In T1-weighted images the uterus presents a uniform, intermediate-low signal, while in T2-weighted images three zones of different signal intensity can be identified: endometrial, junctional and myometrial (**Figs. 6.14, 6.15**).

The central hyperintense zone represents the basal and functional layers of the endometrium and its associated secretions. During the menstrual cycles its thickness various from 1-3 to 3-7 mm. It is thinnest immediately after menstruation and during the follicular phase, and thickens during the luteal phase (**Fig. 6.16**). During menstruation low-signal blood clots can be identified within the endometrial cavity.

The hypointense interface, defines the junctional zone, corresponds with the deepest zone of the myometrium and in woman of fertile age accounts for 20-25% of the myometrial thickness. The junctional zone is hypointense with respect to the more superficial layer of the myometrium given the different cellular composition of the tissue, being characterized by a greater concentration of compact smooth muscle cells and a lesser presence of extracellular matrix than the peripheral zone. There are no significant differences in the myometrial thickness during the menstrual cycle, although the signal intensity does modify, being higher in the central period of the luteal phase due to edema, which tends to decrease the contrast between the junctional zone and the peripheral zone. In this phase the arcuate vessels of the myometrium are also identifiable.

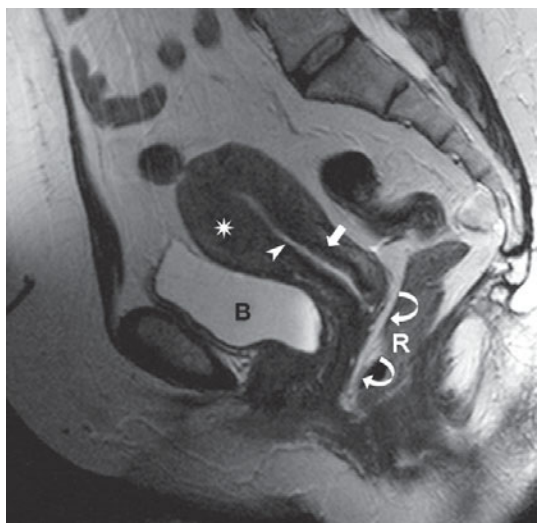

Fig. 6.14. Magnetic resonance. Uterus. T2-weighted sagittal image. The hyperintense signal identifies the endometrial cavity (*arrowhead*), and the hypointense signal the junctional zone (*arrow*). The *asterisk* indicates the myometrium. The *curved arrows* indicate the rectovaginal septum. *B*, urinary bladder; *R*, rectum

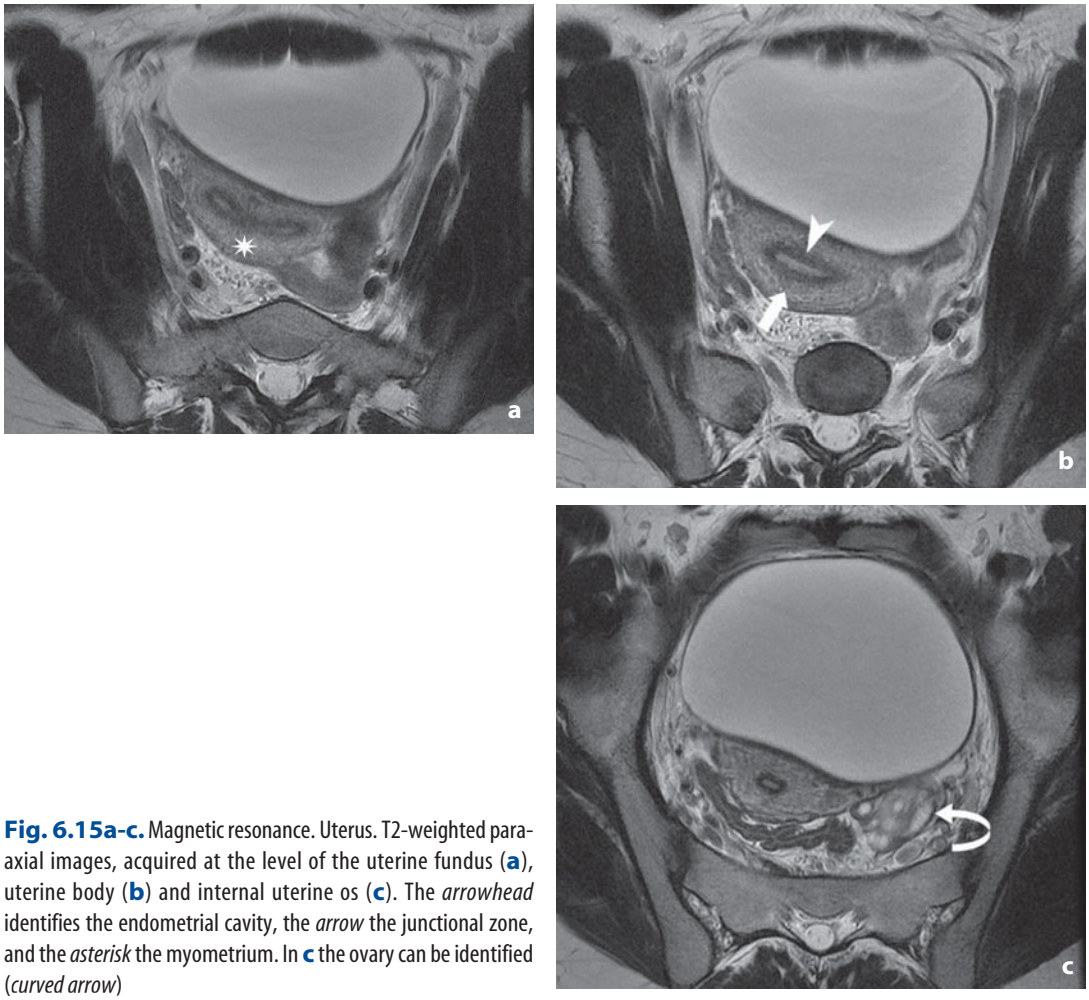

Fig. 6.15a-c. Magnetic resonance. Uterus. T2-weighted paraaxial images, acquired at the level of the uterine fundus (**a**), uterine body (**b**) and internal uterine os (**c**). The *arrowhead* identifies the endometrial cavity, the *arrow* the junctional zone, and the *asterisk* the myometrium. In **c** the ovary can be identified (*curved arrow*)

In postmenopausal women the above-described zonal anatomy is no longer identifiable. The endometrium is thin and the myometrium is characterized by a lower signal intensity than that recorded in woman of fertile age (Fig. 6.17).

In women undergoing HRT the myometrium presents a higher signal intensity in both T1- and T2-weighted images. The junctional zone may prove difficult to identify or even be completely absent. After prolonged HRT the uterine body may appear slightly smaller. The administration of gonadotrofin-releasing hormone analogues tends to decrease estrogen production and therefore produces an involution of the uterus, with marked endometrial atrophy and hypointensity of the myometrial signal (similar to the situation in postmenopausal women). In contrast, estrogen replacement therapy produces a clearly identifiable endometrium, junctional zone and myometrium. In this situation the uterus remains very similar to that of a woman of fertile age.

After the intravenous administration of paramagnetic contrast medium (0.1 mmol/kg) in the normal uterus, the myometrium displays significant enhancement, whereas the junctional zone remains low signal, probably due to its more compact structure and the consequent lesser presence of extracellular spaces.

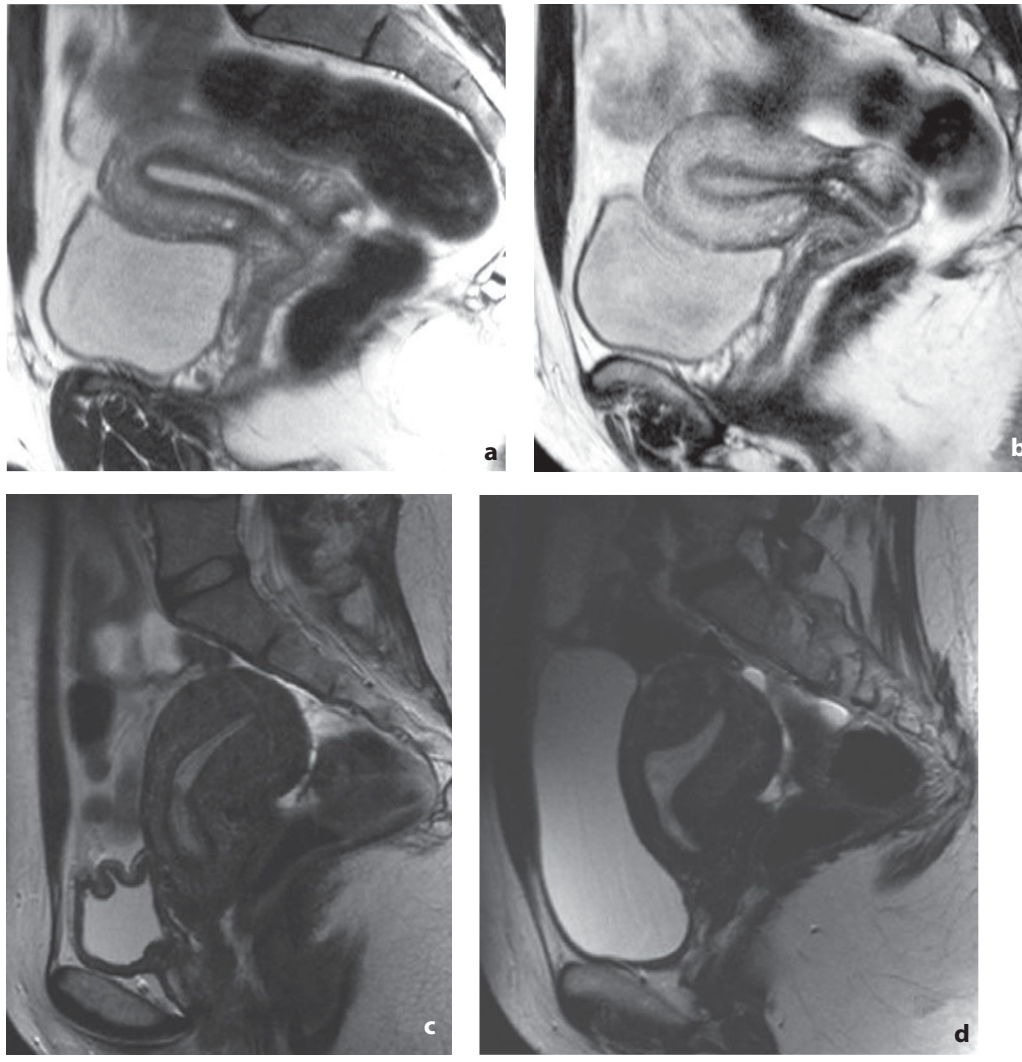

Fig. 6.16a-d. Magnetic resonance. Normal functional anatomy of the endometrium. T2-weighted sagittal images. **a** Follicular phase. **b** Luteal phase in which a slight increase in the thickness of the endometrial cavity can be appreciated with an increase in the signal of the myometrium. The increase in the thickness of the endometrium is more evident in another patient with a retroverted uterus, where image **c** was acquired in the follicular phase and **d** in the luteal phase

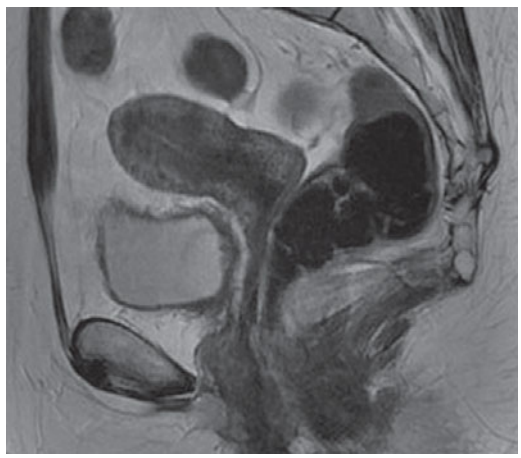

Fig. 6.17. Magnetic resonance. Postmenopausal uterus with reduced volume. The endometrial cavity is reduced to a thin hyperintense line. In this patient the junctional zone is still recognizable, although vague

In addition to the uterine body, the uterine cervix also displays three concentric zones with different signals in T2-weighted images: the cortical zone, the intermediate zone and the peripheral zone. The hyperintense central zone corresponds to the palmate folds and the mucus occupying the cervical canal. The intermediate zone, which corresponds to the deepest part of the fibromuscular stroma, is hypointense due to the higher concentration of smooth muscle cells (as with the description of the intermediate layer of the uterine body). The peripheral zone has a mid-high signal and is the most superficial component of the cervical stroma where smooth muscle cells prevail. In T2-weighted images the pericervical tissue in fertile age women is characterized by medium-high signal intensity and is readily distinguished from the low signal of the cervical stroma (**Fig. 6.18**).

The spatial orientation of the cervix is variable. Its long axis, however, is normally located in the sagittal plane. The cervix is separated anteriorly from the bladder wall by a thin cleavage plane of adipose tissue and posteriorly from the ampulla of the rectum by the rectovaginal fascia.

The administration of contrast medium produces a significant degree of enhancement of both the pericervical tissue and the mucous epithelium, while the dense connective tissue displays only mild enhancement.

The parametrium has intermediate signal intensity in T1-weighted images and a variably higher signal in T2. The suspensory ligaments in contrast appear hypointense in both T1 and T2.

In T1-weighted images the vagina presents intermediate signal intensity, similar to that of the urethra and the rectum. In axial T2-weighted images the anatomy of the

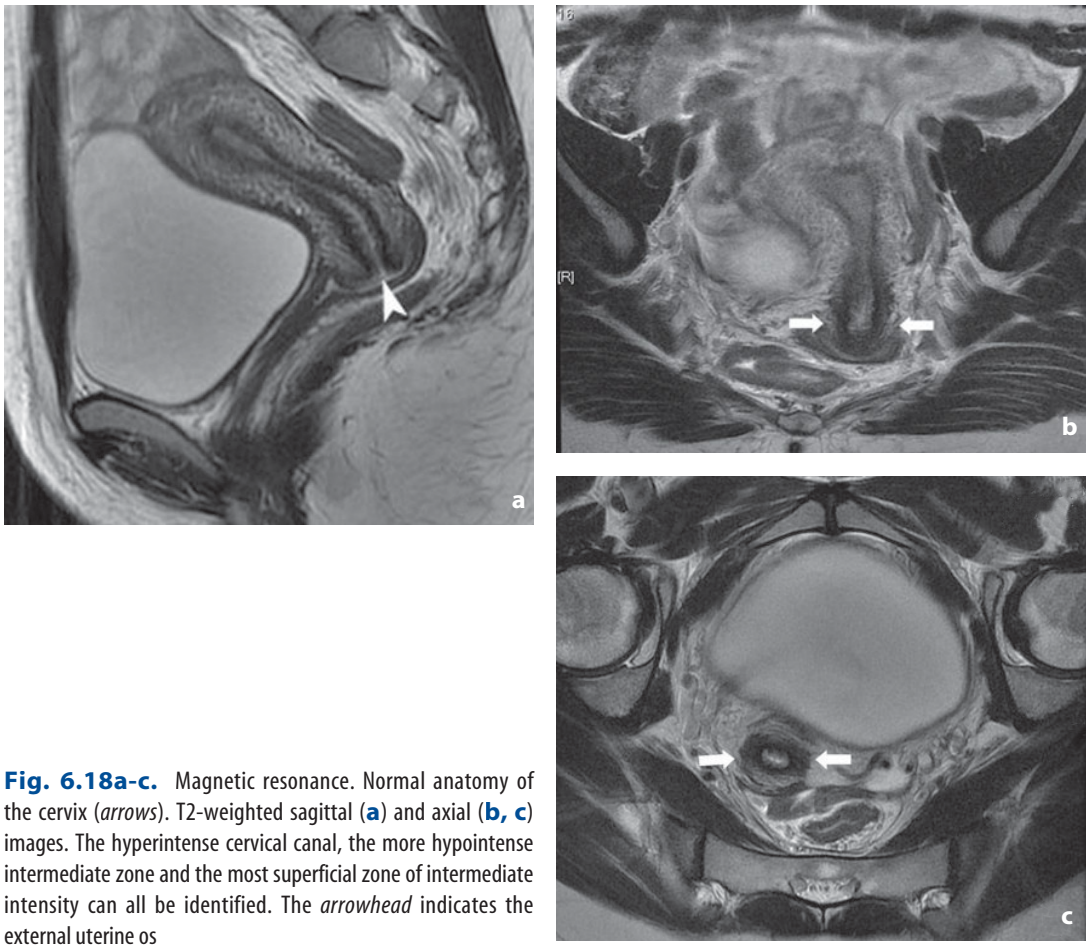

Fig. 6.18a-c. Magnetic resonance. Normal anatomy of the cervix (*arrows*). T2-weighted sagittal (**a**) and axial (**b, c**) images. The hyperintense cervical canal, the more hypointense intermediate zone and the most superficial zone of intermediate intensity can all be identified. The *arrowhead* indicates the external uterine os

vagina can be identified and clearly distinguished from the surrounding structures. In the same sequences the paravaginal vascular spaces have a hyperintense signal. In the sagittal plane the rectovaginal pouch can often be identified (Fig. 6.19).

Not unlike the description of the uterus, hormone stimulation influences the morphologic characteristics and the signal of the vagina, which therefore vary in relation to the menstrual cycle.

In T2-weighted images acquired in the early follicular phase, the vagina appears composed of a wall with a low signal and a hyperintense central area representing the vaginal mucus and epithelium. At the beginning of the luteal phase the thickness of the mucous component increases and in most subjects the vaginal wall presents an intermediate-high signal with a consequent reduction in contrast between the two structures.

In individuals of prepubertal age the vaginal wall appears hypointense in T2-weighted images and the central mucous component can be identified only as a thin hyperintense strip. In woman of postmenopausal age, in the absence of HRT, the vagina appears hypointense, with a very thin central mucous component, and no signs

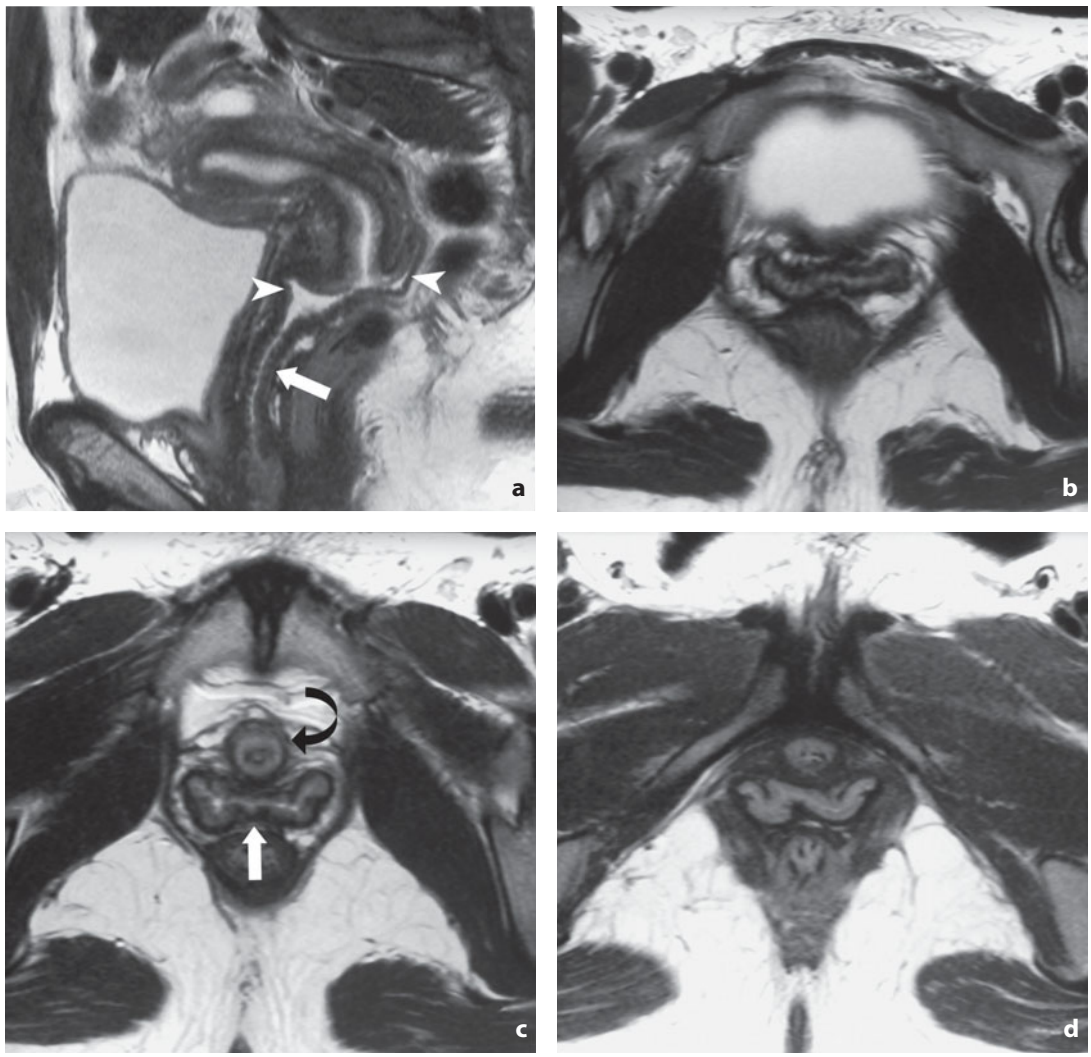

Fig. 6.19a-d. Magnetic resonance. Normal anatomy of the vagina. T2-weighted sagittal (**a**) and axial images at the superior third (**b**), middle third (**c**) and inferior third (**d**). The *arrowheads* indicate the fornices, the *arrow* the vagina and the *curved arrow* the urethra

of vessel congestion can be identified in the paravaginal tissue. If, in contrast, the patient is undergoing HRT, the vagina presents morphologic and signal characteristics similar to those observed in the follicular phase. After the administration of contrast medium both the vaginal wall and the mucous component are enhanced.

Chang SD (2002) Imaging of the vagina and vulva. Radiol Clin North Am 40:637-658

Nalaboff KM, Pellerito JS, Ben-Levi E (2001) Imaging the endometrium: disease and normal variants. RadioGraphics 21:1409-1424

Forstner R (2007) Ovaries and fallopian tubes: normal findings and anomalies. In: Hamm B, Forstner R (eds) MRI and CT of the female pelvis. Springer-Verlag, Berlin

Togashi K (2003) MR imaging of the ovaries: normal appearance and benign disease. Radiol Clin North Am 41:799-811

Part II
Malformation

Clinics and Imaging

7

M.P. Bondioni, S. Milianti, A. Frugoni

Introduction

The urogenital system is frequently the site of congenital anomalies, which occur in 0.2-2% of all live births (Table 7.1). The timely and accurate diagnosis both pre- and postnatally is vital, especially in major malformations, and is aimed at safeguarding renal function, urinary continence and normal sexual function.

Table 7.1. Major urogenital malformations

Kidney	Upper urinary tract	Lower urinary tract	Genitals
♀♂	♀♂	♀♂	♀♂
Numerical anomalies	Double or triple collecting system	Exstrophy of the bladder	Ambiguous genitalia
Fusion and displacement anomalies	Ureteropelvic junction anomalies	Vesical diverticula	
Cystic malformations	Anomalies of the ureter and its course	Persistent urachus	
	Anomalies of the ureterovesical junction	♂	♂
		Double urethra	Ejaculatory duct reflux
		Urethral valves	Hypospadia
		Anterior urethral diverticula	Cryptorchidism, testicular ectopia, retention
		Urethral stricture Cowper's syringocele	
			♀
			Müllerian anomalies
			Urogenital sinus anomalies
			Cloaca
			Vaginal atresia

L. Olivetti, L. Grazioli (eds.), *Imaging of Urogenital Diseases*,

Urogenital malformations account for around 15% of all major congenital anomalies identified in the prenatal period and are found in 0.5% of neonates, half of which undergo surgery in the first year of life.

The association between urinary malformations and renal dysplasia is known, but only since the advent of fetal ultrasonography (US) in the 1990s has it been possible to prenatally identify hypoplastic and dysplastic kidneys, which are associated with malformations of the urinary tract. Today this condition is considered a syndrome: congenital anomalies of the kidney and urinary tract (CAKUT).

The frequent family history and predominance in males, in whom the clinical presentation tends to be more severe, have prompted genetic research. It has been shown that the processes which lead to the formation of the kidneys and the urinary tract are controlled by the complex interaction of a variety of genes. The mutation of one gene can give rise to different malformations, just as the mutation of different genes can cause the same malformation. Since this condition is due to hereditary transmission, different clinical presentations may coexist in the same family group, i.e. major malformations such as renal agenesis, and minor malformations such as pelvic atresia. One of the most studied genes encodes for type-2 angiotensin II receptor (AGTR2), which is expressed in the kidney and urinary tract during embryogenesis and then inactivated. Studies on the DNA of patients with syndromes characterized by ocular defects and renal and urinary tract malformations have identified mutations in the PAX gene family.

This chapter covers the major urogenital malformations. The chief imaging modalities for the diagnosis of these malformations are US and conventional radiography. Second-level techniques, such as computed tomography and magnetic resonance, are generally used in select cases, since the former exposes the patient to a significantly higher dose of ionizing radiation than conventional radiography, whereas the latter involves the use of sedation.

Hinchliffe SA, Chan YF, Jones H et al (1992) Renal hypoplasia and postnatally acquired cortical loss in children with vesicoureteral reflex. Pediatr Nephrol 6:439-444

Sanyannusin P, Shimmentil LA, McNoe LA et al (1995) Mutation of the PAX2 gene in a family with optic nerve colobomas, renal anomalies and vesicoureteral reflux. Nat Genet 9:358-364

Wiesel A, Queisser-Luft A (2005) Prenatal detection of congenital renal malformations by fetal ultrasonographic examination: an analysis of 709,030 births in 12 European countries. Eur J Med Genet 48:131-144

Woolfs AS (2000) A molecular and genetic view of renal and urinary tract malformations. Kidney Int 58:500-512

Renal Malformations

Agenesis

Unilateral renal agenesis is the most frequent anomaly with an incidence of 0.4% in postmortem studies. It more commonly affects the left side, with a male/female ratio of 2:1. In most cases the condition is asymptomatic and generally diagnosed due to malformations affecting the single kidney, such as junction disease, vesicoureteric reflux (VUR), malrotations, and which are encountered in 15-30% of cases. Unilateral renal agenesis is often associated with anomalies of the genitals: in females anomalies of median fusion of the paramesonephric duct occur in over 50% of cases, and in males absence or hypoplasia of the ductus deferens with or without involvement of the testicle is found in around 30% of cases.

The condition is generally an incidental finding during a US examination which fails to identify the kidney in its normal site or along the course of the urinary tract.

When renal agenesis is suspected, intravenous urography and especially scintigraphy are able to confirm the diagnosis. The former demonstrates the absence of contrast medium uptake, the latter the absence of tracer uptake and therefore the absence of renal function. The prognosis depends on the functionality of the single kidney, which usually presents compensatory hypertrophy.

Bilateral renal agenesis or Potter's syndrome is a rare anomaly which is incompatible with life and characterized by severe oligohydramnios and morphologic alterations of the facial skeleton, the limbs and the lungs. Both pre- and postnatal US fail to identify an organ with renal parenchyma. The suprarenal glands in bilateral renal agenesis can take on a cylindrical shape similar to the appearance of a kidney.

Fusion and Displacement Anomalies

Fusion anomalies are the result of anomalous contact between the two early kidneys during organogenesis. They may take the form of crossed fused renal ectopia or contact on the median line, a condition known as horseshoe kidney (**Diagram 7.1**). The latter is the most common fusion anomaly, with an incidence of one case per 1800 postmortem findings. In 95% of cases the fusion involves the lower pole, with a tract known as the "isthmus" composed of fibrous, dysplastic or normal parenchymal tissue.

The horseshoe kidney is generally located lower than normal, and the renal pelves are usually malrotated and lie anteriorly or laterally. The ureters most commonly pass anterior to the isthmus.

The vasculature of the horseshoe kidney is anomalous in 70% of cases, with arteries which may arise directly from the aorta, from the renal artery or even from the inferior mesenteric, common iliac or medial sacral arteries. The isthmus almost always has its own vasculature.

In around one-third of cases the condition is diagnosed incidentally during the course of a US study. In the remaining cases it may present with abdominal pain and of course a mass secondary to hydronephrosis, in that urine flow may be obstructed by the ureters crossing the isthmus or by the presence of anomalous vessels. US is able

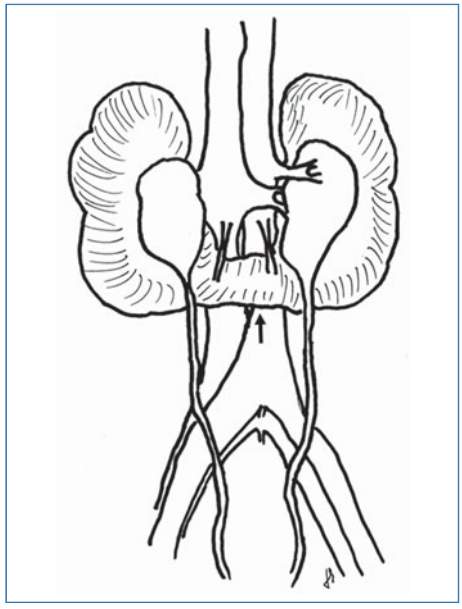

Diagram 7.1. Horseshoe kidney. The fusion of the lower poles on the median line is evident (*arrow*)

to identify the anomalous inclination of the kidneys and highlight the anterior position of the inferior poles which appear fused (Fig. 7.1). Scintigraphy may be useful to precisely locate the organ in the event of hydronephrosis and to correctly evaluate the functionality of the parenchyma.

The incidence of malignant neoplasms is higher in the horseshoe kidney. Wilms tumors in particular are eight times more common than in the normal kidney.

Renal ectopia is a **displacement anomaly** whereby a kidney is not located in its usual position.

Renal ectopia may be simple or crossed. In the first case the ectopic kidney is ipsilateral to its normal position (Diagram 7.2), while in crossed renal ectopia the kidney is located on the side contralateral to the junction of its ureter with the urinary bladder (Diagram 7.3). Simple renal ectopia is very common (1:5000 in postmortem series) and bilateral in 10% of cases. The usual location is pelvic (60%), with the kidney usually irregular and reduced in size. The vasculature may arise from the distal aorta or from the medial sacral, inferior mesenteric or common iliac arteries.

Crossed renal ectopia is more rare and may occur with or without fusion, and involve both or a single kidney. Usually (more than 55% of cases) there are associated malformations. Renal ectopia is usually asymptomatic, although the most frequent symptoms are pain, fever and hematuria, often due to infection.

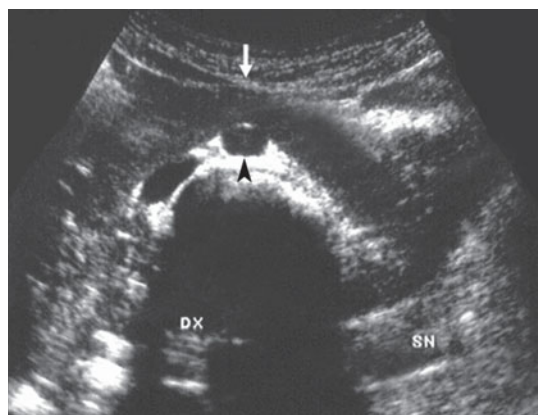

Fig. 7.1. Horseshoe kidney. The axial sonogram shows the anterior fusion of the lower renal poles (*arrow*) in front of the aorta (*arrowhead*), with the structure of the isthmus similar to normal renal parenchyma

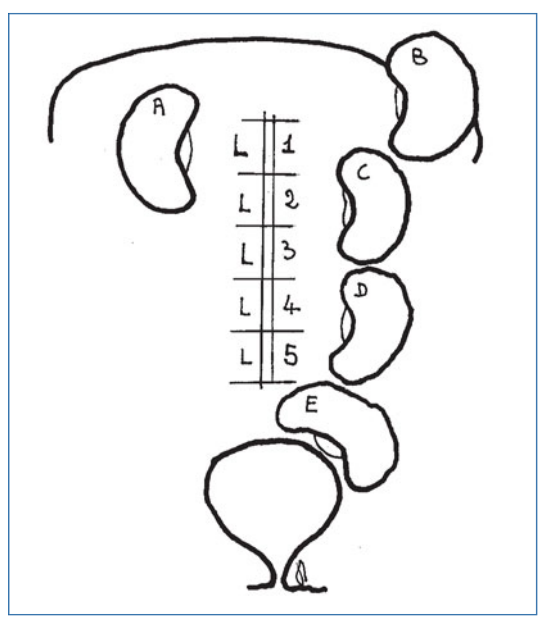

Diagram 7.2. Simple renal ectopia. The diagram shows the position of the normal kidney and the possible sites of the ectopic kidney. *A,* Orthotopic kidney; *B,* Thoracic ectopia; *C,* Abdominal ectopia; *D,* Lumbar ectopia; *E,* Pelvic ectopia

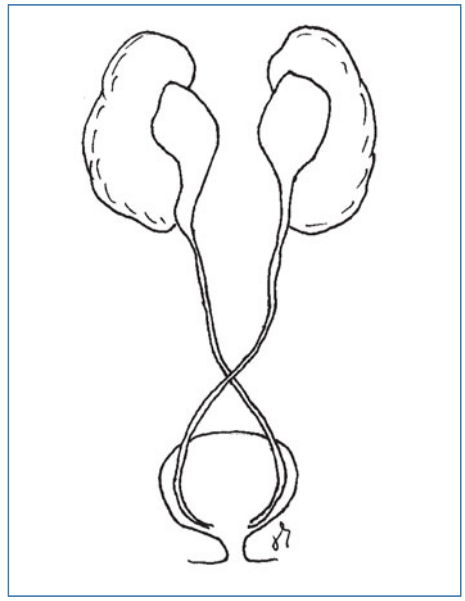

Diagram 7.3. Crossed renal ectopia. The diagram shows the anomalous course of the ureters which cross on the midline. The kidneys are located on the contralateral side of the point of insertion of their ureters in the urinary bladder

In this anomaly US is often useful in identifying the site of the ectopia. However, the technique can be diagnostically limited, in that given the absence of a hyperechoic central hilum the ectopic kidney can mimic an expansive lesion. Conventional urography and now magnetic resonance urography are instead effective in identifying the anomalous position of the organ and the course of the urinary tract. Voiding cystourethrography (VCUG) is a fundamental examination in the diagnosis of these patients due to the elevated incidence of VUR often secondary to the anomalous insertion of the ureter into the urinary bladder (**Figs. 7.2, 7.3**).

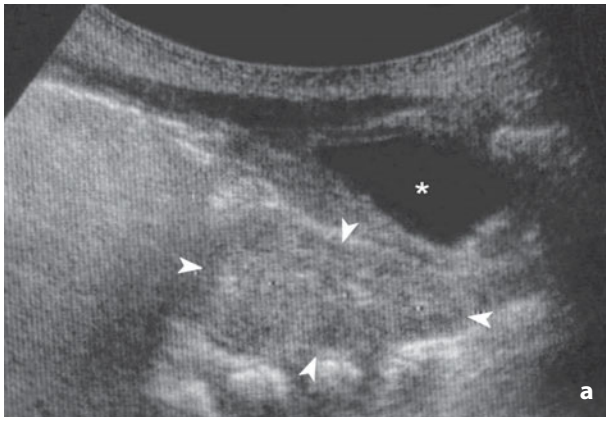

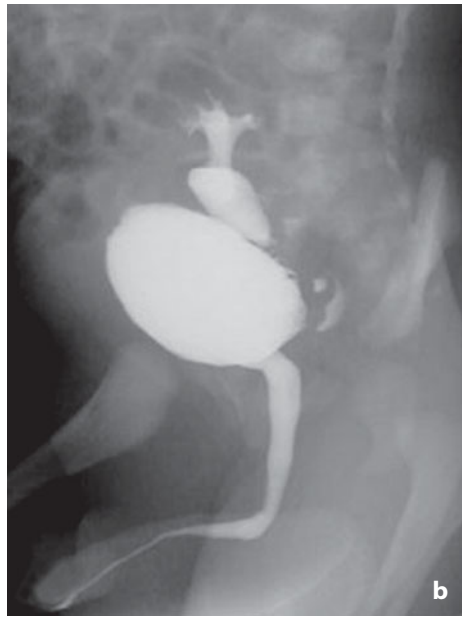

Fig. 7.2a,b. Simple renal ectopia. **a** Longitudinal sonogram shows the kidney located in the pelvis (*arrowheads*) posterior to the urinary bladder (*asterisk*) and anterior to the lumbar vertebrae. **b** Voiding cystourethrography shows vesicoureteric reflux and confirms the left simple renal ectopia located in the pelvis

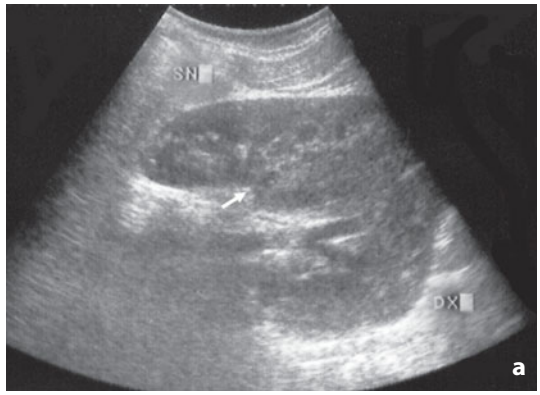

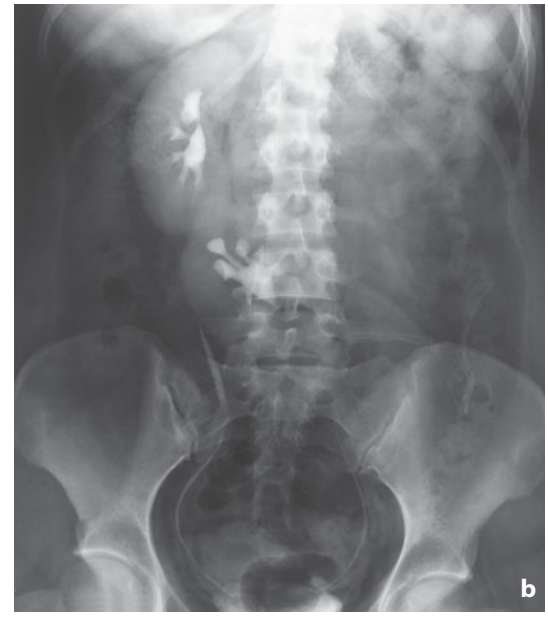

Fig. 7.3a,b. Crossed renal ectopia. **a** Transverse sonogram shows right crossed renal ectopia with the right kidney located in the left hemiabdomen and the upper pole fused to the lower pole of the left kidney (*arrow*). **b** Intravenous urography in the excretory phase confirms right crossed renal ectopia with the ureter inserting in the opposite hemiabdomen

Abeshouse BS, Bhisitkul I (1959) Crossed renal ectopia with and without function. Urol Int 9:63-91

Brum FA, Becker M, Uglione A et al (1997) Polycystic horseshoe kidney. J Urol 158:2229

Campbell MF (1970) Anomalies of the kidney. In: Campbell MF, Harrison GH (eds) Urology. WB Saunders Co., Philadelphia

Cystic Kidney Disease

With reference to the 1987 classification of the American Academy of Pediatrics which is still in use, cystic kidney diseases can be divided into two groups (**Table 7.2**): the inherited forms, which include both the infantile onset and adult onset autosomal dominant polycystic kidney disease, and the noninherited forms, including multicystic dysplastic kidney disease and caliceal diverticula.

Particular attention will be dedicated to multicystic dysplastic kidney, due to its elevated incidence, and caliceal diverticula, due to the difficult differential diagnosis.

Table 7.2. Cystic disease of the kidney: 1987 American Academy of Pediatrics classification

Genetic	Nongenetic
Autosomal recessive (infantile) polycystic kidneys	Multicystic kidney (Multicystic dysplasia)
Autosomal dominant (adult) polycystic kidneys	Multilocular cyst (Multilocular cystic nephroma)
Juvenile nephronophthisis – medullary cystic disease complex	Simple cysts
Juvenile nephronophthisis (autosomal recessive)	Medullary sponge kidney (less than 5% inherited)
Medullary cystic disease (autosomal dominant)	Acquired renal cystic disease in chronic hemodialysis patients
Congenital nephrosis	Caliceal diverticulum (pyogenic cyst)
Cysts associated with multiple malformation syndromes	

Multicystic Dysplastic Kidney Disease

This is the most common cause of an abdominal mass in infants, with an incidence of 1:3000-4000 live births and a bilateral presentation not compatible with life in around 5%. Like renal agenesis the condition is predominant in males and there is a higher occurrence in the left kidney.

The American Academy of Pediatrics has clarified the concept of **dysplasia**, which is always associated with the cysts and is characterized by the presence of primitive ducts and islets of metaplastic cartilage. Three different forms can be identified: (1) the multicystic variant with small cysts and abundant dysplastic stroma (solid cystic dysplasia); (2) the form with large cysts and little stroma (multicystic dysplastic kidney - MCDK); (3) the variant in which the pelvis is still identifiable, known as the hydronephrotic form of MCDK.

The etiology of the condition is not clear: the obstructive hypothesis is the most accredited, although it has not been completely demonstrated. The frequent association with ureteric or pelvic atresia suggests failed meeting between the ureteric bud and the metanephric blastema as a possible cause, although the presence of areas of normal renal parenchyma with collecting ducts in MCDK seems to disagree with this hypothesis. A vascular accident, as with renal agenesis, may play an etiologic role.

Macroscopically the MCDK is usually enlarged and completely substituted by numerous noncommunicating cysts containing citrine liquid, which have a diameter varying from a few millimeters to several centimeters (**Fig. 7.4**). The vascular peduncle is hypoplastic or even absent. The ureter often presents atresia, or terminates with a small ureterocele. Microscopically the cysts are lined with epithelial tissue varying from squamous to columnar embedded in connective tissue with varying degrees of dysplasia and areas of normal nephrogenesis.

In the past the diagnosis of MCDK was suspected in infants presenting an abdominal mass at physical examination. The successive urography would show the absence of uptake of contrast medium in the kidney involved. Today the diagnosis is made with pre- and postnatal US. The identification of rounded anechoic formations of varying size and the absence of a clear renal pelvis and little or no renal parenchyma are diagnostic of MCDK (**Fig. 7.5**). The definitive diagnosis, however, is made with scintigraphy, which confirms the absence of perfusion and lack of function. Given that 10-15% of patients with MCDK have alterations of the contralateral kidney or VUR, the diagnostic protocol generally requires a VCUG be performed.

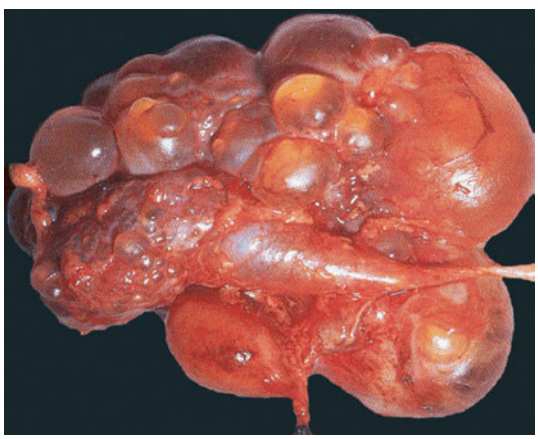

Fig. 7.4. Multicystic kidney. The gross specimen shows structural subversion of the kidney, with normal parenchyma replaced by cysts of variable size

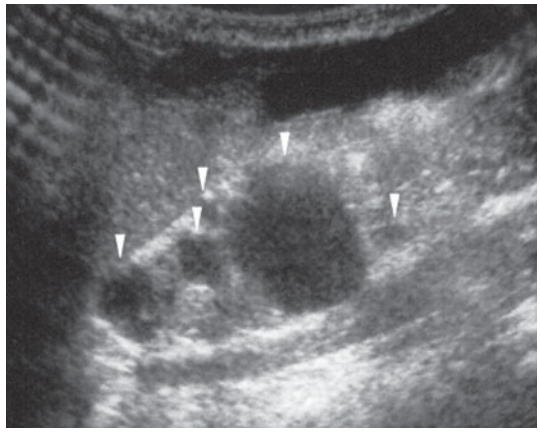

Fig. 7.5. Multicystic kidney. Longitudinal sonogram shows several formations with cystic appearance (*arrowheads*) in the thinned renal parenchyma

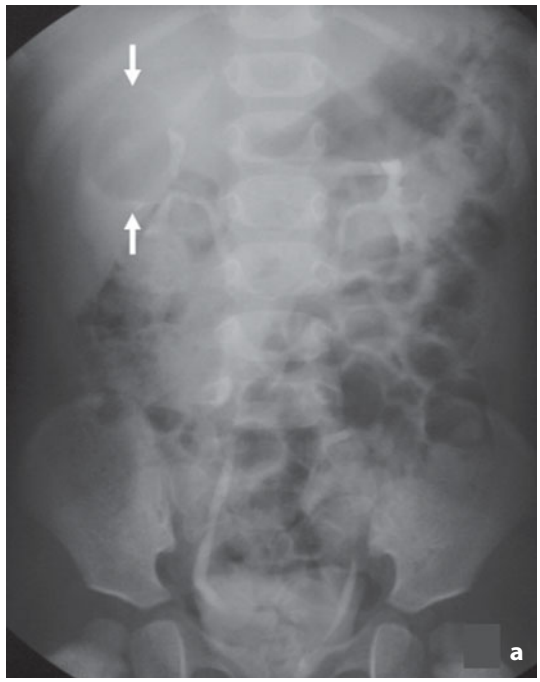

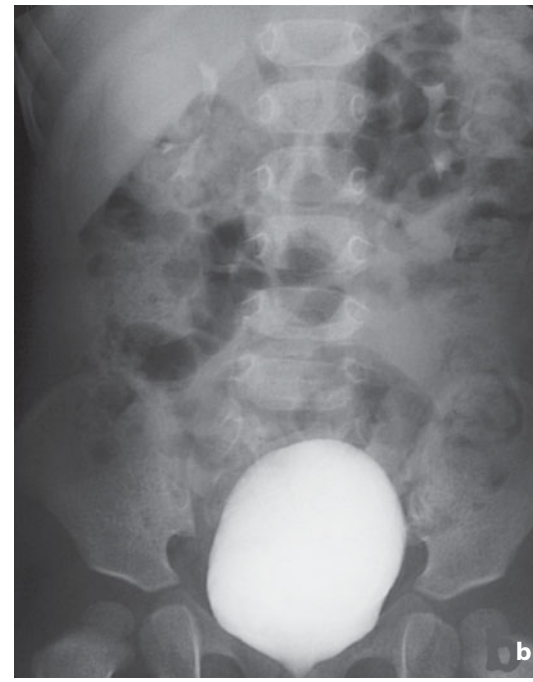

Fig. 7.6a,b. Caliceal diverticula. **a** Urography in the excretory phase shows a rounded structure (*arrows*) connected to the collecting system which in the late phase (**b**) fills with contrast medium

Caliceal Diverticula

These are urine-containing cavities in the renal parenchyma in communication with the renal collecting system through a narrow channel. Usually they are small asymptomatic formations, but in cases of considerable dimensions they can lead to complications with stone formation or urinary tract infection (UTI) or even renal abscess. At US a rounded formation can be appreciated with a cystic-like appearance. Urography or multidetector-row computed tomography (MDCT) are able to visualize the characteristic appearance of the rounded or oval outpouching, with the accumulation of contrast medium, communicating with the collecting system (Fig. 7.6).

Bernstein J (1971) The morphogenesis of renal parenchymal maldevelopment (renal dysplasia). Pediatr Clin North Am 18:395-407

Demertzis J, Menias CO (2007) State of the art: imaging of renal infections. Emerg Radiol 14:13-22

Glassberg KI, Stephens FD, Lebowitz RL et al (1987) Renal dysgenesis and cystic disease of the kidney: a report of the Committee on Terminology, Nomenclature and Classification, Section on Urology, American Academy of Pediatrics. J Urol 138:1085-1092

Matsell DG, Bennet T, Goodyer P et al (1996) The pathogenesis of multicystic kidney disease: insights from the study of fetal kidney. Lav Invest 74:883-893

Malformations of the Upper Urinary Tract

Double or Triple Collecting Systems

These are anatomic variations in themselves asymptomatic which result from the presence of two or three completely separate ureteric buds (complete double or triple collecting systems), which meet the metanephric blastema and divide it into functionally separate districts, or secondary to the more or less early division of the ureteric bud (incomplete double or triple collecting systems). A bifurcation of the ureter proximally produces the variant known as bifid ureter (present in 10% of the population). According to the Weigert–Meyer rule, the ureter which drains the upper pole renal moiety will insert into the urinary bladder more inferiorly and medially, whereas the ureter which drains the lower pole moiety will insert into the urinary bladder more superiorly and laterally.

These variations are often associated with other anomalies. In particular, the lower pole collecting system is often the site of VUR, while the upper pole collecting system is often associated with ectopic ureter or ureterocele (**Diagram 7.4**).

The diagnosis is easily made with US and VCUG. At US the duplex collecting system is characterized by a double central pelvicaliceal system. In general the affected kidney appears longer than the contralateral kidney. In the presence of VUR, which as stated

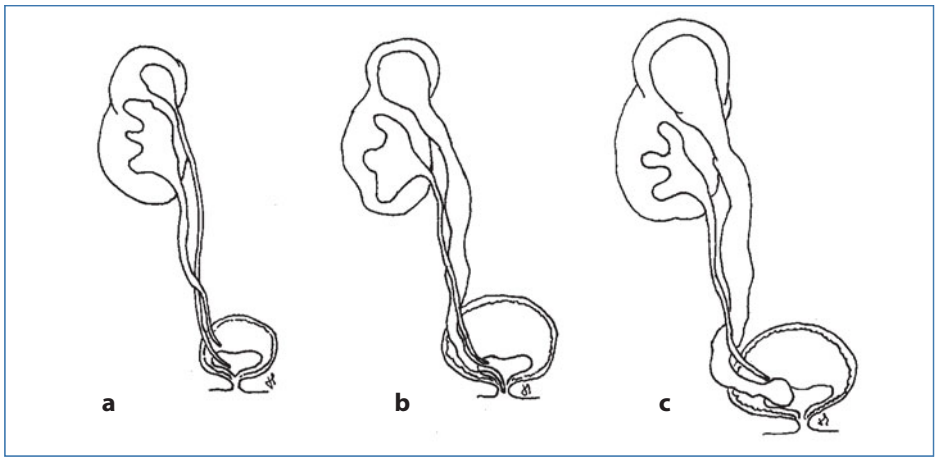

Diagram 7.4. Duplex collecting system. The diagrams show different ureteric variants associated with the anomaly. **a** Double ureter with the lower pole collecting system the site of vesicoureteric reflux. **b** Upper pole collecting system associated with ectopic ureter. **c** Upper pole collecting system associated with ureterocele

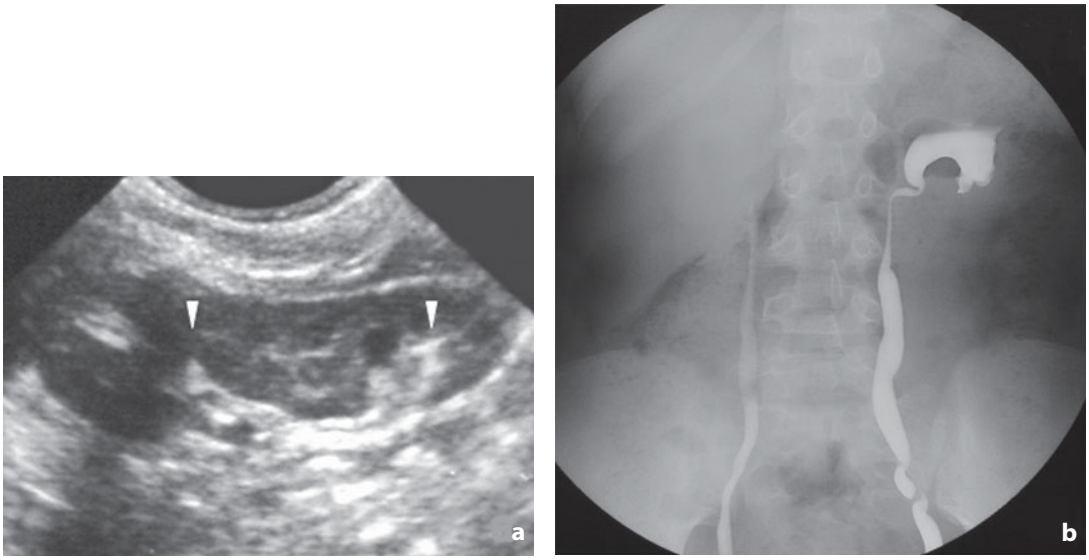

Fig. 7.7a,b. Duplex collecting system. **a** Longitudinal sonogram shows the separation of the central pelvicaliceal system (*arrowheads*) into an upper and lower pole collecting systems. **b** Voiding cystourethrography demonstrates bilateral vesicoureteric reflux with enhancement of the lower pole moiety in the left kidney characterized by an overall reduction in the number of calices

above usually involves the lower pole collecting system, VCUG can confirm the anomalous configuration of the retrograde enhanced urinary tract and accurately evaluate the degree of reflux (Fig. 7.7).

Lee PH, Diamond DA, Duffy PG et al (1991) Duplex reflux: a study of 105 children. J Urol 146:657-659

Anomalies of the Ureteropelvic Junction

Anomalies of the ureteropelvic junction become manifest in conditions of hydronephrosis, i.e. with a more or less marked degree of dilatation of the pelvis and the calices and the possible progressive compression of the renal parenchyma. The anomalies of the urogenital system can be identified as early as the 12th-15th week of gestation, and almost 90% of fetal kidneys can be identified at the 17th-20th week of gestation. Therefore, the search for possible hydronephrosis is one of the fundamental steps of prenatal US. Today the most used classification of hydronephrosis is the one proposed by the Society for Fetal Urology for fetuses beyond the 20th week of gestation (Table 7.3).

Table 7.3. Hydronephrosis: 1993

Grade	Pelvic diameter (anteroposterior)	Calices	Cortex thickness
I	≤10 mm	Normal	Normal
II	10-15 mm	Normal or some dilated	Normal
III	>15 mm	All mildly dilated	Normal
IV	>15 mm	All moderately dilated	Mild reduction
V	>15 mm	All severely dilated	Severe reduction <2 mm

The prenatal study has taken on particular importance given its ability to correlate the degree of hydronephrosis either with its spontaneous resolution or with the probability of the need for surgery. The likelihood that grade I hydronephrosis will resolve spontaneously is 50%, but the probability falls to 3% in grade IV and 0% in grade V (**Fig. 7.8**).

The causes of hydronephrosis can be divided into primary (intrinsic and extrinsic) and secondary. The primary causes, which are very rare, include anomalies of the wall of the ureteropelvic junction and/or the ureters, such as ureteric constriction or hypoplasia, polyps, papillomas, valves, persistent fetal folds and high insertion of the ureter. The most common extrinsic cause is the presence of an anomalous vessel of the lower pole which causes an obstruction, which in most cases is intermittent and is defined as intermittent ureteropelvic junction obstruction. This form accounts for around 20% of cases of hydronephrosis involving ureteropelvic junction alterations. The secondary forms are generally related to high-grade VUR. The consequent tortuous course of the ureter can cause a proximal obstruction.

The most common associated malformations involve the gastrointestinal system (anorectal malformations, esophageal atresia), the central nervous system, cardiovascular system and urinary system (horseshoe kidney, primary megaureter, hypospadia, posterior urethral valve, contralateral renal agenesis and contralateral multicystic dysplastic kidney).

The pre- and postnatal US diagnosis has radically changed the clinical outlook of ureteropelvic junction anomalies. Today children affected by this condition are diagnosed asymptomatic, whereas in the past the hydronephrosis was diagnosed late, often due to the presence of an abdominal mass or the onset of symptoms, such as fever, hematuria with or without renal colic, growth disorders, vomit, dyspepsia and recurrent abdominal pain. US is considered a first level technique in the evaluation of hydronephrosis and the degree of dilatation (**Fig. 7.9**). Color Doppler study can identify the presence of an anomalous vessel, although this finding can be visualized with greater detail with precontrast enhancement T2-weighted and contrast-enhanced gradient recalled echo (GRE) T1-weighted sequences. Premedication with furosemide (1 mg/kg) enables the upper urinary tract to be distended and the concentration of the paramagnetic contrast medium to be diluted. MR is able to fully visualize the malformed urinary tract.

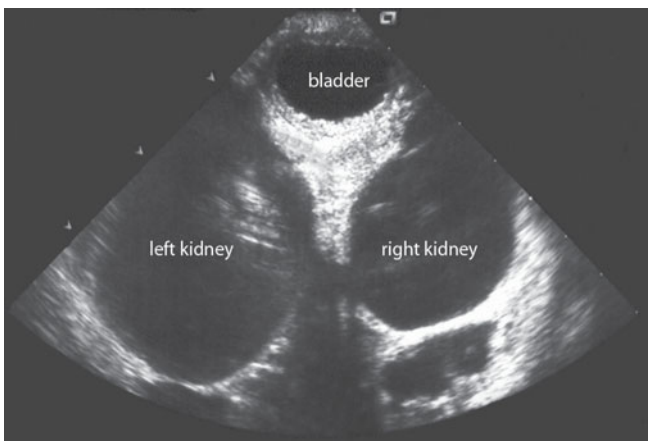

Fig. 7.8. Hydronephrosis. The prenatal sonogram shows marked dilatation of both renal pelves with no evidence of renal parenchyma

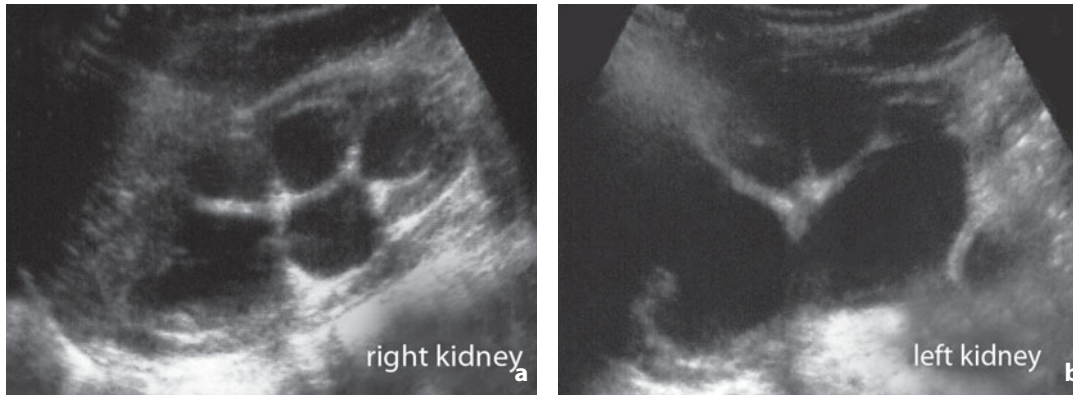

Fig. 7.9a,b. Hydronephrosis. Longitudinal sonogram shows bilateral hydronephrosis with grade IV right (**a**) and grade V left (**b**)

Fernbach SK, Maizels M, Conway JJ (1993) Ultrasound grading of hydronephrosis: introduction to the system used by the Society for Fetal Urology. Pediatr Radiol 23:478-480

Grattan-Smith JD, Jones RA (2006) MR urography in children. Pediatr Radiol 36:1119-1132

Uehling DT, Gilbert E, Chesney R (1983) Urologic implications of VATER association. J Urol 129:352-354

Ectopic Ureter

Ectopic ureter (EU) arises from an anomalous position of the ureteric bud on the mesonephric duct. This anomaly can be divided into two forms: intravesical and extravesical.

In the intravesical form the ureteric outlet is usually more lateral and superior than under normal conditions, beyond the classical trigonal area. VUR is often associated, although the condition may be asymptomatic. EU, however, more commonly refers to the extravesical form, with the outlet of the ureter in the urethra or the genital tract (Diagram 7.5). In particular, the outlet of the ureter may be found in different locations

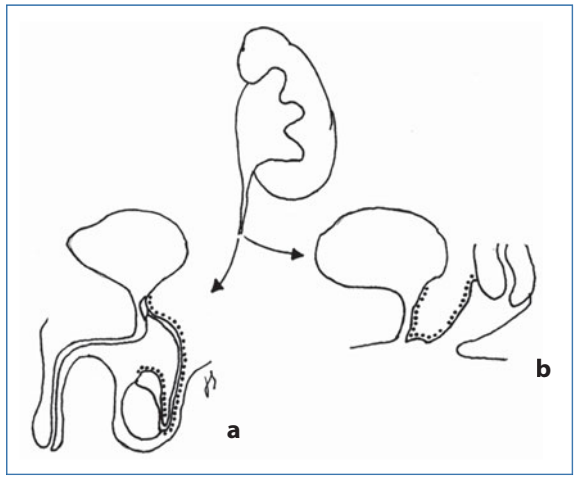

Diagram 7.5. Ectopic ureter. The black dots indicate the possible sites of the ectopic ureteric outlet in males (**a**) and females (**b**)

Table 7.4. Ectopic ureter

Males	Females
Posterior urethra (always above the sphincter)	Urethra (above or below the sphincter)
Ductus deferens	Gartner's duct
Seminal vesicles	Vagina
Epididymis	Uterine cervix - uterus
	Uterine tube

according to sex (Table 7.4). In postmortem series the incidence of ectopia is 1:1900, with a marked prevalence among females (5-6:1). Around 10% of EUs are bilateral. Uni- or bilateral EU associated with a complete duplex collecting system is the most common and least severe form (around 80% of all EU). In contrast, bilateral EU in a single collecting system is the least common but most severe form due to the frequent association with urinary incontinence, urinary bladder hypoplasia and parenchymal compromise. EU both in the single and duplex system is always associated with renal dysplasia with a variable degree of severity but directly proportional to the distance between the ectopic outlet and its normal location. When the EU opens into the genital tract the corresponding collecting system is almost always dysfunctional.

In the most common form, i.e. EU with duplex system in females, incontinence may occur, since the opening of the ectopic ureter is generally located distal to the urethral os.

US may be unable to visualize a duplex system in that the superior system may be too small to identify.

A unilateral duplex system in a female infant with urinary incontinence should always suggest an occult contralateral duplex system with an ectopic ureter draining the upper pole moiety. In cases where VCUG is not diagnostic, in that it fails to demonstrate VUR, CT is able to identify a thin and dysplastic upper pole.

In males EU may open into the rectum, the posterior urethra, the ejaculatory ducts, the seminal vesicles or the ductus deferens. Urinary incontinence will not be present in the latter cases since none of these structures are located below the urethral os. VCUG is able to visualize the termination of the EU or identify a reduced number of calices situated inferior to their normal position.

Campbell MF (1970) Anomalies of the ureter. In: Campbell MF, Harrison GH (eds) Urology. WB Saunders Co., Philadelphia, pp 1487-1670

Braverman RM, Lebovitz RL (1991) Occult ectopic ureter in girls with urinary incontinence: diagnosis by using CT. AJR Am J Roentgenol 156:365-366

Ureterocele

Ureterocele is the cystic dilatation of the terminal, intravesical and submucous tract of the ureter. This malformation is seven times more common in females than in males. The incidence varies in different pediatric postmortem series from 1:500 to 1:4000. The condition is frequently unilateral, with only 10% of cases bilateral. While the etiology is still uncertain, the two most favored hypotheses are the anomalous reabsorption of the tract of the mesonephric duct between the bladder and the ureteric bud or the persistence of the Chwalla membrane which temporarily obstructs the ureterovesical junction and appears between the distal ureter and the urogenital sinus at the 37th day after conception.

Ureterocele wholly contained in the urinary bladder is defined as intravesical, whereas if a portion extends beyond the neck of the bladder the condition is defined as ectopic ureterocele. The ureterocele can be the tributary of a single collecting system, or drain the upper pole of a complete duplex system (the most common form, accounting for 80% of all ureteroceles). In the latter case there is always a degree of dysplasia of the upper renal pole, which may vary to the point of complete dysfunction.

Signs and symptoms of the condition are various. In females the physical examination may reveal a thin-walled cystic formation protruding from the urethral meatus. In this case, as in all cases when the ureterocele exceeds the neck of the urinary bladder, the most significant symptoms are linked to the obstruction of the bladder neck and urethra which influences the emptying of the bladder and causes all the signs of "bladder straining". More commonly ureterocele is identified during a diagnostic US examination for hydroureteronephrosis already identified prenatally. In older children the most common manifestation is UTI.

The diagnosis of intravesical ureterocele is usually made with US or VCUG which in the early filling phase demonstrate a rounded filling defect bounded by a hyperechoic wall in the former and radiotransparent wall in the latter (**Figs. 7.10, 7.11**). At VCUG the contrast medium can be identified filling the urinary tract and the ureterocele, producing the typical rounded or oval appearance known as "cobra head sign" (**Fig. 7.12**).

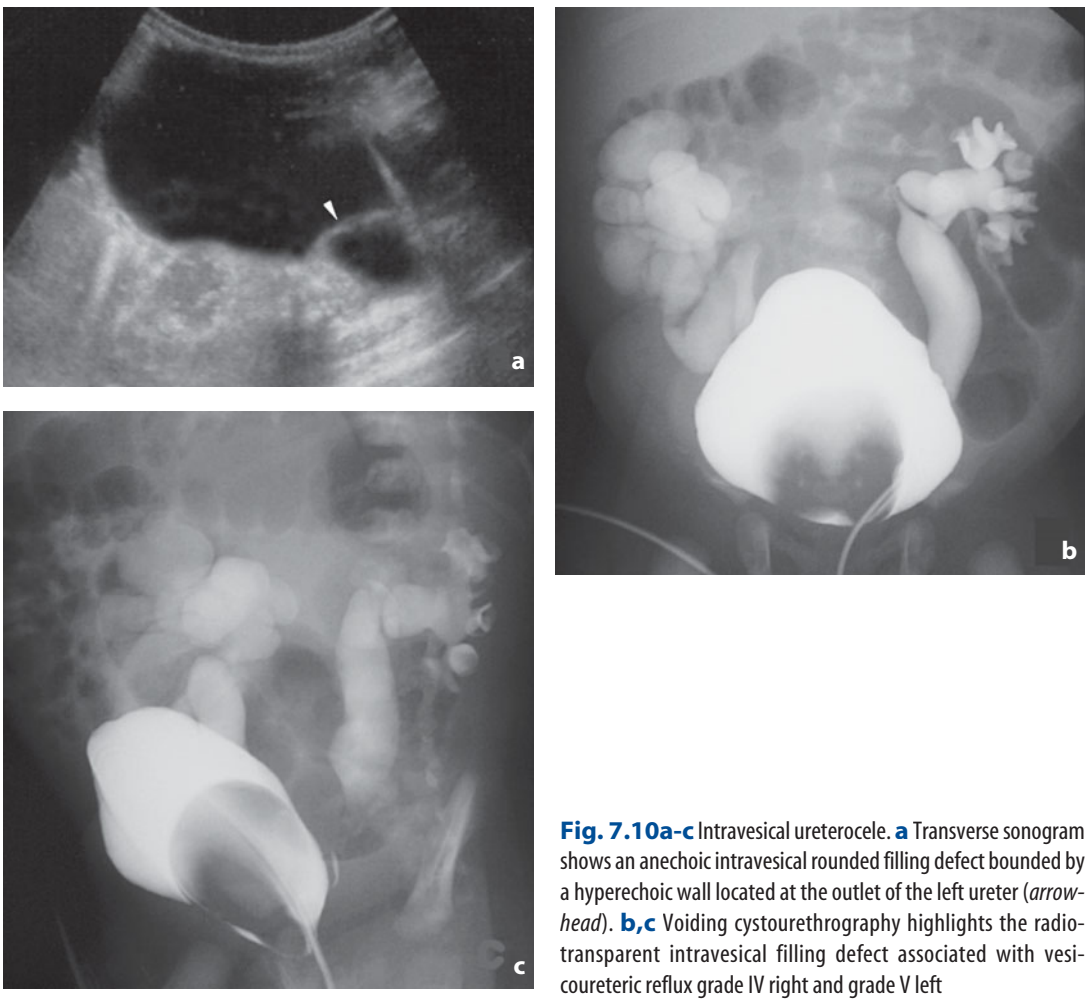

Fig. 7.10a-c Intravesical ureterocele. **a** Transverse sonogram shows an anechoic intravesical rounded filling defect bounded by a hyperechoic wall located at the outlet of the left ureter (*arrowhead*). **b,c** Voiding cystourethrography highlights the radiotransparent intravesical filling defect associated with vesicoureteric reflux grade IV right and grade V left

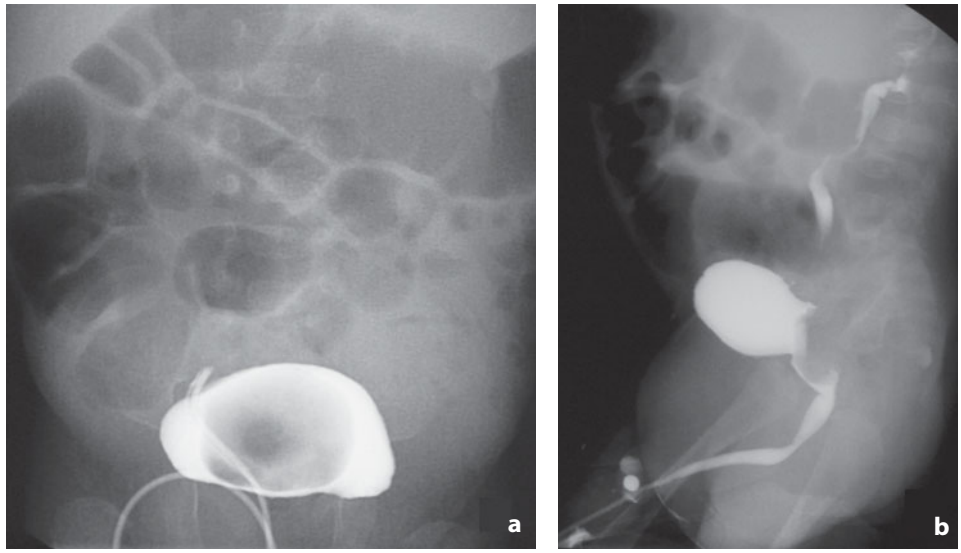

Fig. 7.11a,b. Ectopic ureterocele. Voiding cystourethrography shows a radiotransparent intravesical filling defect which, during voiding, is located beyond the bladder neck. Grade II vesicoureteric reflux can be visualized

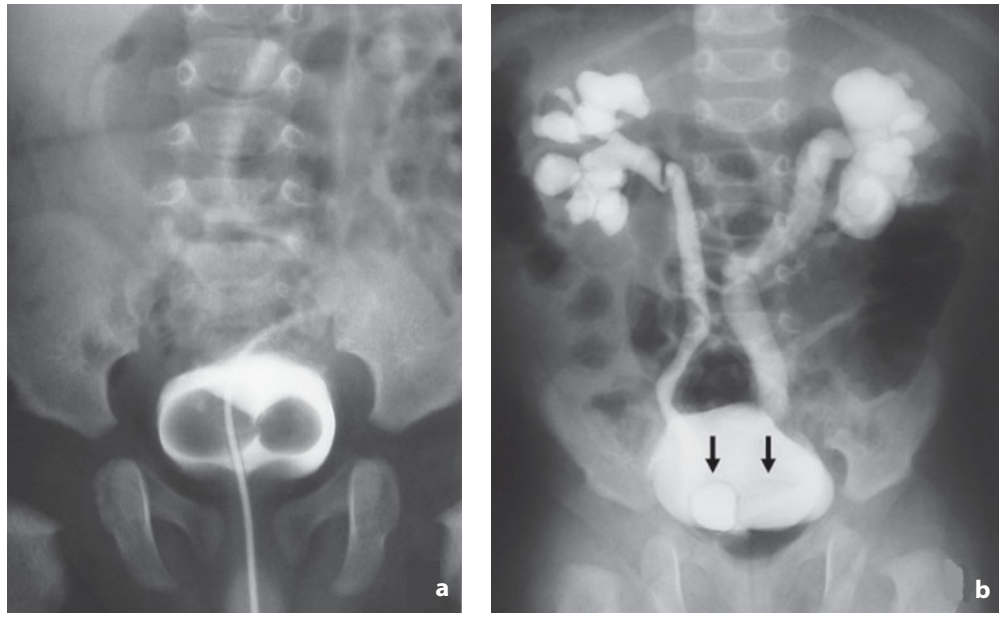

Fig. 7.12a,b. Double ureterocele. **a** Cystography. In the initial filling phase two radiotransparent filling defects are apparent. **b** Urography. In the voiding phase the contrast medium fills the upper urinary tract and the ureteroceles, producing a rounded image on the right and oval on the left (*arrows*) known as cobra head sign

Chwalla R (1927) The process of formation of cystic dilatation of the vesical end of the ureter and diverticula at the ureteral ostium. Urol Cutan Ren 31:499

Stephens FD (1983) Congenital malformation of the urinary tract. Praeger, New York

Anomalies of the Ureterovesical Junction

Anomalies of the ureterovesical junction include conditions which involve the distal tract of the ureter, therefore VUR and megaureter.

Vesicoureteric Reflux

This condition is defined by an anomalous return of urine from the urinary bladder to the ureter and therefore the kidney. VUR is the most common pediatric uropathy. The incidence in children presenting with UTI is around 20-30%. Despite the possibility of spontaneous resolution, the anomaly is potentially serious, in that it is often associated with nephropathy which can be congenital-dysplastic, or secondary to ascending UTIs.

VUR can be divided into five grades (**Table 7.5**) and classified as primary or secondary.

In primary VUR the point of insertion of the ureter into the urinary bladder is vital, since this determines the length and inclination with respect to the bladder wall of the submucosal and intramural segment. These in fact are the anatomic factors, together with the Waldeyer's fascia and the trigone, which enable the ureterovesical junction to behave like a valve and not allow the reflux of urine towards the kidney.

The secondary forms are related to an obstruction during voiding. This can be organic, e.g. in the case of a posterior urethral valve, or functional as in the presence of neurogenic bladder.

The diagnostic suspicion of VUR is generally aroused in the presence of UTI, or following the prenatal US finding of dilatation of the upper urinary tract. In this condition ultrasonography is a technique with limited sensitivity in that it is often negative even in the presence of severe reflux. Occasionally, following recurrent UTIs, parenchymal scarring may be observed, and in the most severe cases the kidney may be reduced in size, with little differentiation between cortex and medulla, indicating dysplasia.

The technique of voiding urosonography (contrast-enhanced US) is becoming increasingly diffuse. This imaging modality is considered substantially reliable in the follow-up of patients with known VUR and in girls, who do not require an accurate study of the urethra. VCUG with pulsed fluoroscopy is still the reference standard in the diagnosis of reflux disease. In addition, the technique is irreplaceable in the functional study of the urinary bladder and the evaluation of the male urethra. Most protocols involve a US and a VCUG being done in patients less than 12 months of age or older patients with recurrent UTIs. In the presence of VUR a renal scintigraphy may be indicated, which is able to evaluate the degree of functional damage.

Table 7.5. Vesicoureteric reflux: classification

Grade I	Thin ureter, with reflux of contrast medium for short tract without enhancement of the pelvis (incomplete reflux)
Grade II	Reflux reaches the pelvis and the calices (complete reflux) without dilatation
Grade III	Complete reflux with mild dilatation of the ureter and the renal cavity
Grade IV	Complete reflux with moderate dilatation of the ureter and the renal cavity
Grade V	Complete reflux with gross dilatation of the ureter and the renal cavities associated with tortuosity of the ureter

Megaureter

The term megaureter often indicates a variety of conditions which have a common presentation of hydroureteronephrosis, i.e. a dilatation of variable degree of the ureter and the intrarenal collecting system. Megaureter can be classified as obstructive (the most common form), refluxing, nonobstructive, nonrefluxing, and obstructive and refluxing.

The classic obstructive form is also defined as primary megaureter. With regard to etiology, the most convincing theory is based on the failed reabsorption of the above-mentioned Chwalla membrane. The clinical presentation is typical of obstructive uropathies, with UTI, abdominal and/or lumbar pain and hematuria. In the more severe forms there may be a palpable mass. At US hydroureteronephrosis is appreciable, and the real-time evaluation is able to visualize active peristalsis to a point close to the distal tract of the ureter, which has an almost normal diameter. VCUG is able to differentiate obstructive and refluxing megaureter, conditions which require a different therapeutic approach. Techniques such as scintigraphy, intravenous urography and magnetic resonance are able to evaluate the degree of dilatation and obstruction as well as residual renal function, expressed in a different manner for each technique as uptake or enhancement of the parenchyma (**Fig. 7.13**).

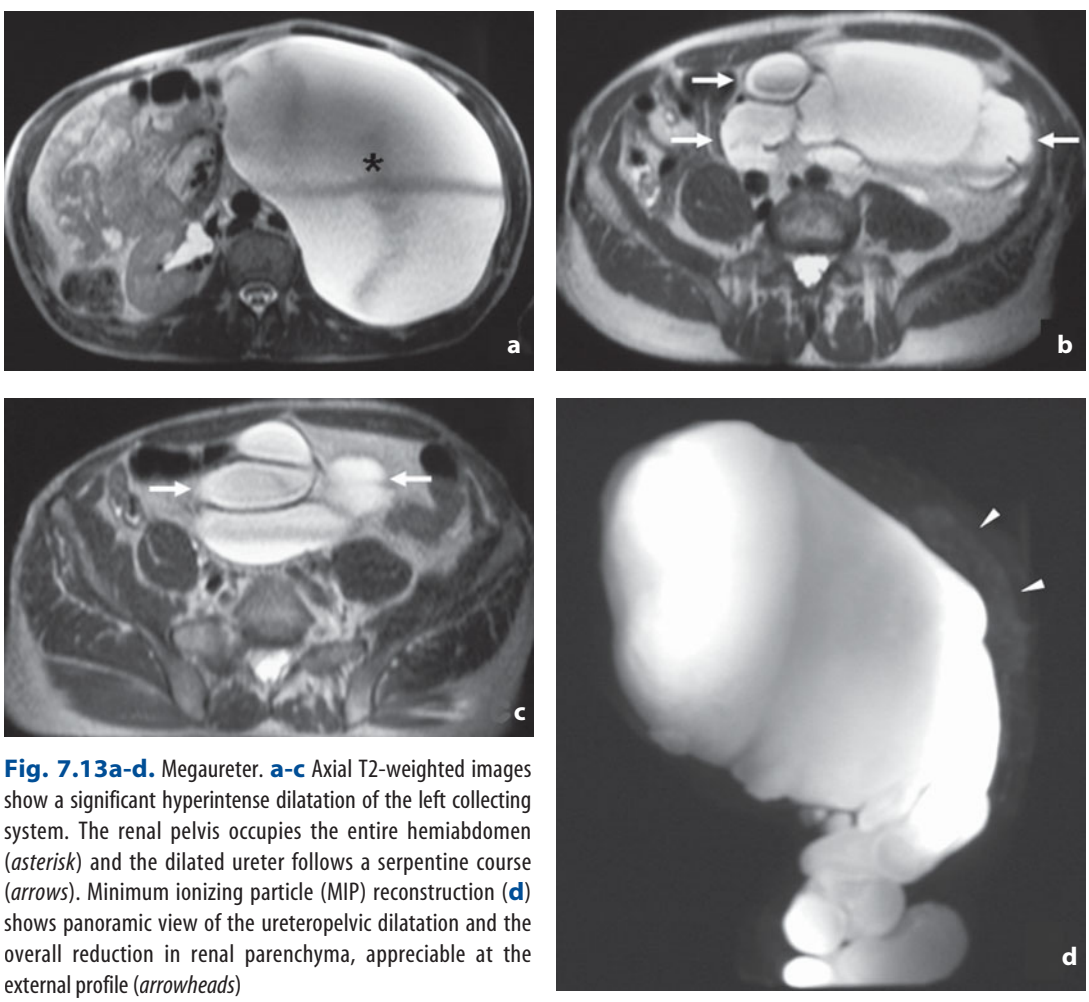

Fig. 7.13a-d. Megaureter. **a-c** Axial T2-weighted images show a significant hyperintense dilatation of the left collecting system. The renal pelvis occupies the entire hemiabdomen (*asterisk*) and the dilated ureter follows a serpentine course (*arrows*). Minimum ionizing particle (MIP) reconstruction (**d**) shows panoramic view of the ureteropelvic dilatation and the overall reduction in renal parenchyma, appreciable at the external profile (*arrowheads*)

Alcaraz A, Vinaixa F, Tejedo-Mateu A et al (1991) Obstruction and recanalization of the ureter during embryonic development. J Urol 145:410-416

King LR (1980) Megaloureter: Definition, diagnosis and management. J Urol 123:222-223

King LR, Stephens FD (1976) Vesicoureteral reflux: history, etiology, and conservative management. In: Kelalis PP, King LR (eds) Clinical pediatric urology. WB Saunders Co., Philadelphia, p 342

Riccabona M, Fotter R (2006) Radiographic studies in children with disorders: what to do and when. In: Hogg R (ed) Kidney disorders in children and adolescents. Taylor and Francis, Birmingham, pp 15-34

Malformations of the Lower Urinary Tract

These malformations are more frequent in males and relatively rare in females.

Urachal Anomalies

The urachus or medial umbilical ligament is a cord-like structure which joins the dome of the bladder to the inferior border of the umbilicus. It is a vestigial structure which in the fetus provides a communication between the primitive bladder and the allantois. At the end of gestation the urachus is usually obliterated. In the absence of complete obliteration the urachus persists in one of four forms: patent urachus, urachal cyst, urachal sinus or urachal diverticulum (**Diagram 7.6**).

In patent urachus a communication remains between the umbilicus and the bladder. This condition is usually evident at birth with a presentation defined as "secreting umbilicus", with urine leaking from the umbilicus during voiding.

Urachal cyst is formed by the incomplete obliteration of the urachus, which leaves one or more patent segments filled with secretions and desquamated epithelium. The cyst usually becomes evident by preadolescence, when it reaches moderate dimensions, or in the presence of infection.

Urachal sinus derives from the distal obliteration of the urachus and its patency at the umbilicus, which results in delayed umbilical scarring and/or leakage of secretions.

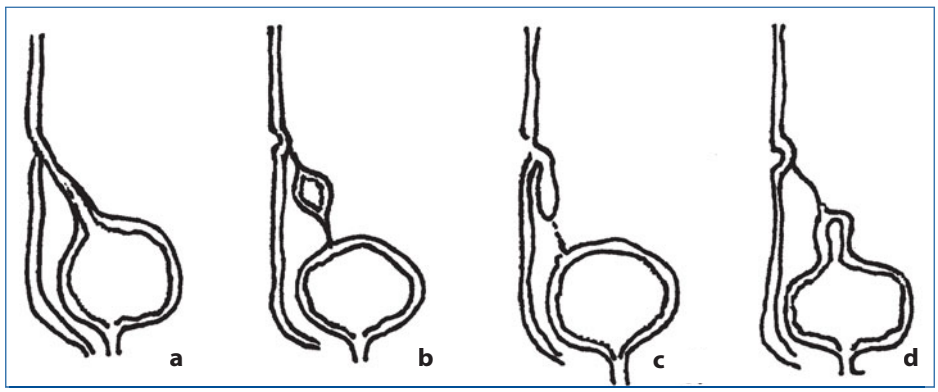

Diagram 7.6. Urachal anomalies. **a** Patent urachus. **b** Urachal cyst. **c** Urachal sinus. **d** Urachal diverticulum

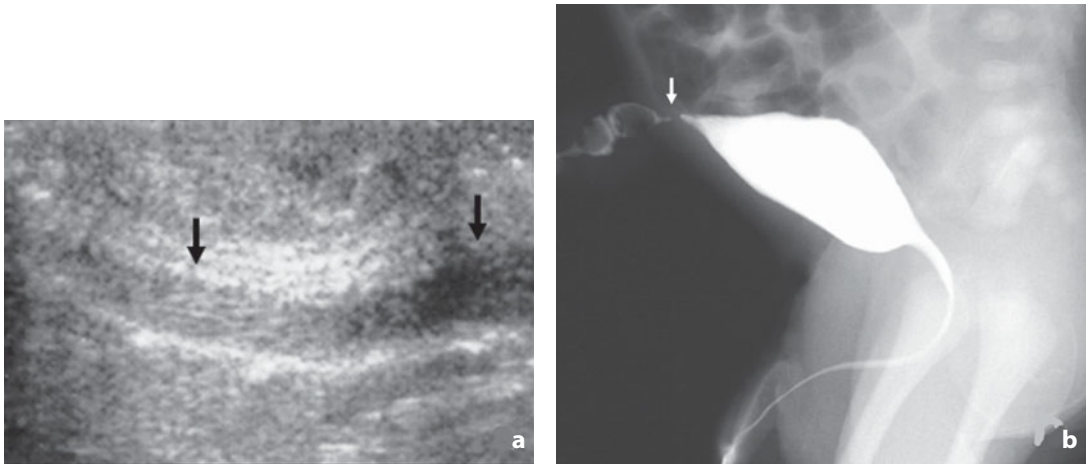

Fig. 7.14a,b. Patent urachus. **a** Longitudinal supravesical sonogram shows an iso-hypoechoic tubular structure (*arrows*) at the site of the medial umbilical ligament. **b** Voiding cystourethrography shows the communication between the bladder and the umbilicus with leakage of contrast medium from the latter (*arrow*)

The obliteration of the urachus only at the umbilicus leads to the creation of urachal diverticulum, which in rare cases can become complicated with the formation of stones or cause UTIs.

These anomalies of the urachus can be readily visualized with US. The technique is able to demonstrate a hypo- or anechoic tubular or cystic structure in connection with the bladder which usually has an elongated appearance. In conditions of complete patency the definitive diagnosis is made with VCUG, with the patient in the laterolateral position during voiding (Fig. 7.14). This technique is able to visualize the connection between the bladder and the umbilicus and the leakage of contrast medium from the latter during voiding.

Chrispin AR, Gordon I, Hall C et al (1980) Diagnostic imaging of the kidney and urinary tract in children. Springer-Verlag, Berlin

Anomalies of the Urinary Bladder

Bladder diverticula are defined as an outpouching of the bladder-wall mucosa through the fibers of the detrusor muscle. They can be congenital or acquired. The former are often single, occasionally bilateral, and usually located in the posterolateral wall of the bladder with no relations with the ureteric outlet (Fig. 7.15). In contrast, paraureteral diverticula (the genesis of which is thought to be caused by a certain laxity of the Waldeyer sheath) are located in close relation with the ureteric outlet. They are therefore constantly associated with VUR (Fig. 7.16). VUR in these cases is usually secondary to the large dimensions of the diverticulum which compresses and incorporates the outlet internally. There are various syndromes associated with vesical diverticula secondary to a congenital laxity of the wall. These include prune belly (lax abdominal wall, dilated urinary tract, bilateral cryptorchidism), Menkes syndrome (copper metabolism disorder, fine wiry hair, severe mental retardation and developmental delay) and Ehlers–Danlos syndrome (cardiovascular anomalies, mental retardation and developmental delay, characteristic facial features).

Acquired diverticula are associated with all the conditions which produce an anomalous increase in intraluminal pressure, such as bladder outlet obstruction, but also in functional alterations, such as hyperactive bladder.

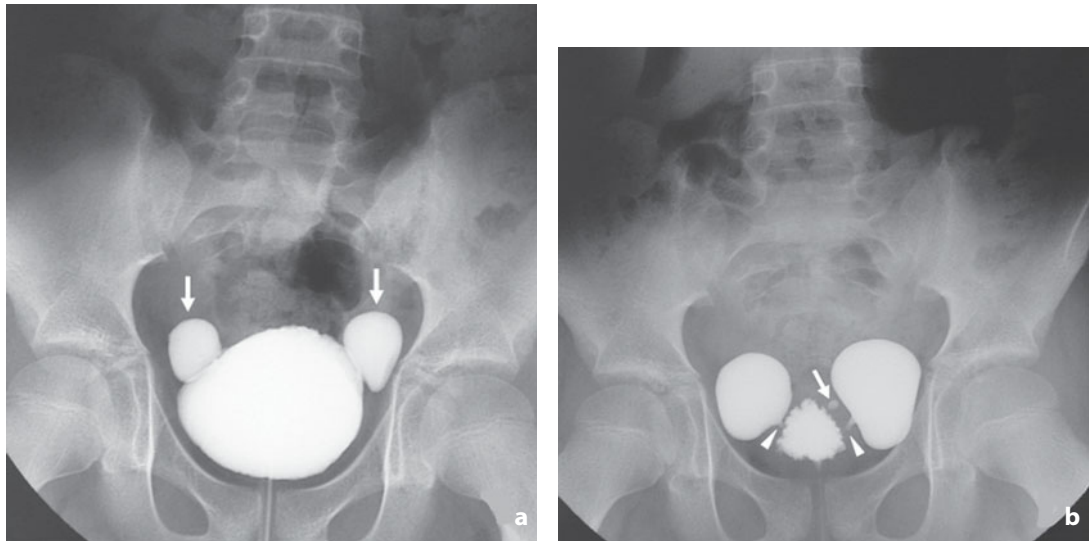

Fig. 7.15a,b. Bladder diverticula. **a** Cystography in the filling phase shows the presence of two large diverticula developing from the posterolateral bladder wall (*arrows*). **b** At the end of spontaneous voiding both diverticula are connected to the bladder with a thin neck (*arrowheads*). In this phase another small outpouching is visible on the left (*arrow*)

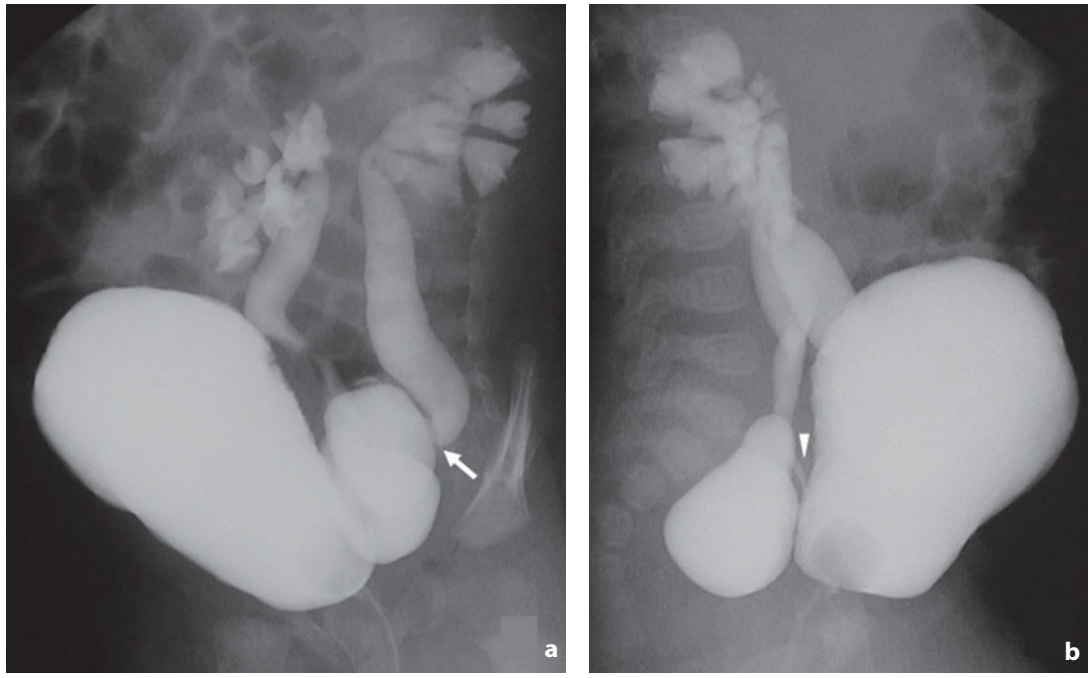

Fig. 7.16a,b. Paraureteral diverticula. Cystography during the filling phase shows two large diverticula associated with vesicoureteric reflux. **a** Left anterior oblique view shows a communication between the ureter and diverticulum (*arrow*). **b** In the right lateral view the ureter courses in front of the diverticulum (*arrowhead*)

Each diverticulum can cause UTIs (due to pooling of urine) or complications with the formation of stones or even become obstructive at the level of the ureterovesical junction or at the neck of the bladder.

US visualizes a hypoechoic formation with a smooth continuous hyperechoic wall. VCUG is able to more precisely evaluate the site, shape, neck and number of even

small diverticula. The technique is particularly indicated for the evaluation of paraureteral diverticula capable of obstructing the urinary tract.

Mollard P (1984) Les diverticules vescicaux. In: Mollard P (1984) Précis d'urologie de l'enfant. Masson, Paris, p 187

Anomalies of the Urethra

Double Urethra

This is a rare anomaly with many variants. For the sake of simplicity the Effmann, Lebowitz and Colodny classification is generally used, which divides these malformations into three variants, the second of which is the most common (**Table 7.6**).

Double urethra can be completely asymptomatic, but in cases of complete double urethra there may also be a double flow and loss of urine (pseudoincontinence). In this variant the accessory urethra can have an epispadiac or hypospadiac meatus. Renal US should be done in patients with suspected urethral malformation, in that there are often associated malformations of the upper urinary tract, such as renal agenesis or hydronephrosis. Retrograde urethrography and, above all, VCUG are able to provide detailed confirmation of the clinical suspicion, in particular by identifying the course of the accessory urethra and the presence of a communication with the main urethra (**Fig. 7.17**).

Table 7.6. Urethral duplication: Effman, Lebowitz and Colodny classification

TYPE I	Blind incomplete urethral duplication (accessory urethra)	
	I A	Distal: opens on the dorsal or ventral surface of the penis but does not communicate with the urethra or bladder
	I B	Proximal: opens from urethral channel and ends blindly in the periurethral tissue
TYPE II	Complete patent urethral duplication	
	II A	Both urethras open onto the glans or one on the glans and one on the penis
	II A 1	Noncommunicating urethras, both arising from the bladder
	II A 2	Second urethra arises from the main urethra
	II B	Single meatus (double urethra arises and terminates in the main urethra)
TYPE III	In cases of duplication of the bladder and the penis	

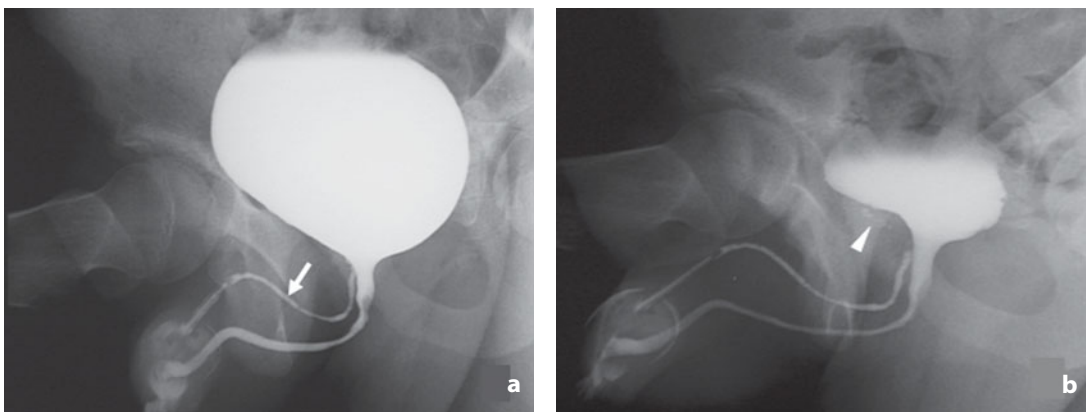

Fig. 7.17a,b. Double urethra. **a** Voiding cystourethrography shows the presence of two urethras, with the main urethra located ventrally. The accessory urethra (*arrow*) is smaller in diameter than the main urethra, arises from the bladder neck and has a separate distal meatus (Type II A1). **b** Noteworthy is the modest ejaculatory duct reflux (*arrowhead*) in the terminal phase of voiding

Cowper's Syringocele

Cowper's syringocele is defined as a possibly cystic dilatation of the excretory ducts of the bulbourethral (Cowper's) glands located at the level of the corpus spongiosum of the urethra and the urogenital diaphragm. These glands secrete a lubricating fluid which facilitates ejaculation and protects the function of the spermatozoa. The ducts can present an anomaly of the junction with the urethra causing a proximal dilatation or reflux.

Maizels proposed the classification of Cowper's syringocele (**Table 7.7**) in relation to its morphology and communication with the urethra. The condition is often asymptomatic, although it can cause voiding disturbance, UTIs and hematuria. If large it can obstruct the urethra. Cowper's syringocele can be readily diagnosed with VCUG, which evaluates its site, morphology and possible communication with the urethra (**Fig. 7.18**).

Table 7.7. Cowper's syringocele: Maizels classification

Type A	Simple syringocele (patent duct, refluent, minimally dilated)
Type B	Imperforate syringocele (duct not communicating with urethra, dilated with cyst-like appearance, intrudes into bulbar urethra)
Type C	Perforated syringocele (patent duct, highly dilated, similar to a diverticulum)
Type D	Ruptured syringocele (like type B, but communicating due to ruptured membrane)

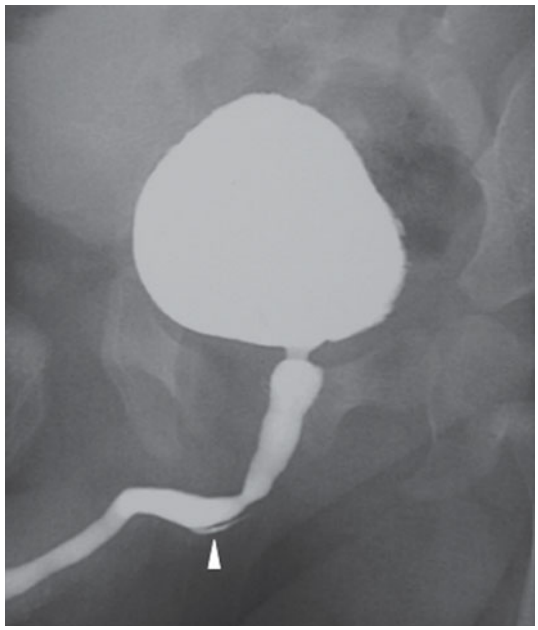

Fig. 7.18. Cowper's syringocele. Voiding cystourethrography shows reflux of contrast material at the bulbous urethra (*arrowhead*)

Posterior Urethral Valves

Posterior urethral valves (PUV) are the most common urethral obstruction, with an incidence of 1 in 5000-8000 live male births against an incidence of 1 in 40,000 reported cases of anterior urethral valves.

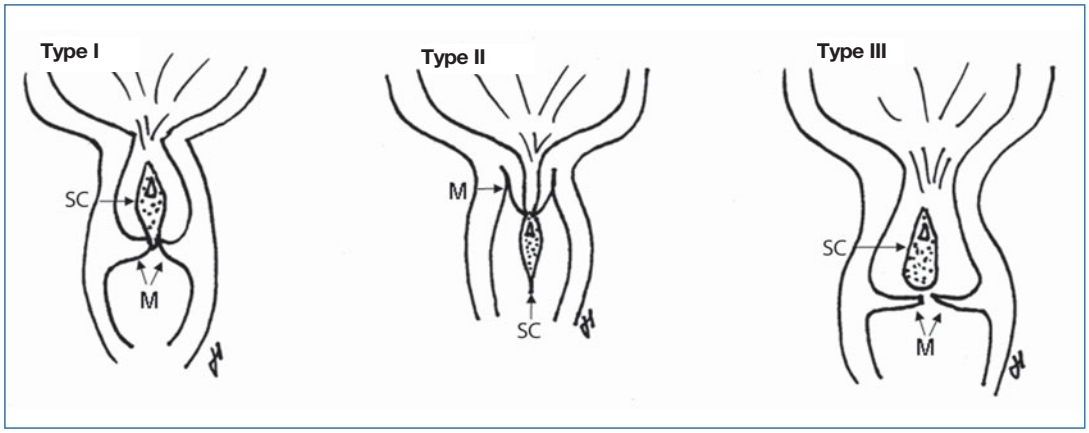

Diagram 7.7. Posterior urethral valves. *M*, membrane; *SC*, seminal colliculus

Originally described by Young in 1919 and classified in three types (**Diagram 7.7**), PUV include a variety of symptoms ranging from the classical severe obstructive presentation in neonates to moderate obstructions which are diagnosed at different life stages.

Type I is the most common, accounting for 95% of PUV, and originates from the anomalous insertion of the mesonephric ducts within the cloaca. It is a sail-like obstructive membrane which courses obliquely from the inferior border of the seminal colliculus and fuses anterolaterally to the most distal portion of the urethral wall (**Fig. 7.19**). They can be very thin, composed of mucosa alone, or thick due to the presence of a stromal component. The orifice is located posteriorly, near to the seminal colliculus, and the degree of obstruction is more or less severe in relation to the size of the valve.

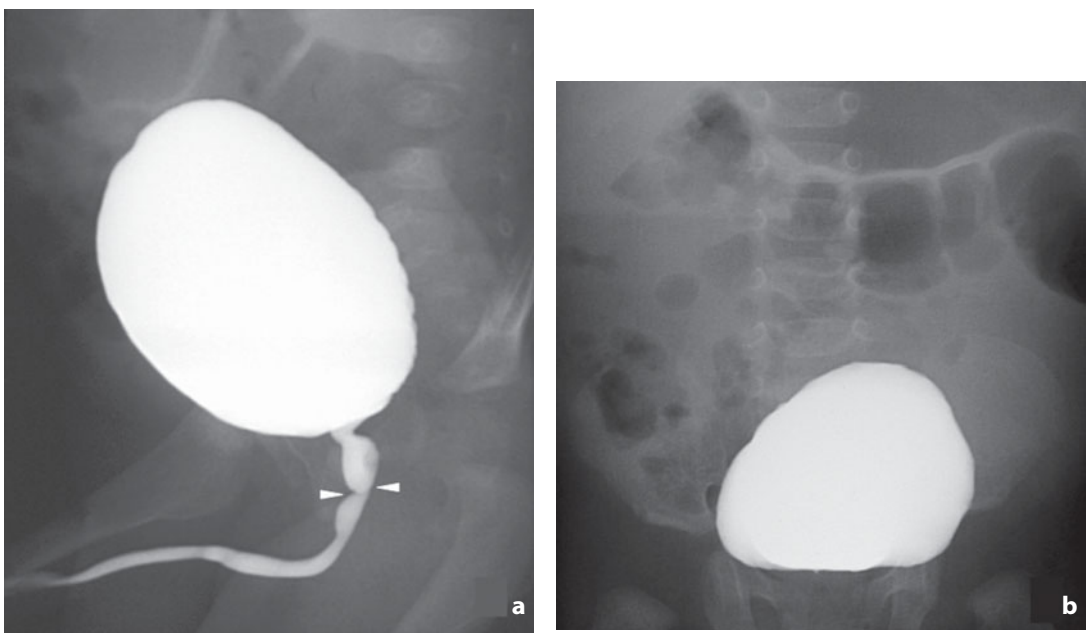

Fig. 7.19a,b. Posterior urethral valve. Type 1 valve. **a** Voiding cystourethrography shows abrupt change in diameter of the urethra (*arrowheads*). **b** Postvoid residual urine secondary to obstruction is a common finding

Type II consists of a mucous fold which courses superiorly from the seminal colliculus to the neck of the bladder. It originates from hypertrophy of the superficial trigonal muscle bundles which extend to the seminal colliculus. This finding is not considered pathologic since it is nonobstructive and frequently encountered in healthy patients.

Type III accounts for 5% of PUV and is characterized by diaphragms with a usually central ostium located distal to the seminal colliculus with which it has no relations. The appearance of this type of valve may be very different in relation to the elasticity of the membrane and the position of the orifice. In terms of embryogenesis, this type of PUV is thought to originate from incomplete regression of the urogenital membrane.

PUV cause an obstruction which drastically influences the development, function and morphology of the urinary system. The evident presentation of this condition occurs with significant obstructions which are already identifiable prenatally. These can occur at the level of the kidney, with alterations of glomerular and tubal function; at the level of the ureters, with a more or less marked dilatation and severe damage of the muscular structures due to VUR or obstruction of the ureterovesical junction (produced by hypertrophy of the interureteric ridge) or both; at the level of the bladder, with morphofunctional modifications (up to megacystis); or at the level of the proximal urethra, with a dilatation of variable degree and functional alterations. Pulmonary hypoplasia, limb deformities and Potter facies may be associated.

The advent and refinement of prenatal US have improved the prognosis of neonates with VUP, with a relatively early diagnosis in the first days of life. US can identify and quantify the dilatation of the urinary tract and the repercussions for the renal parenchyma, which is generally thinned and hyperechoic.

VCUG can confirm and characterize the type of valve, which usually presents as an annular constriction of the urethra, the degree of obstruction and the morphologic modifications of the proximal urinary tract (**Fig. 7.20**).

The alterations at the level of the urethra and bladder correspond to vesicourethral dysfunction (present in 40% of patients). Holmdahl noted that a bladder dysfunction is present at both pre- and postpubertal age in 75% of boys treated for PUV. The associated recurring UTIs are the postnatal factor which determines the progression towards chronic renal insufficiency.

In the child with "minivalves" the obstruction is moderate, occasionally completely compensated by the contractile activity of the detrusor muscle. Clinical presentation in these cases is often limited only to vesicourethral dysfunction. These children may present lower UTIs, which may be recurrent, nocturnal enuresis, daytime urinary incontinence, urinary urgency and frequency. Directly associated with the presence of the valves are disturbances such as hematuria, especially if terminal, dysuria and dribbling.

Anterior Urethral Diverticula

Anterior urethral diverticula are rare malformations which may be secondary to the presence of an anterior urethral valve or cystic dilatation of the periurethral glands or incomplete double urethra. They are saccular outpouchings with a broad neck, located on the ventral wall of the urethra. On occasion they may be of significant size and may be identified by the appearance of a penile or penile-scrotal swelling during voiding.

An anterior urethral diverticulum can cause significant obstruction due to the pressure exerted on the urethra by the increasing volume of the diverticulum. This is the cause and consequence of the pseudovalve which is created at the distal margin of the diverticulum and which in a vicious circle leads to a further increase in the diverticulum.

As with other urethral malformations, retrograde cystography and VCUG are the only radiologic techniques able to visualize the malformation.

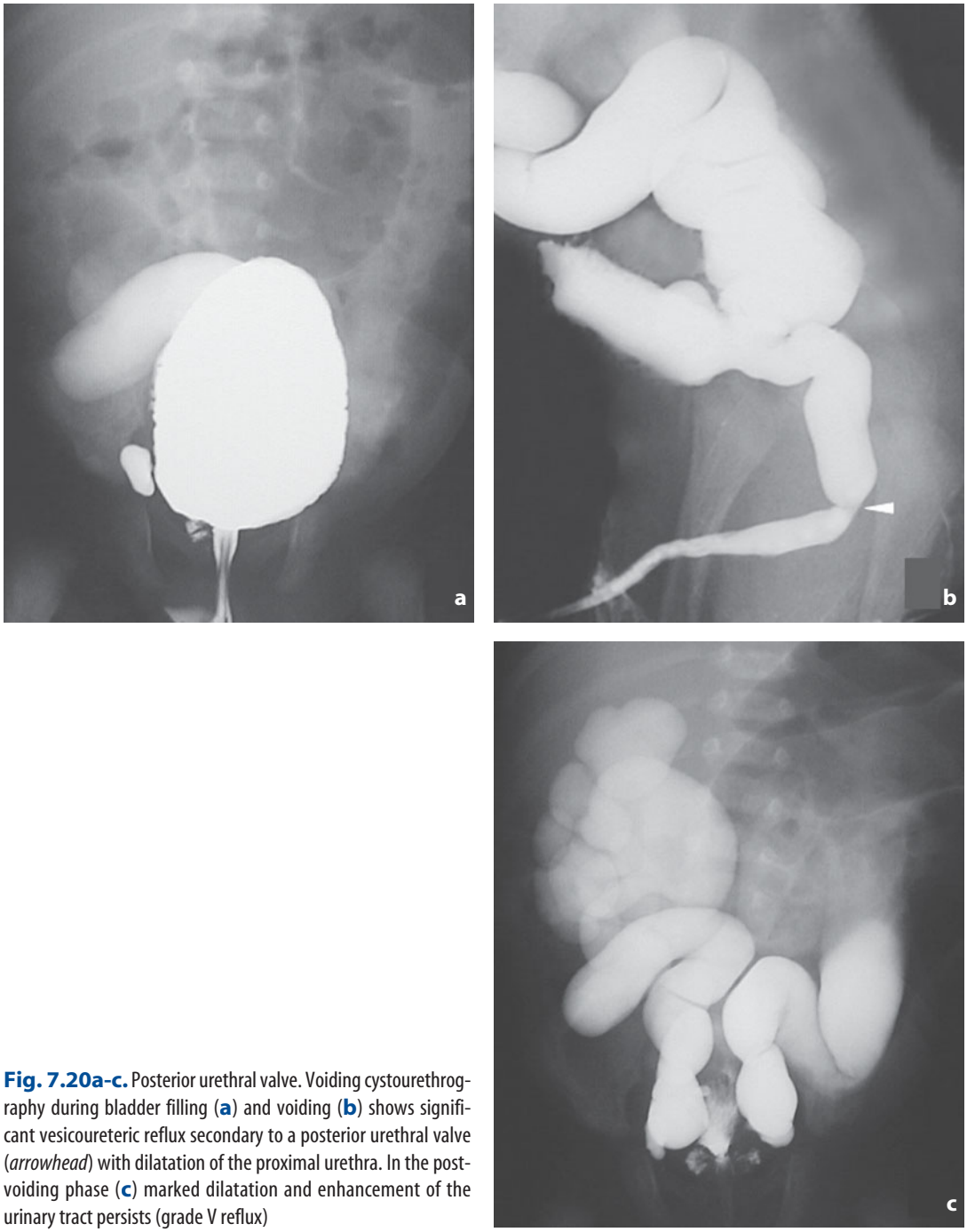

Fig. 7.20a-c. Posterior urethral valve. Voiding cystourethrography during bladder filling (**a**) and voiding (**b**) shows significant vesicoureteric reflux secondary to a posterior urethral valve (*arrowhead*) with dilatation of the proximal urethra. In the postvoiding phase (**c**) marked dilatation and enhancement of the urinary tract persists (grade V reflux)

Urethral Stricture

Congenital forms are much rarer than acquired forms and are found in both sexes, with a prevalence in males. Around 75% of cases affect the bulbous urethra, the point where the proximal urethra (derived from the endoderm) joins with the part originating from the urogenital membrane. According to the degree of obstruction they can be symptomatic from the postnatal period, presenting with a severe alteration of the entire urinary tract (described above for PUV), or with later onset, in which case

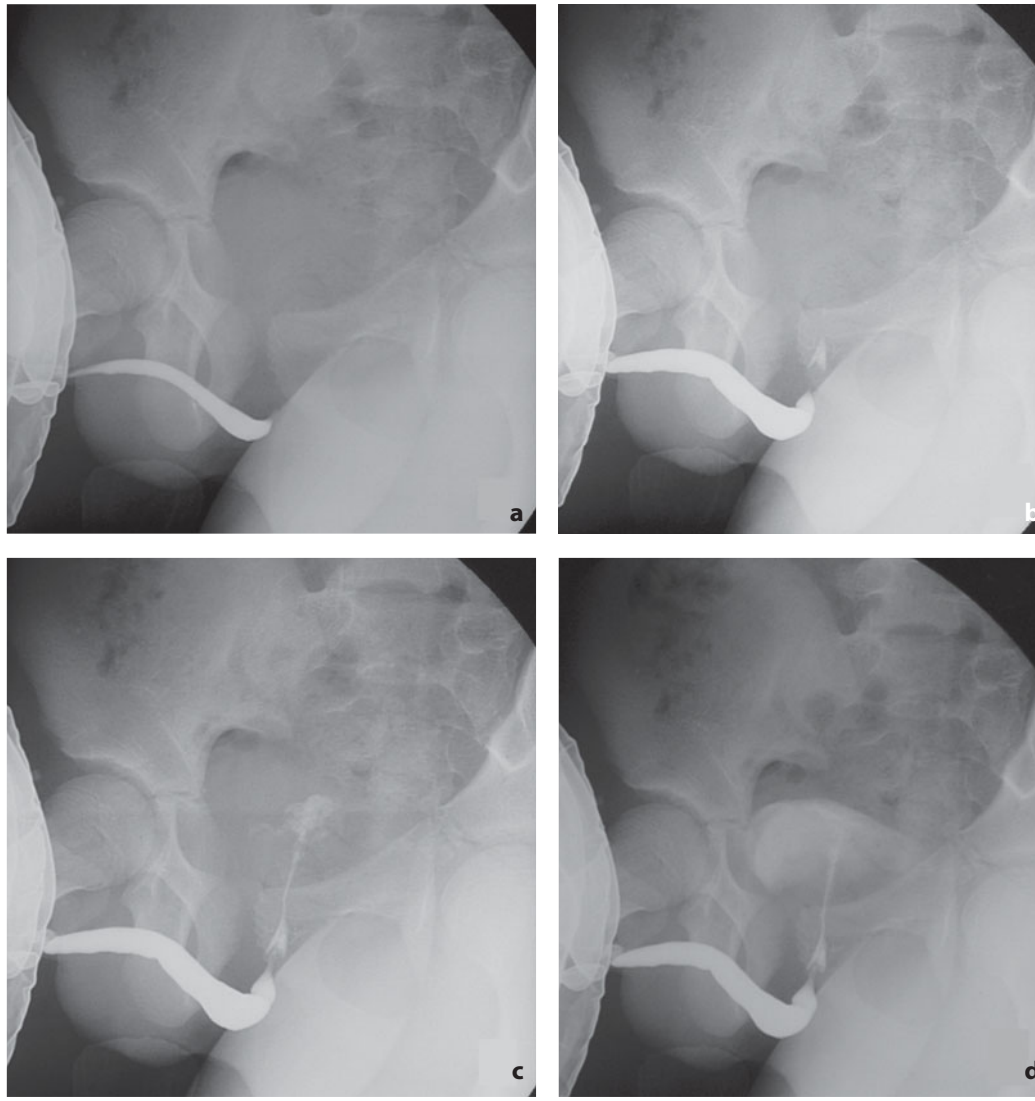

Fig. 7.21a-d. Urethral stricture. **a** Retrograde urethrography in the initial phase shows an arrest in the return of contrast medium at the bulbous urethra. **b-d** The constricted tract is more evident in the following phases

the symptoms are the result of a lower UTI, including voiding disturbances, epididymitis, prostatitis and hematuria (Fig. 7.21).

Effmann EL, Lebowitz RL, Colodny AH (1976) Duplication of the urethra. Radiology 119:179-185

Holmdahl G, Sillén U, Hanson E et al (1996) Bladder dysfunction in boys with posterior urethral valves before and after puberty. J Urol 155:694-698

Maizels M, Stephens FD, King LR et al (1983) Cowper's syringocele: a classification of dilatations of Cowper's gland duct based upon clinical characteristics of eight boys. J Urol 129:111-114

Young HH, Frontz WA, Baldwin JC (2002) Congenital obstruction of the posterior urethra. J Urol 167:265-267

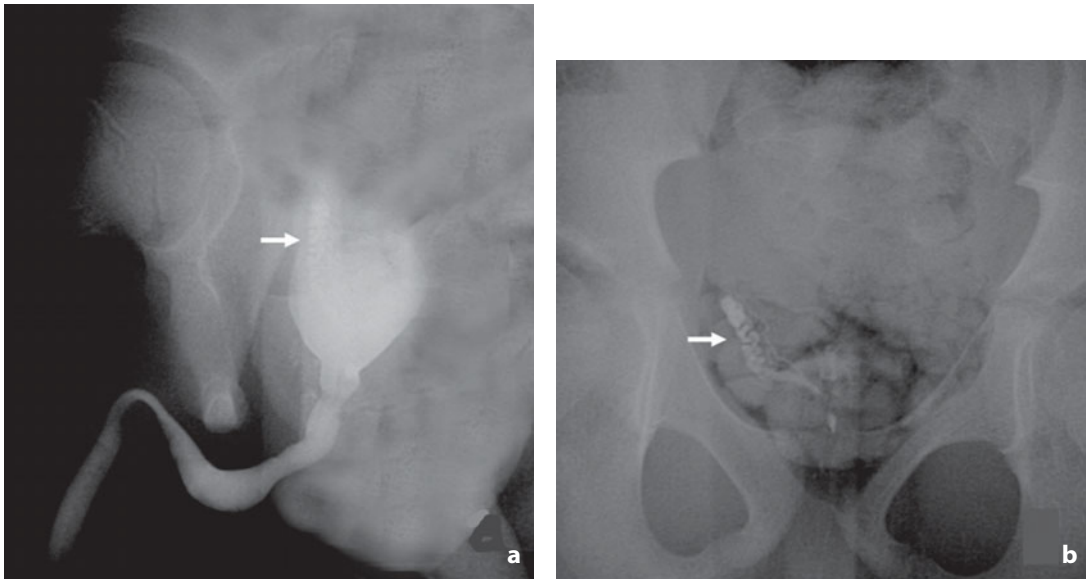

Fig. 7.22a,b. Ejaculatory duct reflux. Voiding cystourethrography during the terminal (**a**) and post- (**b**) voiding phase show retrograde enhancement of the seminal vesicles and the ductus deferens (*arrows*)

Anomalies of the Reproductive System

In males the only anomaly not immediately evident at physical examination, although radiologically identifiable, is ejaculatory duct reflux. This involves an anomalous return of urine from the urethra to the ejaculatory duct, and then to the seminal vesicles and possibly up to the ductus deferens. Often an incidental finding during cystography, it can be the cause of recurrent epididymitis or urethritis (Fig. 7.22). The most common cause is obstruction to the urinary flow located inferior to the prostatic colliculus, although it can also be primary.

There are numerous anomalies of the female reproductive system. Between the 7th and 8th week of gestation the two paramesonephric ducts develop cranially, widening to form the uterine tubes, while caudally they fuse at the median line, migrating downwards to the urogenital sinus where they give rise to the uterus and the superior 4/5 of the vagina. A septum initially separates the two ducts, although it is soon reabsorbed. From the 10th week onwards the early uterus and vagina form a single tubular structure known as the uterovaginal canal. The inferior fifth of the vagina originates from the urogenital sinus.

Uterovaginal agenesis is present in Mayer-Rokitansky-Küster-Hauser syndrome, which is characterized by genital, renal and skeletal anomalies. It has an incidence of 1:4000-5000 neonates with normal 46XX chromosomes and is marked by complete agenesis of the superior 4/5 of the vagina and variable alterations to the uterus and uterine tubes. The uterus may be absent or immaturely formed. A US examination with the bladder fully distended fails to identify the normal impression of the uterus. The ovaries may be normal, ectopic or represented by fibrous bands. The condition is occasionally associated with renal pelvic ectopia.

Vaginal atresia is due to the faulty canalization of the vagina or failed union between the uterovaginal canal and the urogenital sinus. Two anatomic variants have been described: imperforate hymen and transverse septum. Imperforate hymen is the most common form. The condition causes a dilatation of the vagina alone, known as hydrocolpos, or both the uterus and the vagina, known as hydrometrocolpos, due to the accumulation of vaginal and cervical fluids. This condition can manifest as early as the neonatal or even prenatal period due to the presence of a mass, which in some

cases can cause an obstruction of the urinary tract. In the pubescent girl imperforate hymen may manifest with recurrent abdominal pain typically at monthly intervals. Physical examination often reveals protrusion of the completely closed hymen through the vulva. The transverse septum can be located at any point between the hymen and the uterine cervix, but it is usually situated in the inferior third of the vagina. It may be complete or incomplete. In the former, the clinical presentation is similar to imperforate hymen, while the latter may be asymptomatic or cause dyspareunia.

US is able to demonstrate a progressive divergence of the endometrial echoes or a hypoechoic accumulation located in the pelvis as a consequence of fluid retention, whereas visualization of the constricted tract is difficult (**Fig. 7.23**). Magnetic resonance is used as a second-level modality, and is more accurate in defining the exact location and extension of the constricted tract (**Fig. 7.24**).

Septate vagina is caused by a patency defect of the uterovaginal canal or a longitudinal fusion defect between the two mesonephric ducts. In this case a complete or incomplete septum is present, which divides the vagina longitudinally. Two uterine cervices may be present, each afferent to its own hemivagina.

Bicornuate uterus is a condition in which the uterine body is duplicated in two symmetric horns which converge in a single cervical canal. Three subclasses have been described: complete, partial and arcuate. Axial US scans make possible the accurate evaluation of the depth of the separation between the two uterine bodies. A relatively characteristic sign is the two endometrial cavities with an outward fundal concavity (**Fig. 7.25**). Didelphic uterus is defined as the complete duplication of the uterus and the cervix resulting from a complete fusion defect of the mesonephric ducts. Two- and three-dimensional US together with magnetic resonance are able to accurately identify the two separate and diverging uterine horns and the two cervices. In around 75% of cases a vertical septum in the superior segment of the vagina can be identified. In this malformation there may be a transverse vaginal septum generally located in the superior third, which obstructs the canal causing hematometrocolpos (**Fig. 7.26**).

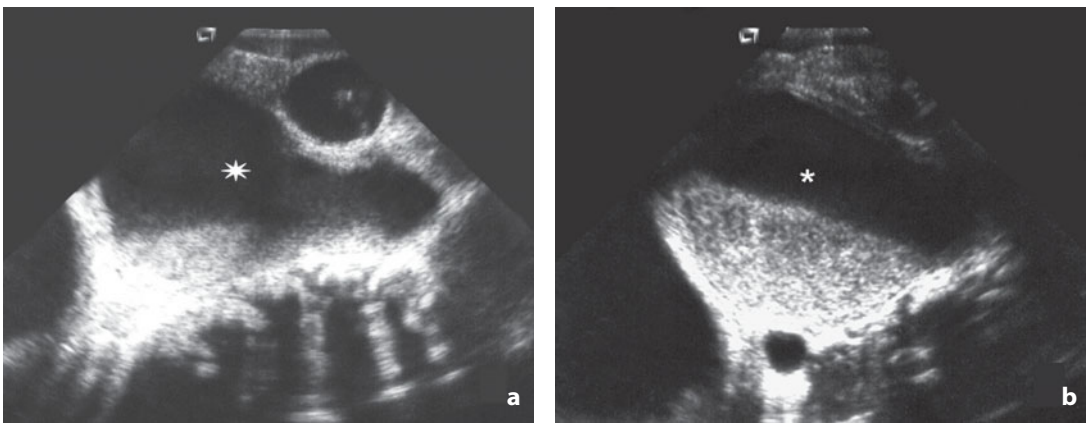

Fig. 7.23a,b. Vaginal atresia. Longitudinal (**a**) and transverse (**b**) sonograms show large pelvic mass (*asterisk*) with nonuniform structure due to collection of fluid with prevalent development in the superior portion and a tapered appearance in the more caudal portion near the constricted tract

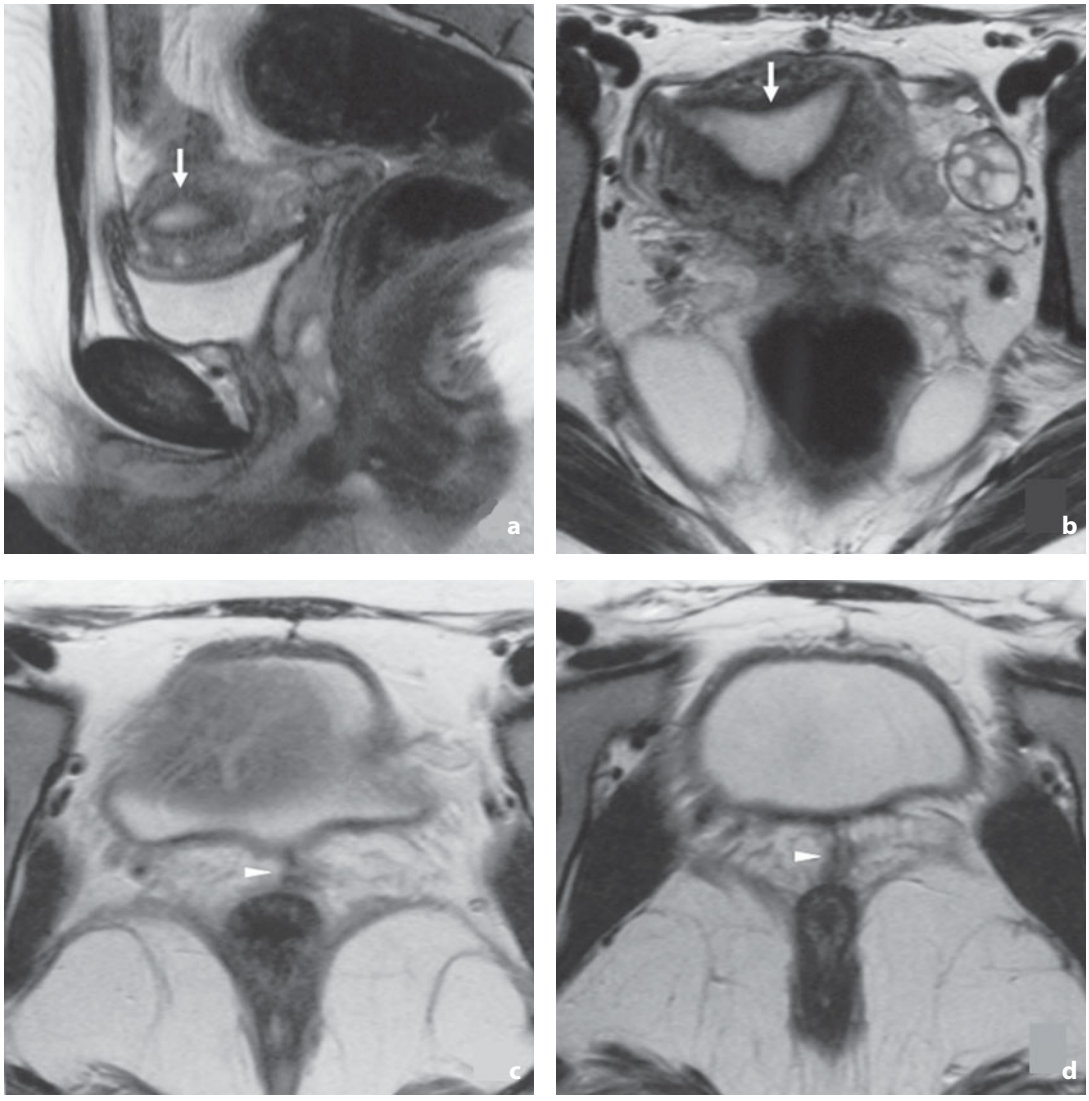

Fig. 7.24a-d. Vaginal atresia. T2-weighted MR scans in the sagittal (**a**) and axial (**b-d**) planes show the collection of fluid in the uterine cavity (*arrow*). The constricted vaginal tract appears as a hypointense tubular structure (*arrowhead*)

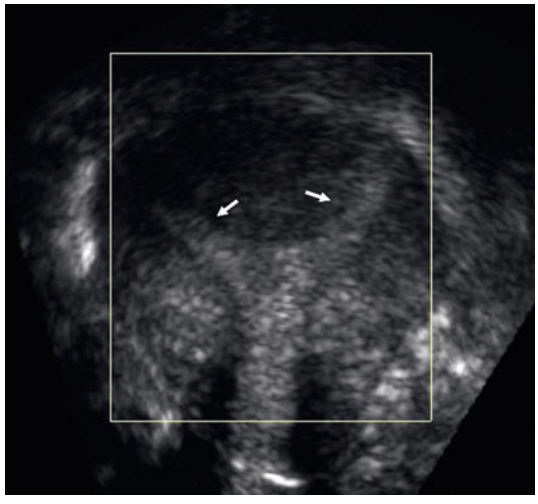

Fig. 7.25. Bicornuate uterus. 3D sonogram shows the double uterine cavity (*arrows*) with a single cervix

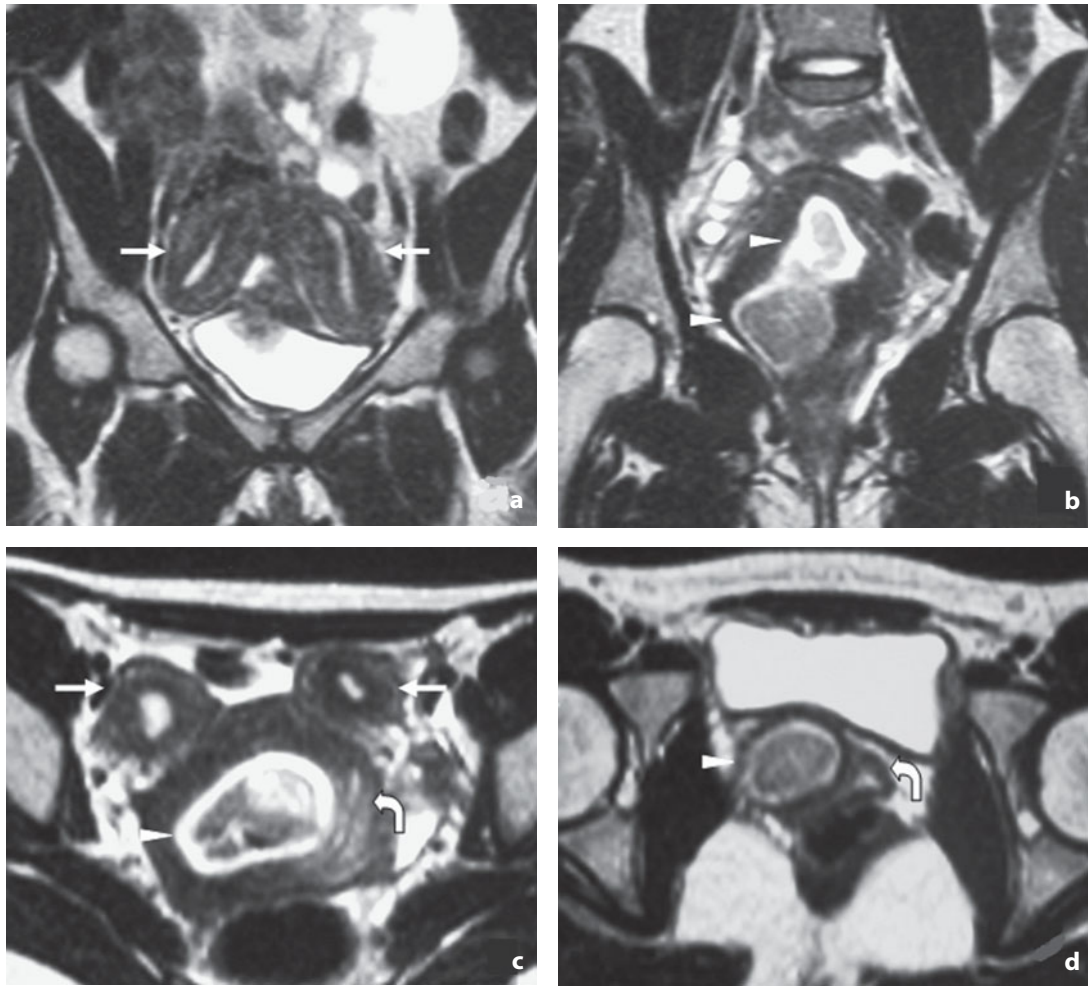

Fig. 7.26a-d. Didelphic uterus with obstructed hemivagina. The coronal (**a,b**) and axial (**c,d**) T2-weighted magnetic resonance images show two separate and diverging uterine cavities with hyperintense endometrium and hypointense myometrium (*arrows*). The right hemivagina dilated by heterogeneously hypointense fluid is discernible, surrounded by a hyperintense ring formed by blood material in various stages of development (*arrowheads*). The left hemivagina shows no signs of obstruction (*curved arrow*)

Cloacal Anomalies

In the embryo at the 4th week of gestation the terminal part of the posterior intestine is dilated to form the cloaca, the common portion of the digestive and genitourinary systems. The amniotic sac and the cloaca are separated by the cloacal membrane. Under normal conditions, at the 6th week of gestation the urorectal septum divides the cloaca into an anterior portion (urogenital sinus) and a posterior portion (anorectal canal). In this way the cloacal membrane is also subdivided into an anterior part, the urogenital membrane, and a posterior part, the anal membrane. The failure of this subdivision gives rise to the clinical condition known as "cloaca", characterized by confluence of the urethra, vagina and rectum into a single common channel. Many anatomic variants exist in relation to the level of confluence of the three structures. Hydrocolpos may be present due to insufficient fluid drainage or the accumulation of urine in the vagina, or even intestinal occlusion. Associated malformations are very

common, especially urinary tract malformations (70%), cardiovascular and digestive tract anomalies, and neural tube defects.

Troiano RN, McCarthy SM (2004) Mullerian duct anomalies: imaging and clinical issues. Radiology 233:19-34

Wilson DA, Stacy TM, Smith EI (1978) Ultrasound diagnosis of hydrocolpos and hydrometrocolpos. Radiology 128:451-454

Part III
Urinary System Disease

Clinical Approach 8

A. Antonelli, A. Cozzoli, C. Simeone, S. Cosciani Cunico

Lithiasis

Urolithiasis is a disease known to mankind since antiquity. In fact lithotomy, i.e. the surgical removal of bladder calculi, is the oldest surgical operation and was practiced by the ancient Egyptians. The prevalence of the condition is still high today, affecting around 10% of the population. Unlike in developing countries, where urinary bladder calculi are the main presentation, in Western countries the upper urinary tract is more commonly involved. Stones located in the bladder are almost always associated with bladder outlet obstruction and only in anecdotal cases with the presence of foreign bodies such as nonabsorbable sutures.

Hereditary and family factors, diet and the environment all interact in a manner that is not fully understood, to form urinary calculi. However, what is certain is that each stone originates from urinary solutes which crystallize and aggregate when an adequate concentration is reached, defined supersaturation. This may be the result of an increased excretion of the solute or an absolute decrease in diuresis, and is influenced by a series of favorable conditions, such as alterations in pH – both in acidity or alkalinity – and a reduction in urinary substances which inhibit lithogenesis (citrate, pyrophosphate and magnesium). Calculi may be classified according to their physical and chemical composition. Most are composed of calcium, followed in order of frequency by uric acid, magnesium ammonium phosphate or struvite, and cystine. Although each type of stone is associated with predisposing pathologic conditions, such as hyperparathyroidism for calcium-based calculi, hyperuricosuria for uric acid calculi, chronic urinary tract infections (UTIs) by urea splitting bacteria for struvite calculi and cystinuria for cystine calculi, in most clinical cases the condition is idiopathic. Therefore, a complete metabolic study should be guided on the basis of the chemical analysis of the stone and is indicated in all cases of high recurrence, young age or known family history of calculosis.

Urinary calculi can have a variety of clinical presentations in relation to their dimensions and site, ranging from completely asymptomatic (microlithiasis of the inferior calices) to acute abdomen (calculi obstructing and rupturing the ureter with extravasation of infected urine). In general, large stones form in the renal cavity without producing pain although they may cause chronic and irreversible damage to the renal parenchyma. In contrast, small-diameter calculi migrate more easily towards the ureteric lumen causing its obstruction with consequent onset of the typical symptoms of renal colic.

Patients with colic report intense lumbar pain with radiation to the flank and the testicle or labia majora, associated with neurovegetative symptoms (nausea, sweating, hypotension). In the expulsive phase irritative voiding symptoms typically appear, which are related to the hyperactivity of the detrusor muscle produced by the irritation of the calculus with intramural location.

UTI in the presence of calculosis can be caused by the condition itself (infected calculosis) or secondary to urinary obstruction. The physical examination reveals

L. Olivetti, L. Grazioli (eds.), *Imaging of Urogenital Diseases*,

marked tenderness at palpation and percussion of the lumbar region, while perineal tenderness may appear in the presence of urinary extravasation. Bladder calculosis manifests with irritative voiding symptoms, hematuria, interrupted voiding or acute retention, if the stone becomes lodged in the bladder neck or the urethra, thus obstructing the passage of urine. Lastly it should be noted that chronic inflammation secondary to prolonged bedridden state (months or years) of patients with large calculi is a predisposing factor for the development of squamous tumors of the urinary tract.

Diagnostic imaging plays a vital role in the characterization and definition of the correct treatment and should investigate the following features:

- ruling out differential diagnoses;
- number and position of the calculi;
- degree of obstruction of the urinary tract;
- degree of compromise of renal parenchyma;
- presence of rupture of the urinary tract;
- presence of malformations.

Pharmacologic therapy can be applied in the treatment of acute pain with non-steroid anti-inflammatory drugs or opioid derivatives, whereas antibiotic therapy is required in the presence of clinically evident UTIs, obstruction or extravasation of urine. In the expulsive phase antispasmodic agents are utilized, as well as drugs used in the treatment of benign prostatic hyperplasia (tamsulosin), which are selective antagonists for the apha-1 adrenergic receptors also identified in the musculature of the intramural ureter. In cases of specific known predisposition, dietary and pharmacologic measures are adopted aimed at inhibiting lithogenesis and crystal aggregation. These include alkalizing the urine (magnesium and/or potassium citrate, sodium bicarbonate), correcting hyperuricosuria (allopurinol) and increasing the solubility of cystine (tiopronin and D-penicillamine). In the presence of severe obstruction of the urinary tract associated with organ dysfunction, infection or rupture, percutaneous nephrostomy or ureteric stenting may be required.

Treatment of calculi over the last twenty years or so has been based on minimally invasive techniques that may be used in combination to reduce the stone to fragments which can then be expelled spontaneously or removed endoscopically. **Table 8.1** summarizes the current consensus of indications. Only a minority of patients with calculi in the upper urinary tract (multiple pyelocaliceal or ureteric), whose calculi are particularly hard or resistant to multiple procedures, or patients with associated malformations (e.g. ureteropelvic junction syndrome, hydrocalix, megaureter) still require invasive surgery. A similar approach may be required in patients with particularly large bladder calculi (**Fig. 8.1**) or associated conditions (significant prostatic hypertrophy, vesical diverticula).

Table 8.1. Current "standard" treatment of urinary calculi

Site and characteristics of calculus	Treatment of choice
Renal pelvic, renal calix and "upper" lumbar ureter ≤1-2 cm	Noninvasive (fluoroscopy- or US-guided extracorporeal shockwave lithotripsy)
"Low" lumbar and pelvic ureter	Intracorporeal (ureteric litholapaxy)
Renal pelvis/calix >2 cm, multiple or complex	Percutaneous (nephrolitholapaxy)
Bladder	Intracorporeal (endoscopic lithotripsy)

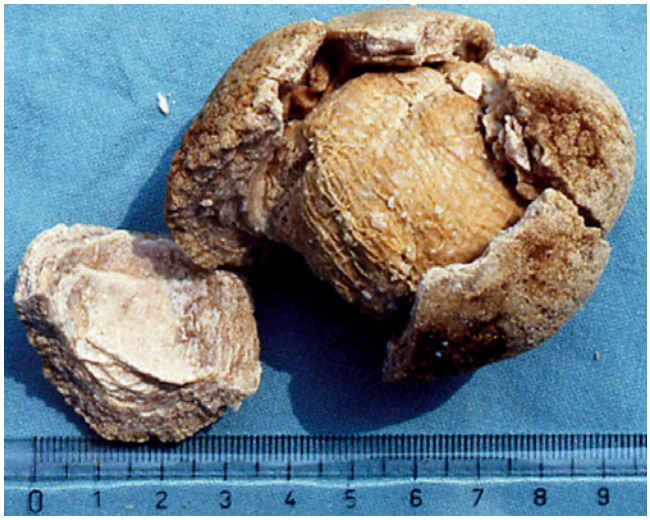

Fig. 8.1. Large bladder calculus removed surgically (cystolithotomy)

Asplin JR, Favus MJ, Coe FL (1996) Nephrolithiasis. In: Brenner BM (ed) Brenner and Rector's the kidney, 5th edn. WB Saunders Co., Philadelphia, pp 1893-1935

Pak CY (1998) Kidney stones. Lancet 351:1797-1801

Parmar MS (2004) Kidney stones. BMJ 328:1420-1424

Westenberg A, Harper M, Zafirakis H et al (2002) Bladder and renal stones: management and treatment. Hosp Med 63:34-41

Inflammation

Although under normal conditions the urinary tract is a sterile environment for its entire course, with the exception of the distal urethra and the meatus, the prevalence of UTIs is relatively high, second only to respiratory system infections. The most common microorganisms involved are Gram-negative aerobic bacteria (*Escherichia coli*, *Klebsiella* species, *Proteus* species, *Enterobacter* species, *Pseudomonas* species) followed by Gram-positive anaerobic cocci, mycetes, viruses and parasites, with differences in geographic distribution or whether the infections are community acquired or nosocomial. The majority of UTIs are ascending infections with access through the external urethral meatus, although hematogenous and probably also lymphatic spread can occur during sepsis or invasive instrumental procedures. The incidence of UTIs is greater in male neonates and the elderly, whereas they are markedly more prevalent in school-age girls and sexually active premenopausal women. This is because the virulence of the germs depends on a series of factors which are differently distributed between the sexes and the different life stages. The main factors include anatomy (short female urethra close to the vaginal and intestinal microbial flora), dietary habits (variations in the composition of urine, alterations to the intestinal flora) and sexual intercourse (direct transmissions of germs from the partner, urethral "trauma"), congenital malformations or acquired conditions capable of altering urinary flow (ureteropelvic obstruction syndrome, vesicoureteric reflux, urethral obstruction, neurogenic bladder), as well as all the conditions that lower the immune system (diabetes, gout, tumors, acquired immunodeficiency, pregnancy, radiotherapy, chemotherapy). An acute onset UTI may present with a broad spectrum of severity ranging from completely asymptomatic (asymptomatic bacteriuria) to fulminant sepsis.

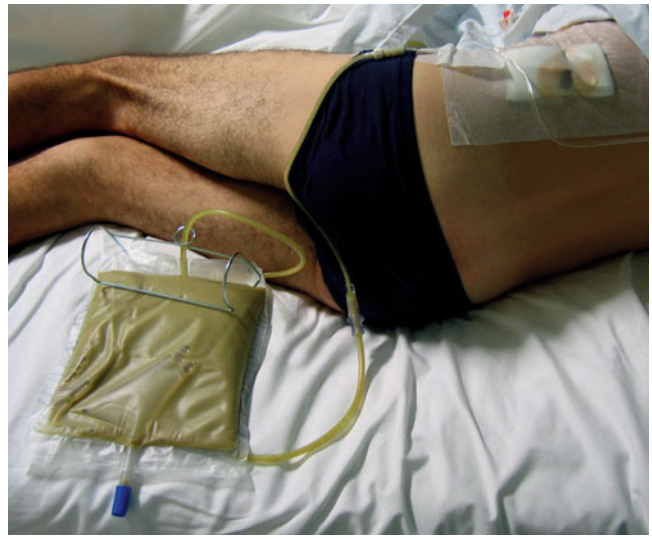

Fig. 8.2. Percutaneous drainage in a patient with obstructive pyelonephritis (the purulent appearance of the urine is evident)

From the clinical and pathophysiologic point of view, lower UTIs (urethritis and cystitis) are distinct from upper UTIs (pyelonephritis and renal abscess). Isolated urethritis is typical in males and is associated with sexual intercourse. It manifests with mild voiding symptoms and urethral secretion, which may possibly be observed during physical examination which nonetheless is absent of other significant findings. Onset can be severe with recurrent urethritis and urethral stricture.

Acute cystitis is the most common UTI in females and, rarely, an isolated phenomenon in males due to associated prostatitis. Patients report intense irritative voiding symptoms (pain, dribbling, frequency), occasionally associated with macroscopic hematuria, with unclear physical examination findings often limited to moderate hypogastric tenderness. Acute pyelonephritis originates prevalently from the reflux of infected urine from the lower urinary tract (ascending pyelonephritis), or as the result of an obstruction of urinary flow in the collecting system involved, e.g. ureteric lithiasis (obstructive pyelonephritis; **Fig. 8.2**). However, hematogenous spread is also possible, especially when infection is bilateral or cases are complicated with corticomedullary abscess formation. Clinical presentation is characterized by acute flank pain, fever and possible severely compromised general status.

Chronic infections (chronic pyelonephritis and cystitis) are less clearly defined. They arise from the failure to eradicate acute infection or the recurrence of less severe infections and may lead to permanent organ damage (renal failure, bladder volume loss).

In addition to physical examination findings, the diagnosis of UTI is guided by laboratory examinations (leukocyturia and leukocytosis) and cell culture (urine culture, ureteric swab). Radiologic examinations play a role in ruling out predisposing malformations, identifying associated conditions (lithiasis, tumors) and evaluating the presence of urinary tract obstructions, renal abscesses or parenchymal scarring.

Treatment consists of the administration of antibiotics, preferably narrow spectrum, with drugs and doses tailored to the site of infection (**Table 8.2**).

Mori R, Lakhanpaul M, Verrier-Jones K (2007) Diagnosis and management of urinary tract infection in children: summary of NICE guidance. BMJ 335:395-397

Nicolle L, Anderson PA, Conly J et al (2006) Uncomplicated urinary tract infection in women. Current practice and the effect of antibiotic resistance on empiric treatment. Can Fam Physician 52:612-618

Table 8.2. First choice antibiotic treatment in urinary tract infections

Infection	Standard treatment protocol
Gonococcal urethritis	Ceftriaxone IM single dose
Nongonococcal urethritis	Azithromycin oral single dose Doxycycline oral 7 days Quinolones oral 7 days
Acute cystitis	Co-trimoxazole oral 3 days Quinolones oral 3 days Amoxicillin-clavulanic acid oral 3 days
Acute cystitis associated with systemic disease or urinary stasis	Same drugs oral 7 days
Acute pyelonephritis	Cephalosporins, quinolones and aminoglycosides IM or IV, alone or in combination, up to 48 h after the temperature comes down and then quinolones or amoxicillin-clavulanic acid oral 7 days

Tumors

Renal Parenchymal Tumors

Renal cell carcinoma (RCC) is one of the most heterogeneous tumors with regard to presentation and clinical course. It accounts for 2-3% of all tumors and around 87% of renal tumors in adults. Onset is prevalently in the sixth or seventh decade of life, although it can be found in patients below 30 years of age. Males are more frequently affected by the disease, with a M/F ratio of around 2-3:1. The causative factor is practically unknown, although a variety of factors have been studied as possible etiologic agents: cigarette smoke and its related carcinogens such as dimethylnitrosamine, air pollutants in urban centers, chronic exposure to cadmium, overuse of drugs containing phenacetin, congenital malformations and genetic predisposition.

A high risk of RCC is found in subjects with von Hippel-Lindau disease, a rare inherited disease characterized by the growth of angiomatous lesions in the cerebellum and retina. In current clinical practice five histotypes of RCC are recognized (**Table 8.3**), distinctive in their microscopic morphology, karyotype and characteristic genomic alterations.

The presenting symptoms of RCC vary widely, but today the diagnosis is increasingly made when the disease is in an early stage, and therefore asymptomatic. The classic triad (hematuria, flank pain and palpable mass) are generally found in cases of advanced disease and present at diagnosis in less than 5% of cases. Most aspecific

Table 8.3. Distribution of tumor histotypes of renal cell carcinoma according to the Heidelberg classification in 1480 patients treated surgically in the period 1983-2007 at the Department of Urology, University of Brescia

Histotype	%
Conventional	84.1
Papillary	8.9
Chromophobe	3.9
Collecting duct	1.3
Unclassified	1.8

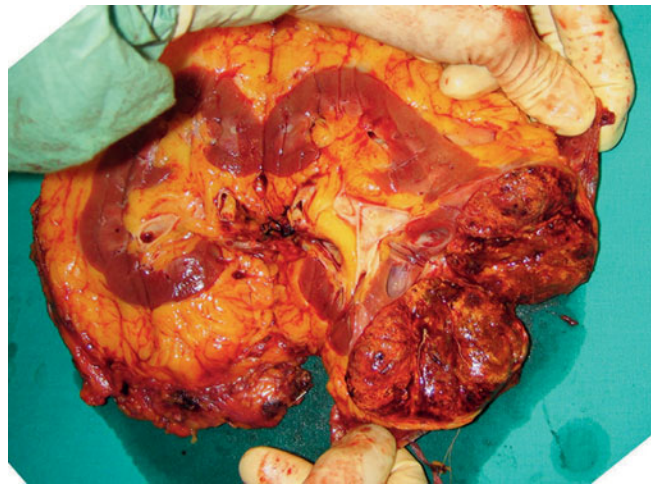

Fig. 8.3. Surgical specimen of radical nephrectomy

symptoms, such as anorexia, asthenia, weight loss and fever fall into the category of paraneoplastic syndromes.

The primary treatment option in RCC is radical nephrectomy, i.e. en bloc removal of the renal fascia and its contents – kidney, suprarenal gland and perirenal fat – as well as the regional lymph nodes after ligation and resection of the renal artery and vein (**Fig. 8.3**). Nephron sparing surgery (removal of only the tumor with sparing of the renal parenchyma) is an absolute indication in the presence of a solitary congenital or surgical kidney, contralateral renal dysfunction or bilateral renal tumors, whereas an elective procedure is applied only in extremely select cases – small localized exophytic renal masses (4 cm or less).

Despite the huge efforts in recent years to find effective treatment methods, the greatest chance of controlling RCCs to date lies in early diagnosis and radical surgery, even though anti-angiogenetic agents have recently produced promising results.

Laber DA (2006) Risk factors, classification, and staging of renal cell cancer. Med Oncol 23:443-454

Ng CS (2006) Radiologic diagnosis and staging of renal and bladder cancer. Semin Roentgenol 41:121-138

Oakley NE, Hegarty NJ, McNeill A et al (2006) Minimally invasive nephron-sparing surgery for renal cell cancer. BJU Int 98:278-284

Wagstaff J (2006) New horizons in the treatment of renal cell cancer. Ann Oncol Suppl 10:x19-22

Tumors of the Renal Pelvis and Ureters

Tumors of the collecting system consist of mainly of transitional cell carcinomas and are histologically similar to the urothelial tumors of the urinary bladder (**Fig. 8.4**). Their incidence does not exceed 5% of all urinary tract tumors. They most commonly manifest from the sixth decade of life onwards, with a male/female ratio of 2:1.

Urothelial tumors of the upper urinary tract follow the natural history of bladder cancer in terms of multifocality and recurrence. However, they differ in their macroscopic development, tending to infiltrate the muscle layer and surrounding tissue

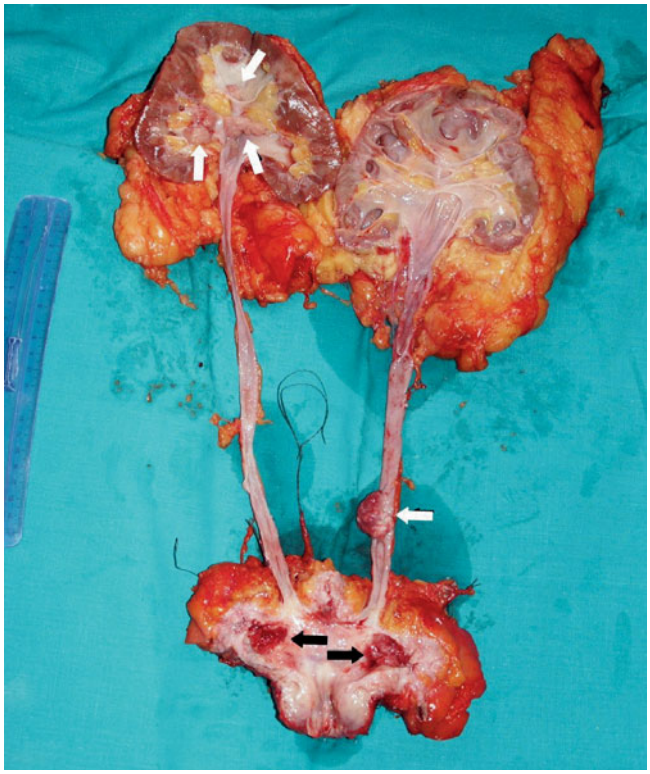

Fig. 8.4. "Panurothelial disease" with tumors in both collecting systems and the bladder (*arrows*)

earlier and in a greater number of cases, thus giving rise to disease at the regional lymph nodes and distant sites. The structure of the upper urinary tract, with its muscle layer markedly thinner than that of the bladder, the site and the lymphatic drainage directly to the lumbar para-aortic lymph nodes are all factors in favor of local-regional growth and distant disease, with a decidedly malignant tendency.

The most common sign which prompts the patient to seek medical advice is gross hematuria (70% of cases), often followed by colic-like pain indicative of urinary tract obstruction by the tumor or blood clot. The finding of a palpable mass and signs and symptoms of cachexia, asthenia, anorexia and weight loss all indicate advanced disease. Urinary cytology, i.e. the study of cell morphology after Papanicolaou staining of the exfoliated urothelial cells found in the urine, is an adjunct to the radiologic techniques used in diagnosis and follow-up.

Primary treatment is surgical, with different strategies and modalities in relation to tumor stage and degree of cellular differentiation. There are two main approaches: open radical nephroureterectomy with excision of the bladder cuff and regional lymph nodes in the presence of an invasive tumor; and segmental ureterectomy with reconstruction of the ureter or tumor excision performed endoscopically in the presence of low-grade lesions. Radiotherapy and neoadjuvant chemotherapy are used in locally advanced and metastatic disease.

Arancibia MF, Bolenz C, Michel MS et al (2007) The modern management of upper tract urothelial cancer: surgical treatment. BJU Int 99:978-981

Catto JW, Yates DR, Rehman I et al (2007) Behavior of urothelial carcinoma with respect to anatomical location. J Urol 177:1715-1720

Bladder Cancer

Tumors of the urinary bladder are the second most common neoplastic lesion of the urinary tract after prostate cancer, accounting for 3-5% of all cancers in adults. Incidence is highest in the sixth decade of life with a male/female ratio of 5:1. The etiology of the disease is the same as tumors of the collecting system, both of which originate from urothelial epithelium. Gross terminal hematuria is the characteristic sign, associated with irritative voiding symptoms when the tumor invades the bladder wall and pelvic pain when the lesion reaches adjacent organs. Bladder cancer can manifest in a broad range of lesions, from superficial papillary tumors with minimal extension to solid ulcerated lesions which progressively invade the bladder wall.

In a category all of its own is carcinoma in situ, which, despite being limited to the mucosa, is highly aggressive due to its growth pattern (flat type of lesion which spreads across the surface and is therefore difficult to detect) and as a result its increased ability for distant diffusion. Bladder endoscopy and biopsy are key aspects for diagnosis, confirming clinical and radiologic suspicion, and treatment planning. For example, surface bladder lesions – Ta or T1, therefore not involving the muscle layer of the bladder – can be treated successfully with endoscopic excision and, where necessary, adjuvant intracavitary chemotherapy, whereas invasive lesions (T2 or above) require radical cystoprostatectomy with pelvic lymphadenectomy in males and anterior pelvic exenteration in females, followed by the creation of a urinary diversion. Systemic neoadjuvant and adjuvant chemotherapy are indicated in locally advanced disease (N+) or metastases, whereas radiotherapy is only used in symptomatic and palliative care.

Dahm P, Gschwend JE (2003) Malignant non-urothelial neoplasms of the urinary bladder: a review. Eur Urol 44:672-681

Epstein JI, Amin MB, Reuter VR et al (1998) The World Health Organization/International Society of Urological Pathology consensus classification of urothelial (transitional cell) neoplasms of the urinary bladder. Bladder Consensus Conference Committee. Am J Surg Pathol 22:1435-1448

Manoharan M, Ayyathurai R (2007) Radical cystectomy for urothelial cancer of the bladder: contemporary advances. Minerva Urol Nefrol 59:99-107

Murta-Nascimento C, Schmitz-Dräger BJ, Zeegers MP et al (2007) Epidemiology of urinary bladder cancer: from tumor development to patient's death. World J Urol 25:285-295

Diagnostic Imaging 9

M.A. Cova, L. Olivetti, L. Grazioli, P. Martingano, F. Stacul

Renal Lithiasis

Clinical Anatomy

Urinary lithiasis is the product of the precipitation of normally soluble substances in the urine, which over time leads to the formation of stones. Many factors play a role in this process, but the main one is the increase in the urinary concentration of the solutes to the point of causing their crystallization. Low urinary volume can also cause precipitation in individuals whose metabolism is normal, since the urinary solution is normally supersaturated.

Urinary stones are composed of a crystalline-organic matrix. The most common stone is formed from calcium oxalate and is generally <2 cm, although stones can be formed from pure calcium phosphate, struvite, pure uric acid and cystine. Stones composed of struvite, pure uric acid and cystine can reach significant dimensions and occupy the entire renal pelvis and calices (staghorn calculus). Calcium oxalate stones are often spiculated and can therefore cause acute pain and hematuria when they pass into the ureter. Cystine and uric acid stones in contrast are relatively smooth.

Even small crystalline aggregates, known as gravel, can migrate along the ureters and cause renal colic.

Renal calculi can be multiple, but in 80% of cases they are unilateral. They can form at any level of the urinary tract, but the most common site is in the kidneys. They can then migrate along the ureter until the diameter becomes too narrow for them to pass, thus causing urinary stasis and classic colicky pain. The stone need not become lodged in the ureter to produce symptoms, in that the irritative action alone and the consequent edema of the ureteric wall are enough to cause stasis.

Many stones, and perhaps most stones, are passed spontaneously without causing any symptoms, especially if they are small with smooth walls.

Renal colic is an excruciating and relentless pain with sudden onset. It often arises in the lumbar region and radiates with the classic loin-to-groin presentation. The pain tends to come in waves, with acute periods interspersed with brief remission. Unlike patients with abdominal pain, the patient with renal colic tends to move constantly in a fruitless search to find a comfortable position. The pain may be associated with nausea and vomiting, intestinal gas, constipation and diarrhea, malaise and lethargy. Frequency, bladder retention and microscopic or gross hematuria may also be present.

Within several hours of onset the urinary obstruction causes a dilatation of the proximal ureter with the development of hydronephrosis. At this stage additional infection may produce pyuria and fever.

Calculosis may also be associated with a more vague presentation of pain or sense of heaviness in the lumbar region with occasional twinges and aspecific vertebral pain.

Renal lithiasis is a disease with a high degree of recurrence: around 75% of patients present again with colicky pain in the following years.

L. Olivetti, L. Grazioli (eds.), *Imaging of Urogenital Diseases*,

Associated with the dilatation of the pelvicaliceal system due to obstruction (hydronephrosis) is a progressive atrophy of the renal parenchyma. The glomerular filtrate begins to back up in the renal interstitium and the perirenal spaces and from here into the lymphatic system. Therefore, glomerular filtration continues for a certain period even in the presence of complete obstruction. The persistence of filtration causes a dilatation of the calices and pelvis. In the presence of complete obstruction the production of urine terminates in a relatively short time, while in cases of partial or intermittent obstruction filtration continues, causing a significant dilatation with progressive shortening of the pyramidal apices, which become sunken. In advanced cases the kidney takes on a cystic-like appearance, with extremely thinned renal parenchyma. The high pressure of the renal pelvis also compresses the vessels in the pyramids, causing a flow reduction in the medulla. This is initially reversible, but over the longer term causes functional damage. The urinary obstruction triggers an inflammatory response which can induce interstitial fibrosis.

Incomplete obstruction, especially with slow development as in the case of staghorn calculi, can be silent or cause only vague disturbances and therefore can persist for a long time, causing irreversible damage to the kidney.

Federle MP, Anne VS, Jen-Sho Chen J et al (2005) Kidney and urinary tract infection and inflammation. In: Federle MP, Jeffrey RB, Desser TS et al (eds) Diagnostic imaging: abdomen, vol III. Amirsys, Salt Lake City, UT, Usa, pp 28-63

Diagnostic Imaging

The patient usually arrives at the emergency room with acute flank pain. The ER physician sends them to radiology to confirm the diagnosis with demonstration of the stone or indirect signs of its presence, or as an alternative the demonstration of urinary or extraurinary tract disease which justifies the symptoms. In the presence of calculi, the findings of interest for the urologist are the identification of the stone, the definition of its site and size, which significantly influence the treatment choice, and lastly the identification of possible complications and the evaluation of the status of the contralateral kidney. In some cases the etiology of the stone can be presumed by the demonstration of predisposing factors for its formation, such as stricture.

It should be recalled that lithiasis is the most frequent cause of renal colic. Other causes include ureteropelvic dyskinesia, a blood clot or a vegetative lesion in the ureter and extrinsic ureteric compression due to tumors or during the course of pregnancy.

Numerous extraurinary conditions can mimic colicky pain, so during the diagnostic study the gastrointestinal tract, the abdominal aorta, the pancreas, the bile ducts and annexes should also be evaluated.

A number of different protocols have been proposed to evaluate acute flank pain which include different imaging modalities.

Plain Abdominal Film

The visualization of a stone depends on the absence of bowel contents, the size, nature and consequent radiopacity of the stone, technical factors, and the presence of nonurinary calcifications. Calcium oxalate stones are markedly radiopaque, cystine and struvite stone are moderately opaque, while uric acid stones are typically radiolucent.

The sensitivity of the plain film radiogram varies, according different studies, from 44 to 77%, with a specificity of 80-87%. Errors may be due to overlying gas, stool or bone (false negatives) and extraurinary calcifications, especially phleboliths and calcified lymph nodes (false positives).

The differential diagnosis can be assisted by a number of imaging characteristics in that urinary stones are polymorphous, solitary and uniformly dense while phleboliths are usually oval or circular with radiolucent centers.

Dalla Palma L, Pozzi-Mucelli R, Stacul F (2001) Present-day imaging of patients with renal colic. Eur Radiol 11:4-17

Urography

Urography is able to obtain the information of the preliminary plain abdominal film together with the information which can be obtained after the administration of contrast medium in the excretory phase. It is able, therefore, to visualize the stone as a radiopacity in the plain film study and as a filling defect in the excretory phase. It is also able to identify indirect signs such as the late or absent enhancement of the pelvis and calices (**Fig. 9.1**) or a dilatation of the collecting system with persistent enhancement of the ureter. In the presence of an acute obstruction of the upper urinary tract

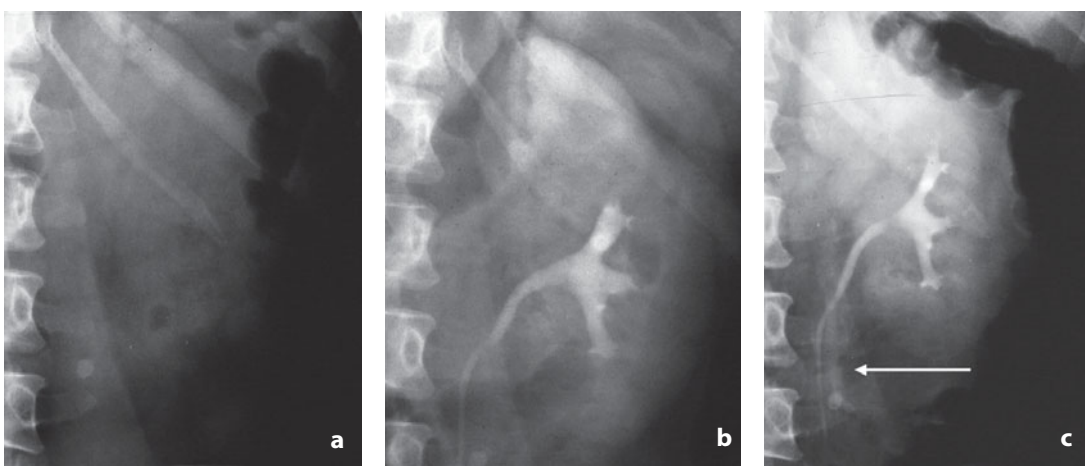

Fig. 9.1a-c. Urography. Ureteric stone in duplex collecting system (patient with left ureteric colic). **a** Plain abdominal film shows a radiopaque formation lateral to the vertebral column at the site of the presumed lumbar ureter. **b** In the excretory phase the opacity is situated outside the enhanced ureter. However, the calices of the upper renal pole, where the nephrogram is more intense (obstructive), are not identifiable. **c** In the delayed phase the ureter of the superior collecting system containing the stone enhances (*arrow*)

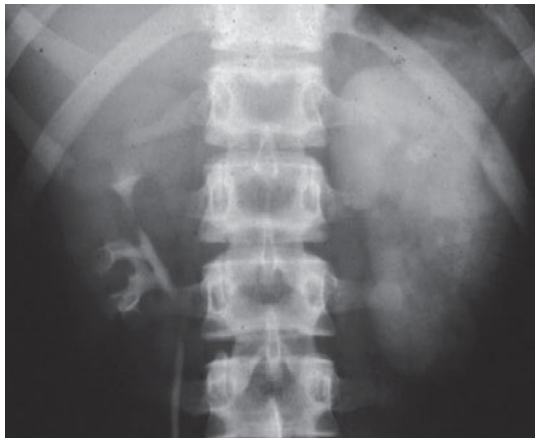

Fig. 9.2. Urography. Obstructive nephrogram (patient with left renal colic). Enlarged left kidney with obstructive-type nephrogram (intense and persistent) and no significant enhancement of the collecting system

the nephrogram may also be altered, which characteristically increases in density over time (obstructive nephrogram) (**Fig. 9.2**).

In the diagnosis of renal colic, urography has a sensitivity of 87-90% and a specificity of 94-100%. These figures made it the most reliable technique until the 1990s, when technologic progress in the field of ultrasonography and computed tomography gradually reduced its importance.

Svedström E, Alanen A, Nurmi M (1990) Radiologic diagnosis of renal colic: the role of plain film, excretory urography and sonography. Eur J Radiol 11:180-183

Ultrasonography

Ultrasonography (US) is able to directly visualize the stone or identify indirect signs such as hyperechogenicity of the kidney, dilatation of the collecting system or a subcapsular fluid collection (**Figs. 9.3-9.6**). The sensitivity in directly visualizing the stone is markedly reduced in the upper and mid segments of the ureter due to the overlying bowel loops, whereas it increases to 67% in the distal segment thanks to the acoustic window provided by the bladder distended with urine.

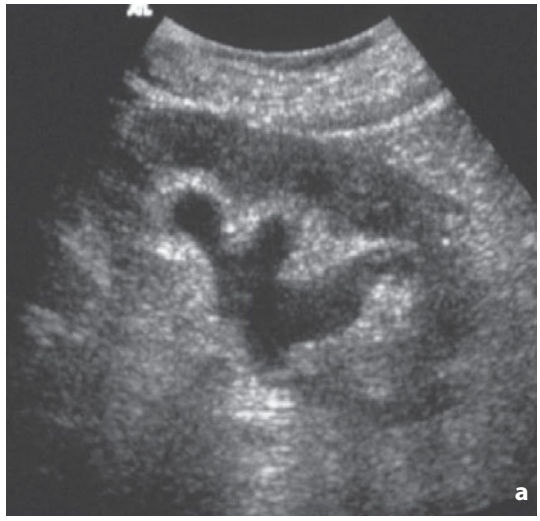

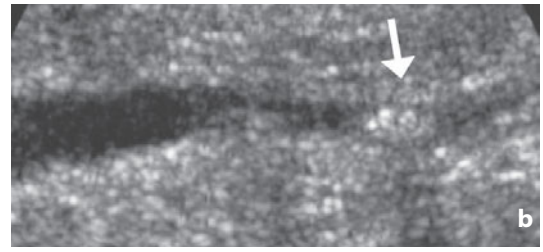

Fig. 9.3a,b. Ultrasonography. Ureteric stone (patient with left renal colic). **a** Moderate dilatation of the pelvis and calices. **b** The dilated ureter continues in the lumbar tract to a stone formation (*arrow*) with evident posterior acoustic shadow

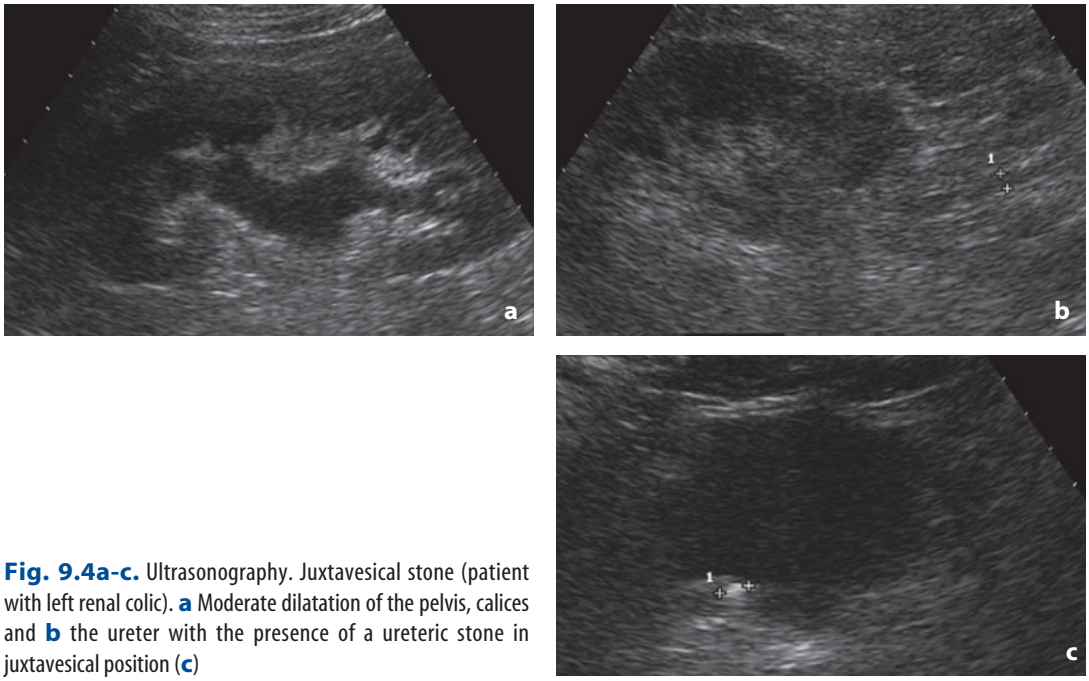

Fig. 9.4a-c. Ultrasonography. Juxtavesical stone (patient with left renal colic). **a** Moderate dilatation of the pelvis, calices and **b** the ureter with the presence of a ureteric stone in juxtavesical position (**c**)

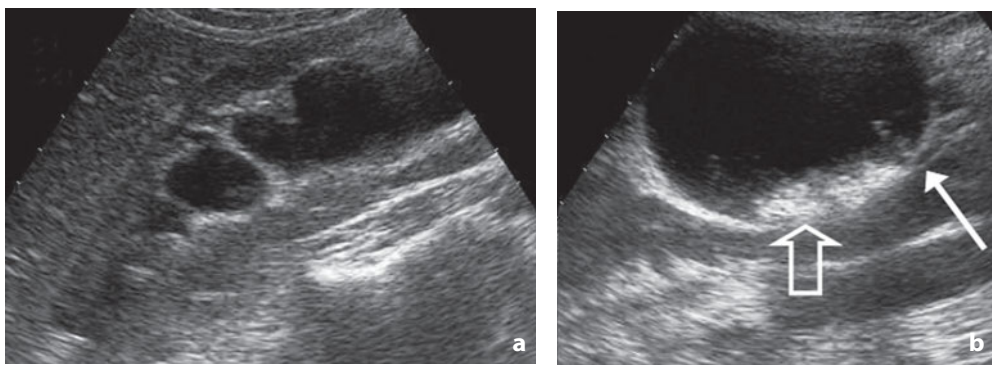

Fig. 9.5a,b. Ultrasonography. Ureteropelvic junction obstruction (patient with right renal colic). US study shows **a** dilatation of the calices and especially **b** the pelvis with the ureter of regular diameter immediately distal to the junction (*arrow*). Obstruction is complicated by multiple stones (*open arrow*)

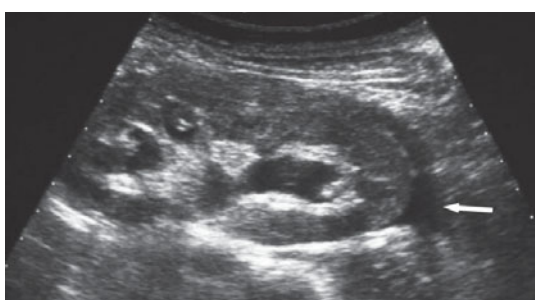

Fig. 9.6. Ultrasonography. Urinoma (patient with left renal colic). Left kidney with dilated pelvis and calices associated with a subcapsular fluid collection at the level of the lower pole attributable to urinoma (*arrow*)

The most important indirect sign is hydronephrosis, which in nonhydrated patients can be identified with a sensitivity of 35-73% and a specificity of 74%. Since several hours are required for the dilatation to become evident, if the patient is not adequately hydrated, up to 20-30% of acute ureteric obstructions may remain unknown. For this

reason the ideal examination technique involves an evaluation of the kidneys, ureters and bladder after slow drip infusion of 500 mL of saline solution or, as an alternative, the oral administration of 500 mL water. In hydrated patients the sensitivity and specificity in identifying hydronephrosis rises to 85% and 100%, respectively.

Diagnostic errors may be committed when obstruction is present and hydronephrosis absent (false negatives) or obstruction is absent and dilatation of the urinary tract is present, which is interpreted as hydronephrosis (false positives) (e.g. in the presence of an anatomically larger ureter).

Doppler can by useful in distinguishing whether a kidney is obstructed or not.

In acute ureteric obstruction vasoactive factors are released which produce a modification of renal hemodynamics with a consequent increase in intrarenal resistance. This can be evaluated by measuring the systolic and end-diastolic velocity peaks at the level of the arcuate arteries. A high resistance index (RI) is suggestive of significant obstruction, whereas a normal RI is correlated with the presence of a nonsignificant obstruction.

The RI in subjects aged between 4 and 60 is on average below 0.70, whereas in elderly patients and in the presence of disease such as renal vein thrombosis, acute renal insufficiency and renal artery stenosis it reaches higher values. Of particular importance is not only the absolute RI, but also the comparison with the RI in the contralateral kidney. The RI in the presence of ureteric obstruction is above 0.70 with a $\Delta RI > 10\%$ between the affected and healthy kidneys.

The literature reports diagnostic accuracy of RI of 90%, although some investigators have suggested it is unreliable.

Color Doppler can be useful for evaluating the ureteric jet of the urine into the bladder. In the presence of severe obstruction it is reduced, less frequent and occasionally with a different direction than the contralateral jet.

US can provide high diagnostic accuracy when it is associated with the plain abdominal film. The association is justified by the better results that the radiogram can obtain in high ureteric stones whereas US is more successful in identifying those located at the ureterovesical junction. US can also provide additional information regarding the renal parenchyma and the bladder, is ideal for follow-up and can also identify alternative causes of acute flank pain such as gallstones, pancreatitis and abdominopelvic masses.

The limitations of US include incomplete visualization of the ureter, operator dependence and interindividual variability.

Grisi G, Stacul F, Cuttin R et al (2000) Cost analysis of different protocols for imaging a patient with acute flank pain. Eur Radiol 10:1620-1627

Heidenreich A, Desgrandschamps F, Terrier F (2002) Modern approach of diagnosis and management of acute flank pain: review of all imaging modalities. Eur Urol 41:351-362

Pepe P, Motta L, Pennini M et al (2005) Functional evaluation of the urinary tract by color-Doppler ultrasonography (CDU) in 100 patients with renal colic. Eur J Radiol 53:131-135

Computed Tomography

Computed tomography (CT) offers numerous possibilities for the evaluation of patients with acute flank pain. In the presence of stones it is able to precisely define the site, size and possible complications. In addition, thanks to its panoramic views the technique is able to identify indirect signs indicating urolithiasis or alternative diagnoses which would explain the symptoms.

The examination is performed with the patient supine. Nonenhanced scans are performed of the entire urinary system from the kidneys to the bladder, which should be sufficiently distended.

With spiral scanners a good compromise between dose delivered to the patient and spatial resolution is achieved using a slice thickness of 3 mm and pitch of 1.6, with a reconstruction thickness of 1.5 mm at 250 mA and 120 kV. In multidetector systems, four-slice acquisitions can be performed with 2.5 mm slice thickness, 1.5 pitch, 120 kV and 30-60 mA based on the physical characteristics of the patent, with automatic tube current modulation to limit radiation exposure. The concept of performing these examinations with a low-dose protocol has in fact been established in the literature. Such protocols are facilitated by the usually high density of the calculi, so that even noisy images can be diagnostic and therefore acceptable.

In addition, curved multiplanar images along the ureter are useful for precisely identifying the ureteric segment of interest (**Fig. 9.7**).

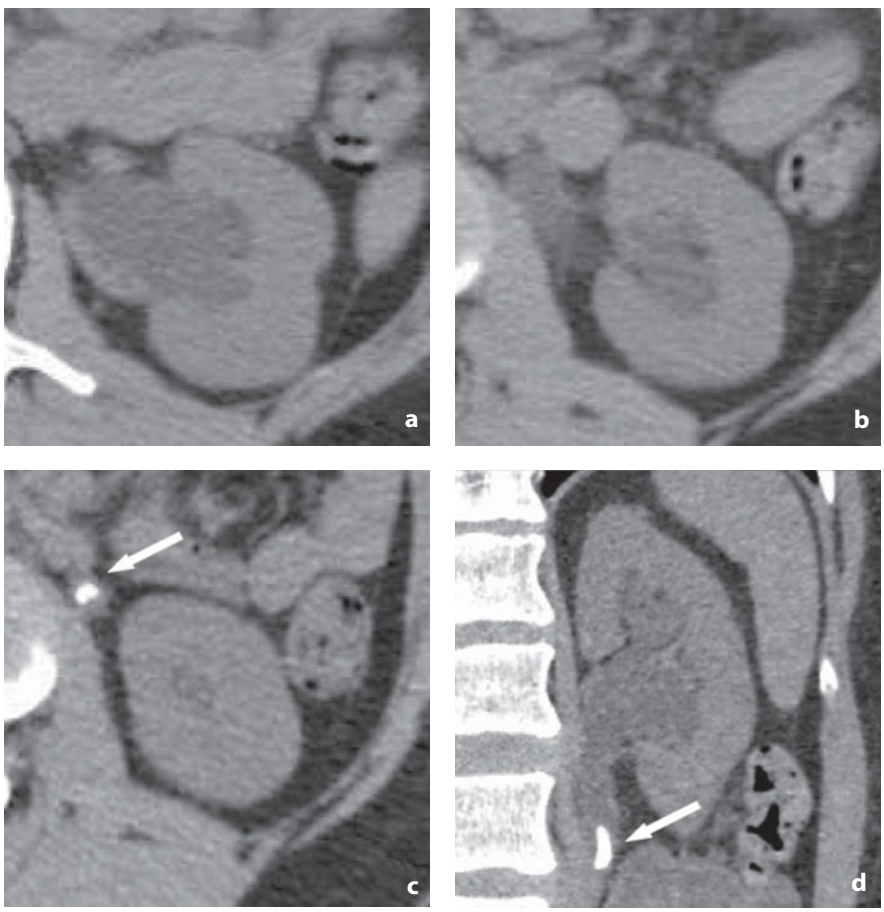

Fig. 9.7a-d. Nonenhanced CT. Ureteric stone (patient with left renal colic). Dilatation of the calices, pelvis (**a**), ureter with periureteric fat stranding (**b**) and stone (*arrow*) in the lumbar segment surrounded by ureteric wall edema (*rim sign*, **c**). The coronal reconstruction precisely shows the maximum dimensions and the site of the stone (*arrow*) (**d**)

The use of contrast medium with image acquisitions in the excretory phase is reserved for very rare cases (**Fig. 9.8**), e.g. in cases of persistent doubt as to whether a calcification is located within the ureter.

All types of stones can be visualized with CT, except for those composed of Indinavir crystals, a protease inhibitor administered to HIV-positive patients.

The literature reports a sensitivity of 94-100% and a specificity of 92-99%.

Possible false positives are due to the incorrect attribution of a phlebolith to the urinary tract. This error can be avoided with the use of multiplanar reconstructions, which are able to demonstrate the comet-tail sign indicating the noncalcified portion of the venous wall adjacent to the phlebolith, and as a last resort the use of contrast media.

Determining whether a calcification belongs to the urinary system or not can be facilitated by the rim sign, i.e. the circumferential soft tissue ring around the ureter at the point of obstruction (**Fig. 9.7**). The sign is not always present, being absent in larger stones, perhaps due to excessive stretching of the wall which limits recognition of the edema.

Indirect signs of stones can help to correctly identify a calcification and recognize the obstruction of the urinary tract in the absence of stones or when these have already been passed.

The estimate of the dilatation of the ureter, rather than being based on absolute values, should be established by comparing it with the contralateral ureter and evaluating the absence of signs of peristalsis, i.e. the uniform dilatation of the entire ureter.

In cases of acute obstruction the dilatation and perhaps the extravasation of the lymphatic vessels contiguous to the ureter and the kidney should be assessed. These appear as periureteric and perirenal fat stranding due to the thickening of the septa between the renal fascia and the renal capsule or between different points of the renal capsule (**Figs. 9.7, 9.9**). The presence of a true opacity in the perirenal space is suggestive

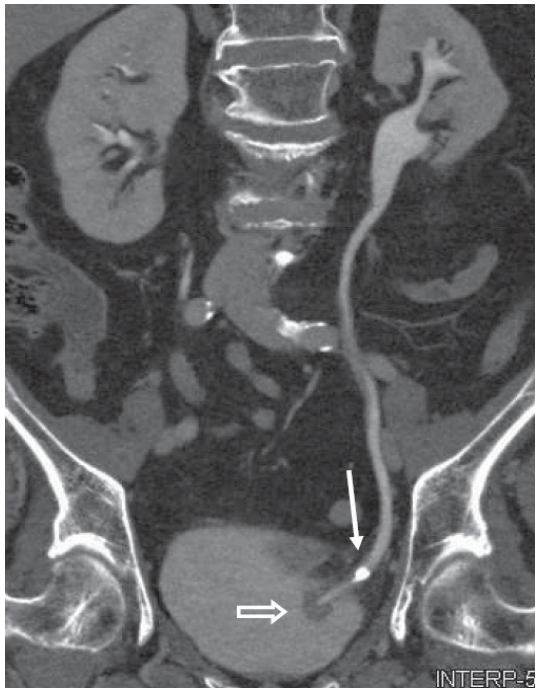

Fig. 9.8. CT urography. Ureteric stone (patient with left renal colic preceded by hematuria). Minimum ionizing particle (MIP) coronal reconstruction. Mild dilatation of the left ureter up to the stone in the pelvic segment in juxtavesical location (*arrow*). A bladder tumor is present at the left ureteric outlet, recognizable as a filling defect (*open arrow*)

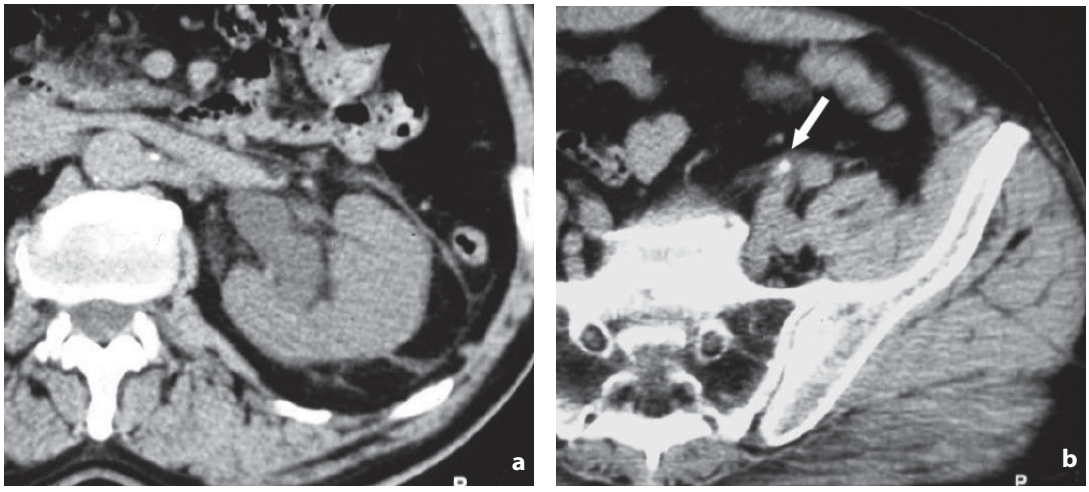

Fig. 9.9a,b. Nonenhanced CT. Ureteric stone (patient with left renal colic). Slight hydronephrosis, thickening of the renal septa and fascia with perirenal (**a**) and periureteric (**b**) stranding. Stone (*arrow*) lodged in the ureter at the crossing with the iliac vessels

of a rupture of the fornices with the consequent formation of a urinoma. The stranding of the fat of the renal sinus is a sign of extravasation of urine at that level. Fat stranding is a sign with a high predictive value, both positive and negative.

Several investigators have reported an increase in kidney dimensions or an increase in parenchymal thickness due to edema as signs secondary to acute obstruction. These signs are not always present and are aspecific, since they can be observed in cases of acute pyelonephritis and renal vein thrombosis, both conditions which present with acute flank pain.

Computed tomography is also useful because it is able to identify other disturbances of the urinary system such as sponge kidney (**Fig. 9.10**), pyelonephritis, renal and perirenal hemorrhage, arteriovenous malformations, ureteropelvic junction obstructions, and ureteric duplication associated with obstruction (**Fig. 9.11**).

The panoramic views provided by CT also enable the identification of extraurinary causes of the symptoms, such as disorders of the gastrointestinal tract, liver, bile ducts, pancreas, aorta or adnexa.

The main role played by CT is to evaluate the size and site of the stone and provide guidance in the clinical management and treatment selection which takes into account the likelihood of the spontaneous passage of the stone, the utility of percutaneous lithotripsy, the placement of a ureteric stent or surgical intervention (**Fig. 9.12**).

The literature has proposed a number of protocols for the study of acute flank pain. In terms of patient management, radiation dose, and diagnostic and therapeutic efficacy, patients should first undergo an abdominal US examination. In cases where diagnostic doubt remains or an anatomic visualization is required for surgical purposes, the preferred second choice is nonenhanced CT with a low-dose protocol for the identification of the stone or secondary signs of its passage. Contrast-enhanced CT is reserved for cases where doubt remains or for the visualization of complications. Urography is no longer performed, not even in select cases, in the light of the greater amount of information provided by CT for comparable costs and a dose delivered to the patient which can be lower than the urography dose when nonenhanced CT is performed, as it is in the large majority of cases.

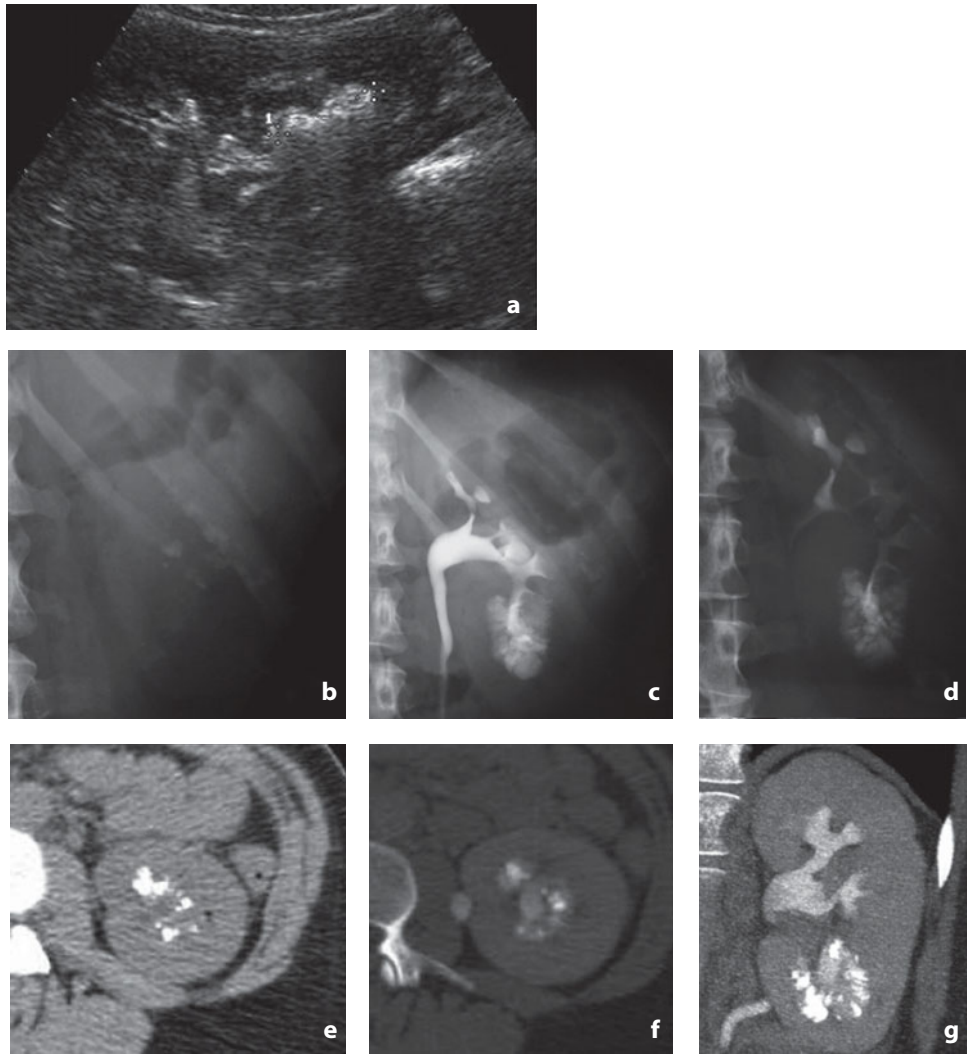

Fig. 9.10a-g. Ultrasonography, urography and CT. Sponge kidney. **a** Sonogram shows a hyperechoic image with posterior acoustic shadowing and lithiasic appearance at the level of the inferior sinus of the left kidney. **b** Plain abdominal film shows minute spotty calcifications in the lower pole of the kidney. **c** At urography multiple papillary streaks and pools of contrast medium distal to the inferior minor calices typical of sponge kidney. **d** Similar appearance in nephrotomography. Of note is the regular morphology of the caliceal fornices. **e** Nonenhanced CT confirms the presence of calcifications. **f,g** Successive low-dose CT urography shows the position of the calcifications outside the pelvicaliceal cavity

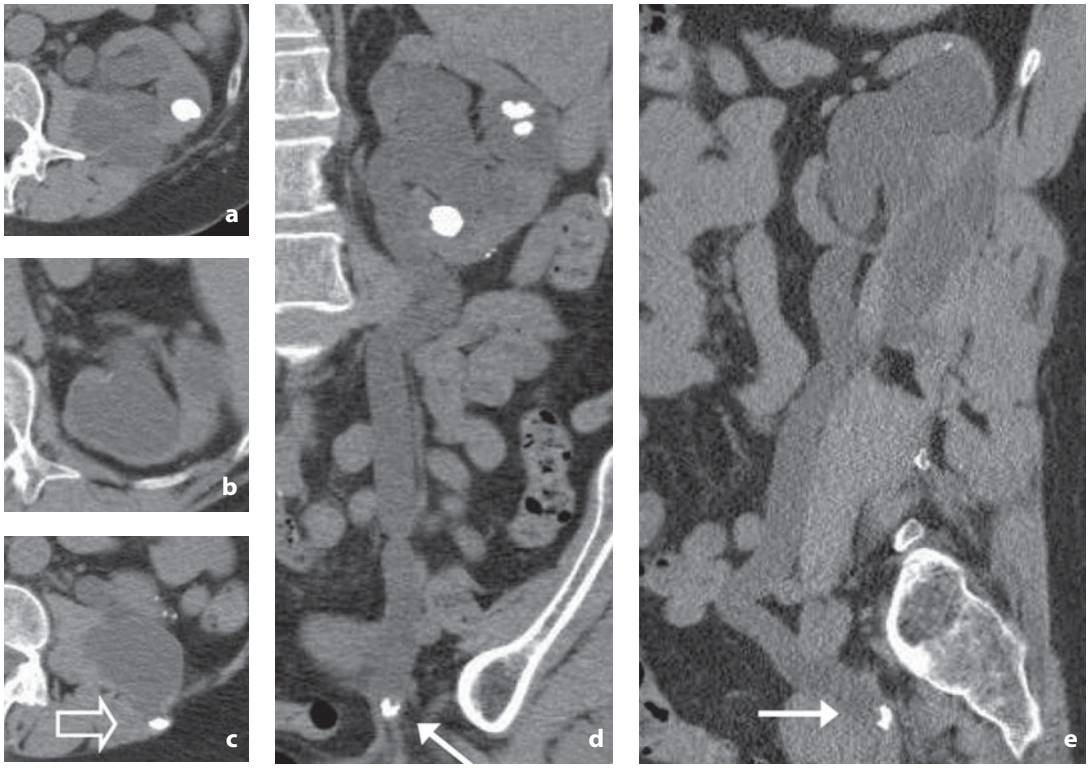

Fig. 9.11a-e. Nonenhanced CT. Complicated lithiasis (patient with left renal colic and fever). **a-c** Native axial and coronal (**d**) and sagittal (**e**) multiplanar reformation (MPR) images. The images show stones in the calices with significant dilatation of the intrarenal cavity and markedly thinned parenchyma. The ureter appears dilated up to the pelvic segment where a stone formation is evident (*arrow*). A voluminous fluid collection is also visible in the iliopsoas muscle associated with the migrated stone (*open arrow*)

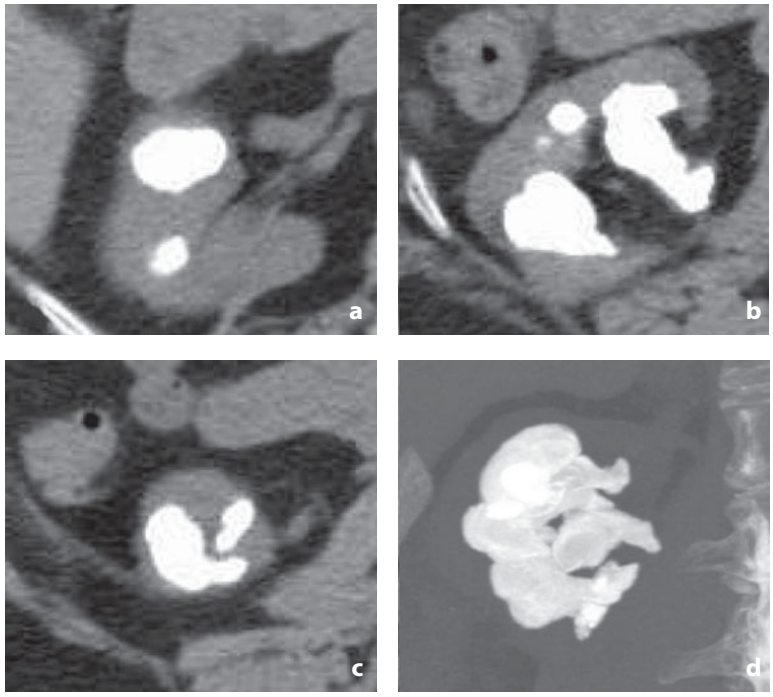

Fig. 9.12a-d. Nonenhanced CT. Staghorn calculus. **a-c** Kidney with staghorn calculus without dilatation of the calices distally in the native axial images and coronal MIP reconstruction (**d**)

Dalrymple NC, Verga M, Anderson KR et al (1998) The value of unenhanced helical computerized tomography in the management of acute flank pain. J Urol 159:735-740

Niall O, Russell J, MacGregor R et al (1999) A comparison of noncontrast computerized tomography with excretory urography in the assessment of acute flank pain. J Urol 61:534-537

Rimondini A, Pozzi Mucelli R, De Denaro M et al (2001) Evaluation of image quality and dose in renal colic: comparison of different spiral-CT protocols. Eur Radiol 11:1140-1146

Sourtzis S, Thibeau Jf, Damry N et al (1999) Radiologic investigation of renal colic: unenhanced helical CT compared with excretory urography. AJR Am J Roentgenol 172:1491-1494

Tack D, Sourtzis S, Delpierre I et al (2003) Low-dose unenhanced multidetector CT of patients with suspected renal colic. AJR Am J Roentgenol 180:305-311

Yilmaz S, Sindel T, Arslan G et al (1998) Renal colic: comparison of spiral CT, US and IVU in the detection of ureteral calculi. Eur Radiol 8:212-221

Renal Inflammation

Clinical Anatomy

Pyelonephritis is an infectious process affecting the kidney, which is caused mainly by Gram, negative bacteria (*E. coli*, *Proteus*, *Pseudomonas*, *Klebsiella* and *Enterococcus* species), whereas less than 20% of cases are caused by Gram, positive bacteria.

The bacteria can reach the kidney by ascending from the lower urinary tract or via hematogenous spread, even from distant foci, or via lymphatic spread along small vessels of the renal interstitium, such as occurs in infections resulting from urinary tract obstructions.

Ascending infections caused by bacteria of the fecal flora are the most common, especially in patients with concomitant urinary tract diseases such as lithiasis or vesicoureteric reflux, thus allowing bacteria which have proliferated in the urinary bladder to ascend to the renal pelvis. Intrarenal reflux allows the bacteria to penetrate the parenchyma through the tubules, especially at the renal poles where the papillae tend to have flattened or concave apices.

Acute pyelonephritis can be defined as a clinical syndrome characterized by lumbar pain and hyperpyrexia, associated with laboratory findings of renal bacterial infection, including leukocytosis, pyuria, bacteriuria and positive urine culture. In anatomopathologic terms pyelonephritis is a bacterial infection of the kidney, with consequent acute inflammation often involving the pelvis and renal parenchyma of both kidneys. This causes suppurative interstitial inflammation with tubular necrosis. Distribution may be patchy with some parenchymal sparing, and may develop to become diffuse or coalesce into focal areas which evolve into abscesses. At the height of inflammation the tubules become clogged with leukocytes which can cause focal intrarenal obstruction. At the same time an intense vasoconstriction of the arteries and arterioles develops within the regions affected by inflammation. In ascending pyelonephritis the distribution is characteristically patchy or lobular, with a clear boundary between the areas involved in and the areas spared from the process. The infected parenchyma presents streaks or yellowish wedge-shaped areas which extend for the entire parenchymal thickness, from the apex of the papillae to the cortical surface. In more severe cases the entire renal parenchyma may be involved.

Hematogenous **abscesses** are found more often in intravenous drug users, in patients with other focal infections and in immunocompromised patients. The most common causative agent is *Staphylococcus aureus*. The initial lesions are usually

multiple, circular and located within the cortex. In more severe cases they may even have a hemorrhagic appearance. At 24-48 h after seeding the lesions expand to involve the medulla and the distinction between hematogenous spread and ascending pyelonephritis can no longer be made.

The natural defenses of the host and antibiotic therapy are usually able to successfully control infection, but in some cases there occurs significant tissue destruction with necrosis and the formation of multiple microabscesses which coalesce into larger abscesses. During the maturation phase granulation tissue develops around the abscess. The renal abscess is usually diagnosed prior to its extension to contiguous organs, but in the event of progression it can extend towards the psoas muscle and into the retroperitoneal space, or towards the superficial planes or in the direction of the peritoneum. Some advanced forms which develop superiorly may involve the pleural cavity to the point of developing an empyema.

Usually the correct diagnosis is made in a relatively early phase and targeted therapy is able to resolve the infection without the development of complications.

The more advanced cases of acute obstructive pyelonephritis may develop **pyonephrosis**, due to the accumulation of purulent fluid in the dilated collecting system.

Both the focal and the diffuse forms of pyelonephritis may regress without permanent damage, an outcome which is relatively frequent in adults, or may lead to renal scarring. In children focal scarring can develop involving the entire layer of parenchyma, while in adults there typically forms a depression on the cortical surface associated with fibrosis and deformation of the underlying calyx.

Emphysematous pyelonephritis is a severe necrotizing form of acute pyelonephritis in which a number of bacteria species provoke the fermentation of glucose present in the tissue with the consequent formation of gas. In 50% of patients a flank mass may be palpable with the typical crepitation of subcutaneous emphysema from the flank to the thigh. The condition progresses rapidly to septic shock with a 50% mortality rate. Ninety percent of patients who develop this form of acute pyelonephritis suffer from poorly controlled diabetes mellitus, while nondiabetic patients are affected by an obstruction of the collecting system due either to a urinary stone or tumor.

Fungal pyelonephritis is very rare and mainly affects immunocompromised or diabetic patients. It results from hematogenous spread to the kidney of fungi, usually *Candida albicans.* Once they have been filtered by the glomerulus the fungi become lodged in the distal tubules causing the formation of multiple cortical and medullary abscesses. The fungal form is associated with a high mortality rate.

Chronic pyelonephritis is a tubulointerstitial inflammation associated with renal scarring, with the involvement of the calices and pelvis. The condition is due to a recurrent or persistent infection with progressive parenchymal destruction, or represents the residue of an earlier infection which has become inactive. Usually it is the result of vesicoureteric or intrarenal reflux in children, although it can be associated with other clinical conditions which lead to stasis, such as chronic obstruction, the presence of urinary stones, neurogenic bladder and urinary diversion.

The term **reflux nephropathy** indicates the disease caused by the sequence of reflux, infection of the upper urinary tract, pyelonephritis and consequent renal scarring. The kidney appears with evident irregular scarring which involves the cortex and medulla above the dilated and clubbed calices. Reflux nephropathy is typically evident in the polar zones. Associated with this pattern are signs of possible new inflammation. The scarring can be focal, but in the event of diffuse distribution the residual parenchyma may undergo compensatory hypertrophy, thus provoking an even more marked deformation of the renal profile with the appearance of a pseudotumor.

In **renal tuberculosis** *Mycobacterium tuberculosis* by its nature causes a chronic infection. After primary infection in the kidney an intraparenchymal nodule (granuloma) is initially formed within the cortex which remains stable and asymptomatic for many years. Then either reinfection or reactivation occurs which leads to extension to

the medulla, i.e. the caliceal system, where it rapidly leads to ulceration with caliceal deformation.

A urine test positive to *M. tuberculosis* will only occur if there is erosion of the calix with opening of the granuloma into the collecting system.

When the granuloma opens into the collecting system the disease may progress in three possible directions: (1) extended cavitation, i.e. open form; (2) fibrosclerosis with the consequent formation of a noncommunicating cavity (closed form), with pericavitary connective tissue closing the neck of the calix and leaving a more or less broad cavity; and (3) a mixed presentation, where both old cavities coexist with initial forms of erosion of the calices caused by recurrent inflammation – the initial phase of fibrosclerosis is followed by the development of new lesions secondary to additional waves of bacteremia. The end result in nontreated forms is the destruction with loss of function and calcification of the entire kidney (tuberculous autonephrectomy).

A particular form of infection is **chronic xanthogranulomatous pyelonephritis**, which is characterized by the destruction and replacement of the parenchyma by foamy macrophages (the definition derives from their high lipid content). It almost always affects a single kidney in a diffuse fashion, causing enlargement of the organ, fibrosis around the renal pelvis, hydronephrosis and characteristic yellowish lobulated masses which replace the parenchyma. With time, the cortex decreases in thickness and can contain multiple abscesses surrounded by xanthoid tissue. Causative agents are commonly *E. coli* and *Proteus* species and result from chronic obstruction: 80% of patients have a staghorn calculus or stone obstructing part of the pelvicaliceal system.

The process may remain confined to the kidney or extend perirenally to involve the pararenal spaces and retroperitoneal structures such as the psoas.

A less common occurrence is focal extension. The expansive form gives rise to swelling which can mimic renal carcinoma.

Chronic pyelonephritis is characterized by vague symptoms with insidious and less characteristic onset than the acute form. The patient comes to the physician's attention in a later phase and the diagnosis is therefore made when renal scarring is already advanced, even with renal failure and reduced renal size.

Hill GS (1989) Uropathology. Churchill-Livingstone, New York, pp 279-429

Kenney PJ (2000) Chronic urinary tract infection. In: Pollack HM, McClennan BL (eds) Clinical urography. WB Saunders Co., Philadelphia, pp 951-975

Medical Research Council Bacteriuria Committee (1979) Recommended terminology of urinary-tract infection. BMJ 2:717-719

Roberts JA (1991) Etiology and pathophysiology of pyelonephritis. Am J Kidney Dis 17:1-9

Diagnostic Imaging

The diagnosis of renal infections is usually made on a clinical basis together with laboratory findings. Diagnostic imaging is reserved for doubtful cases or the study of pyelonephritis in patients who fail to respond to treatment or at high risk of complications, such as diabetic and immunocompromised patients.

The role played by diagnostic imaging regards both the identification of the lesion and evaluation of its intra- and extrarenal extension, and follow-up during treatment. The current guidelines advocate the use of imaging even in noncomplicated cases of pyelonephritis diagnosed with microbiologic studies in males and females who have suffered two or three infections of the upper urinary tract in the space of twelve months. In such cases a US examination is indicated for the study of both the kidney

(and possible associated stone formation) and the lower urinary tract, with the calculation of postvoid residual urine volume and the dimensions of the prostate.

US has good sensitivity. Although it is unable to visualize the renal fascia and is therefore unable to evaluate the perirenal extension of the inflammation, the technique nonetheless plays an important role. The absence of ionizing radiation allows its use during pregnancy and repeated use during follow-up. It is also useful as a guide for drainage placement.

CT is highly sensitive and accurate and has several indications: in cases of persistent septic fever with negative US; after US to better evaluate the extension of the inflammatory process; in follow-up, only in cases where US proves insufficient.

Magnetic resonance (MR) currently only plays a minor role in diagnostic imaging due to its limited availability and elevated costs. It is nonetheless a technique to bear in mind, particularly in children and patients who cannot be administered iodinated contrast material.

Renal 99-Tc DMSA scintigraphy is extremely sensitive and especially useful in children, although it is unable to distinguish the disease pattern, the location of inflammation or the perirenal extension.

Acute Pyelonephritis

In the diffuse form **ultrasonography** is able to identify a kidney with increased parenchymal thickness (Fig. 9.13) and hypo-anechoic areas, whereas in the focal form

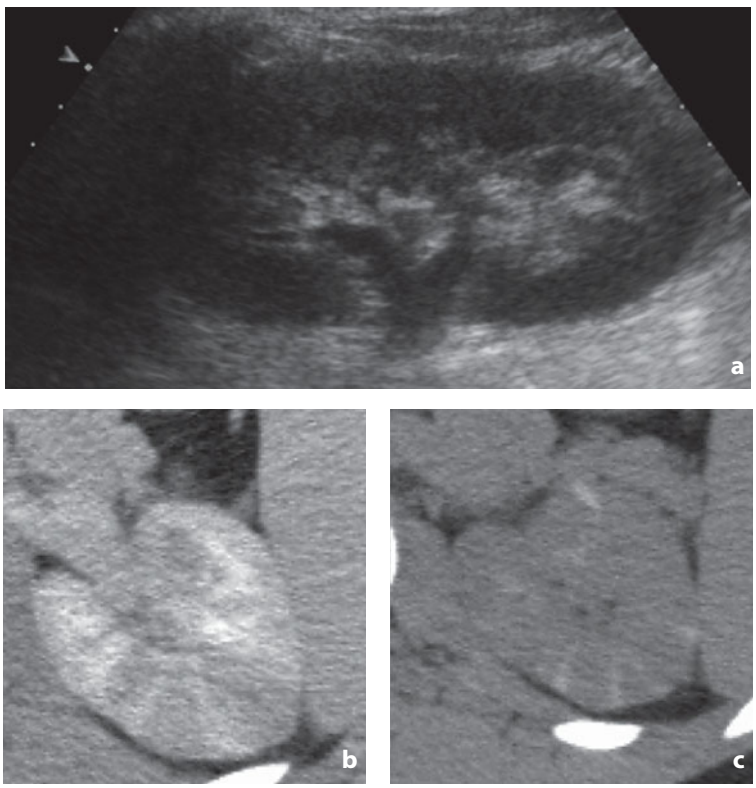

Fig. 9.13a-c. Ultrasonography and contrast-enhanced CT. Acute diffuse pyelonephritis. **a** The US study of the kidney shows a moderate increase in parenchymal thickness. **b** At CT in the nephrographic phase the areas affected by pyelonephritis appear as hypoattenuating wedge-shaped areas with ill-defined margins. **c** In the delayed images, acquired 3 h after contrast medium injection, some of the areas show nonuniform contrast medium uptake (delayed nephrogram)

there appear circular hypoechoic areas with ill-defined margins (**Figs. 9.14, 9.15**). In rare cases there may also be hyperechoic areas if the inflammatory process is hemorrhagic. The adipose tissue of the renal sinus may be less clearly visualized due to imbibition and compression.

US can be useful in suggesting the presence of a congenital anomaly, such as ureteropelvic junction obstruction, and identifying alterations of the renal parenchyma and fluid collections in the perirenal space. There are, however, a number of limitations to the technique. Diffuse thickening is not always identifiable and the evaluation of complications and especially the extension of the inflammatory process is not precise, since the perirenal fascia cannot be recognized.

The use of **Doppler**, especially power Doppler for the visualization of slow flow, can increase sensitivity regardless of the study angle by demonstrating hypoperfusion of the hypoechoic areas which correspond to perilesional edema. False positives may occur at the level of the left upper renal pole due to difficulties encountered in the presence of intestinal gas or overlying ribs. False negatives typically occur in a very early phase when the edema produces a decrease in venous return but as yet no hypoperfusion.

This technique has proven particularly useful in children, thanks to its high sensitivity and specificity, which are comparable to the commonly used technique of 99-Tc DMSA scintigraphy, without the drawbacks of ionizing radiation.

The sensitivity of US appears to be notably increased with the use of contrast media, which enable improved visualization of hypoperfused areas in the renal parenchyma.

In the past acute pyelonephritis was studied with **urography**, a technique which is able to visualize the contours of the renal parenchyma, analyze the nephrographic effect and depict the collecting system. However, the technique is able to identify the infection and some of its complications only on the basis of secondary signs of distortion

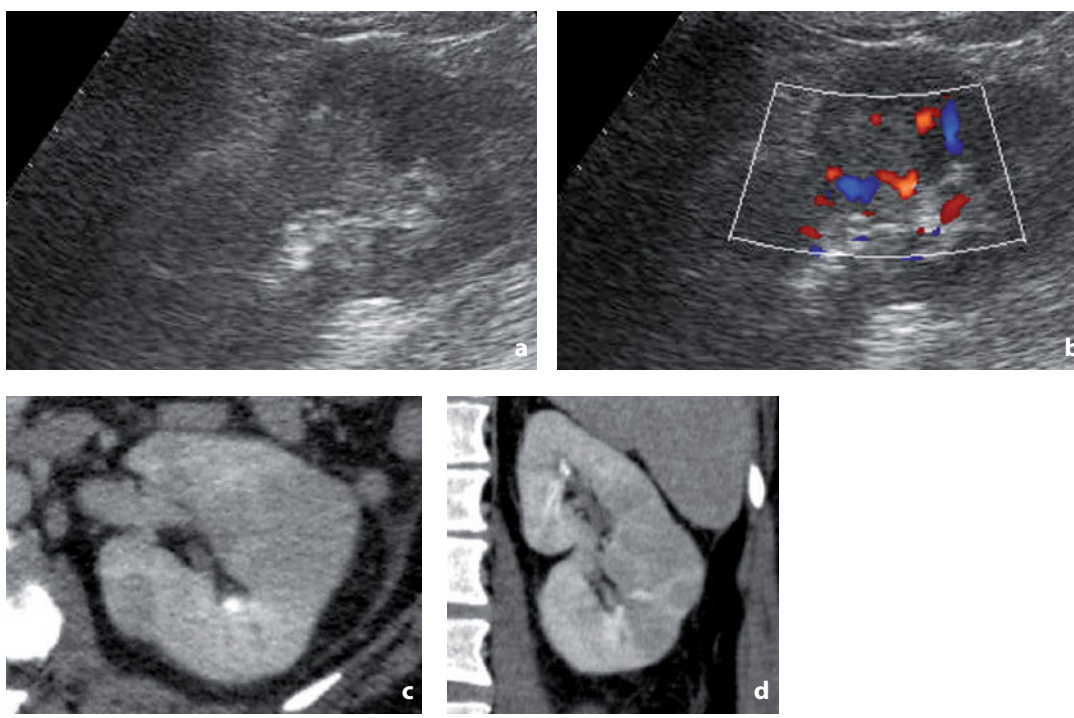

Fig. 9.14a-d. Ultrasonography and contrast-enhanced CT. Acute focal pyelonephritis. **a** The US study shows ill-defined hypoechoic swelling with reduced perfusion at color Doppler (**b**). The contrast-enhanced CT study in the axial (**c**) and coronal (**d**) planes confirms the hypoattenuating lesion with ill-defined margins, which produces a bulge in the renal profile

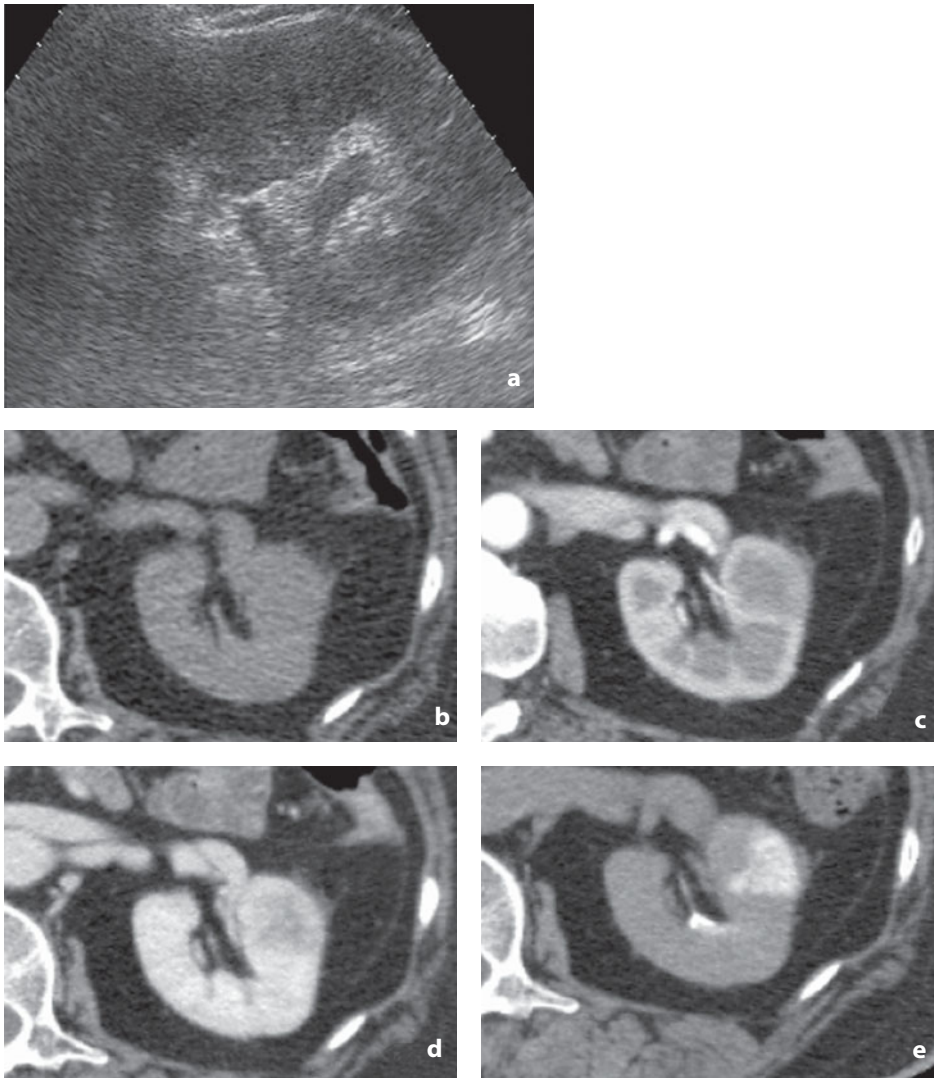

Fig. 9.15a-e. Ultrasonography and contrast-enhanced CT. Acute focal pyelonephritis. **a** The US study shows moderate bulging of the renal profile corresponding to a hypoechoic area with ill-defined margins. **b** The nonenhanced CT image shows slight hypoattenuating swelling with ill-defined margins and perirenal fat stranding. **c,d** After contrast medium injection the presence of a hypoattenuating area is poorly defined in the cortical phase (**c**) but clear in the parenchymal phase (**d**). **e** In the delayed phase, 3 h after contrast medium injection, the formerly hypoattenuating area is now clearly hyperattenuating due to delayed nephrogram resulting from tissue edema and tubular obstruction

of the pelvicaliceal system, such that 75% of urographies are negative even in the presence of pyelonephritis. The findings which can be identified include renal enlargement, compression of the collecting system, and a decreased concentration and delayed excretion of contrast medium, with a striated and persistent nephrogram.

Urography is able to correctly identify the presence of papillary necrosis, an important complication more common in diabetic patients, by the presence of thin streaks and the accumulation of contrast medium at the level of the papillae.

In general, however, urography should be considered a relatively expensive and ineffective technique which exposes the patient to a moderate dose of radiation. It should be avoided in favor of US or CT, which, with the latest multidetector-row scanners and the technique of CT urography, offers a visualization similar to the classic

technique, but associated with precise information on the renal parenchyma which was formerly impossible to obtain.

Except in select cases where an evaluation of the presence of disease favoring the development of acute pyelonephritis is desirable, the study of acute pyelonephritis is performed with conventional **computed tomography**. In particular, nonenhanced scans associated with a parenchymal and a delayed phase acquired after 3-6 h provide important information.

Nonenhanced renal scans are useful in identifying the presence of stone formations or parenchymal calcifications, the presence of gas and, in the rare form of hemorrhagic bacterial nephritis, a hyperattenuating wedge-shaped or oval area. They are also able to demonstrate focal and diffuse enlargement of the kidney due to dilatation and possibly extravasation of the lymphatic vessels. This sign, however, should be evaluated with great caution, in that it is also correlated with renal colic, trauma and prior infection.

After the injection of contrast medium the best phase for evaluating the signs of pyelonephritis is the parenchymal phase. The typical finding is an ill-defined wedge-shaped area which extends from the papilla to the cortical surface (**Fig. 9.15**), with a reduced differentiation between cortex and medulla and associated renal swelling. According to the guidelines of the Society of Uroradiology, all hypoattenuating parenchymal areas on CT should be considered acute pyelonephritis. The disease should then be characterized on the basis of diffuse or focal extension (**Figs. 9.14, 9.15**), the presence of swelling or enlargement of the entire kidney, uni- or bilateral involvement and the presence of complications.

In addition to the hypoattenuation produced by vasospasm, the obstructed tubules and the interstitial edema which characterize the nonfunctioning areas of parenchyma, a striated nephrogram is also distinguishable due to the alternation between functioning tubules and tubules obstructed with leukocytes (**Fig. 9.16**).

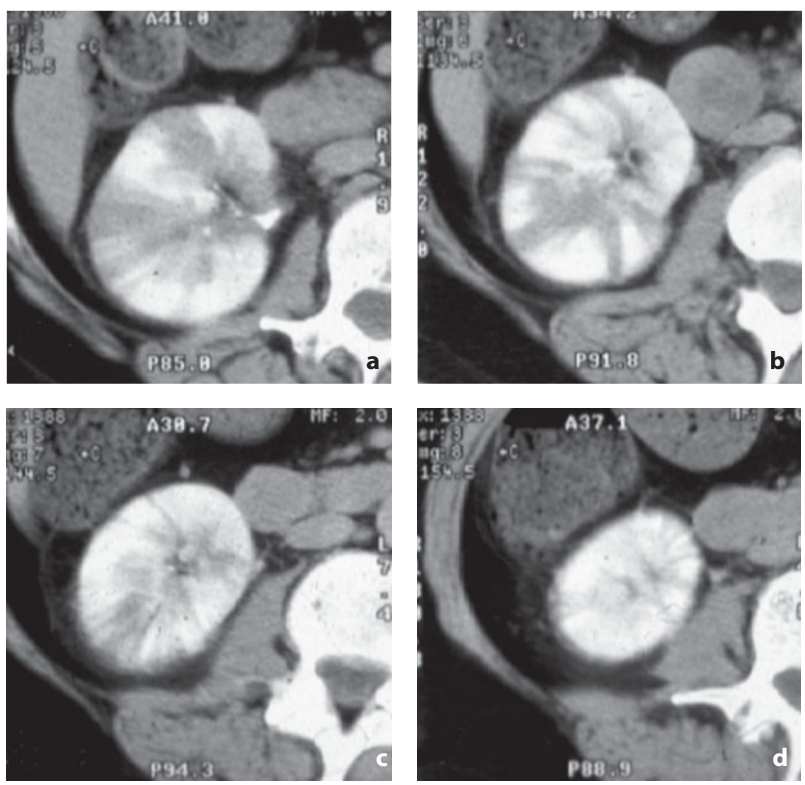

Fig. 9.16a-d. Contrast-enhanced CT. Acute diffuse pyelonephritis. **a-d** A striated nephrogram after contrast medium injection is visible, produced by the alternation of functioning tubules filled with contrast material and tubules clogged with leukocytes. The images also show hypoattenuating wedge-shaped areas resulting from edema and vasospasm (**a, b**)

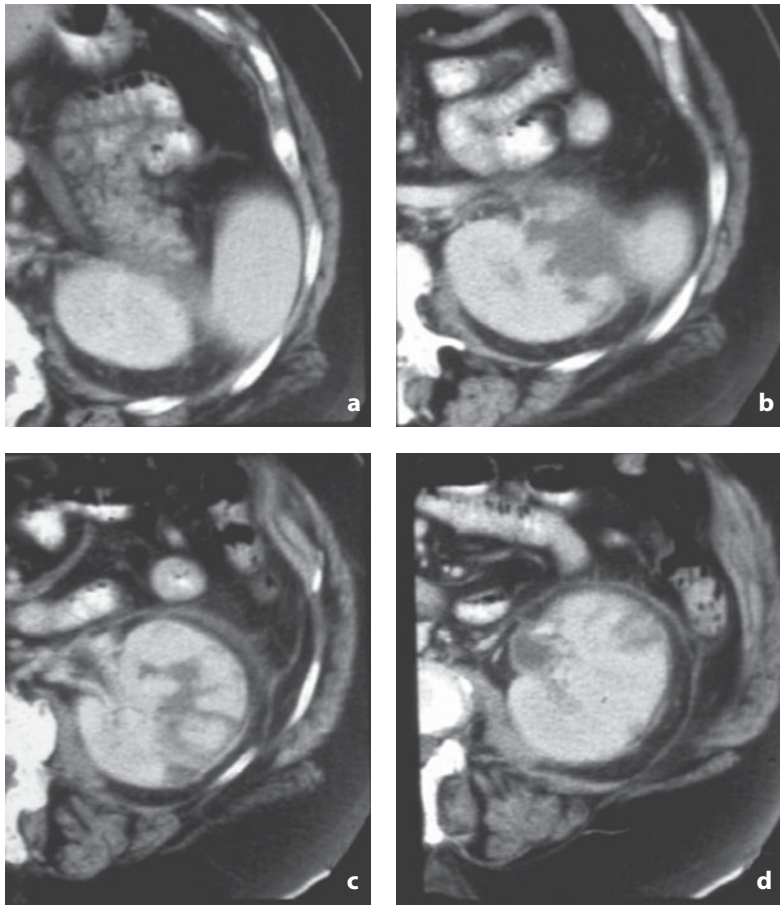

Fig. 9.17a-d. Contrast-enhanced CT. Acute complicated pyelonephritis (diabetic patient). The CT study shows broad hypoattenuating bands indicative of acute pyelonephritis (**c, d**), complicated by liquefaction and extension into the perirenal space (**b**). Ill-defined margins of the anterior perirenal fat can also be seen (**a, b**). The images also show thickening of the anterior renal fascia (**c, d**) and thickening of the wall of the renal pelvis (**d**)

Other CT signs of pyelonephritis are stranding of the renal sinus and perirenal fat, thickening of the renal fascia and caliceal compression by the renal parenchyma and swollen pelvicaliceal wall. CT provides good visualization of the renal fascia and therefore a precise evaluation of the extension of the inflammatory process (**Figs. 9.17, 9.18**).

Delayed CT images acquired at 3 h are useful for a more precise evaluation of extension because the hyperattenuating areas which produce a nonuniform nephrogram in this phase correspond to simple areas of interstitial edema (localized ischemia which can be identified even in areas which earlier appeared healthy) (**Figs. 9.13, 9.15**), whereas those areas which continue to be hypoattenuating represent the real site of infection. The delayed nephrogram is produced on the one hand by localized ischemia due to vasospasm or compression of the arterial bed by the interstitial edema, and on the other by obstruction of the tubules caused by leukocytes and tubule cells.

The follow-up CT study of acute renal infections can be used to evaluate the efficacy of antibiotic therapy. CT studies have demonstrated that despite clinical regression several signs of disease can persist even weeks or months later, and that renal scarring, even in adults, occurs in many more cases than previously thought.

Magnetic resonance (MR) provides good visualization of the kidney, the renal pelvis, the collecting system and the perirenal space. As with CT, the technique can identify enlargement of the kidney and perirenal fat stranding.

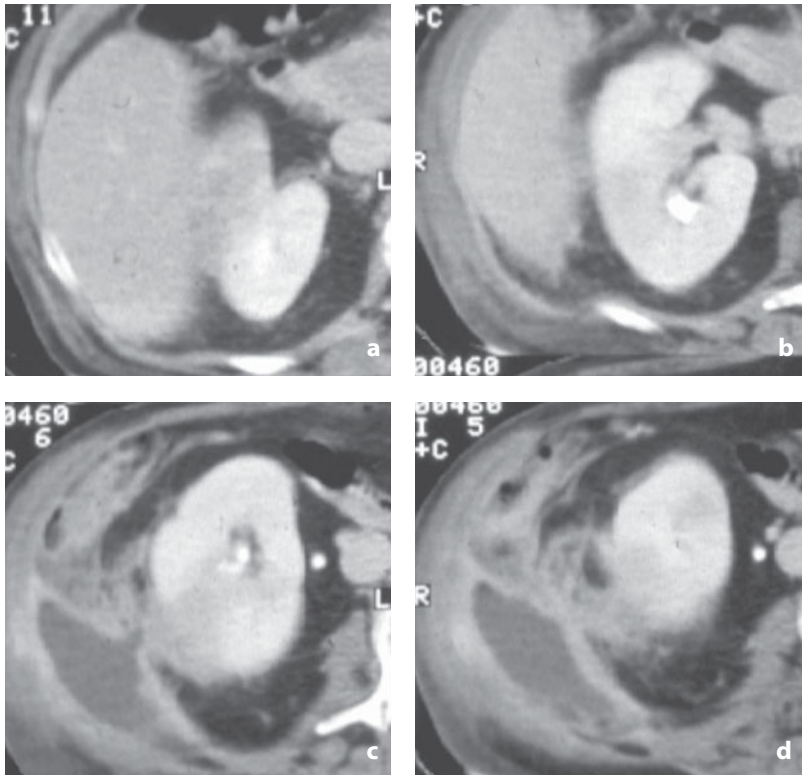

Fig. 9.18a-d. Contrast-enhanced CT. Perirenal abscess. **a-c** The kidney presents a hypoattenuating wedge-shaped area attributable to acute focal pyelonephritis, with associated perirenal fat stranding, thickening of the posterior perirenal fascia and a large posterior perirenal fluid collection (**c,d**)

Parenchymal edema is visualized as areas of low signal intensity in T1-weighted images and elevated signal in T2, with a decreased differentiation between cortex and medulla. Fast inversion recovery sequences after the administration of gadolinium show hyperintensity in the areas of pyelonephritis and low signal in the healthy areas, with a striated pyelogram, thus rendering the lesions readily identifiable which confers the technique a sensitivity comparable, if not superior, to cortical scintigraphy. MR pyelography is also useful for evaluating the dilatation of the pelvicaliceal system and documenting the presence of obstructions.

Browne RFJ, Zwirewich C, Torreggiani WC (2004) Imaging of urinary tract infection in the adult. Eur Radiol 14 [Suppl 3]: E168-183

Kawashima A, Sandler CM, Goldman SM et al (1997) CT of renal inflammatory disease. RadioGraphics 17:851-866

Kim JH, Eun HW, Lee HK et al (2003) Renal perfusion abnormality. Coded harmonic angio US with contrast agent. Acta Radiol 44:166-171

Sakaraya ME, Arslan H, Erkoc R et al (1998) The role of power Doppler ultrasonography in the diagnosis of acute pyelonephritis. Br J Urol 81:360-363

Stunnel H, Buckley O, Feeney J et al (2007) Imaging of acute pyelonephritis in the adult. Eur Radiol 17:1820-1828

Webb JAW (1997) The role of imaging in adult acute urinary tract infection. Eur Radiol 7:837-843

Pyonephrosis

In pyelonephritis **ultrasonography** is able to provide precise information regarding not only the renal parenchyma but also the presence of hydronephrosis and obstruction of the upper urinary tract, as well as to recognize the progression towards pyonephrosis by the presence of echogenic foci in the collecting system, occasionally with a layering of low-amplitude echoes of fluid and debris deposited in the recesses of the collecting system. US is useful for planning the immediate drainage of the renal pelvis with US-guided placement of a percutaneous nephrostomy. A negative US study, however, does not rule out pyonephrosis, since the caliceal distension in the early stages can be minimal, making its identification difficult.

The distinction between hydronephrosis and pyonephrosis at **computed tomography** can be difficult. The presence of debris within the renal pelvis is not always evident, while increased pelvic and ureteric wall thickness, perirenal fat stranding and a certain degree of striated nephrogram can also be present in obstructive uropathy. In general the kidney is enlarged and the nephrogram is reduced or absent. The pyelogram is reduced or absent with dilatation of the pelvicaliceal system and the contrast medium in the renal pelvis distributed above the purulent fluid. Extrarenal extension may also be present. CT is able to visualize the position and morphology of the stone causing the upper urinary tract obstruction. Inflammatory debris and blood clots which may obstruct the collecting system can also be visualized as filling defects.

Magnetic resonance performed with conventional sequences is not able to offer much more than CT in the identification of pyonephrosis. An attenuated signal in T1-weighted images and an increase in signal intensity in T2 can be observed. Occasionally the debris in the collecting system can be visualized. In contrast, diffusion-weighted sequences which study the motion of water molecules are particularly effective. They have demonstrated very high diagnostic accuracy in the differential diagnosis between hydronephrosis and pyonephrosis (in the latter diffusion is reduced due to the viscous contents of the collecting system). These sequences also have the advantage of an acquisition time of several seconds. Lastly, they can also be useful in MR pyelography.

Chan JH, Tsui EY, Luk SH et al (2001) MR diffusion-weighted imaging of kidney: differentiation between hydronephrosis and pyonephrosis. Clin Imaging 25:110-113

Coleman BJ, Arger PH, Mulhern CB Jr et al (1981) Pyonephrosis: sonography in the diagnosis and management. AJR Am J Roentgenol 137:939-943

Fultz PJ, Hampton WR, Totterman SM (1993) Computed tomography of pyonephrosis. Abdom Imaging 18:82-87

Kawashima A, Sandler CM, Goldman SM (2000) Imaging in acute renal infection. Br J Urol Int 86:70-79

Renal Abscesses

Renal abscesses can appear on **ultrasonography** as simple hypo-anechoic fluid collections with well-defined margins and increased transmission of the ultrasound beam (Fig. 9.19). Occasionally signs of their more complex nature are recognizable, such as mobile internal echoes, fluid levels or increased wall thickness. The presence of an acoustic shadow within the cavity is suggestive of the presence of gas.

Computed tomography is able to identify even small fluid areas, an early sign of the development towards the formation of an abscess (Fig. 9.20). The appearance of a hypoattenuating rim, which in this phase surrounds the abscess, confirms the presence of even microabscesses. The mature abscess appears with well-defined borders,

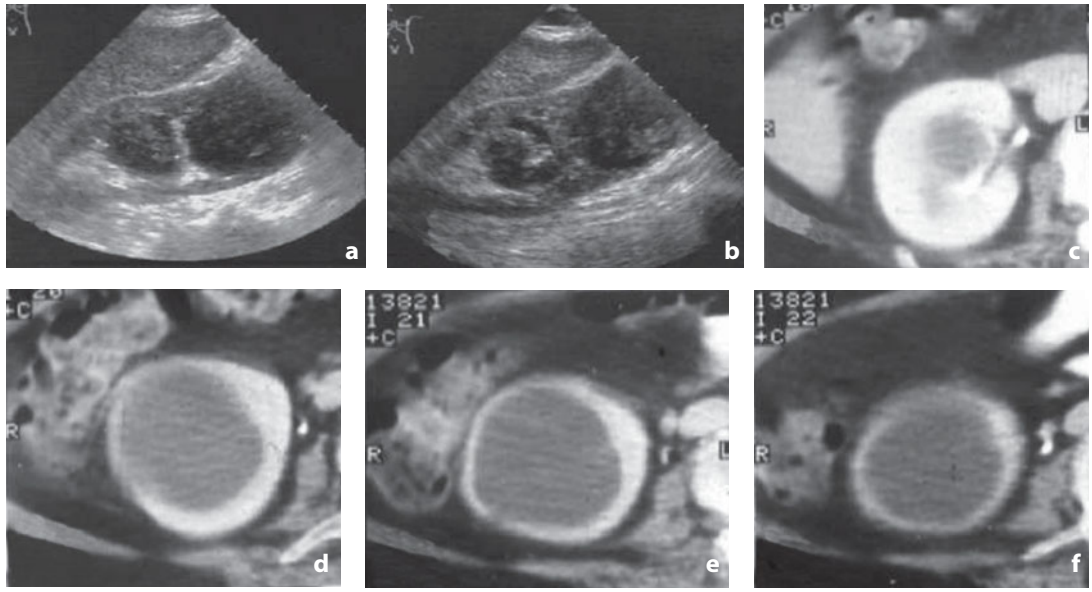

Fig. 9.19a-f. Ultrasonography and contrast-enhanced CT. Renal abscesses. **a, b** The US study shows two hypoechoic collections with several mobile internal echoes and moderate posterior acoustic enhancement. **c-f** On contrast-enhanced CT the abscesses appear as hypoattenuating fluid collections, with above-water attenuation, well-defined margins and nonenhancing in the liquefied area. CT provides an excellent evaluation of the extension of the lesion. In this case the abscesses are confined to the kidney

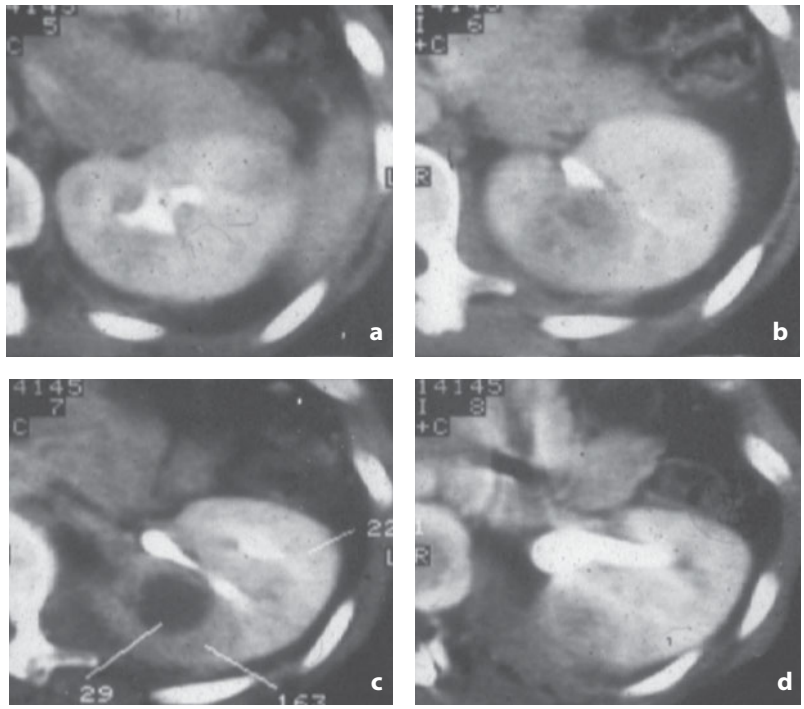

Fig. 9.20a-d. Contrast-enhanced CT. Renal abscess. Adjacent to a calix of the middle system the presence of a hypoattenuating area is identifiable with ill-defined margins due to edema, attributable to focal pyelonephritis. The lesion is complicated by the formation of an abscess, identifiable as an above-water-density lesion with well-defined margins (**d**). Perirenal fat stranding is also appreciable

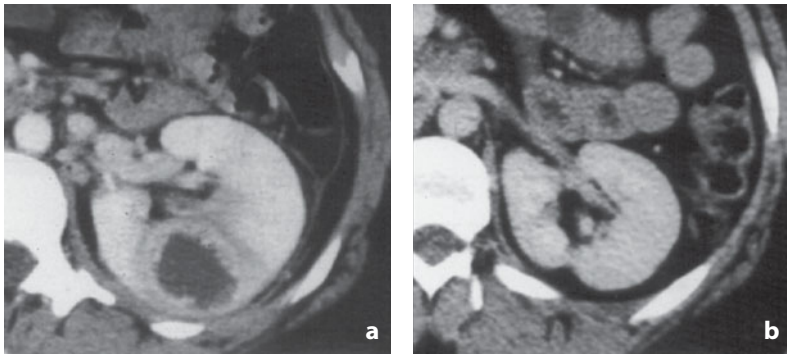

Fig. 9.21a,b. Contrast-enhanced CT. **a** The image shows a rounded lesion, water-like attenuation and a thick irregular wall attributable to an abscess. **b** After medical therapy complete resolution is achieved with residual parenchymal scarring

with an enhancing capsule or pseudocapsule in the delayed views. The CT images help to identify abscesses which respond poorly to medical therapy alone, i.e. those with a diameter >5 cm or which involve more than one organ, for which immediate surgery is warranted. For the other abscesses medical therapy is best begun with immediate CT follow-up to evaluate whether the abscess has regressed (Fig. 9.21) or whether more invasive treatment is warranted.

On **magnetic resonance** images renal abscesses appear as areas of nonuniform low signal intensity in T1-weighted images and elevated signal in T2, in accordance with the quantity of debris and fluid present. Occasionally fluid-fluid levels may be seen. MR is also able to demonstrate the pararenal extension of the lesion.

Browne RFJ, Zwirewich C, Torreggiani WC (2004) Imaging of urinary tract infection in the adult. Eur Radiol 14[Suppl 3]:E168-183

Kawashima A, Sandler CM, Goldman SM (2000) Imaging in acute renal infection. Br J Urol Int 86: S70-S79

Papanicolaou N, Pfister RC (1986) Acute renal infections. Radiol Clin North Am 34:965-995

Emphysematous Pyelonephritis

Plain abdominal film shows gaseous marbling of the entire kidney in 85% of patients. This finding is often incorrectly interpreted as intestinal gas. In the early phases of the disease the gas may be distributed in radial streaks following the orientation of the pyramids, while in more advanced cases the gas tends to have a crescent distribution within the renal fascia.

On **computed tomography** images the appearance of gaseous collections due to the presence of anaerobic organisms is more clear. Multiple bubbles or linear streaks of gas radiating from the papillae can be discerned, while the gas extends by dissecting the layers of interstitium (Fig. 9.22). Associated with these findings are the signs of tissue necrosis and abscess formation described above. The presence of fluid collections within the kidney is a negative prognostic indicator. Three stages of development have been identified, whereby gas is present only in the parenchyma, in the perirenal tissue beyond the perirenal fascia or also involving the contralateral kidney.

In this particular form of pyelonephritis **magnetic resonance** images are not particularly useful, because the presence of gas generates signal loss which is difficult to interpret.

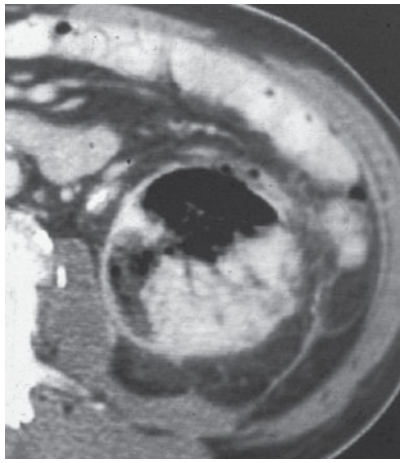

Fig. 9.22. Contrast-enhanced CT. Emphysematous pyelonephritis. In addition to the signs of acute pyelonephritis, such as hyperattenuating areas and perirenal fat stranding, the image shows intrarenal gas

Evanoff GV, Thompson CS, Foley R et al (1987) Spectrum of gas within the kidney: emphysematous pyelonephritis and emphysematous pyelitis. Am J Med 83:149-154

Langston CS, Pfister RC (1970) Renal emphysema. AJR Am J Roentgenol 110:778-786

Fungal Pyelonephritis

Mycetes form a spherical structure within the collecting system which is identifiable with **ultrasonography** as echogenic nodules but without a posterior shadow.

On contrast-enhanced **computed tomography** images aspecific parenchymal hyperattenuating lesions are visible resulting from the formation of multiple microabscesses.

Stapleton A (2002) Urinary tract infections in patients with diabetes. Am J Med 8:80S-84S

Chronic Pyelonephritis

In chronic pyelonephritis, rather than playing a diagnostic role, imaging can be used to establish the severity of renal scarring or to identify the anatomic and functional anomalies which may be underlying the recurrent infection and which facilitate the process.

In cases of reflux nephropathy the renal poles are particularly affected, with scars tending to thin the parenchyma and distort the underlying calices, while the association with dilatation of the caliceal system is not compulsory. In more diffuse forms the affected kidney tends to be small, with distortions of the entire pelvicaliceal system. The surface appears pitted by scarring and occasionally compensatory hypertrophy of the residual parenchyma may lead to the formation of pseudotumoral masses which bulge out from between the fibrous bands.

These findings can be readily detected on US and CT images, whereas urography is less specific, and above all, is only able to examine functioning kidneys.

At **urography** the typical finding is the presence of deep cortical scarring above a clubbed calix since the process involves both the cortex and the medulla. The renal involvement is focal, affecting only several medullary rays, with sparing of the adjacent areas which appear normal. In cases of reflux nephropathy the calices of the renal poles are more commonly affected, with sparing of the midrenal zone. Chronic

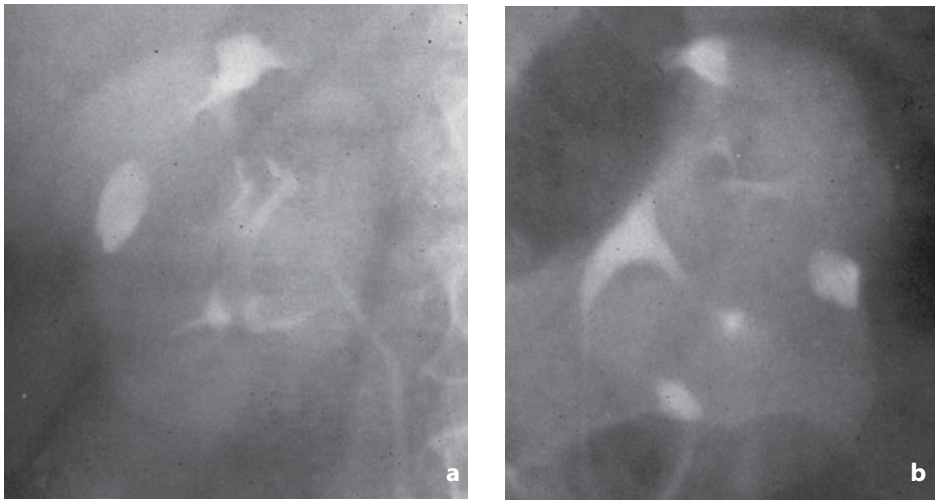

Fig. 9.23a,b. Urography. Bilateral reflux nephropathy. Profound retraction of the external profile of the kidney is evident bilaterally. The corresponding calices appear clubbed

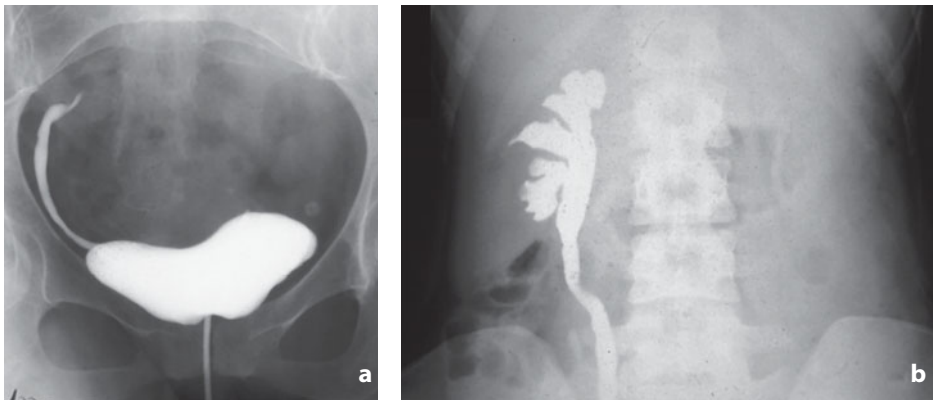

Fig. 9.24a,b. Retrograde cystourethrography. Vesicoureteric reflux. **a** Right vesicoureteric reflux which extends to the level of the kidney where the calices appear dilated and clubbed, typical signs of reflux nephropathy (**b**)

pyelonephritis causes a dilatation of the calices, which may be diffuse, and over time stone formations usually composed of struvite may develop at the papillae.

In reflux nephropathy the calices are dilated and the fornices blunted, and successively the typical clubbed appearance develops (Figs. 9.23, 9.24).

If the inflammatory process also extends to the ureter, the condition becomes known as cystic pyeloureteritis and can be identified by the presence of multiple minute filling defects in the ureter (Fig. 9.25).

The urographic image, however, requires a functioning kidney. Moreover, some conditions such as persistent fetal lobulations and renal infarct scarring can be incorrectly interpreted by a nonexpert radiologist.

Ultrasonography of the kidney affected by chronic pyelonephritis is able to demonstrate the presence of hyperechoic areas which extend from the retracted renal surface to the pelvis, with an increase in echogenicity of the renal sinus and pelvis due to atrophy. Dilatation of the collecting system may also be present. This imaging modality is particularly important in children with recurrent UTIs thanks to the absence of ionizing radiation. In children, decreased parenchymal thickness may not

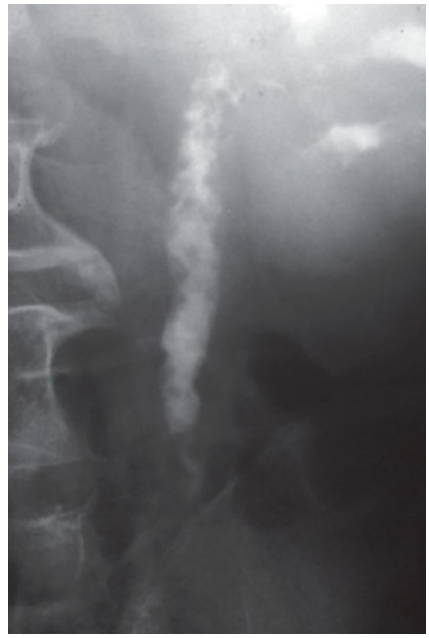

Fig. 9.25. Urography. Cystic pyelonephritis. Multiple minute filling defects can be seen in the left ureter, findings which are compatible with an inflammatory process (cystic ureteritis) and should be included in the differential diagnosis with urothelial productive processes

be associated with cortical retraction. Indirect and aspecific signs of vesicoureteric reflux may include increased wall thickness of the renal pelvis, the ureter and the urinary bladder, and the presence of postvoid residual urine volume.

To date the most appropriate imaging findings of chronic pyelonephritis are provided by **computed tomography**, which has proven to be the most sensitive technique. With CT urography good urographic visualization can be obtained together with direct information regarding the renal parenchyma, vasculature and functionality.

Browne RFJ, Zwirewich C, Torreggiani WC (2004) Imaging of urinary tract infection in the adult. Eur Radiol 14:E168-183

Kenney PJ (1990) Imaging of chronic renal infections. AJR Am J Roentgenol 155:485-494

Riccabona M, Fotter R (2004) Urinary tract infection in infants and children: an update with special regard to the changing role of reflux. Eur Radiol 14:L78-L88

Stokland E, Hellstrom M, Jakobsson B et al (1999) Imaging of renal scarring. Acta Paediatr 88:S13–S21

Stefanidis CJ, Siomou E (2007) Imaging strategies for vescicoureteral reflux diagnosis. Pediatr Nephrol 22:937-947

Renal Tuberculosis

In the advanced stage of disease the **plain abdominal film** can demonstrate the presence of renal calcifications of varying appearance, most commonly amorphous, spotty, lobar or filling the dilated caliceal cavity.

Urography and now **CT urography** are the gold standard for the identification of early signs of renal tuberculosis.

In the initial phase the papillary lesions involve the calix and cause edema of the mucosa. This appearance is represented by loss of definition of the caliceal profile. However, the first generally recognizable sign is the marginal erosion and irregular appearance of the caliceal wall.

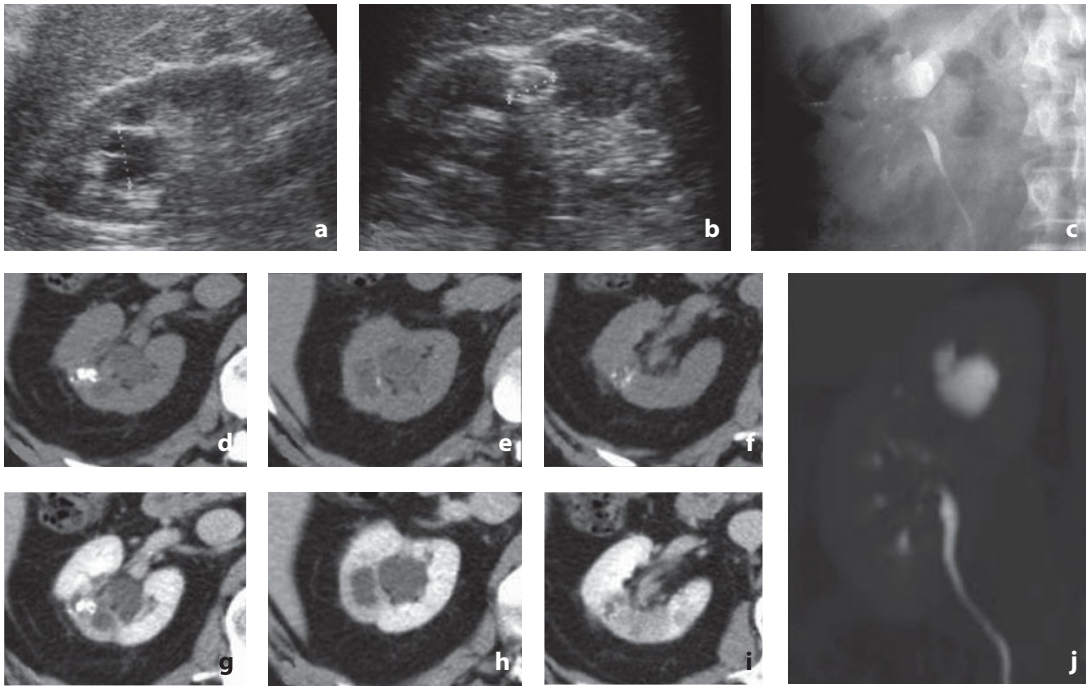

Fig. 9.26a-j. Ultrasonography, urography and CT. Renal tuberculosis. **a** US study shows a bilobular and probably fluid-filled hypoechoic area in the superior sinus and **b** a nodular calcification associated with parenchymal thinning in the mid-third of the kidney, without signs of hydronephrosis. **c** At urography a cavitary image in the superior sinus corresponding to the US findings, and stenosis of the major calices and pelvis. **d-f** Nonenhanced CT images show reduced parenchymal thickness at the mid-upper third of the kidney associated with parenchymal calcifications and hypoattenuating areas in the parenchyma. **g-i** In the same planes after contrast medium injection the cavitations in the parenchyma are appreciable. **j** Coronal reconstruction of the images acquired in the excretory phase shows the amputated calix of the superior system and the proximal cavity

The granuloma increases in size until caseation and rupture into a calix. In this phase the calix is no longer visible, being replaced by a small collection of contrast medium which may be indistinguishable from the papillary necrosis (Fig. 9.26). When evaluating these findings the Hodson line should be borne in mind, i.e. the line which joins all of the calices, to understand whether the dilatation appearing in the image corresponds to the calices or whether it is the result of a cavity in the medulla.

Other signs in the advanced stage of disease include focal scarring, cavitary lesions and infundibular constriction, which causes focal or diffuse nephrosis. The fibrosclerosis which produces the noncommunicating cavitation typically closes the neck of the calix, leaving a more or less wide cavity (Fig. 9.27). This causes the spike-like appearance of the amputated calix (Fig. 9.28) which is different from the irregular amputation caused by tumors.

When the cavity has been completely cleared of the caseous material, distinguishing it from a simple or complex cyst can be challenging. The complete clearance of the central caseation is better evaluated with US than with CT.

The role of **ultrasonography** in renal tuberculosis is secondary. Moreover, in many cases patients come under observation without a confirmed diagnosis. There are two fundamental US patterns: hyperechoic kidney due to the presence of calcifications (Fig. 9.26), infected debris and occasionally abscesses, or hydro- or pyonephrosis associated with dilatation of some or all of the calices, but with a normal-sized renal pelvis. Typical features in tuberculosis are signs of subsequent eruptions, i.e. already cleared cavitations alongside newly formed cavitations which deform the caliceal profile. In advanced cases hydronephrotic-like cavitary areas are observable (Fig. 9.26), which

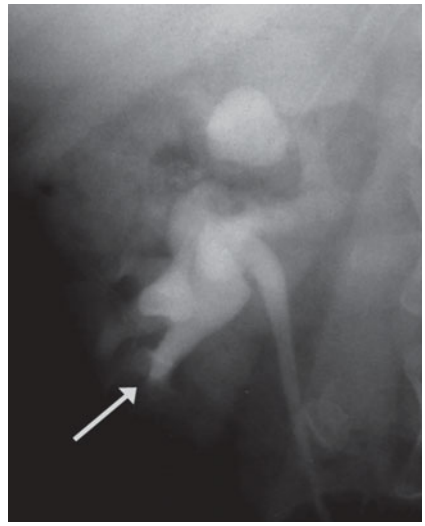

Fig. 9.27. Urography. Renal tuberculosis. Numerous cavitations are evident at the level of the superior sinus with amputated superior major calix. Evident enhancement proximal to the external minor calix of the inferior system indicative of papillary ulceration (*arrow*)

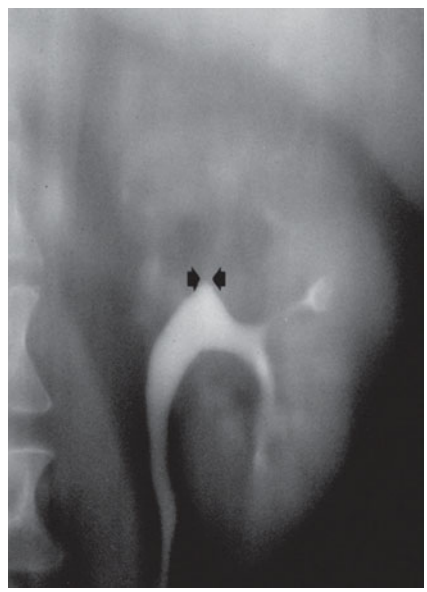

Fig. 9.28. Urography. Renal tuberculosis. Nephrogram shows the spike-like appearance of the amputated superior major calix (*arrows*) with proximal hyperattenuating parenchyma replaced by cavitary lesions

may or may not be clear, and sclerosis involving the entire surrounding renal parenchyma and reduced kidney size.

Thanks to its panoramic views, **computed tomography** is more specific and makes possible the evaluation of the extrarenal extension and the presence of cold abscesses in the adjacent structures, such as the psoas muscle. In the presence of phantom calices, i.e. dilated nonenhancing calices, CT is able to evaluate the proximal structures and therefore more accurately determine whether the caliceal stenosis is caused by tubercular processes or a urothelial tumor, a differential diagnosis which is difficult to make solely on the basis of urographic images.

In advanced cases the kidney is entirely occupied by a cavity communicating with the collecting system and large caseating granulomas, with focal or diffuse scarring of the cortex which is largely calcified and nonfunctioning.

Involvement of the collecting system causes ulcerations, increased wall thickness and fibrosis, with stenosis at various levels causing hydronephrosis or only proximal hydrocalix (Fig. 9.26).

Once the diagnosis of renal tuberculosis has been reached, imaging is required to

monitor the resolution of the condition, to evaluate the loss of renal function (which usually progresses during the lengthy treatment due to the progression of the sclerosis) and then to rule out disease recurrence.

Goldman SM, Fishman EK (1991) Upper urinary tract infection: the current role of CT, ultrasound and MRI. Semin Ultrasound CT MRI 12:335-360

Kim SH (2000) Urogenital tuberculosis. In: Pollack HM, McClennan BL (eds) Clinical Urography. WB Saunders Co., Philadelphia, pp 1193-1228

Wang LJ, Wong JC, Chen CJ et al (1997) CT features of genitourinary tuberculosis. J Comput Assist Tomogr 21:254-258

Xanthogranulomatous Pyelonephritis

Xanthogranulomatous pyelonephritis begins with involvement of the renal pelvis, followed by the medulla, the cortex, the peri- and then pararenal space. The most accredited pathogenesis is infection on an underlying long-term urinary obstruction.

At **ultrasonography** the kidney may appear enlarged with a normal profile, while the parenchymal structures may be altered. In addition, broad and anechoic spaces are present, which may be diffuse or concentrated in a renal sector, and are produced by dilated calices or saccular collections. In the focal form there may be a uniformly hypoechoic mass with associated anechoic cystic foci (**Fig. 9.29**). The study is also able to identify dilatation of the renal pelvis, occasionally with increased wall thickness, and the presence of a large stone responsible for the obstruction favoring the disease.

Computed tomography is the imaging modality of choice for the study of xanthogranulomatous pyelonephritis. In addition to renal enlargement the CT study can identify increased thickness of the fasciae and perirenal fat stranding. The renal parenchyma appears nonuniform, with multiple nonenhancing spherical areas with low attenuation (from -15 to +30 HU, closer to water than to fat) surrounded by an enhancing rim (**Fig. 9.29**). Smaller calcifications may be visible within xanthogranulomatous masses, and occasionally gas pockets produced by an overlying infection of anaerobic bacteria. Excretion of the contrast medium from the affected kidney may be absent.

The disease is classically associated with a staghorn calculus (**Fig. 9.29**), although in 25% of patients no stones are present.

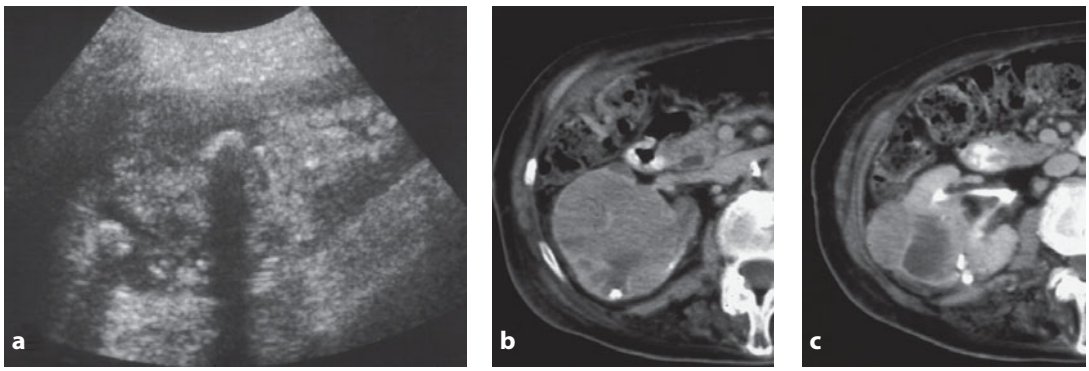

Fig. 9.29a-c. Ultrasonography and contrast-enhanced CT. Xanthogranulomatous pyelonephritis. **a** US study shows renal enlargement limited to the superior sectors associated with several hypoechoic areas and the presence of two stone formations. **b-c** CT images show diffuse and nonuniform hypoattenuation of the superior half of the kidney, with the presence of above-fluid attenuating collections and stone formations. Renal function is conserved, as seen by the presence of contrast medium in the renal pelvis, which demonstrates increased wall thickness

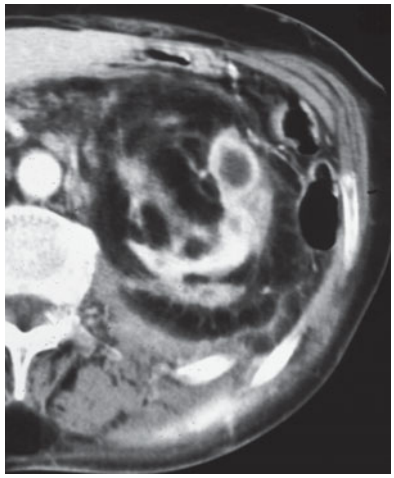

Fig. 9.30. Contrast-enhanced CT. Replacement lipomatosis. The image shows parenchymal atrophy with an increase in renal sinus and perirenal fat and associated stranding. Cysts at the anterior renal lip are also visible

The focal form can mimic the appearance of a tumor due to the presence of a hypoattenuating mass. A hyperattenuating rim may appear in the delayed phase.

There have also been reports of the coexistence of replacement lipomatosis of the renal sinus (**Fig. 9.30**) developed on a reactive basis in patients with chronic renal inflammation (an appearance which can create problems for differential diagnosis).

Magnetic resonance images reflect the presence of xanthomatous cells (lipid-laden) in the granulomatous inflammation. For this reason the solid component can appear extremely hyperintense in T1-weighted images in comparison with the renal parenchyma and similar to intra-abdominal adipose tissue, or isointense to the parenchyma, while in T2-weighted images it appears isointense to the contralateral kidney. There may be hypointense components in T1-weighted images and hyperintense in T2 due to the presence of internal liquid. Fluid-fluid levels might also be identifiable in the cavity due to the presence of fluid, pus and debris. The invasion of perirenal tissue appears hypointense in both T1- and T2-weighted sequences, most likely due to the presence of thick fibrinous exudates.

After administration of contrast medium peripheral enhancement of the cavity can be seen (contrast medium does not pool in the xanthomatous tissue) which is indicative of hypervascularization of the inflamed tissue and increased thickness of the fasciae, thus enabling a more accurate evaluation of disease extent than CT.

These characteristics can be useful, although not compulsory, in the distinction between focal xanthogranulomatous pyelonephritis and renal carcinoma. For this reason an MR study is advisable in doubtful cases prior to performing nephrectomy.

Replacement lipomatosis of the renal sinus is readily identifiable on MR images due to the immediate visualization of the lipid component.

Feldberg MA, Driessen LP, Witkamp TD et al (1988) Xanthogranulomatous pyelonephritis: comparison of extent using computed tomography and magnetic resonance imaging in one case. Urol Radiol 10:92-94

Kenney PJ (1990) Imaging of chronic renal infections. AJR Am J Roentgenol 155:485-494

Laugareil P, Blery M, Despoisse JM et al (1989) Pyélonéphrite xanthogranulomateuse avec prolifération graisseuse de la loge renale. Aspects en tomodensitométrie et IRM. J Radiol 70:295-297

Rabushka LS, Fishman EK, Goldman SM (1994) Pictorial review: computed tomography of renal inflammatory disease. Urology 44:473-480

Ramboer K, Oyen R, Verellen S et al (1997) Focal xanthogranulomatous pyelonephritis mimicking a renal tumor: CT- and MR-findings and evolution under therapy. Nephrol Dial Transplant 12:1028-1030

Verswijvel G, Oyen R, Van Poppel H et al (2000) Xanthogranulomatous pyelonephritis: MRI findings in the diffuse and the focal type. Eur Radiol 10:586-589

Renal cancer

Pathology

The most common renal cancer is the carcinoma (**Fig. 9.31**) (renal cell carcinoma, RCC), which accounts for 3% of all adult cancers and 80-85% of malignant renal tumors, with a higher incidence in North America and Scandinavian countries. Other common histotypes are transitional cell carcinoma of the renal pelvis in adults (15-20%) and nephroblastoma in children. Benign tumors account for only a small percentage of all renal tumors, with the most common being oxyphilic adenoma (oncocytoma) and angiomyolipoma.

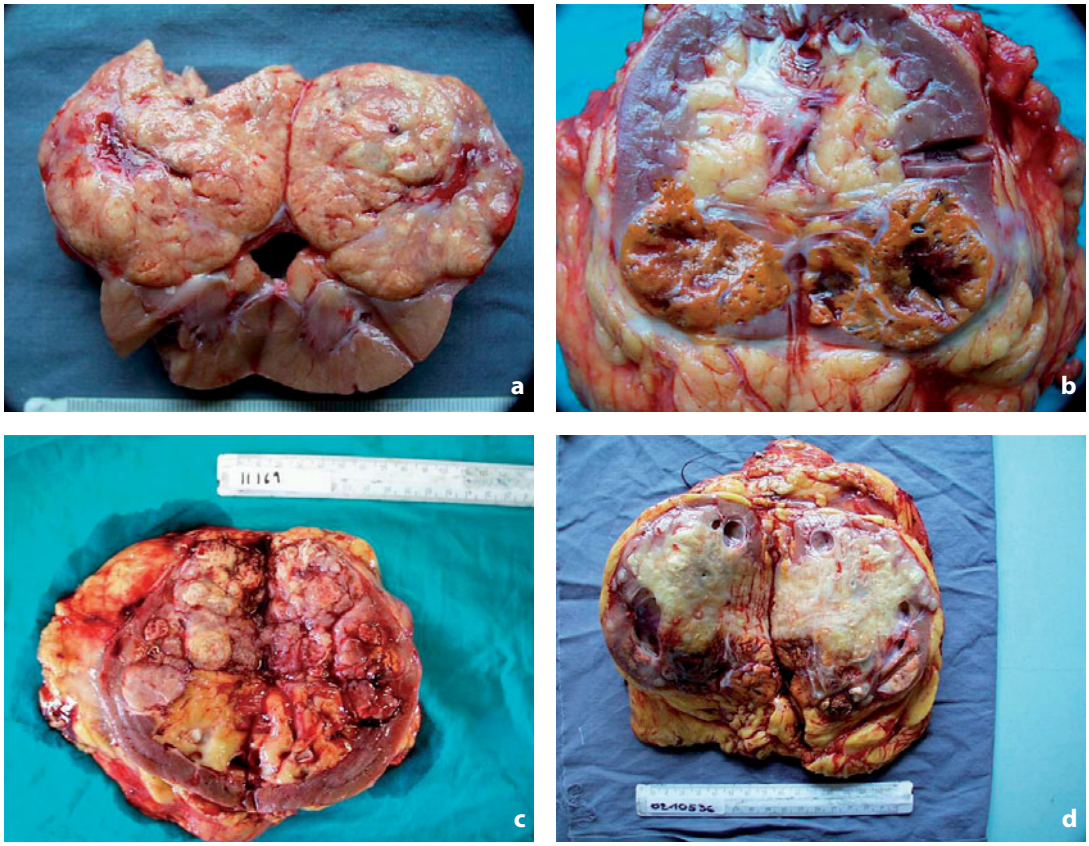

Fig. 9.31a-d. Renal cell carcinoma. Gross anatomy. **a** Well-defined partially exophytic lesion with uniform structure. **b** Lower pole lesion with central necrotic component. **c** Lesion with peripheral thick fibrous capsule. **d** Lesion characterized by different components which determine the nonuniform appearance

Parenchymal Tumors in Adults

Up until several decades ago, all renal masses were defined as hypernephromas or Grawitz tumors after the German pathologist who posed the hypothesis that the tumors arose from residual suprarenal tissue present within the renal parenchyma. At the beginning of the 1970s the demonstration of the origin from the tubules led to the definition of adenoma, a benign tumor <2 cm, and adenocarcinoma, the malignant form classified as clear, granular or mixed cell variants. Following on from the Mainz classification, in 1996 the Heidelberg classification was introduced, which excludes nephroblastoma and metastatic forms to the kidney and subdivides renal tumors on the basis of morphologic appearance and karyotype, i.e. as benign (metanephric adenoma and adenofibroma, papillary renal cell adenoma and renal oncocytoma) and malignant (common or conventional RCC, papillary RCC, chromophobe RCC, collecting duct carcinoma and unclassified, when the lesions shows none of the morphologic features required to classify it amongst the aforementioned categories). The innovative features of this classification allow it to overcome the concept of benignancy and malignancy linked to tumor dimensions (even lesions <3 cm can metastasize) and recognizes an individual karyotype for each histologic group. For example, the group of benign tumors is characterized by a normal karyotype, with the exception of papillary renal cell adenoma characterized by trisomy of chromosomes 7 and 17 and the loss of chromosome Y; common RCC is noted for aberrations of chromosome 3; papillary RCC is characterized by trisomy of numerous chromosomes while chromophobe RCC presents significant alterations of the karyotype; the karyotype of collecting duct carcinoma and the unclassified groups remains in part unknown due to the small number of cases studied.

A variety of classifications exist and are currently in use. In this chapter reference will be made to the classification reported in **Tables 9.1** and **9.2**.

The diagnosis of RCC can be difficult on occasions. In addition to expansive processes of adjacent organs (suprarenal glands), which can simulate RCC, or retroperitoneal mesenchymal tumors which develop with secondary involvement of the kidney, the real clinical-radiologic mimics of RCC are several benign lesions, such as malakoplakia, xanthogranulomatous pyelonephritis (**Fig. 9.32**) and perirenal hemorrhagic cysts. Angiomyolipoma is not a part of this group, although it does pose problems for the differential diagnosis. It is a benign mesenchymal neoplasm composed of adipose tissue, thick-walled vessels and smooth muscle elements in varying proportions. When this triad is present the radiologic diagnosis is uncomplicated. It should however be borne in mind that "monophasic" variants exist, i.e. consisting of only one of these three components, such as the form composed exclusively of spindle-shaped smooth muscle cells, or the epithelioid variant which is particularly problematic because it can be interpreted as a carcinoma.

Diaz JL, Mora LB, Hakam A (1999) The Mainz classification of renal cell tumors. Cancer Control 6:571-579

Kovacs G, Akhtar N, Beckwith BJ et al (1997) The Heidelberg classification of renal cell tumours. J Pathol 183:131-133

Thoenes W, Störkel S, Rumpelt HJ (1986) Histopathology and classification of renal cell tumors (adenomas, oncocytomas and carcinomas). The basic cytological and histopathological elements and their use for diagnostics. Pathol Res Pract 181:125-143

Table 9.1. Histologic classification of tumors and pseudotumoral lesions in adults

Renal cell carcinoma
Renal cortical adenoma
Metanephric tumors
metanephric adenoma
metanephric adenofibroma
metanephric stromal tumor
metanephric adenosarcoma
Oncocytoma
Rare tumors with epithelial and/or parenchymal differentiation
carcinoid
small cell carcinoma
primary neuroectodermal tumor
juxtaglomerular cell tumor
teratoma
nephroblastoma and other "pediatric" renal tumors
multilocular cysts (cystic nephroma)
mixed epithelial-stromal tumor
spiradenocylindroma
Mesenchymal tumors
angiomyolipoma
epithelioid angiomyolipoma
medullary fibroma
leiomyoma
lipoma
hemangioma
lymphangioma
other benign mesenchymal tumors
leiomyosarcoma
liposarcoma
solitary fibrous tumor
hemangiopericytoma
fibrosarcoma and malignant fibrous histiocytoma
rhabdomyosarcoma
angiosarcoma
osteosarcoma
synovial sarcoma
other malignant mesenchymal tumors
Lymphomatous tumors
plasmocytoma
Metastatic tumors
Pseudotumoral lesions
xanthogranulomatous pyelonephritis
inflammatory myofibroblastic pseudotumor
renal pelvic and perirenal cysts

Table 9.2. Histologic classification of renal cell carcinoma

Clear cell
multilocular cysts
Papillary
Chromophobe
Collecting duct
Medullary
Mucinous tubular and spindle cell
Associated with Xp 11.2 translocations/TFE3 gene fusions
Unclassified

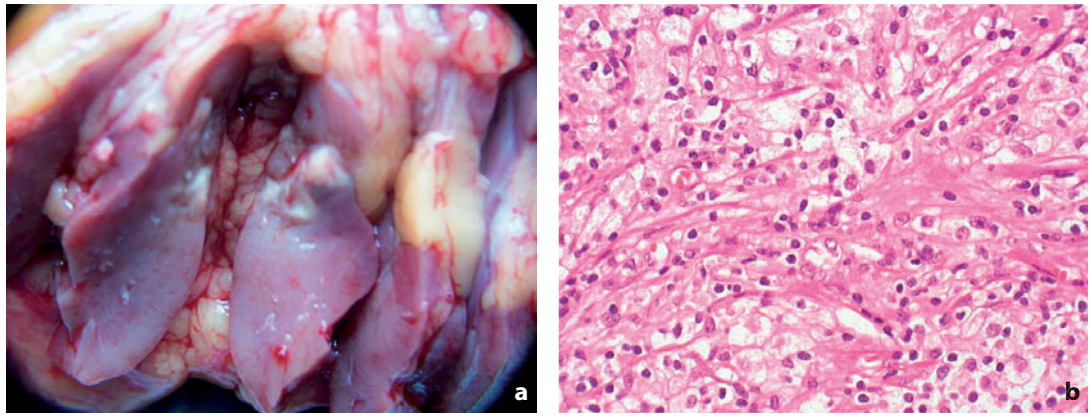

Fig. 9.32a,b. Xanthogranulomatous pyelonephritis. **a** Gross and **b** microscopic anatomy

Parenchymal Tumors in Children: Nephroblastoma

Renal tumors are relatively rare in children, and most cases (more than 90%) are nephroblastoma. The incidence is 1:1,000,000 in subjects below 15 years, with a maximum peak between 3 and 4 years and no difference between sexes. Nephroblastoma accounts for 6-7% of all solid tumors in children, may be familial and is bilateral in 5% of cases. The gross appearance of the tumor is a friable, vascularized and usually voluminous mass (mean 12 cm) covered by its own capsule or a pseudocapsule derived from a thickening of adjacent connective tissue. The cut surface appears heterogeneous due to the irregular alteration of hemorrhagic areas. Microscopically, the characteristic histologic feature is the presence of residual embryonic cells, i.e. the part of the blastic stroma - the renal blastema - which should have completely disappeared by the 34th week of gestation. Nephrogenic rests (abortive tubules and glomeruli) are found at histologic examination in 30-40% of cases. The possible presence of renal blastema rests, potential precursors of nephroblastoma, called for exploration of the contralateral kidney during nephrectomy up to ten years ago. The improvement of imaging techniques has questioned this invasive practice. Nonetheless, follow-up of the remaining kidney is still compulsory due to the possibility of contralateral recurrence.

Other solid parenchymal renal masses in children include mesoblastic nephroma, clear cell sarcoma, rhabdoid tumor and renal cell carcinoma.

Federle MP, Anne VS, Jen-Sho Chen J et al (2005) Kidney and urinary tract infection and inflammation. In: Federle MP, Jeffrey RB, Desser TS et al (eds) Diagnostic imaging: abdomen, vol III. Amirsys, Salt Lake City, UT, Usa, pp 28-63

Rare Parenchymal Tumors

The kidney can be the site for formation of numerous types of benign mesenchymal tumors: angiomas, lipomas, lymphangiomas and various other histologic types which nonetheless have no clinical relevance. Various types of sarcoma can also develop derived from the different types of connective elements in this organ.

Cystic Lesions

The anatomic pathologic definition of a cyst, which radiologically is defined as either simple or complicated, is highly variable. The wall can be fibrotic with intraluminal debris, de-epithelialized fibroepithelial with tubular inclusions or composed of granular tissue or fibrin. A not uncommon finding at the periphery of these cystic lesions or within the thickness of the cystic wall is areas of solid epithelial proliferation which can be attributed to conventional or papillary RCC. The focal nature of these lesions explains in part the frequent false negatives during extemporaneous intraoperative examination. Another problem is the approach to these multilocular cystic lesions, which are characterized by the presence of multiple cystic formations varying in size with fibrous walls. The various cysts are separated by fibrous septa which are often noncommunicating (**Fig. 9.33**). Diagnosis requires study of the epithelial lining, which appears as a single flattened layer in benign multilocular cysts or cystic nephromas, or stratified with parietal nodules of solid epithelial proliferation in the wall of cystic conventional RCC.

Federle MP, Anne VS, Jen-Sho Chen J et al (2005) Kidney and urinary tract infection and inflammation. In: Federle MP, Jeffrey RB, Desser TS et al (eds) Diagnostic imaging: abdomen, vol III. Amirsys, Salt Lake City, UT, Usa, pp 28-63

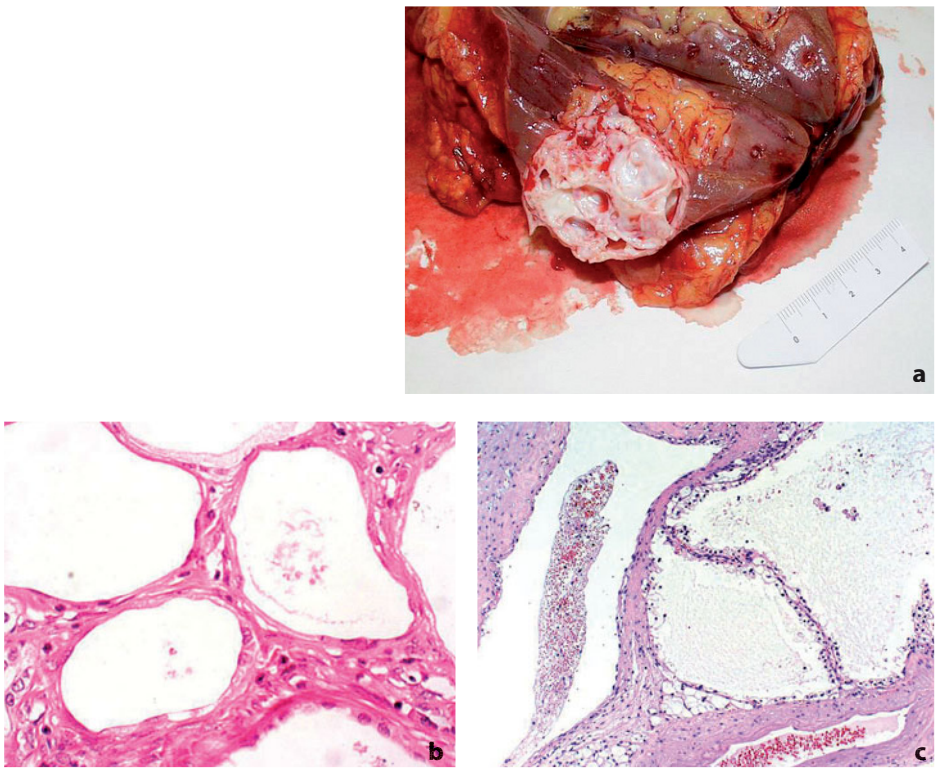

Fig. 9.33a-c. Cystic nephroma. **a** Gross and **b, c** microscopic anatomy

Pelvicaliceal Tumors

These account for less than 10% of all renal tumors. Most (around 90%) arise from the epithelial lining in the form of urothelial or transitional cell carcinomas (TCC). Less frequent are squamous cell carcinoma (5%), and adenocarcinoma (2%) (**Fig. 9.34**). The epithelial tumors are defined as urothelial by the term "urothelium" coined by Melicow in 1945 to describe the epithelial lining of the urinary tract. Urothelium extends from the renal calices to the urethra and is composed of a basal layer of cuboid cells, one or more intermediate layers of similar but larger cells, and a superficial layer of transitional cells, so named because each cell covers several cells of the underlying layer. Lining the transitional cells is a membrane whose integrity is vital for maintaining the tissue impermeable to the toxic component of the urine. The entire surface of the urothelium is exposed to the cancerogenous stimulation of these toxins and this would explain the multicenter distribution of TCC. Some 90-92% of the lesions arise in the urinary bladder, 8-10% in the kidneys (calices and pelvis), around 2% in the ureters (more commonly in the distal segment) and 0.1% in the two proximal thirds of the urethra. Of all urothelial tumors found in the upper urinary tract, 3% occur in the pelvicaliceal cavity, 73% in the distal ureter and the remaining 24% in the mid ureter.

Urothelial tumors can involve the pelvicaliceal cavity in a more or less diffuse manner. However, the extension is not the most important feature. Low-grade TCC tend to have a superficial extension with very little depth, unlike high-grade G3 carcinomas or aggressive variants such as invasive micropapillary carcinoma. Despite appearing small given their limited superficial extension, these lesions can prove to be deeply invasive.

Murphy WM, Grignon DJ, Perlman EJ (2004) Tumors of the kidney, bladder, and related urinary structures. American Registry of Pathology, Washington DC

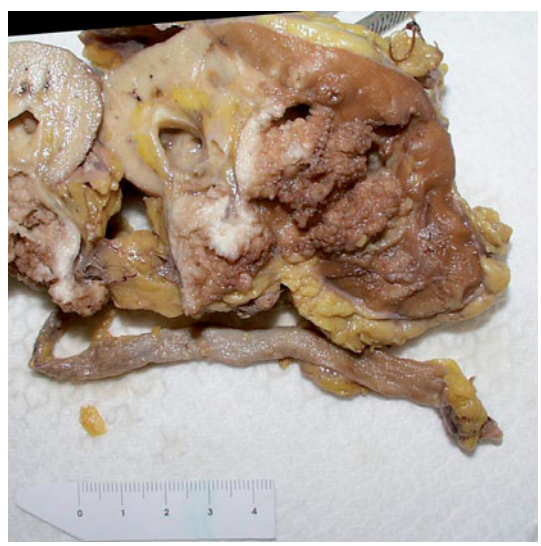

Fig. 9.34. Urothelial carcinoma. Gross anatomy

Diagnostic Imaging

Parenchymal Tumors

The symptoms at onset of renal tumors are moderate and vague or even absent. As a result the diagnosis is often made incidentally at US during examinations performed for other reasons. The classic triad of symptoms - hematuria, palpable mass and abdominal pain - is only present in 10% of cases and generally observed in clinically advanced conditions.

In the presence of disturbances which give rise to suspicion of a tumor or in the case of the incidental finding of a renal lesion, the clinician queries the radiologist for some specific information: (a) the real existence of a renal mass and its dimensions; (b) benign or malignant nature, after differential diagnosis with complicated cystic lesions; (c) unifocal or multifocal nature of the disease; (d) involvement of the ureter; (e) local-regional and distant extension, and in particular involvement of the renal vein and inferior vena cava, knowledge which is indispensable for surgical planning.

Identification

In the diagnosis of renal parenchymal tumors, **urography** with nephrotomography has a sensitivity of 85% in lesions >3 cm. It suffers from severe diagnostic limitations in small tumors, with the sensitivity falling to 20% and 10% in 3 cm and 1 cm lesions, respectively. The role of conventional radiology is therefore marginal.

At **ultrasonography** the lesions are usually circular with associated focal enlargement of the kidney. When this sign is missing in small lesions an evaluation of the relationship between the cortical parenchyma and the pelvic sinus can prove useful, since the former tends to distort the latter (Fig. 9.35). Another useful parameter for identifying a renal lesion is the structure: hyper-, hypo- or anechoic. Hyperechogenicity results from both hypervascularization and hyaline or coagulative necrosis (Fig. 9.36). Hypoechogenicity is generally produced by nonrecent hemorrhagic

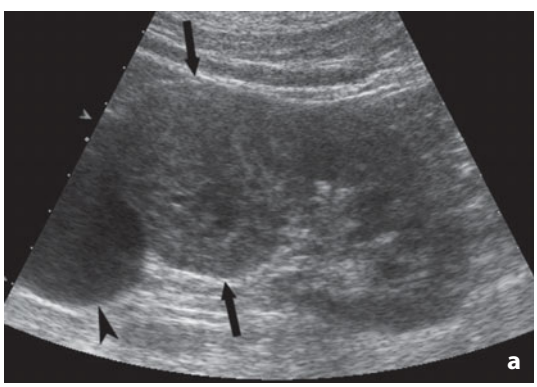

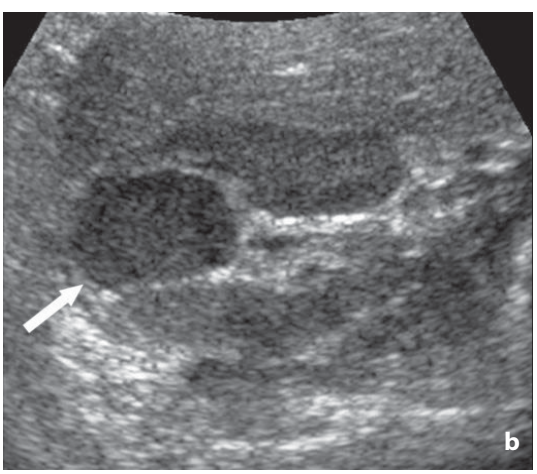

Fig. 9.35a,b. Ultrasonography. Renal cell carcinoma. **a** Isoechoic lesion of the left kidney (*arrows*) with a change in the normal relationship between renal cortex and sinus. Adjacent simple cysts are visible in the upper pole (*arrowhead*). **b** Hypoechoic solid lesion (*arrow*) with distortion of the cortical margin at the pelvic sinus

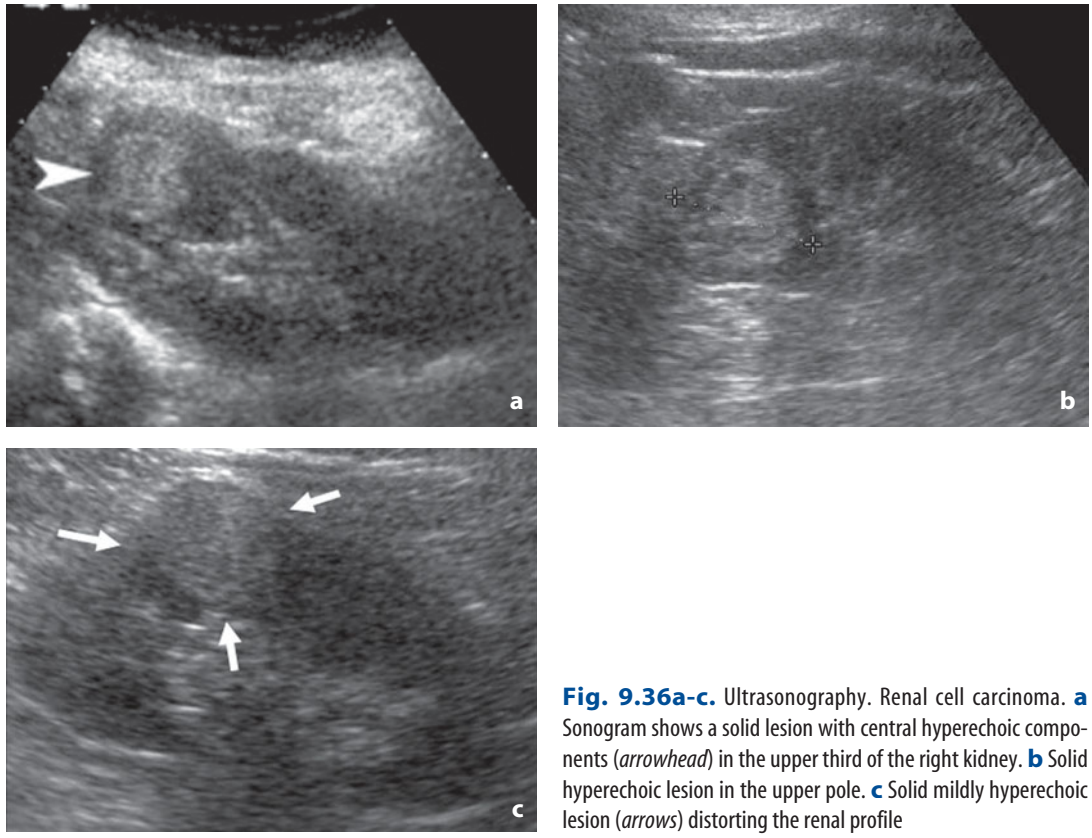

Fig. 9.36a-c. Ultrasonography. Renal cell carcinoma. **a** Sonogram shows a solid lesion with central hyperechoic components (*arrowhead*) in the upper third of the right kidney. **b** Solid hyperechoic lesion in the upper pole. **c** Solid mildly hyperechoic lesion (*arrows*) distorting the renal profile

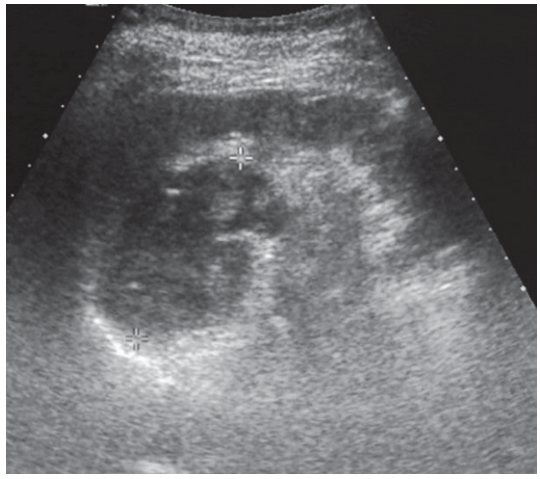

Fig. 9.37. Ultrasonography. Renal cell carcinoma. Solid hypoechoic lesion of the renal lip

necrosis (recent bleeding would appear prevalently hyperechoic) (Fig. 9.37). Anechogenicity is usually correlated with the presence of cystic areas or pseudocysts corresponding to zones of liquefied necrosis (Fig. 9.38).

Color and **power Doppler** can on occasion contribute to the identification of lesions (Fig. 9.39).

Computed tomography (Fig. 9.40) is currently recognized as the best imaging technique for identifying renal parenchymal neoplasms and is without doubt superior to US. CT can identify more and smaller lesions than US, although it is unable to

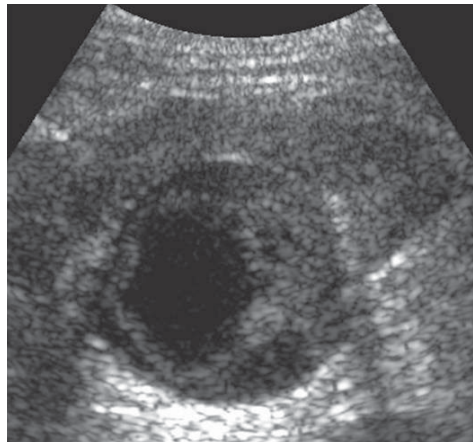

Fig. 9.38. Ultrasonography. Renal cell carcinoma. Solid lesion with heterogeneous structure resulting from necrotic cystic elements

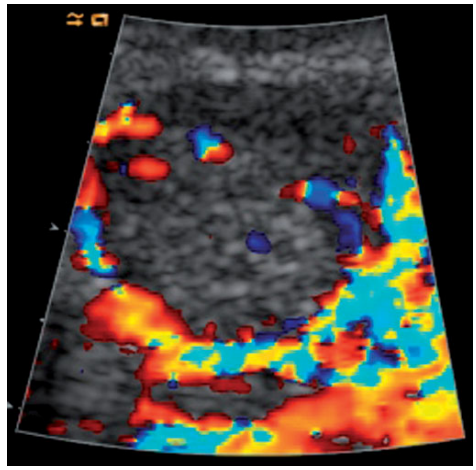

Fig. 9.39. Color Doppler. Renal cell carcinoma. The basket-like appearance of the vessels delimiting the lesion make its identification easier

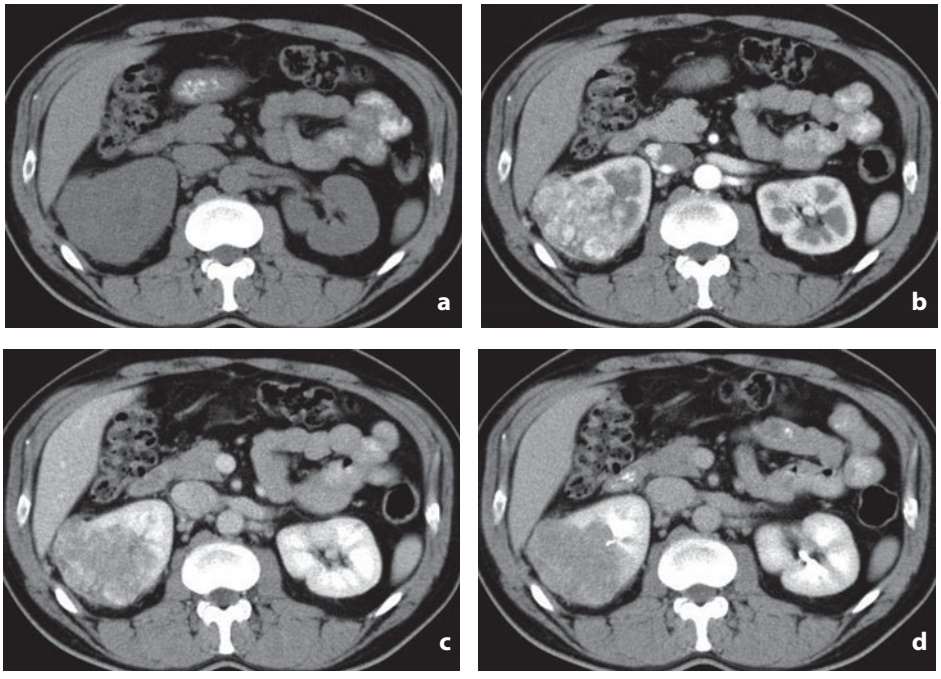

Fig. 9.40a-d. Computed tomography. Renal cell carcinoma. Contrast-enhanced dynamic study in the **a** baseline, **b** arterial, **c** venous and **d** delayed phase. Lesion located in the mid third of the right kidney

improve on their characterization. In fact, lesions within the range of 10-35 mm are correctly characterized by CT and US in 82% and 80% of cases, respectively. However, it should be borne in mind that a negative CT (and also a negative US) does not rule out the presence of a lesion <1.5 cm.

It is rather unlikely that today or in the near future **magnetic resonance** will play much of a role in the identification of renal lesions, a role which is reserved for US and CT.

Characterization

There are two fundamental aims to the characterization of solid renal lesions: to distinguish a renal tumor from normal anatomic variants or pseudotumoral lesions which can mimic a neoplasm (e.g. lobar dysmorphism or fetal lobulations) and to differentiate benign from malignant forms.

For the differential diagnosis of solid renal lesions gray-scale **ultrasonography** uses a number of signs, including echogenicity, the presence of a peripheral anechoic halo, posterior signal attenuation and the presence of intratumoral cystic formations. Nonetheless, these findings are not pathognomonic. Although a hyperechoic mass is highly suggestive of an angiomyolipoma and although RCCs are frequently hypo- or isoechoic, up to 30% of all RCCs and especially those <3 cm can appear hyperechoic at US, and therefore with a similar appearance to the "classic" angiomyolipoma. Uniform echotexture may suggest a diagnosis of oncocytoma (in some cases a hypoechoic stellate scar has been reported, although this is a rare finding, especially in lesions <3 cm). Nonetheless, 35% of carcinomas can appear uniform in the same manner as oncocytoma.

The rationale behind using **color Doppler** in the characterization of RCC lies in the presence of newly formed vessels which influence the development of the tumor itself. This vasculature is characterized by the presence of arteriovenous fistulae and the development of sinusoids. The fistulae produce a brusque acceleration of blood flow due to the significant pressure gradient, and color Doppler is able to identify vessels with elevated flow velocity. Sinusoids, on the other hand, are situated in the center of the mass, and due to the typical absence of musculature in these vessels their flow is slow, producing a low-resistance Doppler pattern with little systolic-diastolic excursion.

Power Doppler can prove useful in the identification of pseudotumoral masses (including prominent renal columns, cortical dysmorphisms, fetal lobulations, areas of compensatory hypertrophy) in that they are characterized by vasculature that is very similar to normal parenchyma).

Contrast-enhanced ultrasonography does not appear to add much to the accuracy of the characterization of solid renal lesions. The real utility of contrast media in the standard diagnostic protocol of these lesions still needs to be defined, while also bearing in mind their cost-benefit ratio.

Computed tomography can suggest a growth pattern is infiltrative rather that expansive (in the latter the tumor is bounded by a pseudocapsule). On the basis of a number of characteristics, CT is able to differentiate between a conventional clear cell RCC, sarcomatoid carcinoma, metastasis (in cases of a positive history of a primary tumor at another site), TCC, squamous cell carcinoma and lymphoma. There are no CT signs able to suggest more complex or rare cases, such as adult nephroblastoma, collecting duct carcinoma or Bellini duct carcinoma. In daily practice sporadic cases may be included in the differential diagnosis, e.g. xanthogranulomatous pyelonephritis or the more common complicated cysts.

Magnetic resonance has without doubt an important role to play in the characterization of renal lesions. Thanks to the efficacy of the dynamic study (**Fig. 9.41**) performed with the injection of paramagnetic contrast medium, the increase in signal intensity can be measured over time and the vasculature of small lesions can be evaluated, a finding which can label a neoplasm malignant.

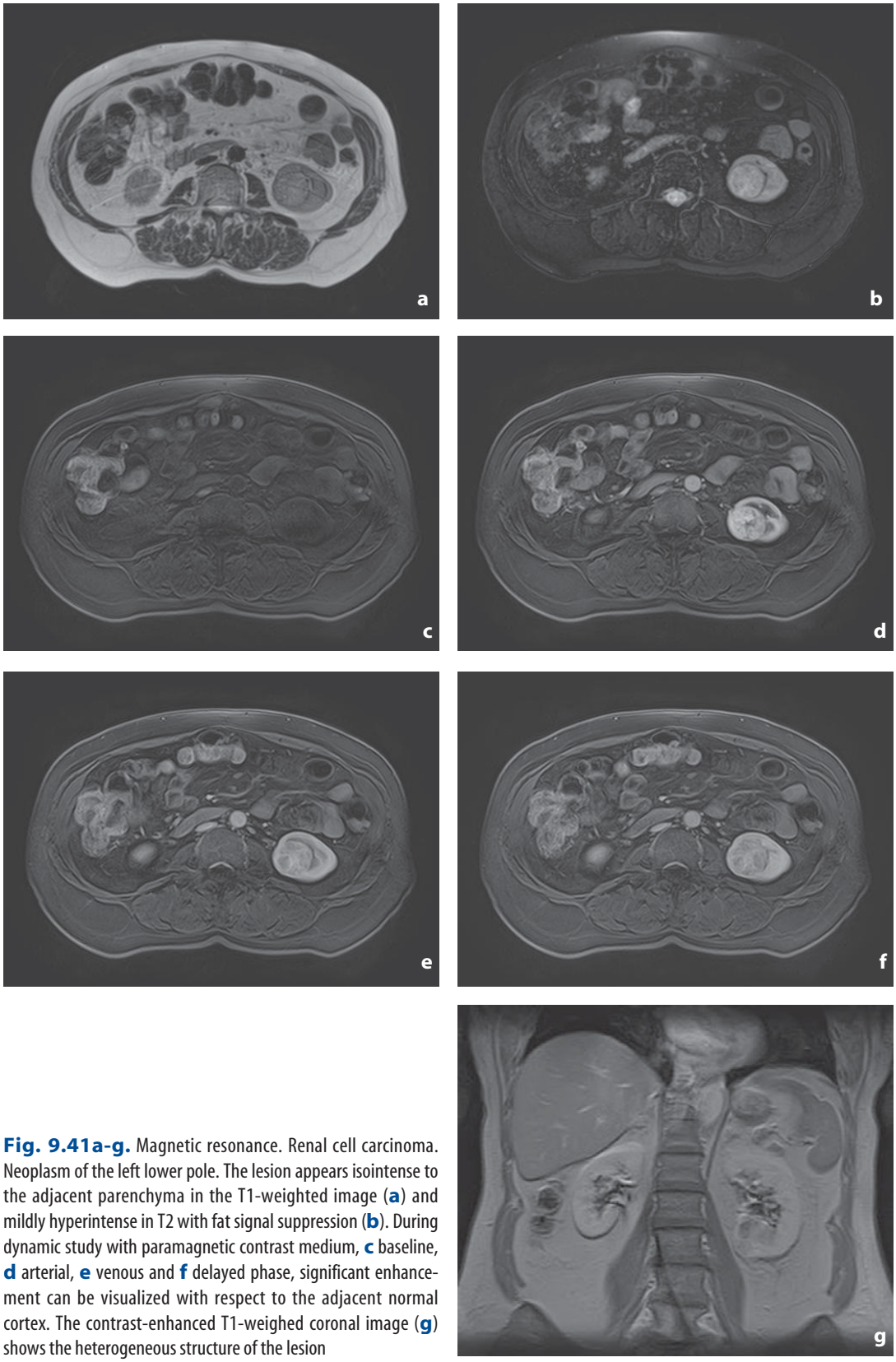

Fig. 9.41a-g. Magnetic resonance. Renal cell carcinoma. Neoplasm of the left lower pole. The lesion appears isointense to the adjacent parenchyma in the T1-weighted image (**a**) and mildly hyperintense in T2 with fat signal suppression (**b**). During dynamic study with paramagnetic contrast medium, **c** baseline, **d** arterial, **e** venous and **f** delayed phase, significant enhancement can be visualized with respect to the adjacent normal cortex. The contrast-enhanced T1-weighed coronal image (**g**) shows the heterogeneous structure of the lesion

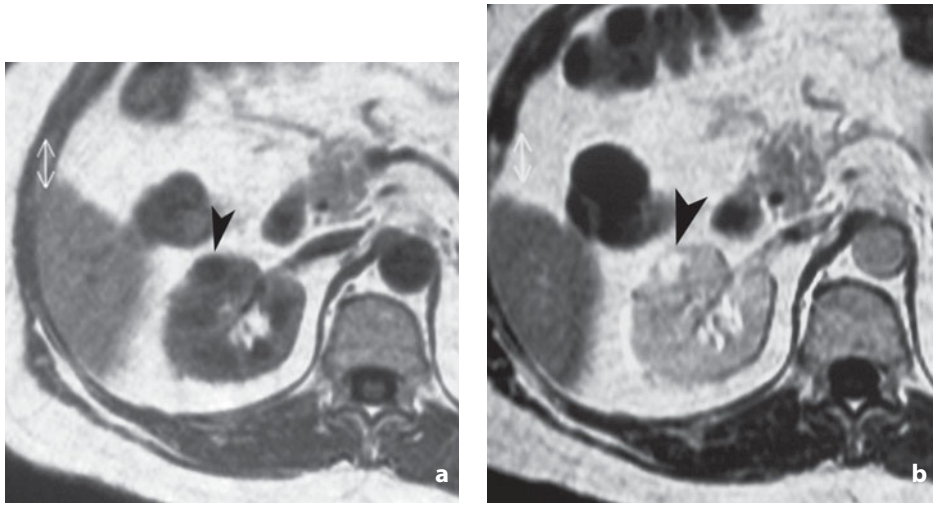

Fig. 9.42a,b. Magnetic resonance. Carcinoma of the anterior lip of the right kidney. The approximately 1 cm lesion (*arrowhead*) appears **a** hypointense in T1 and **b** hyperintense after contrast medium injection

In T1-weighted images medium to large lesions can appear hypo-isointense or even weakly (but never clearly) hyperintense. In T2-weighted sequences the appearance is hypo- and hyperintense (Fig. 9.42). The main characteristic of larger lesions is their heterogeneous structure, which is particularly notable in contrast-enhanced images. The MR signs are very similar to CT signs in both morphology and signal characteristics. In the larger lesions MR can also play a role in contributing to the characterization of doubtful lesions.

MR is able to resolve the problems CT has with complex cysts, i.e. small lesions with calcified walls, in which the absence of enhancement (confirmed by comparison with the rapid increase in signal intensity of the normal parenchyma) can help make the diagnosis of benign lesions.

The appropriateness of or need to perform imaging-guided biopsy to characterize a focal renal lesion is today limited to well-defined cases: doubtful or discordant imaging findings; critical clinical conditions (patients with a single kidney or renal insufficiency); multifocal and/or bilateral lesions; positive history of cancer; lymphoma; and trauma. As these indications suggest, biopsy plays an effective role only when accurate planning for nephron-sparing surgery is required or when there are conditions to seriously consider a differential diagnosis alternative to primary renal neoplasm.

Staging

Of all the available prognostic factors, tumor extension at diagnosis is the most important element for predicting disease progression (indeed, 5-year survival is 60-90% in cases of organ-confined lesions, whereas it falls to 5-10% with distant spread). As a result, **computed tomography** plays a key role and still today can be considered the best imaging modality for staging RCC according to two possible classifications: the Robson classification or the TNM classification (Table 9.3). The former and earlier of the two is also the simpler classification. It has significant limitations with regard to stage III disease, which combines a heterogeneous group of patients with different prognoses. For example, patients with invasion of the inferior vena cava are definite candidates for radical surgery, whereas patients with lymph node metastasis usually only undergo palliative resection. The somewhat more complicated TNM

Table 9.3. Classification of renal cell carcinoma according to the Robson and TNM systems

	Robson classification Stage	TNM classification Stage
Tumor confined to kidney		
<7 cm	I	T1
≥7 cm		T2
Invasion of perirenal fat	II	T3a
Tumor thrombi	IIIA	
renal vein		T3b
inferior vena cava below diaphragm		T3c
inferior vena cava above diaphragm		T4b
Metastases to regional lymph nodes	IIIB	N1-N3
Direct invasion of adjacent viscera	IVA	T4a
Distant metastases	IVB	M1a-d

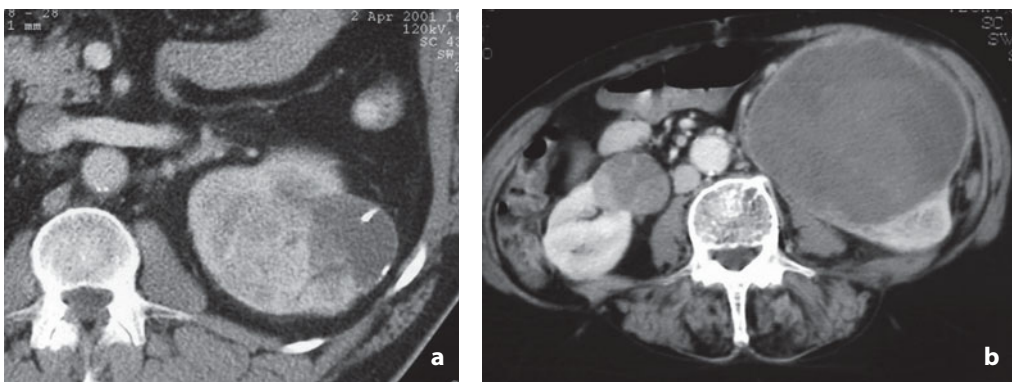

Fig. 9.43a,b. Computed tomography. Renal cell carcinoma. **a** Stage T1. Solid mass <7 cm in the left kidney. **b** Stage T2. Solid mass >7 cm in the mid third of the left kidney. A synchronous lesion <7 cm is also appreciable in the right kidney

classification provides better prognostic indications of tumor extension and is currently the most used.

Size differentiation (lesion less than or greater than 7 cm) classifies a lesion as either T1 or T2 (Fig. 9.43). Diagnostic difficulties can arise in the differentiation between stage T2 - confined to the capsule - and stage T3a - extracapsular extension of the tumor. The most specific CT parameter for classifying a solid mass as T3a (however with sensitivity <46%) is provided by the identification of a solid enhancing nodule in the perirenal fat, which possibly behaves in a similar manner to the primary lesion (Fig. 9.44). Stranding and increased thickness of perirenal fat are not necessarily signs of tumor spread, since they are identifiable in 50% of patients with lesions confined to the capsule and may be produced by edema, vascular congestion or prior inflammation. These diagnostic limitations of CT, however, do not influence patient management, since stage T3a is a candidate for both radical and nephron-sparing nephrectomy.

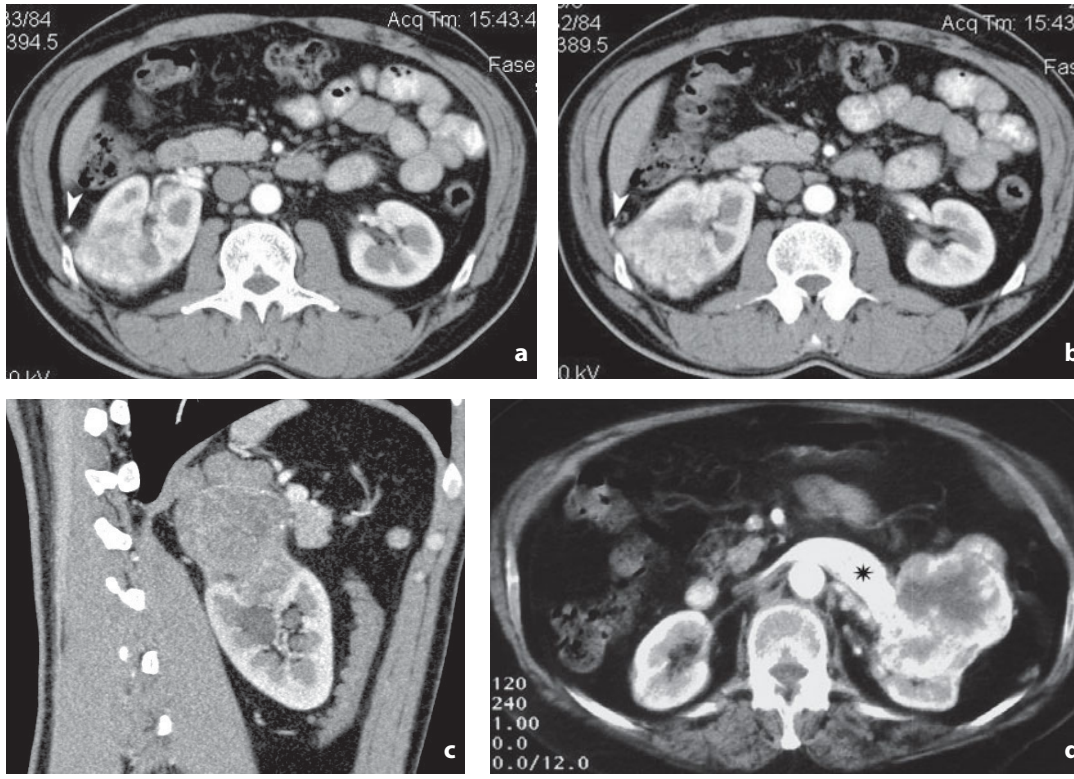

Fig. 9.44a-d. Computed tomography. Renal cell carcinoma. **a, b** Stage T3a neoplasm of the upper third of the right kidney: small solid lesion in the perirenal fat (*arrowhead*). **c** Different case, stage T3a. Solid mass in the upper renal pole of left kidney, with solid nodules in the perirenal fat indicating extracapsular extension. **d** Solid mass, stage T3b. Corticomedullary phase of dynamic study. The image shows a parenchymal neoplasm of the left anterior renal lip invading the renal vein (*asterisk*)

Involvement of the inferior vena cava is demonstrated by extension of the renal vein thrombus into the vena cava itself, where it becomes evident as an intraluminal defect. An indirect sign is the presence of paravertebral collateral circulation. Special attention should be paid to avoid incorrectly interpreting nonenhanced return flow as a thrombus. Defining the level of the thrombus (intrahepatic, retrohepatic, supradiaphragmatic) is important because this influences the surgical approach adopted. Until a few years ago magnetic resonance appeared to be the imaging modality of choice for defining stage T3c. Today multidetector-row CT can provide the same diagnostic information, thanks to the equally effective coronal and sagittal reconstructions. A persistent difficulty for both techniques is the evaluation of invasion of the inferior vena cava wall.

The evaluation of invasion into the adjacent viscera, and in particular into the liver, can be challenging (**Figs. 9.45, 9.46**). Although the absence of a cleavage plane increases the probability of tumor invasion, it is not a pathognomonic sign of invasion as it can be seen without later intraoperative confirmation in some 15% of patients. The only certain sign is focal attenuation alterations in the adjacent organ.

The diagnosis of lymph node metastasis in RCC is based essentially on the size of the nodes. As a result it is encumbered with the limitations of diagnostic imaging which are also well-known in other tumors: micrometastases in otherwise normal-size

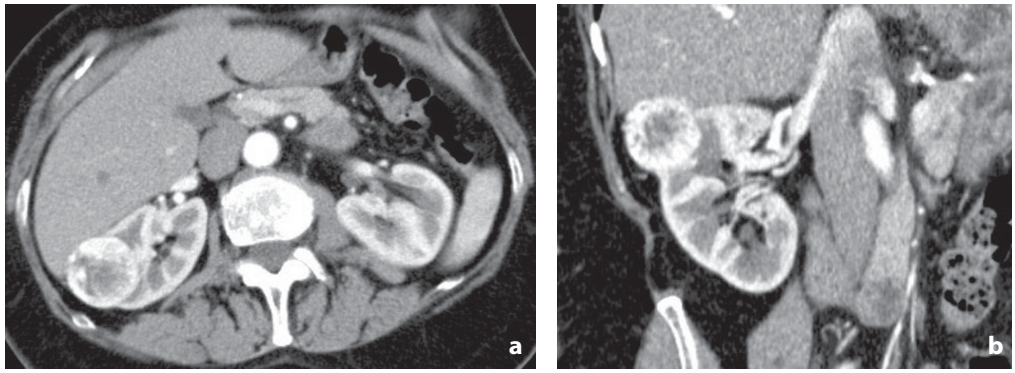

Fig. 9.45a,b. Computed tomography. Renal cell carcinoma. The stage T4 lesion shows no evident cleavage planes with the liver; probable invasion of the hepatic capsule

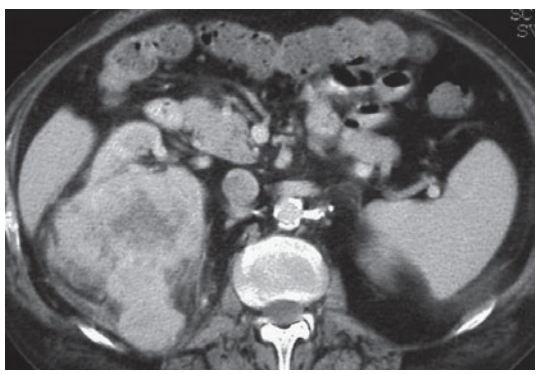

Fig. 9.46. Computed tomography. Renal cell carcinoma. Stage T4 lesion of the lower renal pole with invasion of the paravertebral musculature

lymph nodes, and lymph nodes suspicious of secondary localization but which are in reality only inflamed.

Computed tomography remains the most immediately used imaging modality for the evaluation of distant metastases (lungs, liver, skeletal system) (**Figs 9.47, 9.48**). It should be recalled that in addition to direct extension, the suprarenal glands can be the site of hematogenous seeding.

Prando A, Prando D, Prando P (2006) Renal cell carcinoma: unusual imaging manifestations. RadioGraphics 26:233-244

Sheth S, Scatarige JC, Horton KM et al (2001) Current concepts in the diagnosis and management of renal cell carcinoma: role of multidetector CT and three-dimensional CT. RadioGraphics 21:S237-S254

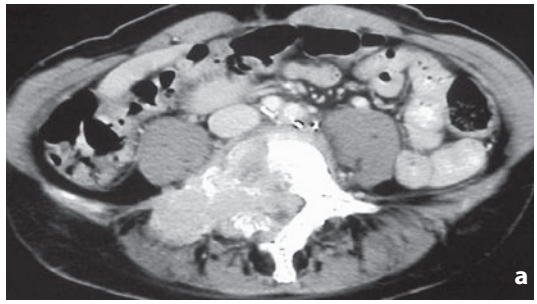

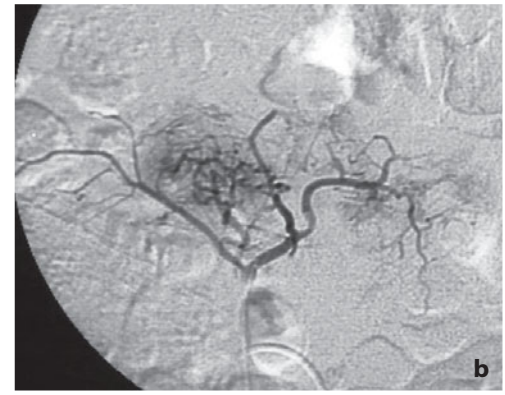

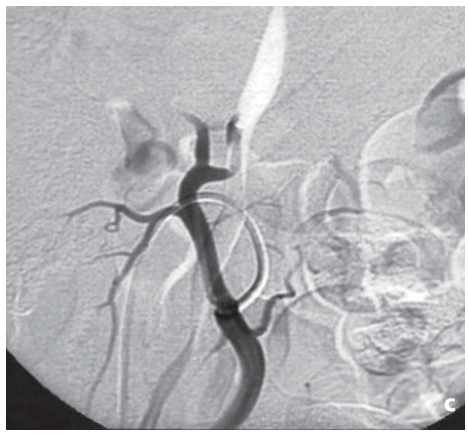

Fig. 9.47a-c. Computed tomography and arteriography. Bone metastasis from renal cell carcinoma. **a** Secondary lesion of the body of L5. **b** Image shows vascularization of the lesion by vessels arising from the right lumbar branch. **c** Deafferentation of the vascular pole after selective embolization

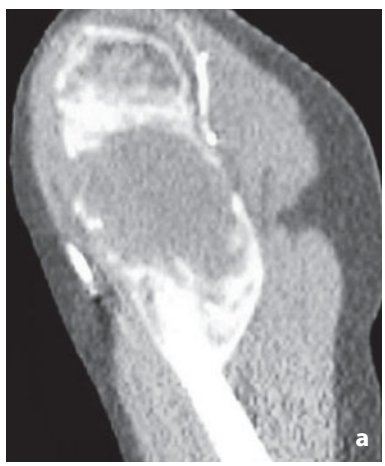

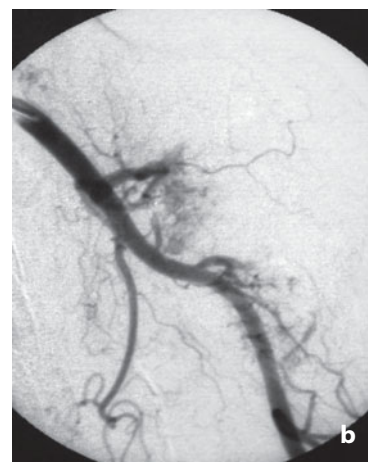

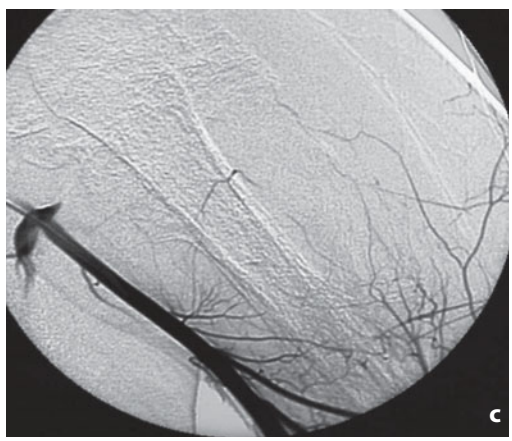

Fig. 9.48a-c. Computed tomography and arteriography. Bone metastasis from renal cell carcinoma. Secondary localization of the left humerus (**a**) supplied by vessels arising from the circumflex humeral artery (**b**). **c** Preoperative selective embolization

Parenchymal Tumors in Children

In most cases nephroblastoma appears on **ultrasonography** as a very large mass which completely overrides the normal structure of the kidney or spares only a part of it. Any healthy tissue is generally separated from the lesion by a thin hypoechoic rim composed of healthy compressed parenchyma.

The structure of the lesion is rather heterogeneous owing to the presence of numerous necrotic hypoechoic areas alternating with hyperechoic areas corresponding to viable portions of the tumor itself (Fig. 9.49). In 10% of cases calcified flecks are visible. The calculation of lesion volume is important particularly in follow-up and is done by summing the two transverse diameters and the longitudinal diameters.

Color Doppler is able to evaluate the intratumoral vasculature as well as define the position and patency of the renal vein and the inferior vena cava, with the rare finding of thrombus extension to the right atrium.

On **computed tomography** images (Fig. 9.50) both before and after contrast medium administration, nephroblastoma generally appears heterogeneous owing to the alternation of hypoattenuating and hyperattenuating areas representing tumor zones with increased vascularity. In the urographic phase of the study the renal origin of the mass can be further confirmed by neoplastic incorporation of the enhanced calices. The pelvicaliceal cavities lose their normal distribution, appearing distorted, either stretched apart or squashed together and flattened, thus losing their radiopacity. Occasionally invasion is seen. The identification of vascular invasion and possible lymph node and distant metastases is relatively easy.

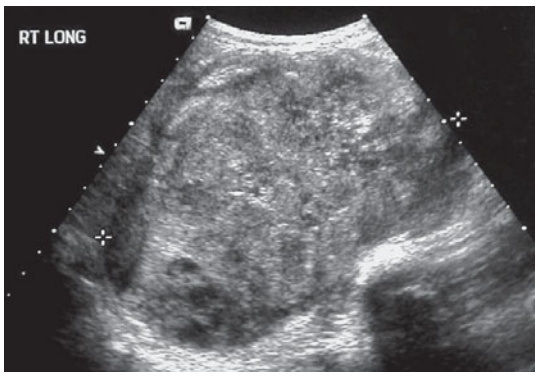

Fig. 9.49. Ultrasonography. Nephroblastoma. Heterogeneous mass completely overrides the structures of the right kidney

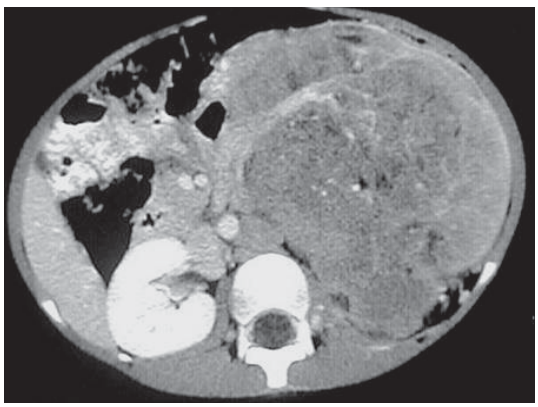

Fig. 9.50. Computed tomography. Nephroblastoma. Large neoplasm arising from the kidney occupies the entire left hemiabdomen

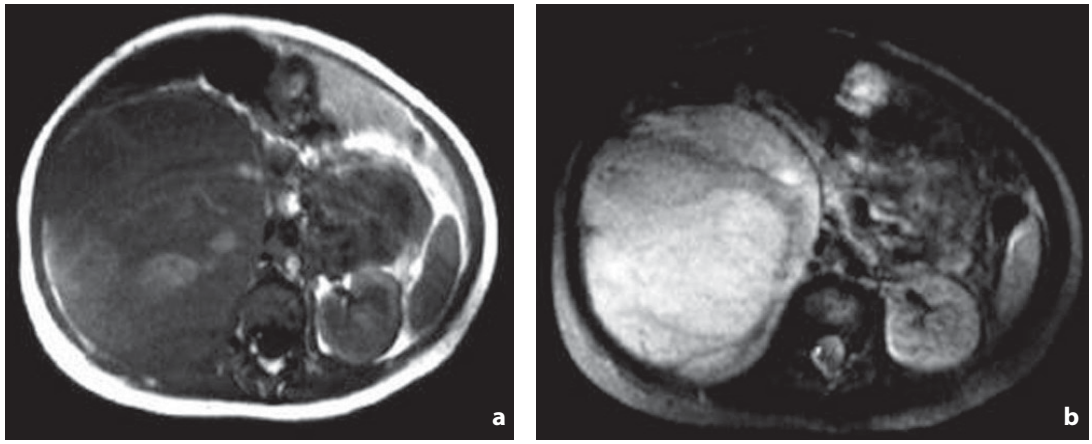

Fig. 9.51a,b. Magnetic resonance. Nephroblastoma in right kidney. The lesion appears prevalently hypointense in T1 (**a**) and hyperintense in T2 (**b**)

On **magnetic resonance** images (**Fig. 9.51**) nephroblastoma usually appears as heterogeneously hypointense in T1-weighted sequences and heterogeneously hyperintense in T2. This imaging modality also has no difficulties in demonstrating invasion of the inferior vena cava.

Angiography is not indicated in unilateral nephroblastoma, with the diagnosis and extension of the tumor being adequately demonstrated with noninvasive imaging modalities. The technique is, however, requested in cases of bilateral tumor, neoplasm in a single kidney (congenital or acquired) or in horseshoe kidney. Abdominal aortography and selective renal arteriography have the sole aim of providing a vascular map to aid the surgical approach, which needs to be as conservative as possible.

In terms of differential diagnosis, nephroblastoma, with its large necrotic component, should be distinguished from a benign lesion such as multilocular cystic nephroma. The latter is characterized by numerous cystic areas separated by thin septations which at US appear well-defined and hyperechoic with no evidence of solid elements. Such elements, in contrast, are highly present in nephroblastoma. The differential diagnosis should also include nephroblastomatosis, a lesion of dubious malignancy which is thought to be a precursor of nephroblastoma. Nephroblastomatosis can be characterized by its uniform structure which is well visualized on both US and CT images.

Lowe LH, Isuani BH, Heller RM et al (2000) Pediatric renal masses: Wilms tumor and beyond. RadioGraphics 20:1585-1603

Cystic Tumors

The kidney is an organ that is frequently affected by cystic lesions. Cysts may be simple dysplastic, congenital or acquired, parasitic or neoplastic in nature. Post-mortem studies have shown that more than 50% of people under the age of 50 have one or more cysts, while some 35-36% of individuals above the age of 50 are found to have a cyst on CT.

The radiologic diagnosis of cysts is certain when the appearance is perfectly anechoic at US, uniformly hyperattenuating on CT images and the wall is smooth, regular and almost invisible. In such cases no further diagnostic study is required. However, this is not the case with complicated cysts. These lesions are called complicated due to their morphologic appearance (septated, wall nodularity, intracystic hemorrhage, overlying inflammation) which renders their characterization difficult. These findings can in fact be found in benign dysplastic, malignant and vascular formations, as well as in lesions resulting from infective-inflammatory processes and trauma.

In 1986 Bosniak proposed a classification (**Table 9.4**) of renal cysts based on CT appearance (which can nonetheless be easily adapted to US and MR) which divides cysts into four categories of increasing risk of malignancy and therefore requiring different therapeutic approaches.

Category I refers to the classic benign cyst. For these lesions the diagnosis is conclusive without need for additional examinations. Category II includes different types of cysts: cysts complicated by the presence of septations (few and thin) with wall nodules (few and regular); multiple cysts adjacent to one another separated by normal renal tissue; high-density nonenhancing cysts which therefore appear hypoattenuating in the nephrographic phase - the content of these lesions is hemorrhagic, highly viscous, proteic or colloidal. The typical appearance of these cysts at US together with the CT findings is diagnostic of benign lesions, also in this case requiring no follow-up.

Table 9.4. Bosniak classification of renal cysts

Bosniak category	Characteristics
I	Simple benign cyst with hair-thin wall, no septations, calcifications or solid elements. The cyst is a nonenhancing lesion with water density
II	Benign cyst with hair-thin septations. Small calcifications may be present in the walls or septations. The <3 cm cyst is a uniformly hyperattenuating nonenhancing lesion with sharp margins
IIF	These cysts contain more hair-thin septations. The septations or wall may be minimally enhancing. Septation or wall thickness may be slightly increased. The cysts may contain dense nodular calcifications but no solid enhancing elements. Included in this category are totally intrarenal, high-density, nonenhancing lesions ≥3 cm. The lesions generally have sharp margins
III	Indeterminate cysts with thick and irregular walls or enhancing septations
IV	Malignant cystic lesions with enhancing solid elements

Bosniak category III cysts (Fig. 9.52) have thick and irregular septations, multiple and irregular calcifications and thick irregular walls. Around 80% of these lesions are malignant and require surgery. Category IV includes clearly malignant solid cystic lesions with numerous cystic or necrotic elements and enhancing wall nodularity (Fig. 9.53).

In 1997 Bosniak modified the previous classification because some category II lesions had in the meantime been encountered with neoplastic characteristics. This led to the introduction of category IIF (where F stands for follow-up) which includes a subset of minimally complicated lesions due to the presence of calcifications considered

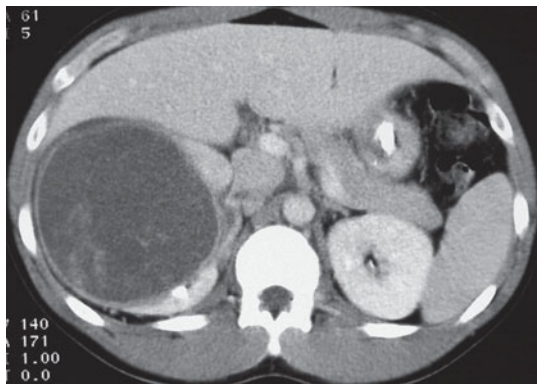

Fig. 9.52. Computed tomography. Bosniak category III renal cyst. Cystic lesion of the right kidney with hyperattenuating septations after contrast enhancement

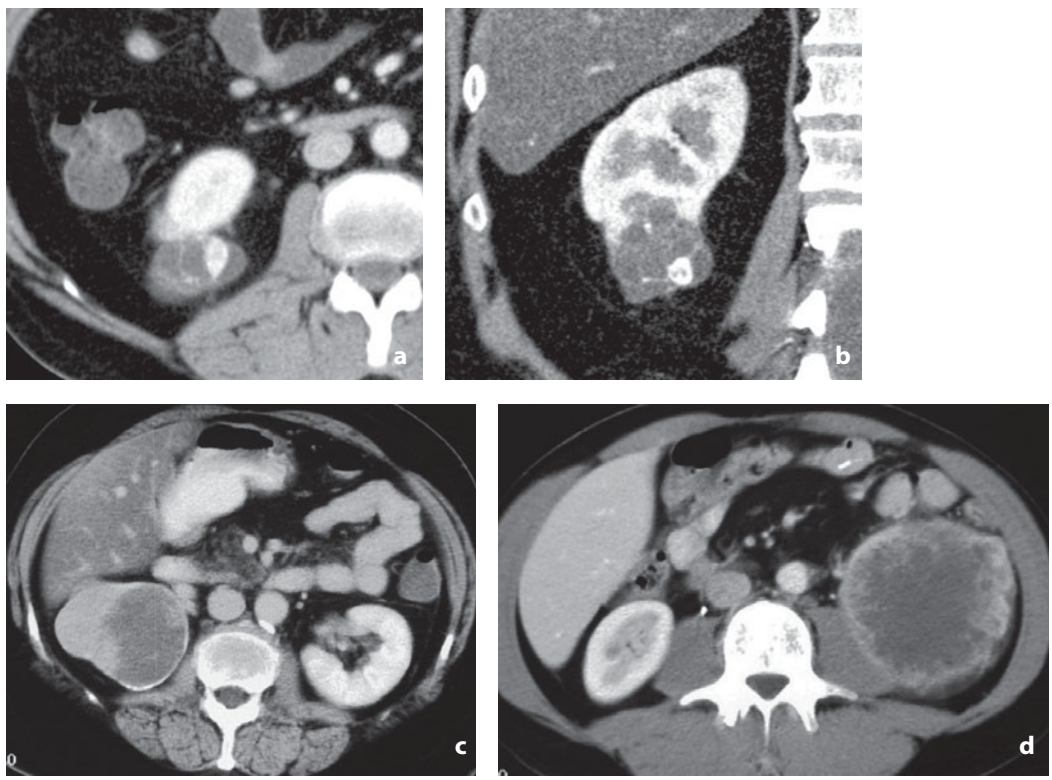

Fig. 9.53a-d. Computed tomography. Bosniak category IV renal cyst. Hypervascular nodule and septations in cystic lesion of lower right renal pole. **a** Axial scan and **b** coronal reconstruction. Histologic diagnosis: clear cell carcinoma. **c** Right renal cystic lesion with solid elements which in the venous phase show enhancement similar to the adjacent normal parenchyma. **d** Cystic lesion of left kidney with solid hyperattenuating elements after contrast enhancement

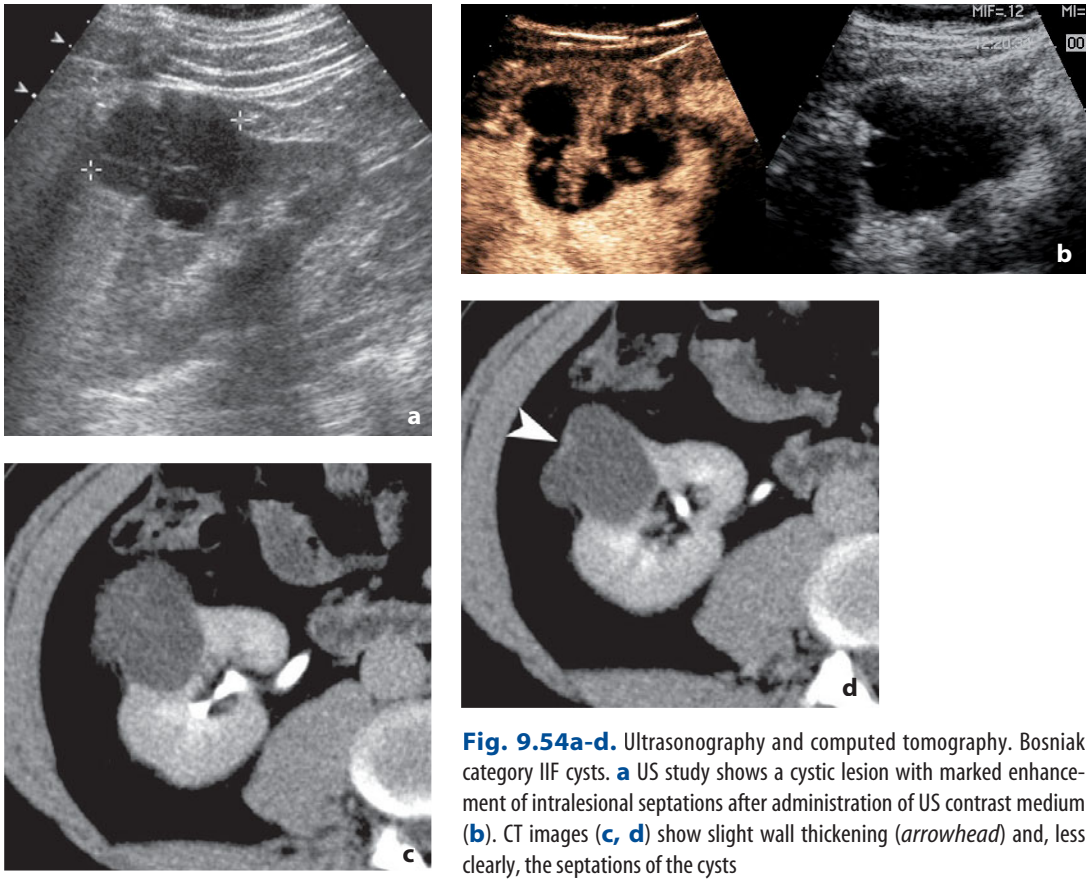

Fig. 9.54a-d. Ultrasonography and computed tomography. Bosniak category IIF cysts. **a** US study shows a cystic lesion with marked enhancement of intralesional septations after administration of US contrast medium (**b**). CT images (**c, d**) show slight wall thickening (*arrowhead*) and, less clearly, the septations of the cysts

significant or septations subjectively considered thickened or more numerous (**Fig. 9.54**).

The Bosniak classification provides a standard for the therapeutic management of complicated cystic lesions. This is based on the probability that the lesion is malignant given its structural irregularity. When the classification is closely adhered to it achieves an accuracy of 84-93% in the differential diagnosis between benign and malignant lesions. Moreover, the classification of each lesion is subjective and therefore influenced by interobserver variability. In addition to being subject to interpretation and experience of the operator, diagnostic accuracy is correlated with the diameter of the lesions, the imaging modality used and the possibility of correlating the findings of different imaging techniques.

The role of **imaging-guided biopsy** in complicated cysts has been broadly debated. Biopsy is usually considered inappropriate for performing differential diagnosis between benign and malignant lesions because internal hemorrhage frequently hampers evaluation of the cell characteristics. In contrast, other investigators suggest that biopsy significantly modifies the therapeutic approach by avoiding the need for surgery in 70% of cases.

In the setting of complicated renal cysts the differential diagnosis should also include parasitic forms. In 2-4% of cases (usually in pastoral areas such as Sicily or Sardinia) *Echinococcus granulosis* can parasitize the kidney, with various radiologic appearances: cystic wall nodularity in plain abdominal films; renal masses which compress the calices and which opacify during urography if they are open in the collecting system; multilocular cysts on US with thick septations and occasionally internal alterations produced by debris; on CT images calcifications within the mass

or multilocular cysts with nonenhancing septations. Wall nodularity can be considered pathognomonic. The cysts may be filled with smaller cysts with an almost completely solid complicated appearance and some residual fluid. At times they appear as hyperattenuating cysts with a solid appearance on US. *Echinococcus* cysts cannot be easily classified in the Bosniak system and since they are nonenhancing lesions they cannot be included in category IV. The diagnosis can be challenging, but must be considered in patients with complicated cysts originating from geographic areas with a high prevalence of echinococcosis.

Bosniak MA (1986) The current radiological approach to renal cysts. Radiology 158:1-10

Bosniak MA (1991) Difficulties in classifying cystic lesions of the kidney. Urol Radiol 13:91-93

Bosniak MA (1994) How does one deal with a renal cyst that appears to be Bosniak class II on a CT scan but has sonographic features suggestive of malignancy (e.g. nodularity of wall or a nodular or irregular septum). AJR Am J Roentgenol 163:216

Bosniak MA (1997) Diagnosis and management of patients with complicated cystic lesions of the kidney. AJR Am J Roentgenol 169:819-821

Hartman DS, Choyke PL, Hartman MS (2004) From the RSNA Refresher Courses: a practical approach to the cystic renal mass. RadioGraphics 24:S101-S115

Pelvicaliceal Tumors

Urography can identify transitional cell carcinoma (TCC) (as well as parenchymal lesions which infiltrate the pelvicaliceal system) according to several characteristic presentations:

- filling defect (35% of cases) either single (**Figs. 9.55, 9.56**) or multiple (**Fig. 9.57**) which may appear as smooth, irregular or stippled;
- filling defects with proximal distension of the calix (oncocalix) (25% of cases);
- filling defect with obliteration, stenosis or amputation of the calix (20%);
- hydronephrosis (6%);
- nonvisualized kidney or delayed enhancement of the collecting system (13%).

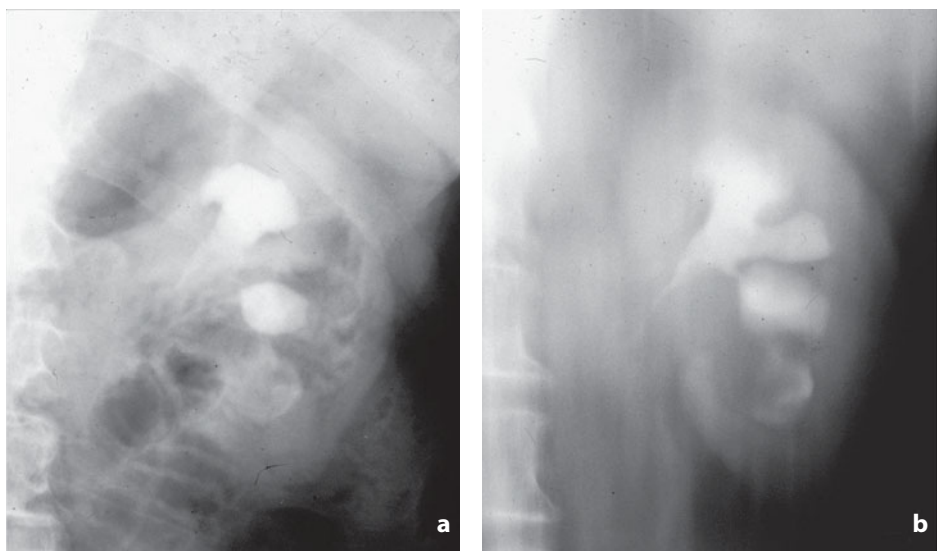

Fig. 9.55a,b. Urography (**a**) and tomography (**b**). Transitional cell carcinoma. Left kidney. Filling defect of the pelvis with stenosis of the collecting system of the dilated upper caliceal system

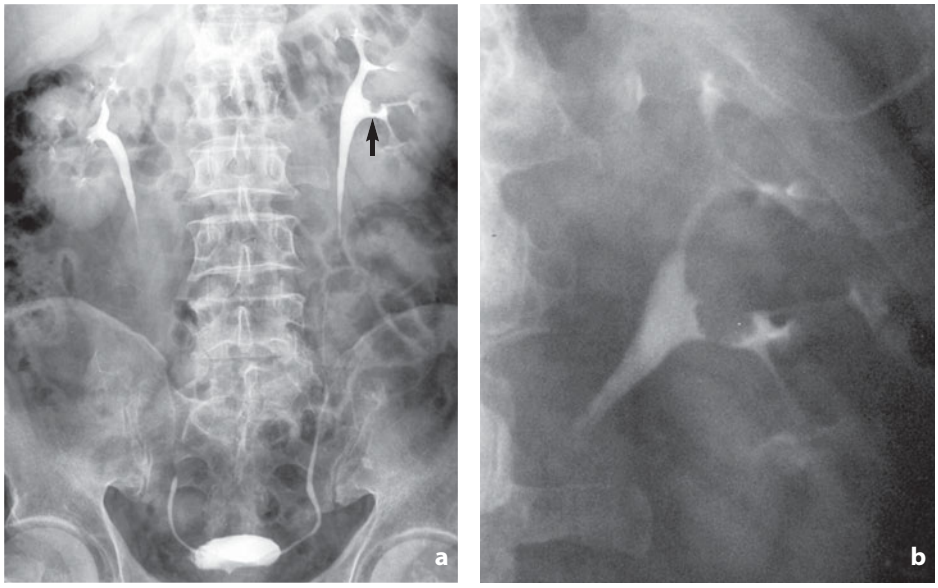

Fig. 9.56a,b. Urography. Transitional cell carcinoma. **a** Radiograph performed at end perfusion. At the level of the upper pole calices a round filling defect can be appreciated with attachment to the major calix wall (*arrow*). **b** Detailed radiography. Lesion with attachment to pelvic wall is confirmed, with lobulated margins and absent caliceal retrodilatation

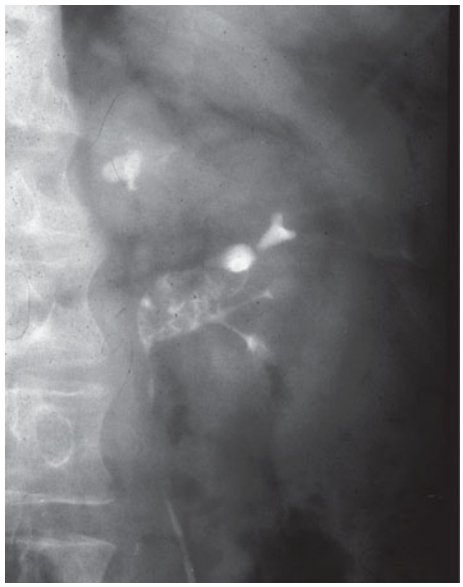

Fig. 9.57. Urography. Transitional cell carcinoma. Multiple filling defects in the renal collecting system

Urography is obviously unable to identify the extraluminal extension of the lesion, which can only be performed with digital tomographic techniques. Its sensitivity in identifying TCC ≥3 cm is above 85%, although this falls drastically for smaller lesions (10-20%). In the setting of conventional radiology TCC is included in the differential diagnosis with other conditions which produce filling defects or pelvicaliceal distortions:

cystic pyelitis (Fig. 9.58), coagulations, kidney stones, papillary necrosis, scarring stenosis and tumors of the renal parenchyma with invasion of the pelvis.

Retrograde pyelography (Figs 9.59, 9.60) is able to study the collecting system of a functionally excluded kidney, better define the extension of a tumor already visualized with other techniques, and perform biopsies with brushing for cytologic evaluation. The mucous surface of the calices or pelvis has an irregular, nodular or papillary appearance. A characteristic sign of a pelvic tumor is the reflux of contrast medium from the cavities to the renal interstitium resulting from the functional exclusion of renal parenchyma.

Ultrasonography is the first-choice imaging technique in the study of patients with hematuria, even though its ability to detect the lesion is inferior to CT. The technique

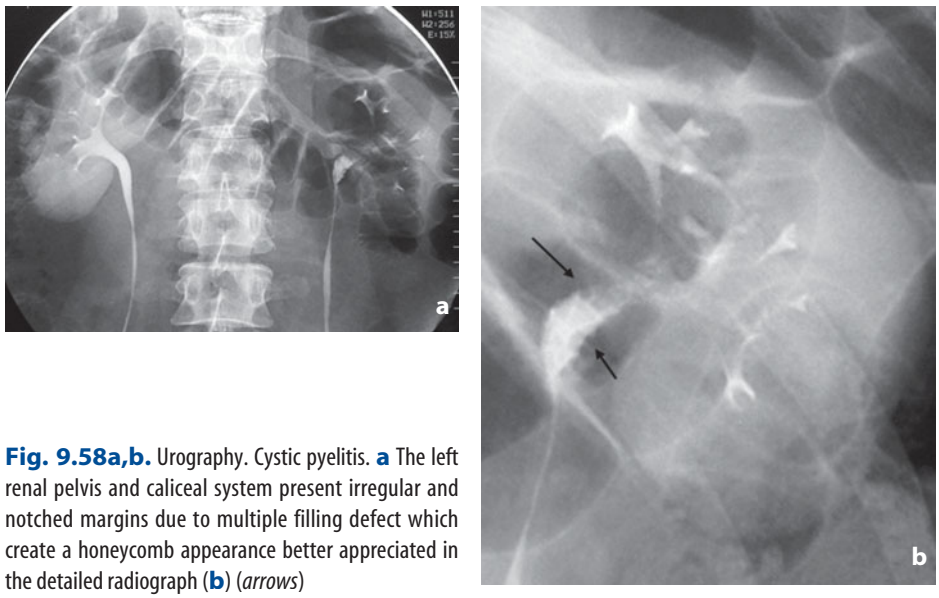

Fig. 9.58a,b. Urography. Cystic pyelitis. **a** The left renal pelvis and caliceal system present irregular and notched margins due to multiple filling defect which create a honeycomb appearance better appreciated in the detailed radiograph (**b**) (*arrows*)

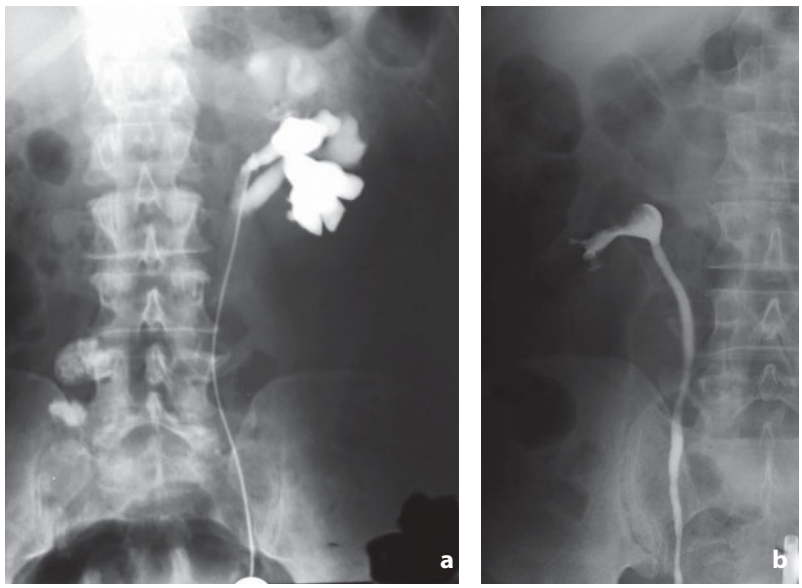

Fig. 9.59a,b. Retrograde pyelography. Transitional cell carcinoma. **a** Amputation of the superior renal pole caliceal system of the left kidney. **b** Different case. Filling defect of the renal pelvis and amputation of the mid and superior caliceal systems of the right kidney

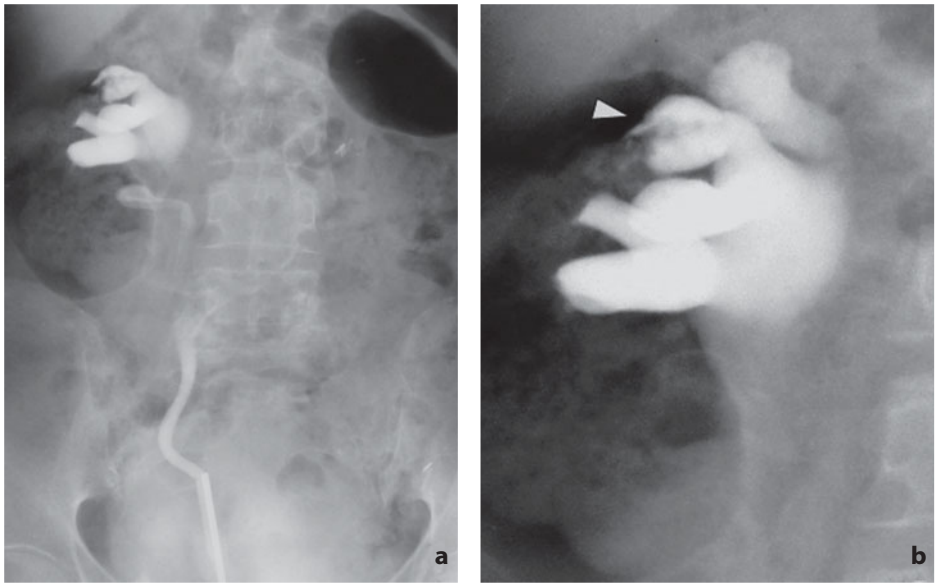

Fig. 9.60a,b. Retrograde pyelography. Caliceal transitional cell carcinoma. Patient previously having undergone left nephrectomy subsequent to urothelial neoplasm. A superior calix of the right kidney shows irregular and notched margins (**a**). The detailed image performed several minutes later (**b**) also shows a filling defect (oncocalix)

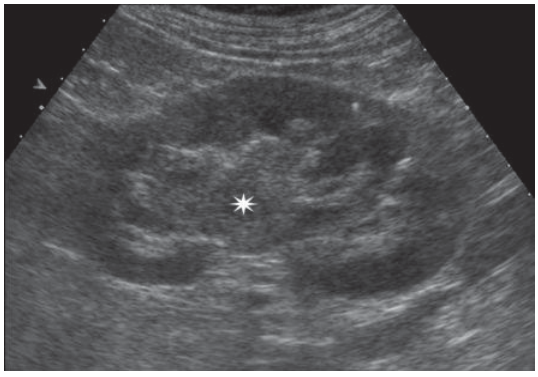

Fig. 9.61. Ultrasonography. Transitional cell carcinoma. Solid centropelvic lesion (*asterisk*) extending into the mid and superior caliceal systems

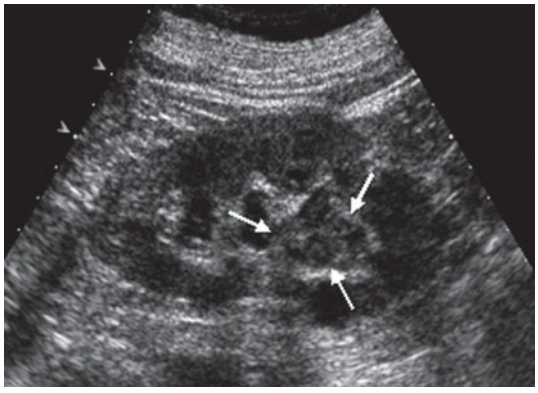

Fig. 9.62. Ultrasonography. Transitional cell carcinoma. Sonogram show an ill-defined solid iso-hyperechoic lesion at the level of the inferior caliceal system (*arrows*)

often identifies urothelial lesions as incidental findings during the course of an examination for other reasons. Caliceal TCC often appears as a moderately hyperechoic lesion in the central renal sinus with or without associated hydronephrosis (Figs. 9.61, 9.62). Occasionally highly malignant lesions appear with heterogeneous

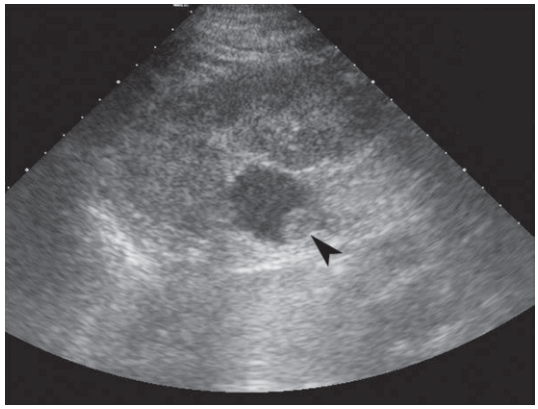

Fig. 9.63. Ultrasonography. Transitional cell carcinoma. Solid lesion in the right renal pelvis (*arrowhead*)

echotexture. Even though the lesion invades the renal parenchyma, the renal profile tends to remain normal. TCC of the pelvis appears as an iso-hyperechoic lesion with good through transmission which remains stationary with changing position of the patient (Fig. 9.63). In some cases the lesions does not appear on US and the diagnostic suspicion is based entirely on secondary signs, such as a shift or distortion of the interface of normal structures, or dilatation of a caliceal system or the pelvis.

The use of **color Doppler** and second-generation **ultrasonographic contrast media**, both widely used in the characterization of renal parenchymal lesions, provides no particularly useful information. The evaluation of blood flow and microcirculation in fact is unable to contribute much in these hypovascular lesions.

CT urography has recently been proposed as a replacement for the conventional technique. Even though the American College of Radiology is still in favor of urography as the technique of choice for the study of hematuria, many centers have completely abandoned the technique in preference for CT. The CT urographic study is performed in two or more dynamic phases. An initial baseline examination to rule out stone formations is followed by a delayed arterial or early corticomedullary phase acquired 15-25 s after the injection of contrast medium, which is especially useful in identifying vascular anomalies. The nephrographic phase used for the study of the renal parenchyma begins at 80-140 s after the injection of contrast medium. The final excretory phase is acquired at 4-8 min and enables study of the collecting system and the bladder.

TCCs ≥1 cm can be visualized in the baseline examination as solid or cystic-like lesions with attenuation values between 8 and 40 HU, location in the renal pelvis or a calix, and a round, plaque-like or arborescent appearance. In the arterial and venous phases of the dynamic study there is a moderate but significant increase in the attenuation values of the lesion (around 30 HU). TCC is identified in the excretory phase as a sessile, nodular filling defect with lobulated margins. Other possible patterns include pelvicaliceal irregularity, focal or diffuse wall thickening and exclusion of caliceal systems. Occasionally dilatation of a calix, hydronephrosis and/or delayed enhancement of the collecting system may be the only signs of the presence of a lesion (Figs. 9.64-9.68). At times oncocalix may be observed, i.e. a dilated calix filled with a TCC. The presence of clots in the collecting system (usually hyperattenuating in the baseline images and nonenhancing after contrast medium injection) can suggest a hemorrhagic lesion. When the tumor is invasive, its extraluminal growth can be identified with invasion of the perirenal pelvic fat and/or psoas muscle. In addition, multidetector-row CT is able to study its precise anatomy and relations with the arterial and venous vessels.

The differential diagnosis should include pelvicaliceal inflammatory processes

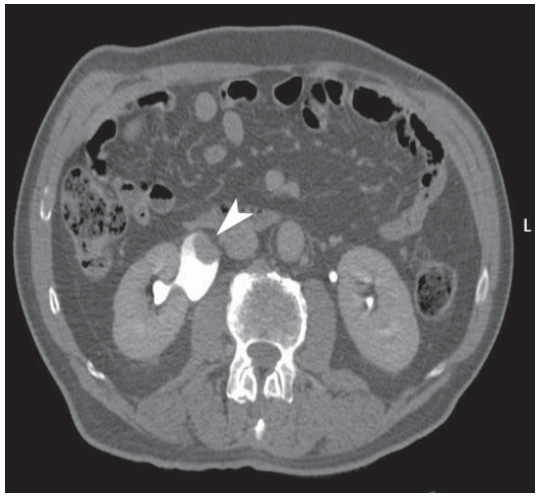

Fig. 9.64. Computed tomography. Transitional cell carcinoma. Same case as Figure 9.63. Solid lesion in the right renal pelvis (*arrowhead*)

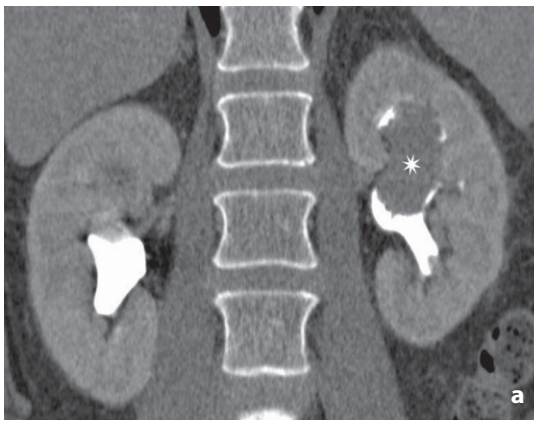

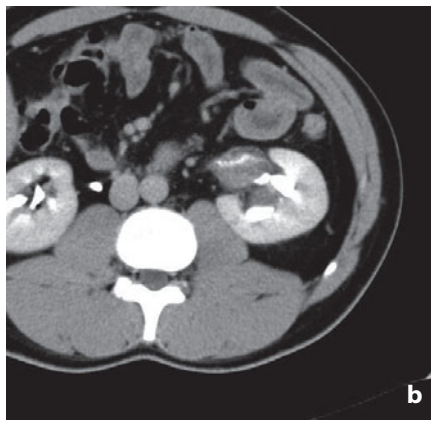

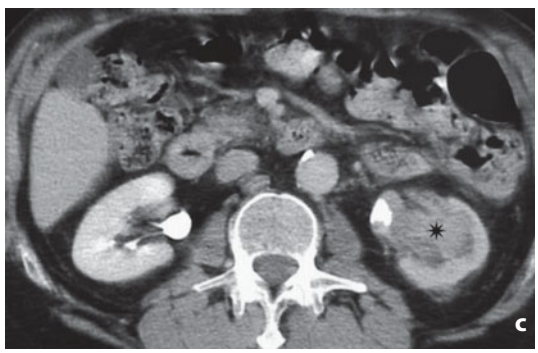

Fig. 9.65a-c. CT urography, excretory phase. Transitional cell carcinoma. **a** Lesion (*asterisk*) in the mid and superior caliceal systems. **b** Lesion in the renal pelvis. **c** Solid mass in the pelvis with invasion of the renal sinus (*asterisk*)

which can produce wall thickening and heterogeneity of the surrounding adipose tissue.

MR urography is especially indicated in children, pregnancy and patients with known allergies to iodinated contrast medium. The study can be either static or dynamic. Static examination is done with heavily T2-weighted images to exploit the hyperintense signal of the static or semistationary fluids, such as urine in the event of stenosis of the collecting system. Dynamic study can be done with or without an

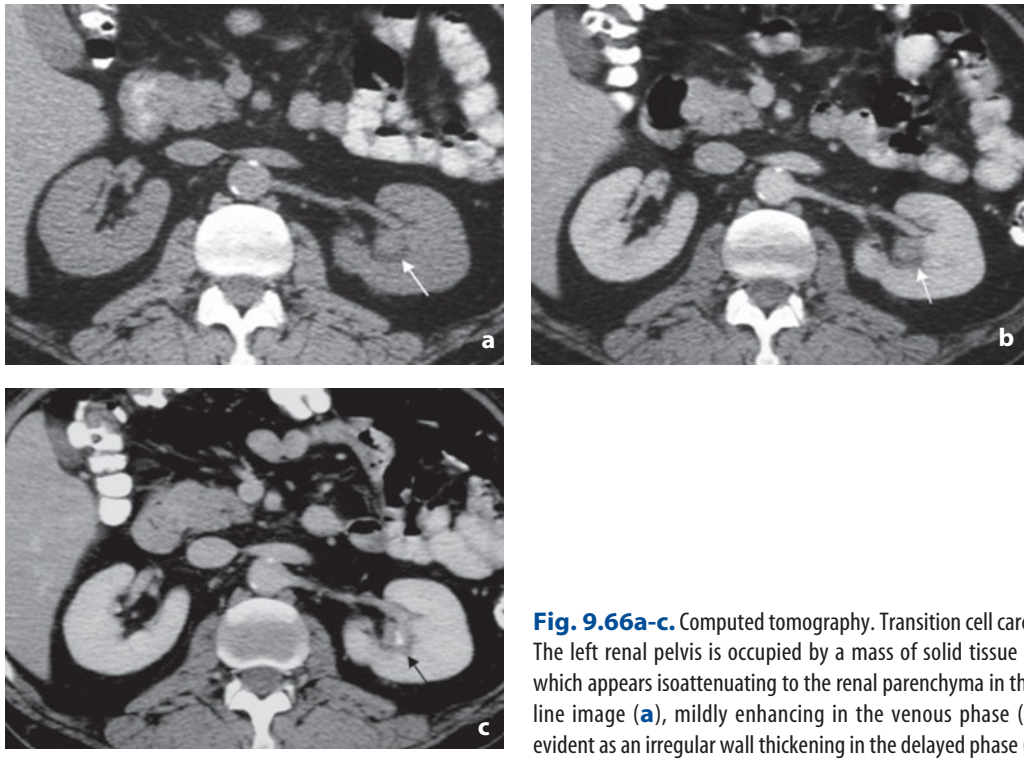

Fig. 9.66a-c. Computed tomography. Transition cell carcinoma. The left renal pelvis is occupied by a mass of solid tissue (*arrow*) which appears isoattenuating to the renal parenchyma in the baseline image (**a**), mildly enhancing in the venous phase (**b**) and evident as an irregular wall thickening in the delayed phase (**c**)

associated diuretic agent and is performed after the injection of gadolinium, which is concentrated in the collecting system during the delayed phase.

Like on CT images, tumors of the pelvicaliceal cavities appear on MR urography as filling defects with a vegetative polypoid appearance and irregular or stippled margins. Their attachment, which is readily identifiable at the level of the pelvis, is more challenging in lesions arising from the calices or collecting ducts due to the limited size of their lumina. TCC appears isointense to renal parenchyma in T1- and T2-weighted images, and hypointense to urine in T2-weighted images, making its identification simple in the event of dilatation of the pelvicaliceal cavity. Despite being hypovascular, the lesion may appear moderately enhancing after contrast medium administration.

As with CT, the MR differential diagnosis of TCC includes renal pelvis blood clots, staghorn calculus and fragments of papillae. In these cases the baseline MR sequences are vital for making a confident diagnosis.

MR is infrequently used for identifying transitional cell carcinoma of the upper urinary tract, for obvious reasons. These include limited availability of and access to scanners, lengthy acquisition times (thus requiring patient compliance), propensity to artifacts (even though the development of fast sequences has closed the gap with CT), spatial resolution inferior to CT (although compensated for by the elevated contrast resolution), and difficulty in identifying very small lesions or lesions with a plaque-like growth pattern.

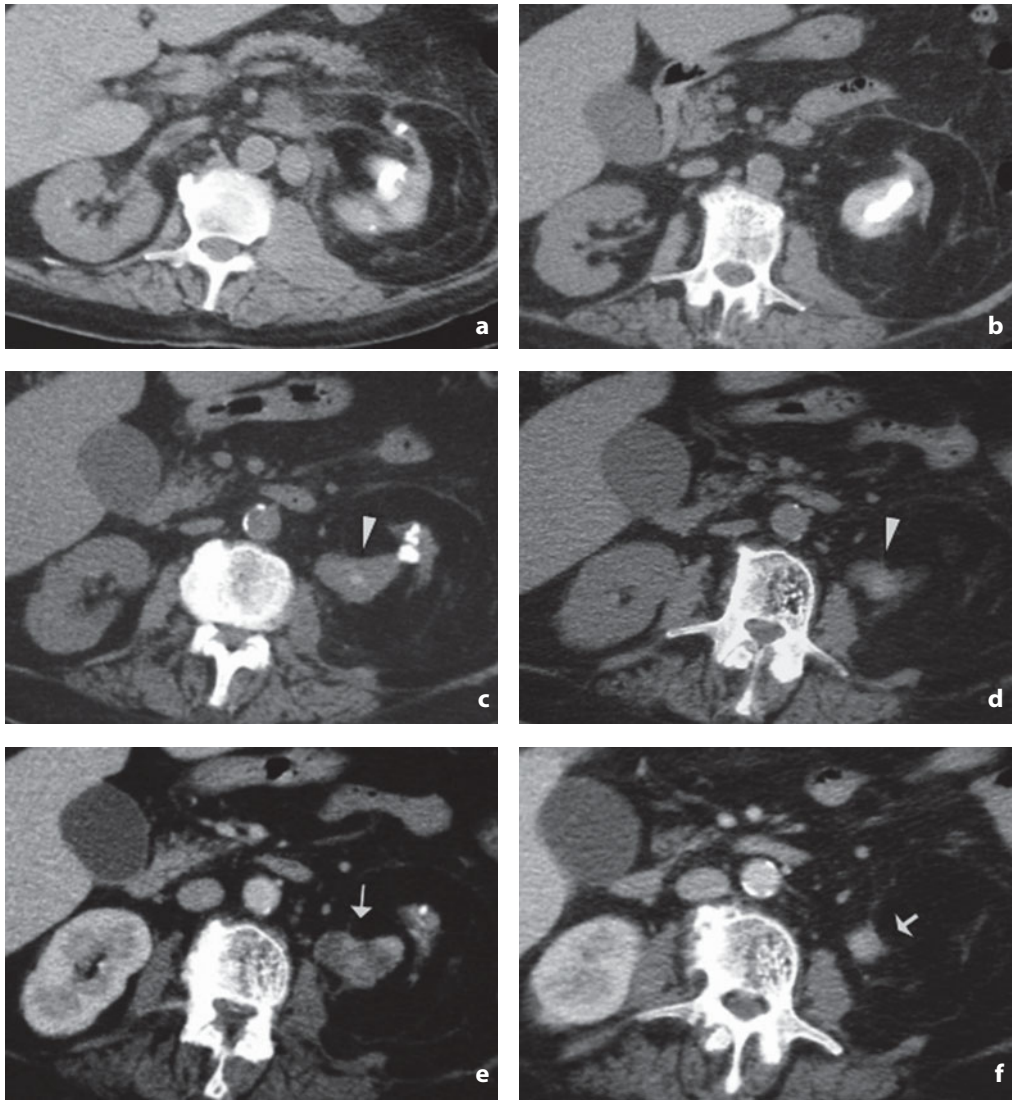

Fig. 9.67a-f. Computed tomography. Transitional cell carcinoma in kidney with staghorn calculus. In the baseline scans (**a-d**) the left renal pelvis is occupied by stones and the ureteropelvic junction, with the proximal segment of the ureter, appears distorted and with solid attenuation (*arrowhead*). After contrast medium injection, the venous phase images show the heterogeneous enhancing pelvic mass (**e**) and solid tissue occupying the proximal segment (**f**) of the ureteric lumen (*arrows*)

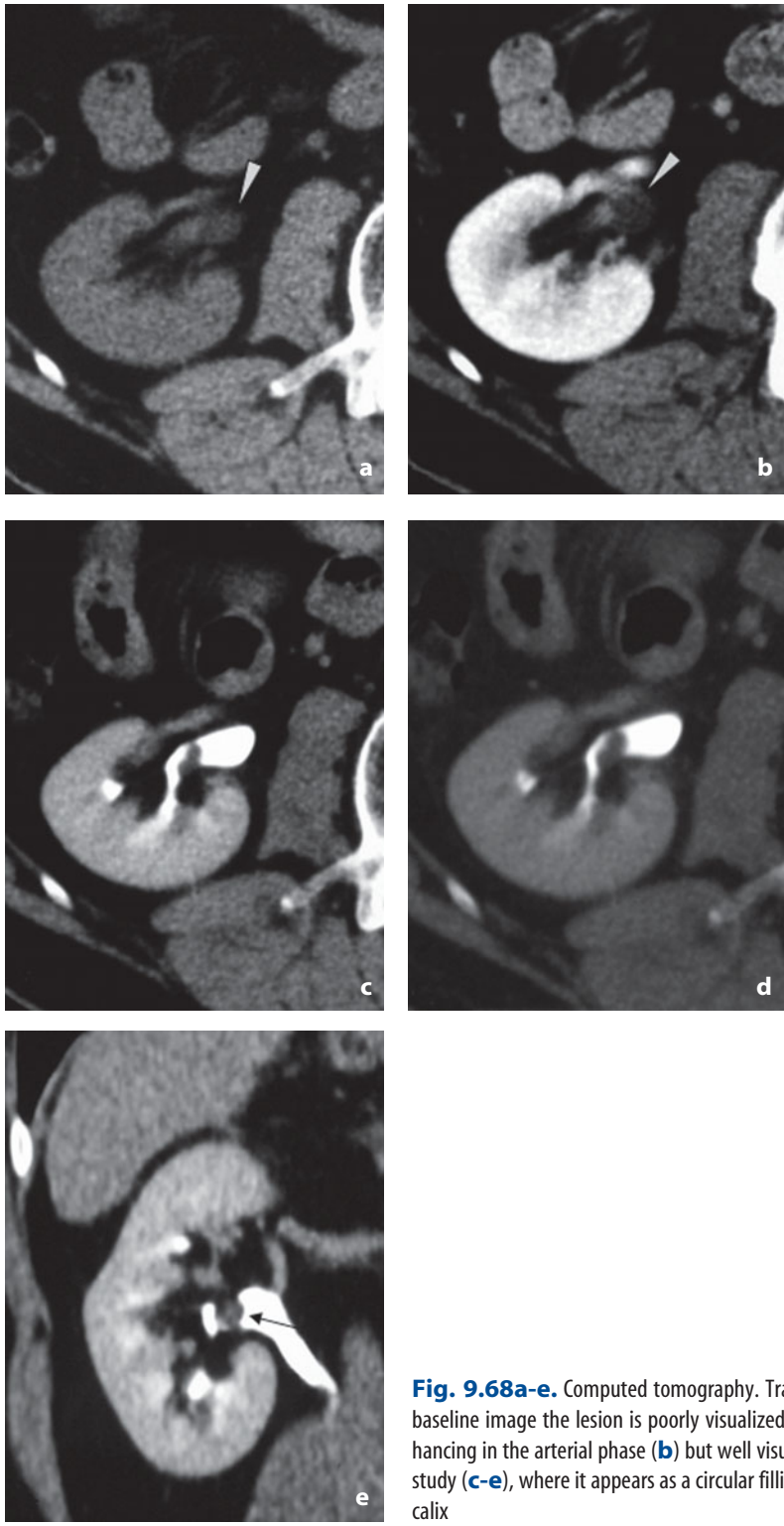

Fig. 9.68a-e. Computed tomography. Transitional cell carcinoma. **a** In the baseline image the lesion is poorly visualized (*arrowhead*). The mass is nonenhancing in the arterial phase (**b**) but well visualized in the delayed phase of the study (**c-e**), where it appears as a circular filling defect attached to the wall of a calix

Table 9.5. TNM classification of upper urinary tract transitional cell carcinoma

Stage	Histopathology
Tx	Occult primary tumor
T0	No evidence of primary tumor
Tis	Carcinoma in situ
Ta	Papillary noninvasive carcinoma
T1	Carcinoma involves subepithelial connective tissue
T2	Carcinoma invades the muscularis
T3	Carcinoma invades beyond muscularis into periureteric or peripelvic fat or into renal parenchyma
T4	Carcinoma invades adjacent organs or extends through the kidney into perirenal fat
Nx	Regional lymph nodes cannot be assessed
N0	No regional lymph node metastasis
N1	Metastasis in a single lymph node, ≤2 cm in greatest dimension
N2	Metastasis in a single lymph node 2-5 cm in greatest dimension; or multiple metastatic lymph nodes, none >5 cm in greatest dimension
N3	Metastasis in a lymph node >5 cm in greatest dimension
Mx	Presence of distant metastasis cannot be assessed
M0	No distant metastasis
M1	Distant metastasis

Staging of TCC (Table 9.5) is defined at diagnosis and influences the incidence of distant metastases, local recurrence and, of course, survival. Lesions in the initial stages (T0-T2) are confined by the renal capsule and do not invade the pelvic fat. The more advanced lesions invade and obliterate the adipose and adjacent tissues. Common sites of distant metastases are the lungs and bone. Conventional radiography and US are unable to evaluate the degree of transmural invasion. This can only be done with CT and MR.

Browne RF, Meehan CO, Colville J et al (2005) Transitional cell carcinoma of the upper urinary tract: spectrum of imaging findings. RadioGraphics 25:1609-1627

Ureteric Tumors

Pathology

Primary tumors of the ureter are rare, accounting for 6% of all cancers of the urinary system. Most are malignant and the most common histotype is transitional cell carcinomas (TCC) (91%). These lesions are prevalent in males with onset between 50 and 80 years of age. They can be preceded by benign or low-grade malignant papillomas. They are bilateral synchronous in 2-9% of cases and metachronous in 11-13%. Up to 50% of patients with ureteric cancer develop a lesion of the urinary bladder of the same histotype within two years of treatment of the initial tumor. In contrast, 2% of patients with bladder TCC have a synchronous lesion in the upper urinary tract whereas 6% develop one thereafter.

Other primary malignant tumors of the ureter include squamous cell carcinoma (8%), adenocarcinomas, undifferentiated carcinomas and sarcomas.

The ureter can also be the site of secondary lesions, either by direct extension (dislocation, encasement of retroperitoneal lymphomas, invasion of carcinomas of the bladder, prostate or uterine cervix) or much more rarely by hematogenous seeding (invasion of periureteric fat, involvement of the wall or submucosal nodules from distant tumors).

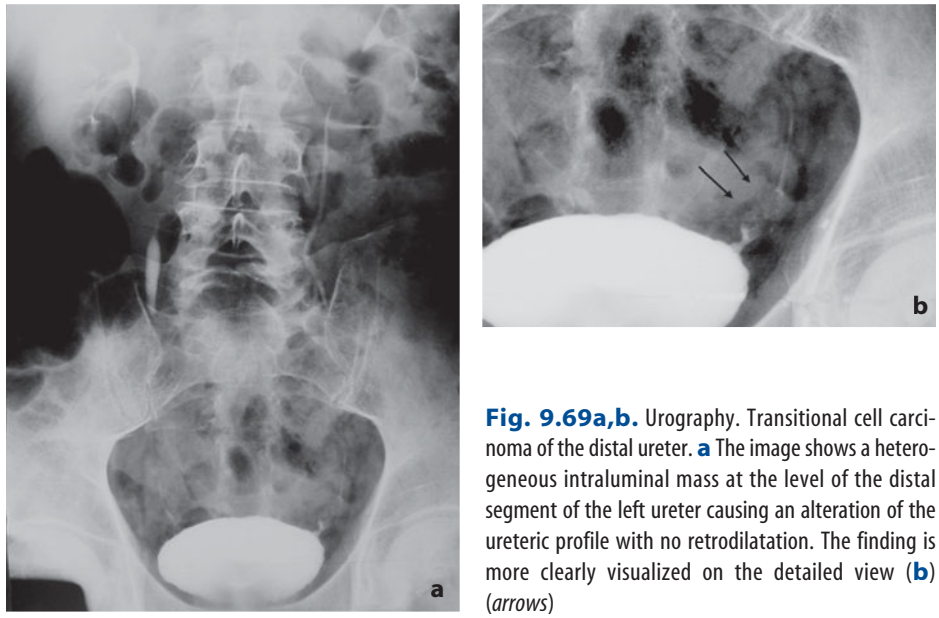

Fig. 9.69a,b. Urography. Transitional cell carcinoma of the distal ureter. **a** The image shows a heterogeneous intraluminal mass at the level of the distal segment of the left ureter causing an alteration of the ureteric profile with no retrodilatation. The finding is more clearly visualized on the detailed view (**b**) (*arrows*)

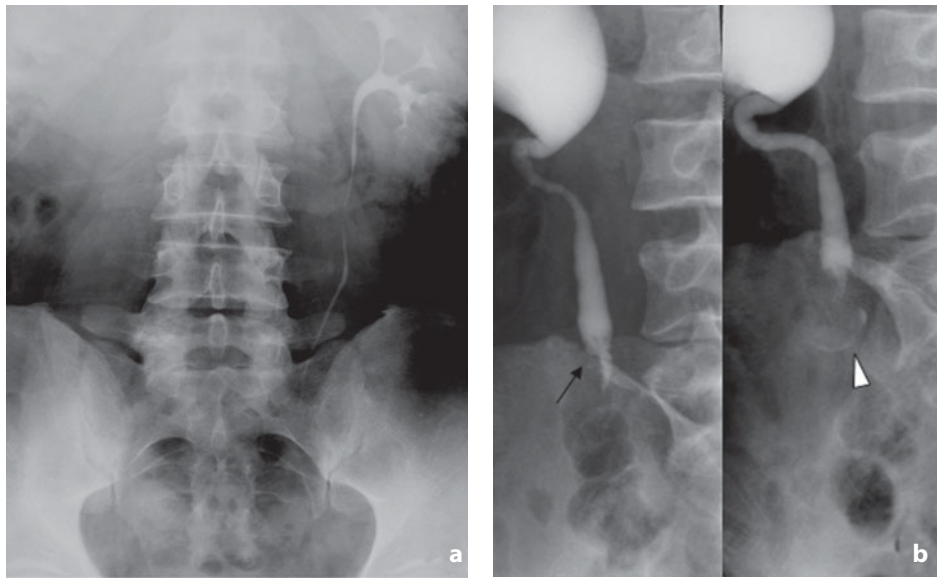

Fig. 9.70a,b. Urography. Ureteric tumor. **a** End-perfusion image shows loss of function of the right kidney. **b** After several hours there is marked dilatation of the right renal pelvis and the proximal segment of the ureter which comes to a sudden stop, with irregular margins (*arrow*). Note the characteristic goblet sign (*arrowhead*)

Diagnostic Imaging

Identification

Urography has for many years been the most widely used technique for the diagnosis of ureteric TCC. Characteristic signs are a single or multiple filling defects (33% of cases) (Fig. 9.69), delayed excretion of iodinated urine (25%), hydronephrosis or hydroureteronephrosis (25%). In a limited number of cases a ureteric TCC can go unobserved. Benign eccentric or encircling lesions can mimic malignant tumors, even though the latter tend to present a fixed appearance with irregular margins (Fig. 9.70).

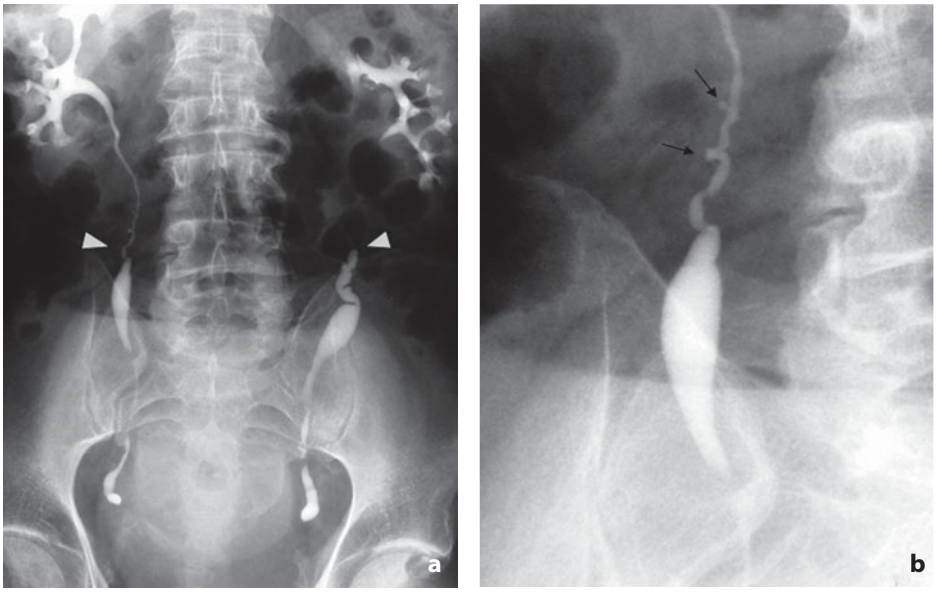

Fig. 9.71a,b. Urography. Cystic fibrous dysplasia of the ureter. **a** Bilateral ureteric stricture (*arrowheads*) with distal dilatation of the lumen. **b** The detailed image shows some diverticular formations (*arrows*)

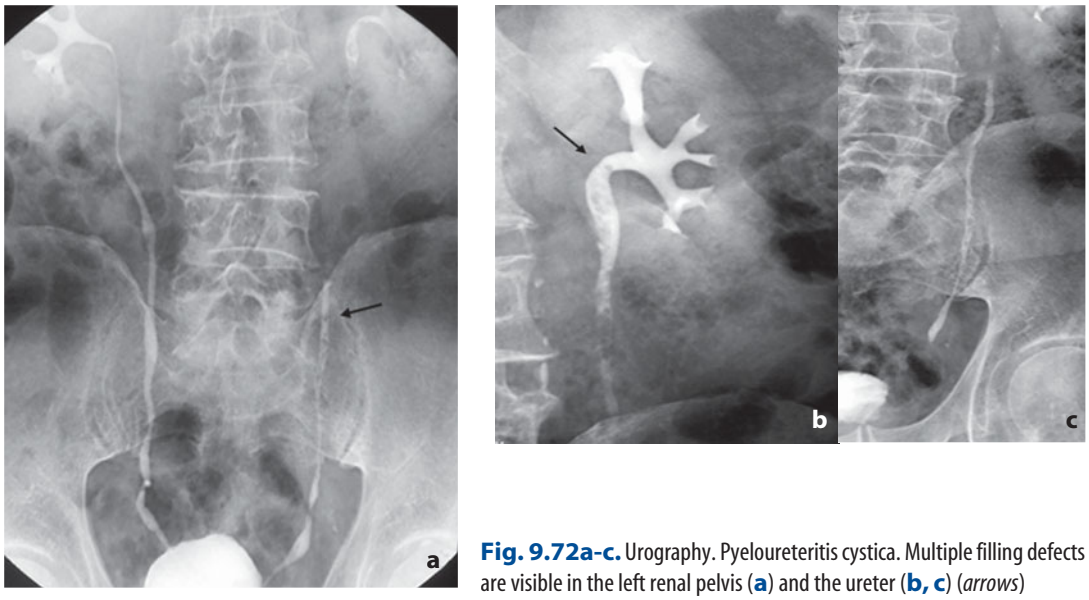

Fig. 9.72a-c. Urography. Pyeloureteritis cystica. Multiple filling defects are visible in the left renal pelvis (**a**) and the ureter (**b, c**) (*arrows*)

Other conditions, however, should be included in the differential diagnosis, such as pyeloureteritis cystica, which can cause filling defects and/or stricture (**Figs. 9.25, 9.71, 9.72**). Urography is also limited in other areas: by causing hydroureteronephrosis and compromising the excretory function of the kidney, chronic stricture can undermine the study of the collecting system and in cases of ureteropelvic obstruction hinder the visualization of a possible distal synchronous lesion.

Retrograde pyelography is considered the examination of choice for the study of ureteric tumors. The technique is invasive (performed during cytoscopy) and enables the study of lesions considered suspicious on urography. The procedure is indicated in cases of renal failure or known allergic reactions to contrast media. TCC appears as an intraluminal polypoid defect with dilatation of the proximal segment of the ureter.

A rather characteristic feature of TCC is the goblet sign, i.e. the champagne-glass-like configuration of the focally and distally dilated ureter at the intraluminal defect. A rare finding is the Bergmann sign, when a retrograde catheter is placed in the "goblet" below the lesion.

Ultrasonography is decidedly limited in these cases, since it is rarely able to study the entire ureter even when it is dilated. The technique is only able to evaluate the proximal segment when dilated and the vesicoureteric junction with the urinary bladder distended. The diagnosis of tumors may be suspected when there is an obstruction with dilatation of the pelvicaliceal cavities, and is therefore based on secondary signs (**Fig. 9.73**). One technique still under development and currently used in very few centers is based on the use of miniaturized intraluminal transducers to perform ureterorenoscopy.

Hydroureteronephrosis is a common finding in CT. In some cases the tumor can manifest as a mass of solid tissue (≥5 cm) with an attenuation value above urine in baseline images, or more commonly as a filling defect or wall thickening in the excretory phase (**Figs. 9.74-9.76**). Other useful CT findings for the identification of ureteric tumors are eccentric or concentric thickening of the ureteric walls, lumen stricture, invasion of the adjacent structures (wall thickening and enhancement together with periureteric fat stranding are especially indicative of extramural tumor spread).

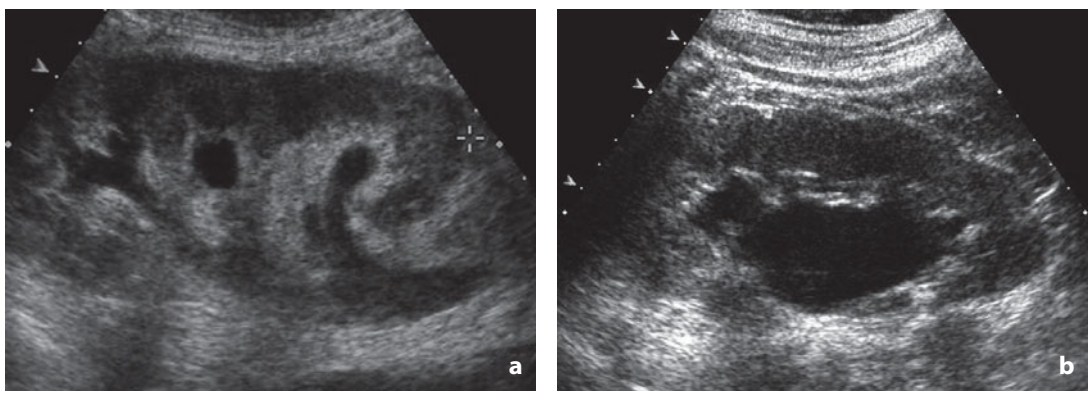

Fig. 9.73a,b. Ultrasonography. Ureteric tumor. In these two patients the ureteric tumor is manifest with secondary signs of pelvicaliceal hypotony (**a**) and hydronephrosis (**b**)

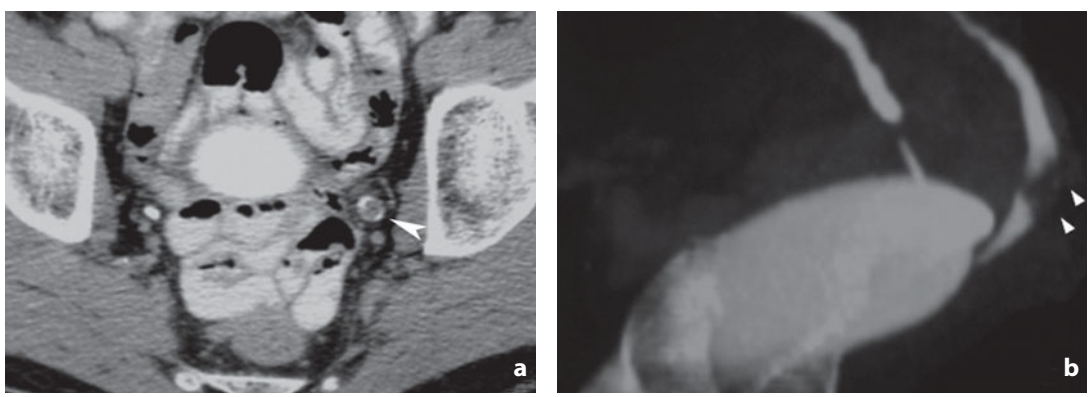

Fig. 9.74a,b. Computed tomography. Distal ureteric tumor. Examination performed in the excretory phase. **a** Nonobstructive filling defect is discernible in the left ureteric lumen (*arrowhead*). **b** MIP reconstruction confirms the filling defect in a urographic-like image

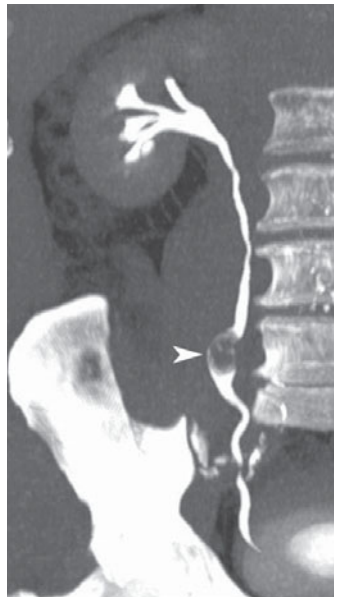

Fig. 9.75. CT urography. Transitional cell carcinoma. Irregular filling defect (*arrowhead*) at the mid-third of the right ureter

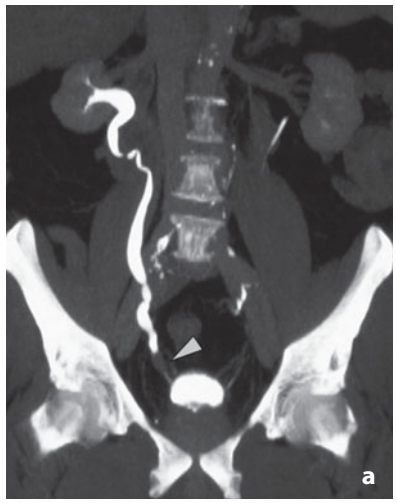

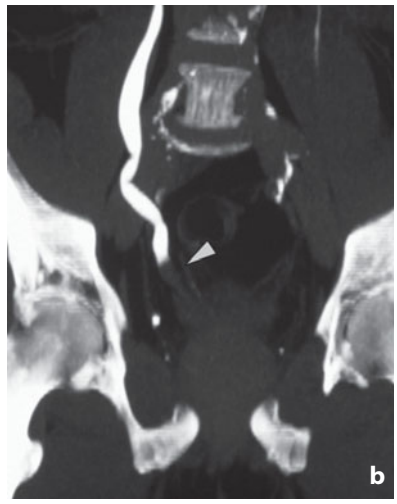

Fig. 9.76a-c. CT urography. Distal ureteric tumor. **a,b** MIP and **c** shaded surface display (SSD) reconstructions. Filling defect in the right ureter (*arrowhead*), with proximal dilatation of the collecting system

CT urography enables differential diagnosis between TCC, renal stones, blood clots and periureteric edema due to stasis (Fig. 9.77).

On **MR urography** the lesion also appears as an intraluminal filling defect (with consequent dilatation of the collecting system proximally) or nonobstructive, in which case the goblet sign described above may be visible. This is useful in differential diagnosis with obstructive calculi, since in the latter the lumen distal to the obstruction appears threadlike or stenotic. In addition, TCC typically appears as an irregular intraluminal defect whereas a calculus displays regular and well-defined margins. The differential diagnosis between a tumor and a small stone can nonetheless be challenging. In this case paramagnetic contrast medium, which should produce at least slight enhancement of TCC, is not always helpful. In baseline sequences in fact, TCC has signal intensity similar to that of the psoas muscle in T1-weighted images, and slightly higher in T2.

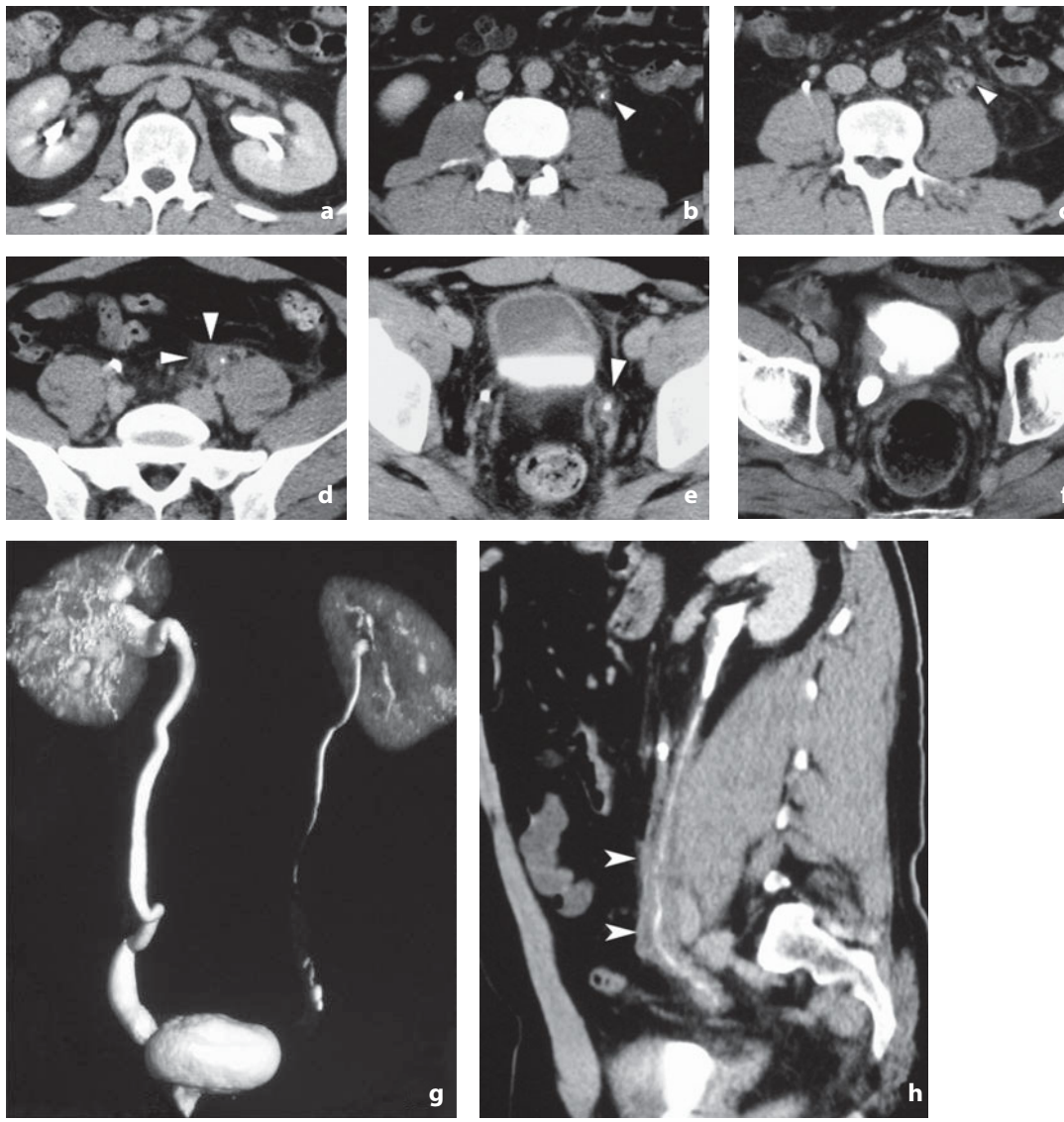

Fig. 9.77a-h. Computed tomography. Ureteric compression due to venous stasis. **a-f** Delayed phase of the dynamic study. Images show left ureteric wall thickening (*arrowheads*), marked edema of the surrounding adipose tissue and reduction of the ureteric lumen. Stenosis of the ureteric outlet can also be seen in the SSD (**g**) and 3D reconstruction (**h**)

The presence of periureteric fat stranding can be a sign of extramural spread of the tumor, even though prior inflammation, surgery or radiotherapy can mimic this condition (prior inflammation can nonetheless be characterized by its low signal in T2-weighted images).

Staging

As with renal TCC, only CT and MR are able to evaluate the transmural invasion of the tumor. Lesions in the initial stages (T0-T2) are confined by the muscle layer and do not invade the periureteric fat. The more advanced lesions invade and obliterate the adipose and adjacent tissues. Sites of distant metastasis of ureteric tumors are most commonly the lungs and bone.

Winalski CS, Lipman JC, Tumeh SS (1990) Ureteral neoplasms. RadioGraphics 10:271-283

Wong-You-Cheong JJ, Wagner BJ, Davis CJ (1998) Transitional cell carcinoma of the urinary tract: radiologic-pathologic correlation. RadioGraphics 18:123-142

Bladder Cancer

Pathology

Bladder cancer (**Fig. 9.78**) is histologically classified in epithelial (95%) and nonepithelial (mesenchymal) (**Table 9.6**). Between 80% and 90% of the former are urothelial

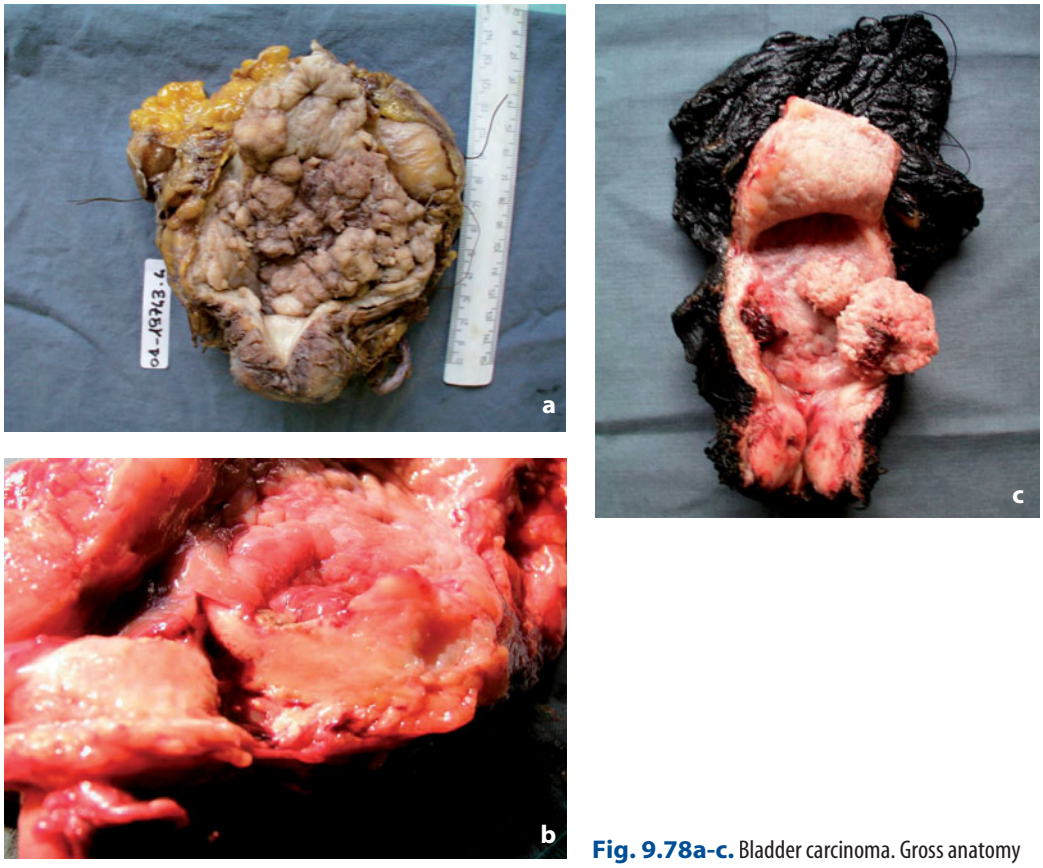

Fig. 9.78a-c. Bladder carcinoma. Gross anatomy

Table 9.6. Histologic classification of bladder cancer

Epithelial tumors	Mesenchymal tumors
Urothelial (transitional cell) tumor Papilloma inverted exophytic	Mesenchymal tumors benign malignant
Papillary urothelial neoplasm of low malignant potential	Pheochromocytoma (paraganglioma)
	Lymphoma
Carcinoma low-grade high-grade	Plasmocytoma
Carcinoma in situ	Germ cell tumors
Dysplasia / atypical cells Variants of urothelial carcinoma	Non-neoplastic conditions Metaplasia Inflammation "Cystitis" Amyloidosis Hamartomas Vascular lesions, etc.
Squamous cell carcinoma	
Adenocarcinoma	
Villous tumor	
Poorly differentiated small-cell carcinoma	
Rare tumors Carcinoid Melanoma Lymphoepithelial carcinoma Large cell neuroendocrine carcinoma Spindle and giant cell carcinoma Plasmacytoid / lymphomatoid carcinoma Rhabdomyoma Basaloid carcinoma	

lesions which range from benign papillomas to carcinoma in situ and even invasive carcinoma. Other epithelial forms in descending order of incidence are squamous cell carcinoma (2-15%) and adenocarcinomas (<2%), while small-cell/neuroendocrine carcinoma, carcinoid and melanoma are rare. Since they arise from the superficial lining of the bladder wall, the epithelial forms often appear as irregular intraluminal defects. Indeed, lesions with a papillary appearance are more often papillomas, inverted papillomas, papillary urothelial neoplasms of low malignant potential (PUNLMP), and low- and high-grade papillary carcinomas. PUNLMP is a histologic form recently introduced to the World Health Organization classification. It describes a small unifocal lesion which never invades or metastasizes and with a recurrence rate of 35% and a progression to a higher stage in 11% of cases. Other patterns of epithelial tumors include a nodular and sessile appearance, the latter being more typical of reactive urothelial hyperplasia, atypical dysplasia and carcinoma in situ.

Mesenchymal tumors can be benign (leiomyoma, paraganglioma, fibroma, plasmocytoma, hemangioma, solitary fibrous tumor and lipoma) or malignant (rhabdomyosarcoma, leiomyosarcoma, lymphoma and osteosarcoma).

Up to 90% of bladder cancers are situated at the level of the lateral walls, posterior

wall or trigone. The remaining 10% are found at the dome or the bladder neck. Around 60% are unifocal and at cystoscopic diagnosis 50% measure <2.5 cm. At cystoscopic diagnosis 10% of bladder cancers are metastatic, 20% are invasive and the remaining 70% are characterized by a papillary appearance and a long history of repeated recurrences after resection, without, however, progressing towards malignancy. In fact only 20% of subjects with initial noninvasive disease develop a malignant lesion and only 2% of patients die from bladder cancer.

Murphy WM, Grignon DJ, Perlman EJ (2004) Tumors of the kidney, bladder, and related urinary structures. American Registry of Pathology, Washington

Diagnostic Imaging

Identification

In conventional radiography, morphologic study of the urinary bladder is performed with **cystography**, which can be **antegrade** (during the terminal phase of urography), **retrograde** (with enhancement of the viscera via a urethral catheter) or **micturating** (with documentation of bladder dynamics and visualization of the urethra during voiding). Bladder cancers generally appear as filling defects, irregularities in the mucous pattern and/or wall rigidity, which can be visualized in radiographs acquired in several views and best with low or mid filling and postvoid (**Figs. 9.79-9.82**).

Ultrasonography is a key examination. Provided that it is adequately distended, the urinary bladder can be well evaluated with a suprapubic approach. Lesions projecting into the lumen can have variable echogenicity and sometimes (6–7%) with internal calcifications. The margins of the tumor can be irregular due to necrosis or ulceration (**Fig. 9.83**). The differential diagnosis with blood clots, which are mobile with changing patient position, is generally immediate. More challenging is the comparison with nodular endometriosis, prostatectomy outcomes or ureterocele. Greater difficulty is encountered in identifying invasive lesions of the bladder wall, which generally only moderately into the lumen and only appear with focal thickening or rigidity of the

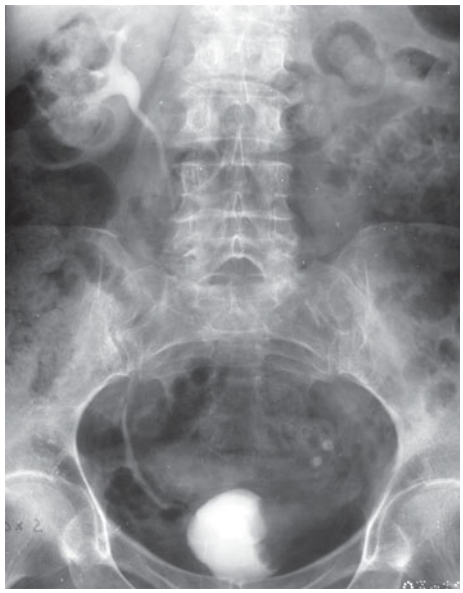

Fig. 9.79. Urography. Bladder cancer. Large filling defect with irregular margins involving almost half of the bladder lumen, most likely attached to the left lateral wall. The functional exclusion of the left kidney is suggestive of involvement of the ipsilateral distal ureter

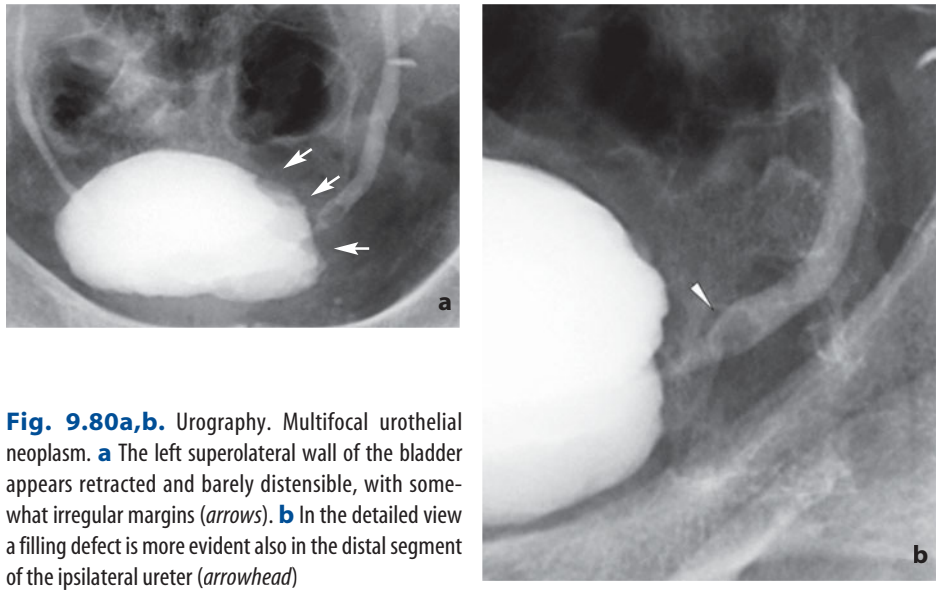

Fig. 9.80a,b. Urography. Multifocal urothelial neoplasm. **a** The left superolateral wall of the bladder appears retracted and barely distensible, with somewhat irregular margins (*arrows*). **b** In the detailed view a filling defect is more evident also in the distal segment of the ipsilateral ureter (*arrowhead*)

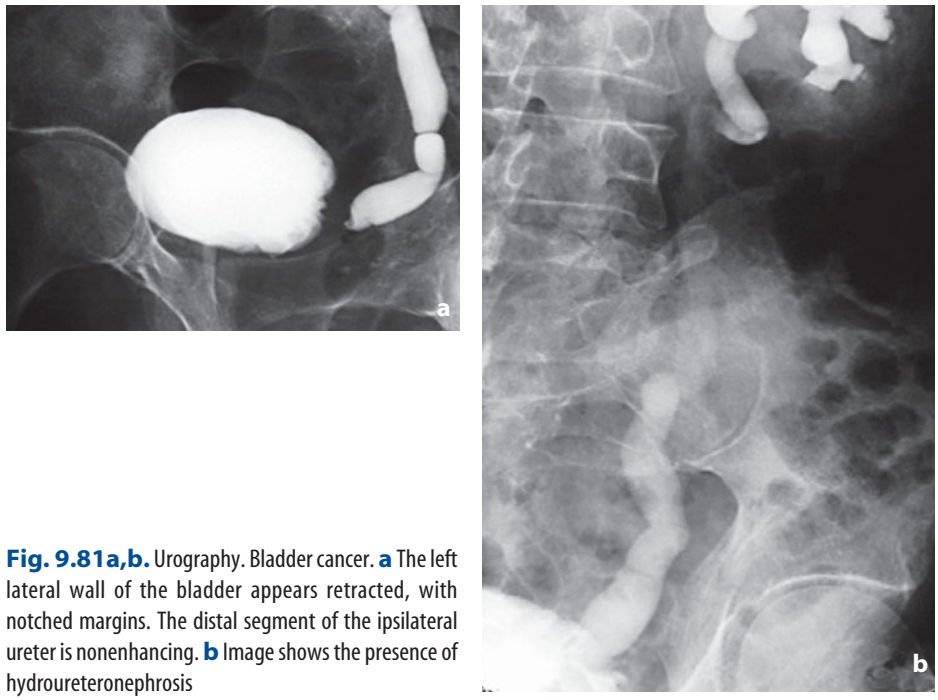

Fig. 9.81a,b. Urography. Bladder cancer. **a** The left lateral wall of the bladder appears retracted, with notched margins. The distal segment of the ipsilateral ureter is nonenhancing. **b** Image shows the presence of hydroureteronephrosis

bladder wall (making differential diagnosis with cystitis difficult). A particular feature of the US examination is its ability to visualize tumors located in bladder diverticula (especially in post-voiding scans). These tumors can pass unobserved in urography or cystoscopy if the neck of the diverticulum is particularly narrow. The use of transrectal or transvaginal transducers is particularly effective for the study of tumors arising in the proximity of the bladder neck.

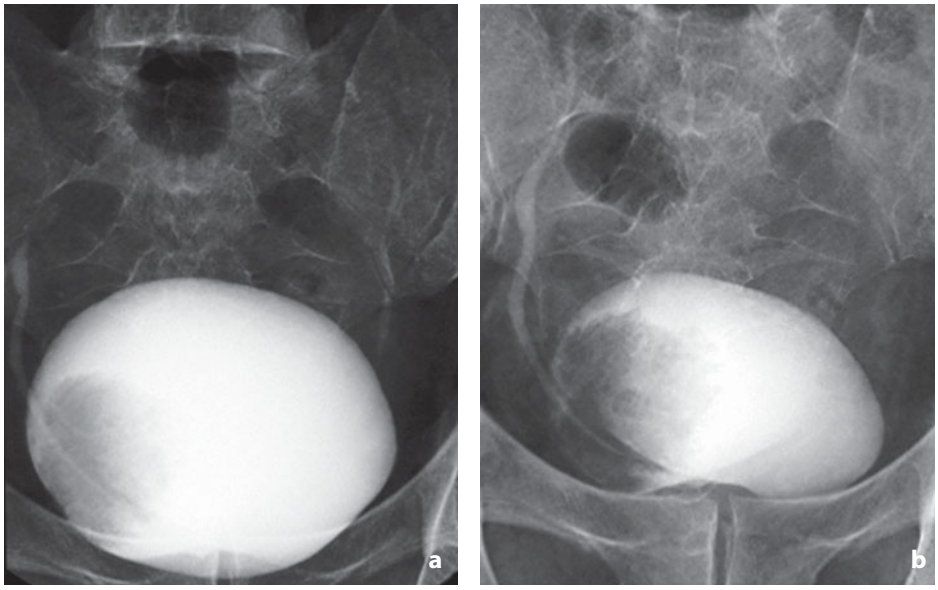

Fig. 9.82a,b. Urography. Bladder cancer. **a** Cystographic study reveals a significant filling defect which is particularly evident in the oblique view (**b**), arising from the right inferolateral wall of the bladder

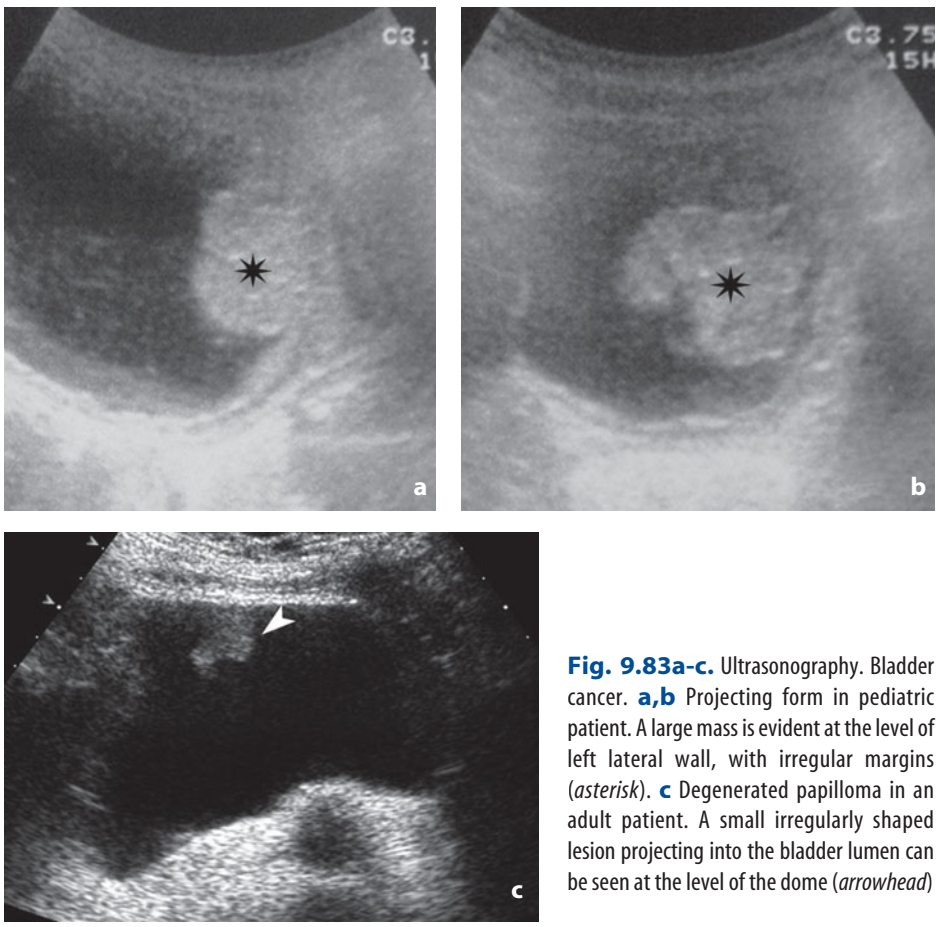

Fig. 9.83a-c. Ultrasonography. Bladder cancer. **a,b** Projecting form in pediatric patient. A large mass is evident at the level of left lateral wall, with irregular margins (*asterisk*). **c** Degenerated papilloma in an adult patient. A small irregularly shaped lesion projecting into the bladder lumen can be seen at the level of the dome (*arrowhead*)

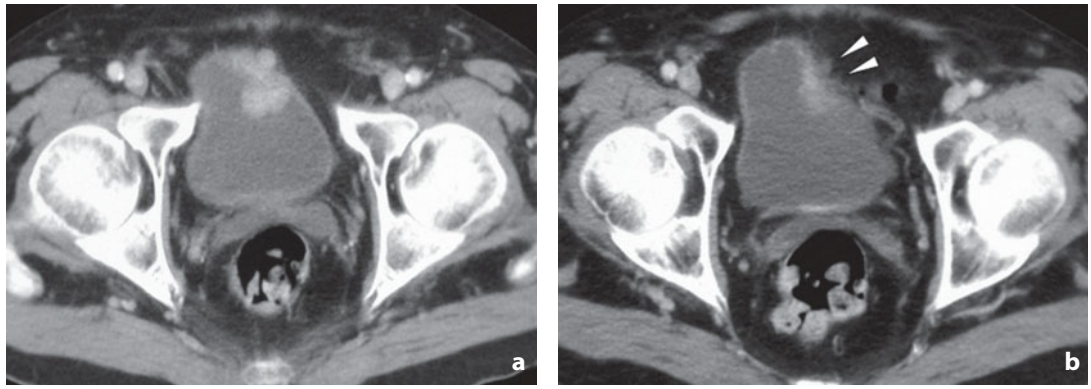

Fig. 9.84a,b. Computed tomography. Bladder cancer. **a** The mass attached to the left anterolateral wall is moderately enhancing after injection of contrast medium in the venous phase of the dynamic study. **b** Probable invasion of the perivesical fat (*arrowheads*)

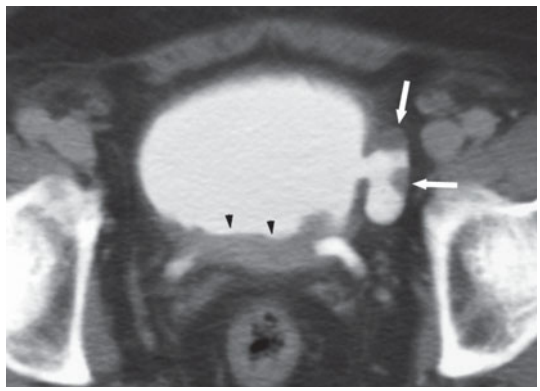

Fig. 9.85. Computed tomography. Bladder cancer. In the late phase of the dynamic study a diverticulum with a narrow neck can be visualized. Filling defects with their base attached to the wall of the diverticulum itself are present (*arrows*). Nonuniform thickening of the posterior bladder wall is also visible (*arrowheads*)

The role of **computed tomography** and **magnetic resonance** is not to identify bladder cancer, since this is already performed by cystography, ultrasonography and cystoscopy. The exception to this rule is in special cases, such as small suspected lesions of the bladder dome and urachal carcinoma (a rare carcinoma originating from urachal rests). In order to perform a good evaluation of the bladder both techniques require good distension of the organ.

On nonenhanced CT images bladder cancer generally appears as a solid hyperattenuating mass protruding into the bladder lumen with the base attached to the wall, or as a focal thickening of the wall which appears rigid or retracted. Calcifications are rarely observed. A sign of tumor extension beyond the bladder wall is given by the nonuniform appearance of the adipose tissue surrounding the organ which, if minimal, can be difficult to differentiate from reactive lymphangitis (**Fig. 9.84**). After the administration of contrast medium the lesion may enhance in the venous phase, becoming more visible with attenuation values higher than those of the healthy bladder wall. In this phase the possible involvement of lymph nodes, adjacent organs and/or distant metastases (to the liver, lungs or bone) is also evaluated. In the late phase of the dynamic study, when the bladder is opacified by iodinated urine, the lesion appears as a filling defect and the possible involvement of the urethral outlets as well as the presence of other lesions along the course of the urinary tract can be better evaluated (**Figs. 9.85, 9.86**).

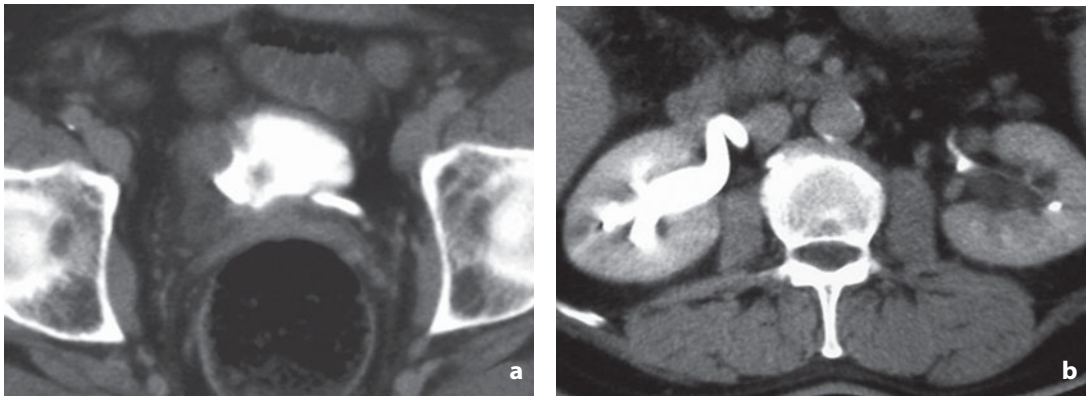

Fig. 9.86a,b. Computed tomography. Bladder cancer. **a** The late phase of the dynamic study shows wall thickening at the right lateral aspect of the bladder. **b** The ipsilateral ureteric outlet is probably involved due to retrodilatation of the ureter

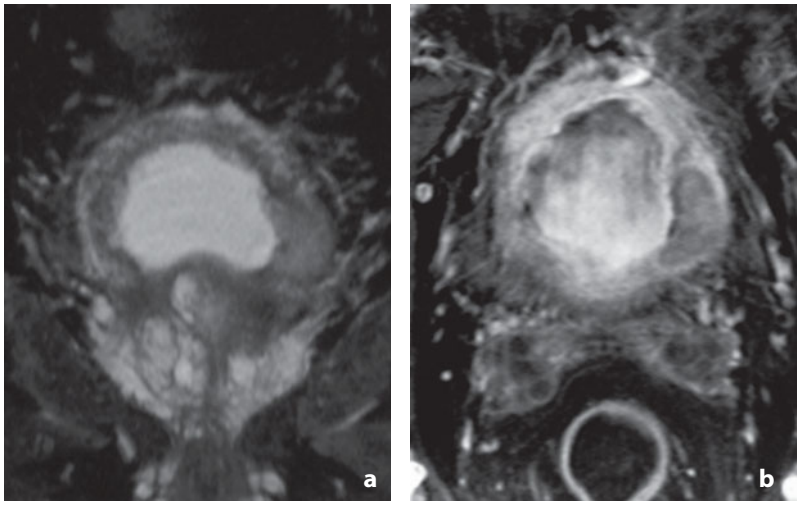

Fig. 9.87a,b. Magnetic resonance. Transition cell carcinoma of the bladder. **a** T2-weighted image shows thickening of the left lateral bladder wall. **b** After administration of gadolinium-based contrast medium the local extension of the disease is visible, appearing to involve all layers of the bladder wall while remaining confined to the organ (stage T2b)

Virtual cystoscopy, which today can be performed using multidetector-row CT with dedicated software, has been suggested as a useful technique in the identification of dubious plaque-like lesions.

Magnetic resonance (Figs. 9.87–9.89) T2-weighted images can be used to differentiate neoplastic tissue from the adjacent healthy bladder wall, the signal of which is not quite as high as that of the lesion. In T1-weighted sequences the invasive neoplastic tissue (intermediate signal intensity) can be identified within the muscular wall of the bladder (low signal intensity). T1-weighted sequences with fat saturation can also be used to evaluate the presence of invasion of the perivesical fat (Fig. 9.90). The injection of paramagnetic contrast medium can help to identify a lesion with invasive growth, which appears moderately enhancing in the dynamic phases of the study. In particular, the increase in signal intensity of the lesion during the arterial phase is more intense than that of the muscular structures of the bladder wall, thus making possible improved evaluation of the presence and local extension of the disease. There are, however, problems with both CT and MR in the differential diagnosis with postradiotherapeutic wall thickening and/or retraction, and in conditions of increased wall thickness arising from inflammatory pseudotumors (Fig. 9.91).

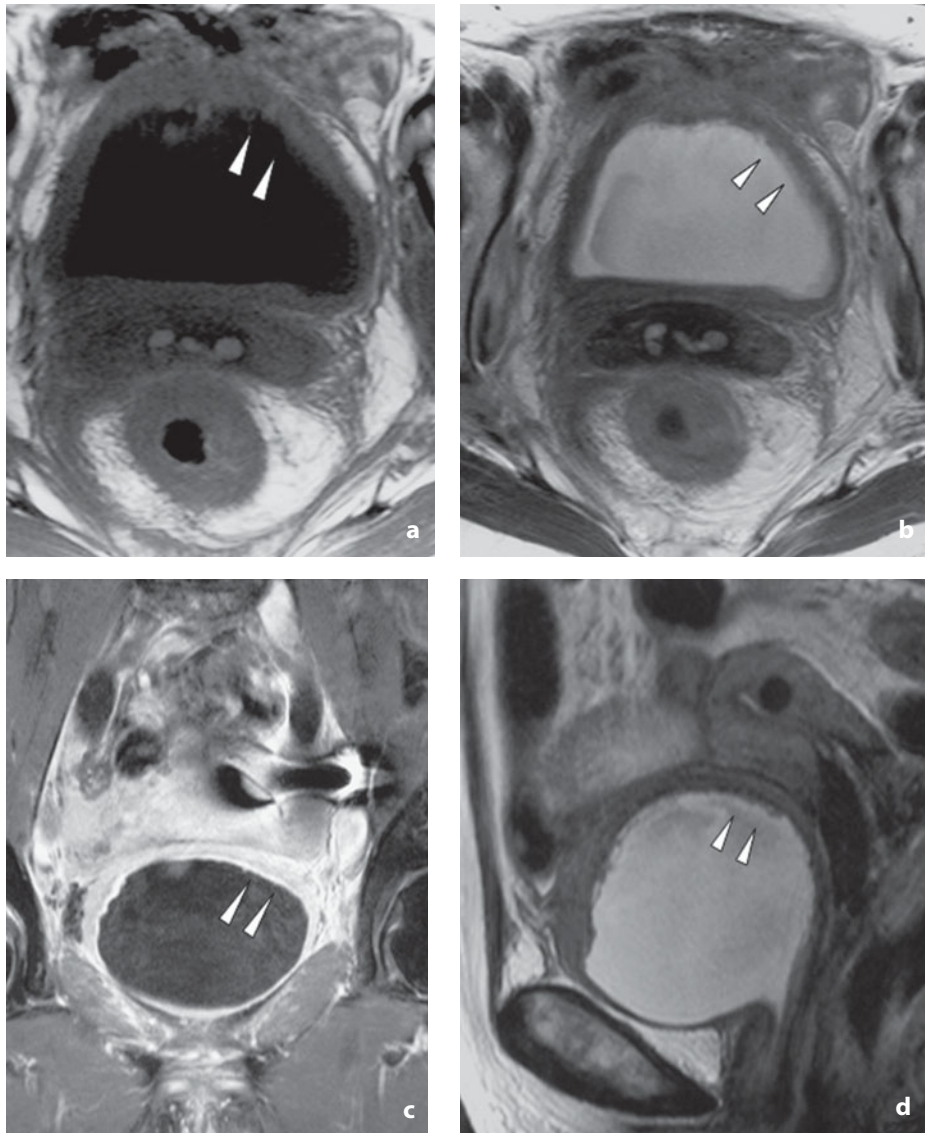

Fig. 9.88a-d. Magnetic resonance. Bladder cancer, stage T1. T1-weighted (**a**) and T2-weighted (**b**) images show slight eccentric thickening of the bladder wall (*arrowheads*). The finding is confirmed in the coronal T1-weigthted (**c**) and sagittal T2-weighted (**d**) images

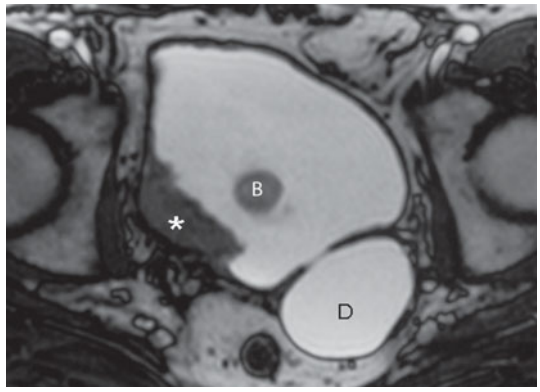

Fig. 9.89. Magnetic resonance. Bladder cancer. T2-weighted sequence shows an evident broad-based lesion projecting into the bladder lumen at the right posterolateral aspect (*asterisk*). A large diverticulum (*D*) is visible with the neck at the left posterolateral wall. *B*, balloon of the bladder catheter

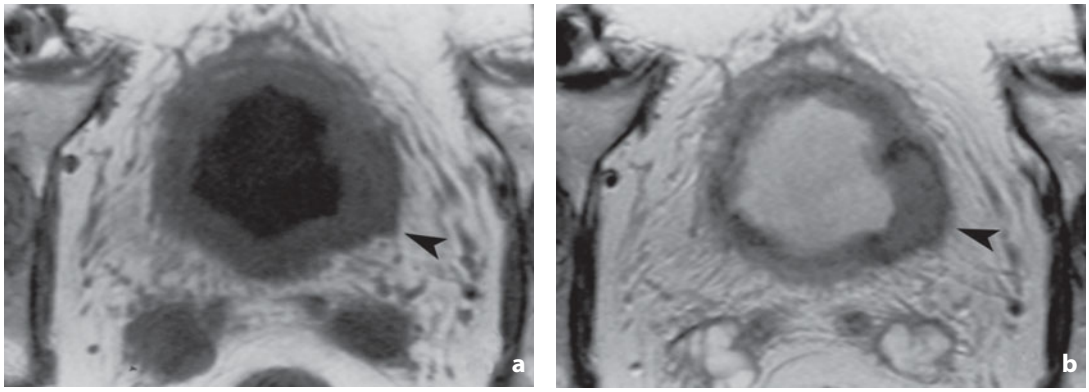

Fig. 9.90a,b. Magnetic resonance. Bladder cancer. **a** T1-weighted sequence shows concentric bladder wall thickening with irregularities of the left posterolateral profile (*arrowhead*). **b** The finding, which can be attributed to invasion of the adipose tissue (stage T3) is better visualized in the contrast-enhanced T1-weighted image

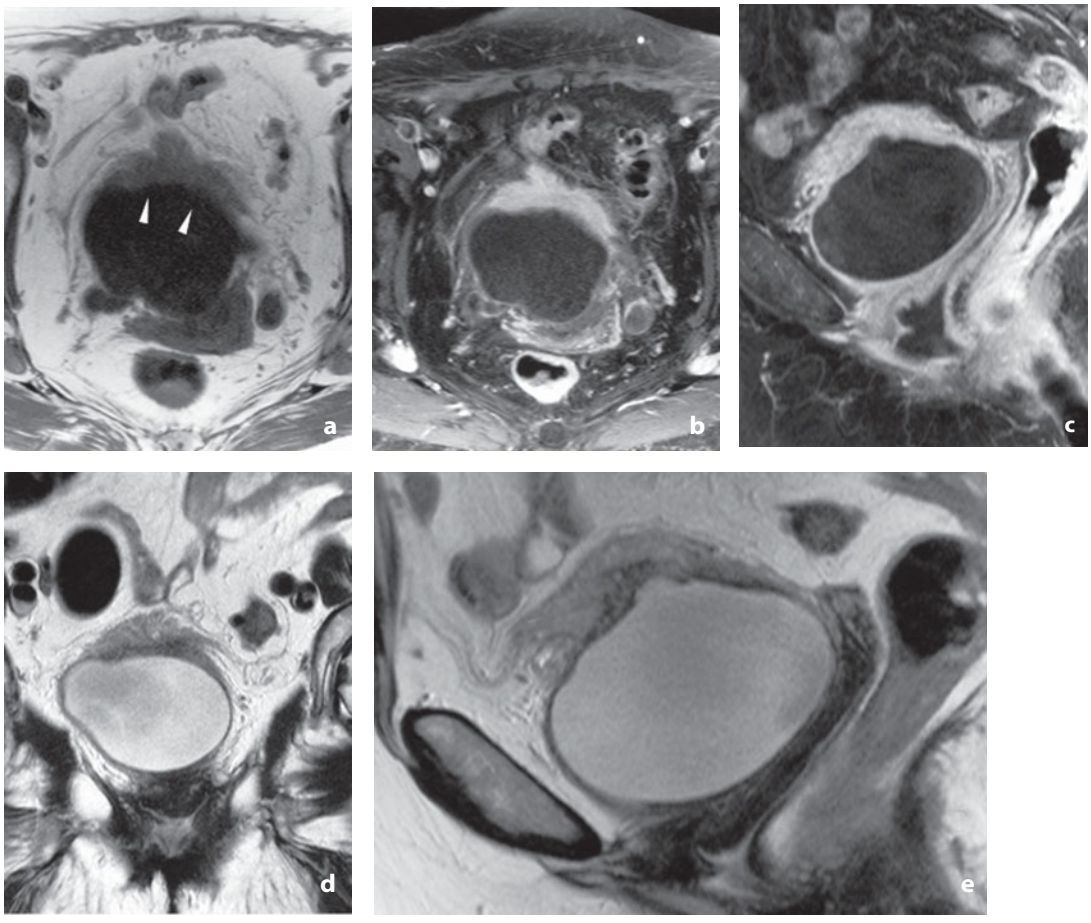

Fig. 9.91a-e. Magnetic resonance. Bladder pseudotumor. **a** Baseline T1-weighted image shows nonuniform plaque-like thickening at the bladder dome (*arrowheads*). **b** After contrast medium injection with fat saturation, marked enhancement of the lesion is appreciable, evident also in the contrast-enhanced sagittal T1-weighted sequence (**c**) and the coronal and sagittal T2-weighted images (**d,e**). Differential diagnosis with an invasive bladder cancer is challenging

Staging

CT is able to evaluate the extension of a tumor to adjacent organs (T4), the presence of suspected lymph node metastasis (N1–N3) or distant metastasis (M1). Although CT and **MR** are similar in the study of advanced disease (T3–T4, presence of pathologic lymph nodes and distant metastasis), the staging of bladder cancer (**Table 9.7**) is preferably entrusted to MR, since it is better able to evaluate the dome, base and neck of the bladder than CT, and provides more accurate information regarding the disease in the early stages (T1-T2). One obstacle to local staging of bladder cancer with MR is the frequent presence of perilesional edema, which can lead to an overstaging of disease. Other technical limitations include overdistension of the bladder, chemical shift artifacts and partial volume artifacts.

To provide complete staging MR often uses images with a broader field of view with T1- and T2-weighted sequences, thus enabling the possible identification of pathologic lymph nodes. In this regard superparamagnetic iron-oxide contrast media are currently being tested. The contrast media are taken up by the reticuloendothelial system and provide not only morphologic but also functional information, which is

Table 9.7. Classification of bladder carcinoma according to the Jewett-Strong and TNM systems

Jewett-Strong	TNM	Histologic finding
0	T0	No evidence of primary tumor
0	Tis	Carcinoma in situ
0	Ta	Papillary tumor confined to the epithelium (mucosa)
A	T1	Tumor invades subepithelial connective tissue (lamina propria)
B1	T2a	Tumor invades superficial muscle (internal half)
B2	T2b	Tumor invades superficial muscle (external half)
C	T3	Tumor invades perivesical fat
D1	T4a	Tumor invades adjacent organs
D1	T4b	Tumor invades pelvic or abdominal wall
D1	N1	Metastasis in a single lymph node ≤2 cm
D1	N2	Metastasis in a single lymph node >2 ≤5 cm or in multiple lymph nodes ≤5 cm
D1	N3	Metastasis in a single lymph node >5 cm
D2	N3	Lymph node metastasis above the common iliac bifurcation
D2	M1	Distant metastasis

useful in differential diagnosis between a reactive and pathologic lymph node. The rationale is based on the fact that unlike metastatic lymph nodes, reactive lymph nodes contain Kupffer cells such that after contrast medium administration they are characterized by a significant loss of signal (**Figs. 9.92, 9.93**).

Wong-You-Cheong JJ, Woodward PJ, Manning MA et al (2006) From the Archives of the AFIP: neoplasms of the urinary bladder: radiologic-pathologic correlation. RadioGraphics 26:553–580

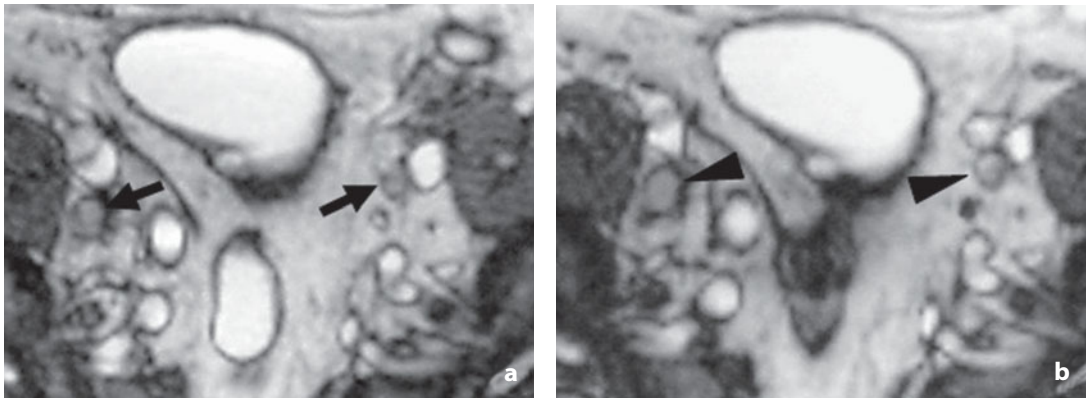

Fig. 9.92a,b. Magnetic resonance. Metastatic lymph nodes. Patient with bladder cancer. **a** Prior to contrast medium administration several internal iliac lymph nodes of dubious pathology are visible (*arrows*). **b** After injection of USPIO-based contrast medium there is no signal loss given the absence of reticuloendothelial-system cells in these lymph nodes and their replacement by neoplastic tissue (*arrowheads*)

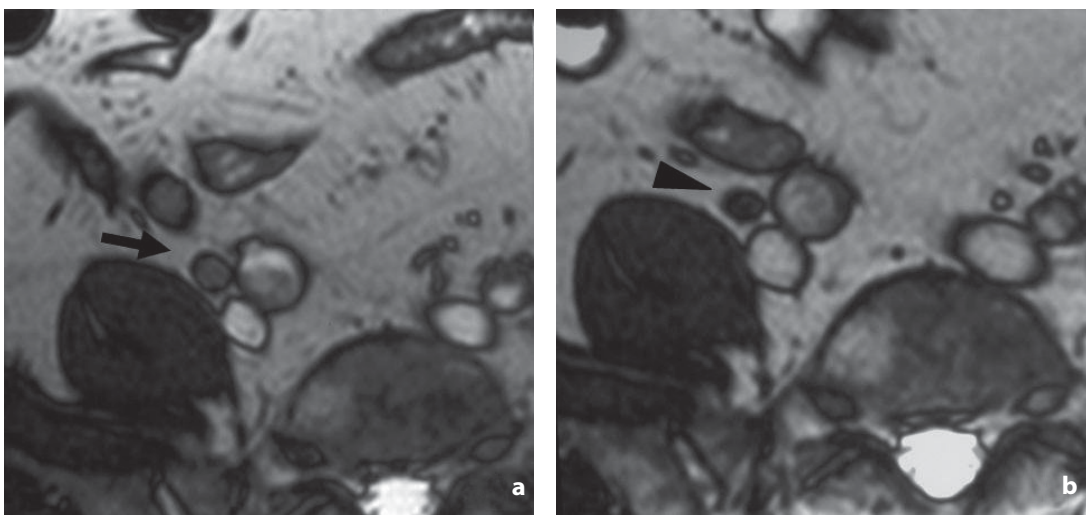

Fig. 9.93a,b. Magnetic resonance. Inflammatory lymph node. Patient with bladder cancer. **a** The nonenhanced image shows a lymph node suspicious in size and morphology (*arrow*). **b** After injection of USPIO-based contrast medium uniform signal loss can be appreciated due to the accumulation of iron-oxide particles in the cells of the reticuloendothelial system present in the normal lymph node (*arrowhead*)

Part IV
Disease of the Male Reproductive System

Clinical Approach to Prostate Disease

10

D. Zani, C. Simeone, S. Cosciani Cunico

The prostate is the largest gland annexed to the male reproductive system and is made up of a glandular and stromal component. The former, as described by McNeal, can be subdivided into three zones: central, transition and peripheral. The nonglandular part consists of the periprostatic sphincter, the anterior connective tissue and the prostatic capsule.

The periprostatic sphincter consists of a cylinder of smooth muscle fibers surrounding the proximal segment of the prostatic urethra. The peri-urethral region is situated within this sphincter and constitutes a very small part of the gland.

Inflammation

Inflammatory prostatic disease is plagued by a certain degree of controversy due to terminological and classification difficulties. The etiology is often uncertain, as are the pathophysiologic mechanisms in the absence of specific clinical characteristics. Prostatitis is classically subdivided into acute bacterial prostatitis, chronic bacterial prostatitis, chronic nonbacterial prostatitis and prostatodynia. More recent classifications include the 1995 National Institutes of Health (NIH) classification, which further subdivides the categories of inflammation and introduces the concept of chronic pelvic pain syndrome (**Table 10.1**). Reference is made to this syndrome in the 2002 International Continence Society (ICS) classification, which sees chronic pelvic pain syndrome subdivided according to whether the genesis is urologic (vesical, urethral, penile, prostatic, scrotal), anorectal, neurologic or muscular.

Table 10.1. Classification of prostatitis according to the National Institutes of Health (1995)

Type	Name	Definition
I	Acute bacterial prostatitis	Acute infection of the prostate
II	Chronic bacterial prostatitis	Recurrent infection of the prostate
III	Chronic prostatitis / chronic pelvic pain syndrome	Absence of demonstrable infection
IIIa	Inflammatory	Presence of leukocytes in prostatic secretions
IIIb	Noninflammatory	Absence of leukocytes in prostatic secretions
IV	Asymptomatic inflammatory prostatitis	Absence of symptoms, histologic finding of inflammation

L. Olivetti, L. Grazioli (eds.), *Imaging of Urogenital Diseases*,

Acute Prostatitis

The most common pathogens involved in the genesis of acute bacterial forms are Gram negative, while Gram-positive forms are rarer. *Chlamydia trachomatis* plays an important role in younger patients.

Onset is usually sudden and symptoms include painful micturition, frequency and urgency, with the possibility of complete urinary retention. The urinary symptoms are accompanied by fever and bodily aches and pains.

Digital rectal examination (DRE) reveals an enlarged and tender prostate, while single or multiple foci may be palpated only in cases of prostatic abscess. Transrectal ultrasonography (TRUS) is usually not required to confirm the clinical suspicion, although it can be used to identify abscess collections.

Antibiotic therapy may be guided by an antibiogram in cases of positive findings at urine culture. Instrumental examinations and especially endoscopy are contraindicated in this phase, and should urinary drainage be required transurethral catheterization is best avoided in favor of suprapubic cystostomy.

Chronic Prostatitis

Since this definition often includes clinical presentations which are varied, with changeable and often subtle symptoms and a difficult etiology, establishing the real incidence of the disease is challenging. The diagnostic criteria are varied and poorly codified. Particularly relevant are both irritative and obstructive voiding symptoms associated with pain.

Chronic bacterial forms of prostatitis which have been definitively diagnosed account for a minority of cases and are so defined when the etiologic agent responsible for the infection, usually Gram negative, has been identified. The role of Gram-negative bacteria is still the subject of debate, whereas forms secondary to *Chlamydia* and *Mycoplasma* species are possible.

In nonbacterial chronic prostatitis the urine culture is negative, while an elevated number of leukocytes are found in the urine after prostatic massage indicating inflammation.

Prostatodynia groups together patients reporting characteristic voiding symptoms, especially irritative symptoms, but without positive urine culture or an elevated number of leukocytes in the urinary sediment.

Diagnosis of the type of chronic prostatitis is perhaps best performed with the Meares-Stamey test. Inflammation is defined on the basis of finding 10 leukocytes per high-powered field. The test should be integrated with urine culture in the search for *Chlamydia* and *Mycoplasma* species.

If there is clinical suspicion of a functional problem with detrusor/sphincter instability and/or hyperactivity of the perineal muscle, the diagnostic procedures can be integrated with uroflowmetry or a urodynamic study. TRUS can identify tissue heterogeneity with prostatic calcifications. The seminal vesicles may even be dilated with septal thickening.

The course of antibiotic therapy (with broad spectrum or targeted antibiotics based on the antibiogram) should be long. In chronic forms antibiotic therapy is often administered in cycles associated with antiinflammatories, anticholinergics and/or alpha blockers to reduce symptoms.

Abrams P, Cardozo L, Fall M et al (2002) The standardisation of terminology of lower urinary tract function: report from the standardisation subcommittee of the International Continence Society. Neurourol Urodyn 21:167-178

Nickel JC, Weidner W (2000) Chronic prostatitis: current concepts and antimicrobial therapy. Infect Urol 13:22-28

Pavone Macaluso M, Di Trapani D, Pavone C (1991) Prostatitis, prostatosis and prostalgia. Psychogenic or somatic disease? Scand J Urol Nephrol 138:77-82

Roberts RO, Jacobson DJ, Girman C et al (2002) Prevalence of prostatitis like symptoms in a community based cohort of older men. J Urol 168:2467-2471

Roberts RO, Lieber NM, Bostwick DG et al (1997) A review of clinical and pathological prostatitis syndromes. Urology 49:809-821

Benign Prostatic Hyperplasia

Benign prostatic hyperplasia (BPH) indicates a pathophysiologic alteration which occurs at the level of the periurethral glands. Incidence increases with age, varying from 17% in the fifth decade of life to 37% in the seventh.

The etiopathogenesis of BPH appears to be multifactorial, with possible causes including hormones, growth factors and diet.

Testosterone is without doubt the most investigated androgen, being definitely involved in the genesis of BPH. The mechanism involves the synthesis of dihydrotestosterone (DHT) from testosterone circulating in the prostate, by the action of 5-alpha-reductase. Since this enzyme is principally located in the epithelium and stroma, the final action on these cells is an increase in proliferation and an alteration in apoptosis. Estrogens also appear to play a key role, causing an increase in the synthesis of both 5-alpha-reductase and the receptors for DHT.

The main growth factors include soluble proteins and peptides, such as fibroblastic growth factor, which regulate the stroma/epithelium/intercellular matrix interaction and are able to influence the proliferative and apoptotic processes of the prostate.

A diet rich in vegetable fiber, phytoestrogens and flavonoids is correlated with an extremely low incidence of BPH, as seen in Asian populations. These substances act as competitive receptor blockers on estrogenic receptors, thus inhibiting 5-alpha-reductase and angiogenetic mechanisms.

The pathophysiologic changes do not always produce clinical symptoms. These tend to be correlated with either a partial or total mechanical obstruction secondary to the increased size of the gland (as typically occurs in hyperplasia of the middle lobe), or a functional component, such as hyperactivity of the alpha adrenergic receptors present to a greater extent in the fibromuscular part of the prostate. Lower urinary tract symptoms define the voiding symptoms that can be present simultaneously, although they may be perceived with varying intensity by the patient.

Voiding symptoms can be broadly divided into obstructive and irritative. Obstructive symptoms include painful micturition, weak urinary stream, abdominal straining, hesitancy and postvoiding dribble. Irritative symptoms include frequent diurnal and nocturnal urination, urgency and intermittent, painful micturition. The former are typically present in BPH, whereas the latter are more frequently due to conditions involving the detrusor, such as aging and ischemia.

Precisely defining the symptoms reported by the patient can be challenging, which is why a number of symptom scores have been proposed, some of which also investigate quality of life. The most used is the International Prostate Symptom Score. Patient history and clinical examination, as well as urine analysis, creatininemia and prostate specific antigen (PSA) testing, comprise the minimum work-up for clinical evaluation of the patient.

The usual imaging technique is either suprapubic US or TRUS, which should be integrated with the evaluation of the postvoid residual. Uroflowmetry can be particularly useful for evaluating the reduction in urinary flow, but this should be correlated

with the nomogram relative to the patient's age, as well as with the volume voided. The urodynamic pressure flow study is a second-level diagnostic examination which can be used to orient therapy, particularly in possible cases of surgery.

BPH is a progressive condition with regard to the increase in the volume of the gland and the reduction in flow. The risk factors regarding a possible degeneration of the condition include age (>50 years), prostatic volume (>30 g), urinary flow (<12 mL/s), PSA (>1.4 ng/mL) and an American Urology Association score >7. Acute or chronic urinary retention, calculi and vesical diverticuli, hematuria and recurrent infections are the leading possible complications in the natural history of these patients.

Treatment of BPH involves the use of two classes of drugs: 5-alpha-reductase inhibitors and alpha blockers. The former (finasteride, dutasteride) act by blocking the synthesis of DHT from testosterone, thus inhibiting cellular growth and proliferation and, over the long term, even reducing prostatic volume and improving urinary flow. Alpha blockers (alfuzosin, tamsulosin, terazosin) act on the alpha receptors, relaxing the smooth muscle of the prostate and obtaining a more rapid improvement of symptoms.

A wide variety of invasive treatments have been proposed. Open surgery is usually reserved for the larger adenomas, at least larger than 50 g. In cases of lesser volume, endoscopy and resection of the adenoma is still the reference standard. This is despite the development of numerous other technological advancements in recent years, none of which have proved to be competitive with the traditional techniques in terms of efficacy and long-term success.

AUA Practice Guidelines Committee (2003) AUA guideline on management of benign prostatic hyperplasia. Chapter 1: Diagnosis and treatment recommendations. J Urol 170:530-547

Girmar GJ, Jacobsen SJ, Tsukamoto T et al (1998) Health related quality of life associated with lower urinary tract symptom in four countries. Urology 51:428-436

Jacobsen SJ, Girman CJ, Guess HA et al (1995) New diagnostic and treatment guidelines for benign prostatic hyperplasia. Arch Intern Med 155:477-481

Mebust WK, Holtgrewe HL, Cockett ATK (1989) Transurethral prostatectomy: immediate and postoperative complication. A cooperative study of 13 participating institutions evaluating 3885 patients. J Urol 41:243-247

Walsh PC, Retik AB et al (1998) Campbell's urology, 7th ed. WB Saunders Co., Philadelphia

Prostate Cancer

Carcinoma of the prostate has become the most prominently diagnosed malignant tumor. It is responsible for the second highest number of deaths from cancer in the United States and is the solid tumor most correlated with age. The highest incidence is found among African-Americans, in whom the tumor tends to be more aggressive and is diagnosed at an earlier age.

The neoplasm develops in the peripheral zone of the prostate. Initial alterations occur in the prostatic acini, known as prostatic intraepithelial neoplasia (PIN). This is characterized by a progressive dysplasia of the prostatic epithelium with the basement membrane intact. Demonstration of invasion of the basement membrane is essential for the diagnosis of carcinoma of the prostate. The stroma apparently plays an important role in the invasion of the basement membrane by releasing growth factors and metalloprotease. Once invasion has been established, grading is performed with the Gleason score, which is based on the tendency of a certain tumor to form glandular-type structures. Gleason identified five stages of tumor differentiation, numbered progressively from 0 to 5. Due to the marked heterogeneity of the

neoplastic cellular component, the Gleason score is assigned to the two predominant typologies present in the sample.

Tumor spread most frequently occurs via the prostatic capsule, involving the periprostatic tissue and seminal vesicles. The tumor may also invade the bladder, at the level of the trigone, with possible involvement of the ureteric orifices and consequent bilateral hydroureteronephrosis, renal insufficiency and anuria if the obstruction is complete. Invasion of the rectum is decidedly less common since the rectovesical fascia appears to provide an effective barrier against tumor spread. Sites of distant metastases include the obturator lymph nodes and bone, especially the vertebral column and the pelvis. In advanced stages the metastases may involve lymph nodes and organs at other sites.

DRE is able to evaluate the prostate, especially in the peripheral zone where most tumors arise. Asymmetry of the lobes and an increase in the consistency or presence of nodules on the surface of the gland should give rise to suspicion of carcinoma. However, DRE alone tends to understage the disease, with a sensitivity of 57–68% and a specificity ranging from 44 to 96% based on the experience of the operator.

The diagnosis of prostate cancer has radically changed since the introduction and diffusion of PSA testing. This organ-specific marker has made possible an earlier diagnosis when the tumor is contained within the prostatic capsule and is therefore susceptible to radical treatment. However, the normal range for the marker is nonuniform: some investigators have suggested 0–2.5 ng/mL, while others have proposed 0–4.0 ng/mL. Estimates suggest that with a PSA value between 2.5 and 4.0 ng/mL the positive biopsy rate is 27%, whereas with a PSA value between 4 and 10 ng/mL the positive biopsy rate varies from 42% to 64% in patients above 50 years. With a PSA between 4 and 10 ng/mL the disease is extracapsular, while with a PSA >20 ng/mL the disease is metastatic in 80% of cases. Prostatic biopsy can be performed with either a transperineal or transrectal approach. Regardless of the access chosen, it has been shown that at least 8–12 cores need to be taken. This improves the diagnostic reliability with respect to the classic sextant scheme of six cores.

Treatment of prostate cancer depends on whether the tumor stage is localized, locally advanced or metastatic. In young patients and when the tumor is confined to the capsule, radical prostatectomy may be indicated which can be performed with the nerve sparing technique to reduce the rate of possible complications: erectile deficit and urinary incontinence. Laparoscopic techniques and the recently introduced robotic procedures seem to produce results comparable to open surgery. As an alternative, external conformational radiotherapy appears to guarantee the same control over the disease. This can also be the treatment of choice when the disease is locally advanced. Brachytherapy may be a valid alternative in localized tumors and small prostates. In elderly patients with localized disease a further treatment option may be watchful waiting.

In metastatic disease the treatment of choice is androgen suppression. Anti-androgenic therapy in the past was performed with bilateral orchidectomy, but today is carried out with the use of antiandrogens and luteinizing hormone-releasing hormone (LH-RH) agonists, either used individually or in association. Chemotherapy may be indicated in patients who demonstrate hormone-refractory disease. The results are usually modest, with a limited increase in survival curves.

Abbas F, Scardino PT (1997) The natural history of clinical prostate carcinoma. Cancer 80:827-833

American Urological Association (AUA) (2000) Prostate specific antigen (PSA) best practice policy. Oncology 14:267-280

Bil Axelson A, Holmberg L, Ruutu M et al (2005) Radical prostatectomy versus watchful waiting in early prostate cancer. N Engl J Med 352:1977-1984

Gleason DF (1997) Histologic grading and clinical staging of prostatic carcinoma. In: Tannenbaum M (ed) Urologic pathology: the prostate. Lea & Febiger, Philadelphia, pp 171-198

Mundy GR (1997) Mechanism of bone metastases. Cancer 80:1546-1556

Scardino PT (1989) Early detection of prostate cancer. Urol Clin North Am 16:635-655

Sooriakumaran P, Khaksar SJ, Shah J (2006) Management of prostate cancer. Part 2: localized and locally advanced disease. Expert Rev Anticancer Ther 6:595-603

Diagnostic Imaging of the Prostate

11

L. Olivetti, L. Grazioli

Inflammation

Pathology

Due to its high incidence, inflammation of the prostate is a significant clinical problem which still has not been clearly defined. Prostatitis is a generic term which may be misused in daily practice and offered as a diagnosis based solely on clinical findings without precise data from the physical examination. In an attempt to clear up some of the confusion regarding painful benign conditions of the prostate and to create a common terminological framework, in 1978 Drach proposed a classification based on clinical and laboratory findings which is still valid:

- acute bacterial or viral prostatitis (and prostatic abscess);
- chronic bacterial prostatitis, usually secondary to an incompletely eradicated acute form;
- chronic nonbacterial prostatitis, characterized by no history of urinary infection and constant sterility of the prostate secretions, which is puruloid due to the presence of macrophages;
- prostatodynia, a condition similar to the chronic inflammatory form but with no history of urinary infections and normal prostatic secretions.

Acute prostatitis can manifest with massive congestion, edema and suppuration of the entire gland or with small and disseminated abscesses or with broad areas of liquefied necrosis. When these characteristics are diffuse there follows an increase in volume of the prostate, which proves to be soft and tender. The typical histologic features relate to the duration and intensity of the inflammation and range from a slight stromal infiltrate of lymphocytes to leukocyte collections in the glandular lumen, even to the point of necrosis. Inflammatory episodes may undergo complete regression with scarring, or conversely become chronic with obstruction of the excretory ducts allowing infection to continue in small abscesses.

Chronic prostatitis is characterized by an inflammatory process represented by numerous lymphocytes, plasma cells, macrophages and neutrophils. Aggregates of lymphocytes may also be found in the prostate of elderly subjects without the presence of chronic inflammation, given the absence of pathognomonic cells of infection (macrophages and leukocytes).

Granulomatous prostatitis, a sequela of acute and chronic forms, is characterized by thickening of the prostate secretions, marked focal lesions consisting of a large nodular infiltrate of epithelioid histiocytes mixed with leukocytes, lymphocytes, plasma cells and multinucleated giant cells. These granulomas contain neither foci of caseation necrosis nor acid-resistant bacteria, both of which are present when granulomatous prostatitis is supported by a tubercular process that is almost always secondary to an infection of another part of the urogenital system (usually the urinary bladder or kidney).

L. Olivetti, L. Grazioli (eds.), *Imaging of Urogenital Diseases*,

Diagnostic Imaging

Acute Prostatitis and Prostatic Abscess

Acute bacterial or viral forms of prostatitis are distinguished by clear clinical symptoms: rapid onset of fever with chills, perineal, testicular and penile pain, dysuria (frequency, nocturia, obstructive urinary tract syndromes). Upon palpation the prostate is boggy and extremely tender, while the urine is rich with bacteria and leukocytes. In the presence of such clear findings an **ultrasonography (US)** is rarely indicated and only if there is suspicion of prostatic abscess. In fact, despite being clinically easy to diagnose, acute prostatitis is often completely silent at US. In general, the shape and the symmetry of the gland are well defined, while the echogenicity is lower than normal, particularly in the central periurethral region. The borders of the gland are well defined with an increase in the vasculature of the periprostatic adipose tissue. However, a loss of definition of the profile is not rare, produced by foci of inflammation mimicking the capsular and extracapsular invasion of carcinoma. Multiple irregularly distributed hypoechoic areas are often found, particularly in the McNeal peripheral zone.

In contrast, US can play an important role in the early diagnosis of a prostatic abscess. Abscesses are rarely primary and generally a late complication of acute prostatitis in subjects with lowered immune systems (patients suffering from diabetes, uremia, immunosuppression) who undergo repeated urethral catheterization. The abscess collections tend to spontaneously drain into the urethra, the rectum and the periprostatic adipose tissue. The symptoms are often masked, with moderate fever, recurrent urinary infections, epididymitis, dysuria and perineal pain. Palpation is often negative. A rare finding is fluctuation caused by the fluid under tension in the cavity of the abscess.

At US the abscess appears in an early phase as an anechoic heterogeneous lesion with fine intraluminal echoes produced by necrotic tissue and fibrin deposits. The margins, which initially are well defined, become progressively irregular (**Fig. 11.1**). If left untreated, the inflammation tends to involve the entire gland, which turns into an abscess sac. US is able not only to diagnose but also to guide drainage of the collection with the successive necessary controls (cell and microbiologic culture). The study can also guide the needle for antibiotic lavage and, where necessary, document the presence of fistula with contrast medium.

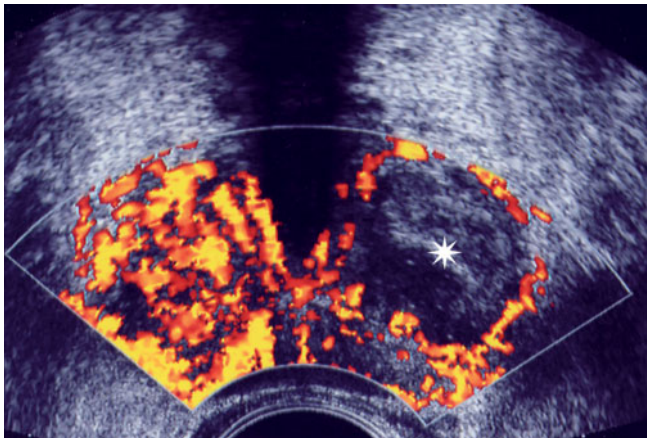

Fig. 11.1. Ultrasonography. Transrectal approach. Acute prostatitis with abscess formation. Sonogram shows a heterogeneous and prevalently hypoechoic area due to necrosis in the left lobe with absence of vasculature at power Doppler (*asterisk*)

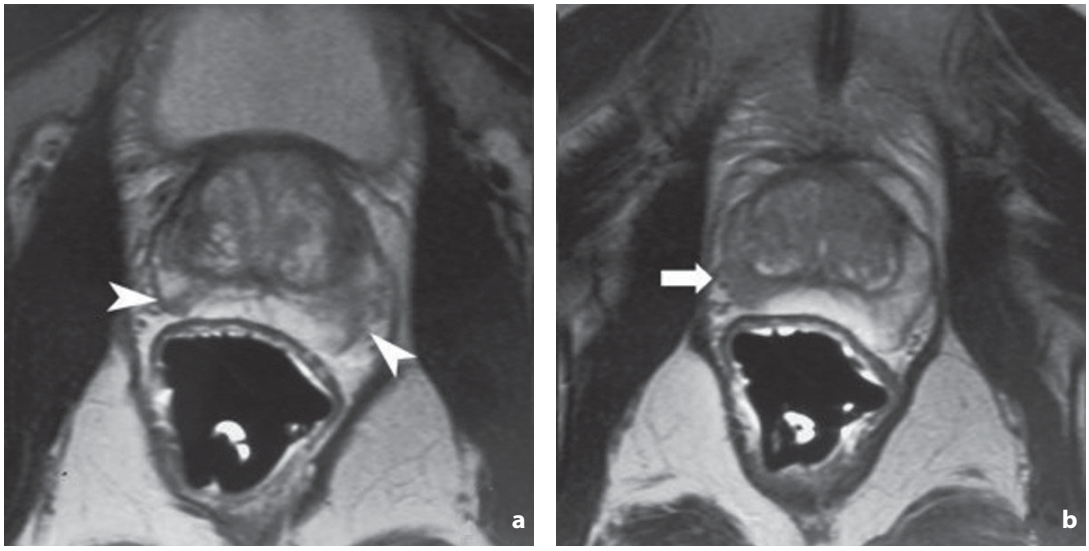

Fig. 11.2a,b. Magnetic resonance. Chronic prostatitis. **a** Axial T2-weighted image acquired at the middle third of the gland. In the peripheral zone, which is slightly asymmetric due to a retraction of the margin, a vague area of hypointensity can be seen (*arrowheads*) indicating postinflammatory tissue which in image **b** has a compact pseudonodular appearance (*arrow*), making differential diagnosis with carcinoma challenging

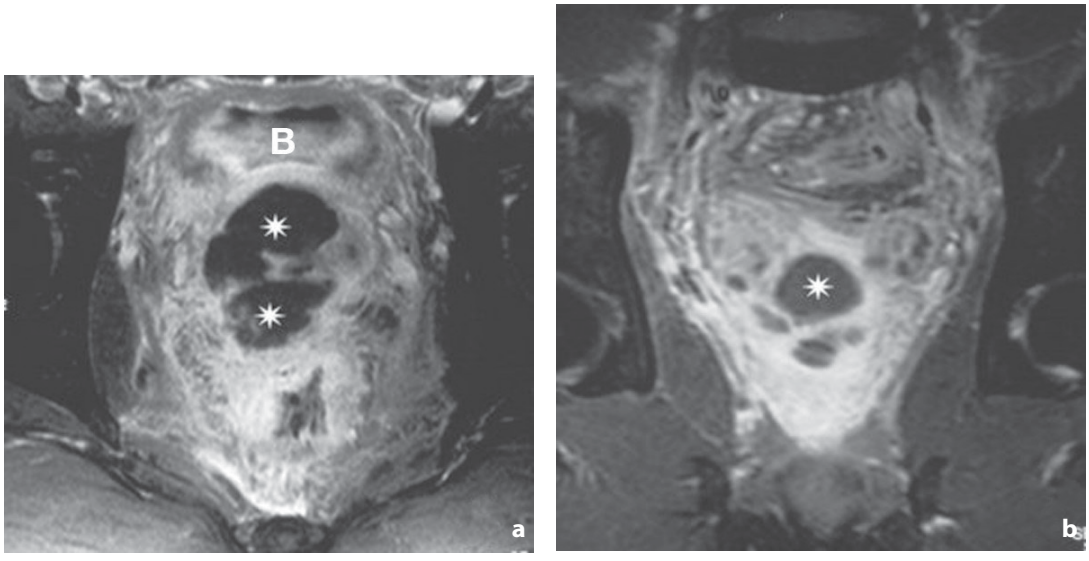

Fig. 11.3a,b. Magnetic resonance. Axial (**a**) and coronal (**b**) T2-weighted images. Complete subversion of the prostatic area by a necrotizing inflammatory process (*asterisks*) which involve the surrounding soft tissue with significant edema. *B*, urinary bladder

Other imaging modalities usually have no diagnostic indication in acute prostatitis, or in the chronic form (Fig. 11.2). A possible diagnostic niche is prostatic abscess. **Magnetic resonance (MR)** is able to identify intraglandular fluid collections and on the basis of signal intensity define the more-or-less corpuscular nature of the fluid. The principal advantage lies in its ability to evaluate whether the abscess has exceeded the anatomic boundaries of the capsule (Fig. 11.3).

Chronic Prostatitis

Bacterial or nonbacterial forms of chronic prostatitis, characterized by urinary disturbances typically of the irritative type and only rarely the obstructive type, usually manifest with one of the following three US presentations:

- absence of evident alterations; the gland appears normal (by far the most common presentation);
- alternating areas of hypo-, iso- or hyperechoic areas in one or both lobes;
- focal lesions (hypo-, iso- and hyperechoic) without being site-specific.

The presence of focal lesions, especially when associated with palpable areas, should always indicate biopsy.

The US appearance tends to change over time due to fibrous, fibrocalcific or calculous involution of the inflamed tissue. The latter two are easily identifiable even on computed tomography images (**Figs. 11.4, 11.5**). A particular kind of chronic inflammation is nonspecific granulomatous prostatitis, which can be subdivided into eosinophilic and non-eosinophilic. This form is characterized by an increase in prostate specific antigen (PSA) and a palpable tumor-like mass with a US appearance similar to carcinoma (focal hypoechoic areas, initially homogeneous). The capsule can appear invaded due to extension of the inflammatory process to the immediately

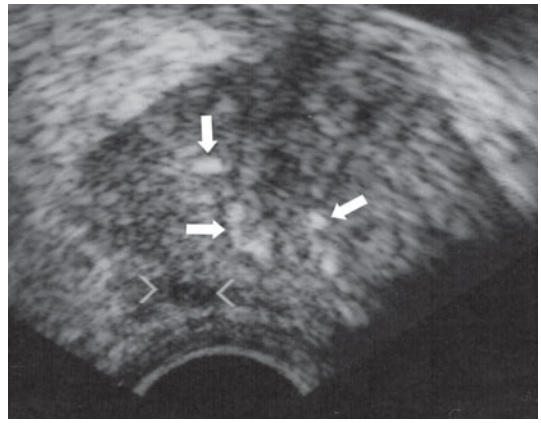

Fig. 11.4. Ultrasonography. Transrectal approach. The structure of the prostate appears coarser than normal, with numerous small calcifications (*arrows)*. In the peripheral zone two *landmarks* indicate the presence of a focal lesion, which after US-guided biopsy proved to be adenocarcinoma

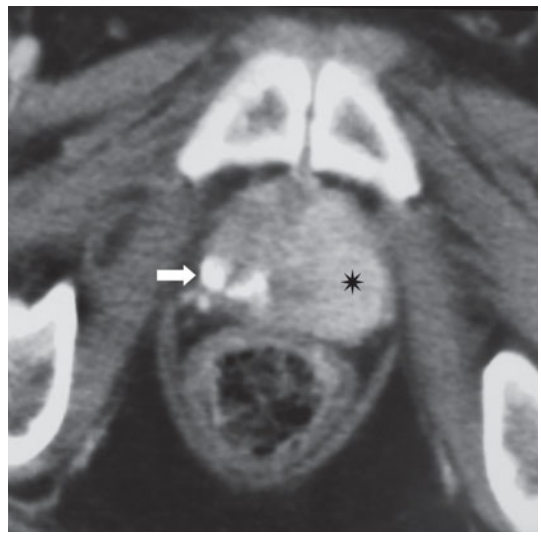

Fig. 11.5. Computed tomography. Axial contrast-enhanced scan. Chronic prostatitis with large calcifications (*arrow)* in the right lobe. The hyperattenuation of the left lobe (*asterisk*) is indicative of inflammatory recurrence

adjacent adipose tissue. In fact pseudoinfiltrative appearances coexist, due to the presence of inflammatory cells and edema in the loose periprostatic tissue. In these cases the granulomatous prostatitis is difficult to distinguish from carcinoma, especially if clinical findings (i.e. rectal palpation) are suspicious for tumor, thus making biopsy necessary.

A relatively frequent finding associated with chronic prostatitis is calculosis characterized by high-energy echoes which in large stones are accompanied by the classic acoustic shadow. Calcified chronic prostatitis, especially in young subjects, can give rise to inflammation of the ductus deferens and seminal vesicles or can cause a purely mechanical obstruction to the flow of seminal fluid in one or both ejaculatory ducts due to scarring and retraction or compression from adjacent calculi, with consequent sterility.

Hyperplasia

Pathology

Benign prostatic hyperplasia (BPH), also known as nodular hyperplasia and benign prostatic hypertrophy (technically a misnomer, since hypertrophy only indicates an increase in the volume of an organ and not in cellularity, as is the case here), is characterized by the presence of nodules which originate in the intrasphincteric periurethral and central transition zone. The nodules tend to form lobes which compress the peripheral zone, causing progressive atrophy and transformation into a pseudocapsule, which is useful as a surgical cleavage plane. Hyperplasia may be macroscopically present as:

- median lobe (commissural lobe, third lobe) usually posterior, with subtrigonal development;
- bilobar, symmetrical or asymmetrical (arising from the transition zone);
- trilobar, symmetrical or asymmetrical (the fusion of the above two presentations);
- subcervical lobe (special form of the median lobe, pedunculated, obstructing the bladder outlet with a ball-valve mechanism);
- anterior commissural lobe (rare).

The nodules are differentiated as a result of glandular proliferation and dilatation, or stromal, fibrous or muscular hyperplasia. Therefore, as a result of the prevalence of one or another appearance, five histologic types can be identified: stromal, muscular, fibromuscular, fibroadenoma and fibromyoadenoma (the latter being the most common). In 25% of cases areas of recent or prior infarction are present. Inflammatory infiltrates and areas of metaplasia, dysplasia and cystic degeneration are not uncommon findings (**Fig. 11.6**).

There is no strong association between the degree of hyperplasia and the extent of urethral obstruction, which instead arises from the combination of several factors including the location of the nodules and concomitant congestion, inflammation and infarction. Obstruction is followed by progressive compensatory hypertrophy of the detrusor muscle, with straining producing micro- and macrodiverticula of the bladder. Increased postvoid residual secondary to weakening of the detrusor promotes sepsis, the formation of calculi and the dilatation of the ureters (hydroureteronephrosis) due to their constriction in the intramural segment of the hypertrophic muscular wall, and incontinence (vesicoureteric reflux) or stenosis due to postinflammatory scarring and retraction.

Fig. 11.6. Histologic specimen. This gross section of the prostate shows large adenoma with heterogeneous structure due to the presence of retention cysts. The peripheral zones are compressed and thinned

Diagnostic Imaging

The principal role of **conventional radiology** with the techniques of urography or cystography is to evaluate the repercussions of BPH on the urinary bladder, which tends to be more-or-less elevated with impression on the bladder base near the neck. The shape of the impression varies: arched, with a large-radius downward curve if the whole of the prostate is enlarged; bilobar and heart-shaped, if the hyperplasia only involves the lateral lobes; concave downwards, but with a short-radius median curve if the hyperplasia is limited to the median lobe (**Fig. 11.7**). The bladder usually presents alterations due to urinary retention (column-cell appearance, diverticuli). In advanced cases vesicoureteric reflux and hydroureteronephrosis may be found. The prostatic urethra appears lengthened, diverted and constricted due to compression by the lateral lobes of the prostate, but does not present irregular margins.

US has the role of defining:

- the overall volume of the prostate;
- the volume of the adenoma and its changes after medical therapy;
- the presence of small adenomas which compress the neck of the bladder or the urethra above the seminal colliculus and which can be the cause of severe lower urinary tract symptoms (LUTS);
- the urinary dynamics and the postvoid residual.

Some information can initially be obtained with suprapubic US, although it is common knowledge that transrectal ultrasonography (TRUS) enables the best measure not so much of the whole gland but of the hyperplastic portion. This is particularly useful in monitoring pharmacologic therapy or in view of transurethral resective surgery (comparison between estimated weight of the adenoma and weight of the resected tissue). The weight is calculated using the ellipsoid formula (A×B×C)×0.523 (**Fig. 11.8**).

The transverse view on TRUS shows progressive loss of the normal triangular shape of the prostate which over time tends to become ovoid and then rounded due to the increase in the two diameters, especially the sagittal diameter. A clear difference can be appreciated between the external and the internal peripheral zones, where the structure is influenced by the nodule or nodules present. If these are plainly adenomatous the structure is hypoechoic. It becomes hyperechoic in cases with a higher muscular and stromal component (**Fig. 11.9**). Hyperechoic areas resulting from scarring secondary to prior infarction may also be seen within the adenoma, or hypoechoic areas due to a mixture of adenomatous nodules or recent infarcts in the context

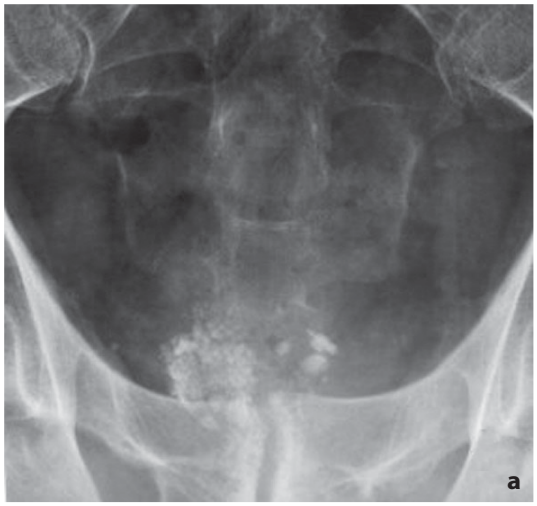

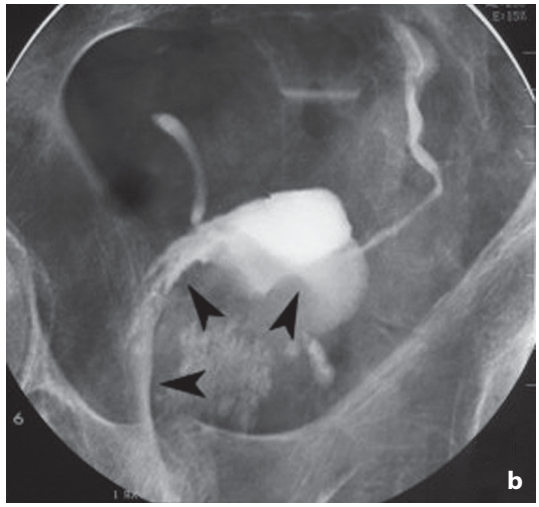

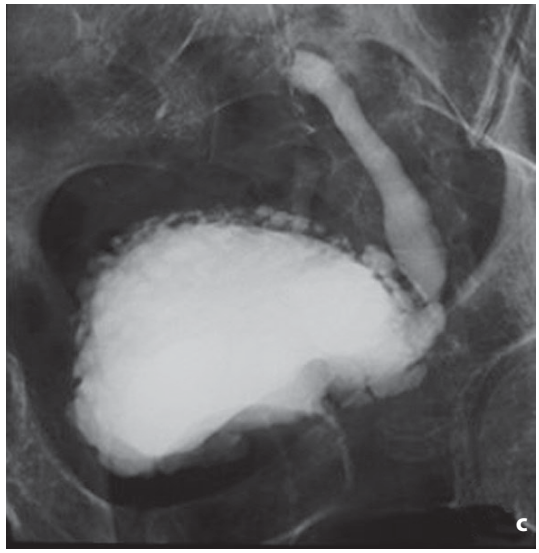

Fig. 11.7a-c. Urography. **a** Plain film radiography shows numerous small calcifications in the prostate area. **b** The early filling phase shows a significant bilobar heart-shaped impression on the bladder floor (*arrowheads*) resulting from an enlarged prostate. **c** Different case. The adenoma causes hypertrophy of the bladder wall with a diffusely irregular appearance due to numerous intramural diverticuli. Moderate retrodilatation of the left ureter can also be seen

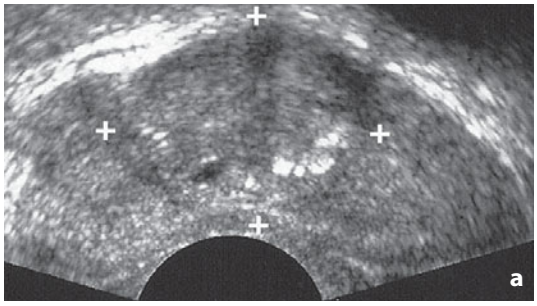

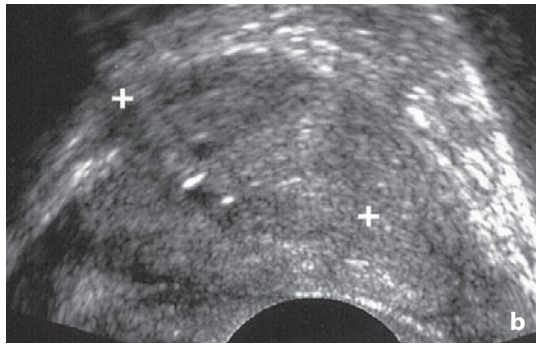

Fig 11.8a,b. Ultrasonography. Transrectal approach, axial (**a**) and sagittal (**b**) scans. Benign prostatic hyperplasia. The *crosses* placed at the margins of the adenoma are used to calculate the weight

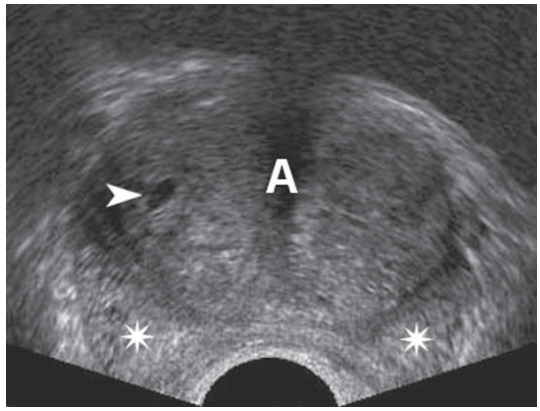

Fig. 11.9. Ultrasonography. Transrectal approach. Prostatic hyperplasia. The adenoma (*A*) displays a nodular appearance with heterogeneous structure. A hypoechoic ring separates it from the peripheral zone (*asterisks*). The *arrowhead* indicates a small retention cyst

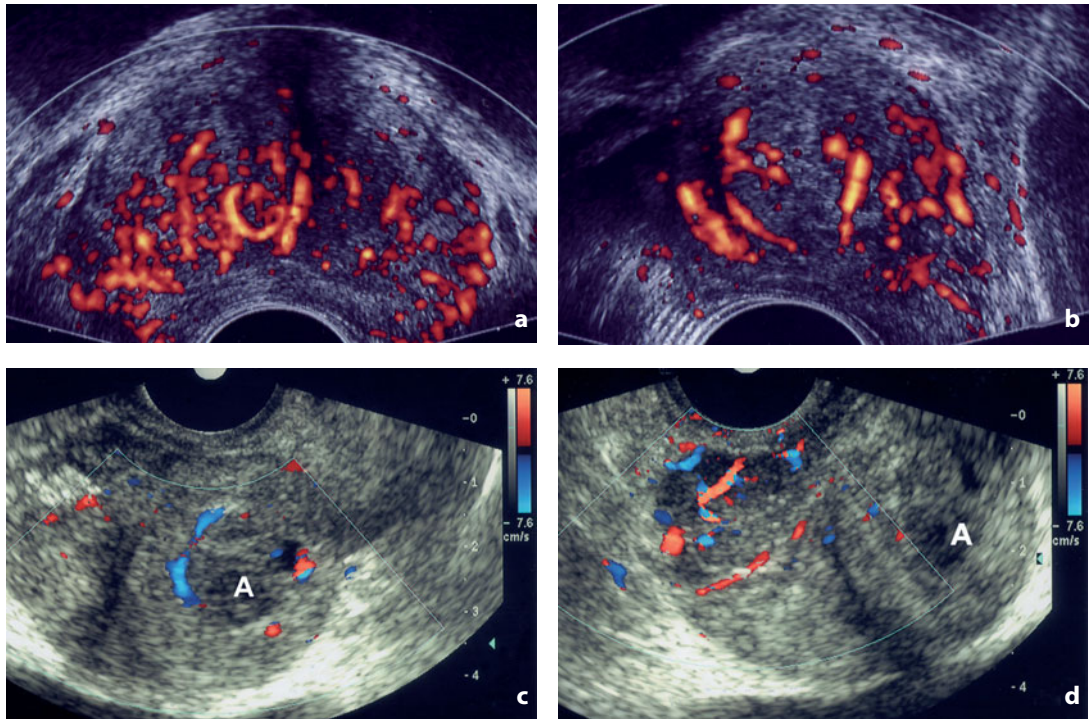

Fig. 11.10a-d. Power and color Doppler. Vasculature of the prostatic adenoma. **a, b** Power Doppler. **a** Axial scan. **b** Sagittal scan. The adenoma appears significantly more vascular than the peripheral zone. **c, d** Color Doppler shows increased vascularity in the area of the adenoma (*A*) which is, however, less than that identified in the carcinoma present in the right peripheral zone

of a stromal nodule. Retention cysts and calcifications are also common, distributed along the pseudocapsule or inscribed within the adenoma, along the urethra with an arching course. The prostatic capsule or, more exactly, the external profile of the gland, appears linear without deformations or interruptions.

In contrast to the transverse scan, the longitudinal view makes possible the study of the relations of the urethra above the seminal colliculus with hyperplastic nodules, and, although challenging, the study of the profile of the urethra during voiding, thus identifying the degree of compression on the urethra by the nodule.

The use of **color** and **power Doppler** offers no diagnostic advantages. Generally they show an increase in vascularity, particularly in young patients, as well as compression and dislocation of the vessels by the larger-sized nodules (Fig. 11.10).

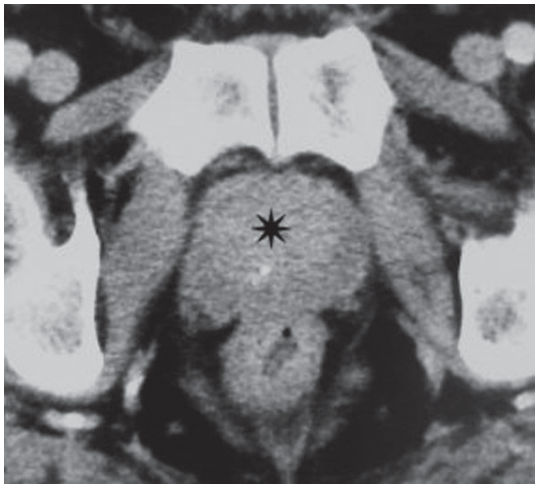

Fig. 11.11. Computed tomography. Prostatic adenoma. The lesion (*asterisk*) is recognizable due to the increased hyperattenuation with respect to the peripheral zone

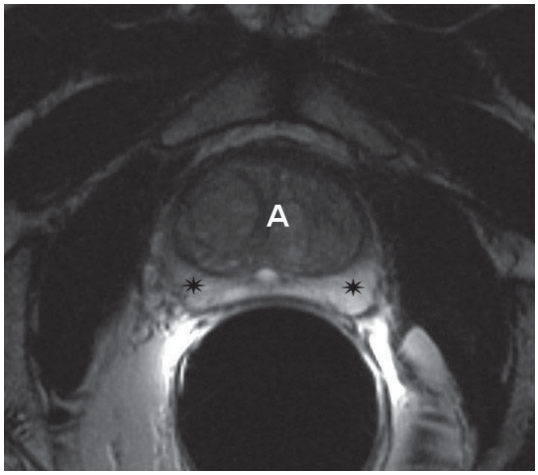

Fig. 11.12. Magnetic resonance. Axial T2-weighted image. Prostatic adenoma. In the central portion of the adenoma (*A*) a heterogeneous multinodular structure can be discerned with initial compression on the peripheral zone (*asterisks*), from which it is well differentiated

Given its inability to differentiate the zonal anatomy of the prostate, **computed tomography** in the study of BPH can do little more than demonstrate a generic increase in the volume of the gland which may be nonuniform owing to the presence of calcifications (Fig. 11.11). In contrast, **magnetic resonance (MR)** is able to visualize BPH very well, especially with the use of intraluminal coils. In T2-weighted sequences the adenoma can be easily separated from the peripheral portion of the gland, thus making an evaluation of its size and morphology possible, as well as providing information regarding its leiomyomatous or cystic glandular nature (Fig. 11.12). Although there is no indication for the use of MR in the study of BPH, the imaging characteristics of the condition need to be known to avoid interpretation errors, since almost all patients with adenocarcinoma also have prostatic hyperplasia.

The imaging modalities currently used in the study of patients with BPH who come under medical observation with LUTS include pelvic US with a suprapubic approach, TRUS for the direct study of the prostate, renal US and urography performed with the traditional technique or, better still, with CT.

According to the Consensus Conference organized in 2004 by the Italian Association of Urologists (AURO), suprapubic pelvic US is highly efficient and plays a central role, thanks to its ability to:

- evaluate postvoid residual (an index of the possible progression of the disease and a predictor of the failure of medical therapy);

- define the dimensions of the prostate (with results very similar to those obtained with the more complex transrectal approach);
- visualize the thickness of the bladder wall (the weight of the bladder wall which can be derived from the technique is thought to be a reliable indicator of the early onset of acute urinary retention).

TRUS is only recommended in candidates for minimally invasive surgery, to provide precise anatomopathologic information.

Renal US in association with an abdominal plain film is only indicated in patients with retention and/or suspected involvement of the upper urinary tract. In line with other American and European guidelines, according to AURO renal US is useful in patients with symptoms of BPH associated with hematuria, urinary tract infections (UTIs), renal insufficiency and prior surgery. The guidelines emphasize the low sensitivity of this modality in identifying small lesions of urothelial origin.

Urography is today considered of limited usefulness in clinical practice and is generally substituted by renal US performed in association with the plain abdominal film. In the presence of concomitant hematuria, performing CT urography and cystoscopy is advisable for the study of the upper and lower urinary tracts, respectively.

Gozzi G, Conti G, Peroni R et al (2005) Consensus conference about imaging of benign prostatic hypertrophy. Radiol Med 110:179–189

Grossfeld GD, Coakley FV (2000) Benign prostatic hyperplasia: clinical overview and value of diagnostic imaging. Radiol Clin North Am 38:31–47

Malignant Neoplasms

Pathology

Adenocarcinomas account for over 95% of all malignant neoplasms of the prostate (**Fig. 11.13**). In 3% of cases the tumor arises from the prostatic ducts and is differentiated in transitional or squamous carcinoma (metaplastic variant of transitional cell carcinoma), intraductal carcinoma and endometrioid carcinoma. The rarer forms include sarcomas (rhabdomyosarcoma, leiomyosarcoma, fibrosarcoma, chondrosarcoma, etc.), carcinosarcomas, carcinoids and lymphomas. In rare cases the prostate can also be the site of metastases.

Although no prostatic zone is immune from neoplastic transformation, the most frequent site of origin of adenocarcinomas is the lateral posterior peripheral zone (70% of cases). Less commonly affected are the central and transition zones (30%). Multifocality is not rare, and may be explained by either a multifocal origin or intraprostatic diffusion/metastasis.

In the initial phase with typical onset in the peripheral zone, the adenocarcinoma displays nodular growth. Obstructed by the capsule and the rectoprostatic fascia posteriorly and by frequent hyperplasia anteriorly, the tumor encounters minimal resistance to its expansion along the longitudinal axis with invasion of the apex and seminal vesicles. Further progression is characterized by invasion of the anterior gland and the capsule with involvement of the neurovascular bundle, of the bladder wall and rectum. The first lymph nodes to become involved are the periprostatic and obturator nodes. The tumor progressively involves the external iliac and hypogastric lymph nodes, and then the common iliac and periaortic nodes. Sites of distant metastasis of the adenocarcinoma include bone, the liver and the lungs, with the brain and other sites being less common. The prevalence of metastases to the axial skeleton and the pelvis, which in the past was attributed to neoplastic diffusion via the vertebral veins, is today more correctly justified by regional arterial flow and not by specific venous drainage.

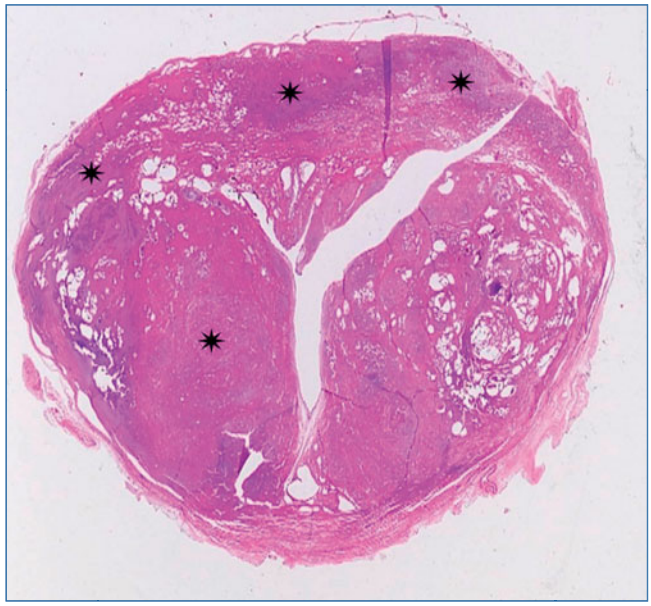

Fig. 11.13. Histologic specimen. The *asterisks* indicate the multifocal adenocarcinoma which on the left has also infiltrated the central zone

Table 11.1. Gleason classification

Grade 1	Tumor composed of well-defined individual glandular nodules, closely arranged, uniform and separate from each other
Grade 2	Tumor still relatively well defined, but with possible minimal extension of the neoplastic acini to the periphery of the tumor nodule in the noncancerous prostatic tissue
Grade 3	Tumor infiltrates the noncancerous prostatic tissue; the gland shows marked variation in size and organization
Grade 4	Markedly atypical cells with extensive infiltration into surrounding tissues
Grade 5	Tumor presents no glandular differentiation; composed of sheets of undifferentiated cancer cells

The cytologic and histologic features can be statistically correlated with prognosis. For this reason a number of grading systems have been proposed, with differentiated classes on the basis of the cytologic, cytohistologic and histologic appearance. The most widespread system currently in use for the evaluation of histologic grade is the Gleason score. The classification system is structured in relation to the cytologic characteristics of the prostatic adenocarcinoma cells as well as the glandular organization, and recognizes five different grades (Table 11.1). The score is defined by the combination of the primary, predominant grade and the secondary grade. Its range is potentially from 2 (1+1) to 10 (5+5). A score of 2–4 in biopsies is rare: these are generally lesions present in the transition zone which are sampled during transurethral resection of the prostate (TURP). The Gleason grade is reported for each individual biopsy sample and the biopsy with the highest grade is considered representative of the Gleason score of the patient. Patients can have a well-differentiated tumor (Gleason

score 2–4), moderately differentiated (5–7) or poorly differentiated (8–10). However, it should be borne in mind that a Gleason score of 4+3=7 is different from 3+4=7, because, although the sum is the same, in reality the first case has a higher primary grade. In a minority of cases, in addition to the primary and the secondary grades, the tumor also shows a tertiary grade which is higher than the other two. Despite being less represented, this tertiary grade needs to be included (and added to the primary grade) in the Gleason score, since a small focus of high-grade carcinoma present in the biopsy may correlate with a significant presence in the entire prostate, thus influencing prognosis. Therefore, 3+4+5=8 and not 7, and 2+3+4=6 and not 5.

The application of the Gleason score is unreliable in the evaluation of tumors which have been subject to neoadjuvant hormone therapy or radiotherapy. In these cases it is better to refer to the pretreatment Gleason biopsy.

The Gleason score is constantly used in the definition of classes at risk, i.e. of prognostic nomograms together with the PSA value and the clinical stage of the disease.

Diagnostic Imaging

Identification

Adenocarcinoma of the prostate can be verified following TURP performed for the treatment of BPH. Nonetheless, identification usually occurs following a series of procedures set in motion by the incidental finding of an altered PSA value in asymptomatic patients, or less frequently during digital rectal examination (DRE) and/or TRUS performed for reasons other than cancer screening (usually for the evaluation of BPH).

Leaving aside a detailed analysis of the topic for the appropriate chapter, discussion of the imaging features will nonetheless benefit from some introductory remarks regarding PSA and DRE, which make up an important part of tumor staging.

PSA Assay

As PCA3 testing has not become a part of routine clinical practice, PSA (glycoprotein produced mainly by the prostate) can currently be considered the only marker used on a routine basis in patients with prostate disease. PSA is however nonspecific, since it can be elevated in the presence not only of malignant lesions, but also of benign ones (hyperplasia, acute inflammation, infarction, urinary retention), as well as after several diagnostic procedures such as DRE itself, cytoscopy and prostatic biopsy (in the latter case increases of up to 50 times may be observed with a slow return to normal values in 30–60 days). Therefore, when we want to evaluate therapy-induced changes in PSA, the assay should be done prior to DRE, TRUS and instrumental procedures in the rectum and colon (rectoscopy or colonoscopy). In addition, a period of four weeks should pass after prostatic biopsy if the measured serum PSA is to be considered reliable. On the other hand, PSA levels in the bloodstream can decrease following the use of several drugs utilized in the treatment of BPH. Considering the prevalence of prostate cancer in the population affected by BPH, a drug-induced reduction in PSA can compromise the diagnostic utility of the marker in the presence of malignant tumor. Therefore, to exclude the concomitant presence of the latter, the following is advisable: baseline measurement prior to the beginning of treatment, successive six-monthly monitoring and further diagnostic procedures if a decrease in PSA >50% is not observed or if PSA levels rise over time.

PSA is generally evaluated with reference to a threshold value calculated on the basis of the distribution of the marker in normal subjects. The threshold value used is 4 ng/mL, although this value may be considered conventional since it is characterized by low positive and negative predictive values. This is due to several reasons, including patient age (PSA tends to increase in the elderly) and the overlap between

patients with neoplasm confined to the prostate and patients with BPH, who present values ranging from 4 to 10 ng/mL.

The sensitivity, specificity and positive predictive value of PSA in the identification of prostate cancer varies from study to study. The sensitivity of the test in patients with a PSA value of 4 ng/mL in fact fluctuates between 67.5% and 80%. This means that around 20–30% of cancers fail to be diagnosed when PSA is the only diagnostic test used. The specificity of the test varies from 60% to 70% with PSA >4 ng/mL.

Since 1991 prostatic biopsy has been recommended for total PSA (tPSA) values >4.0 ng/mL. In fact, prior to the 1990s there had been much debate regarding the appropriateness of performing biopsy in patients with tPSA values between 4 and 10 ng/mL in the presence of a negative DRE and normal TRUS. During the second half of the 1990s, however, it became clear that the possibility of encountering carcinoma of the prostate in patients with tPSA of 4–10 ng/mL ranged from 20% to 30%.

The possibility of a positive biopsy for prostate cancer can be correlated with tPSA values. The probability of carcinoma in patients with tPSA of 0.0–4.0 ng/mL is 10%, and in 90% of cases the tumor is confined to the prostate. With a tPSA of 4.0–10.0 ng/mL the probability of carcinoma is 25% with the tumor confined to the prostate in 70% of cases. With a tPSA >10.0 ng/mL the probability of carcinoma is 50%, with the tumor confined to the prostate in 50% of cases.

Since 10–15% of patients with tPSA between 2.5 and 4.0 ng/mL can have prostate cancer, it has recently been proposed to lower the normal tPSA threshold from 4 to 2.5 ng/mL. However, there is no broad consensus in the literature in this respect, such that the current proposal is to use a cutoff of 2.5 ng/mL in subjects with a family history of carcinoma of the prostate, an elevated tPSA for their age and an anomalous finding at DRE.

Age-adjusted PSA

Adjusting the PSA value on the basis of patient age has been introduced to improve the sensitivity of the marker in young subjects and the specificity in the elderly. The correlation of PSA values by age does not guarantee an acceptable increase in sensitivity and specificity.

PSA Ratio

Serum PSA exists in various forms, even though most of it is in complex with protease inhibitors such as alpha 1-antichymotrypsin and only a small amount is present in the free form. The ratio between free PSA (fPSA) and tPSA is defined PSA ratio. The percentage of fPSA is lower in subjects with prostate cancer. Therefore, the percentage of fPSA can be useful in determining which patients should undergo prostatic biopsy. It has been demonstrated that the percentage of fPSA can increase the specificity of tPSA in subjects with a tPSA between 2.5 and 10 ng/mL. The sensitivity and specificity of the percentage of fPSA are independent of the age of the subject undergoing the examination.

PSA Velocity and PSA Doubling Time

One possible method for rendering tPSA more efficient is to use repeated measurements over time to distinguish benign lesions from malignant ones on the basis of the different rates of change in the two situations. The rationale behind this approach is that men with carcinoma of the prostate will display a faster increase in PSA than those without prostate cancer.

PSA velocity measures the changes in PSA over one year, thus making possible a longitudinal evaluation of serum PSA levels. In the first half of the 1990s the concept was introduced that an increase in tPSA greater than 0.75 ng/mL per year is suggestive of carcinoma.

PSA doubling time measures the rate of change in a different manner, using a logarithmic formula to calculate the time it takes for PSA to double in value. The formula

is: log (2×t) divided by log (final PSA)–log (initial PSA). PSA doubling time is expressed in months. The limitations to using PSA velocity and PSA doubling time are linked to the inter- and intralaboratory variations in determining PSA values and in biologic variations of tPSA in single individuals unrelated to the underlying disease but linked to drugs, foodstuffs, and physical and sexual activity.

PSA Density

PSA density refers to the tPSA divided by the prostate volume expressed in cubic centimeters. PSA density was developed in an attempt to evaluate the importance of prostate volume, in light of the fact that an increase in prostate volume related to BPH can produce an increase in tPSA even in the absence of carcinoma. The calculation can be made in terms of the total prostate volume (PSA density) or in terms of the volume of the transition zone, the site of BPH (PSA transition zone density).

Normally, in subjects with a tPSA between 4 and 10 ng/mL a normal PSA density value is 0.15. There are nonetheless disadvantages in using PSA density in clinical practice. The value obtained is in fact dependent on the variations in the PSA assay and the accurate TRUS evaluation of the prostate volume. There is also a considerable overlap of patients with a PSA density below 0.15 who have BPH, prostatitis or carcinoma.

cPSA

Currently it is possible to assay PSA in complex with alpha 1-antichymotrypsin (cPSA). One of the theoretical advantages is being able to perform a single assay, thus reducing the variability of the two assays required for calculating the PSA ratio (tPSA and fPSA). Despite this theoretical advantage, both the initial retrospective studies and the successive prospective studies have failed to demonstrate the superiority of cPSA over the PSA ratio.

Digital Rectal Examination

DRE is often the first diagnostic approach to the patient presenting symptoms related to prostate disease. DRE is able to assess anal sphincter tone, the state of rectal fullness, the size, consistency and configuration of the prostate, the persistence of the median ridge, the symmetry between the two lobes, the tenderness of the gland and possible presence of a nodule whose site, margins, surface and consistency can be defined.

An abnormal rectal finding is defined as an increase in compactness possibly associated with irregularities of the surface or margins of the prostate. DRE is only able to identify tumors of moderate size arising from the peripheral zone. The examination fails to identify formations which, due to their central site, limited dimensions and consistency, do not cause palpable alterations. It should also be borne in mind that in addition to carcinoma other nonmalignant conditions (calculosis, prostatitis, tuberculosis, infarction, post-biopsy reactions and even hyperplastic nodules) can produce increases in focal consistency and/or modifications of the margins of the prostate.

The presence of an abnormal rectal finding is an indication for prostatic biopsy. In around 18% of cases the diagnosis of prostatic carcinoma is made exclusively on the basis of this finding. On the other hand, DRE alone does not have adequate diagnostic accuracy and should be associated with the PSA assay. In addition, a number of studies have shown that DRE should be performed in subjects with a tPSA greater than or equal to 1 ng/mL: 14–30% of subjects with a suspicious DRE and PSA between 1 and 4 ng/mL are found to have carcinoma at biopsy.

DRE can therefore be considered a first-line diagnostic procedure, being simple and noninvasive. The technique has the significant disadvantages of interoperator variability and an inability to appreciate the entire prostate. As a result, the procedure is never used alone to formulate the diagnosis of carcinoma of the prostate. Often there is in fact no correlation between DRE and the biopsy findings, since around 38% of

patients who undergo radical prostatectomy have been shown to have a neoplasm which does not cause anomalies in the consistency of the gland that can be identified at palpation.

Transrectal Ultrasonography of the Prostate

The suprapubic US study is absolutely inadequate at differentiating areas of variable echogenicity within the prostate. Therefore, the examination needs to be performed with a transrectal approach.

Clinical and anatomopathologic studies have definitively shown that small carcinomas of the prostate (<2 cm) arising in the peripheral zone in most cases appear as hypoechoic lesions with well-defined margins with respect to the surrounding tissue (**Fig. 11.14**). Although in a small percentage of cases (from 2.5 to 7.2% according to different studies) TRUS alone is able to identify the nonpalpable carcinoma in patients with PSA <4 ng/mL, the US appearance described above cannot be considered pathognomonic because in the peripheral zone:

- hypoechoic foci can be the result of acute inflammation, chronic inflammation and infarction (once a nodule has been identified, the positive predictive value of TRUS improves significantly when the finding is integrated with DRE and the PSA value; **Table 11.2**);
- the neoplasm can appear isoechoic in one-third of cases, similar to the adjacent parenchyma, such that the diagnosis is only reached thanks to the finding of volume asymmetry between the two lobes or the TRUS finding of a bulge corresponding to a nodule appreciable at DRE;
- in not exceptionally rare cases the tumor can appear hyperechoic, resulting from a particular histologic variety known as prostatic comedocarcinoma (**Fig. 11.15**).

In addition, as stated above 30% of prostate cancers originate in the central or transition zone, where they are difficult to identify with TRUS.

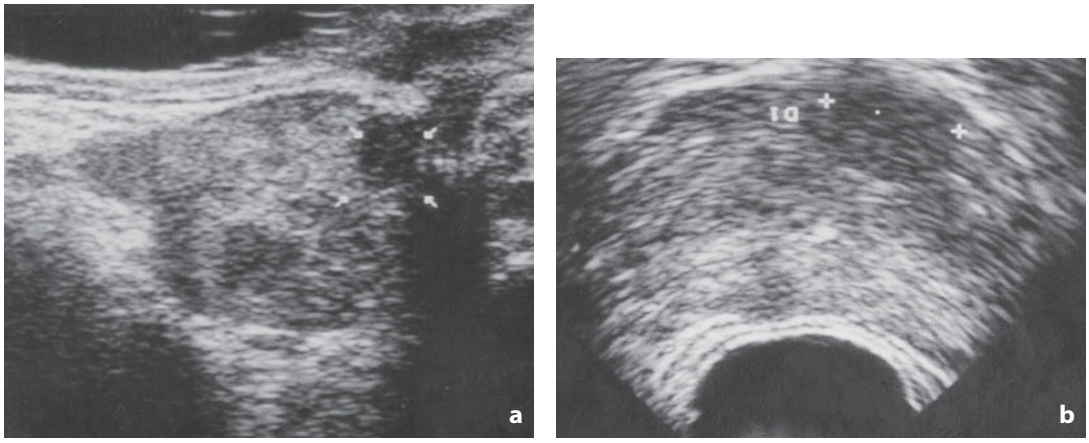

Fig. 11.14a,b. Ultrasonography. Transrectal approach. Prostatic adenocarcinoma. **a** Sagittal scan. A hypoechoic focal lesion with well-defined margins is apparent in the peripheral zone bounded by *small arrows*. **b** Axial scan. The nodule is identifiable by the greater hypoechogenicity

Table 11.2. Positive predictive value (PPV) for carcinoma of the prostate of a hypoechoic nodule identified in the peripheral zone of the prostate when the TRUS finding is integrated with the PSA value and digital rectal examination (DRE)

		PPV
Elevated PSA	DRE +	71%
Normal PSA	DRE +	26%
Elevated PSA	DRE –	34%
Normal PSA	DRE –	5%

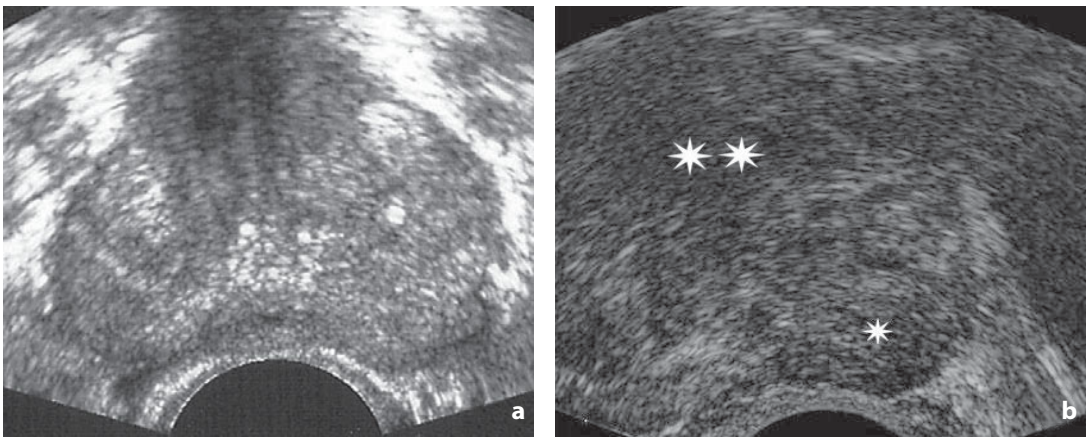

Fig. 11.15a,b. Ultrasonography. Transrectal approach. Prostatic adenocarcinoma. **a** Isoechoic lesion. Patient with PSA 8 ng/mL. The random biopsies show the presence of adenocarcinoma in the right peripheral zone. A centrally located trilobar adenoma is also visible. **b** Detailed view of hypoechoic lesion (*asterisk*) located in the peripheral zone of the left lobe. At US-guided targeted biopsy granulomatous prostatitis is diagnosed. The gland shows diffusely coarse echotexture prevalently hypoechoic in the central zone (*double asterisk*)

Bounded posteriorly by the capsule and the rectoprostatic fascia and anteriorly by frequent hyperplastic nodules, the neoplasm tends to grow along the line of least resistance to the infiltrative process. Therefore, it develops longitudinally and laterally, transforming itself from a nodule into a plaque, all the while remaining hypoechoic (Fig. 11.16). Only in the later phases, i.e. when the neoplastic tissue grows from the peripheral zone towards the central zone, does the echotexture change from hypoechoic to a mixture of sparse hypoechoic malignant areas and hyperechoic benign areas produced by fibrotic glandular parenchyma or calcification incorporated by the growing tumor tissue.

The carcinoma, therefore, originates as hypoechoic and tends towards mixed, since the echogenicity is influenced by the preexisting disease: the progressive infiltration of prior areas of calcified or fibrocalcified prostatitis (i.e. predominantly stromal hyperplasia) produces the mixed-hyperechoic type of echotexture.

The use of **color and power Doppler** has not shown significant improvements in the ability to identify prostate cancer. The hypothesis of identifying neoplastic areas which are occult in B-mode has not been supported by clinical findings, probably because the tumor is poorly vascular. Even though sensitivity and positive predictive value in some studies are improved by the technique, specificity continues to be too low to avoid biopsy.

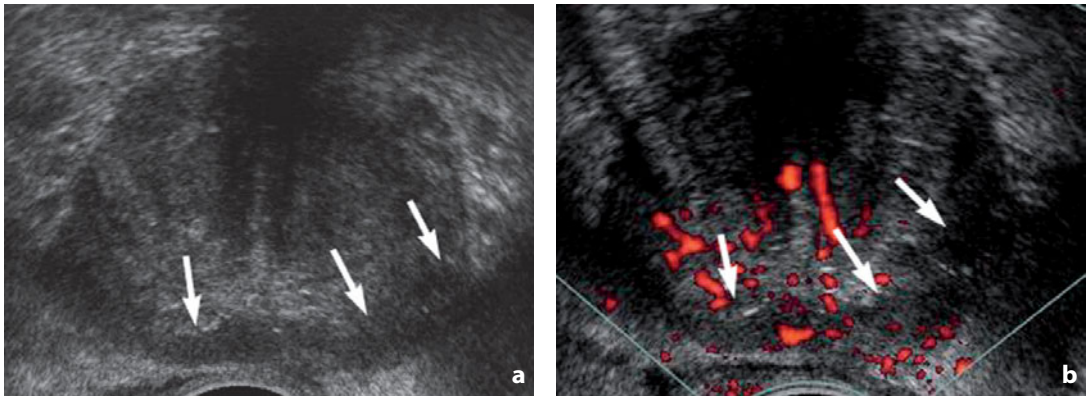

Fig. 11.6a,b. Color Doppler. Prostatic adenocarcinoma. **a** The tumor (*arrows*) shows plaque-like infiltration of the diffusely hypoechoic peripheral zone. **b** Vascularity at power Doppler is only slightly higher than in the central portion of the gland, the site of adenoma

A recent development in US imaging of the prostate has been the use of contrast media with or without color Doppler, with the aim of identifying intratumoral neovascularization in the sonographically suspicious or poorly vascular areas. Nonetheless, their use does not seem to be decisive in the differential diagnosis between carcinoma and chronic granulomatous prostatitis.

Each of the procedures currently used in the identification of carcinoma of the prostate (PSA, DRE, TRUS) has limitations which can be improved with the integrated approach, without, however, guaranteeing the necessary diagnostic reliability. This is why the definitive diagnosis of the tumor is delegated to the histology obtained from biopsy.

Prostate Needle Biopsy

Prostate biopsy should be performed in all cases in which there is suspicion of malignancy, i.e. in the presence of a palpable nodule, hypoechoic lesion, PSA >10 ng/mL, PSA 4–10 ng/mL with PSA ratio <15%, PSA density >0.15 or PSA velocity >1 ng/mL. The procedure is always performed under TRUS guidance, with a 14–18 gauge needle and a transrectal or transperineal approach. The former is simpler, thanks to the use of the guide device (mounted on the end-fire transducer) and the trace indicated on the computer monitor; the technique is less painful and requires the administration of antibiotics before and after the biopsy to avoid infection. The latter technique has the advantage of the absence of contamination, thus avoiding possible prostatitis.

The biopsy technique differs in relation to the indication. In cases with suspicious PSA and negative DRE and TRUS, sampling is performed with a random technique in an attempt to systematically biopsy the prostate.

The classic sextant technique described by Hodge and performed with a transrectal approach involves the selection of six sites on the prostate for needle insertion, three per lobe, two of which (one per lobe) are in the central zone. The observation of a small number of carcinomas which escape detection with this technique has led to a series of modifications with regard to both the number and the sites of needle insertion. Various proposals have been made, including the systematic five region prostatic biopsy promoted by Eskew: in addition to the six needle cores in the Hodge technique there are three in the central region and two in both lateral regions for a total of thirteen. In the fan-shaped technique proposed by Bosner and performed with a transperineal approach to the apex, the inclination of the needle varies in successive passages, producing the characteristic pattern which gives the technique its name (Fig. 11.17).

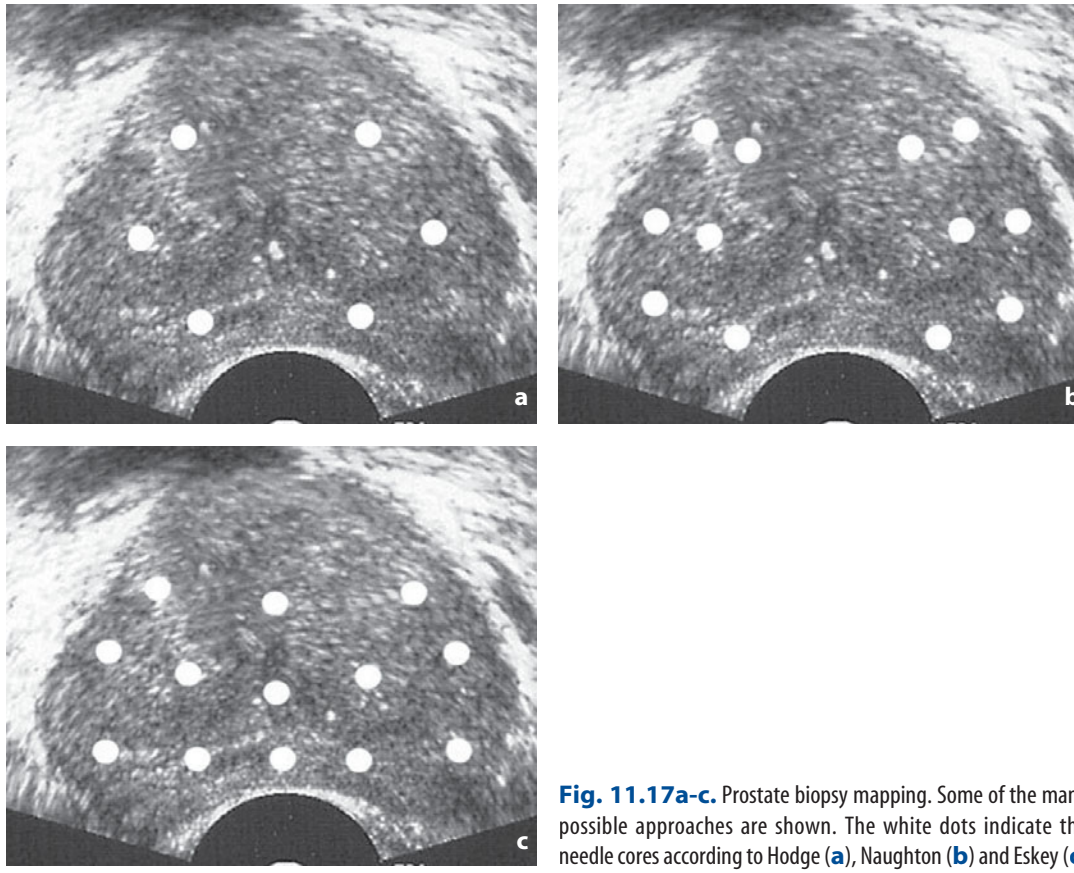

Fig. 11.17a-c. Prostate biopsy mapping. Some of the many possible approaches are shown. The white dots indicate the needle cores according to Hodge (**a**), Naughton (**b**) and Eskey (**c**)

Regardless of the technique used, the number of cores to be taken has still not been unanimously defined, even though increasing the number obviously involves improving diagnostic accuracy. In clinical practice there appears to be general agreement that 8–10 cores, at least two of which are in the transition zone, is a good compromise between diagnostic accuracy and patient discomfort.

In cases with a positive DRE or TRUS, US-guided targeted biopsy is performed (**Fig. 11.18**). Nonetheless, associating the technique with the standard sextant protocol is considered indispensable for identifying imperceptible foci and for achieving a biopsy definition of the tumor volume. This is an important parameter in tumor staging based on nomograms which take into account PSA, biopsy grading and the number of positive cores.

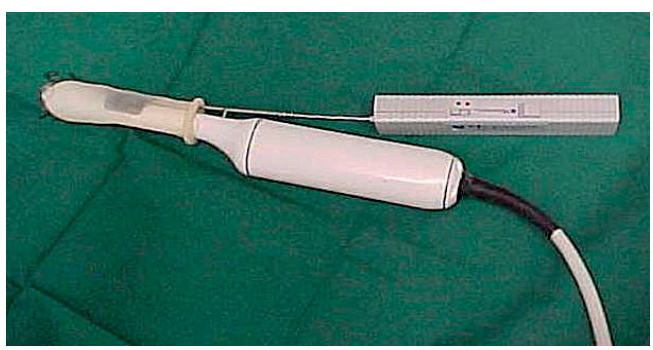

Fig. 11.18. Transducer and biopsy gun for US-guided procedures

Should the first mapping prove negative, a further biopsy is indicated in patients with a persistently high PSA and/or the appearance of clinically suspicious areas at DRE or TRUS. A further biopsy is also indicated in cases where a previous biopsy has shown the presence of high-grade prostatic intraepithelial neoplasia (HGPIN) or atypical small acinar proliferation (ASAP), findings which are histologically predictive of the presence or development of invasive disease.

The identification of prostatic adenocarcinoma is therefore based on the PSA assay, DRE and TRUS, with the definitive diagnosis being made with prostatic needle biopsy. Nevertheless, the lesion may also be identified with CT and MR.

Computed Tomography

Unlike US and MR, CT is unable to differentiate the zonal anatomy of the prostate: the central and peripheral zones have the same signal. There is therefore no rationale for using the technique in the study of the prostate, and in particular in identifying adenocarcinoma. Prostate cancer may nonetheless be an incidental finding on CT scans performed for other reasons (**Fig. 11.19**).

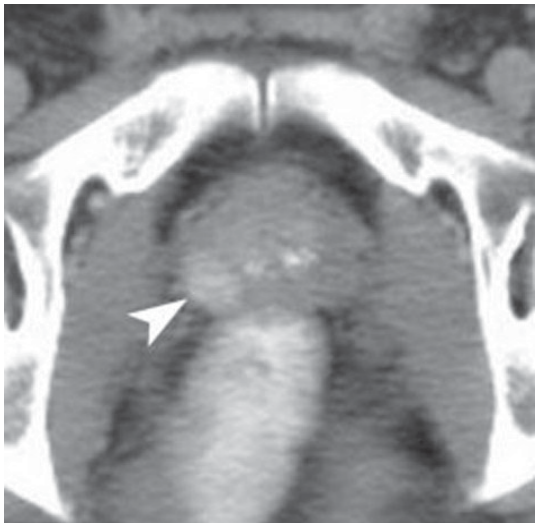

Fig. 11.19. Computed tomography. Prostatic carcinoma. Incidental finding of a lesion (*arrowhead*) in the left lobe. The nodule appears hyperattenuating after contrast medium injection

Magnetic Resonance

Rather than being used in the identification of lesions, MR plays a role in the localization of the neoplasm and can provide a wide variety of information. This includes (1) improving the diagnosis by targeting the biopsy towards suspicious areas in patients defined as highrisk at PSA despite having had previous negative US-guided biopsies; (2) evaluating the presence of tumor in the neurovascular bundle when planning surgical excision; (3) improving the results of laparoscopic prostatectomy; (4) planning intensity-modulated radiation therapy; (5) correctly guiding therapy towards less-invasive procedures such as cryosurgery and brachytherapy; (6) monitoring the dimensions and development of the tumor in patients who choose not to be treated (watching and waiting).

The visualization and identification of adenocarcinoma, however, depends on the type of sequence used. On T1-weighted images the hypointense lesion cannot be identified, and although in T2 the signal is substantially similar, regardless of the magnetic

field, the coil used (preferably intraluminal) and the site of the lesion (whether central or peripheral), the lesion can be easily identified. This is because the peripheral zone is hyperintense in T2-weighted sequences such that the hypointense adenocarcinoma is clearly visible in most cases (**Figs. 11.20, 11.21**).

MR is even able to identify neoplastic nodules situated in the central zone, especially with the use of an endorectal coil. In fact, the precise indication for the use of the endorectal coil is in subjects with increased PSA and negative DRE and TRUS. The identification of a neoplastic nodule with MR in these cases can in fact avoid the need for irritating random biopsies. On the other hand, the finding of a hypointense nodule is not pathognomonic since a hypointense signal can be present in postbiopsy hemor-

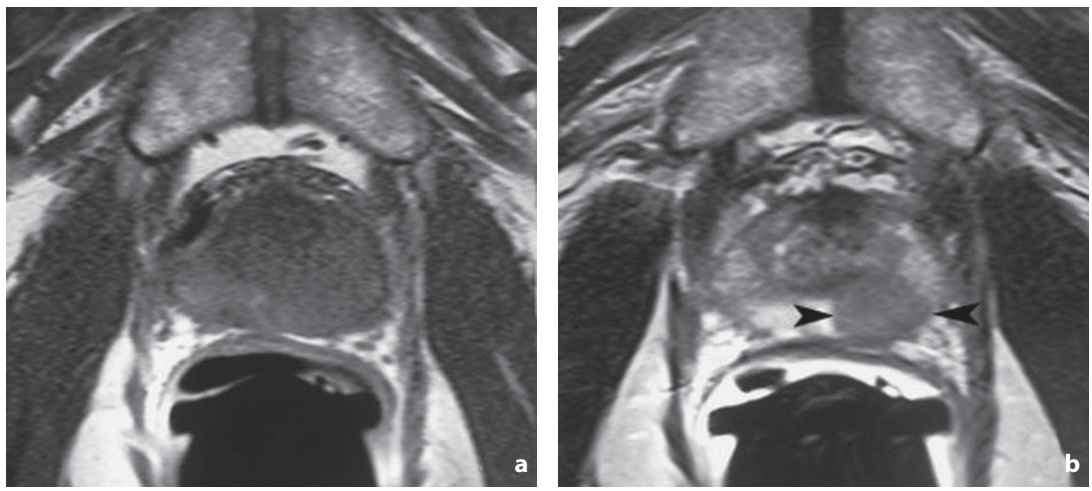

Fig. 11.20a,b. Magnetic resonance. Signal characteristics. Prostatic carcinoma. **a** Axial T1-weighted image. The lesion is isointense to the adjacent tissue and therefore cannot be identified. **b** Axial T2-weighted image shows the well-defined hypointense nodule (*arrowheads*) in the context of the hyperintense peripheral zone

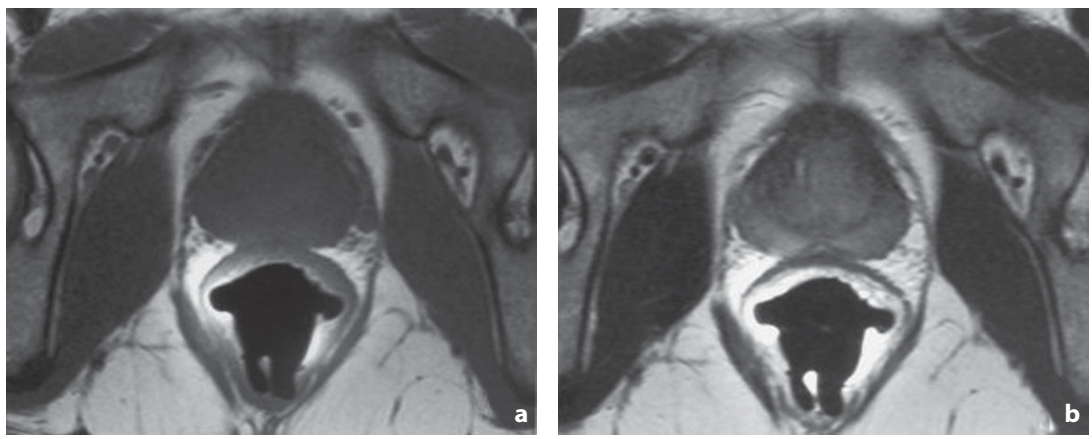

Fig. 11.21a,b. Magnetic resonance. Signal characteristics. Prostatic carcinoma. **a** Axial T1-weighted image. The lesion is isointense to the adjacent tissue and therefore cannot be identified. **b** Axial T2-weighted image shows the hypointense lesion diffusely infiltrating the peripheral zone which is no longer recognizable in its normal hyperintensity

rhage, prostatitis, intraglandular dysplasia and heterotopic nodule of BPH. In order to improve the identification of adenocarcinoma the use of extracellular interstitial paramagnetic contrast medium has been proposed (**Fig. 11.22**). However, the pre- and postcontrast-enhanced T1-weighted images alone are not always adequate for differentiating malignant from benign tissue, and therefore differentiating the neoplastic nodule in the presence of BPH, since both show the same pattern of enhancement. By exploiting perfusion differences it may be possible to distinguish the two by performing a dynamic study with T1-weighted sequences. These can be slow with low temporal resolution (30 s) but high spatial resolution (which generally produces high sensitivity and low specificity), or they can be fast with high temporal resolution (1-4 s) and low spatial resolution (which produces low sensitivity and high specificity). Lesions in the peripheral zone can be identified with the first technique, which in evaluating the presence of early-stage clinically significant neoplasms achieves elevated sensitivity around 90%. This is equivalent to or sometimes higher than the reference standard of random biopsies (six or eight cores with 14 gauge needle), even for PSA levels <10 ng/mL. In most cases, therefore, current practice tends to prefer the use of high-spatial-resolution sequences, which at least seem to improve staging.

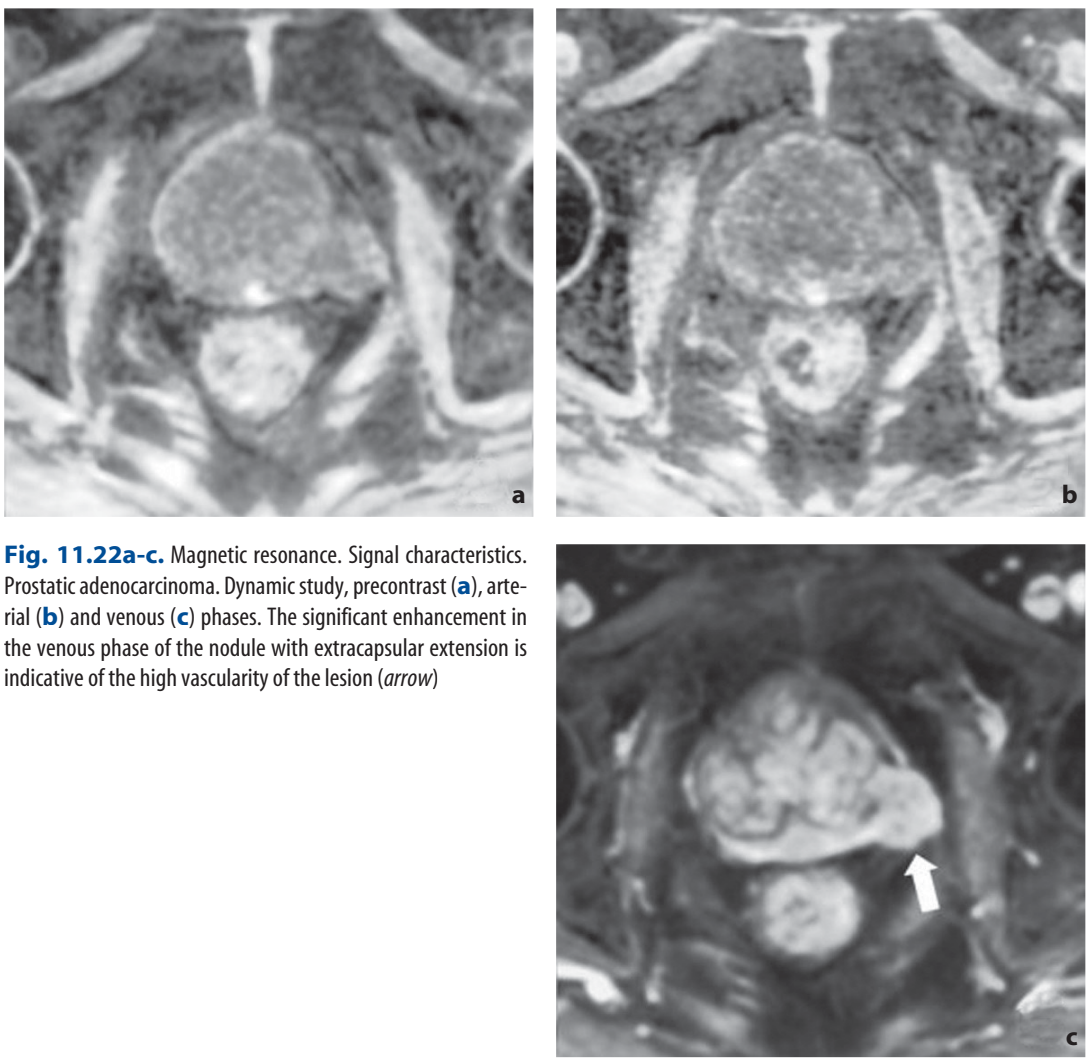

Fig. 11.22a-c. Magnetic resonance. Signal characteristics. Prostatic adenocarcinoma. Dynamic study, precontrast (**a**), arterial (**b**) and venous (**c**) phases. The significant enhancement in the venous phase of the nodule with extracapsular extension is indicative of the high vascularity of the lesion (*arrow*)

Contrast enhancement in the context of the neoplastic lesion can be evaluated with semiquantitative analysis of the signal intensity (time to appearance, maximum signal intensity, shape of the enhancement curve and area below it in a set time, usually 60-90 s after arrival, wash-out gradient), or with a quantitative analysis of the concentration of contrast medium in the tissue based on the use of pharmacokinetic models (calculation of extracellular extravascular volume, volume transfer constant, diffusion ratio constant). In reality, due to computational difficulties quantitative analysis is never used in routine clinical practice in favor of semiquantitative analysis, and is of little use due to the difficulties in making comparisons between different patients and different scanners.

Regardless of the technique used, dynamic studies together with T2-weighted images are less accurate in identifying central lesions than lesions originating in the peripheral zone.

In view of these limitations, special attention has been paid to **MR spectroscopy (MRS)**, which is the only noninvasive technique able to quantitatively identify the chemical substances in the body. The images can be acquired with a high static field magnet and using a body coil for pulse transmission and a surface coil positioned at the level of the pelvis for signal reception. Alternatively, an endorectal coil connected to a phased array coil positioned on the pelvis can be used. The choice of a surface coil may be preferable to avoid the discomfort of an intraluminal coil and to improve the image quality degraded by artifacts specific to endorectal coils (coil flair, straight line, glandular distortion). The individual voxels of the volume selected are represented two-dimensionally on a grid overlying the corresponding T2-weighted images.

The rationale behind the use of MRS is provided by the demonstration of elevated levels of choline and low levels of citrate in the carcinoma. This is the opposite of normal prostate tissue, where the concentration of citrate is high and choline is low. The low concentrations of citrate in the tumor are the result of changes in cellular function and tissue architecture. In fact the neoplastic cells are less able to synthesize citrate and the normal glandular epithelium is substituted by the newly formed tissue. High concentrations of choline, which is a component of the cellular membranes, are found in carcinoma of the prostate due to the irregular multiplication of the tumor membranes.

Analysis of the spectroscopic curve is performed with appropriate software, which calculates the area below the citrate, choline and creatinine peaks. To identify the presence of cancer, the ratio between the area below the choline plus creatinine peaks and the area below the citrate peak is calculated. The presence of cancer is hypothesized when the ratio (>0.75) of (Cho+Cr)/Cit in the suspicious zone deviates by more than 2 standard deviations (SD) with respect to the value obtained in the healthy reference zone. A ratio (>0.86) of (Cho+Cr)/Cit greater than 3 SD with respect to the value of the normal zone is defined as the definite presence of neoplasia. The voxels with a ratio less than 0.75 are defined as normal tissue of the peripheral zone (**Fig. 11.23**).

In identifying tumor, MRS has a specificity which is significantly higher than MR alone. A positive finding at MR and MRS indicates a high probability of the presence of tumor (positive predictive value 88-92%), whereas a negative result rules out disease with a slightly lower probability. Recent studies have evaluated the possibility of establishing a correlation between tumor aggressiveness measured with the Gleason score and the concentration levels of choline and citrate in the neoplasm. A marked reduction to the point of absence of the citrate peak has been observed in cases of high-grade Gleason tumors and a smaller reduction in the peak in low-grade Gleason tumors. This finding can most likely be explained by the lesser presence of glandular structures (producers of citrate) in poorly differentiated tumors. It has also been shown that small low-grade tumors (Gleason 4 and 5) might not be identified due to the slight alterations of citrate and choline. Initial clinical studies with high-intensity magnetic fields (3T) have shown improved spectral resolution and a substantial increase in the detection and characterization of prostatic carcinoma.

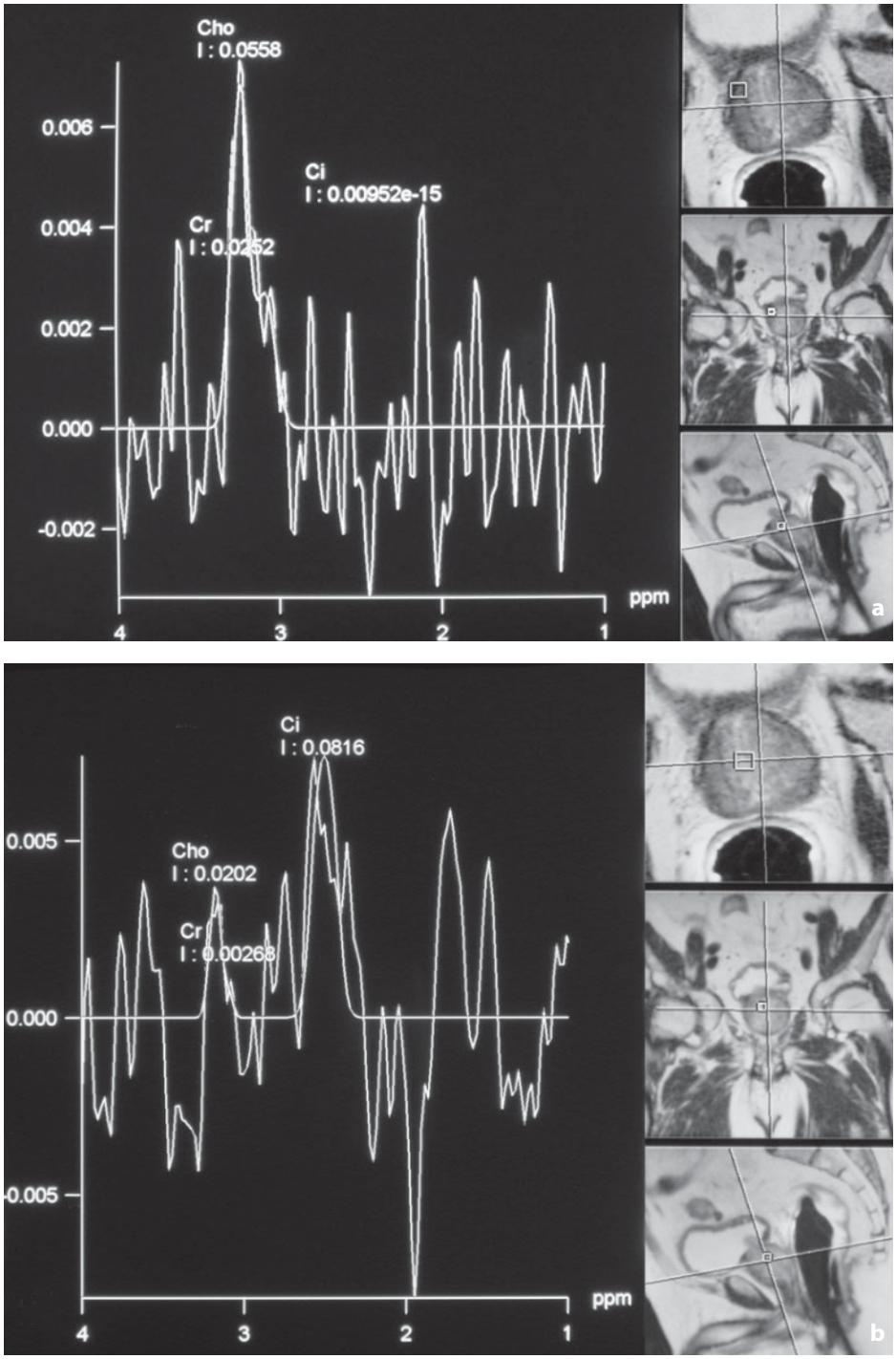

Fig. 11.23a,b. MR spectroscopy. In image **a** the spectrum is sampled at the site of the tumor in the peripheral zone. The (Cho+Cr)/Cit ratio is greater than 0.75. Compare this finding with image **b** which shows the same ratio at the level of the central adenomatous zone

Choi YJ, Kim JK, Kim N et al (2007) Functional MR imaging of prostate cancer. RadioGraphics 27:63-75

Choyke PL (2006) Prostate cancer imaging: past, present, future. RSNA categorical course in diagnostic radiology. Genitourinary Radiology, pp 35-41

Hambrock T, Padhani AP, Tofts PS et al (2006) Dynamic contrast-enhanced MR imaging in the diagnosis and management of prostate cancer. RSNA categorical course in diagnostic radiology. Genitourinary Radiology, pp 61-77

Hricak H, Choyke PL, Eberhardt SC et al (2007) Imaging prostate cancer: a multidisciplinary perspective. Radiology 24:28-53

Shukla-Dave A, Hricak H (2006) MR spectroscopy of prostate cancer: current practices and techniques. RSNA categorical course in diagnostic radiology. Genitourinary Radiology, pp 53-60

Staging

Staging of prostatic adenocarcinoma is performed according to the TNM system (**Table 11.3**) or the Whitmore–Jewett classification (**Table 11.4**) and involves clinical examination and diagnostic imaging. **Table 11.5** demonstrates a possible protocol for the integration of imaging modalities and optimization with prognostic factors such as the Gleason score and PSA.

Table 11.3. TNM classification of prostate cancer

Evaluation of primary tumour
- **TX** Primary tumour cannot be assessed
- **T0** No evidence of primary tumour
- **TI** Clinically inapparent tumour not palpable or visible by imaging
  - T1a Tumour incidental histologic finding in 5% or less of resected tissue (for other reasons)
  - T1b Tumour incidental histologic finding in more than 5% of resected tissue
  - T1c Tumour identified by needle biopsy (e.g., because of elevated PSA)
- **T2** Clinically appreciable tumour (palpable) confined within the prostate
  - T2a Tumour involves one half of one lobe or less
  - T2b Tumour involves more than half of one lobe, but not both lobes
  - T2c Tumour involving both lobes
- **T3** Tumour extends through the prostatic capsule (if infiltration of the capsule is only partial the tumour should still be classified T2)
  - T3a Extracapsular extension (unilateral or bilateral)
  - T3b Tumour invades one or both seminal vesicles
- **T4** Tumour is fixed or invad adjacent structures other than the seminal vesicles: bladder neck, external sphincter, rectum, etc.

Evaluation of regional lymph nodes
- **NX** Regional lymph nodes cannot be assessed
- **N0** No regional lymph node metastasis
- **N1** Regional lymph node metastasis

Evaluation of distant metastasis
- **MX** Distant metastasis cannot be assessed
- **M0** No distant metastasis
- **M1** Distant metastasis
  - M1a Non-regional lymph nodes metastasis
  - M1b Bone (s)
  - M1c Other site (s)

Note: A tumour found in one or both lobes by needle biopsy, but which is not palpable or visible by imaging is classified T1c.
Invasion into the prostatic apex or into (but not beyond) the prostatic capsule is classified T2 and not T3.
The regional lymph nodes are the pelvic lymph nodes, i.e. those located at the aortic bifurcation: common, internal and external iliac, and obturator lymph nodes

Table 11.4. Whitmore–Jewett classification of prostate cancer

STAGE A. Microscopic, nonpalpable, clinically silent tumor
A1 Well differentiated single focus
A2 Moderately or poorly differentiated multifocal lesions

STAGE B. Macroscopic, palpable intracapsular tumor
B1 Tumor present in a single lobe and ≤1.5 cm
B2 Tumor >1.5 cm or multiple nodules in both lobes

STAGE C. Extracapsular extension but still clinically localized
C1 Extension to the seminal vesicles but not to the pelvis
C2 Extension to the pelvis possibly causing urinary retention due to urethral obstruction

STAGE D. Metastasis
D1 Metastasis limited to three lymph node sites
D2 More extensive lymph node metastasis and extrapelvic (e.g. bone) metastasis

Table 11.5. Diagnostic and staging protocol of carcinoma of the prostate optimized in accordance with prognostic factors. DRE, digital rectal examination; TRUS, transrectal ultrasonography; GI, Gleason; GIS, Gleason score

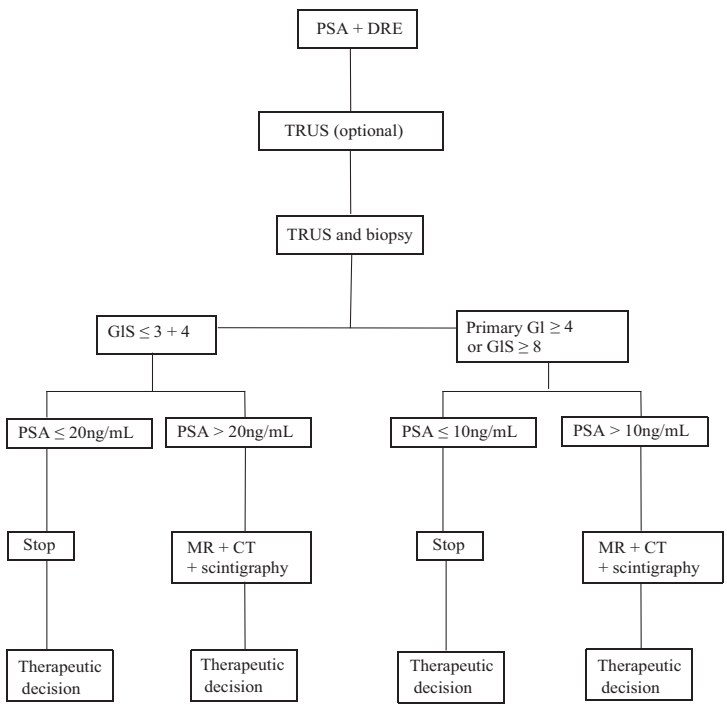

Digital Rectal Examination

DRE is completely subjective with a wide margin of error, such that 30–50% of clinical T2 tumors prove to be T3, while some 10% of cases diagnosed as T3 are reclassified T2 after surgery. Despite this wide margin of error, DRE is widely used because it is cheap and nonetheless highly specific in T3 and T4 advanced forms. Large study populations have shown that very few patients with intracapsular tumor at DRE are excluded inappropriately from surgery.

Transrectal Ultrasonography of the Prostate

Sensitivity and specificity of the technique are limited by the difficulty in identifying isoechoic lesions located in the central zone of the prostate. The ability to evaluate extracapsular extension and invasion of the seminal vesicles is marginally greater, but not significantly, than for DRE.

Capsular invasion can be deduced when a restricted irregularity of the glandular margin or interruption of the hyperechoic line corresponding to the periprostatic adipose tissue is observed (**Fig. 11.24**). Data in the literature vary widely: sensitivity 50–92%, specificity 46–91% and diagnostic accuracy 58–86%. Two important multicenter prospective studies have shown that TRUS is no better than DRE regarding extracapsular extension of the disease.

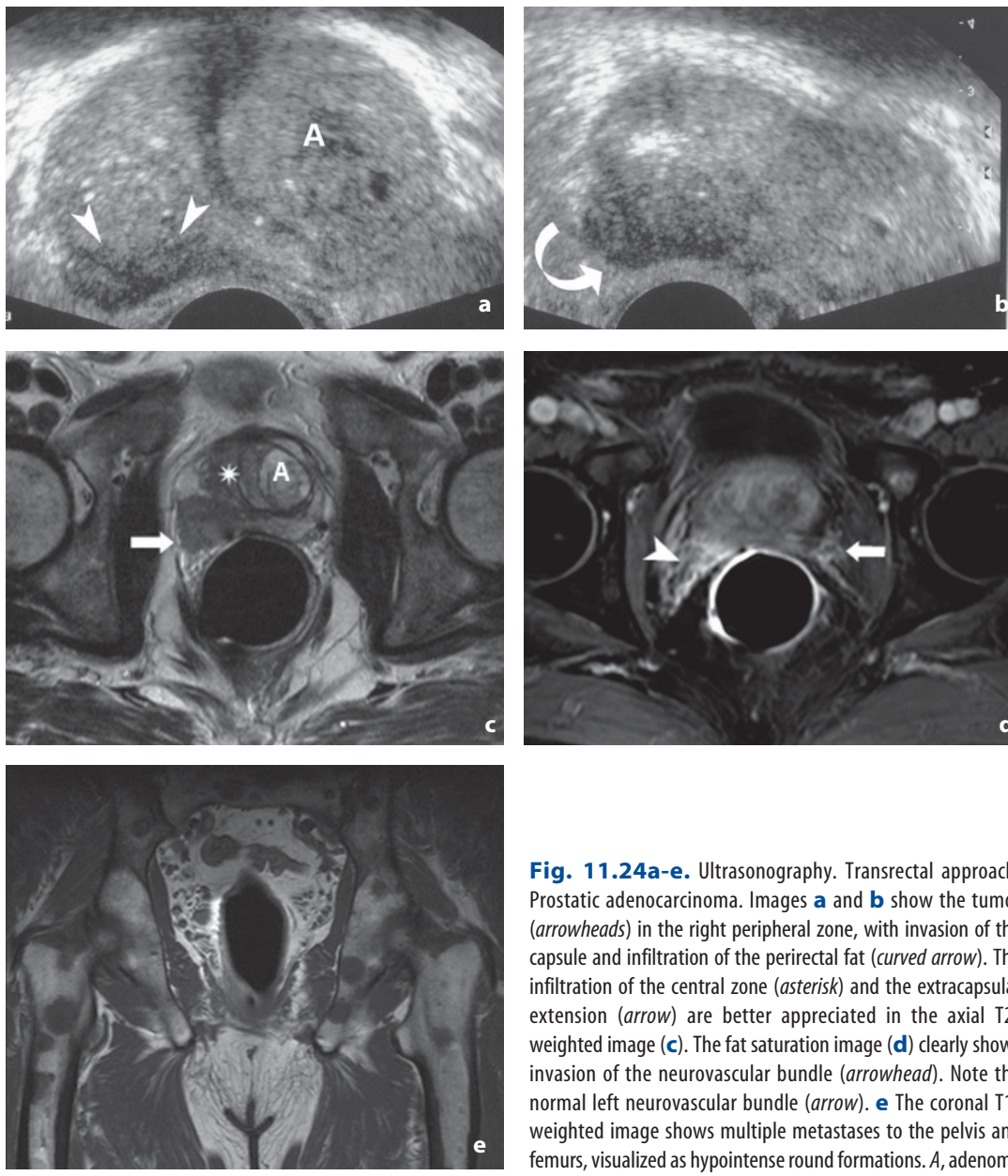

Fig. 11.24a-e. Ultrasonography. Transrectal approach. Prostatic adenocarcinoma. Images **a** and **b** show the tumor (*arrowheads*) in the right peripheral zone, with invasion of the capsule and infiltration of the perirectal fat (*curved arrow*). The infiltration of the central zone (*asterisk*) and the extracapsular extension (*arrow*) are better appreciated in the axial T2-weighted image (**c**). The fat saturation image (**d**) clearly shows invasion of the neurovascular bundle (*arrowhead*). Note the normal left neurovascular bundle (*arrow*). **e** The coronal T1-weighted image shows multiple metastases to the pelvis and femurs, visualized as hypointense round formations. *A*, adenoma

Invasion of the neurovascular bundle can be diagnosed with a sensitivity of 66% and specificity of 78% in patients with visible carcinoma.

Defining the degree of invasion of the seminal vesicles is, however, more challenging, especially in the initial forms (sensitivity 22–60%, specificity 88% and accuracy 78%). Involvement of the seminal vesicles, which tends to occur earlier when the tumor is located near the prostatic base, can be identified with the following findings:

- presence of a hypoechoic halo around the ejaculatory ducts, an expression of tumor spread along the periductal connective tissue;
- disappearance of the acute angle between the seminal vesicles and the prostate where they penetrate the gland;
- direct extension of the carcinoma in the vesicle in cases of extensive tumors.

Computed Tomography

CT is currently the reference standard for the study of regional lymph nodes, although it can also provide information regarding the regional evaluation of advanced disease and be helpful in the search for distant metastases (**Fig. 11.25**). With PSA values <20 ng/mL it is highly unlikely for abdominal and pelvic CT to be positive. The examination is nonetheless indicated in cases of a PSA >20 ng/mL or in patients with a primary Gleason >4 or a Gleason score ≥8 and PSA >10 ng/mL.

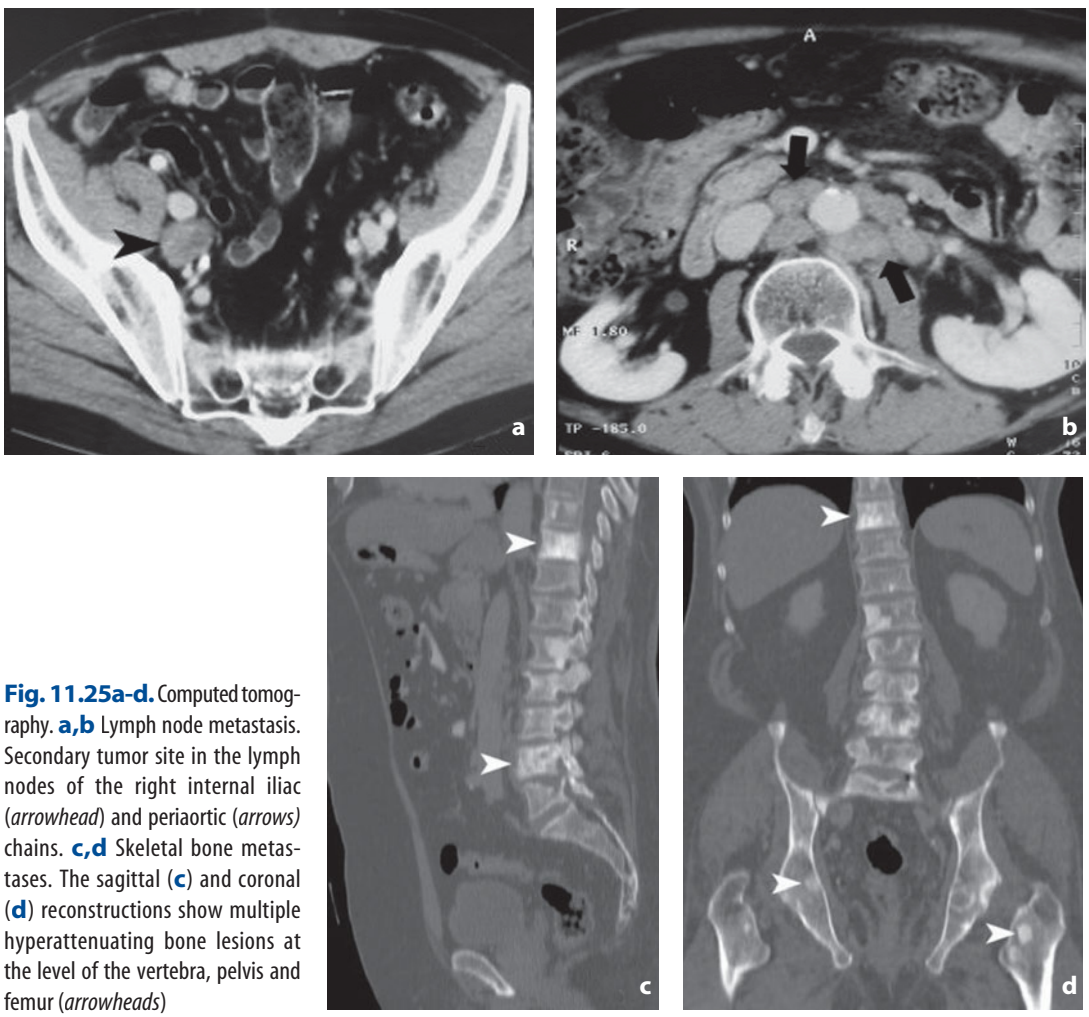

Fig. 11.25a-d. Computed tomography. **a,b** Lymph node metastasis. Secondary tumor site in the lymph nodes of the right internal iliac (*arrowhead*) and periaortic (*arrows*) chains. **c,d** Skeletal bone metastases. The sagittal (**c**) and coronal (**d**) reconstructions show multiple hyperattenuating bone lesions at the level of the vertebra, pelvis and femur (*arrowheads*)

Magnetic Resonance

In the staging of known cancer MR plays a leading role in the diagnostic imaging of carcinoma of the prostate.

MR has the advantage of being able to evaluate both the T and the N factors in staging. The versatility of the technique has considerably improved over the years thanks to surface phased array and endorectal coils.

Studies performed by McNeal demonstrate that the volume of carcinoma of the prostate is correlated with the aggressiveness of the tumor, which is expressed by extracapsular extension, invasion of the seminal vesicles and the incidence of lymph node metastases. In general, tumors with a volume less than 1 cm are confined within the prostate, whereas tumors greater than 3 cm frequently display extraprostatic spread. The disappointing results of TRUS in defining tumor volume derive from the isoechogenicity of more-or-less extensive portions of the tumor, which therefore cannot be fully evaluated. In contrast, the use of endorectal coils allows MR to obtain highly accurate volume measurements of carcinoma of the prostate, especially when located in positions of crucial importance for surgical treatment, such as the apex (**Fig. 11.26**).

Technological development has enabled a diagnostic accuracy of 75–90% for extracapsular extension to be achieved (results vary due to the equipment used and the experience of the radiologist interpreting the data). The prostatic capsule is visualized in T2-weighted images as a thin hypointense line between the hyperintensity of the peripheral zone and the periprostatic fat (often a chemical shift artifact contributes to forming the image of the capsule). The diagnosis of intracapsular carcinoma (stage T2) is simple when a thin layer of hyperintense tissue corresponding to normal peripheral tissue is maintained between the tumor and the capsule containing it. When instead the hypointense tumor comes into contact with the similarly hypointense capsule, reaching a diagnosis of capsular infiltration is difficult (**Fig. 11.27**).

Various signs have been proposed for the diagnosis of extracapsular extension

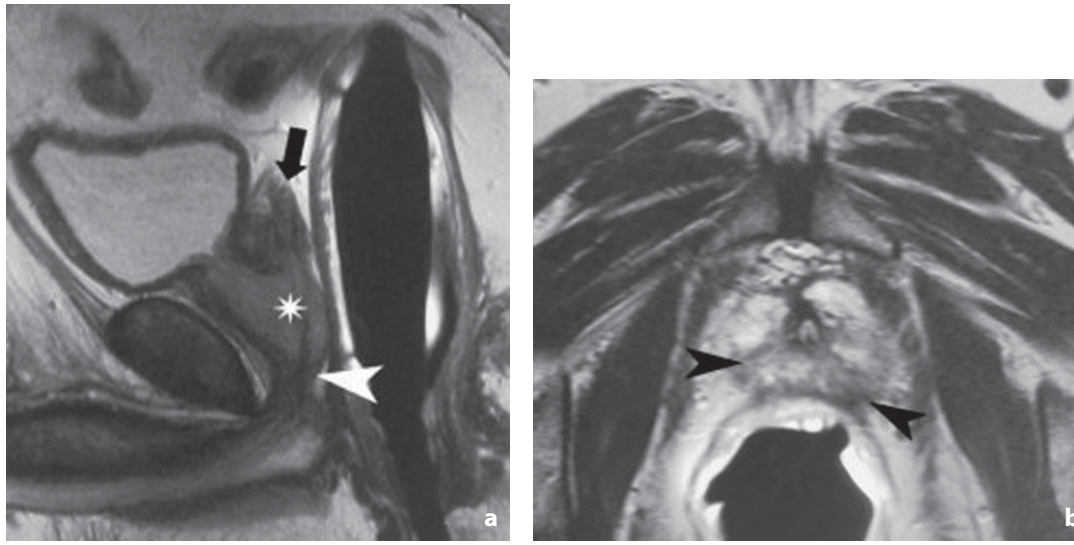

Fig. 11.26a,b. Magnetic resonance. Sagittal (**a**) and axial (**b**) T2-weighted images. Adenocarcinoma of the prostatic apex. The images show extensive tumor (*asterisk*) infiltrating the gland from the base to the apex (*arrowhead*) involving the seminal vesicles (*arrow*)

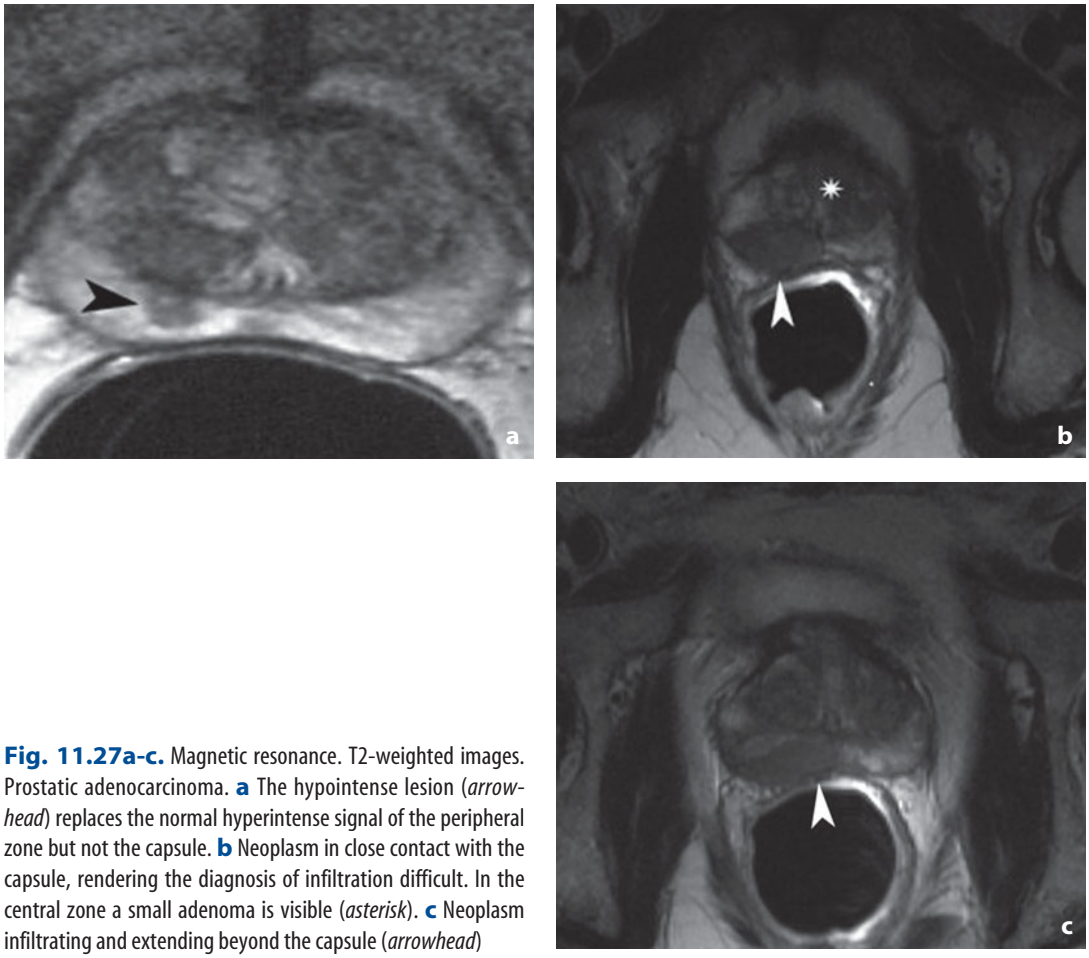

Fig. 11.27a-c. Magnetic resonance. T2-weighted images. Prostatic adenocarcinoma. **a** The hypointense lesion (*arrowhead*) replaces the normal hyperintense signal of the peripheral zone but not the capsule. **b** Neoplasm in close contact with the capsule, rendering the diagnosis of infiltration difficult. In the central zone a small adenoma is visible (*asterisk*). **c** Neoplasm infiltrating and extending beyond the capsule (*arrowhead*)

(stage T3a): contact with the capsule >12 mm; protrusion with rounded margins of the glandular borders; deformation or interruption of the capsular profile; tissue layering in the periprostatic fat; obliteration of the rectoprostatic angle and asymmetry of the neurovascular bundle (**Fig. 11.28**). The sensitivity of the technique is not particularly high (around 50-60%), although specificity is higher (82-95%). High specificity is particularly important in MR imaging to avoid excluding patients on the basis of false positives from potentially curative surgical procedures. Microscopic extension is virtually impossible to evaluate with diagnostic imaging techniques, which is the most important factor reducing the accuracy of the technique.

When there is no extension to the neurovascular bundle, nerve sparing extracapsular prostatectomy can be performed to conserve erectile function. The neurovascular bundle appears in T1-weighted images as a minute hypointense layer in the periprostatic fat at the posterolateral angles of the gland. However, it is not visible in its entire course, particularly at the prostatic apex. Therefore, invasion is certain when the neurovascular bundle is absent in its usually identifiable portion. In contrast, invasion cannot be excluded in the tracts where the neurovascular bundle is not normally visualized (**Fig. 11.29**).

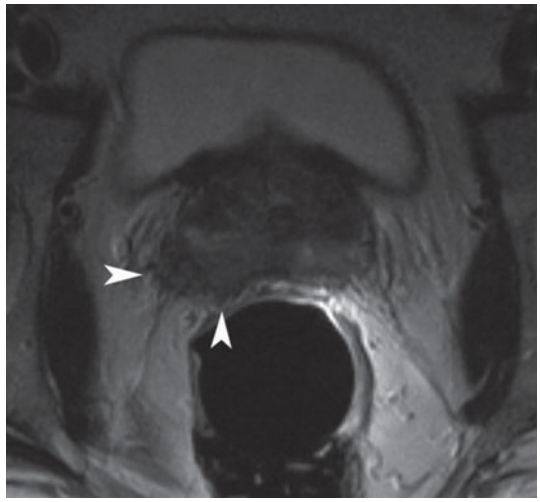

Fig. 11.28. Magnetic resonance. Axial T2-weighted image. Prostatic adenocarcinoma, stage T3a with invasion of the perirectal fat. On the right the lesion interrupts the hypointense signal of the prostatic capsule and extends into the perirectal fat with irregular margins (*arrowheads*)

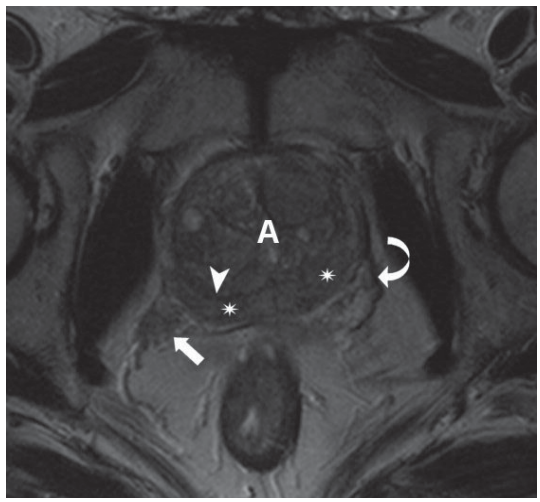

Fig. 11.29. Magnetic resonance. Prostatic adenocarcinoma, stage T3a with invasion of the neurovascular bundle. The normal hyperintense signal of the peripheral zone is completely replaced by the hypointense signal of the carcinoma (*asterisks*), which can be seen with irregular margins invading the right neurovascular bundle (*arrow*). An adenoma (*A*) is visible in the central zone with a recognizable surgical pseudocapsule (*arrowhead*). Note also the normal left neurovascular bundle (*curved arrow*)

With respect to US, MR is better at identifying invasion of the seminal vesicles (stage T3b), with sensitivity of around 80% and specificity around 93%. In T2-weighted images the seminal vesicles normally display a clearly hyperintense signal. Initial involvement can be appreciated as hypointense wall thickening in some tracts of the vesicle. Evident invasion instead is visualized by a hypointense signal within the seminal vesicle (**Fig. 11.30**).

With regard to the N parameter, noncontrast-enhanced MR has limited sensitivity and specificity, being unable to differentiate between an enlarged lymph node caused

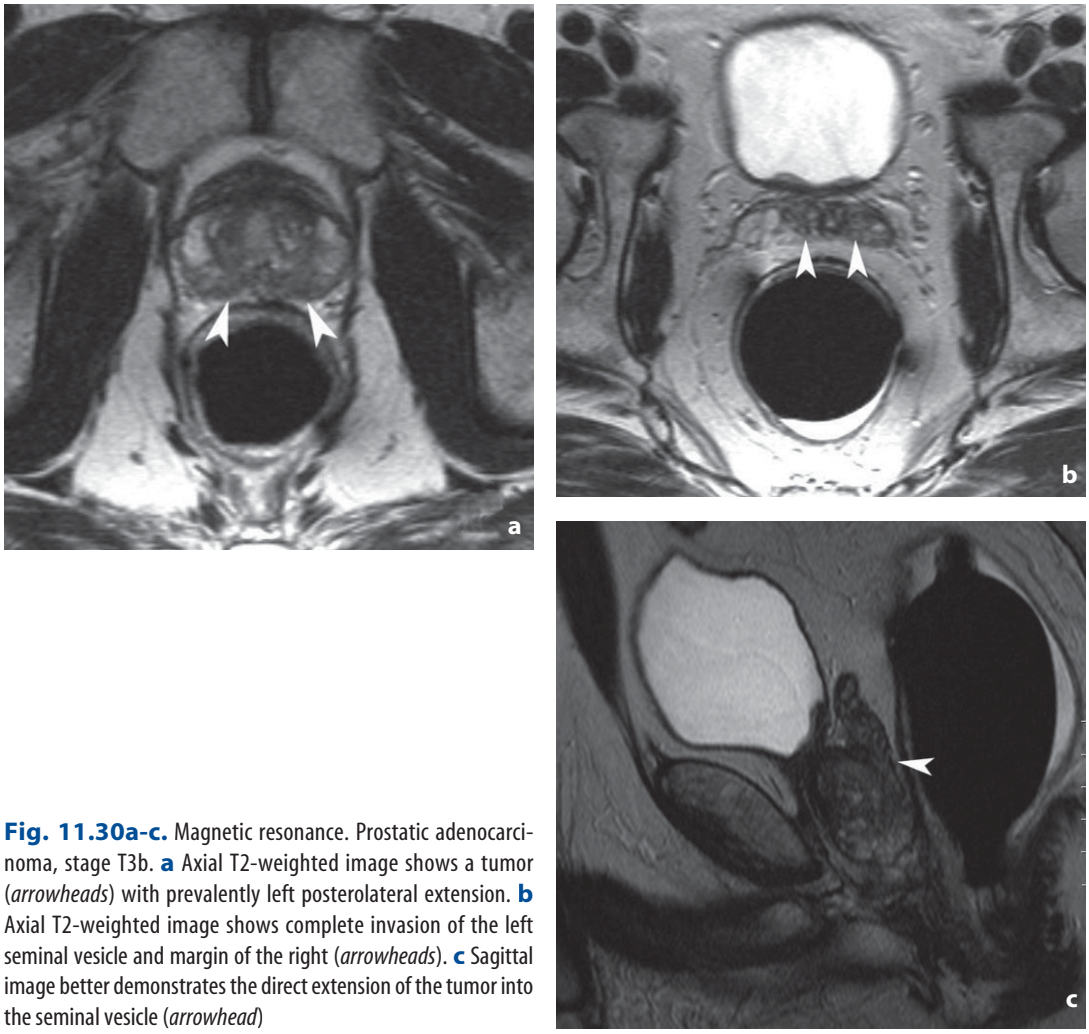

Fig. 11.30a-c. Magnetic resonance. Prostatic adenocarcinoma, stage T3b. **a** Axial T2-weighted image shows a tumor (*arrowheads*) with prevalently left posterolateral extension. **b** Axial T2-weighted image shows complete invasion of the left seminal vesicle and margin of the right (*arrowheads*). **c** Sagittal image better demonstrates the direct extension of the tumor into the seminal vesicle (*arrowhead*)

by a reactive process and a normal-sized lymph node with micrometastases (**Fig. 11.31**). The technique is improved with the use of contrast media with reticuloendothelial uptake, which is engulfed by the macrophages present in normal or inflamed lymph nodes lower the signal of the nodes. This of course does not occur in metastatic lymph nodes since the macrophages have been replaced by neoplastic tissue which fails to take up the contrast medium. It has been shown that MR lymphangiography increases sensitivity from 0 to 41% and from 29 to 96% in the identification of lymph nodes <5 mm and between 5 and 10 mm, respectively (**Figs. 11.32, 11.33**).

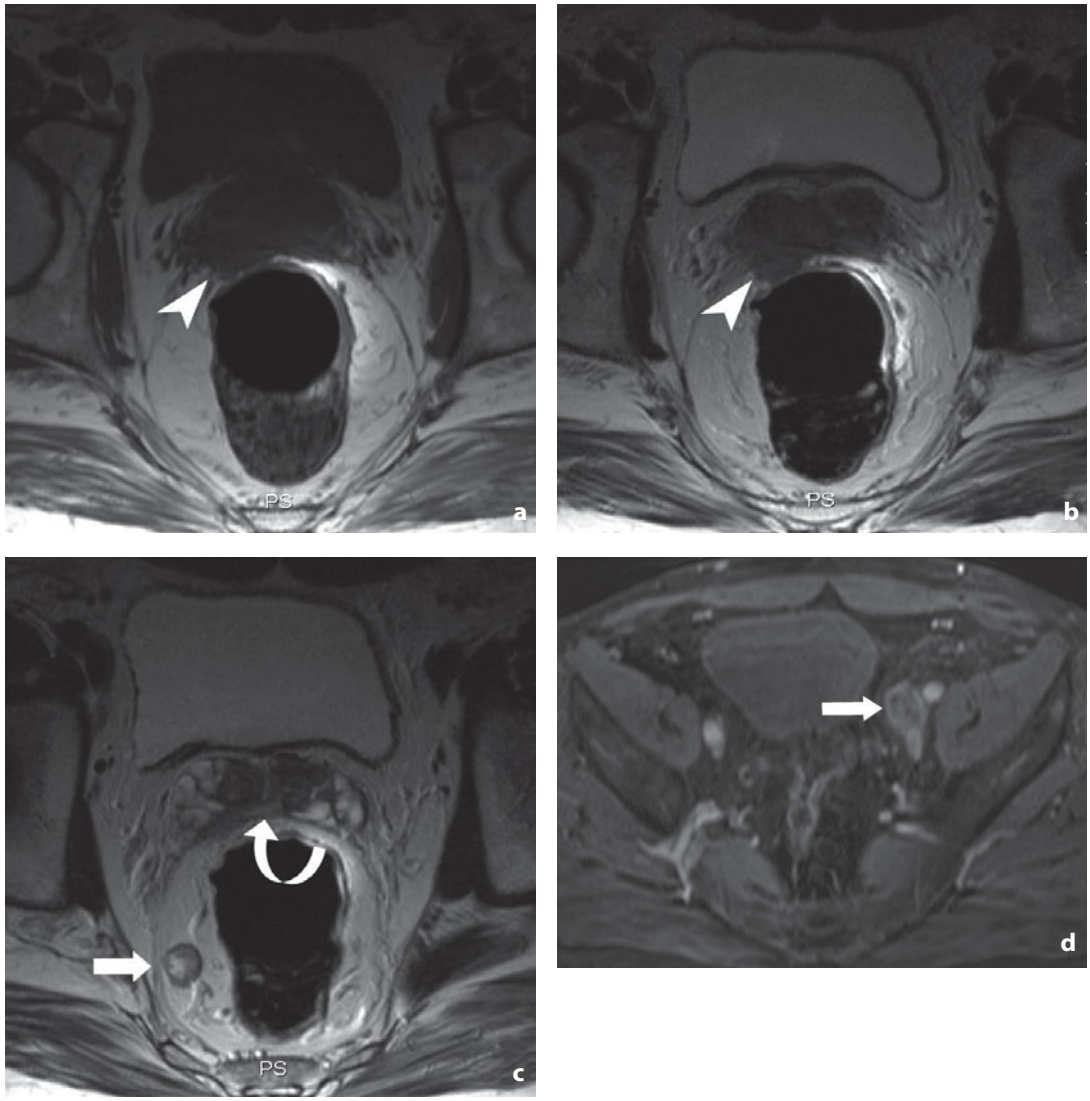

Fig. 11.31a-d. Magnetic resonance. Lymph node metastasis in T3b carcinoma of the prostate. Axial T1- (**a**) and T2-weighted images (**b,c**) show the tumor invading the perirectal fat (*arrowheads*) and the seminal vesicles (*curved arrow*) with lymph node metastasis (*arrow*) in the right ischiorectal fossa. **d** Another necrotic metastatic lymph node (*arrow*) can be visualized in the left external iliac chain

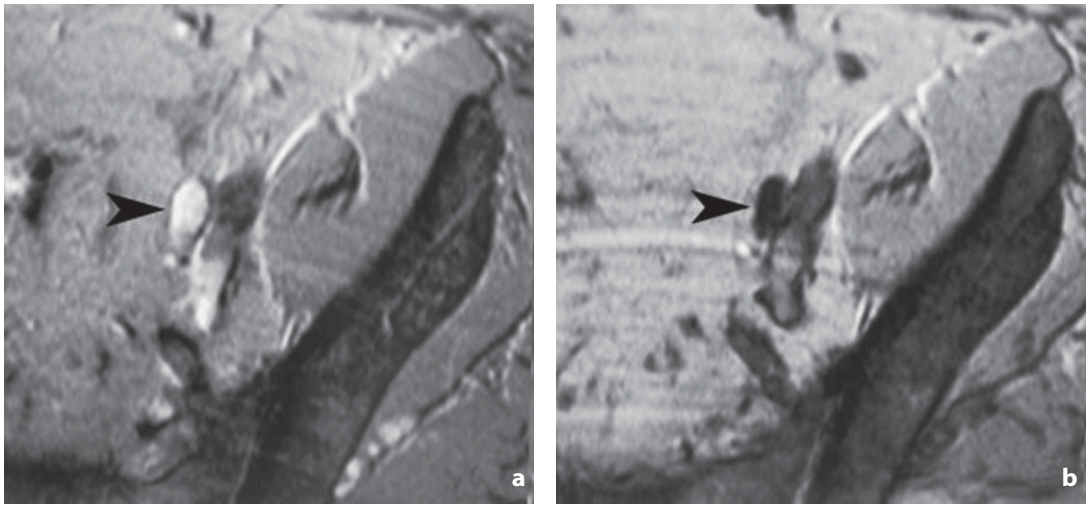

Fig. 11.32a,b. Magnetic resonance lymphangiography. Study with reticuloendothelial uptake contrast medium (USPIO). True negative lymph node verified at biopsy following lymphadenectomy. **a** Nonenhanced image shows an enlarged lymph node in the left obturator chain (*arrowhead*) which, after contrast medium administration, (**b**) shows marked signal loss. On the basis of the signal pattern the lymph node is classified reactive

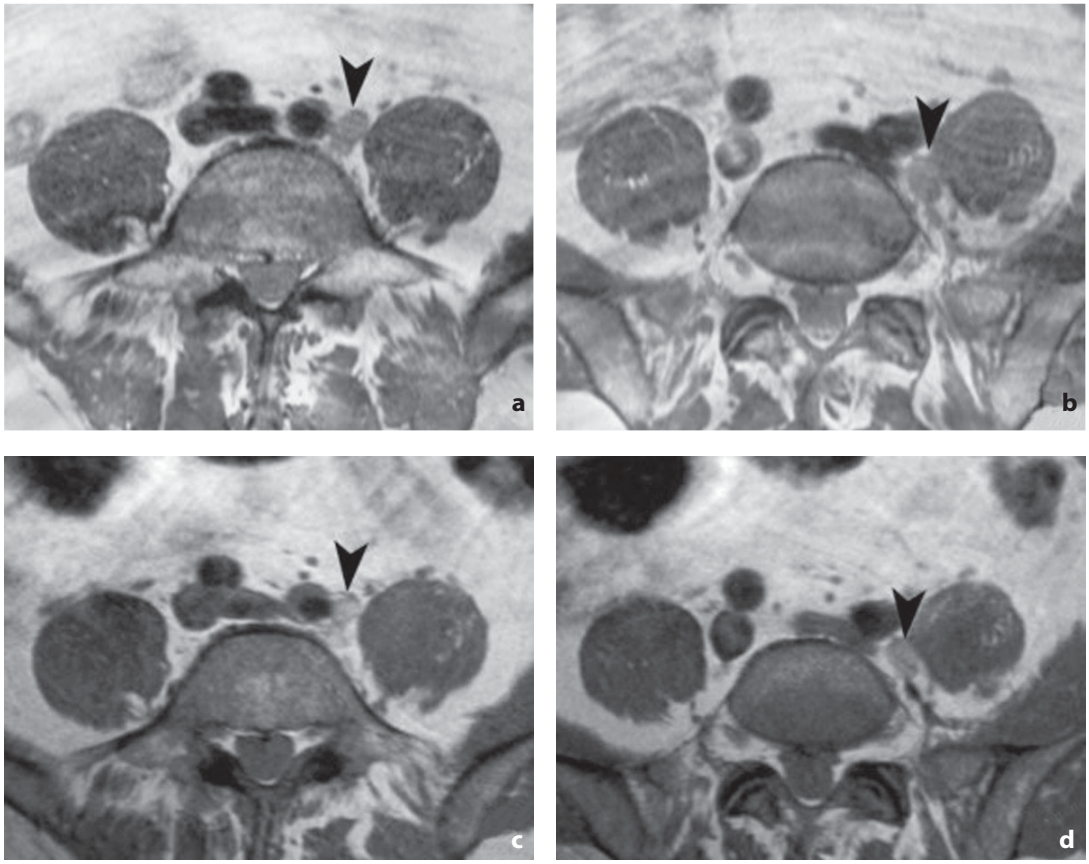

Fig. 11.33a-d. Magnetic resonance lymphangiography. Study with reticuloendothelial uptake contrast medium (USPIO). True positive lymph node verified at biopsy following lymphadenectomy. **a,b** Nonenhanced image shows two morphologically borderline lymph nodes in the left common iliac chain (*arrowheads*) which, after contrast medium administration, (**c,d**) show no significant signal loss. On the basis of the signal pattern the lymph nodes are classified metastatic

Bone Scintigraphy

This is the current reference standard for the evaluation of bone metastases (Fig. 11.34). A positive scintigraphy is highly uncommon with PSA levels below 20 ng/mL. The examination is therefore indicated in patients with PSA >20 ng/mL or with clinically staged disease ≥T3 or a primary Gleason ≥4 or a Gleason score ≥8 and PSA >10 ng/mL. Bone scintigraphy is also indicated in patients with bone pain or with elevated levels of alkaline phosphatase.

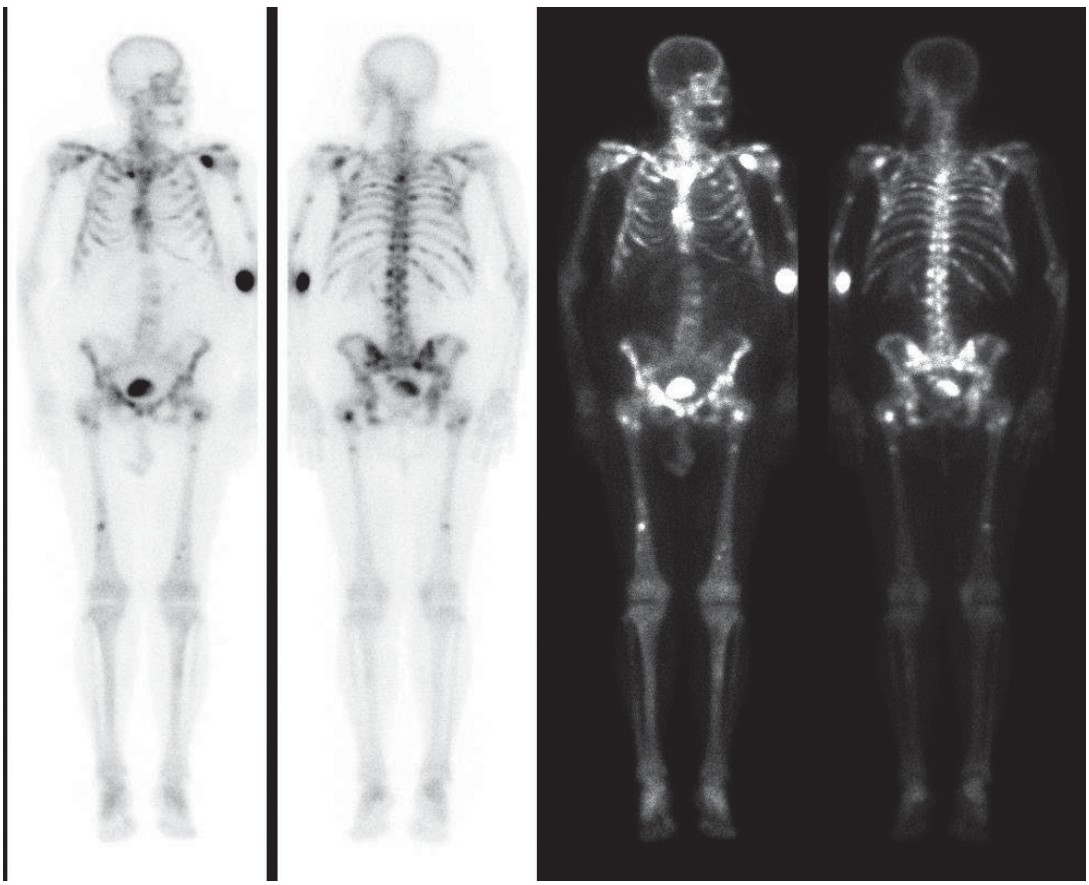

Fig. 11.34. Bone scintigraphy. Anteroposterior and posteroanterior views in different gray-scales. Bone metastasis in patient with advanced carcinoma of the prostate. Multiple bone metastases prevalently in the vertebral column and pelvis documented by increased radiotracer uptake

Positron Emission Tomography (PET) and CT-PET

This examination is particularly promising with the use of choline as a tracer and appears to improve the accuracy of the clinical staging of the lymph nodes. Its role in the diagnostic phase has not been completely defined as yet. It may therefore be proposed for the search for adenopathy in select patients, whereas its more widespread use for the moment is limited to controlled studies (Fig. 11.35).

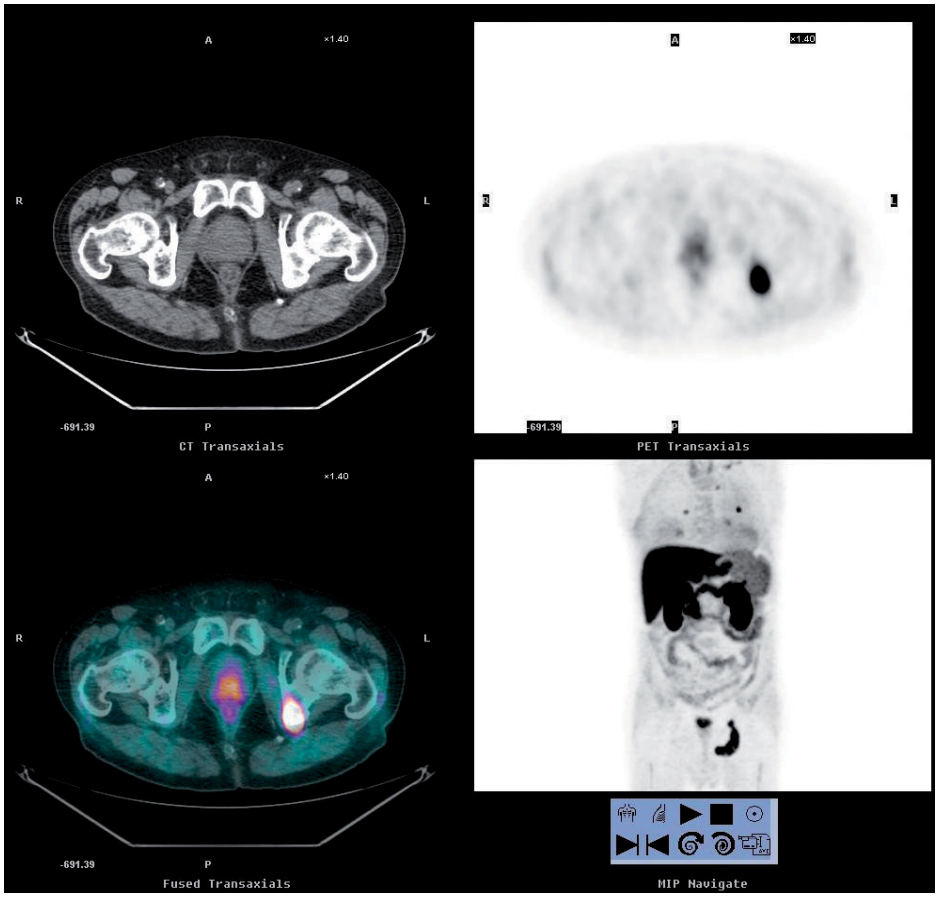

Fig. 11.35. CT-PET with choline. In addition to pathologic hyperaccumulation in the prostate (due to tumor), tracer uptake (metastasis) can also be visualized in the left ischiopubic ramus and in both lungs

Laparoscopic Lymphadenectomy

Surgical staging of pelvic lymph nodes is currently not indicated if not in the setting of radical surgery (prostatectomy). The exclusive use of this technique for lymph node staging is currently inadvisable.

Claus FG, Hricak H, Hattery RR (2004) Pretreatment evaluation of prostate cancer: role of MR imaging and 1H MR spectroscopy. Radiographics 24:S167-180

Fuchsjäger M, Shukla-Dave A, Akin O et al (2008) Prostate cancer imaging. Acta Radiol 49:107-120

Hricak H, Choyke PL, Eberhardt SC (2007) Imaging prostate cancer: a multidisciplinary perspective. Radiology 243:28-53

Presti JC Jr (2000) Prostate cancer: assessment of risk using digital rectal examination, tumor grade, prostate-specific antigen, and systematic biopsy. Radiol Clin North Am 38:49-58

Yu KK, Hricak H (2000) Imaging prostate cancer. Radiol Clin North Am 38:59-85

Clinical Approach to Testicular Disease

12

S. Cosciani Cunico, T. Zanotelli, M. Scanzi

Inflammation

The infectious forms of epididymitis and orchiepididymitis are among the most frequent causes of acute scrotal pain, which is in differential diagnosis with spermatic cord torsion.

Epididymitis is an ascending infection from the urethra along the ductus deferens. Whereas in the fifth decade of life coliform bacterial infections predominate alongside the increasing incidence of prostatic hyperplasia, in younger males (below 35 years) epididymitis is more commonly caused by sexually transmitted diseases (*Chlamydia trachomatis* and *Neisseria gonorrhoeae*). Specific or fungus etiology is more common in immunocompromised subjects. Infection by lymphatic spread is very rare. Infection may be secondary to endourethral instrumentation or fostered by the presence of an indwelling bladder catheter.

Acute inflammation of the testicle (orchitis) generally manifests as orchiepididymitis – the infection in fact involves the testicle arriving from the epididymis. Orchitis without epididymitis is rare and secondary to a systemic infection which reaches the testicle via hematogenous or lymphatic spread. In adolescents and young men orchitis is associated with a viral mumps infection and is bilateral in 10% of cases.

The diagnosis of epididymitis, which is most commonly unilateral, is made clinically with a typical presentation: scrotal pain with scrotal skin thickening, fever and urinary frequency, urgency or dysuria secondary to urinary infection. Physical examination reveals an enlarged epididymis with induration, particularly at the level of the lower pole. In the event of orchiepididymitis there is also a marked testicular enlargement and induration, such that at palpation in the acute phase it is difficult to differentiate the epididymis as an anatomic entity separate from the testis. Pain is particularly sharp and radiates along the spermatic cord to the groin. Areas of diminished firmness may be identified as a sign of abscess formation, and reactive hydrocele may be present. Laboratory examinations reveal leukocyturia and leukocytosis.

Recurrent acute episodes can result in chronic forms characterized by epididymal enlargement and induration, with irregular margins and possibly extensive areas of fibrosis. In these cases pain tends to be moderate. This clinical presentation, particularly in young men, can be the manifestation of tuberculosis most commonly originating from the prostate. Such cases are rare, but should be considered in immunocompromised patients or subjects from at-risk geographical areas.

In younger patients and adolescents the differential diagnosis especially includes spermatic cord torsion. The onset of pain is generally more acute than with infection which in any case is rare below 16 years. Even at the physical examination torsion may mimic an infection, but in the typical presentation the testicle is raised towards the inguinal canal and the spermatic cord is not completely palpable.

Another cause of acute scrotum in adolescents can be the torsion of one of the small testicular or epididymal appendices. In this case the pain is more localized, even though spermatic cord torsion is often included in the differential diagnosis.

L. Olivetti, L. Grazioli (eds.), *Imaging of Urogenital Diseases*,

Acute scrotum is a condition of surgical urgency. In cases of doubtful torsion the patient should undergo surgical exploration in the shortest possible time after the onset of symptoms.

Altaffer LF III, Steele SM Jr (1980) Torsion of testicular appendages in men. J Urol 124:56-57

Cinman AC (1982) Genitourinary tuberculosis. Urology 20:353-358

Joly-Guillou ML, Lasry S (1999) Practical recommendations for the drug treatment of bacterial infections of the male genital tract including urethritis, epididymitis and prostatitis. Drugs 57:743-750

Naber KG, Bergman G, Bishop MC et al (2001) EAU guidelines for the management of urinary and male genital tract infections. Eur Urol 40:576-588

Witherington R, Jarrell TS (1990) Torsion of the spermatic cord in adults. J Urol 143:62-63

Testicular Cancer

Tumors of the testicle account for 1–2% of all malignant tumors in males and the large majority (90–95%) are made up of primary solid malignant lesions arising from germ cells. In terms of epidemiology the peak incidence in relation to age occurs between 20 and 35 years. Incidence may vary according to the histologic type: the peak for choriocarcinoma is 20–30 years, for teratoma and embryonal carcinoma 25–35 years, and for seminoma 35–40 years, whereas spermatocytic seminoma, lymphoma and other secondary tumors peak after 50 years. In addition to histologically monotype tumors, i.e. tumors with a single histotype, mixed forms are possible and are characterized by a variable composition of several histotypes in different percentages.

Although the etiology remains ill-defined, a number of risk factors have been identified. The most prominent among these is cryptorchidism. Some 7–10% of patients with testicular cancer have a history of not necessarily homolateral cryptorchidism. In these patients the risk is greater for the intra-abdominal testicle than it is for an inguinal cryptorchid testis, and orchidopexy does not reduce the risk of cancer.

The most common presentation of testicular cancer is a painless hard lump on the affected testis. Some 10% of patients present with acute pain secondary to hemorrhage or tumor infarction, while 30–40% report persistent dull pain in the scrotum, perineum or lower abdomen. Patients typically seek medical advice with a delay of 3–6 months from the onset of local symptoms. Around 10% present with symptoms of metastatic spread (cervical mass from metastasis to the supraclavicular lymph nodes; respiratory problems caused by pulmonary metastasis; dorsolumbar pain due to secondary localizations in the retroperitoneal lymph nodes which compress the nerve roots or from bone metastases; gastrointestinal problems arising from retroduodenal metastases).

Physical examination reveals either a completely hard testicle or a hard painless nodule in the testis. Reactive hydrocele may be present. Palpation of the abdomen, the neck and the inguinal region should be performed in the search for possible sites of metastasis. The chest should also be examined, in that gynecomastia is found in 5% of patients with germ cell tumors and in a higher percentage in subjects with tumors of the gonad interstitium (Leydig cell and Sertoli cell tumors).

Testicular germ cells produce protein markers which are relatively specific and easy to measure in the serum. Especially useful is alpha-fetoprotein (AFP) and beta-human chorionic gonadotropin (beta-HCG). These markers enable the diagnosis, staging and evaluation of therapeutic response. They are useful prognostic indicators and are used in follow-up. In addition, there is a correlation between marker and tumor histotype. In fact AFP can be elevated in patients with embryonal carcinoma (70% of cases), yolk sac tumor (75% of cases), and teratocarcinoma, whereas it is normal in pure

seminoma and choriocarcinoma. Beta-HCG is increased in 100% of patients with choriocarcinoma, 50–60% of patients with embryonal carcinoma, 25% of patients with yolk sac tumor and 5–10% of patients with pure seminoma. The half-life of the two markers (5–7 days for AFP and 24–36 h for beta-HCG) is of vital clinical importance, since elevated or rising levels post-treatment (whether surgical or nonsurgical) are indicative of persistent disease. Moreover, normal preoperative levels of the markers do not rule out the possibility of a testicular germ cell tumor.

Clinical staging of patients with testicular carcinoma is crucial both for diagnosis and for therapeutic planning and prognostic evaluation. The necessary clinical-instrumental findings include: serum tumor marker assay (AFP and beta-HCG), scrotal ultrasonography, abdominal and pelvic computed tomography, chest radiography or computed tomography. Although numerous classifications are currently in use, they are to a large extent modifications or extensions of the original staging system proposed by Boden and Gibb in 1951. This classification subdivides tumor extension into three stages: stage I, tumor limited to the testicle; stage II, tumor extends beyond the testicle but is contained within the regional lymph nodes; stage III, disease spread beyond the retroperitoneal lymph nodes (e.g. pulmonary, visceral, brain, bone).

Initial treatment of malignant tumors of the testicle, regardless of histology, is radical inguinal orchidectomy. Since these tumors are sensitive to radio- and chemotherapy, the percentage of recovery is very high, even in advanced cases of disease.

Batata MA, Chu FC, Hilaris BS (1982) Testicular cancer in cryptorchids. Cancer 49:1023-1030

Javadpour N (1983) Multiple biochemical tumour markers in seminoma. A double-blind study. Cancer 52:887-889

Johnson DE (1976) Epidemiology of testicular tumours. In: Johnson DE (ed) Testicular tumours, 2nd edn. Medical Examination Publishing Co, Flushing, NY, pp 37-46

Mostofi FK (1973) Testicular tumors: Epidemiologic, etiologic and pathologic features. Cancer 32:1186-1201

Schottenfeld D, Warshauer ME, Scherlock S et al (1980) The epidemiology of testicular cancer in young adults. Am J Epidemiol 112:232-246

Diagnostic Imaging of the Testicle

13

L.E. Derchi, E. Capaccio, A. Podestà

Radiologists play a fundamental role in the evaluation of patients with testicular disease. Imaging can in fact provide highly effective information which responds to clinical queries regarding the presence of lesions, their intra- or extratesticular location and whether they are bilateral. In some cases imaging is even able to identify the nature of the lesions. The most appropriate techniques are ultrasonography (US) and magnetic resonance (MR). Plain film radiology and computed tomography (CT) may be used in rare cases in the search for gas or calcifications in the scrotal tissue.

Study Technique and Radiologic Signs

Ultrasonography

US is the first choice technique in the study of the testicle and often it is conclusive. The study should be performed with high-frequency and high-definition transducers with the Doppler module. The testicle appears oval in shape with smooth borders and uniform echotexture composed of fine echoes with intermediate reflectivity. The hyperechoic mediastinum testis can be visualized at the periphery of the testicle, appearing elongated in longitudinal scans and triangular in shape in axial scans. Adjacent to it the mildly hypoechoic rete testis can sometimes be discerned with a striated appearance. The tunica albuginea surrounding the testis appears as a thin hyperechoic line around the organ (**Fig. 13.1**). The intraparenchymal arteries are always visible with the recurrent rami radiating towards the periphery. Flow signals have low resistance with the diastolic component well represented. The resistance index (RI)

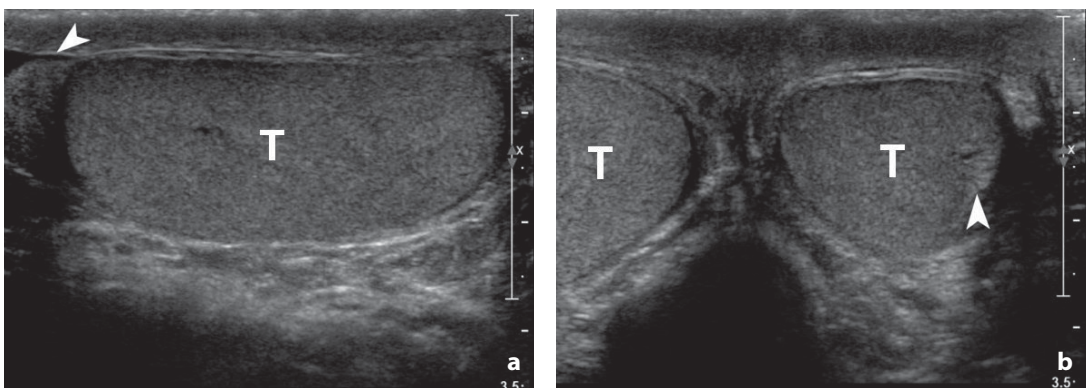

Fig. 13.1a,b. Normal anatomy. Ultrasonography of the normal testicle (*T*). **a** Sagittal scan. **b** Axial scan. The testicle shows uniform echotexture, with small echoes of mid-high intensity. **a** The head of the epididymis is visible cranially to the testicle (*arrowhead*). **b** The mediastinum testis can be visualized as a mildly hyperechoic image roughly triangular in shape at the periphery of the testis (*arrowhead*)

L. Olivetti, L. Grazioli (eds.), *Imaging of Urogenital Diseases*,

varies from 0.48 to 0.75, with a mean value of 0.62. An arterial vessel (transtesticular artery) can be identified passing through the testicle in 54% of cases, sometimes accompanied by a vein. The other intratesticular veins cannot be easily visualized (Fig. 13.2).

The epididymis appears as an elongated structure attached to the testicle with an echogenicity slightly lower than that of the latter. The different segments – head, body and tail – can be readily identified. The epididymal vessels can only be visualized with modern equipment. They appear as small vascular signals with greater arterial resistance than the intratesticular vessels (Fig. 13.3).

The finding of a small quantity of liquid within the tunica vaginalis is normal. The presence of liquid makes possible the visualization of one or more appendages of the testicle and/or the epididymis. These four structures are a few millimeters in size and correspond to remnants of the embryonic ducts. The appendix testis (hydatid of Morgagni) is located at the upper pole of the testicle, in the groove between the testis and the head of epididymis. The appendix epididymis is attached to the head of the epididymis.

The examination should be performed together with palpation of the scrotum. This allows the transducer to be directed towards palpable anomalies and the correlation of physical and US findings.

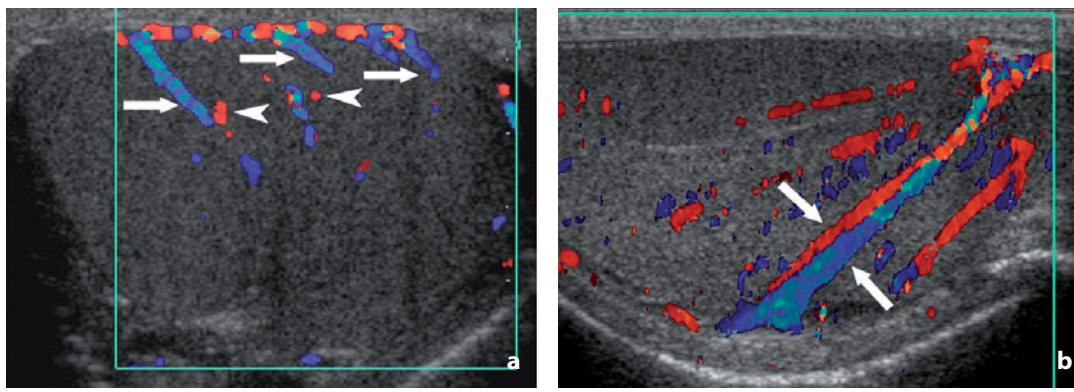

Fig. 13.2a,b. Normal anatomy. Normal intratesticular vessels. **a** Sonogram shows the vessels which from the periphery run within the testis (*blue vessels – arrows*). The *arrowheads* indicate the recurrent rami radiating towards the periphery. **b** A transtesticular artery and corresponding vein are well visualized (*arrows*)

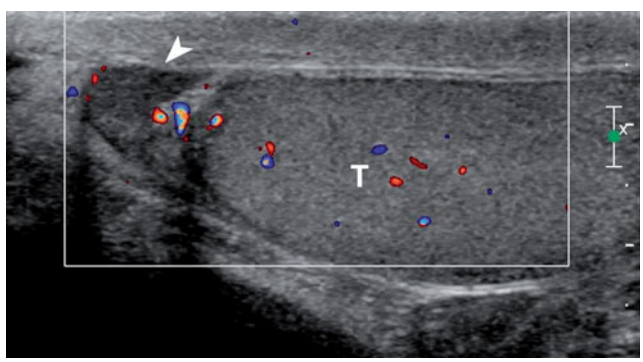

Fig. 13.3. Normal anatomy. Sagittal scan of a normal testicle (*T*). The head of the epididymis (*arrowhead*) can be seen at the upper pole. Color Doppler demonstrates the presence of vessels within both the testis and the epididymis

Magnetic Resonance

MR is used as a complementary examination to US. The technique is indicated in three clinical situations: disagreement between US and clinical findings; presence of inconclusive US findings; and suspected diffuse neoplastic testicular involvement.

The study is performed with surface coils using T1- and T2-weighted sequences, often followed by contrast-enhanced T1-weigthted sequences. The testicle appears as a uniform structure with intermediate signal intensity in T1 and elevated intensity in T2 (intensity greater than the subcutaneous adipose tissue). The tunica albuginea appears as a thin hypointense line surrounding the organ. The mediastinum testis can be identified in the axial images, where it appears triangular in shape with a hypointense signal with respect to the surrounding testicular parenchyma (**Fig. 13.4**). The epididymis can be identified by its shape. Its structural appearance is mildly hypointense with respect to the testicle in T1-weighted sequences and markedly hypointense with respect to the testicle in T2 (**Fig. 13.5**). When present the liquid in the vaginal cavity has high signal intensity in T2-weighted images, greater than the testicular parenchyma.

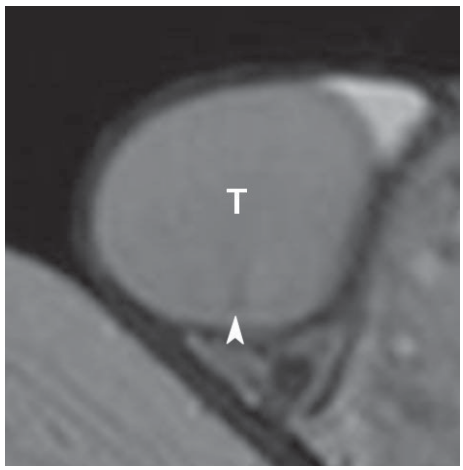

Fig. 13.4. Normal anatomy. Axial T2-weighted MR image of the normal testicle (*T*). The structure of the organ is homogeneous. The mediastinum testis (*arrowhead*) is hypointense in appearance

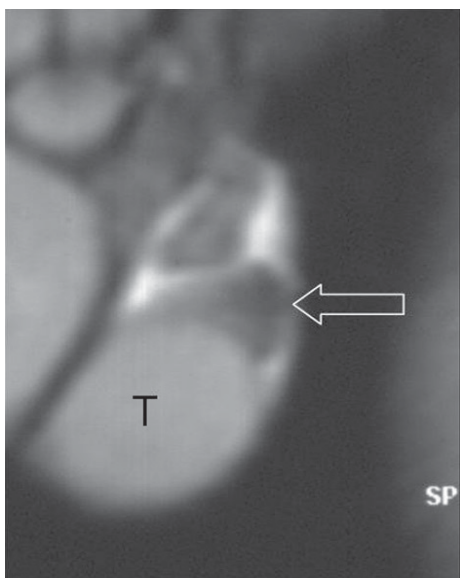

Fig. 13.5. Normal anatomy. Sagittal T2-weighted MR image of normal testicle and epididymis. The testicle (*T*) shows a homogeneous structure. The head of the epididymis (*arrow*) appears hypointense

Dogra VS, Gottlieb RH, Oka M et al (2003) Sonography of the scrotum. Radiology 227:18-36

Middleton WD, Bell MW (1993) Analysis of intratesticular arterial anatomy with emphasis on transmediastinal arteries. Radiology189:157-160

Muglia V, Tucci S Jr, Elias J Jr et al (2002) Magnetic resonance imaging of scrotal diseases: when it makes the difference. Urology 59:419-423

Oyen RH (2003) Scrotal ultrasound. Eur Radiol 12:19-34

Serra AD, Hricak H, Coakley FV et al (1988) Inconclusive clinical and ultrasound evaluation of the scrotum: impact of magnetic resonance imaging on patient management and cost. Urology 51:1018-1021

Pathologic Findings

Acute Scrotum

This term covers a number of conditions characterized by pain, swelling and/or reddening of the scrotum. The differential diagnosis between the different causes can be challenging on a purely clinical basis. Imaging therefore plays a crucial role. The most common causes vary on the basis of the age of the patient: torsion of the testicle or of one of the testicular appendages or the epididymis is prevalent in children, whereas acute infection is more common in adults.

Torsion of the Spermatic Cord

Differentiating spermatic cord torsion from acute inflammation is an important and urgent diagnostic dilemma. The former can in fact lead to infarction of the testicle within several hours. Therefore it requires immediate treatment.

The speed with which infarction can take place varies in relation to the degree of torsion. If this is 90°, hemorrhagic infarction develops slowly over several days resulting from an obstruction to the venous and lymphatic drainage of the testicle. In contrast, a torsion of 720° occludes arterial flow to the organ and causes infarction in a few hours. Between these two extremes there are of course intermediate degrees of torsion and times to the appearance of infarction. The US findings (size, shape, structure, vasculature) vary in relation to the degree of torsion and the time elapsed between the beginning of the clinical event and the examination.

It should be recalled that during the examination the contralateral asymptomatic testicle can be used for a comparison of both morphology and vasculature.

The testicle tends to progressively increase in volume and develop a diffusely irregular hypoechoic structure. The torsed spermatic cord can also be identified at the upper pole of the testis as a nonuniform formation with a corkscrew appearance. The findings develop in a relatively late phase and analysis of the vascularity seems to be the most sensitive instrument for performing the diagnosis. The absence of vascularity on color Doppler is a sign of torsion (only very rare cases of false positives associated with vasculitic processes have been described). This finding has a sensitivity of 86% (**Fig. 13.6**). In milder cases of torsion intraparenchymal arterial flow is reduced, but still present, with the possibility therefore of false negatives. In order to avoid this problem, a spectral flow analysis of the arterial signals should be performed. The examination is not easy to perform and may require a prolonged study. In conditions of an obstruction of venous flow an increase in intratesticular arterial resistance is created. By comparing the signals obtained bilaterally, a reduced diastolic compo-

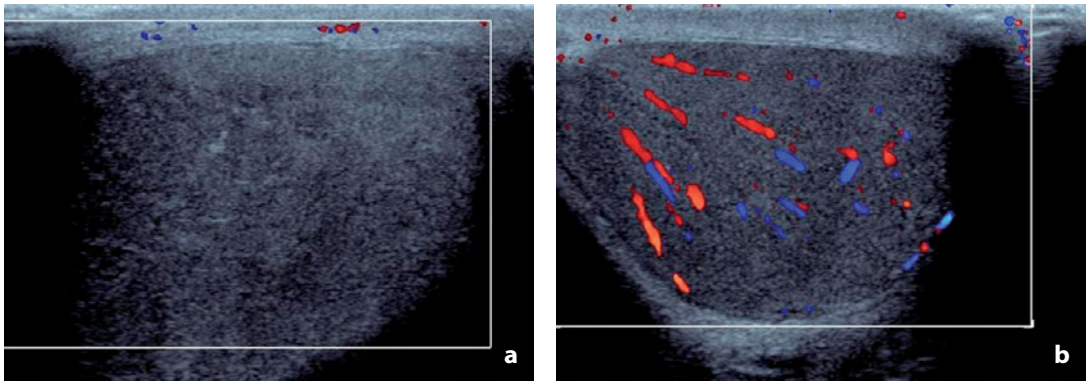

Fig. 13.6a,b. Right spermatic cord torsion. **a** The right testicle appears enlarged, mildly hypoechoic and diffusely heterogeneous, with no signs of internal vasculature. **b** The contralateral testicle is normal in appearance with easily identifiable internal vessels

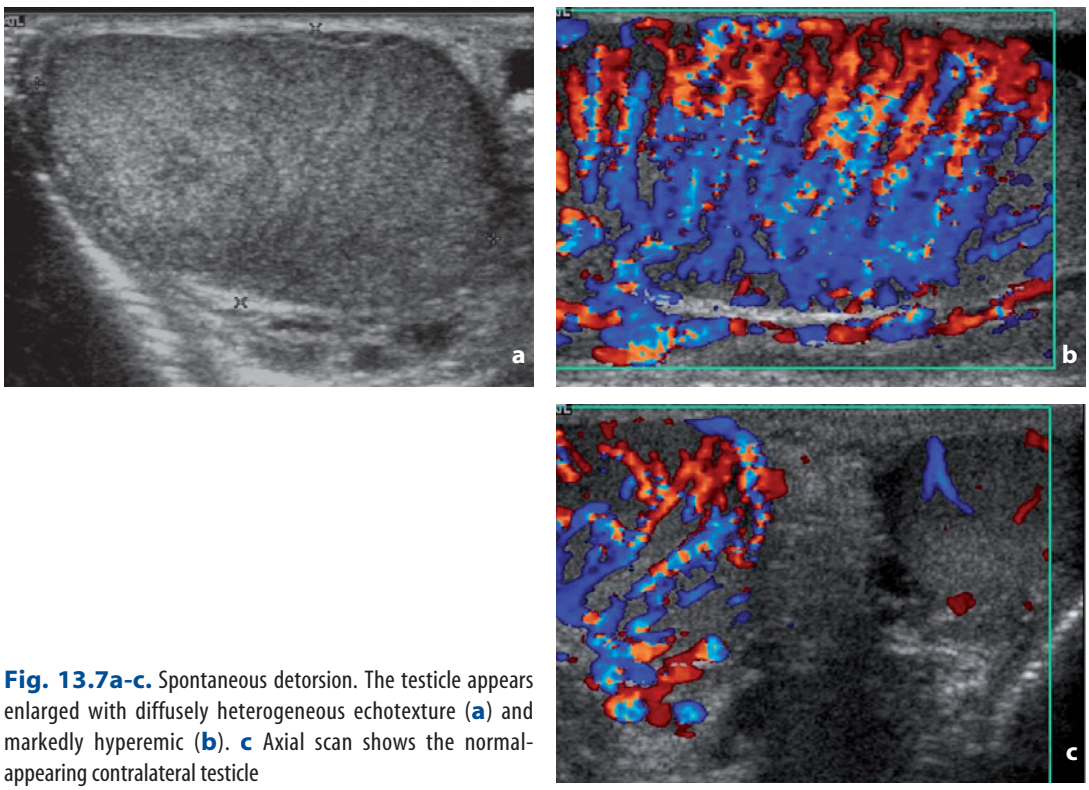

Fig. 13.7a-c. Spontaneous detorsion. The testicle appears enlarged with diffusely heterogeneous echotexture (**a**) and markedly hyperemic (**b**). **c** Axial scan shows the normal-appearing contralateral testicle

nent in the arterial signals of the torsed testicle can be demonstrated and therefore the condition can be identified. An RI greater than 0.75 is definitely pathologic. The normal RI varies between 0.48 and 0.75, with a mean value of 0.62. Comparative analysis is therefore crucial.

Spermatic cord torsion can resolve spontaneously. A US study performed immediately after detorsion may show a swollen, nonuniform and diffusely hyperemic testicle, a finding which can be confused with an inflammatory process. The case history is fundamental for the correct diagnosis (Fig. 13.7).

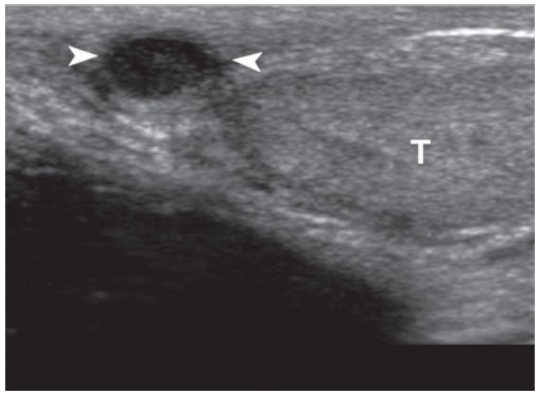

Fig. 13.8. Torsion of the appendix testis in pediatric patient. The testicle (*T*) shows normal volume and echotexture. Intraparenchymal flow on color Doppler is normal. In proximity to the head of the epididymis a hypoechoic nodule can be identified (*arrowheads*)

Torsion of the Appendix Testis and Appendix Epididymis

The appendices of the testicle and the epididymis can be subject to isolated torsion and not associated with testicular torsion. Several studies have shown that this is the most frequent torsion in pediatric patients. Differentiation is possible with US by demonstrating that both testicles have normal vascular appearance and that there is a round nodular formation >5 mm in proximity to the testicle with variable echogenicity (iso- or hypoechoic). The formation is nonvascular in appearance on color Doppler without the presence of internal flow (**Fig. 13.8**).

Acute Epididymitis and Orchitis

Inflammation of the male reproductive system is, in most cases, the result of an ascending infection originating at the level of the prostate or the urinary system. The infection progressively involves, in order, the ductus deferens, the spermatic cord, the head, body and tail of the epididymis and lastly the testicle. US can be performed at any time during this process, so findings vary accordingly. In funiculitis findings are aspecific and consist of a mild enlargement of the spermatic cord due to edema. In epididymitis there is frequently an enlargement of the portion involved, with hypervascularity at color Doppler. Thickening of the adjacent scrotal wall is often associated. The finding of hypervascularity is of paramount importance, in that it can precede enlargement of the epididymal region involved in the inflammatory process. In addition, given the relatively low vascularity shown on color Doppler in the normal epididymis, it is a clear finding. The inflamed epididymis generally appears hypoechoic and heterogeneous (**Fig. 13.9**). Hyperechoic areas within the inflamed epididymal parenchyma have been correlated with hemorrhage, whereas areas with a liquid and generally corpuscular appearance are indicative of abscess collections. The latter are often hypoechoic like the inflamed epididymal parenchyma (**Fig. 13.10**) and can be readily visualized on color Doppler due to the absence of an internal vascular signal. Some 20-40% of epididymal infections extend to the testicle. In these cases the testicle appears enlarged, hypoechoic and in general diffusely heterogeneous. Here, too, color Doppler is able to demonstrate hypervascularity of the region involved (**Fig. 13.11**). In particular, the intratesticular venous vessels can be easily identified, while spectral analysis reveals an elevated diastolic component in the arterial flow (low resistance).

It should be borne in mind that the hypoechoic and heterogeneous appearance of testicular and epididymal inflammatory lesions is not pathognomonic. Diffuse hypoechogenicity can also be the expression of lymphoma or leukemic invasion of the testicle. In subjects with known myeloproliferative disease the diagnosis of

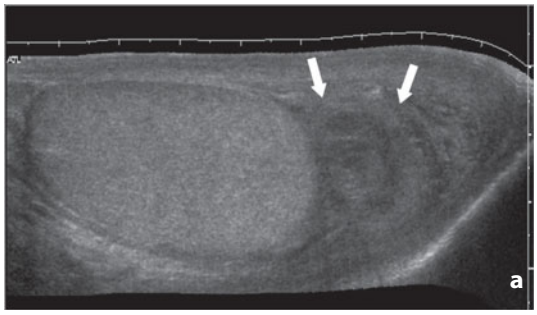

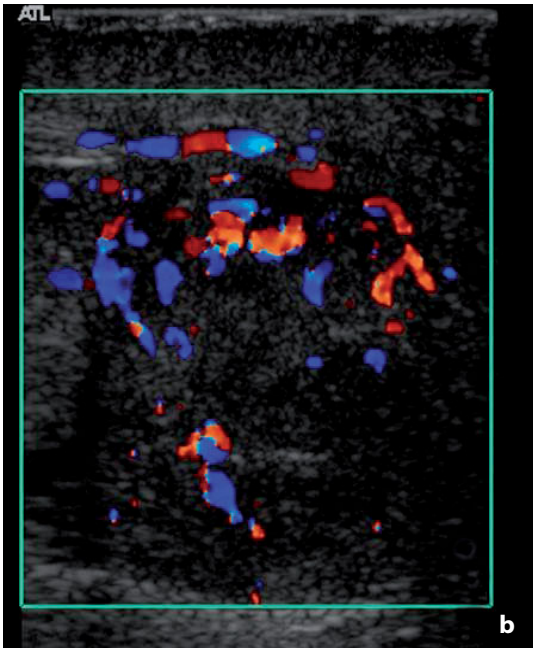

Fig. 13.9a,b. Acute epididymitis of the tail. **a** Sonogram shows an enlarged tail appearing hypoechoic and heterogeneous (*arrows*). Scrotal wall thickening can also be visualized. **b** Color Doppler demonstrates marked hypervascularity

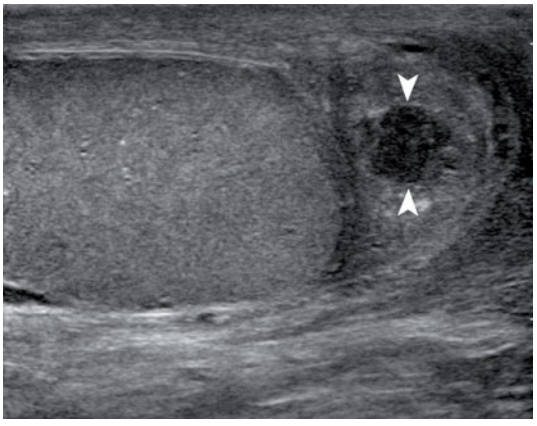

Fig. 13.10. Epididymal abscess. A liquid area is visible in the tail of epididymis (*arrowheads*) which shows no vascular supply on color Doppler

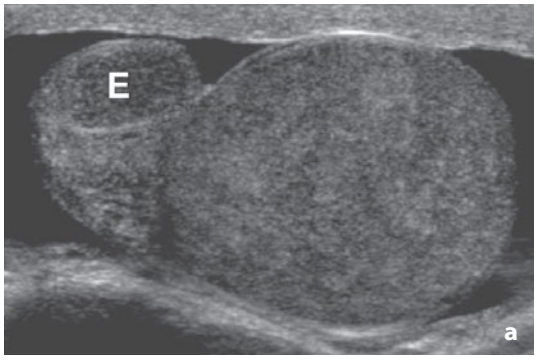

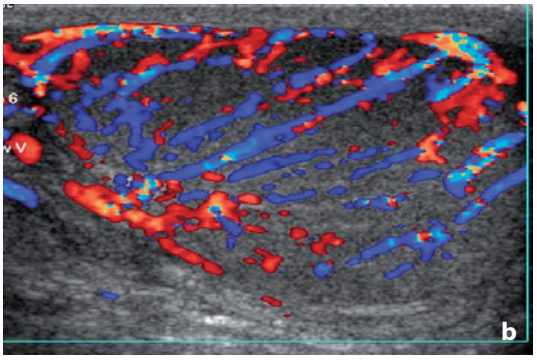

Fig. 13.11a,b. Orchiepididymitis. **a** Sonogram shows a mild enlargement of the head of epididymis (*E*) and the testis, which appears hypoechoic with heterogeneous echotexture. **b** The color Doppler study shows diffuse hypervascularity

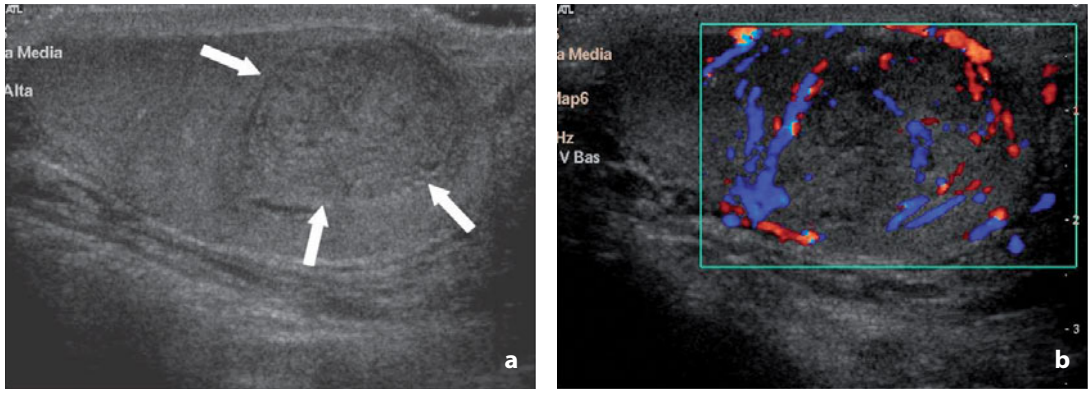

Fig. 13.12a,b. Focal orchitis. **a** In a clinical setting of inflammation a rounded intratesticular formation can be seen (*arrows*) with internal vasculature at color Doppler (**b**)

orchiepididymitis should be made only after ruling out a neoplastic process. In addition, testicular inflammatory alterations can occasionally have a focal appearance which can be difficult to recognize, being indistinguishable from a neoplasm (Fig. 13.12). At the level of the epididymis the inflammation can produce a nodular image which compresses the testicle and can mimics a testicular lesion. When presented with images of nodular appearance, even in the clinical setting of inflammation, the progression of the lesion during therapy should always be monitored to definitively rule out the diagnosis of a malignant lesion.

A number of complications are associated with orchiepididymitis. Parenchymal edema which develops during testicular inflammatory alterations causes an enlargement of the testicle. The tunica albuginea surrounding the testicle is not very extensible, such that in severe cases of edema the increase in intratesticular pressure can cause occlusion of the intraparenchymal venous vessels. The combination of these factors explains how severe orchitis can develop hemorrhagic infarction. High resistance arterial signals can suggest the development of this condition. Other complications include intratesticular abscesses, which appear as corpuscular liquid areas with a peripheral hypervascular halo: pyocele appears as echogenic fluid within the tunica vaginalis.

Chronic Epididymitis and Orchitis

Recurrent epididymal infections can give rise to chronic conditions, with persistent pain and enlargement of the portion involved, which is often hyperemic on color Doppler, but which displays less evident flow than in the acute phase of disease. Particular attention should be paid to differentiation between these lesions and space-occupying lesions of the testicle (Fig. 13.13). Correlation with patient history is crucial for establishing a correct diagnosis.

The epididymis and the testicle can be affected by granulomatous inflammatory diseases, such as tuberculosis, syphilis or parasitosis. Differential diagnosis with regard to aspecific lesions can be challenging. Patient history and the findings of physical examination and laboratory tests are also fundamental in these cases.

It should be recalled that granulomatous lesions also are mostly ascending lesions originating from the urinary tract. They therefore affect first the epididymis and then the testicle, where they may also manifest as nodular formations. Although they are similar in appearance to neoplastic lesions, the associated alterations to the

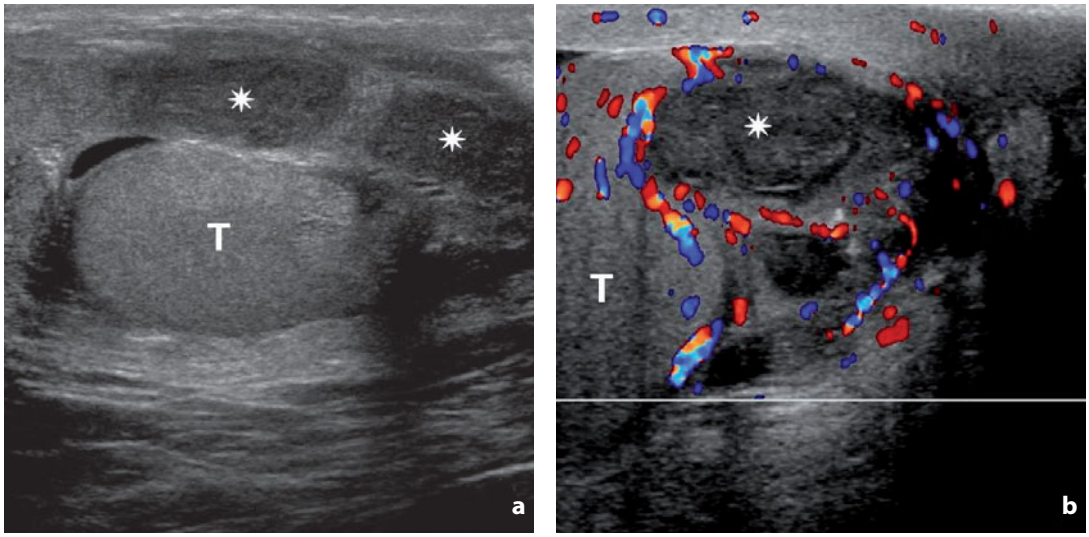

Fig. 13.13a,b. Chronic epididymitis. **a** Sonogram shows a completely enlarged epididymis (*asterisks*). **b** A nodular formation (*asterisk*) is visible in the tail, with peripheral hyperemia which compresses the testicle, mimicking a space-occupying lesion. *T*, testicle

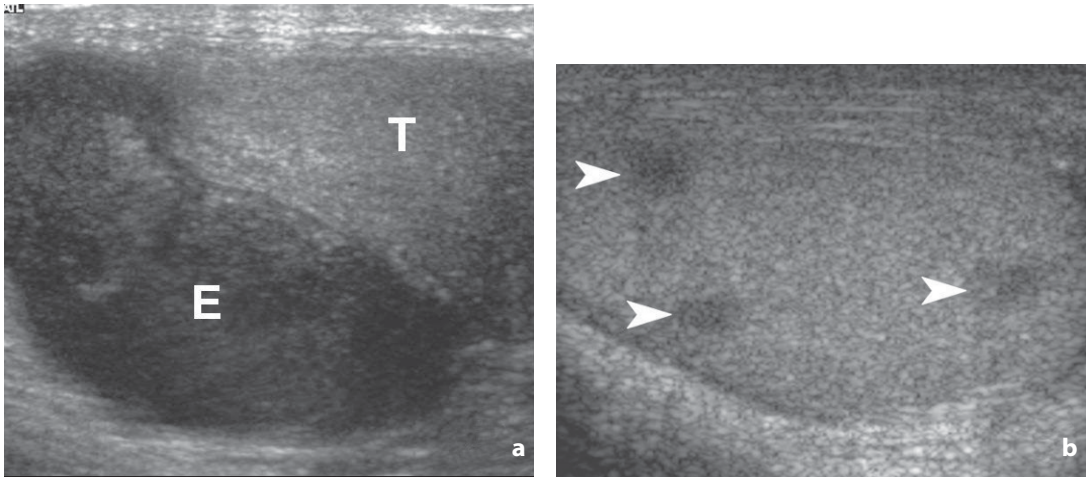

Fig. 13.14a,b. Tubercular epididymitis. **a** The epididymis (*E*) appears completely enlarged, with hypoechoic and uniform echotexture. **b** Tubercular orchitis manifesting with small hypoechoic intraparenchymal nodules (*arrowheads*) is indistinguishable from a multinodular neoplastic lesion. The inflammation was, however, associated with an enlarged epididymis and the patient had a clinical history of tubercular infection

epididymis and testicle are indicative of an inflammatory etiology, thus orienting the patient towards biopsy and not orchidectomy (Fig. 13.14).

Fournier Gangrene

Fournier gangrene is a form of necrotizing fasciitis of the tissues of the perianal region and the scrotal wall. It is a clinically serious condition correlated with high mortality. Risk factors include diabetes and immunodeficiency. The necrotizing process commonly arises from lesions of the anal canal or the perianal region and can extend

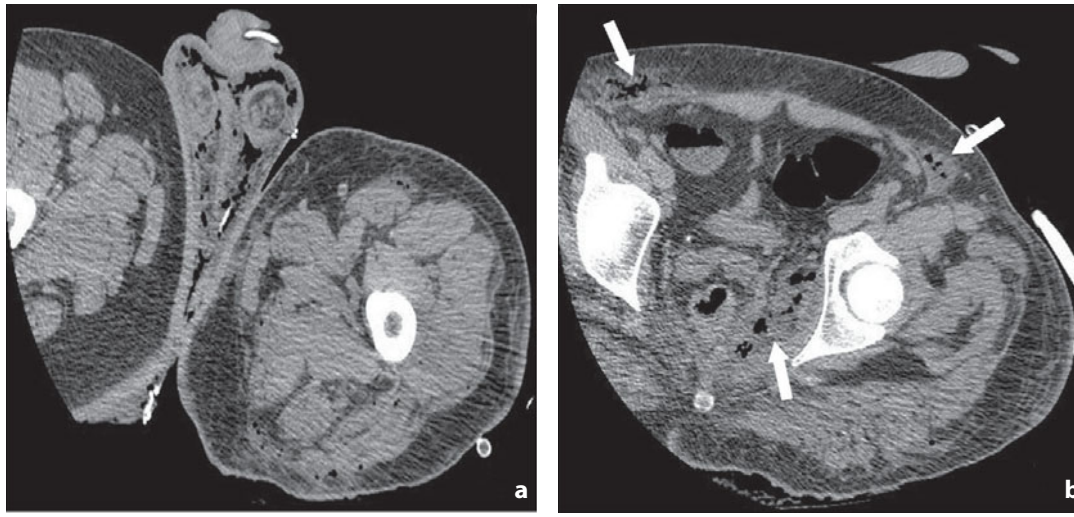

Fig. 13.15a,b. Fournier gangrene. CT scan of the pelvic and perineal region. **a** The presence of gas within the scrotum can be readily identified. **b** Image shows a collection of air bubbles in the region of the left obturator and the presence of gas in the inguinal region bilaterally (*arrows*)

to the pelvis with an uncontrollable clinical course. Fournier gangrene is characterized by the presence of air in the perineal tissue, which facilitates the diagnosis. Although US can identify edema of the perianal tissue and scrotum, CT is the best technique for defining the presence and real extent of the lesion (**Fig. 13.15**).

Chung JJ, Kim MJ, Lee T et al (1997) Sonographic findings in tuberculous epididymitis and epididymo-orchitis. J Clin Ultrasound 25:390–394

Cohen HL, Shapiro MA, Haller JO et al (1992) Torsion of the testicular appendages: sonographic diagnosis. J Ultrasound Med 11:81–83

Dogra V, Bhatt S (2004) Acute painful scrotum. Radiol Clin North Am 42:349–363

Dogra VS, Rubens DJ, Gottlieb RH et al (2004) Torsion and beyond: new twists in spectral Doppler evaluation of the scrotum. J Ultrasound Med 23:1077–1085

Dogra VS, Smeltzer JS, Poblette J (1994) Sonographic diagnosis of Fournier's gangrene. J Clin Ultrasound 22:571–572

Farriol VG, Comella XP, Agromayor EG et al (2000) Gray-scale and power Doppler sonographic appearances of acute inflammatory diseases of the scrotum. J Clin Ultrasound 28:67–72

Lin EP, Bhatt S, Rubens DJ et al (2007) Testicular torsion: twists and turns. Semin Ultrasound CT MR 28:317–328

Rajan DK, Scharer KA (1994) Radiology of Fournier's gangrene. AJR Am J Roentgenol 163:649–655

Stavros T, Rapp C, McGrath J (2000) Color duplex sonography of acute scrotal pain. In: Bluth EJ, Arger PH, Benson CB et al (eds) Ultrasound. A practical approach to clinical problems. Thieme, New York, pp 135–152

Strauss S, Faingold R, Manor H (1997) Torsion of the testicular appendages: sonographic appearance. J Ultrasound Med 16:189–192

Vijayaraghavan SB (2006) Sonographic diagnosis of acute scrotum: real time whirlpool sign, a key sign of torsion. J Ultrasound Med 25:563–570

Testicular Cancer

Risk Factors

Imaging plays an extremely important role in evaluating patients with risk factors for developing testicular cancer. A periodic US examination in these subjects is useful for demonstrating nonpalpable lesions in an early stage.

Patients having undergone orchidectomy for testicular cancer have a risk of developing a tumor in the contralateral testicle that is 20 times higher than in the general population. A family history (first degree relative) positive for testicular cancer increases the risk six times. Even patients with infertility problems have an increased risk of tumor. Testicular biopsy in infertile men shows a prevalence of "in situ" tumor in 0.4-1.0%, even in the absence of a history of cryptorchidism. Testicular cancer is a not infrequent incidental finding on US performed for infertility problems. Similarly, the risk of testicular cancer is higher in subjects with cryptorchidism, even in the contralateral testicle in cases of unilateral cryptorchidism.

There is another finding, identifiable only on US, which can be considered a risk factor: testicular microlithiasis. In the absence of alterations of the adjacent parenchyma, the condition is characterized by minute hyperechoic foci which at histologic analysis correspond to microliths of the seminiferous tubules composed of a calcified core with surrounding layers of glycoprotein (**Fig. 13.16**). The prevalence of microlithiasis is unknown. Most studies are retrospective, and report this diagnosis in 0.6-0.9% of cases. Two prospective studies (which evaluated symptomatic patients with scrotal problems) reported microlithiasis in 2% and 18.1% of patients. This entity has been subdivided into classic testicular microlithiasis (>5 microliths per testicle) and limited testicular microlithiasis (<5 microliths). The lesions can also be bilateral.

Microlithiasis is a relatively common finding in patients with testicular cancer. Middleton reports that testicular cancer was present in 3/40 (8%) patients with classic testicular microlithiasis and in 9/155 subjects (5.8%) with limited testicular microlithiasis. Only 3/884 patients (0.3%) without microlithiasis had tumor. Testicular microliths have also been observed in other conditions, such as cryptorchidism, infertility, Klinefelter syndrome and testicular atrophy, all being conditions where a testicular dysgenesis is present. Indeed, the condition of dysgenesis rather than microliths themselves puts the testicle at risk of cancer. Although it seems reasonable to offer

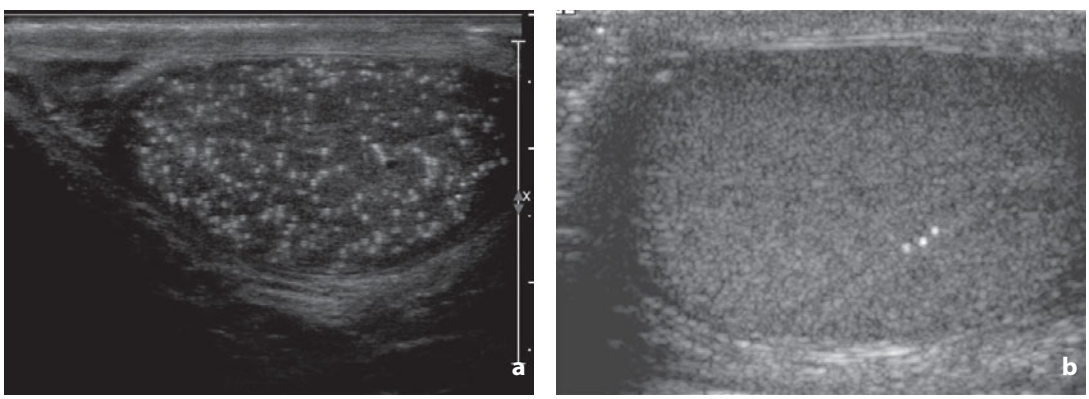

Fig. 13.16a,b. Testicular microlithiasis. Sonograms show the presence of small hyperechoic foci with no acoustic shadow and without associated structural anomalies of the surrounding parenchyma. In **a** the alteration appears diffuse, while in **b** the microlithiasis is located in the center of the testicle, with three small hyperechoic foci

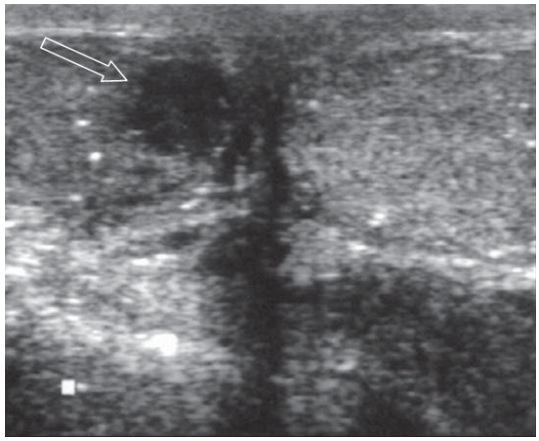

Fig. 13.17. Young patient with a history of right cryptorchidism. The right testicle appears smaller than the left and is characterized by the presence of a hypoechoic neoplastic nodule (*arrow*). Several microliths can also be identified bilaterally

these patients US monitoring, there is no consensus in the literature regarding the timing and effectiveness of such a strategy (Fig. 13.17).

Diagnostic Imaging

Ultrasonography has almost absolute sensitivity in the identification of focal testicular lesions and is therefore considered the technique of choice in such cases of clinical suspicion. With a sensitivity of 98%, US can identify the intra- or extratesticular site of palpable masses, and has an elevated ability to discriminate the cystic or solid nature of lesions.

In most cases extratesticular lesions and cysts are benign. In addition, the diagnosis of cysts can only be made in the presence of completely anechoic lesions without septation. Testicular tumors can in fact present liquid or hemorrhagic and necrotic areas. The literature describes a case of a purely cystic formation which at follow-up showed the growth of a wall nodule, thus revealing the real neoplastic nature of the lesion.

On US, testicular tumors appear as space-occupying nodular lesions. In most cases they are hypoechoic, although hyperreflective and liquid areas may be present. In general, the heterogeneous echotexture correlated with areas of necrosis is more evident in larger lesions (Fig. 13.18).

On **color Doppler** lesions larger than 1.6 cm appear hypervascular (Fig. 13.19). The absence of vascular supply in larger formations may suggest the non neoplastic nature of the lesion.

Testicular tumors have an irregular vascular supply. This characteristic can be useful in the relatively uniform diffuse infiltration of the testicle, where only the altered vascularity can suggest the presence of a neoplasm.

On the basis of the US appearance the different types of lesions cannot be differentiated. Seminomas, especially when small, commonly have uniform hypoechoic echotexture, whereas other germ cell tumors are often heterogeneous, with internal liquid collections and irregular margins. These structural characteristics are linked to the presence of intralesional necrosis and/or hemorrhage, a common finding in all types of cancers (Fig. 13.20).

On **magnetic resonance** images the tumors appear as nodular formations with different signal intensity from the surrounding parenchyma, especially in T2-weighted sequences. Their structure is generally heterogeneous due to intratumoral necrosis or hemorrhage. MR can easily identify the tunica albuginea and therefore just as easily diagnose its neoplastic involvement. Although seminomas generally appear

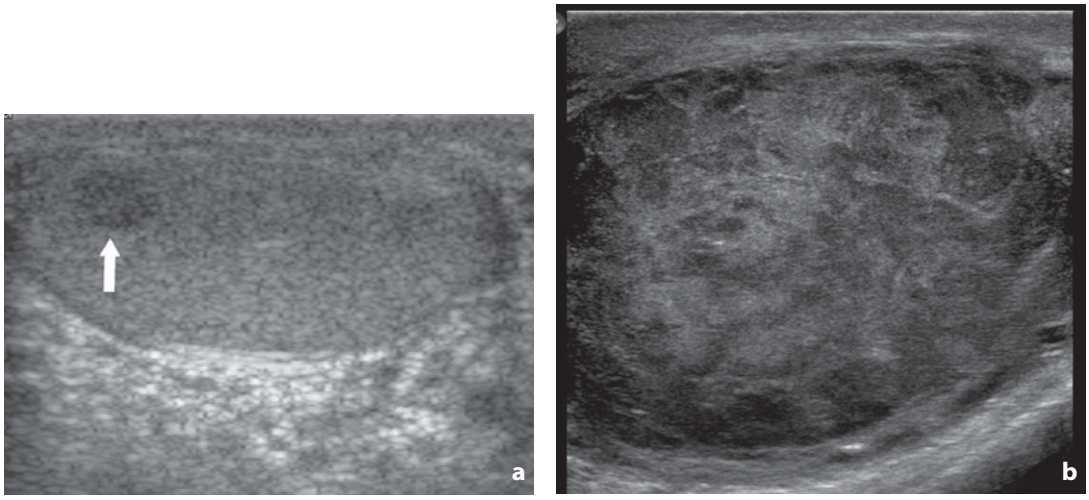

Fig. 13.18a,b. Seminoma. **a** Small hypoechoic lesion with homogeneous echotexture (*arrow*). **b** The tumor with solid appearance and diffusely heterogeneous involves the entire testicle

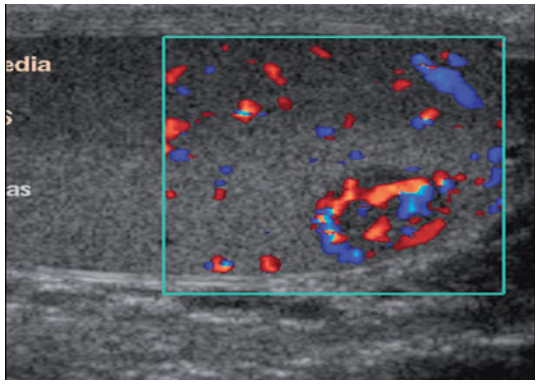

Fig. 13.19. Seminoma. Lesion of around 2 cm appears hypervascular on color Doppler

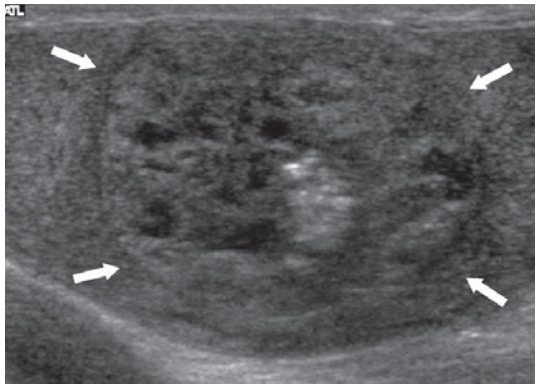

Fig. 13.20. Choriocarcinoma. Large heterogeneous lesion (*arrows*) with some liquid areas and central hyperechoic zone

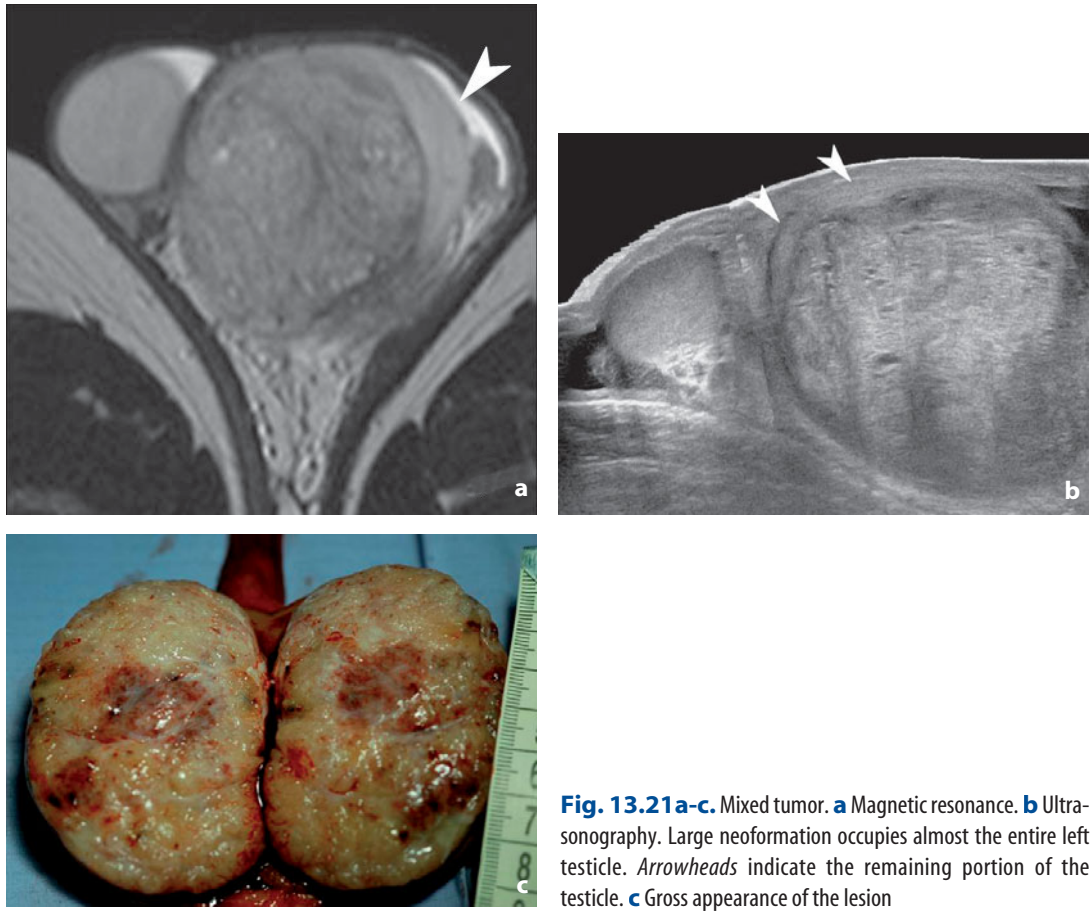

Fig. 13.21a-c. Mixed tumor. **a** Magnetic resonance. **b** Ultrasonography. Large neoformation occupies almost the entire left testicle. *Arrowheads* indicate the remaining portion of the testicle. **c** Gross appearance of the lesion

more homogeneous than nonseminomatous tumors, the type of lesion cannot be characterized with certainty (Fig. 13.21). This also holds for both US and MR with regard to stromal cell tumors, whose nature cannot be definitively identified with imaging modalities.

Recent developments in ultrasonographic contrast media do not seem to make a differential diagnosis possible between different testicular tumors. The use of contrast media in MR in some cases can help distinguish a simple cyst from a tumor with a prevalently cystic appearance, which may show areas of contrast enhancement. Similar applications for ultrasonographic contrast media have not been described.

Imaging is particularly useful in patients with nonpalpable testicular lesions. Between 2% and 4% of cases of testicular tumors are bilateral (synchronous or metachronous). US exploration of the contralateral testicle that is normal at palpation is therefore crucial for correct staging of the patient at diagnosis and, in postoperative patients, for identifying metachronous lesions at an early stage.

In patients with secondary lesions, which, due to their location (lungs, retroperitoneal and supraclavicular lymph nodes), suggest a primary testicular lesion, US (and MR) can identify a nonpalpable tumor and in some cases the presence of a small hyperechoic area with a scar-like appearance (thick with acoustic shadow). Although aspecific, the latter finding can be the expression of a small tumor residue or a regressed tumor (likely due to insufficient neovascularization to guarantee adequate blood supply) (Fig. 13.22).

In clinical practice a focal intratesticular lesion with solid appearance should, in the first instance, be considered malignant. In most cases the nature of the lesion should be ascertained with a histologic examination of the surgical specimen.

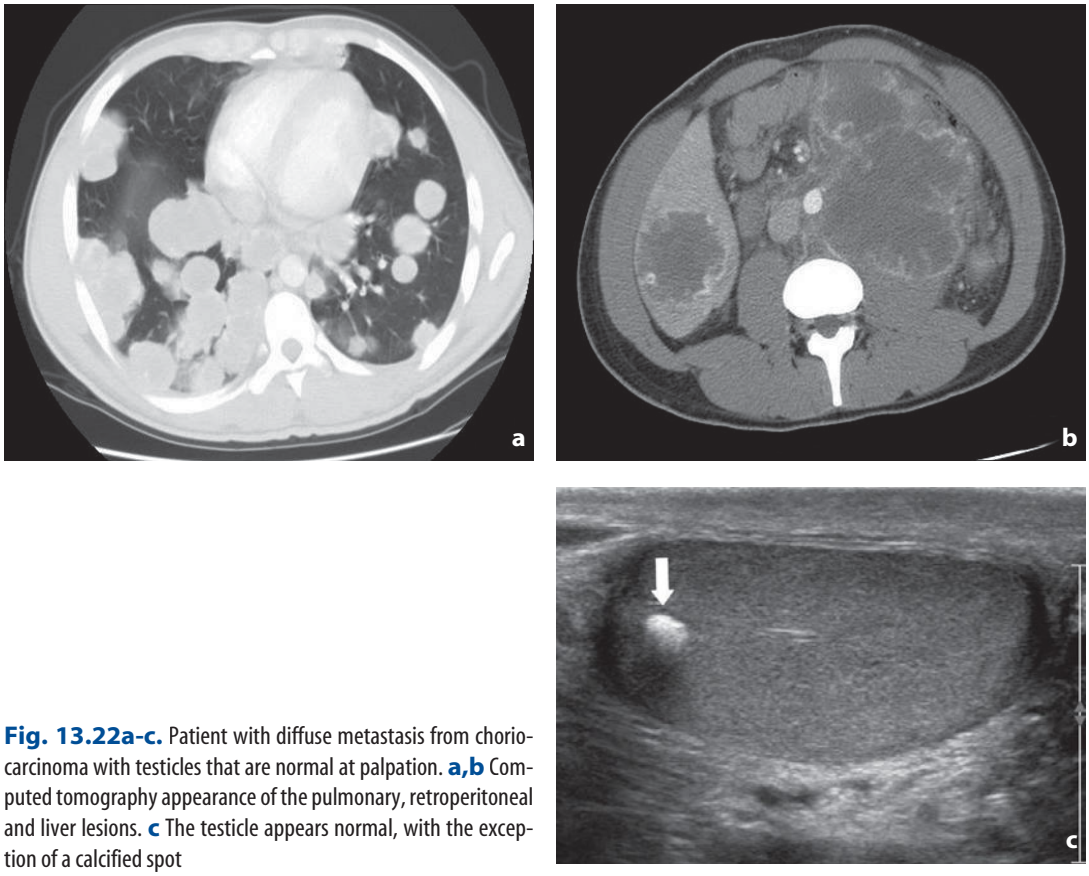

Fig. 13.22a-c. Patient with diffuse metastasis from choriocarcinoma with testicles that are normal at palpation. **a,b** Computed tomography appearance of the pulmonary, retroperitoneal and liver lesions. **c** The testicle appears normal, with the exception of a calcified spot

Benign Intratesticular Focal Lesions

Not all space-occupying lesions identifiable on US and/or MR are malignant tumors. There are benign inflammatory lesions and tumors which can mimic a malignant lesion. Careful analysis of the characteristics, in close correlation with the findings of the physical examination and the clinical history, can help in the differential diagnosis, validating the hypothesis of the benign nature of the lesion and therefore suggesting biopsy be performed before excision, or delaying the histologic examination in favor of comprehensive follow-up.

Testicular Cysts

These are relatively frequent. They can be subdivided in to cysts of the tunica albuginea, which are superficial and easily palpable, and parenchymal cysts, which are generally located in proximity to the mediastinum testis and are nonpalpable when small. The diagnosis is easily made with US and MR (Fig. 13.23). As stated above, for a lesion to be classified a simple cyst it must be completely anechoic without wall irregularities. Testicular tumors, and especially teratomas, can appear with large internal cystic areas. In doubtful cases, a contrast-enhanced MR examination can help in demonstrating enhancement of the solid component and correctly orienting the diagnosis.

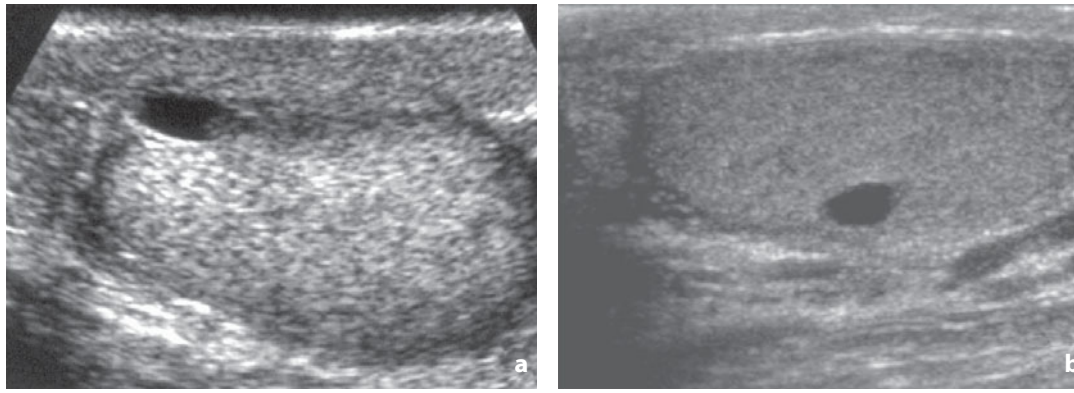

Fig. 13.23a,b. Testicular cysts. **a** A cyst of the tunica albuginea can be identified on the surface of the testicle. **b** A nonpalpable intraparenchymal cyst can be identified in proximity to the mediastinum testis

Cystic Ectasia of the Rete Testis

This is a relatively common and easily identifiable condition. It appears as a series of small liquid collections with tubular appearance, divided by thin and regular septations located at the level of the mediastinum testis (Fig. 13.24). It appears to arise from an obstruction to the spermatic pathway and is often associated with spermatocele. Its importance lies in the need for an accurate differential diagnosis with prevalently cystic tumors. The latter have liquid collections of varying size, with irregular shape and thick and irregular internal walls and septations. In doubtful cases short-term follow-up tends to be definitive.

Epidermoid Cysts

These are rare benign tumors which account for 1% of all testicular neoplasms. Possibly bilateral, they are true cysts filled with caseating material, distributed in concentric layers. On US they appear as round lesions with well-defined and occasionally calcified borders. Internally they are hypoechoic with a concentric layered appearance. There are no signs of vascular supply on color Doppler. On MR images epider-

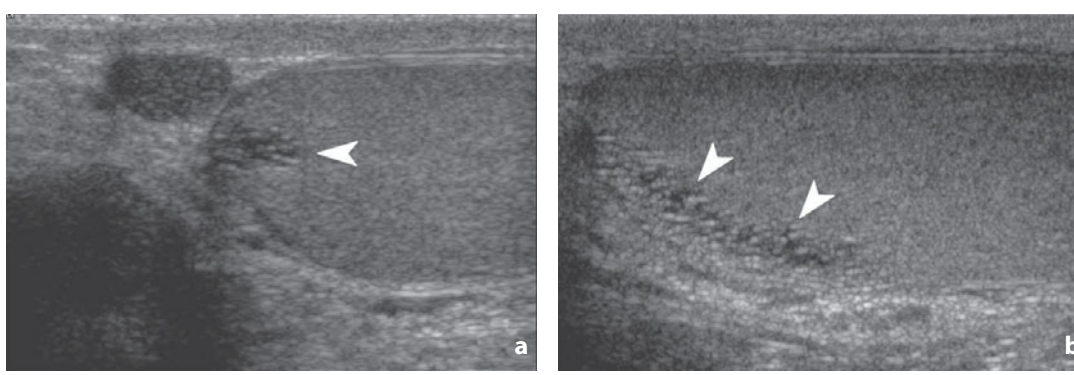

Fig. 13.24a,b. Cystic ectasia of the rete testis. Axial (**a**) and sagittal (**b**) sonograms. The alteration (*arrowheads*) situated at the mediastinum testis appears as a collection of small liquid formations with a tubular appearance and separated by thin septations

moid cysts appear as concentric circles with a hypointense periphery and a hyperintense central portion in both T1- and T2-weighted sequences. The imaging appearance of these lesions is often diagnostic and can therefore orient therapy towards enucleation rather than orchidectomy.

Focal Inflammatory Alterations

Inflammatory alterations to the testicle can take on a focal characteristic, with a hypoechoic, edematous or liquid (abscess-like) appearance. On the basis of structural appearance alone the inflammatory nature of the lesions cannot be recognized. On color Doppler imaging the inflamed zones are hypervascular in appearance. A definitive differential diagnosis with neoplastic lesions is therefore not possible. The inflammatory nature of the lesion can only be suggested on the basis of patient history, physical examination and at imaging by the frequent association with alterations of the epididymis. Around 15% of patients with malignant lesions show symptoms mimicking inflammation. The patient should therefore undergo comprehensive follow-up after therapy.

Focal Traumatic Lesions

Testicular trauma can produce a focal alteration to the testicle. In traumatized patients with the possibility of testicular rupture the therapy is surgical. The procedure involves exploration and suture of the testicle. Around 15% of patients with testicular tumor are diagnosed following a trauma. This can be the result of two causes: the presence of a tumor within the testis which renders it prone to rupture even in the event of a minor trauma; following the trauma, the particular attention paid to the testicle, which prompts self-palpation and/or seeking medical advice. Once again, in cases of a focal lesion in a testicular trauma which does not undergo surgical treatment, comprehensive follow-up is required.

Testicular Infarction

Testicular infarction can also present as a focal lesion. This condition seems to be particularly common in patients with diabetes, orchitis, endocarditis, leukemia, coagulopathies, vasculitis or following trauma. The typical appearance is a roughly triangular alteration with absent vascular supply. In addition, lesions may be rounded in appearance, with only a reduction and not disappearance of internal vascularity. Absent or reduced vascular supply is a finding which may suggest a non-neoplastic nature of the lesion. At follow-up testicular infarction tends to diminish in size. Chronic lesions can present internal calcifications.

Bilagi P, Sriprasad S, Clarke JL et al (2007) Clinical and ultrasound features of segmental testicular infarction: six year experience from a single centre. Eur Radiol 17:2810-2818

Cittadini G, Gauglio C, Pretolesi F et al (2004) Bilateral epidermoid cyst of the testis: sonographic and MRI findings. J Clin Ultrasound 32:370-372

Dogra VS, Gottlieb RH, Oka M et al (2003) Sonography of the scrotum. Radiology 227:18-36

Hamm B (1997) Differential diagnosis of scrotal masses by ultrasound. Eur Radiol 7:668-679

Hortsman WG, Melson GL, Midldeton WD et al (1994) Testicular tumors: findings at Doppler US. Radiology 191:561-564

Kim W, Rosen MA, Langer JE et al (2007) US-MR imaging correlation in pathologic conditions of the scrotum. RadioGraphics 27:1239-1253

Langer JE, Ramchandani P, Siegelman ES et al (1999) Epidermoid cysts of the testicle: sonographic and MR features. AJR Am J Roentgenol 173:1295-1299

Middleton WD, Teefy SA, Santillan CS (2002) Testicular microlithiasis: prospective analysis of prevalence and associated tumor. Radiology 224:425-428

Miller FN, Sidhu PS (2002) Does testicular microlithiasis matter - A review. Clin Radiol 57:883-890

Miller FNAC, Rosairo S, Clarke JL et al (2007) Testicular calcification and microlithiasis: association with primary intratesticular malignancy in 3,477 patients. Eur Radiol 17:363-369

Oyen RH (2002) Scrotal ultrasound. Eur Radiol 12:19-34

Tackett RE, Ling D, Catalona WJ et al (1986) High resolution sonography in diagnosing testicular neoplasms: clinical significance of false positive scans. J Urol 135:494-496

Tartar VM, Trambert MA, Balsara ZN et al (1993) Tubular ectasia of the rete testis: sonographic and MR imaging appearance. AJR Am J Roentgenol 160:539-542

Winter TC (2002) There is a mass in the scrotum: what does that mean? In: Cooperberg PL (ed) RSNA Categorical Course in Diagnostic Radiology: Findings at US – what do they mean? RSNA 283-293

Woodward PJ, Sohaey R, O'Donoghue MJ et al (2002) Tumors and tumorlike lesions of the testis: radiologic-pathologic correlation. RadioGraphics 22:189-216

Part V
Oncologic Recurrences of the Male Reproductive System

Clinical Approach 14

S. Cosciani Cunico, A. Moroni, G. Mirabella, C. Simeone

Tumors of the male urogenital system are frequent (with an incidence in the United States of 25%). They usually have a long latency period and a high percentage of post-therapy survival. Patients affected by malignant urogenital lesions therefore require a long period of monitoring to identify recurrence of disease requiring adjuvant or salvage treatment as early as possible. The task of the urologist is to identify a strategy which on the one hand guarantees patient safety and on the other maintains costs within acceptable levels. This is prompted by the fact that apart from clinical and laboratory findings, patient follow-up principally consists of radiologic examinations.

Bradford T, Montie J, Hafez KS (2006) The role of imaging in the surveillance of urologic malignancies. Urol Clin N Am 33:377-396

Jemal A, Murray T, Ward E et al (2005) Cancer statistics, 2005. CA Cancer J Clin. 55:10-30

Kidney

Patients who undergo nephrectomy or renal sparing surgery due to localized tumor may develop local, lymph node or distant recurrence in 25-50% of cases. Staging and grading are commonly used as prognostic factors which are adapted to orient follow-up. The most common sites of distant metastases are the lungs, bone and abdominal organs. Some 6.7-7.6% of pulmonary metastases are diagnosed on the basis of symptoms. A periodic chest radiograph is commonly indicated as well as a computed tomography (CT) scan in the event of anomalous findings. In the absence of signs, symptoms or tumor marker alterations, abdominal recurrences are usually diagnosed with ultrasonography (US) or CT. In general, in the presence of brain or bone metastases clinical signs or alterations of tumor markers appear, prompting a brain CT or bone scintigraphy.

Janzen NK, Kim HL, Figlin RA et al (2003) Surveillance after radical or partial nephrectomy for localized renal cell carcinoma and management of recurrent disease. Urol Clin N Am 30:843-852

Rabinovitch RA, Zelefsky MJ, Gaynor JJ et al (1994) Patterns of failure following surgical resection of renal cell carcinoma: implications for adjuvant local and systemic therapy. J Clin Oncol 12:206-212

Stephenson AJ, Chetner MP, Rourke K et al (2004) Guidelines for the surveillance of localized renal cell carcinoma based on the patterns of relapse after nephrectomy. J Urol 172:58-62

L. Olivetti, L. Grazioli (eds.), *Imaging of Urogenital Diseases*,

Upper Urinary Tract

Tumors of the upper urinary tract account for 5% of urothelial tumors. The incidence of recurrence has been reported in various studies between 8.7% and 42%, with a mean time to appearance between 7 and 18 months. The possibility of recurrence both in patients who have undergone conservative treatment and those who have undergone nephroureterectomy should be borne in mind not only in the upper urinary tract, but in the entire urothelium. Patients should therefore be monitored with periodic urinary cytology and urethrocystoscopy. Investigating the presence of regional lymph node or distant recurrences by integrating clinical findings with plain chest film and abdominal CT is useful in patients with advanced disease.

Deligne E, Colombel M, Badet L et al (2002) Conservative management of upper urinary tract tumors. Eur Urol 42:43–48

Jabbour ME, Smith AD (2000) Primary percutaneous approach to upper urinary tract transitional cell carcinoma. Urol Clin N Am 27:739–750

Urinary Bladder

Bladder cancer is the most common urologic tumor after carcinoma of the prostate. At diagnosis 74% of tumors are superficial, 19% invade the muscle layer and 3% are metastatic. After endoscopic resection in patients with superficial lesions, monitoring basically consists of urinary cytology and endoscopic examinations. The debate over the utility of performing a periodic urography in asymptomatic patients is still open, with some authors only recommending this option in the presence of elevated risk factors for recurrence, such as high-grade disease, multifocality, multiple recurrences or carcinoma in situ.

The literature reports local recurrences after cystectomy for invasive malignant lesions in 5–19% of patients, distant recurrence in 6–22% of patients and combined in 8–13% of patients. Distant recurrences usually appear in the pelvic cavity, bone, lungs and liver. Distant recurrences in the upper urinary tract may occur in 2.4–6.6% of cases with an interval of 30–80 months after cystectomy. Recurrences are diagnosed because they are symptomatic in 26–76% of patients. Only in 10% of cases is the CT diagnosis made in the absence of symptoms or anomalous laboratory findings. The frequency of follow-up should be based on the stage of the disease, with many authors recommending prolonged follow-up. Imaging mainly consists of CT or magnetic resonance (MR) with urographic reconstructions which highlight possible complications related to urinary deviation. These include calculi or obstructions, which may be asymptomatic in up to 80% of cases. There are currently no clear clinical indications for the use of positron emission tomography (PET).

Bradford TJ, Montie JE, Hafez KS (2006) The role of imaging in the surveillance of the urologic malignancies. Urol Clin N Am 33:377–396

Herr HW, Bochner BH, Dalbagni G et al (2002) Impact of the number of lymph nodes retrieved on outcome in patients with muscle invasive bladder cancer. J Urol 167:1295–1298

Kuroda M, Meguro M, Maeda O et al (2002) Stage-specific follow-up strategy after cystectomy for carcinoma of the bladder. Int J Urol 9:126–133

Oosterlink W, Lobel B, Jakse G et al (2002) Guidelines on bladder cancer. Eur Urol 41:105–112

Prostate

The global survival rates for prostate cancer, regardless of the stage of disease, is 92% at 10 years and 61% at 15 years. The widespread use of the prostate specific antigen (PSA) assay has increased the diagnosis of low-risk tumors. Therefore, follow-up of prostate cancer needs to be over the long-term. The role of imaging has still not been clearly defined. In most cases an increase in PSA or the presence of signs and symptoms, such as bone pain, are indicators of progression and recurrence of disease.

The monitoring of patients undergoing hormone suppression therapy generally consists of conducting a periodic PSA assay and monitoring signs and symptoms, with bone scintigraphy and CT reserved for the onset of the latter. In patients who have undergone radical prostatectomy follow-up consists of a periodic PSA assay. When this is within the normal range and in the absence of signs and symptoms, no further examinations are required.

Bone scintigraphy is instead indicated in patients with an elevated PSA without clinical signs of recurrence. The findings of the examination depend largely on the PSA value, since the probability of a positive examination is below 5% with a PSA below 40–45 ng/mL.

The role of CT has still not been clearly defined. Some authors suggest performing the technique only in the presence of PSA values above 4 ng/mL, others only with PSA velocity greater than 0.2, even though CT confirms the presence of local recurrence in only 36% of cases documented by biopsy. Other authors have reported 100% sensitivity and specificity of MR in diagnosing local recurrence. There is some doubt regarding the role of fluorodeoxyglucose FDG-PET in distinguishing fibrosis from recurrence and in quantifying the response to treatment. A more promising technique appears to be PET with C-11 acetate.

US-guided peri-anastomotic biopsy may be indicated in the clinical suspicion of local recurrence in view of radiotherapy, bearing in mind that many authors have obtained similar results with radiotherapy performed after positive biopsies, and empirically, after negative biopsies. The management of post-radiotherapy patients is also substantially based on PSA values, where the biochemical indicator of recurrence is defined as three consecutive increases in PSA.

Cher ML, Bianco FJ Jr, Lam JS et al (1998) Limited role of radionuclide bone scintigraphy in patients with PSA elevations after radical prostatectomy. J Urol 160:1387-1391

Koppie TM, Grossfeld GD, Nuddell DM et al (2001) Is anastomotic biopsy necessary before radiotherapy after radical prostatectomy? J Urol 166:111-115

Messing EM, Thompson I Jr (2003) Follow-up of conservatively managed prostate cancer: watchful waiting and primary hormonal therapy. Urol Clin N Am 30:687-702

Nelson JB, Lepor H (2003) Radical prostatectomy. Urol Clin N Am 30:703-723

Shvarts O, Han KR (2002) PET in urologic oncology. Cancer Control 9:335-342

Testicle

Testicular cancer is the most commonly diagnosed malignant lesion in males aged between 15 and 44 years in developed countries. Stage I seminoma is classically treated with radical orchidectomy followed by radiotherapy on the lumbar aortic lymphonodes, even though many authors do not perform adjuvant radiotherapy in favor of comprehensive follow-up. After radical orchidectomy alone the rate of recurrence at the lumbar aortic lymphonodes varies from 13% to 19%. Recurrence most frequently occurs between 13 and 17 months. In patients who undergo radiotherapy the rate of recurrence is 3–6% of cases. Obviously follow-up is more comprehensive in

the first group, with clinical evaluation, study of tumor markers and chest/abdominal/pelvic CT or abdominal/pelvic CT with plain chest film every 3–4 months for the first 3 years, whereas in radiotherapy-treated patients the time interval is every 6 months for the first year. The frequency of follow-up is then reduced in both groups, although the duration of monitoring has still not been unequivocally established.

Patients with stage IIa and IIb seminomatous tumors generally undergo chemotherapy. The guidelines of the European Association of Urology suggest monitoring every 4 months in the first 2 years. CT diagnoses residual disease after chemotherapy in 30% of cases in advanced stages (IIc and III). PET could be a useful complementary examination to CT given its ability to differentiate between tumor tissue and fibrotic or necrotic tissue. Despite returning false positives and false negatives, PET has proven to be more specific than CT, thus enabling discrimination between patients indicated for surgery and those who should be keep under close surveillance.

Patients with stage I nonseminomatous lesions undergo radical orchidectomy and retroperitoneal lymphadenectomy or chemotherapy. In recent years the option of comprehensive follow-up after orchidectomy alone has become increasingly popular, thanks to the effectiveness of chemotherapy in saving a large percentage (70%) of excised negative lymph nodes. The percentage of recurrence in patients who undergo lymphadenectomy is 10–13%, with recurrence most frequently in the lungs, whereas the rate in patients who undergo comprehensive follow-up is 24–30%, with recurrence in the lungs in 5% of cases. In patients who undergo chemotherapy the recurrence rate is 1–5%, in most cases retroperitoneal.

Patients with stage II disease who undergo chemotherapy after lymphadenectomy have disease-free survival in 97–100% of cases, whereas those who undergo chemotherapy after radical orchidectomy have recurrence rates, even late recurrence, between 11% and 17%. The role of PET is still a matter of debate, although it appears less effective than in seminoma. It may have a role to play as a complement in patients with CT findings and discrepant tumor markers.

Hendry WF, Norman AR, Dearnaley DP et al (2002) Metastatic nonseminomatous germ cell tumors of testis: results of elective and salvage surgery for patients with residual retroperitoneal masses. Cancer 94:1668–1676

Laguna MP, Pizzocaro G, Klepp O et al (2001) EAU guidelines on testicular cancer. Eur Urol 40:102–110

Livesey JE, Taylor B, Mobarek N et al (2001) Patterns of relapse following radiotherapy for stage I seminoma of testis: implications for follow-up. Clin Oncol 13:296

Purdue MP, Devesa SS, Sigurdson AJ et al (2005) International patterns and trends in testis cancer incidence. Int J Cancer 115:822–827

Spermon JR, Roeleveld TA, van der Poel HG et al (2002) Comparison of surveillance and retroperitoneal lymph node dissection in stage I nonseminomatous germ cell tumors. Urology 59:923–929

Spermon JR, Witjes JA, Kiemeney LA (2004) Efficacy of routine follow-up after first-line treatment for testicular cancer. World J Urol 22:235–243

Penis

Penile cancer is the rarest of the male urogenital tumors. The most important indicators for inguinal lymph node recurrences are tumor stage, tumor grade and the presence at onset of lymphatic invasion. There are relatively few recommendations in the literature regarding the clinical management of patients after partial or total penectomy with or without inguinal lymphadenectomy. In patients who undergo

lymphadenectomy with involvement of the lymph nodes, clinical monitoring should be integrated with frequent chest/abdominal/pelvic/inguinal CT. However, imaging is not required in cases of negative lymph nodes or in patients who were assessed as not requiring inguinal lymphadenectomy.

Solsona E, Algaba F, Horenblas S et al (2004) EAU guidelines on penile cancer. Eur Urol 46:1–8

Diagnostic Imaging 15

L. Olivetti, G. Voltini

Knowledge of the mechanisms, risk factors and times at which a recurrence of a malignant tumor occurs in a local-regional or distant site are fundamental elements for correct interpretation of images. Therefore, each of the following sections dedicated to the oncologic recurrence of tumors of the kidney, urinary bladder, prostate and testicle is preceded by a brief presentation of those elements.

Kidney

Introduction

Around 5% of patients who have undergone nephrectomy for carcinoma suffer local recurrence. This is generally correlated with incomplete tumor resection, positive surgical margins or the presence of lymph node metastasis.

Secondary sites of distant spread are present in 30% of cases at diagnosis. After nephrectomy 20-30% of patients with local disease are subject to metastasis within 3 years. Metastases can in fact appear after a lengthy period of time, making this a distinctive feature of renal cell carcinoma which is found in 11% of patients surviving 10 years or more after surgery.

Dissemination occurs via lymphatic or hematogenous spread. The lung is the organ most commonly affected (50-60%), with other sites (in decreasing order of incidence) being the bone, liver, contralateral kidney and/or adrenal gland, and brain. Collateral retrograde venous flow of the lumbar veins in the vertebral plexus of Batson is particularly important for explaining metastases to the bone and brain.

The T stage at diagnosis is the single most important prognostic indicator. Large tumors with local-regional invasion and/or venous thrombosis have a higher incidence of distant metachronous metastasis. The degree of differentiation, the presence of lymph node metastases and the sarcomatoid appearance of the tumor are other important elements in determining the likelihood of recurrence. In contrast, a long interval free of disease is a favorable indicator of survival. With inclusion of the above-mentioned risk factors, attempts have been made to construct nomograms capable of predicting the probability of 5-year disease-free survival and defining the correct strategy in the follow-up of these patients.

Diagnostic Imaging

Computed Tomography

Computed tomography (CT) is without doubt the best imaging modality for evaluating tumor recurrence at local-regional or distant sites. Like the primary tumor, secondary lesions are highly vascular. In order to produce images of high diagnostic

L. Olivetti, L. Grazioli (eds.), *Imaging of Urogenital Diseases*,

quality a number of features need to be taken into consideration. These include performing an initial study of the parenchymal organs from the diaphragm to the pubic symphysis in the arterial phase, with successive extension of the study to the lungs and re-evaluation of the abdomen and pelvis in the venous phase. Special attention should be paid to the surviving kidney for the presence of contralateral lesions, particularly in subjects with hereditary renal cell carcinoma and von Hippel-Lindau disease.

The retroperitoneal anatomy is significantly altered after nephrectomy, with dislocation of the colon, small intestine and tail of the pancreas in the empty renal space. Therefore opacification of the jejunal-ileal loops with oral contrast medium is suggested.

Local-regional recurrence manifests as a mass which often invades the quadratus lumborum muscle or the psoas and dislocates or invades the adjacent structures (**Fig. 15.1**). Superior extension can involve the adrenal gland if this was spared during the prior surgical procedure. In cases of partial nephrectomy the recurrence can manifest as markedly enhancing intraparenchymal renal nodules.

The lymph nodes adjacent to the vascular peduncle are frequently involved and are an important predictor of distant metastasis.

Multifocal metastases are a common finding. Pulmonary metastases are associated with the spread of lesions to other sites in 50-60% of cases. Bone metastases are in all cases lytic and have a preference for the axial skeleton from the 12th thoracic vertebra to the pelvis (**Fig. 15.2**).

In addition to the common sites listed in the introduction, secondary lesions (particularly late onset lesions more than 10 years after surgery) can involve atypical sites such as the pancreas, bronchi, muscles, peritoneum and intestine (**Figs. 15.3-15.5**). The common feature once again is hypervascularity, which produces the clinical presentation (hemoptysis, enterorrhagia, etc.) and the imaging pattern (e.g. enhancement of a secondary lesion in the pancreas enables differentiation with ductal adenocarcinoma).

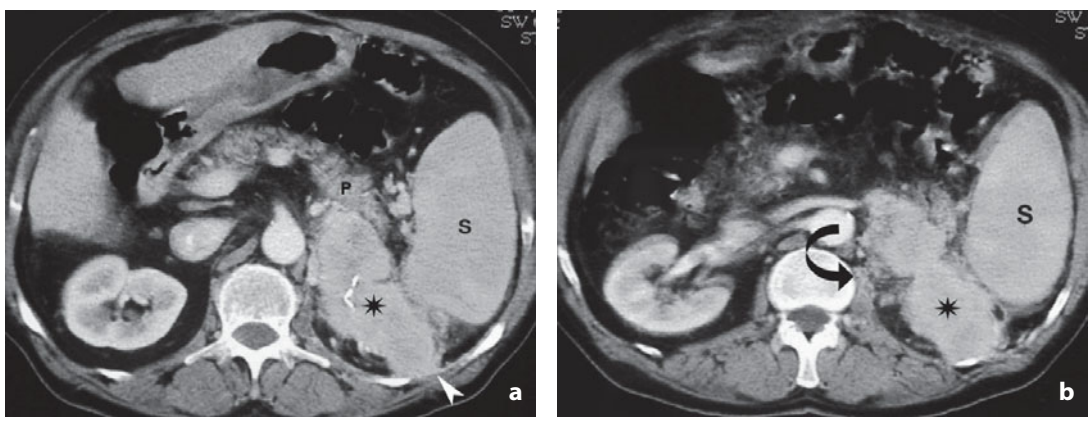

Fig. 15.1a,b. Computed tomography. Local-regional recurrence following left radical nephrectomy. The images show a large mass (*asterisk*) growing in the empty renal space, invading the transverse fascia (*arrowhead*) and in contact with the spleen (*S*), the tail of the pancreas (*P*) and the ileo-psoas muscle (*curved arrow*)

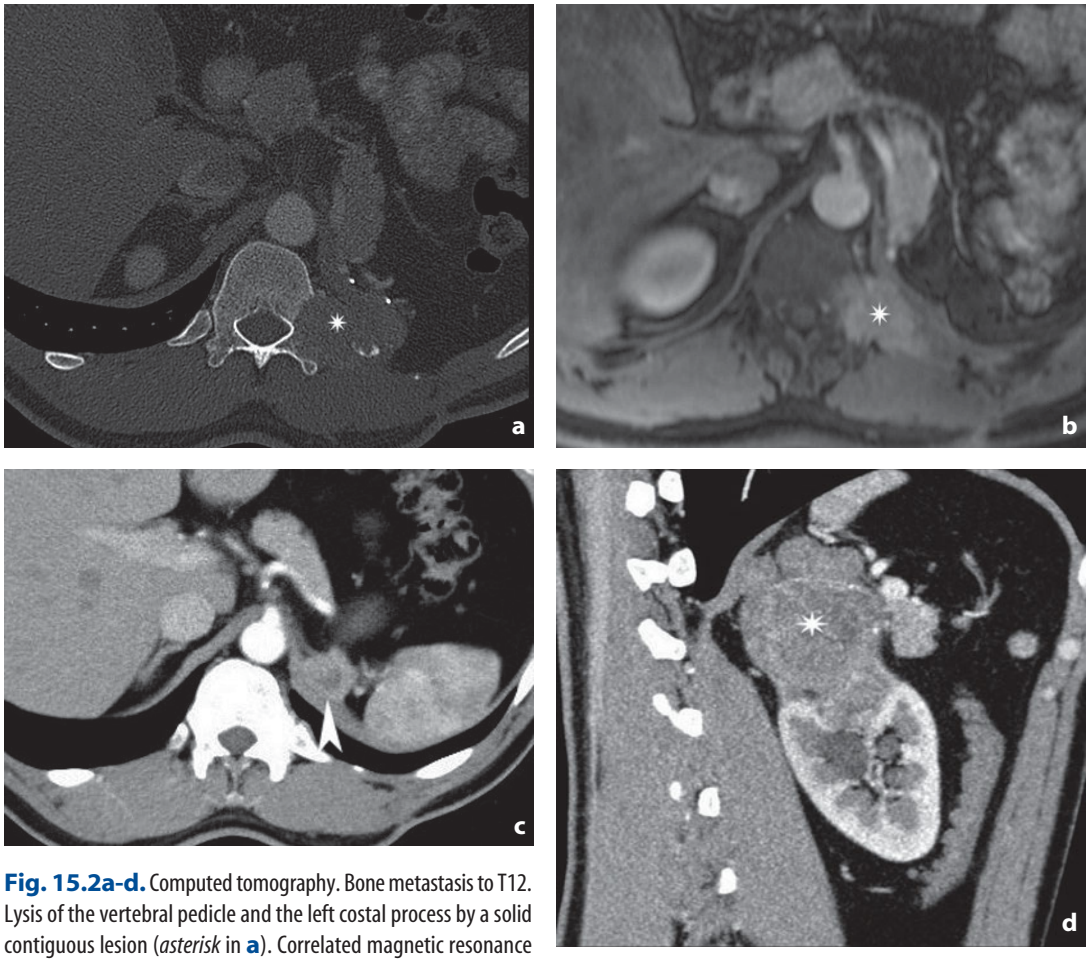

Fig. 15.2a-d. Computed tomography. Bone metastasis to T12. Lysis of the vertebral pedicle and the left costal process by a solid contiguous lesion (*asterisk* in **a**). Correlated magnetic resonance image (**b**). Patient history: previous resection of local-regional recurrence (*arrowhead* in **c**) of a T3a renal cell carcinoma (*asterisk* in **d**)

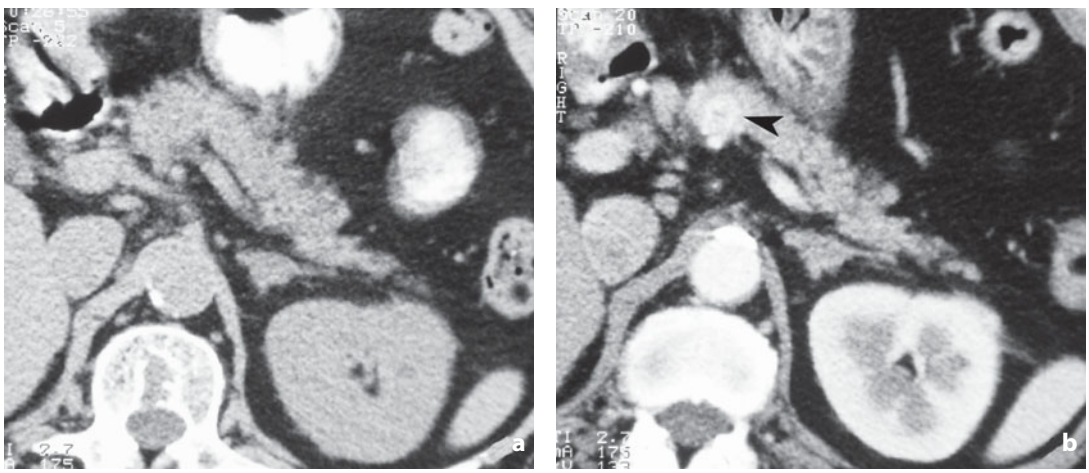

Fig. 15.3a,b. Computed tomography. Pancreatic metastasis following right nephrectomy. Axial nonenhanced (**a**) and enhanced (**b**) images in the arterial phase. The latter shows a hypervascular nodule at the level of the isthmus (*arrowhead*)

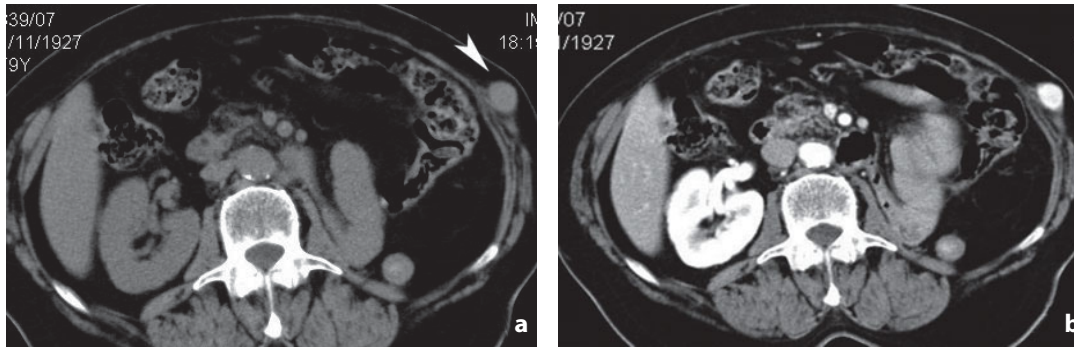

Fig. 15.4a,b. Computed tomography. Axial nonenhanced (**a**) and enhanced (**b**) images. Muscle metastasis of renal cell carcinoma following left radical nephrectomy. A solid enhancing nodule (*arrowhead*) can be identified in the left abdominal wall at the level of the oblique muscles

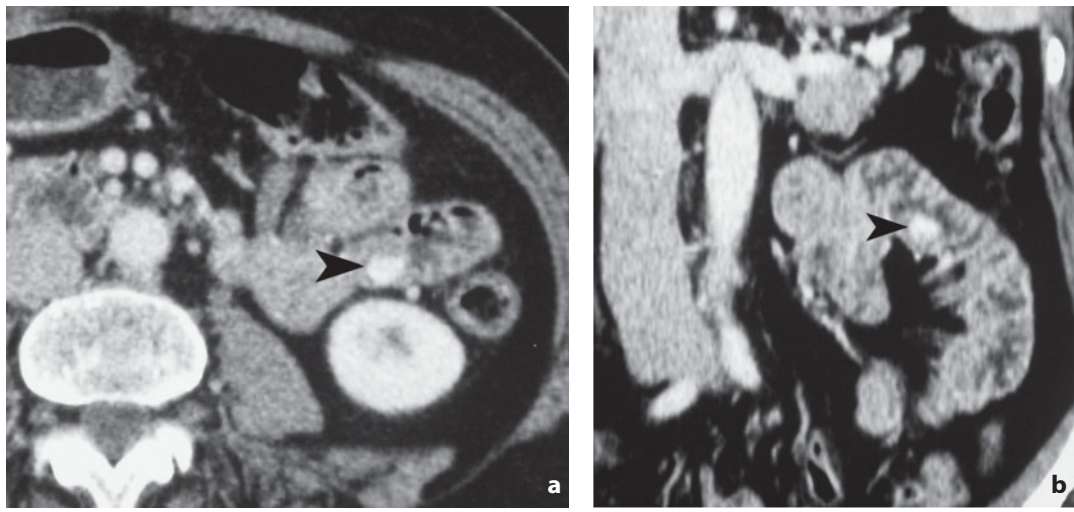

Fig. 15.5a,b. Computed tomography. Intestinal metastasis following right nephrectomy. Patient with melena. The axial image (**a**) and coronal reconstruction (**b**) of the arterial phase of the dynamic study show a hypervascular lesion (*arrowhead*) at the level of the first jejunal loop

Magnetic Resonance

Magnetic resonance (MR) of the abdomen and pelvis is indicated in subjects with compromised renal function or prior adverse reaction to iodinated contrast media (**Fig. 15.6**).

CT-PET

PET with F-18 fluorodeoxyglucose has a potential role in cases where the findings of other imaging techniques are inconclusive. In relation to specificity and positive predictive value of the technique, a positive result is strongly suggestive of local-regional or distant recurrence, whereas a negative finding cannot reliably rule out the recurrence of disease.

Griffin N, Gore ME, Sohaib SA (2007) Imaging in metastatic renal cell carcinoma. AJR Am J Roentgenol 189:360-370

Scatarige JC, Sheth S, Corl FM et al (2001) Patterns of recurrences in renal cell carcinoma: manifestations on helical CT. AJR Am J Roentgenol 177:653-658

Zhang J, Lefkowitz RA, Bach A (2007) Imaging of kidney cancer. Radiol Clin North Am 45:119-147

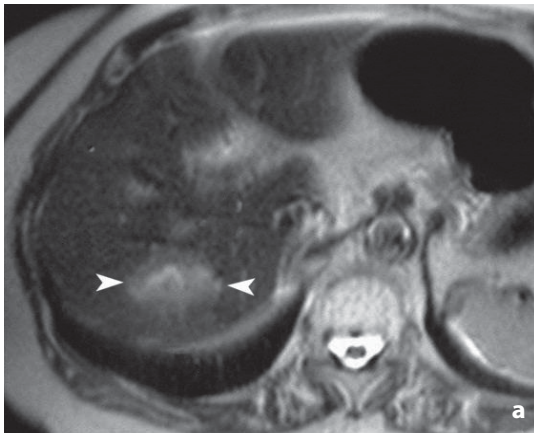

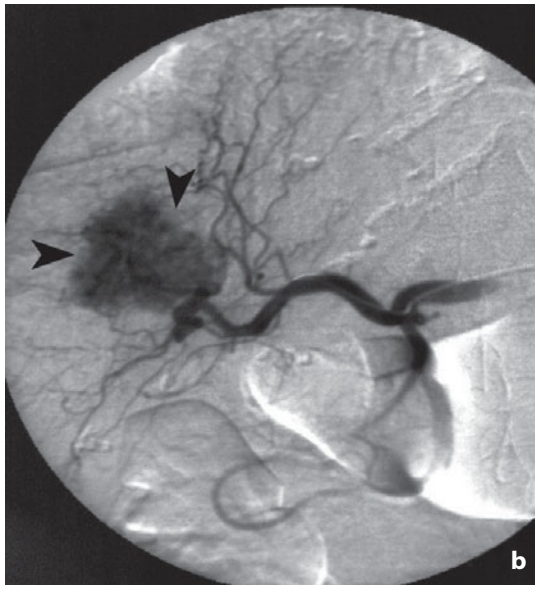

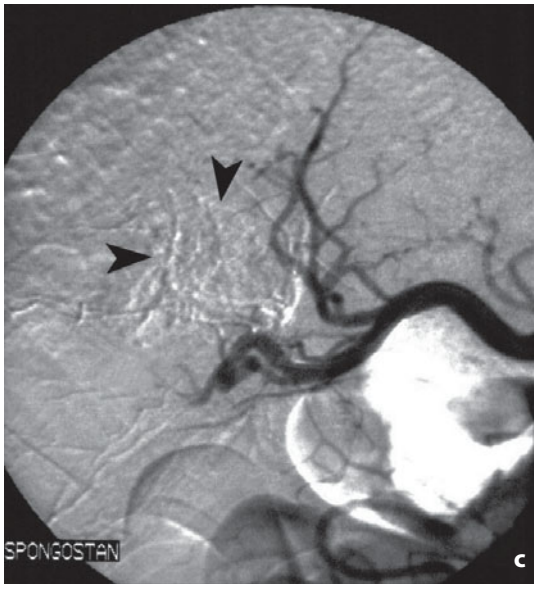

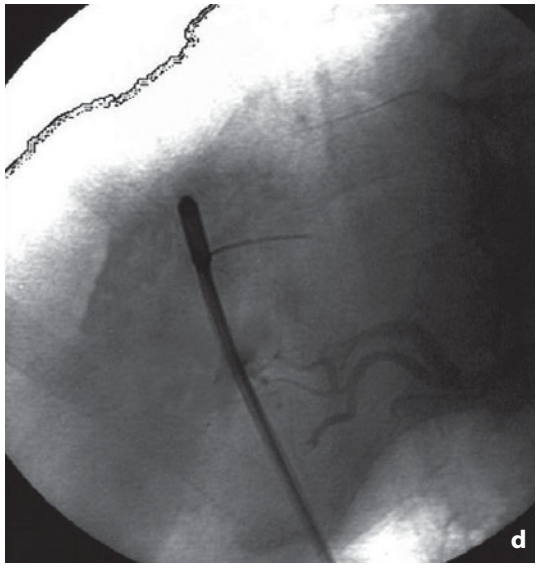

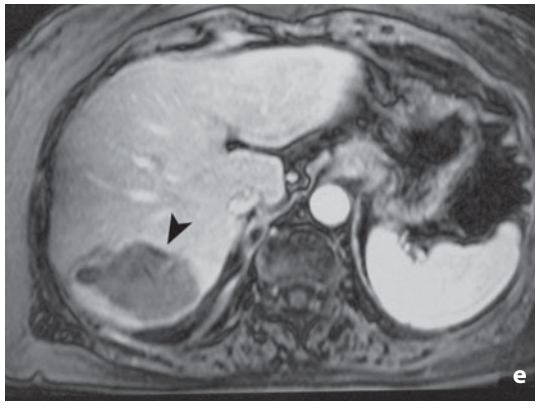

Fig. 15.6a-e. Magnetic resonance. Liver metastasis following right nephrectomy for renal cell carcinoma. Mild renal insufficiency. Lesion (*arrowheads*) of segment VII of the liver confirmed with MR and visible in the T2-weighted image (**a**). The lesion is hypervascular as demonstrated by diagnostic angiography (**b**) prior to combined treatment of stop-flow (**c**) and radiofrequency thermoablation (**d**). At follow-up, the arterial phase of the dynamic MR study (**e**) shows the complete necrosis of the lesion

Urinary Bladder

Introduction

It is no easy task identifying an adequate imaging technique for the lifelong monitoring and evaluation of disease recurrence in patients with bladder cancer. The histologic nature of the tumor (urothelial), in fact, suggests it should be considered as affecting the entire urinary tract rather than simply one of its organs.

This chapter takes into consideration only the local and distant recurrences (extra-urinary tract) of bladder cancer, leaving other chapters for description of the imaging techniques (loopography, CT urography, etc.) required for the evaluation of metachronous lesions of the upper urinary tract.

Following radical cystectomy, the incidence of disease recurrence varies from 5% to 37% of cases. These take the form of local pelvic recurrence (45%), secondary sites at the pelvic lymph nodes (33%) and distant metastases (11%).

Diagnostic Imaging

Computed Tomography

After intraluminal resection of the primary neoplasm the follow-up to identify local recurrence, which often is only superficial, can be managed with endoscopic techniques. **Cystoscopy** with biopsy is the reference standard. It is nonetheless expensive and invasive, and obviously is unable to evaluate the upper urinary tract. **Urinary cytology** has high specificity (>90%) but poor sensitivity (<50%) for low grade tumors.

The role of **ultrasonography** in this setting is marginal. **Computed tomography** has some limitations in that transurethral resection and radiotherapy produce wall thickening, edema and consequent enhancement of the mucous and submucous layers, an appearance which is similar to local recurrence. The time interval, the presence and growth of a lesion in the shape of a mass are decisive elements which help the interpretation of the images (Fig. 15.7).

CT has the advantage of being able to evaluate the entire urinary tract with high spatial resolution, which is particularly useful when bacillus Calmette-Guérin (BCG) has been used in the treatment of superficial lesions. Some patients can in fact manifest a granulomatous systemic reaction in the form of nodules which can compromise the kidneys, bladder and prostate. When located in the kidney, the lesions appear hypoattenuating with a heterogeneous structure. In the bladder they typically appear intramural, possibly enhancing, while in the prostate their appearance is very similar to a carcinoma (this is also true for digital rectal examination findings and the increase in prostate specific antigen PSA). The diagnosis can be made on the basis of the response to therapy, i.e. the reduction and even disappearance of the lesions after BCG instillation.

Magnetic Resonance

As with the kidney, MR is indicated in patients with non-severely compromised renal function or with known adverse reactions to iodinated contrast material. The technique is, nonetheless, encumbered by a number of limitations, such as lengthy examination times and the need for injection of diuretics and saline solution to better extend the collecting system. In identifying and characterizing local recurrence, MR has the advantage of multiple examination parameters, and elevated spatial and contrast resolution. Recent studies in perfusion and diffusion have underlined further potential of the technique in oncology.

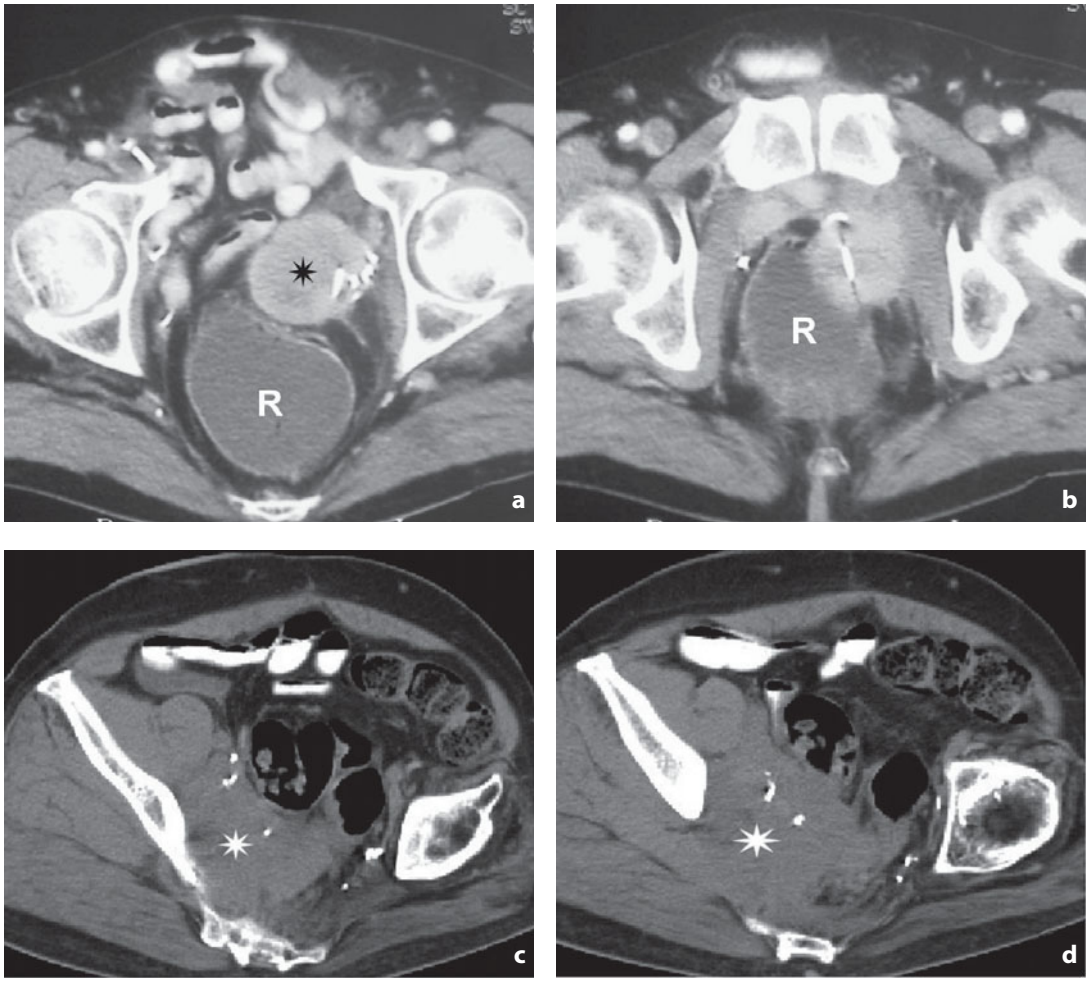

Fig. 15.7a-d. Computed tomography. Local recurrence after radical cystectomy. **a,b** Round nodule (*asterisk*) corresponding, with a metal clip of a prior surgical procedure. **c,d** Different patient. Extensive recurrence (*asterisk*) involving the right hemipelvis. *R*, rectum

In addition, studies have highlighted the ability of the technique (95% accuracy, 93% sensitivity and 100% specificity) to predict the response to chemotherapy of advanced lesions on the basis of the time to enhancement of the tumor and the lymph node metastases. The enhancement is correlated with neoangiogenesis and therefore the aggressiveness of the neoplasm.

Zhang J, Gerst S, Lefkowitz RA et al (2007) Imaging of bladder cancer. Radiol Clin North Am 45:183-205

Prostate

Introduction

Adenocarcinoma of the prostate is the most common malignant neoplasm and the second highest cause of death from cancer in males in the United States. The options for cure of the clinically localized lesion include radical prostatectomy, cryosurgery and radiotherapy (with external irradiation, brachytherapy or a combination of the two).

Despite the excellent therapeutic results, there is still no method for determining the extent of the tumor with certainty. Almost 50% of patients are understaged in terms of extracapsular extension of the disease, and of these, 30-40% show progression of the disease after treatment.

After prostatectomy, 50% of patients with a preoperative PSA >10 ng/mL or a postoperative Gleason score >7 are affected by recurrence within 7 years of surgery. Risk is correlated with preoperative PSA, stage and postoperative Gleason score as well as the positive or negative status of the resection margins. Approximately 35% of patients suffer from recurrence if the tumor is pT3, i.e. if the histologic examination finds extracapsular extension of the tumor. Patients with positive resection margins, regardless of the stage of disease, have a 25% likelihood of recurrence at 5 years. In contrast, patients with disease contained within the prostate after radical prostatectomy have a 10-year disease-free survival rate of 85%.

The distinction between local and distant recurrence is crucial for the choice of treatment. Patients with local recurrence may benefit from adjuvant chemotherapy or cryotherapy, whereas subjects with distant recurrence, regardless of the presence of local recurrence, require systemic therapy with hormone suppression. The precise localization of the distant recurrence is not clinically relevant, since in this phase most patients receive the same treatment. Nonetheless, it can prove useful in determining the timing of systemic therapy, intermittence of hormone suppression therapy and monitoring of the response to treatment.

There are several imaging techniques available for evaluating recurrence of prostate cancer. These must take into consideration the PSA assay and digital rectal examination (DRE), both of which were covered in Chapter 14, but which still require some brief introductory remarks to recall their key features prior to discussion of the radiologic techniques proper.

PSA

PSA is still the most sensitive indicator for evaluating how radical the surgical procedure has been and the likelihood of tumor recurrence. An increase in PSA following radical prostatectomy, radiotherapy or cryosurgery is the first and most reliable indicator of the recurrence of disease. In fact, if PSA is normal, DRE is negative and there are no symptoms of bone pain, then there is no indication for performing diagnostic imaging.

PSA is unable to reliably differentiate between local and distant recurrence (a positive PSA assay could even be due to normal glandular tissue left in situ, not so much after radical prostatectomy, but after radiotherapy or cryosurgery). Some studies have attempted to perform a differential diagnosis on the basis of the pattern of PSA increase. Local recurrence is suggested when PSA increases after 24 months from treatment, the PSA velocity is low and the PSA doubling time is >6 months, whereas distant metastasis is more likely in the presence of an early (<10 months) increase in PSA, high PSA velocity and PSA doubling time <6 months.

PSA after Radical Prostatectomy

After radical surgery, if there are no unknown sites of disease, the PSA value should be normal with the traditional measurement systems. The appropriate PSA value and the criteria for defining disease progression have not yet been standardized. However, a cutoff level below 0.2 ng/mL should not be used, as it is clear that such values are not associated with disease progression.

An abnormal PSA value after surgery could be due to the following causes:

- residual healthy glandular tissue (highly unlikely);

- residual disease, when PSA is >0.2 ng/mL at 8 weeks after surgery with a confirmed increase at the following measurement;
- biochemical recurrence of disease, when PSA progressively increases to >0.2 ng/mL in at least two successive measurements performed with intervals of not less than 2 weeks. These conditions codify residual or recurrent disease, respectively. However, since higher threshold levels of PSA correspond with higher specificity for disease recurrence, waiting for PSA to reach 0.4 ng/mL is a prudent measure prior to indicating salvage therapy.

PSA after Radiotherapy

Recurrence after radiotherapy or cryosurgery is much more difficult to characterize since the prostate is left in situ.

From the outset the evaluation of the PSA trend as an indicator of the state of disease is controversial. A decrease in PSA in terms of initial values in fact does not have a constant time course. Normally there is a slow and progressive reduction in PSA, until a constant minimum is reached (the so-called nadir). The time required varies from 17 to 32 months. The nadir value is the fundamental reference point for evaluating the possible failure of radiotherapy in terms of biochemical recurrence, defined by the American Society for Therapeutic Radiology and Oncology (ASTRO) as three consecutive increases in PSA, after three months of reaching the nadir value, regardless therefore of any threshold value. The time of recurrence is defined as halfway between the nadir value and the time to the first increase. The sensitivity and specificity of the increase in predicting the effective clinical recurrence, whether local or distant, is 60% and 72%, respectively.

The guidelines proposed by ASTRO also include the following observations:

- biochemical recurrence does not justify in itself the beginning of therapy, in that it is not equivalent to clinical recurrence;
- biochemical recurrence is nonetheless an adequate endpoint for evaluating the results of clinical studies;
- no definition of biochemical recurrence has proven to be a valid substitute for survival or clinical recurrence;
- the nadir is a highly predictive prognostic factor, but there is no cutoff which distinguishes therapeutic success from failure.

Digital Rectal Examination

Although it is undoubtedly useful in screening for carcinoma of the prostate, DRE is unreliable in evaluating local recurrence after prostatectomy or radiotherapy.

After radical prostatectomy the prostatic fossa should be empty at palpation, such that for DRE to be positive the presence of a certain volume of disease is required. In addition, the pelvic anatomy is inevitably modified in the resected patient, thus rendering difficult the differentiation between recurrence and fibrous tissue. This explains why 42% of patients with biochemical recurrence and negative DRE after radical prostatectomy are found to be positive at anastomotic biopsy. Similarly, after radiotherapy the small and restricted prostate renders differential diagnosis between recurrence and fibrosis at DRE difficult.

Diagnostic Imaging

Transrectal Ultrasonography

Transrectal ultrasonography (TRUS) is without doubt a useful technique. Its sensitivity increases significantly with rising PSA levels.

The pelvic anatomy after radical prostatectomy has been well described with TRUS. Tissue which is usually hyperechoic and symmetrical, with well-defined margins is often recognizable at the bladder neck and is attributable to the vesicourethral anastomosis (Fig. 15.8). Exactly at that site, local recurrence appears as a solid hypoechoic mass, or in 30% of cases isoechoic and therefore poorly visualized (Fig. 15.9).

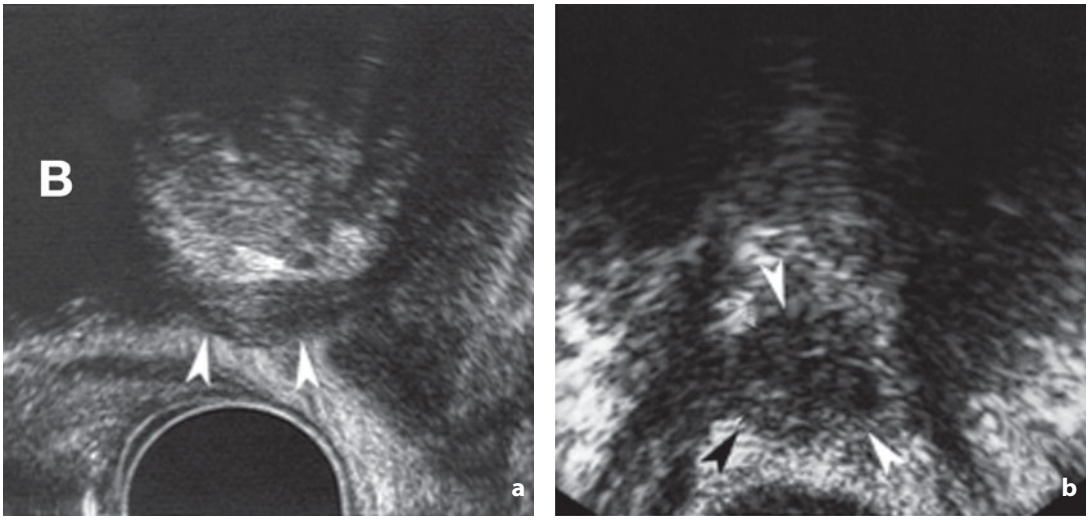

Fig. 15.8a,b. Ultrasonography. Normal postoperative anatomy following radical prostatectomy. **a** The *arrowheads* in the longitudinal scan indicate the urethra. **b** The *arrowheads* in the axial scan indicate the symmetrical vesicourethral anastomosis. *B*, urinary bladder

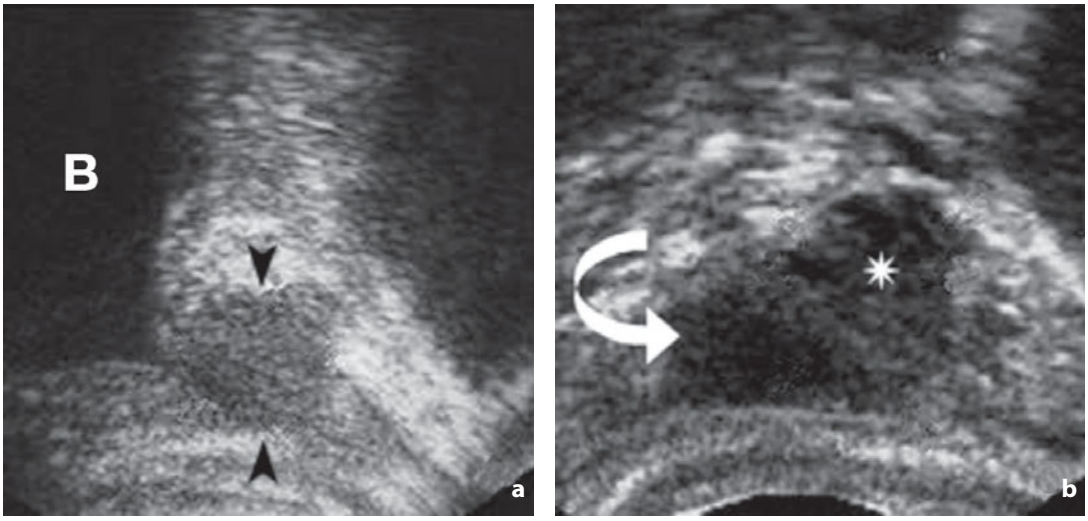

Fig. 15.9a,b. Ultrasonography. Local recurrence following radical prostatectomy. **a** The *arrowheads* in the longitudinal scan indicate a hypoechoic nodule at the level of the vesicourethral anastomosis. **b** The *asterisk* in the axial scan of another patient indicates the presence of a hypoechoic lesion with ill-defined margins located to the left of the vesicourethral anastomosis (*curved arrow*). B, urinary bladder

Identifying residual or recurrent disease with TRUS after radiotherapy is challenging. When visualized the lesion appears hypoechoic in the peripheral zone. The sensitivity of the technique does not exceed 50%, since post-actinic fibrosis distorts the normal tissue planes and renders the prostate small and hyperechoic.

After cryosurgery the prostate has a vague appearance following the post-freezing death of the cells. In contrast, poorly frozen areas appear clearer and can therefore be monitored over time to evaluate the possible onset of recurrence which appears hypoechoic.

The real advantage of TRUS is its use to guide biopsy.

After radical prostatectomy only 25% of patients are found to be positive at biopsy with PSA <1 ng/mL. The percentage increases with an increase in the biochemical marker. There is still no agreement on the length of time after radical radiotherapy that biopsy may appear positive.

Computed Tomography

CT is not indicated in the evaluation of local recurrence. The sensitivity of the technique is around 36% and in any case can only identify lesions >2 cm.

CT is better used in the search for distant lymph node metastases (pelvic and retroperitoneal) in patients with biochemical recurrence and no evidence of disease recurrence in the pelvic or distant sites. It has been shown that in 75% of patients who have undergone radical prostatectomy and pelvic lymphadenectomy the usual caudocranial pattern of the progression of lymph node metastases is not respected. In fact secondary retroperitoneal adenopathies are commonly present in the absence of pelvic lymph node involvement (**Fig. 15.10**).

CT has replaced lymphangiography and is preferable to MR due to its easier accessibility, greater examination speed, possibility of guiding biopsy procedures and, on the basis of the results of the latter, use in the planning of radiotherapy. Lymph node metastases are in fact a determining factor in the definition of a therapeutic strategy. This therefore includes the use of CT-guided biopsy (although not always possible and not free from morbidity) in an attempt to make a cytologic/histologic diagnosis.

The diagnostic criterion used by CT (and MR for that matter) is based on size. With a cutoff of 1 cm the sensitivity of the technique in different studies varies from 27% to 75%, whereas specificity is between 66% and 100%. With a cutoff of 7 mm and the use of guided biopsy several studies have reported a sensitivity of 78% and specificity of 100%.

In addition to evaluating the presence of lymph node metastases, CT is also able to identify metastases to the viscera and bone (**Fig. 15.11**).

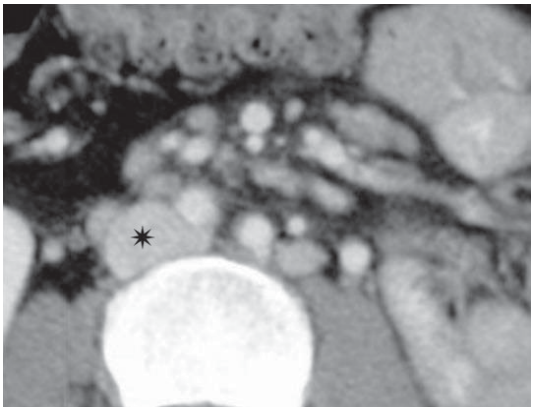

Fig. 15.10. Computed tomography. Retroperitoneal lymph node metastases after radical prostatectomy. Enlarged lymph nodes are recognizable at the level of the root of the mesentery and with retroperitoneal aortocaval and right paracaval location. The largest lymph nodes are located at this site (*asterisk*)

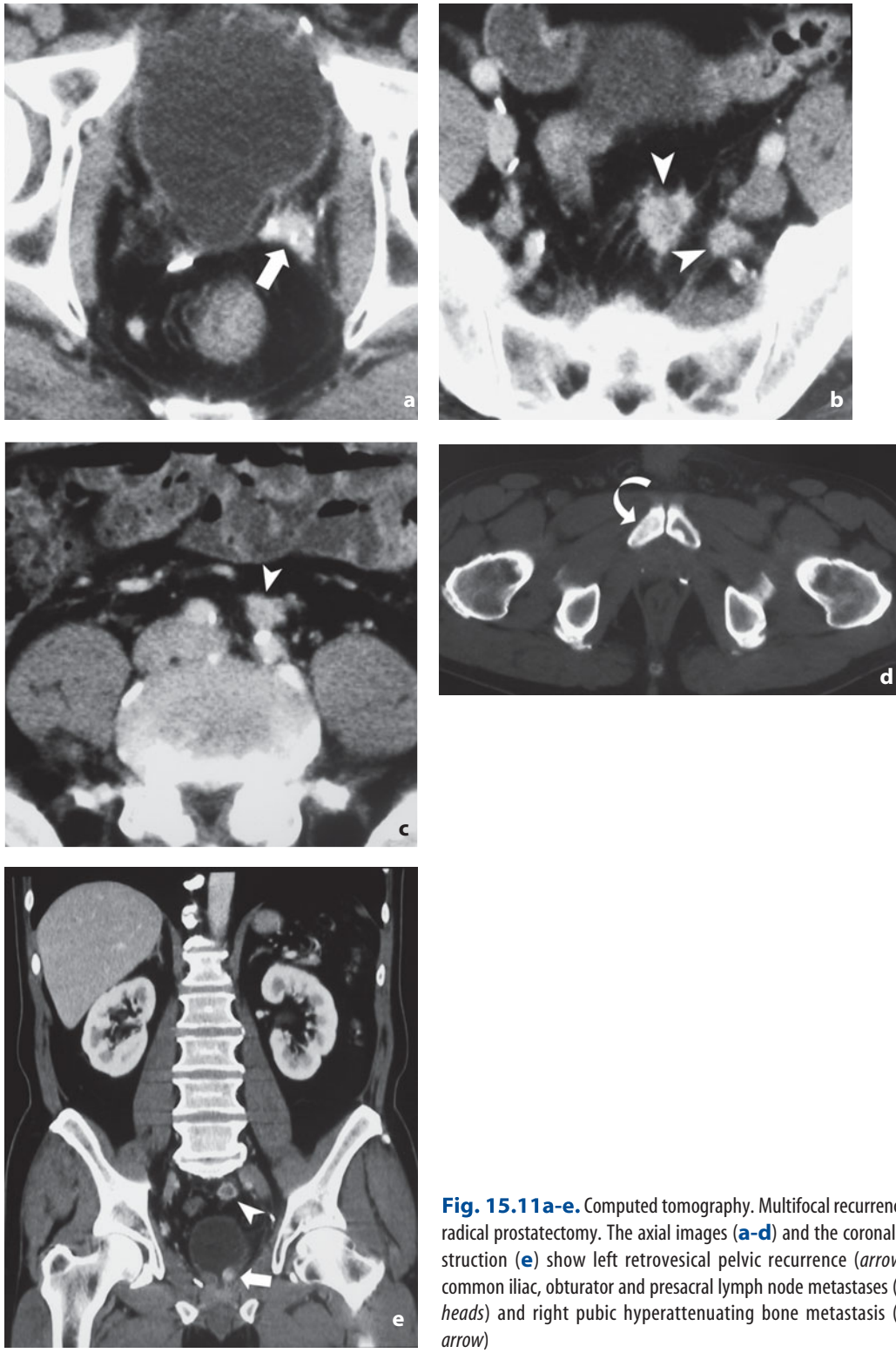

Fig. 15.11a-e. Computed tomography. Multifocal recurrence after radical prostatectomy. The axial images (**a-d**) and the coronal reconstruction (**e**) show left retrovesical pelvic recurrence (*arrow*), left common iliac, obturator and presacral lymph node metastases (*arrowheads*) and right pubic hyperattenuating bone metastasis (*curved arrow*)

Magnetic Resonance

MR can be used to identify local recurrence and lymph node and distant metastases (Fig. 15.12). After radical prostatectomy, the former appear isointense in T1-weighted images and mildly hyperintense in T2 with respect to the adjacent levator ani muscle. The lesions are mildly enhancing after contrast medium administration (Fig. 15.13). The sensitivity of MR in identifying the lesions has been reported as 95%, with specificity 100%. In one study, local recurrence was perianastomotic in 29% of patients, retrovesical in 49%, in the lumen of conserved seminal vesicles in 22% and in the anterior or posterior surgical margins in 9% of cases. The mean diameter of the lesions was 14 mm (range 8–45 mm) with PSA levels varying from absent to 10 ng/mL.

MR is able to clearly demonstrate residues of the seminal vesicles, which do not contribute to raising PSA levels, but can create difficulties for differential diagnosis at DRE or TRUS (Fig. 15.14).

Post-actinic fibrosis also renders difficult the MR identification of residual or recurrent malignancy with the prostate in situ. In T2-weighted images, tumor tissue appears hypointense to the adjacent peripheral gland and mildly hyperintense to the levator ani muscle.

Where available, MR spectroscopy is increasingly used in the differential diagnosis between normal and pathologic glandular tissue. One study has shown that MR imaging (68%) and spectroscopy (77%) are more sensitive than DRE (16%) and sextant biopsy (48%) in evaluating external postradiotherapy recurrence. MR spectroscopy (78%), however, is less specific than the other three techniques (90%).

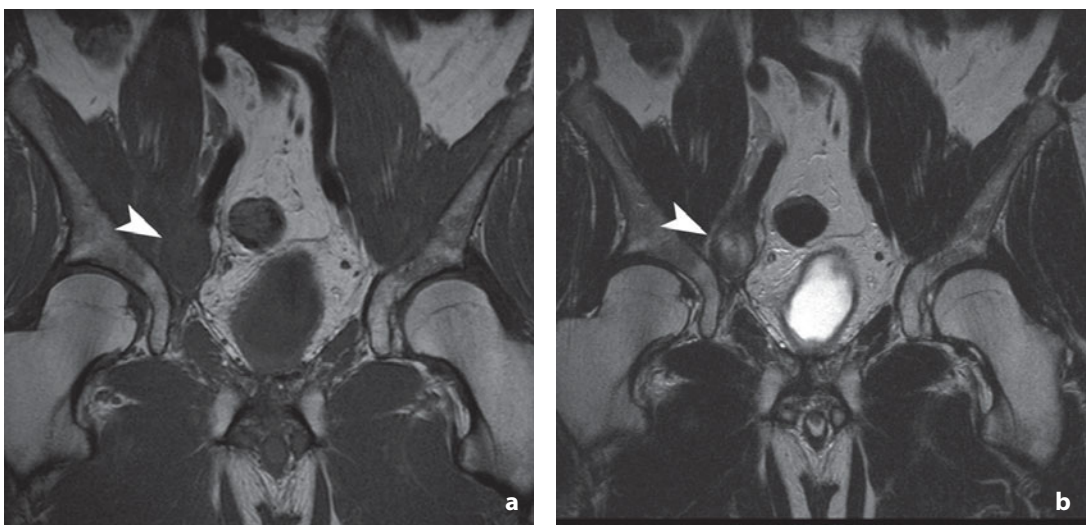

Fig. 15.12a,b. Magnetic resonance. Lymph node metastasis after radical prostatectomy. Coronal T1-weighted (**a**) and T2-weighted (**b**) images show an enlarged lymph node with heterogeneous signal intensity at the level of the right external iliac chain (*arrowhead*)

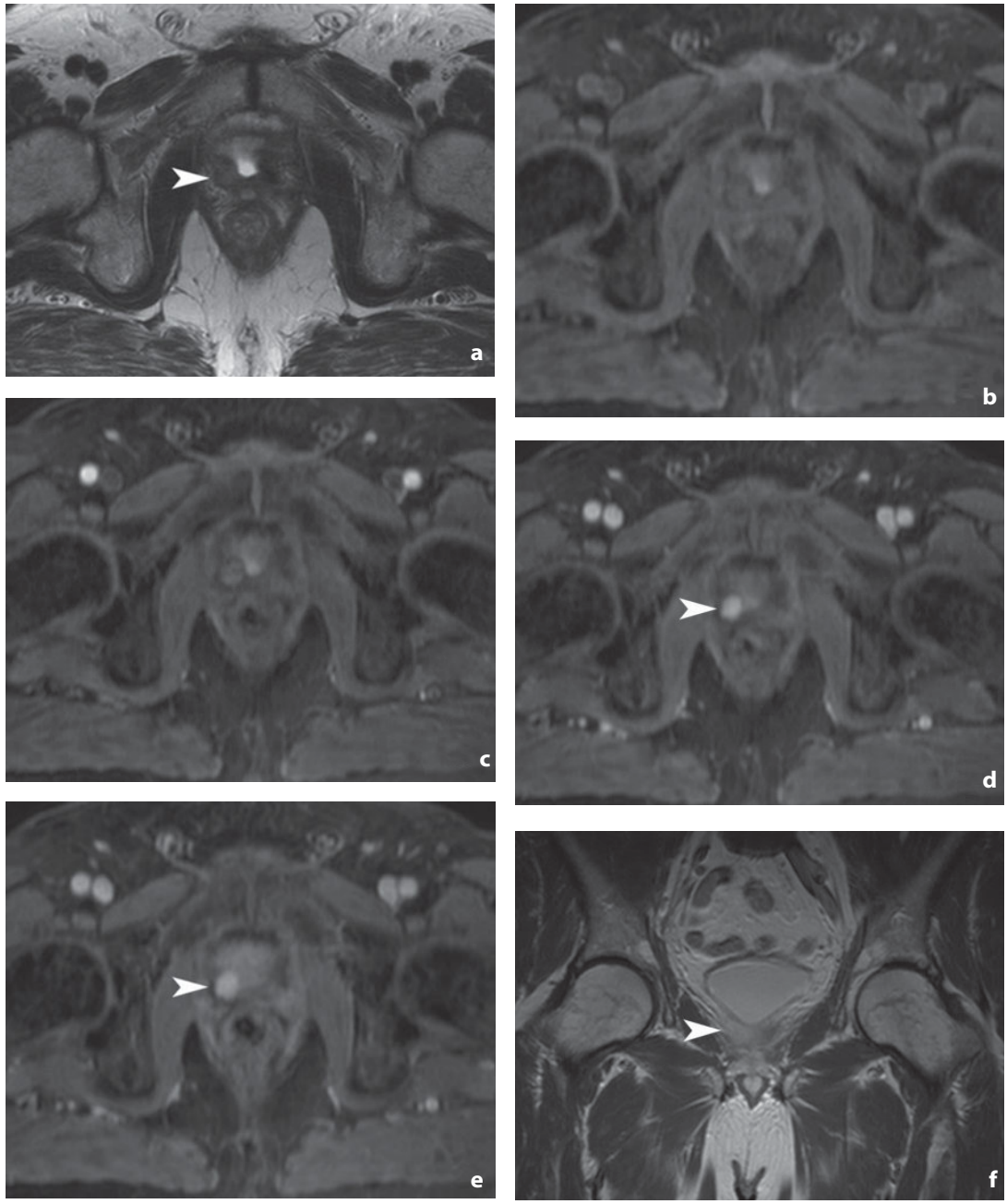

Fig. 15.13a-f. Magnetic resonance. Local recurrence after radical prostatectomy and biochemical recurrence. T2-weighted image (**a**) shows mild asymmetry of the vesicourethral anastomosis due to the presence on the right of a nodule (*arrowhead*) with intermediate signal intensity. In the venous (**d**) and late (**e**) phase of the dynamic study with paramagnetic contrast medium (**b-e**), the lesion appears markedly enhanced. The lesion is well visualized also in the coronal image after contrast administration (**f**)

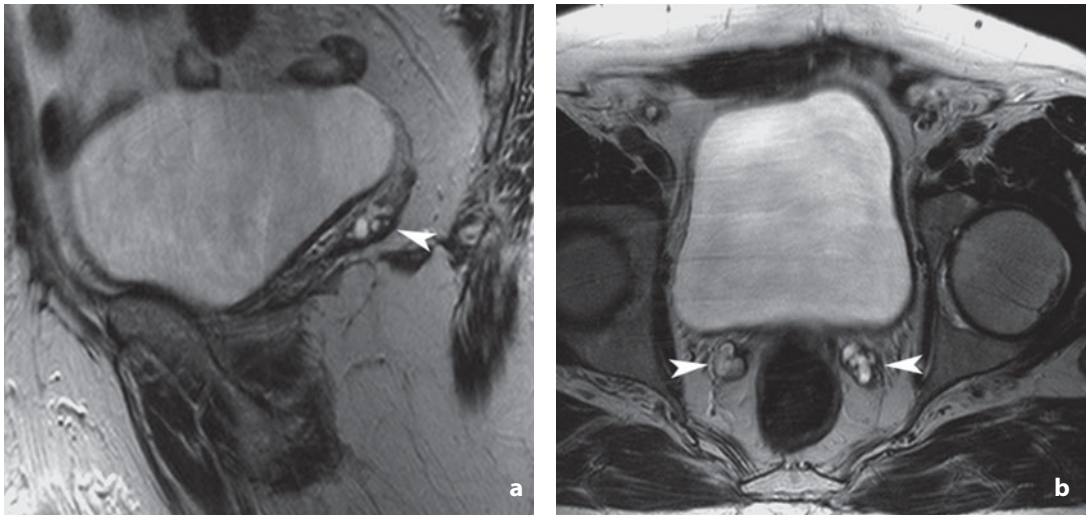

Fig. 15.14a,b. Magnetic resonance. Sagittal (**a**) and axial (**b**) T2-weighted images. Residues of the seminal vesicles (*arrowheads*) after radical prostatectomy

Bone Scintigraphy

Adenocarcinoma of the prostate preferentially metastasizes to the axial skeleton (pelvis, sacrum, vertebral column, ribs) and the long bones.

Despite the potential of CT and MR (**Figs. 15.15, 15.16**), scintigraphy with 99m-technetium is still the standard technique for identifying bone metastases. In patients with biochemical recurrence, a negative bone scintigraphy indicates that the recurrence is in the prostatic fossa, whereas a positive study indicates the presence of distant disease requiring systemic therapy (**Fig. 15.17**).

Scintigraphy is not indicated in the absence of specific bone pain or elevated PSA. In fact, a positive scintigraphy is unlikely when PSA values are <30–40 ng/mL. Only rare cases have been reported of bone metastases in patients with normal PSA after radical prostatectomy.

The diagnosis is simple, being based on the uptake of the radiotracer. False negative results are rare. False positives are more common, due to Paget's disease, arthrosis, prior trauma or fibrosis of the marrow, all of which are relatively frequent in middle-aged subjects. In doubtful cases other imaging techniques can be used. Plain film radiography can be useful to rule out a number of obvious conditions such as fractures or Paget's disease. More difficult and select cases may benefit from MR, with its higher sensitivity and specificity (superior spatial resolution being taken for granted) than scintigraphy. The typical MR pattern of bone metastases is low signal in T1 and high signal in T2. However, many high-density bone lesions present with low signal in both T1- and T2-weighted images.

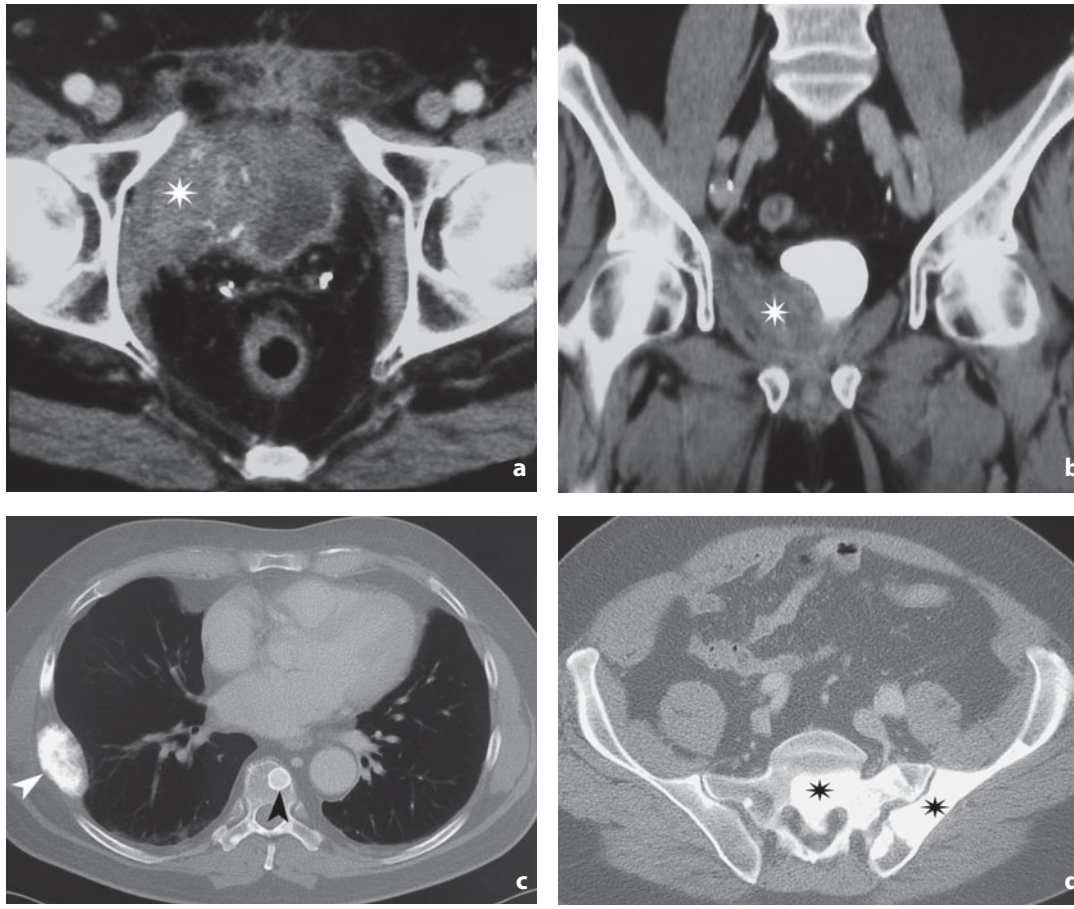

Fig. 15.15a-d. Computed tomography. Local recurrence and bone metastases after radical prostatectomy. Axial image (**a**) and coronal reconstruction (**b**) show large recurrence (*asterisk*) causing an impression on the urinary bladder. Hyperattenuating bone lesions are also present in the rib, vertebra (*arrowheads* in **c**), sacrum and left iliac (*asterisks* in **d**)

Imaging with monoclonal antibodies

Imaging with monoclonal antibodies (capromab pendetide) is indicated in biochemical recurrence after radical prostatectomy or radiotherapy when local or distant recurrence cannot be identified with standard imaging techniques. Despite the theoretical assumption of a high affinity between antibodies and neoplastic prostate tissue, data in the literature are discordant, with sensitivity ranging from 44% to 92% and specificity from 36% to 86%. In essence the technique does not appear to offer significant advantages over traditional scintigraphy in the identification of bone metastases.

CT-PET

The use of CT positron emission tomography (CT-PET) is still being validated. The technique has a sensitivity of 65% in the evaluation of bone metastases. With regard to the evaluation of local recurrence in post-prostatectomy patients, the technique is limited by spatial resolution limitations. In patients treated with radiotherapy, CT-PET is limited by the relatively high uptake of the tracer by the hyperplastic prostate. In addition, tracer uptake in the urinary bladder tends to mask the prostatic fossa.

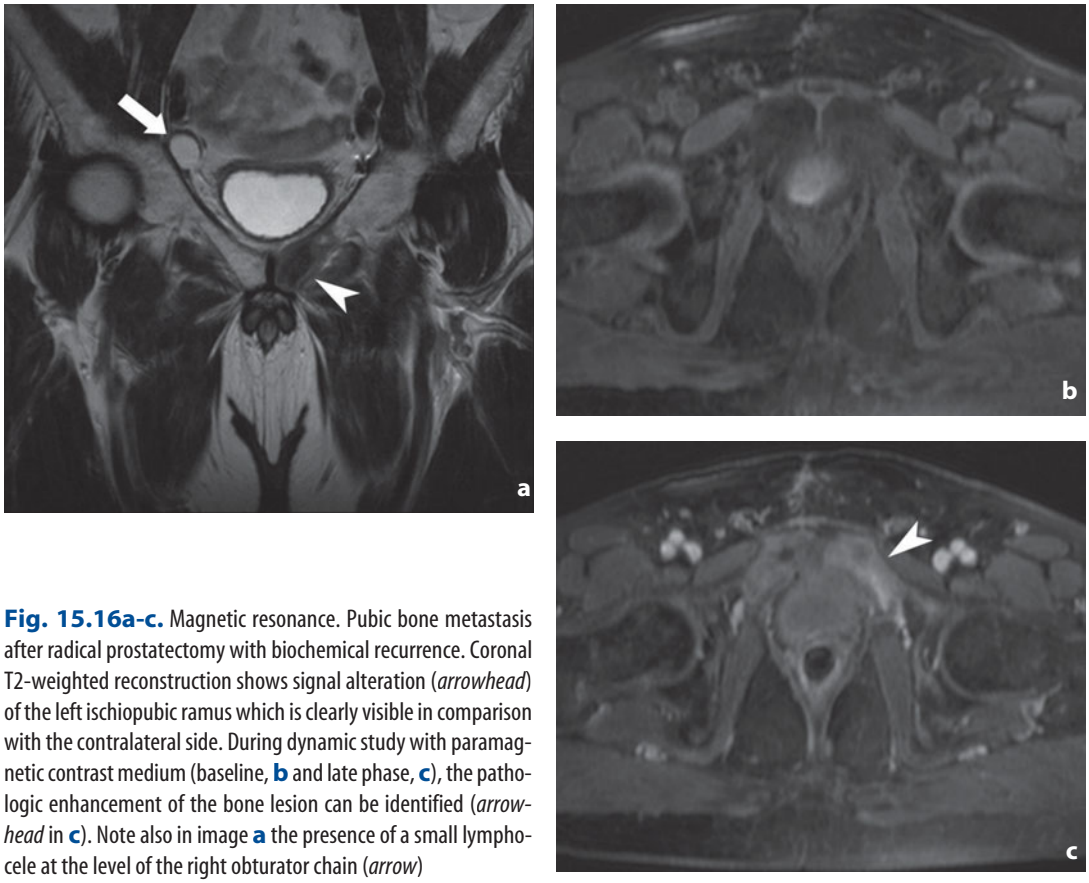

Fig. 15.16a-c. Magnetic resonance. Pubic bone metastasis after radical prostatectomy with biochemical recurrence. Coronal T2-weighted reconstruction shows signal alteration (*arrowhead*) of the left ischiopubic ramus which is clearly visible in comparison with the contralateral side. During dynamic study with paramagnetic contrast medium (baseline, **b** and late phase, **c**), the pathologic enhancement of the bone lesion can be identified (*arrowhead* in **c**). Note also in image **a** the presence of a small lymphocele at the level of the right obturator chain (*arrow*)

In a study performed in post-prostatectomy patients with biochemical recurrence, CT-PET identified local or distant disease in 31% of the 91 patients with biochemical recurrence. Improved results are expected with the use of 11C-choline as a tracer (**Fig. 15.18**).

Akin O, Hricak H (2007) Imaging of prostate cancer. Radiol Clin North Am 45: 207-222

Grossfeld GD, Li YP, Lubeck DP et al (2002) Patterns of failure after primary local therapy for prostate cancer and rationale for secondary therapy. Urology 60:57-62

Hanlon AL, Hanks GE (2000) Scrutiny of the ASTRO consensus definition of biochemical failure in irradiated prostate cancer patients demonstrates its usefulness and robustness. American Society for Therapeutic Radiology and Oncology. Int J Radiat Oncol Biol Phys 46:559-566

Nudell DM, Wefer AE, Hricak H et al (2000) Imaging for recurrent prostate cancer. Radiol Clin North Am 38:213-228

Pucar D, Sella T, Schöder H (2008) The role of imaging in the detection of prostate cancer local recurrence after radiation therapy and surgery. Curr Opin Urol 18: 87-97

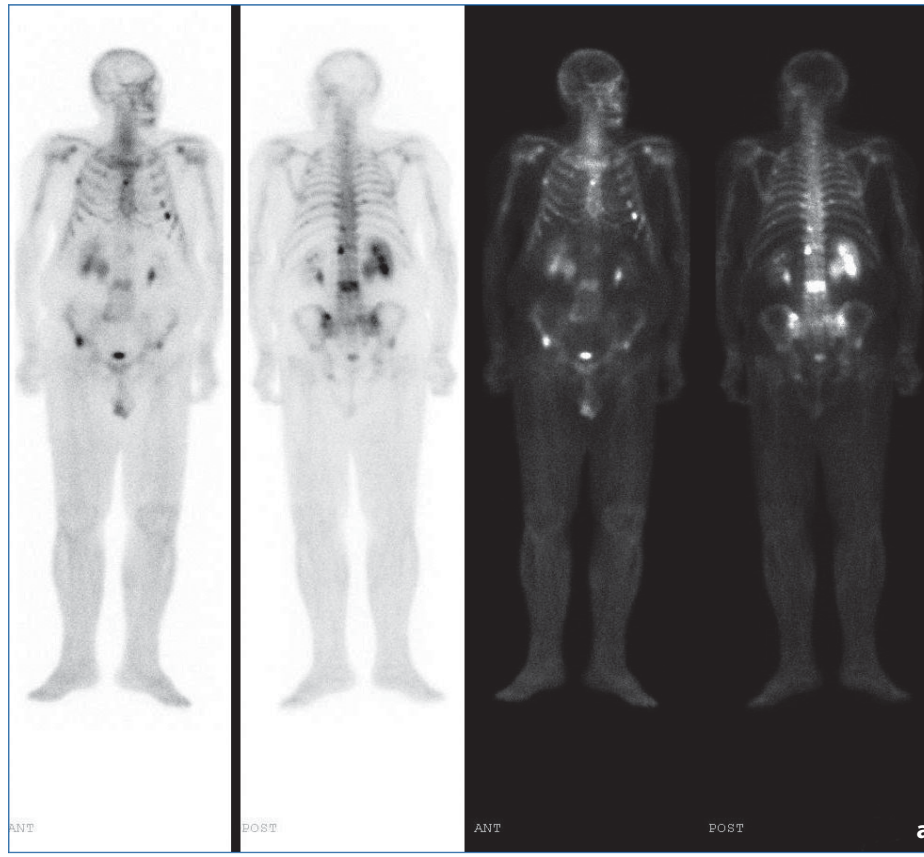

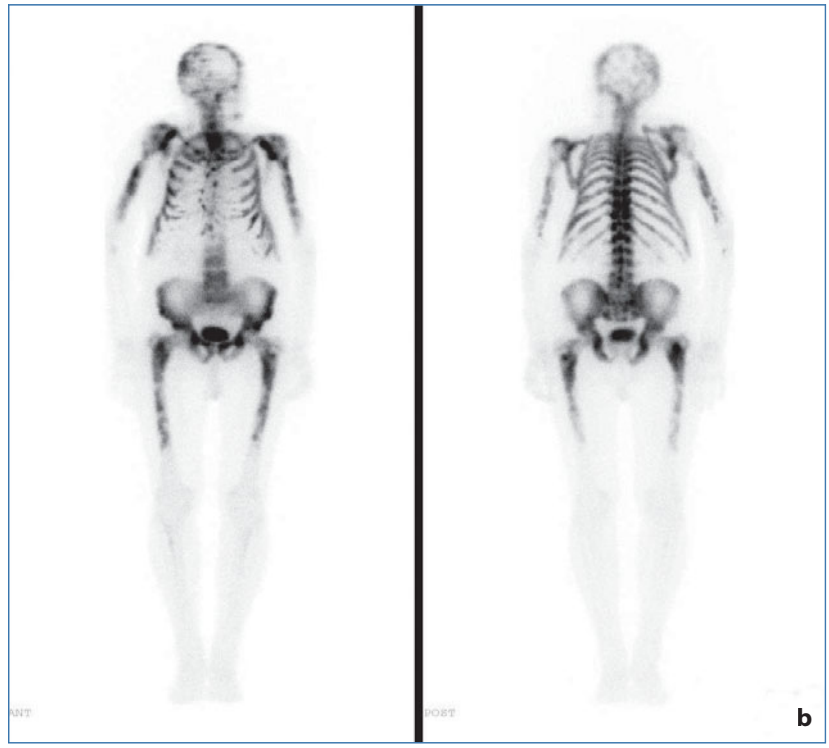

Fig. 15.17a,b. Bone scintigraphy. **a,b** Anteroposterior and posteroanterior views in different gray-scales. Post radical prostatectomy. Multiple bone metastases prevalent in the vertebral column and pelvis are identifiable by marked uptake of the radiotracer

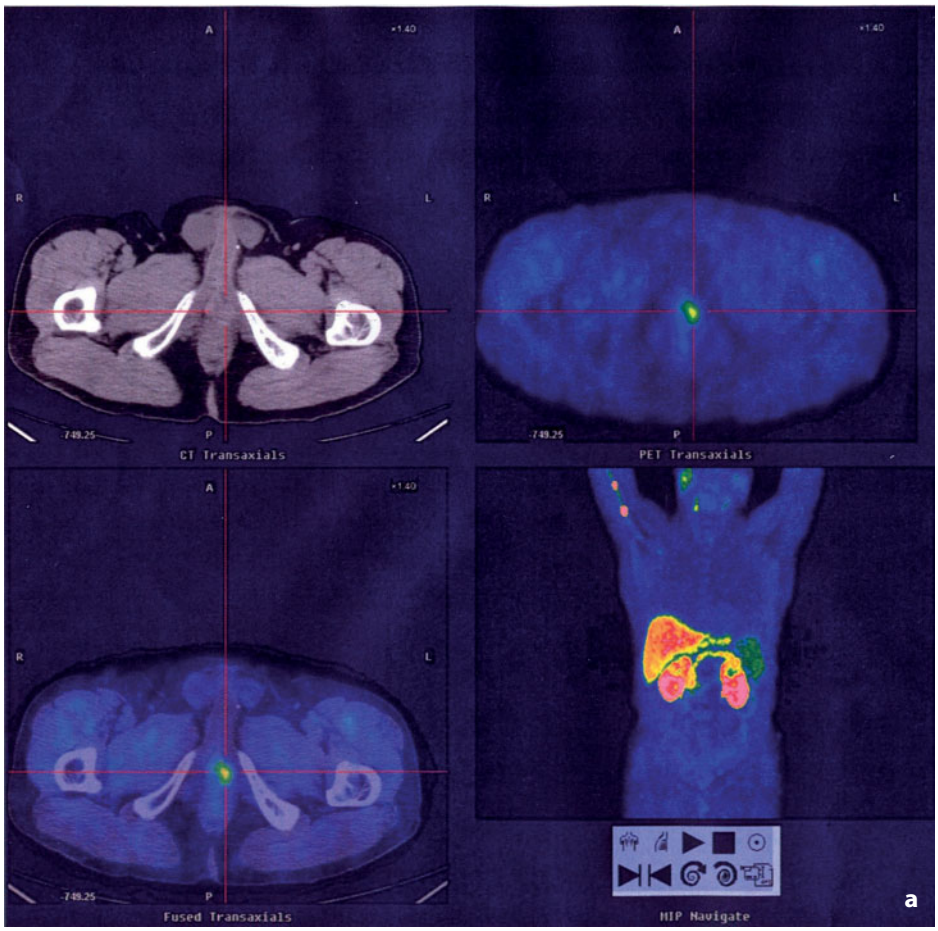

Fig. 15.18a,b. CT-PET with choline. Local recurrence after radical prostatectomy. **a** CT-PET shows a focus of radiotracer uptake at the vesicourethral anastomosis. **b** In the corresponding sagittal T2-weighted MR image the *arrowhead* indicates the nodule. *B*, urinary bladder

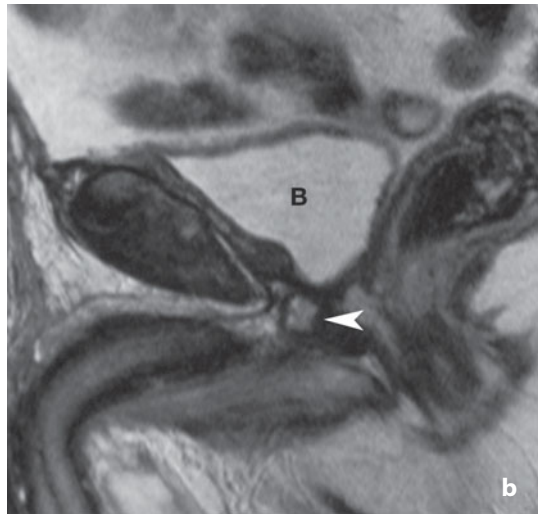

Testicle

Accurate staging at diagnosis and improving multimodal therapy (surgery, radiotherapy and chemotherapy, especially with cisplatin) have reduced the incidence of recurrence and brought disease-free survival to above 90% in all stages of germ cell tumors. This is in spite of the fact that recurrence after 2 years is chemoresistant and has unfavorable prognosis.

In general, seminomas tend to recur more frequently than nonseminomatous tumors. Most recurrences appear within 24 months of treatment and can involve the contralateral testicle or any other organ. In 2-4% of cases the recurrence can manifest very late, with intervals exceeding 30 years.

Optimal follow-up has not been defined. In general, check-ups are recommended every 3-4 months in the first 3 years, every 6 months at 4-7 years and each year thereafter. Follow-up includes tumor marker assays (β-HCG, AFP, LDH), chest radiography, abdominal-pelvic CT extended – according to some authors – to the chest and the supraclavicular region given the multifocality (30% of patients) and the predilection for lung metastases in lesions such as yolk sac tumor.

In recurrences, the main symptom (specific only in 35% of cases) is lumbar pain. Clinical presentation with compression of the urinary tract is uncommon. Therefore, the primary factor suggesting recurrence is biochemical, usually entailing an increase in AFP values.

Even though recurrence of germ cell tumors has been reported in the brain (especially with choriocarcinoma), cervical and thoracic vertebrae, liver and pelvis, the most common site (50-80% in different study populations) is retroperitoneal, regardless of the initial stage and primary treatment. Therefore, **computed tomography** is the imaging modality of choice, given its ability to identify metastases to the paraaortic and aortocaval lymph nodes, as well as along the iliac chain in some cases. A characteristic feature of choriocarcinomas, unlike other germ cell tumors, is the presence of a hemorrhagic component within the recurrences.

Carver BS, Motzer RJ, Kondagunta GV et al (2005) Late relapse of testicular germ cell tumor. Urol Oncol 23:441–445

Jewett MA, Grabowski A, McKiernan J (2003) Management of recurrence and follow-up strategies for patients with nonseminoma testis cancer. Urol Clin North Am 30:819–830

Woodward PJ, Sohaey R, O'Donoghue M et al (2002) From the archives of the AFIP: tumors and tumorlike lesions of the testis: radiologic-pathologic correlation. RadioGraphics 22:189–216

Part VI
Female Pelvic Floor

Female Pelvic Floor Dysfunction: Clinics and Imaging

16

G. Minini, F. Franco, S. Zanelli

Introduction

Female pelvic floor dysfunction essentially consists of pelvic organ prolapse, also known as uterovaginal prolapse. This term indicates the descent, through the urogenital hiatus of the pelvic floor, of the vagina, uterus, bladder, rectum and possibly bowel loops to a varying degree and association.

Prolapse of the bladder is defined as cystocele, of the rectum rectocele, of the uterus hysterocele or hysteroptosis and of the bowel loops, through the herniated rectouterine pouch, enterocele or colpocele.

An understanding of the anatomy and support system of the pelvic organs is fundamental for demonstrating the causes leading to the anomalous condition and for defining the correct surgical approach.

Anatomy of the Pelvic Floor

The pelvic floor consists of the musculofascial layers which sustain the pelvic organs and their support structures. It is characterized by a urogenital hiatus through which the urethra, vagina and rectum are in communication with the exterior, thus enabling the functions of evacuation and childbirth.

The fibroconnective structures (fascia and ligaments) play a passive role, whereas the pelvic muscles, essentially consisting of the pelvic diaphragm (levator ani muscle) and the perineal membrane and which contract in response to sudden increases in intra-abdominal pressure (coughing, sneezing, etc.), play an active role in the support system of the pelvic organs.

The pelvic diaphragm consists of the levator ani muscle, which is made up of two components: the iliococcygeus and pubococcygeus muscles. The more slender iliococcygeus muscle originates from the pelvic wall bilaterally at the level of the tendinous arch of levator ani, which extends between the pubis and the ischial spine and inserts into the median raphe posterior to the rectum. The posterior margin of this muscle fuses with the fibers of the coccygeus muscle at the level of the sacrospinous ligament. The thicker, sling-shaped pubococcygeus or puborectalis muscle originates from the pubis and is anchored to the lateral walls of the vagina and rectum. Some of the fibers of this muscle course posterior to the rectum forming a kind of sling which pulls it towards the pubis. Different portions of the muscle can be identified, which take their names from their site of insertion (pubovaginalis, puborectalis, pubococcygeus). For this reason, several authors (Lawson 1974, Zacharin 1985) prefer renaming it the pubovisceral muscle. Upon contraction the pubovisceral muscle compresses the vagina, urethra and rectum against the pubis, thus guaranteeing continence. Some muscle fibers are connected with the endopelvic fascia surrounding the vagina and urethra. Thanks to this relationship between the pelvic organs, fascia and muscle, and the continuous state of tonic contraction of the levator ani muscle, constant support

L. Olivetti, L. Grazioli (eds.), *Imaging of Urogenital Diseases*,

to the urethra and its effective closure is guaranteed in the event of a sudden increase in intra-abdominal pressure. The levator ani muscle is in fact characterized by basal tone regardless of the voluntary contractile capacity. This plays a crucial role in supporting and stabilizing the organs which rest upon the surface of the pelvic floor. In the presence of sudden changes in intra-abdominal pressure, the striated musculature of the pelvic diaphragm pulls the organs towards the pubis. This closes the urogenital hiatus, through which pass the urethra, bladder and rectum, and provides an almost horizontal platform upon which they may rest.

The perineal membrane, or urogenital diaphragm, is a fan of muscles oriented transversally which covers the anterior surface of both the urethra and the distal third of the vagina, surrounding the anterior (urogenital) triangle of the pelvic outlet. It inserts laterally into the ischial-pubic rami at around 2 cm from their caudal margin. The perineal membrane fuses medially with the lateral walls of the vagina and inferiorly with the fibrous center of the perineum. According to studies performed by Oelrich in 1983, the perineal membrane is made up of three components. The urethrovaginal sphincter muscle is the deep portion which completely surrounds the vagina and seems to converge with the superficial muscles of the membrane, the bulbospongiosus muscle and the superficial transverse perineal muscle. The compressor urethrae muscle, with fibers which in part surround the vagina and two-thirds of the urethra, composes the intermediate portion. Lastly, the external urethral sphincter is the most superficial portion and is characterized by fibers that completely surround the proximal and intermediate thirds of the urethra. The function of the perineal membrane is to prevent prolapse of the perineal body and the lateral vaginal walls when the levator ani muscle is relaxed, or in the event of an increase in intra-abdominal pressure. This support function is, however, linked to the resistance of the connective tissue composing the perineal membrane. The function of the anterior portion of the perineal membrane in relation to urinary continence is controversial.

The perineal body is an irregular mass of fibromuscular and elastic tissue located in the median plane between the vagina and rectum and ischial tuberosities. Anteriorly it fuses with the vaginal wall, whereas laterally it receives fibers from the perineum, the external anal sphincter and the perineal membrane which connects it with the ischial-pubic rami. The posterior attachment of the perineal body is given by the anococcygeus raphe which joins the external anal sphincter to the coccyx. Support of the pelvic outlet is linked to the continuity of the perineal membrane with the ischial-pubic rami and the perineal body. Tearing during childbirth left unrepaired tends to weaken the support provided by the perineal membrane.

The connective component, which is prevalently composed of collagen fibers, elastin and a certain amount of smooth muscle, is distributed throughout the pelvic cavity in a number of ways. It forms ligaments and fascia which surround the pelvic organs and anchor them to the walls of the pelvic cavity. The ligaments are generally solid, well-defined neurovascular structures surrounded by fibro-areolar connective tissue. They have a precise function of anchorage of the organs to the walls of the pelvic cavity and include the cardinal ligaments and uterosacral ligaments.

The pelvic connective tissue is organized in thin layers, known as the endopelvic fascia. This covers the muscular structures and viscera and has the function of supporting, strengthening and binding the pelvic organs.

The endopelvic fascia and ligaments act to stabilize the pelvic organs, but they also have a vital role in the support system in the event of a deficit of the muscular component. The more cranial portion of this complex support system is given by the cardinal and uterosacral ligaments, which continue caudally with the pubocervical fascia (anteriorly) and the rectovaginal fascia (posteriorly). The cardinal ligament originates from the greater sciatic foramen and is prevalently composed of perivascular connective tissue which surrounds the uterine artery and vein throughout their course. The uterosacral ligament originates from the 2nd-4th sacral vertebra and is composed of smooth muscle tissue and fibrous tissue. Both ligaments, which despite having

different terminations cannot be considered separate structures, insert into the uterine cervix forming the pericervical ring, and in part cover the upper third of the vagina, thus creating valid support for both the structures within the pelvic floor. The pubocervical fascia and the rectovaginal fascia, which are the caudal extension of the uterosacral/cardinal complex, fuse with the adventitial layer of the vagina, bladder and rectum, thus contributing to the support of these organs to the pelvic wall.

The pubocervical fascia extends laterally (paravaginal fascia) and inserts into the tendinous arch of the pelvic fascia, a fibrous thickening extending from a point located around one centimeter from the median line and one centimeter below the pubic arch, up to the ischial spine. The rectovaginal fascia, or rectovaginal septum, is composed of fibromuscular tissue and joins superiorly with the uterosacral/cardinal complex and inferiorly with the perineal body.

Pelvic support is guaranteed by the interaction between the pelvic musculature and the endopelvic fascia. The connective tissue, by forming ligaments and fascia, anchors the organs to the walls of the pelvic cavity and stabilizes them, fusing with the muscular layers of the individual organs. The muscular component, particularly the levator ani muscle with its basal tonic contraction, guarantees a plane upon which the pelvic organs may lie, and by contracting and compressing the vagina, the bladder and the rectum against the pubic symphysis, is able to maintain normal continence of those organs.

Epidemiology and Pathogenesis of Pelvic Organ Prolapse

Estimates suggest that for every 10,000 women, 10–30 undergo surgery for pelvic organ prolapse. However, several studies have reported a prevalence of prolapse (even mild) in up to 48% of women. The real prevalence of 2nd grade or higher vaginal prolapse seems to be 2–4%. The incidence of surgery for prolapse increases with age.

The interaction between the different components – muscular and connective – is responsible for normal pelvic support. Damage to one or the other of these elements can contribute to the genesis of pelvic organ prolapse.

Childbirth is the main cause of pelvic organ prolapse and urinary stress incontinence, while a shortage of estrogens, chronic pulmonary disease and chronic constipation are considered the most common risk factors involved in pelvic floor dysfunction. The hypothesis of a multifactorial etiopathogenesis would justify the finding of prolapse and/or incontinence in women who have borne no children or who present none of the above-mentioned risk factors (**Table 16.1**).

Neuromuscular damage of the levator ani muscle as a result of childbirth would appear to validate the role of vaginal delivery as the main causative factor leading to the genesis of prolapse. Numerous electromyographic studies conducted on patients affected by prolapse and/or urinary incontinence have reported a higher percentage of denervated fibers in these women than in normal subjects.

Advanced age also leads to a physiologic decrease in the density of muscle fibers and progressive denervation. Pelvic muscle damage seems to be correlated with multiparity, the type of delivery (dystocia), the lengthening of the second stage of labor, third-grade perineal tears and macrosomia.

Abnormalities of the collagen and connective tissue, and therefore of the ligaments and fascia covering the pelvic muscles, are an important etiopathogenetic factor which could justify the development of pelvic organ prolapse in nulliparous women. During delivery the uterine cervix undergoes enzymatic degradation of the collagen and elastin, which translates into a reduction in cervical resistance to enable the passage of the fetus. The proximity of the uterine support structures and the upper third of the vagina with the cervix suggests that the fascia and the ligaments undergo the same process of degradation.

Table 16.1. Causative factors of pelvic organ prolapse

Local factors	
Congenital	- pouch colon - neuromuscular (spina bifida) - connective tissue alterations (urinary bladder extroversion) - congenital short vagina
Acquired	- obstetric causes - hormonal causes
General factors	- obesity - cough - constipation - heavy work activities

Endopelvic Fascial Defects

The role of the endopelvic fascia in the support system of the pelvic organs has been receiving increasing attention in recent years. In particular, the American School, based on the theories of Baden, Walker and Richardson, according to whom the specific pelvic support defects are at the basis of specific defects of the pelvic organs, have developed a current of diagnosis and treatment of pelvic organ prolapse based on the identification and repair of endopelvic fascial defects.

Specific defects of the endopelvic fascia, both anteriorly and posteriorly, can be lateral, medial and transversal.

A lateral defect is the result of a detachment of the pubocervical and rectovaginal fascia from the tendinous arch or white line of pelvic fascia which courses from the ischial spine to the pubis. Anteriorly a lateral defect can be subdivided into a periurethral and paravesical defect, with outcomes in urethrocele and cystocele, respectively, with or without urinary stress incontinence. Posteriorly, detachment of the rectovaginal fascia from its lateral anchorage to the fascia of the levator ani muscle causes rectocele.

A median defect is caused by a rupture along the median line of the pubocervical fascia or posteriorly in the rectovaginal fascia. The consequent cystocele, in a manner similar to rectocele, is characterized by the loss of normal vaginal rugae. This type of prolapse is commonly associated with problems of urinary retention, and in the case of rectocele, difficultly evacuating the rectum.

A transversal defect is the underlying cause of a herniation which develops at the level of the anterior and/or posterior space of the vaginal fornix. The condition originates from a detachment from the pericervical ring of the pubocervical fascia anteriorly, and from the rectovaginal fascia posteriorly (**Table 16.2**).

Table 16.2. Classification of endopelvic fascial defects

Fascial defects of the anterior segment	
	right lateral
	left lateral
	median
	transverse
	puborectal
Fascial defects of the superior segment	
	cardinal/uterosacral complex
	superior paravaginal (Delancey level I)
Fascial defects of the posterior segment	
	right lateral
	left lateral
	median
	high transverse
	low transverse

Classification

A systematic description and classification of pelvic organ prolapse are useful for documenting the severity of the problem and for establishing a common approach to treatment. A number of classifications have been proposed in the literature. Systems which are still used today include The Halfway System developed by Baden and Walker in 1972 and the more complex ordinal quantitative system proposed by the International Continence Society (ICS), which tends to establish an accurate method of measurement to better understand the various alterations.

The classification of pelvic support defects with the Baden and Walker method (Halfway System) defines the degree of prolapse of the various segments with respect to a number of fixed reference points, which are: the plane of the ischial spine, the plane of the hymen, the plane of the maximum descent of the prolapsed organ (beyond the vaginal canal). The plane of the ischial spine (which in a normal vaginal profile projects into the upper third of the vagina) is the level of the normal anatomic position. The plane of the hymen is grade two descent. The plane of maximum descent is the maximum displacement possible outside the vaginal canal, and defines grade four descent. Grade one and grade three descent are an intermediate position of the prolapsed segment, i.e. "halfway", between 0-2 and 2-4. In women with normal pelvic support, under conditions of maximum strain the uterine cervix or the vaginal vault projects to the level of the ischial spines, whereas the urethra, the urinary bladder, the rectouterine pouch and the rectum do not pass beyond the upper half of the vagina.

The Baden and Walker classification can be summarized as follows:

Grade 0 normal, the protrusion does not reach the middle of the vagina
Grade 1 the protrusion is halfway between the ischial spines and the hymen
Grade 2 the protrusion reaches the hymen
Grade 3 the protrusion is halfway beyond the hymen
Grade 4 the protrusion is completely beyond the hymen

This classification identifies three anatomic segments of the vaginal profile: anterior, superior and posterior. All three segments need to be evaluated at the same time and their grade of anatomic position defined, regardless of whether the prolapse appears to involve only one of them. The evaluation of each segment should define the position of the urethra and bladder anteriorly, the position of the cervix and posterior fornix (rectouterine pouch) superiorly, and the rectum (posterior vaginal wall) and perineum posteriorly.

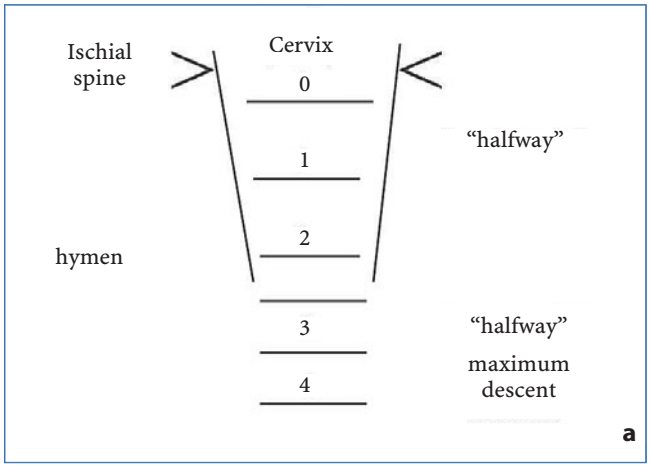

Halfway system	0	1	2	3	4	note
Urethra						
Urinary bladder						
Cervix						
Rectouterine pouch						
Rectum						
Perineum						

b

Fig. 16.1a,b. Classification of pelvic organ prolapse according to Baden and Walker (Halfway System) (**a**). Outline for attributing the numeric score (**b**)

Each specific site of the relative segment should be evaluated and graded according to the general 0-4 scale (Fig. 16.1).

The quantitative-descriptive system proposed by the ICS enables a precise evaluation of the pelvic support defect of each individual patient, expressed in centimeters, without assigning a "degree of severity". For a detailed presentation of the classification the reader is invited to consult specific texts.

Pelvic Organ Prolapse and Correlated Disease

Urinary Incontinence and Prolapse

A common clinical finding is the concomitant presence of prolapse and voiding problems (50% of cases).

It should however be noted that the two clinical presentations are not always associated, i.e. there are many patients with pelvic organ prolapse without urinary incontinence or other voiding disturbances, just as there are cases of voiding problems in the absence of pelvic support defects.

However, the pathogenetic factors responsible for prolapse (multiple deteriorations of the support structures) are often similar to those responsible for urinary incontinence. This explains how the pathogenesis, but most of all the surgical and non-surgical treatment, of the two entities have many common features.

Other factors to recall, albeit briefly, include:

- urinary incontinence can be aggravated by the appearance of pelvic organ prolapse;
- urinary incontinence may be present in the latent state, i.e. be masked by the presence of prolapse. This situation is not always easy to identify and occurs, for example, in cases of obstructive cystocele, i.e. when there is a large cystocele which

under tension, compresses the urethra and bladder neck, thus impeding the outflow of urine under stress;
- urinary incontinence can manifest after surgery to repair prolapse (bladder neck suspension with vaginal approach, colpoplasty), which alters the situation created by the obstructive colpocele and leads to a situation that until then was only potential.

In order to explain the etiologic relationship between prolapse of the anterior vaginal wall and urinary incontinence, a brief discussion of *transmission of abdominal pressure to the urethra* is required.

This phenomenon is particularly important in women. It originates from the intra-abdominal site of the proximal urethra and is a critical factor in the pathophysiology of *urinary stress incontinence.*

The pressure inside a normally situated, nonprolapsed urethra is greater than the bladder pressure. When the urethra is in its normal intra-abdominal position, a sudden increase in abdominal pressure (e.g. cough) causes an equal increase in pressure according to Laplace's law, in both the bladder and the upper two-thirds of the urethra. In this fashion the positive urethrovesical pressure gradient is maintained and so too is continence.

Recently a new mechanism of urinary incontinence has been defined, known as "urethral support". Under normal conditions the urethra, and especially the mid-cranial portion (i.e. the more important part from a functional point of view), is supported by the muscular-fascial structures of the anterior pelvic floor (pubocervical fascia, perineal membrane, pubourethral ligaments). In the event of a pressure increase the urethra is "compressed" against those structures, which if intact maintain the urethra in its place and enable its collapse and angulation with respect to the bladder base, with its subsequent closure. A good illustration of the concept is a garden hose. When the tube is trodden on, the flow of water within it is interrupted only if the hose rests on a solid "floor". If instead the hose is lying on sand, it will "sink in" under the weight, not collapse, and maintain the flow of water. The aim of modern urinary stress incontinence surgery lies precisely in restoring valid suburethral support against which the urethra may be "compressed" and therefore closed.

Pelvic organ prolapse may also negatively influence bladder emptying, causing acute and chronic urinary retention which may progress into high-grade hydroureteronephrosis and renal insufficiency (obstructive cystocele).

Gastrointestinal Dysfunction and Prolapse

The two pathologic intestinal presentations most frequently correlated with pelvic organ prolapse are alterations of continence and alterations of anorectal evacuation.

Fecal incontinence more commonly affects women with prolapse than the normal population, with an incidence of 17% of patients, and particularly, with the concomitant presence of urinary incontinence, sphincter hypotony or irritable bowel syndrome. Some 20% of patients with prolapse have a lengthened intestinal transit time. The use of imaging modalities such as defecography enables the visualization of associated pathologic conditions such as enterocele, rectal prolapse, invagination, etc.

Abrams PA, Cardozo L, Khoury S et al (2005) Incontinence. Health Publication Ltd, Paris

Baden WF, Walker TA (1972) Genesis of the vaginal profile. Clin Obstet Gynecol 15:1048

DeLancey JOL (1986) Correlative study of paraurethral anatomy. Obstet Gynecol 68:91-97

DeLancey JOL (1988) Structural aspects of extrinsic continence mechanism. Obstet Gynecol 72:296-301

Gosling JA (1985) The structure of the female lower urinary tract and pelvic floor. Urol Clin North Am 12:207

Lawson JO (1974) Pelvic anatomy. I. Pelvic floor muscles. Ann R Coll Surg Engl 54:244-252

Lawson JO (1974) Pelvic anatomy. II. Anal canal and associated sphincter. Ann R Coll Surg Engl 54:288-300

Norton PA (1993) Pelvic floor disorders. The role of fascia and ligaments. Clin Obstet Gynecol 36:926-938

Richardson AC (1993) The rectovaginal septum revisited: its relationship to rectocele and its importance in rectocele repair. Clin Obstet Gynecol 36:978-983

Pelvic Organ Prolapse: Imaging

Introduction

According to the literature, some 50% of women above 50 years of age have some degree of relaxation of the pelvic floor. Only 20% of these are symptomatic with the clinical problems associated with pelvic organ prolapse: voiding disturbances, incontinence, dyschezia.

Insufficient pelvic support at the origin of prolapse can involve three compartments:

- anterior, involving the urethra and urinary bladder;
- middle, involving the vagina and the uterus;
- posterior, involving the rectum and the rectouterine pouch.

In this setting the use of diagnostic imaging is often required for an accurate evaluation and correct treatment planning, in that the clinical examination can underestimate the degree of the condition.

Diagnostic imaging is called on to not only establish the integrity of the anatomic support structures responsible for the stasis of the endopelvic organs, but also to highlight the dysfunctions which can alter the relations between the same structures and which often become manifest only following a precise functional request.

On the basis of this premise, the choice of imaging modality in this clinical setting is based not only on the specific clinical request and considerations of invasiveness and cost, but also on the need of a dynamic-functional approach.

The imaging modalities currently available have a number of advantages and disadvantages.

Conventional radiology (cystourethrography, colpo-cysto defecography) performed with the use of contrast medium for the visualization of endopelvic organs offers the best morphofunctional evaluation of the urethra, the bladder neck and the rectum. However, the study cannot obtain information regarding the support system, if not indirectly. In most cases the radiographic study is limited to the evaluation of one or at most two pelvic compartments, whereas most support deficits are multicompartmental.

Ultrasonography enables the simultaneous visualization of the endopelvic organs, but only in the sagittal plane. In addition, the study is unable to offer a satisfactory exploration of the muscular and ligamentous support structures.

Magnetic resonance is able to provide a panoramic exploration, with the highest detail of the endopelvic organs and support structures, but is limited in the dynamic-functional examination.

Voiding Cystourethrography

Radiographic visualization of the urinary bladder after filling with iodinated contrast medium associated with the study of the urethra during voiding (VCUG) provides useful information for the characterization of forms of bladder prolapse. When the prolapse is associated with urinary disturbances the technique is especially useful in the study of incontinent patients. VCUG can also provide supplementary information in the presence of concomitant disease (tumors, fistulas, vesicoureteric reflux).

The bladder is filled via a catheter and distended until a strong voiding urge is felt by the patient. Sonographic studies have shown how the position and mobility of the vesicourethral junction are influenced by the degree of bladder filling. For this reason at least 300 mL of contrast medium should be introduced into the bladder.

The morphologic study is performed with the patient supine, in the anteroposterior and lateral views. In this particular clinical setting oblique views generally do not provide additional information.

At rest the distended bladder presents clear margins and is rounded in appearance. Lateral views are the most effective in outlining the profile of the bladder base, which normally appears rectilinear with an oblique course backwards and upwards. The site of the internal urethral orifice is easily identifiable situated at the passage between the anterior third and middle third of the bladder base, immediately above the plane passing through the inferior profile of the pubic symphysis. The static study is integrated with dynamic radiographs performed during provocative maneuvers (cough, strain, contraction), with the aim of indirectly evaluating, through modification of the position and morphology of the bladder, the pelvic support system in contraction and relaxation induced by the Valsalva maneuver.

Study of the voiding phase is performed in the lateral view, preferably with the patient seated. Voiding in the upright position is for many women an added embarrassment and can influence the results of the study.

The criteria for differentiating normal conditions from the presence of an alteration to the system of bladder support are numerous and include both quantitative (**Figs. 16.2, 16.3**) and qualitative parameters.

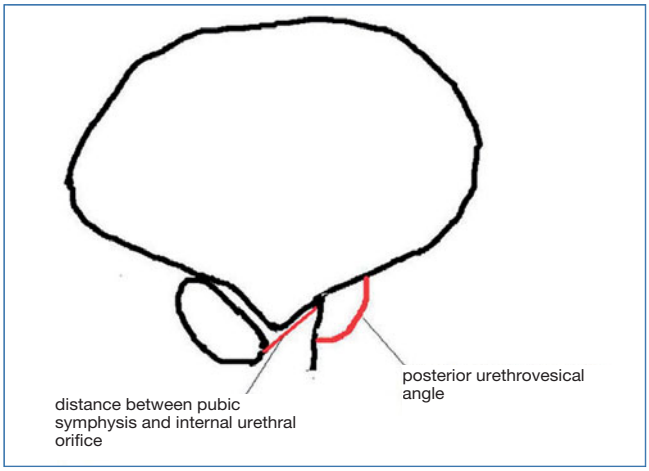

Fig. 16.2. Quantitative evaluation parameters of cystography

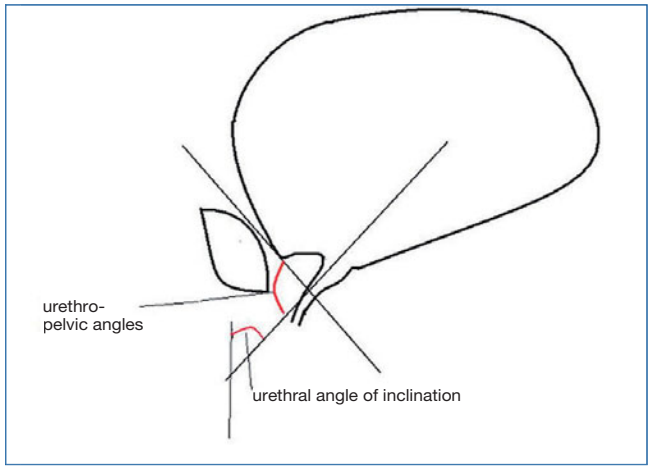

Fig. 16.3. Quantitative evaluation parameters of cystography

Quantitative Parameters

- Posterior vesicourethral angle: this is defined as the intersection between a tangent to the posterior margin of the urethra and a tangent to the bladder trigone. The normal value is less than 115°.
- Urethral inclination angle: this is defined as the angle of intersection between the posterior urethral axis and the vertical plane (the latter obviously varies with the degree of inclination of the patient). The normal value is less than 45°.
- Urethropelvic angle: this is measured during voiding, and is formed by the intersection between the urethral axis and the line joining the internal profile of the pubic symphysis with the inferior profile of the obturator foramen.
- Distance between internal urethral orifice and pubic symphysis: this is measured in conditions of rest and in the normal subject is around 30 mm. The threshold considered to be pathologic is 20 mm.

Qualitative Parameters

These include:
- morphology of the profile of the bladder base;
- identification of the point of greatest descent of the bladder base, anterior or posterior with respect to the internal urethral orifice;
- appearance of the bladder neck and urethra.

On the basis of the findings, bladder support defects can be divided into the following two categories.

Anterior Bladder Wall Support Defects

These are characterized by a reduction in the distance between the internal urethral orifice and the inferior profile of pubic symphysis, with values below 20 mm. In this event the bladder neck at rest or under strain has a funnel-shaped appearance (Fig. 16.4).

The anatomopathologic substrate is linked to a deficit of the fascial and ligamentous support system of the bladder (pubourethral and pubovesical ligaments).

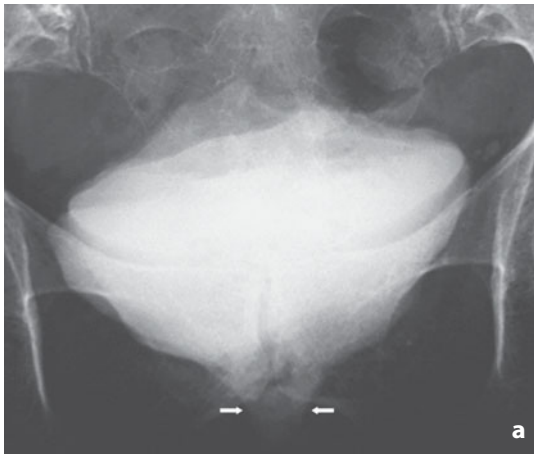

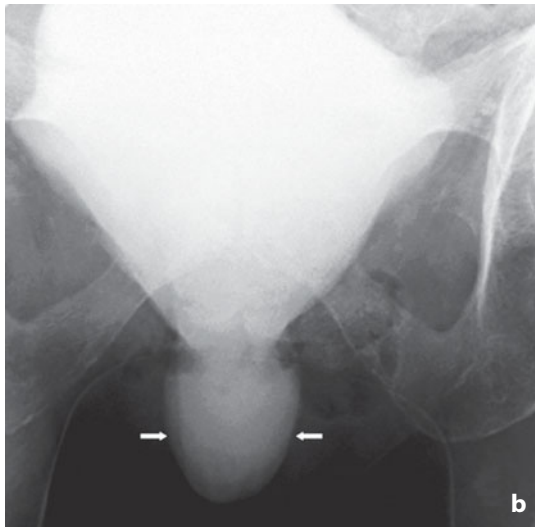

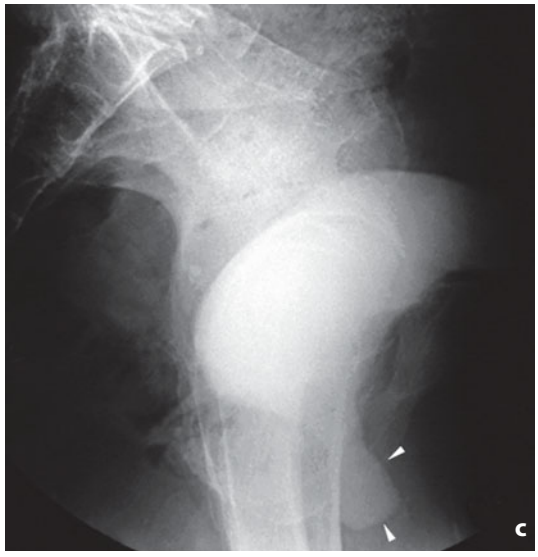

Fig. 16.4a-c. Cystography. **a** AP view at rest shows a lowering of the bladder base with a funnel-shaped appearance of the neck (*arrows*) due to a support defect of the anterior wall. **b** The descent of the bladder base exceeds the landmark of the ischial tuberosity. **c** Lateral view shows the prolapse of the anterior portion of the bladder base (*arrowheads*)

Posterior Bladder Wall Support Defects

These are believed to be the result of a deficit of the muscular support system and in particular of the pubovesical portion of the pubococcygeus muscle. In this category of alterations of the support system occurs an abnormal descent of the posteroinferior portion of the bladder base (Fig. 16.5) with a consequent reduction in the posterior vesicourethral angle (≤70°).

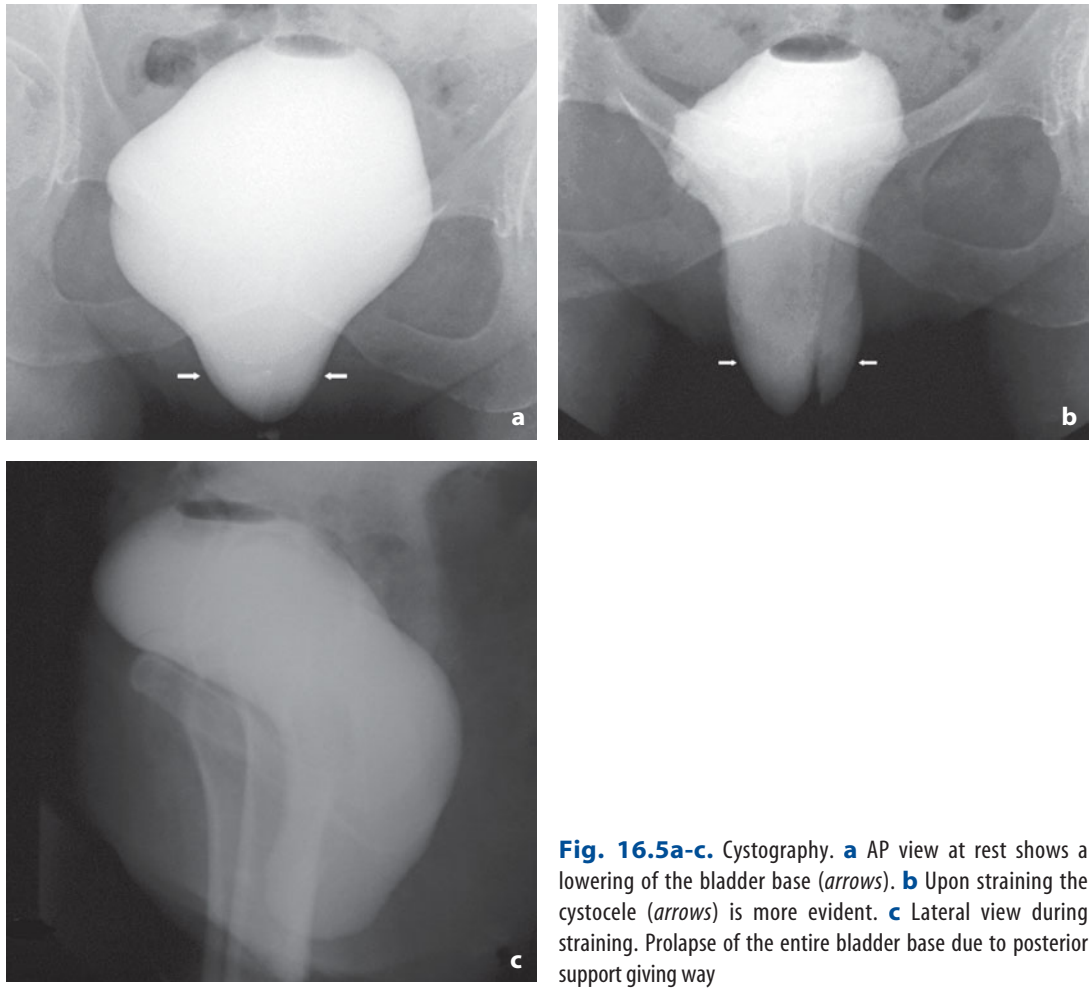

Fig. 16.5a-c. Cystography. **a** AP view at rest shows a lowering of the bladder base (*arrows*). **b** Upon straining the cystocele (*arrows*) is more evident. **c** Lateral view during straining. Prolapse of the entire bladder base due to posterior support giving way

Defecography

The first contrast-enhanced studies of the dynamic modifications of the pelvic floor and the rectum that occur during defecation were performed in the 1950s, although standardization of the technique came about in the 1980s with the studies by Mahieu. The rectum is opacified with barium contrast medium of a density high enough to mimic feces. The quantity of barium paste introduced varies from 120 to 300 mL in different studies.

The examination is performed with the patient seated on a special commode and images being acquired at rest, during straining, contraction, and evacuation and in the post-evacuation phase. The images are acquired with cineradiography (at least 2 radiographs per second) or videorecording to limit the equivalent dose delivered to the patient (4–9 mSv).

The mobility of the pelvic floor is evaluated in the various phases of the study with reference to the position of the anorectal junction with respect to the pubococcygeus line, which joins the inferior profile of the pubic symphysis at the last mobile segment of the coccyx. The significant threshold for prolapse is reached when the distance between the anorectal junction and the pubococcygeus line during straining or evacuation exceeds 7 cm. Other authors prefer to quantify the descent of the rectum with reference to the ischial tuberosity. In this case the pathologic threshold is 4 cm.

The descent of the anterior wall of the rectum, which exceeds the tangent to the anterior profile of the anal canal of the rectum by more than 2 cm with protrusion into

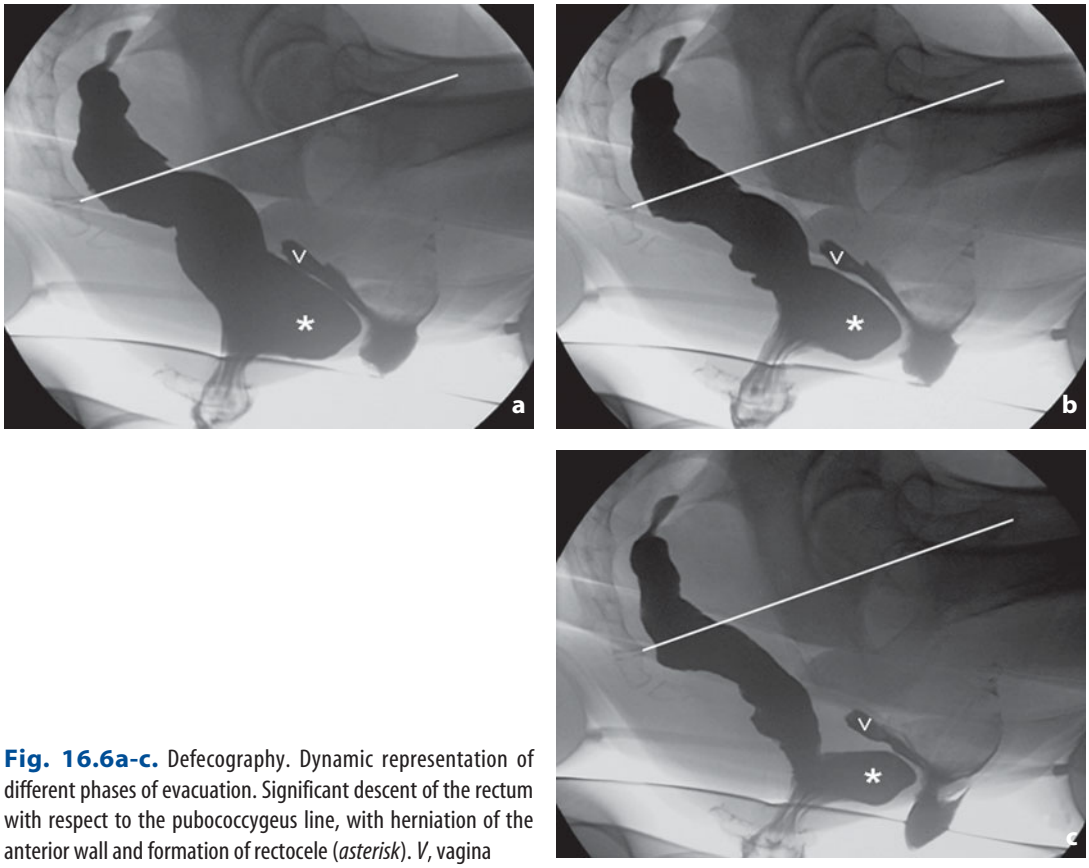

Fig. 16.6a-c. Defecography. Dynamic representation of different phases of evacuation. Significant descent of the rectum with respect to the pubococcygeus line, with herniation of the anterior wall and formation of rectocele (*asterisk*). *V*, vagina

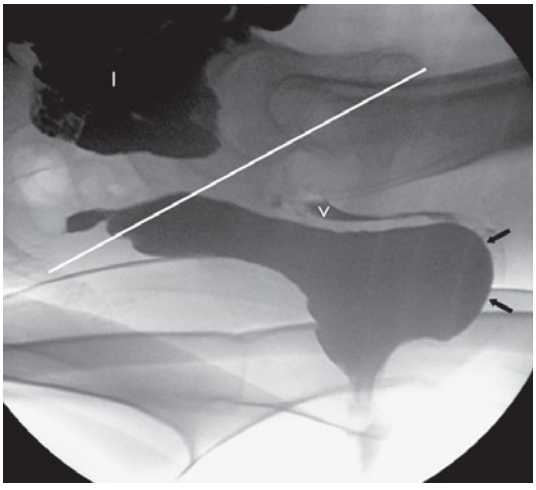

Fig. 16.7. Defecography in the evacuation phase. Abnormal descent of the rectum with respect to the pubococcygeus line with herniation of the anterior wall (*arrows*) and imprint on the vagina (*V*). The orally opacified loops of the small intestine (*I*) do not exceed the plane of the pubococcygeus line

the vaginal lumen, produces rectocele, which is frequently associated with prolapse (Fig. 16.6). Vaginal opacification during defecography improves the diagnostic sensitivity of the examination.

Abnormal descent of the small bowel through the rectovaginal septum with interposition between the rectum and bladder and consequent obstruction of defecation constitutes enterocele. In order to identify this anomaly with defecography the bowel loops need to be opacified with barium contrast medium 1–2 h before the examination (Fig. 16.7). This is, however, rarely performed due to the lengthening of diagnostic time.

Ultrasonography

US was first used in the urogynecologic setting in the 1980s and soon became a permanent feature of the examinations used in the diagnostic protocol of prolapse and associated disease. The advantages of US over other medical and imaging techniques (limited invasiveness, low cost, availability of devices, absence of ionizing radiation and contrast media, no catheter requirement) have made it the technique most accepted by both patients and operators. Its disadvantages are operator dependence, difficulty in defining the fascial and muscular support structures, and the fact that although US is able to visualize a number of pelvic organs and structures, it can only identify one anatomic landmark: the pubis.

US study of the pelvis is performed with different modalities. The choice of approach is based on the experience of the operator and the availability of appropriate equipment.

The use of **transabdominal US** is limited to patients with obstructive cystocele in the quantification of the postvoid residue and the evaluation of possible hydronephrosis.

Intraluminal US makes use of an end-fire transducer with a frequency of 5–9 MHz which can be used transvaginally or transrectally. It should be borne in mind that during the transvaginal approach the pressure exerted by the transducer can interfere with the correct visualization of the anatomy of the vaginal neck and the urethra. Therefore, despite being more invasive and less well tolerated by the patient, the transrectal approach is often preferred, especially when the US study is performed together with other urodynamic examinations. Intraluminal US is able to obtain a visualization of the endopelvic organs (bladder, uterus, urethra, pubis) in the sagittal plane.

In addition to end-fire transducers, mechanical and electronic radial intraluminal probes are also used, especially in transrectal evaluation of the anal sphincter and the puborectal muscle, but these also provide detailed visualization of the urethra.

Transperineal US makes use of "convex" transducers with frequencies of 3–6 MHz. Lastly, **introital US** utilizes a sector transducer with frequencies of 5–8 MHz, whereby the transducer is placed between the labia minora in contact with the vaginal opening. These two approaches enable a more panoramic view of the pelvis.

Evaluation of the bladder neck and urethra can be performed with the patient in the supine position, with lower limbs slightly abducted, or in the seated position or even with the patient erect. The study in the seated position, however, requires dedicated transducers to ensure adequate contact between the transducer and the perineum.

Although bladder mobility is maximum with the patient in the erect position, comparative studies indicate that variations in the position of the bladder and the bladder neck linked to patient position are mild.

US study is not limited to dynamic evaluation of the morphology and position of the endopelvic organs at rest and during provocative maneuvers, but also involves performing several measurements to obtain parameters of quantitative evaluation (**Fig. 16.8**), the most important of which are:

- **retrovesical angle** (β), measured by the intersection of the axis of the urethral canal with the tangent of the bladder base;
- **position of the inner urethral orifice**, calculated with reference to the pubic symphysis by a system of Cartesian coordinates proposed by Schaer in which the x-axis represents the median line passing through the pubic symphysis and the y-axis is reconstructed by tracing a line perpendicular to the x-axis at the level of the inferior profile of the pubic symphysis. The exact position of the internal urethral orifice is therefore calculated by measuring the distance Dx, which separates the bladder neck from the y-axis, and the distance Dy, which separates the bladder neck from the x-axis. To identify the position of the bladder neck the transition point between the superior anterior urethral wall and the bladder is taken as a reference.

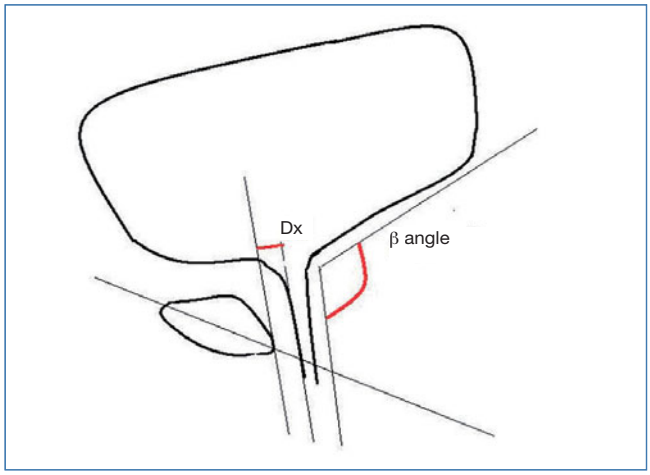

Fig. 16.8. Ultrasonography parameters of quantitative evaluation

As an alternative to the method described, the position of the internal urethral orifice can be calculated according to the method proposed by Creighton. This involves measuring the line which separates the bladder neck and the inferior margin of the pubic symphysis and calculating the angle, known as the pubourethral angle, formed between this line and the median line passing through the pubic symphysis. The accuracy of both methods has been validated in the literature.

In order to maximize the accuracy and reproducibility of the US study, the ICS has formulated recommendations for standardizing the study, which include:

- position of the patient: supine to maximize comfort, seated or erect to improve the evaluation of the bladder neck;
- bladder filling: 300mL;
- provocative maneuvers: the study should be conducted not only at rest, but also during the Valsalva maneuver, which induces relaxation of the pelvic muscles and better enables evaluation of the organ descent (**Figs. 16.9, 16.10**); during voluntary contraction to evaluate the pelvic muscle tone, e.g. after rehabilitative therapy; during reflexive contraction induced by cough;
- measurements: these should include definition of the position of the internal urethral orifice and the retrovesical angle.

Once these conditions have been satisfied, the data in the literature show that the intra- and interobserver variability are not statistically significant.

The current limitations of the technique include the visualization of the endopelvic organs only in the sagittal plane, the insufficiently panoramic views and only partial visualization of the muscular and ligamentous support structures. However, these may be partially overcome in the future thanks to technologic developments and the availability of US devices able to perform a three-dimensional study. Recent developments in 3D techniques have opened up new prospects in the diagnostic setting, for example enabling detailed visualization of structures such as the striated sphincter and the submucosal vascular plexus of the urethra (**Fig. 16.11**).

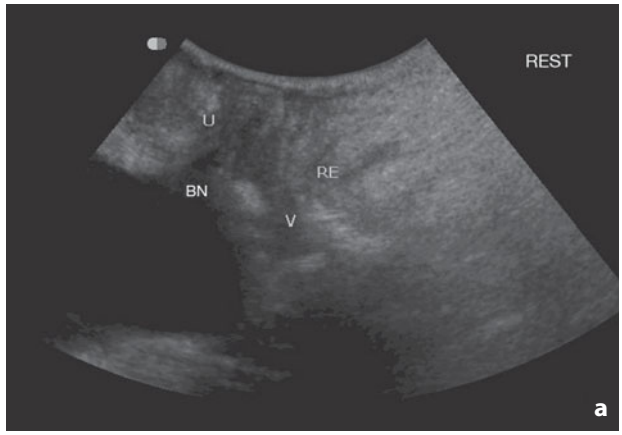

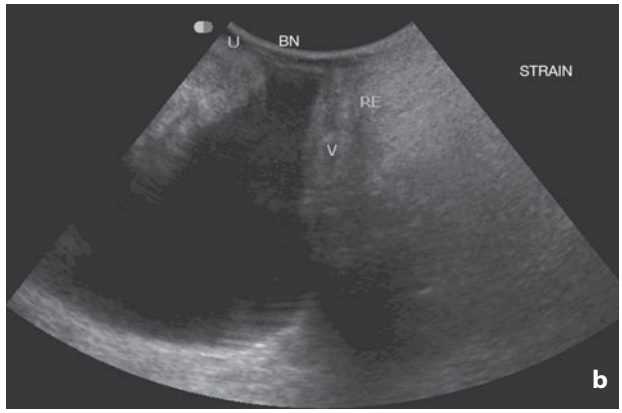

Fig. 16.9a,b. Introitus ultrasonography. **a** Median sagittal scan at rest. The relations between the pelvic organs are normal. **b** Under stress a descent of the bladder base is visible, which reaches the perineal plane, with the urethra in near horizontal position (cystocele). *BN*, bladder neck; *U*, urethra; *V*, vagina; *RE*, rectum

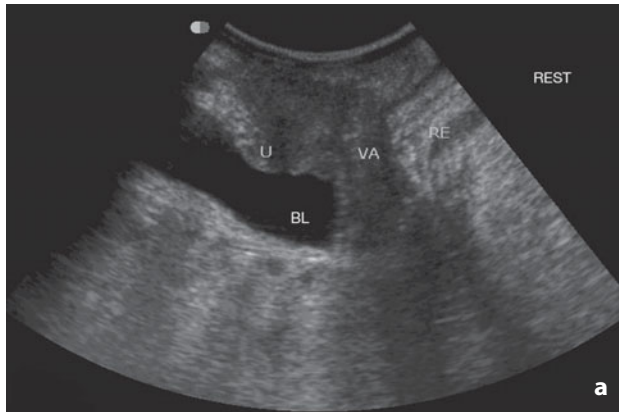

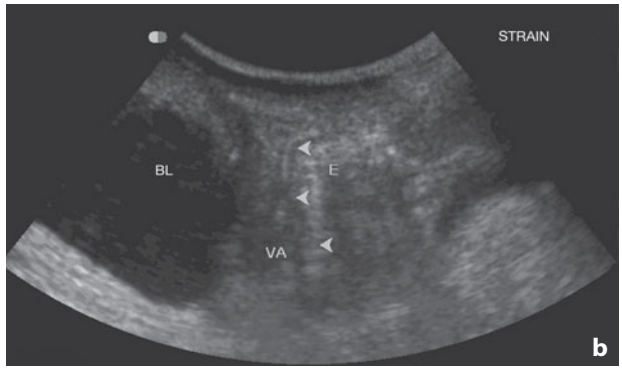

Fig. 16.10a,b. Introitus ultrasonography. **a** At rest panoramic view of the pelvic organs which preserve their normal appearance. **b** During straining enterocele appears (*E*) with herniation of bowel loops in the rectovaginal septum and an imprint on the posterior vaginal wall (*arrowheads*). *BL*, urinary bladder; *U*, urethra; *VA*, vagina; *RE*, rectum

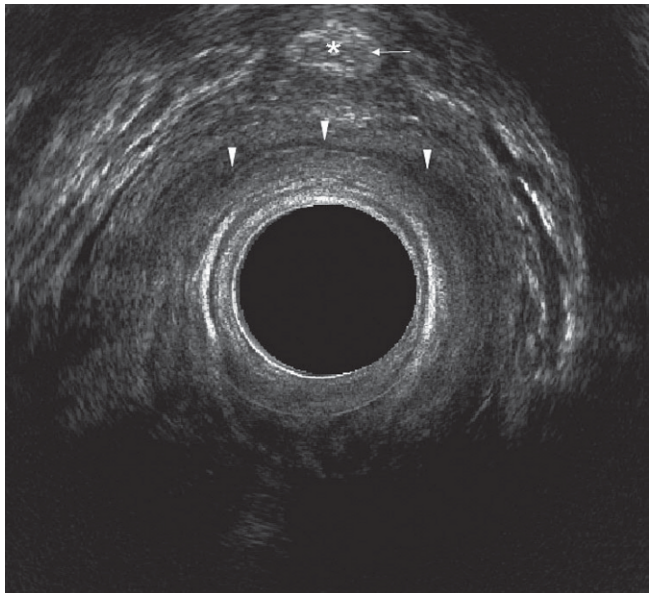

Fig. 16.11. 3D ultrasonography with electronic rotating transrectal transducer. Scan above the plane of the sphincter at the level of the hiatus of the levator ani muscle. Axial view of the vagina (*arrowheads*) and the urethra (*U*) with detailed visualization of the submucosa (*arrow*)

Magnetic Resonance

Pelvic floor dysfunctions have a complex anatomic substrate: cystocele, uterine prolapse, rectocele and enterocele often tend to coexist and even patients who have clinical signs and symptoms related to a specific pelvic region often suffer from multicompartmental alterations. The diagnosis of concomitant abnormalities is absolutely necessary for treatment planning – reconstructive surgery risks not obtaining the desired results when the defects of the respective compartments are not corrected.

Magnetic resonance (MR) is the only imaging method able to bring together the features of accurate and multiplanar views of all the pelvic organs and muscles in a single noninvasive examination without the use of ionizing radiation.

Study with surface coils and conventional T1-weighted sequences and T2-weighted spin echo sequences is able to accurately define the anatomy of the pelvic organs and fibromuscular and ligamentous support system and to identify possible concomitant disease.

The use of endovaginal coils enables a more detailed visualization of the anatomy of the urethra. However, distortion of the normal anatomy caused by the pressure exerted by the coil constitutes a limitation to the technique.

The accuracy of conventional MR is contrasted by the impossibility of performing a dynamic study in the search for prolapse or giving way of the pelvic muscles due to the excessively long acquisition times. The relatively recent introduction of fast "single shot" sequences characterized by sufficient temporal resolution (acquisition time 1-2 s) has made a dynamic-functional study possible. Dynamic MR utilizes single, shot fast spin echo, half-Fourier snapshot turbo spin echo (HASTE) or true fast imaging steady-state precession (true FISP) sequences. The acquisitions are performed in the sagittal plane at the level of the median line, with a slice thickness of 6-10 mm and are repeated at rest, during voluntary contraction and during straining. In this manner a sequence of images is obtained which can be continuously re-evaluated at the workstation (cine MR).

Indications in the literature enable a protocol to be drawn up which limits the study time to 15 min and which includes:

- a morphologic study with T2-weighted fast-spin echo sequences acquired in the axial plane to define the pelvic anatomy and identify the presence of concomitant disease;
- a dynamic study with median sagittal and possibly also coronal acquisitions at rest, during contraction and during straining.

Variations in the position of the endopelvic organs is evaluated with reference to precise anatomic landmarks (**Fig. 16.12**).

The **pubococcygeus line** joins the inferior margin of the pubic symphysis with the last mobile joint of the coccyx, which corresponds to the point of insertion of the levator ani muscle. This line represents the plane of the levator ani muscle.

The **H line** bounds the distance between the inferior margin of the pubic symphysis and the insertion of the pubococcygeus muscle in the rectum. This line represents the breadth of the hiatus of the pubococcygeus muscle, which surrounds the urethra, the vagina and the rectum.

The **M line**, perpendicular to the pubococcygeus line at the intersection point of the H line with the rectum, enables the degree of descent of the levator ani muscle to be measured in relation to the pubococcygeus line.

In the normal population, during straining the breadth of the hiatus of the pubococcygeus muscle, which corresponds to the H line, has values less than 6 cm. The descent with respect to the pubococcygeus line (M line) does not exceed 2 cm.

In descending perineum syndrome a lengthening of the H line and the M line is observed. The degree of relaxation of the pelvic floor is classified as follows:

Grade 1 (mild): H line 6-8 cm; M line 2-4 cm
Grade 2 (moderate): H line 8-10 cm; M line 4-6 cm
Grade 3 (severe): H line 10 cm and above; M line 6 cm and above.

The position of the endopelvic organs in the normal subject, both at rest and during straining, is above the H line. Exceeding this anatomic landmark constitutes prolapse, which is classified as follows:

Grade 1 (mild): exceeding the H line by up to 2 cm
Grade 2 (moderate): exceeding the H line by 2-4 cm
Grade 3 (severe): exceeding the H line by more than 4 cm.

In dysfunction of the support system of the anterior and middle compartments, in which cystocele and vaginocele occur (**Figs. 16.13, 16.14**), other characteristic features may be observed:

- descent of the vesicourethral junction and the vaginal vault below the pubococcygeus line during straining;
- horizontal position of the urethra with a vertical inclination angle of the urethra >30°;
- vesicourethral angle >115%;
- lengthening of the H line which exceeds 5 cm;
- lengthening of the M line which exceeds 2 cm;
- convex appearance of the levator ani muscle recognizable in axial and coronal planes.

Dysfunction of the support system of the posterior compartment manifests in rectocele (**Fig. 16.15**), which is frequently associated with enterocele. The characteristic features of rectocele are:

- abnormal descent of the rectum and the rectovaginal septum;
- herniation of the anterior wall of the rectum due to the rectovaginal septum giving in, with protrusion exceeding the plane tangent to the anterior wall of the anal canal by at least 2 cm;
- lengthening of the M line by at least 2 cm.

In enterocele a herniation of the peritoneum is observed in which the bowel loops become lodged between the rectum and the vagina, exceeding the reference of the

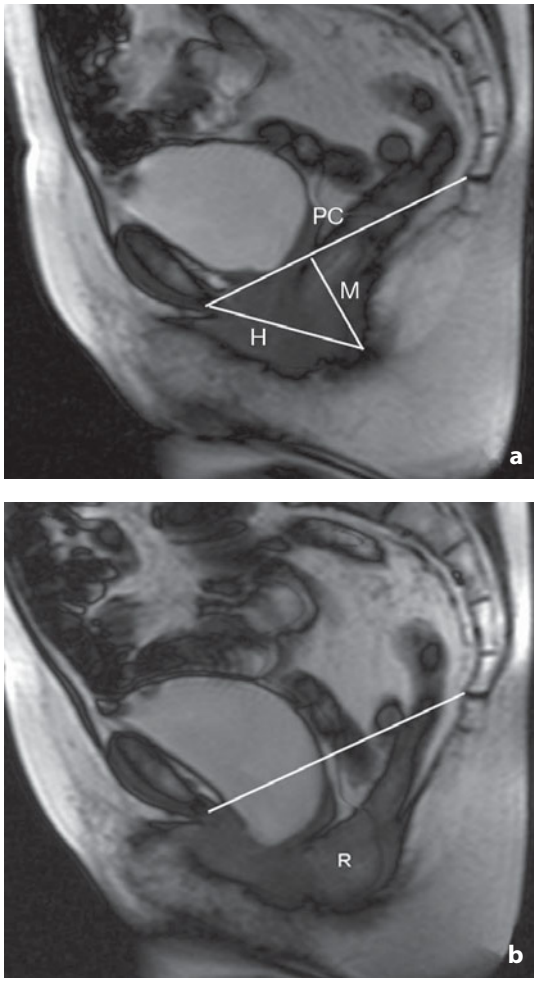

Fig. 16.12a,b. Dynamic magnetic resonance of the pelvis. Median sagittal scan with T2-weighted "single-shot" true FISP sequences. **a** At rest, the position of the pelvic organs is normal with respect to the reference pubococcygeus (*PC*), *H* and *M* lines. **b** During straining the bladder base descends beyond the pubococcygeus line producing grade 1 cystocele. Rectocele (*R*) is also identifiable

pubococcygeus line by at least 2 cm. A more rare occurrence is involvement of the sigmoid colon (sigmoidocele).

MR is the reference standard for the identification of enterocele. The sensitivity of the technique (87%) is higher than that of defecography and clinical examination.

In the examination of rectocele the rectum needs to be filled with gel and the dynamic study needs to be performed in the evacuation phase as well. Once these conditions have been met, the sensitivity in identifying rectocele is very high, although the performance of MR is still significantly inferior to defecography in identification of the mucous lesions frequently associated with this condition, such as mucous prolapse and invagination.

Despite its numerous advantages, MR is still not used in the routine diagnostic protocol of prolapse. The main limitation to the technique lies in the fact that in most cases the study can only be performed in the supine position and therefore in non perfect physiologic conditions. The seated position is only possible with open magnet systems. There is agreement in the literature for indicating the technique only in select cases, e.g. when physical examination is difficult, in the search for occult enterocele, or in cases of failed surgical repair to identify dysfunction in other compartments.

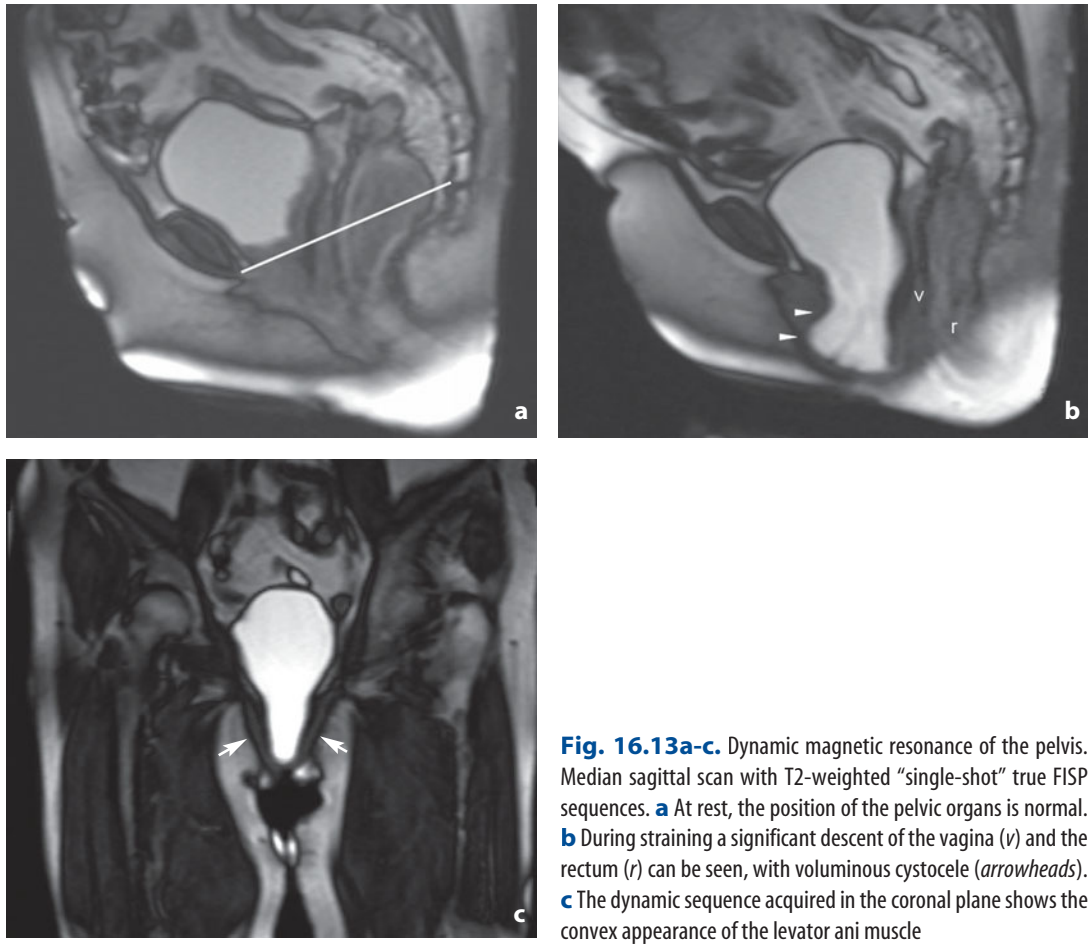

Fig. 16.13a-c. Dynamic magnetic resonance of the pelvis. Median sagittal scan with T2-weighted "single-shot" true FISP sequences. **a** At rest, the position of the pelvic organs is normal. **b** During straining a significant descent of the vagina (*v*) and the rectum (*r*) can be seen, with voluminous cystocele (*arrowheads*). **c** The dynamic sequence acquired in the coronal plane shows the convex appearance of the levator ani muscle

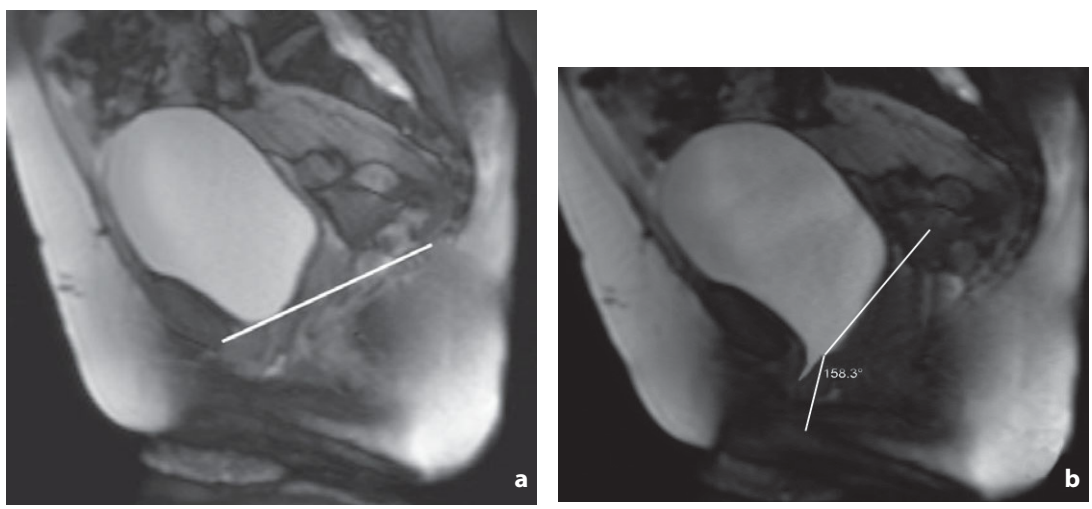

Fig. 16.14a,b. Dynamic magnetic resonance of the pelvis. Median sagittal scan with T2-weighted "single-shot" true FISP sequences. **a** At rest, the position of the pelvic organs is normal. **b** During straining a nonsignificant descent of the bladder base can be seen, but with involuntary loss of urine and increase in the posterior vesicourethral angle

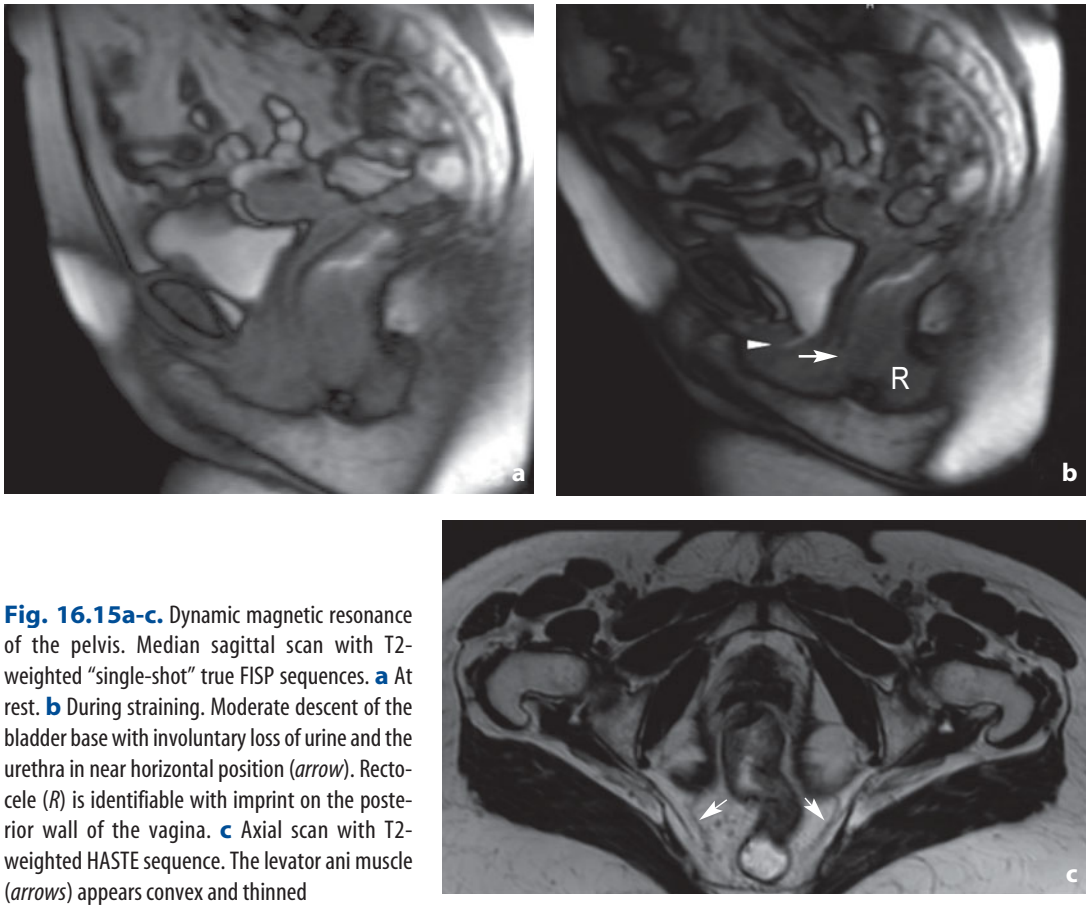

Fig. 16.15a-c. Dynamic magnetic resonance of the pelvis. Median sagittal scan with T2-weighted "single-shot" true FISP sequences. **a** At rest. **b** During straining. Moderate descent of the bladder base with involuntary loss of urine and the urethra in near horizontal position (*arrow*). Rectocele (*R*) is identifiable with imprint on the posterior wall of the vagina. **c** Axial scan with T2-weighted HASTE sequence. The levator ani muscle (*arrows*) appears convex and thinned

Bartram C (2003) Dynamic evaluation of anorectum. Radiol Clin North Am 41:425-441

Brubaker L, Heit MH (1993) Radiology of the pelvic floor. Clin Obstet Gynecol 36:952-959

Creighton SM, Pearce JM, Stanton SL (1992) Perineal video-ultrasonography in the assessment of vaginal prolapse. Br J Obstet Gynecol 93:310-313

Dalpiaz O, Curti P (2006). Role of perineal ultrasound in the evaluation of urinary stress incontinence and pelvic organ prolapse: a systematic review. Neurourol Urodyn. 25:301-306

Fielding JR (2002) Practical imaging of pelvic floor weakness. RadioGraphics 22:295-304

Gufler H, De Gregorio G, Allmann KH et al (2000) Comparison of cystourethrography and dynamic MRI in the determination of bladder neck descent. J Comput Assist Tomogr 24:382-388

Kelvin FM, Maglinte DD, Hale DS et al (2000) Female organ prolapse: a comparison of triphasic dynamic MR imaging and triphasic fluoroscopic cystocolpoproctography. AJR Am J Roentgenol 174:81-88

Maglinte DD, Kelvin FM, Fitzgerald K et al (1999) Association of compartment defects in pelvic floor dysfunction. AJR Am J Roentgenol 172:439-444

Olesen KP (1983) Descent of the female urinary bladder. A radiological classification based on colpo-cysto-urethrography. Dan Med Bull 30:66-84

Pannu HK (2004) MRI of pelvic organ prolapse. Eur Radiol 14:1456-1464

Tubaro A, Carter J (2002) The standardisation of ultrasound imaging of the bladder. www.icsoffice.org

Wetsby M, Ulmetsen U, Asmussen M (1983) Dynamic urethrocystography in women. Urol Int 38:329-336

Part VII
Disease of the Female Reproductive System

Endometriosis, Pelvic Pain: Clinics and Imaging

17

G.M. Ciravolo, F. Rampinelli, G. Morana, A. Guarise

Introduction

Endometriosis is one of the most common diseases in gynecology, even though its epidemiology is still relatively unknown. This derives from the fact that the diagnosis of endometriosis, according to current clinical opinion, should be made through the "direct" or surgical visualization of the disease or through histologic confirmation. Deeply infiltrating endometriosis (DIE) (>5 mm) is the most complicated and symptomatic form and is found in 30-40% of patients with endometriosis. Often the disease involves the uterosacral ligaments, the rectouterine pouch, the retrocervical tissue, the bladder, the ureter, the vagina and the intestine.

Cornillie F, Oosterlynck D, Lauweryns JM et al (1990) Deeply infiltrating pelvic endometriosis: histology and clinical significance. Fertil Steril 53:978-983

Koninckx PR, Meuleman C, Demeyere S et al (1991) Suggestive evidence that pelvic endometriosis is a progressive disease, whereas deeply infiltrating endometriosis is associated with pelvic pain. Fertil Steril 55:759-765

Rectovaginal Endometriosis

This is the most important form of DIE and consists of endometrial nodules (in which the fibrous component is prevalent) located within the connective tissue of the anterior rectal wall and the vagina. The rectovaginal lesion may extend to the superficial muscular layer or more deeply to the mucosa of the rectum and/or vagina.

Intestinal Endometriosis

This is the most common extragenital location of endometriosis and accounts for 3-37% of all cases. The sites affected by the disease, in decreasing order of frequency, are the rectosigmoid (74%), rectovaginal septum (12%), ileum (7%), cecum (4%) and appendix (3%). Endometriosis of the rectosigmoid, therefore, accounts for some 70% of all intestinal forms and is associated in 80% of cases with genital endometriosis. Intestinal endometriosis is typical in women of fertile age, with an elevated frequency between 25 and 40 years.

The course of the disease may be asymptomatic if confined to the external layer of the intestinal wall, i.e. the serosa, and is without infiltrative growth. However, under the influence of the hormone cycle the endometrial tissue can proliferate and invade the intestinal wall, generating clinical symptoms of irritation and obstruction related above all to postprandial intestinal movement or defecation. The main symptoms are cramping pain, abdominal distension, flatulence, painful tenesmus, hyperperistalsis and progressive constipation. Intestinal obstruction is a possible complication

L. Olivetti, L. Grazioli (eds.), *Imaging of Urogenital Diseases*,

of endometriosis. McGuff has identified the following forms of obstruction:
- annular, characterized by a concentric restriction of the intestinal lumen;
- polypoid submucosal infiltration;
- scarring with angulation;
- combined infiltration and torsion.

The highly challenging diagnosis involves an accurate patient history, clinical examination and imaging techniques capable of providing adequate preoperative information.

McGuff P (1948) Endometriosis as a cause of intestinal obstruction. Surg Gynec Obstet 86:273-288

Vercellini P, Chapron C, Fedele L et al (2004) Evidence for asymmetric distribution of lower intestinal tract endometriosis. BJOG 111:1213-1217

Weed J, Ray JE (1987) Endometriosis of the bowel. Obstet Gynecol 69:727-730

Endometriosis of the Urogenital Tract

This form has an incidence of 1.2% with a ratio between the urinary bladder, ureter and urethra of 40:5:1. It is usually associated with scattered localizations elsewhere in the pelvis, although in these patients the symptoms related to the urinary tract may be the first and sometimes the only ones. Ureteric endometriosis is rare, with an incidence of 0.1-1% of all women affected by endometriosis. Due to the association with asymptomatic renal obstruction, the literature reports an incidence of loss of renal function and subsequent nephrectomy between 23% and 47%. Although cases have been described of bilateral ureteric involvement in patients with extensive pelvic endometriosis, the lesion is mostly asymmetric and commonly involves the distal segment of the left ureter. Ureteric endometriosis can be subdivided into extrinsic, which is the most common form (80%) and occurs when the glandular and stromal endometrial tissue is within the submucosa and the adventitia, and intrinsic (20%), which occurs when the uroepithelium and the submucosa are involved.

Stillwell TJ, Kramer SA, Lee RA (1986) Endometriosis of ureter. Urology 28:81-85

Yates-Bell AL, Molland EA, Pryor JP (1972) Endometriosis of the ureter. Br J Urol 44:58-67

Yohannes P (2003) Ureteral endometriosis. J Urol 170:20-25

Imaging

The gross anatomopathologic appearance is rather variable and depends on a number of factors, including the duration of the disease and the location of the lesions – whether superficial or deep – with respect to the peritoneal surface. Therefore, even the ultrasonography (US) and magnetic resonance (MR) appearances reported in the literature are extremely variable.

The morphology is heterogeneous, with disease manifesting as a neoformation proper located within the pelvic cavity or viscera, or simply as a defect of the peritoneal surface. Alternatively, lesions may be nodular and/or cystic and variable in size and number. Rarely, pelvic-peritoneal endometriosis may appear as multiple polypoid masses which invade the entire pelvic cavity mimicking a malignant tumor.

The US appearance is influenced by the structure of the endometrial implants, which most commonly are nodular (secondary to reactive fibrosis) or cystic (secondary to hemorrhage), by their size, which may vary from a few millimeters to several centimeters, and by the presence or absence of adhesions. The lesions may

involve different anatomic sites and tend to be more easily identifiable when they involve structures which can be more easily accessed with US. They are generally hypoechoic, which can render their distinction from the adjacent structures or the loose connective tissue containing them difficult. At other times they have a mixed appearance due to the presence of echogenic nodules, whereas on rare occasions they may appear hyperechoic.

The MR appearance of endometriosis is instead influenced by the characteristics of the hemorrhagic content of the lesions, and especially by the time elapsed between the hemorrhagic episode and the time of examination (**Diagram 17.1**).

The main morphologic appearances of the lesions are listed below as identified by both imaging techniques. Multiple appearances are often identified in the same patient.

a) Small nodules (several millimeters in diameter) are most commonly located in the rectovaginal septum and less frequently in the vesicovaginal septum. The identification of lesions of the rectovaginal septum occurs especially when they have a hypoechoic appearance (**Fig. 17.1a**), since the identification of hyperechoic lesions is much more rare (**Fig. 17.1b**). The MR study with fat saturation is able to identify these small lesions as small foci of signal hyperintensity in T1-weighted sequences (**Fig. 17.2**).

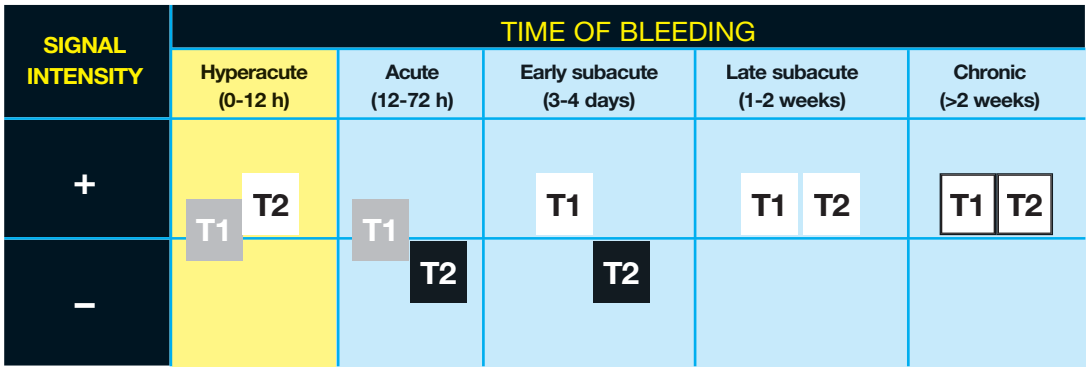

Diagram 17.1. Different content of haemoglobin degradation products, related to the time of bleeding, influence the imaging findings of endometriosis on *T1* and *T2* weighted images. The followings are the aspects of the endometriotic cysts in relation to the time of bleeding: *hyperacute phase*, the lesion is hypo-isointense on T1 and hyperintense on T2 weighted images; *acute phase*, the lesion is hypo-isointense on T1 and hypointense on T2 weighted images; *early subacute phase*, the lesion is hyperintense on T1 and hypointense on T2 weighted images; *late subacute phase*, the lesion is hyperintense on T1 and T2 weighted images; *chronic phase*, the lesion is hyperintense on T1 and T2 weighted images with a hypointense rim.

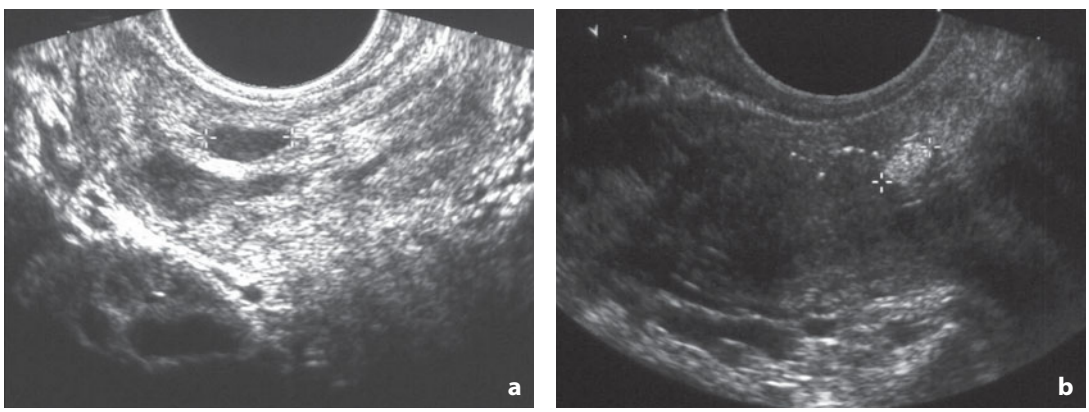

Fig. 17.1a,b. Transrectal ultrasonography. Endometriosis of the rectovaginal septum. Hypoechoic (**a**) and hyperechoic (**b**) solid endometrial nodule can be identified in the rectovaginal septum (*crosses*)

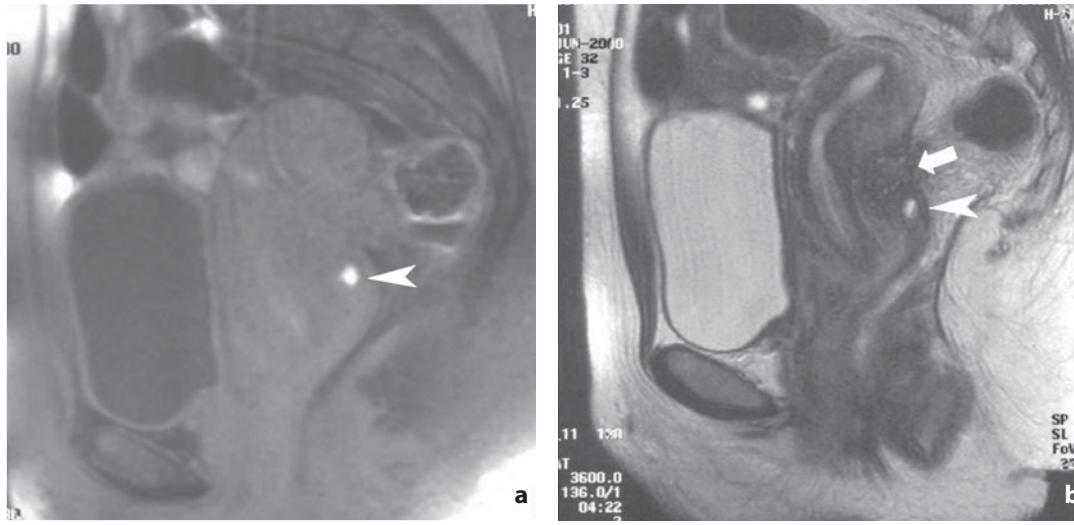

Fig. 17.2a,b. Magnetic resonance. Endometriosis of the posterior vaginal fornix. Straightened retroflex uterus. Small endometrial nodule in the posterior vaginal fornix (*arrowhead*) appears hyperintense in both the T1-weighted sequence with fat-signal suppression (**a**) and the T2-weighted sequence (**b**) in which the blood-fluid level is better identifiable. An adjacent plaque of uterine adenomyosis can also be seen (*arrow*)

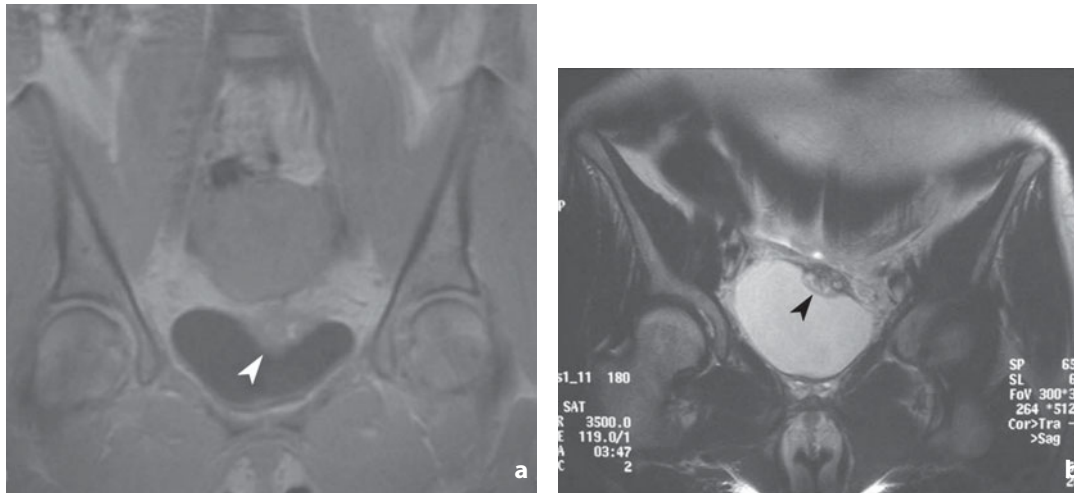

Fig. 17.3a,b. Magnetic resonance. Bladder endometriosis. Solid nodule in the superior bladder wall modifying the appearance of the mucosal surface. The nodular lesion (*arrowhead*) appears isointense to the muscular wall in the T1-weighted sequence (**a**) with hyperintense internal microfoci, and hyperintense in the T2-weighted sequence (**b**)

b) Large nodules (diameter >1.5-2 cm) can be found in various sites. Their US appearance is prevalently hypoechoic. On MR, solid fibrotic nodules are characterized by intermediate signal intensity in T1-weighted sequences. Foci of signal hyperintensity may be identified within the lesions. The lesions are enhancing after the administration of contrast medium, with bladder lesions presenting this appearance in most cases (**Fig. 17.3**).

c) Laminar lesions, like the small nodules, can be identified mainly in relation to the thickness of the rectovaginal septum and can have variable thickness up to appearing as a plaque proper. These lesions also have a hypoechoic appearance on US (**Fig. 17.4**). On MR they are characterized by signal hyperintensity in T1-weighted sequences and variable signal in T2. Both techniques have difficultly identifying laminar lesions situated at the peritoneal level (**Fig. 17.5**).

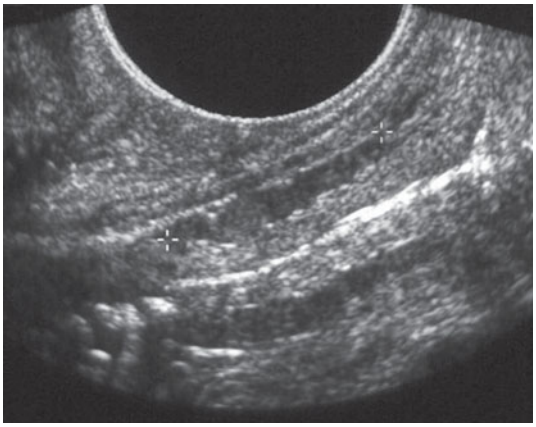

Fig. 17.4. Transrectal ultrasonography. Endometriosis of the rectovaginal septum. A solid hypoechoic plaque is visible in the rectovaginal septum (*crosses*)

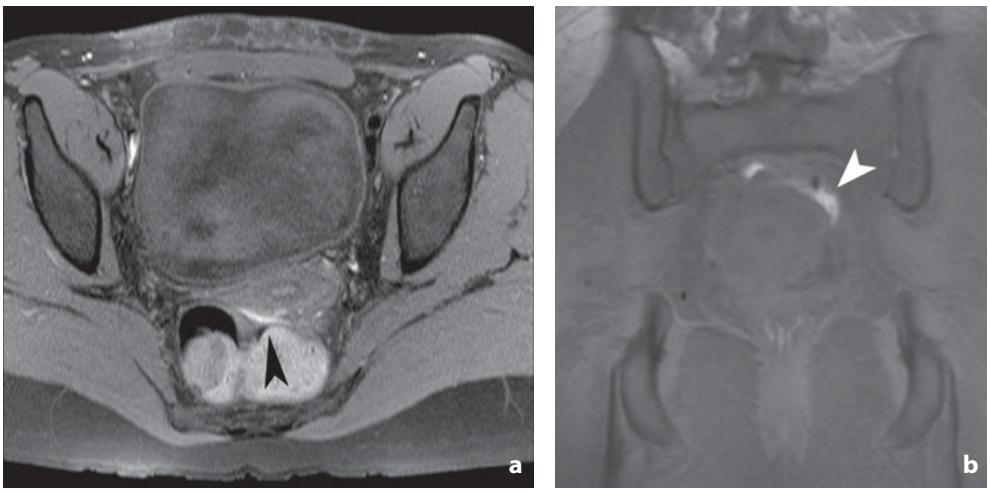

Fig. 17.5a,b. Magnetic resonance. Peritoneal endometriosis. Axial (**a**) and coronal (**b**) T1-weighted image with fat signal suppression show endometriosis with laminar appearance (*arrowhead*)

d) Cystic lesions can have a diameter varying from a few millimeters to several centimeters and a markedly heterogeneous appearance on US and MR. Endometrial cysts (also known as endometriomas) commonly involve the ovary, the normal tissue of which can be partially or completely replaced. Bilateral involvement occurs in 30–50% of cases. The cysts rarely have a diameter exceeding 10 cm. Larger formations are often the expression of neoplastic degeneration.

Only rarely is the content of the cysts exclusively liquid. More often it is made up of a chocolate-colored dense or semi-liquid material, hence the name "chocolate cyst". On US the lesion may appear as a simple thin-walled cyst (**Fig. 17.6a**), or as a complex cyst (**Fig. 17.6b,c**) or even as a solid adnexal mass. The typical finding on suprapubic and intraluminal US is a cystic mass with homogeneous, diffuse, low-level internal echoes with increased through-transmission (**Fig. 17.6a**).

In addition, the cysts tend to be well-encapsulated and over time form a fibrous capsule with numerous adhesions. These formations, which are essentially found at the level of the ovary, can mimic other lesions with a similar appearance: functional cysts, abscess, hemorrhagic luteal body, neoplasm or dermoid cysts.

More rarely the endometriomas may appear completely anechoic and occasionally present fluid-fluid levels. Color Doppler study is able to demonstrate flow around, but not within, these masses (**Fig. 17.6c**). This is also the case with simple cysts, so it is an aspecific finding.

On MR the endometriomas typically appear as a hyperintense mass (signal the same or higher than fat) in T1-weighted sequences and hypointense (usually with a progressive decrease in signal intensity towards the sloping portions: "shading effect") in T2-weighted sequences. This sign is highly specific and is due to the stratification of the high-viscosity contents derived from repeated episodes of hemorrhaging (Fig. 17.7). In some cysts a hypointense rim may be observed in T1- and T2-weighted sequences due to the presence of fibrous walls containing hemosiderin-laden macrophages (Fig. 17.8). This fibrous capsule enhances with the administration of contrast medium due to its highly vascular structure.

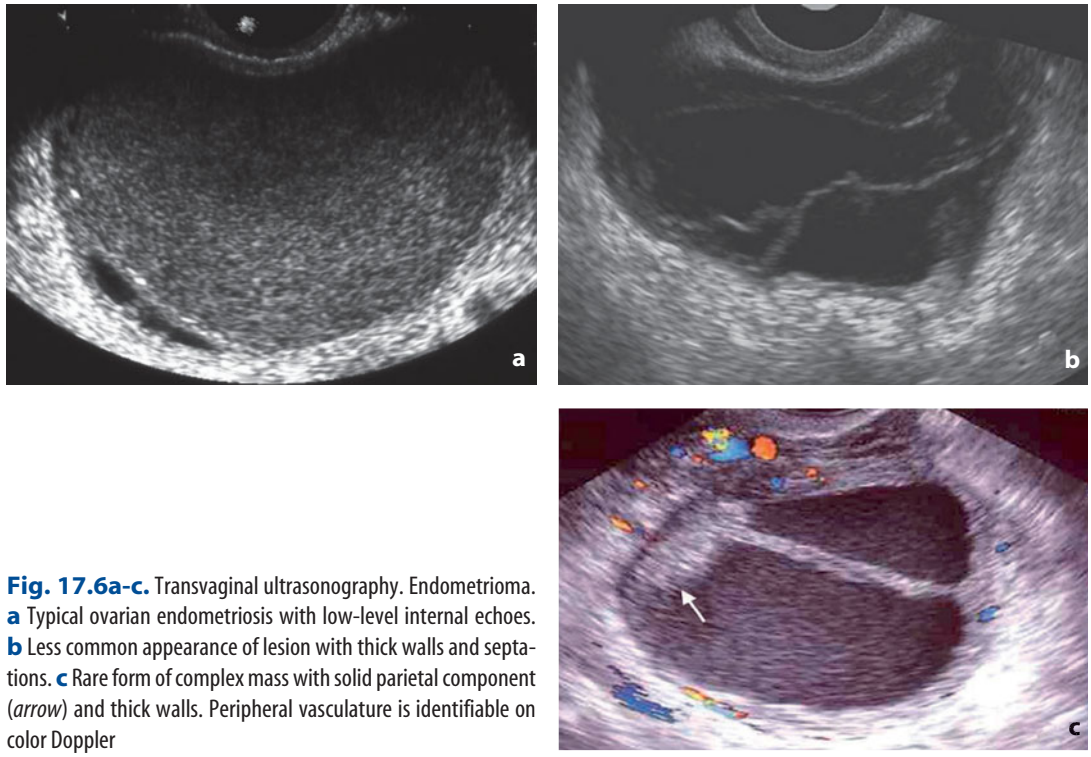

Fig. 17.6a-c. Transvaginal ultrasonography. Endometrioma. **a** Typical ovarian endometriosis with low-level internal echoes. **b** Less common appearance of lesion with thick walls and septations. **c** Rare form of complex mass with solid parietal component (*arrow*) and thick walls. Peripheral vasculature is identifiable on color Doppler

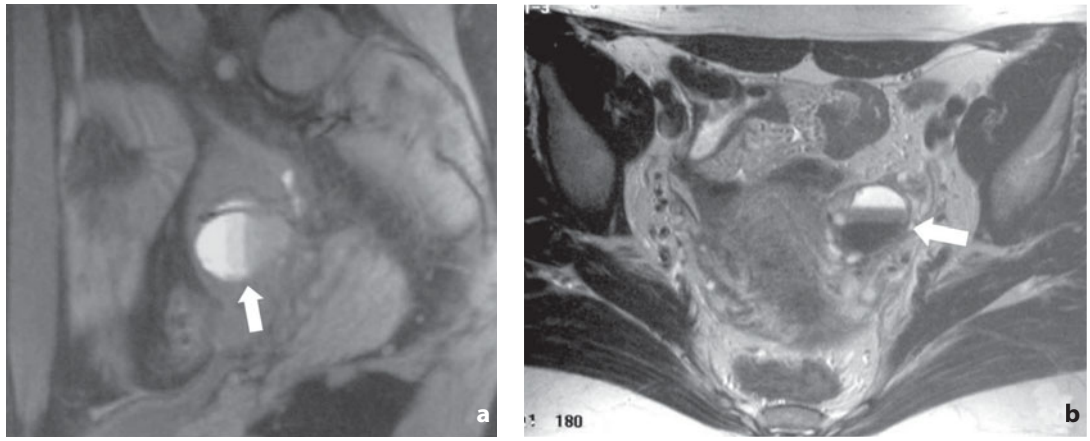

Fig. 17.7a,b. Magnetic resonance. Endometriosis. Sagittal (**a**) and axial (**b**) images show stratification of signal in the presence of layered deposits of blood material indicative of recurrent hemorrhage. There is progressive signal loss towards the sloping portions of the endometriomas (*arrow*) where the concentration of hemosiderin is greater and the cystic component is denser

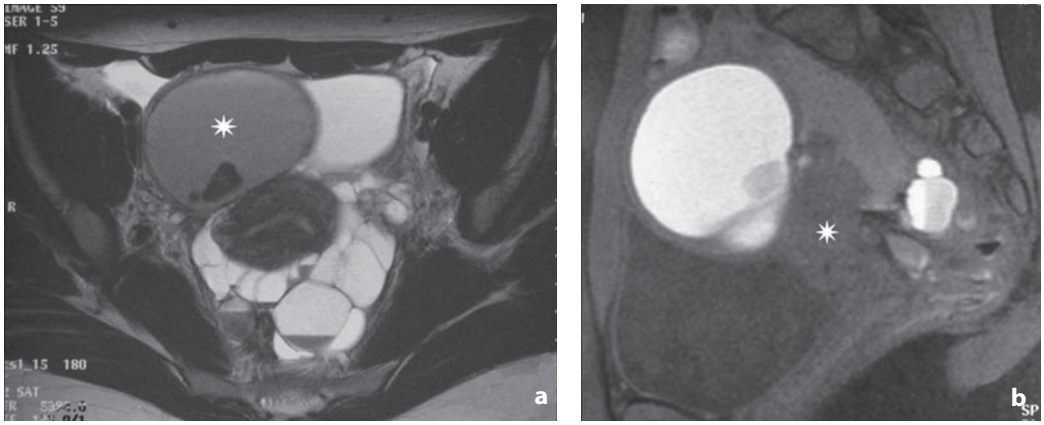

Fig. 17.8a,b. Magnetic resonance. Severe endometriosis. **a** The rectouterine pouch and vesicouterine space are occupied by multiple cystic formations with varying signal in the T2-weighted image. The largest (*asterisk*) demonstrates the shading effect (progressive signal hypointensity towards the sloping portions) and has thick walls with a clot in the dependent position. **b** Different case. The rectouterine pouch is occupied by a solid hypointense mass with spiculated margins. Adjacent to it is an endometrioma with thick walls contained in another cystic formation (perforated cyst), (*asterisk*)

Even when very small, endometrial cysts tend to perforate. In other words, the cystic wall ruptures with the consequent formation of another collection outside the former, with respect to which it is usually completely isolated (Fig. 17.8b). This justifies the finding of multilocular cysts, often arising from the ovary but adhering to adjacent structures. Multilocular cysts ("perforated cysts", Fig. 17.8b) tend to originate from cysts whose blood material is produced by recent hemorrhaging and is responsible for the characteristic signal of acute hematomas (signal hypointensity in T1- and T2-weighted sequences) and from cysts which present the classic signal of endometrial cysts (hyperintensity in T1-weighted sequences).

e) Complex neoformations are prevalently located at the ovaries and the rectouterine pouch (Fig. 17.8). For the most part they are large cystic formations characterized on US (Fig. 17.6c) and MR (Fig. 17.8a) by a solid and usually parietal components. This appearance is difficult to differentiate from a tumor mass, thus requiring its removal and histologic appraisal in order to rule out malignant transformation (endometrioid carcinoma). On US they appear with dense liquid material and complex echotexture due to the presence of both hypo- and hyperechoic areas and particularly thick walls or solid chips within the cystic formation.

Bennett GL, Slywotzky CM, Giovanniello G (2002) Gynecologic causes of acute pelvic pain: spectrum of CT findings. RadioGraphics 22:785-801

Brosens IA (1998) Endometriosis: current issues in diagnosis and medical management. J Reprod Med 43:281-286

Carbognin G, Guarise A, Minelli L et al (2004) Pelvic endometriosis: US and MRI features. Abdom Imaging 29:609-618

Fried AM, Kenney CM 3rd, Stigers KB et al (1996) Benign pelvic masses: sonographic spectrum. RadioGraphics 16:321-334

Kupfer MC, Schwimer SR, Lebovic J (1992) Transvaginal sonographic appearance of endometriomata: spectrum of findings. J Ultrasound Med 11:129-133

Woodward PJ, Sohaey R, Mezzetti TP Jr (2001) From the Archives of AFIP. Endometriosis: radiologic-pathologic correlation. RadioGraphics 21:193-216

Comparison of Diagnostic Modalities

Ultrasonography and Magnetic Resonance

Sensitivity in the diagnosis of endometriosis of both intraluminal US and MR is essentially similar, particularly in the case of ovarian occurrence. The accuracy of combined transvaginal US (TVUS) and transrectal US (TRUS) in evaluation of endometriosis in the posterior compartment is 92%. The only study present in the literature comparing classic laparoscopic staging by the American Fertility Association and MR staging showed agreement in 94% of cases. Although MR is able to accurately evaluate the first two parameters of laparoscopic staging, a major limitation resides in evaluation and assessment of the extent of adhesions. Confirmation of the findings reported by Zanardi et al. is provided by a study by Bazot et al.: sensitivity, specificity, positive predictive value, negative predictive value and diagnostic accuracy of MR in the evaluation of DIE are 90.3%, 91%, 92.1%, 89% and 90.8%, respectively. With regard to the individual localizations, US is more reliable in the study of the rectovaginal septum thanks to the intraluminal approach, which also favors the identification of lesions of the rectal and vaginal wall.

However, both US and MR cannot easily demonstrate, if at all, disease arising from the broad and uterosacral ligaments. TRUS partially overcomes the limited field of view with TVUS, given the absence of the obstacle to passage of the transducer in the pelvic cavity represented by the vaginal fornices. While the sensitivity of the two techniques is similar, or slightly in favor of US in pelvic occurrences, it is completely to the advantage of MR in suprapelvic sites, especially in the liver (**Fig. 17.9**), ureters (**Fig. 17.10**) and along the spinal nerve root (**Fig. 17.11**). The difference is justified by the higher power of resolution of intraluminal US study for pelvic lesions, localized in the field of view of the ultrasound beam, and by the greater ability to explore and discriminate tissue provided by MR study. The diagnostic specificity of the two techniques is instead markedly different and clearly in favor of MR, with a value of 97% in the diagnosis of endometriomas. MR is able to identify the lesions largely because of the presence of blood and therefore the products of its degradation. With fat saturation in the T1-weighted sequences, adnexal lesions can be identified by differentiating hemorrhagic masses (hyperintense) from lesions containing liquid or fat, such as teratomas (hypointense, **Fig. 17.12**).

Intestinal involvement of endometriosis begins from the serosa in the direction of the intestinal lumen, and therefore the findings of sigmoidoscopy can be completely normal. Colonoscopy, therefore, has sensitivity below 60% and so does not play a crucial role in the diagnosis of endometriosis. It has been demonstrated that TVUS and TRUS have the same accuracy in the diagnosis of rectal wall involvement. Therefore the study should preferably begin with TVUS and be completed with TRUS in the event of doubt or for surgical planning. Sensitivity and negative predictive value of TRUS and MR in the diagnosis of rectal involvement in the presence of DIE are in favor of the former (97% vs. 76.5%). On MR the abnormality of the anterior wall of the rectum and sigmoid colon is indicated by the disappearance of the adipose tissue located between the uterus and the rectum, and the presence of wall thickening with the possible appearance of fibrous masses with spiculated margins and signal hypointensity in T2-weighted images (**Fig. 17.13**).

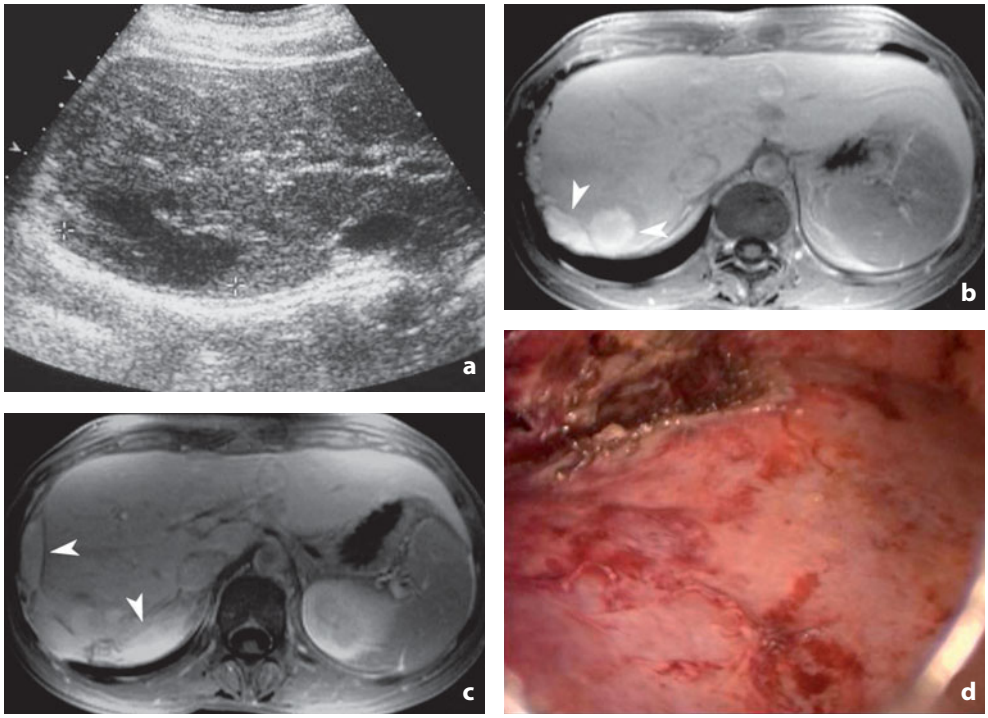

Fig. 17.9a-d. Ultrasonography and magnetic resonance. Hepatic endometriosis. **a** Sonogram shows hypoechoic subcapsular areas in the posterior sectors of the right lobe (*crosses*). The T1-weighted MR sequences with fat signal saturation (**b, c**) confirm the presence of hyperintense confluent hemorrhagic collections (*arrowheads*) with capsular and subcapsular location and confirmed at laparoscopy (**d**) as endometrial implants

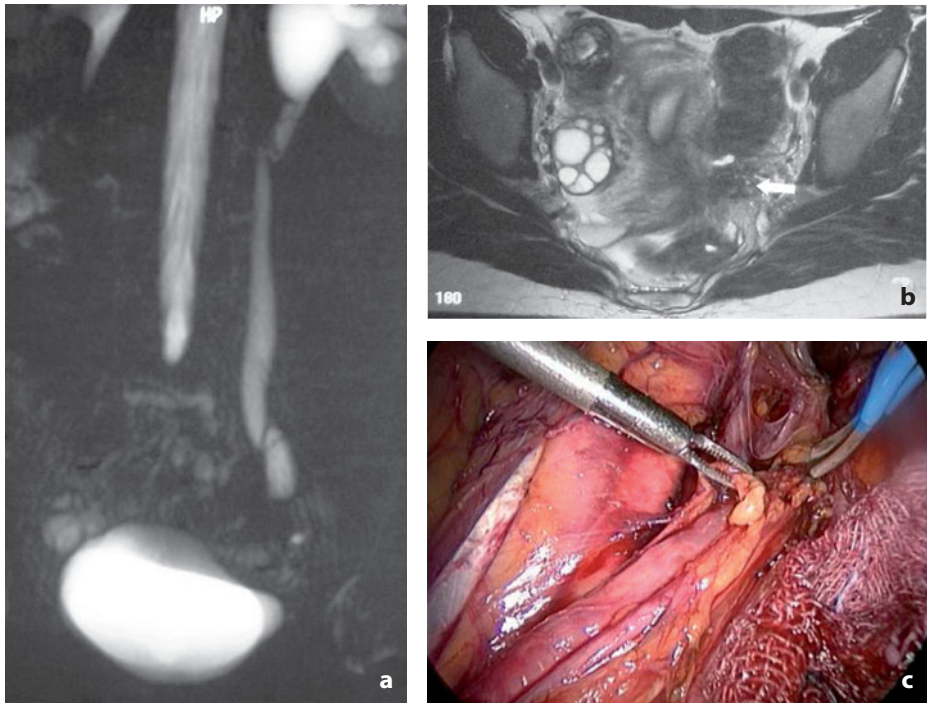

Fig. 17.10a-c. Magnetic resonance. Ureteric endometriosis. **a** MR urography shows the dilatation of the left pelvis and ureter. **b** T2-weighted sequence shows the distal segment of the ureter surrounded by a solid mass (*arrow*) with irregular margins and low signal intensity. Laparoscopy (**c**) confirms the distal ureteric obstruction as a solid endometrial plaque

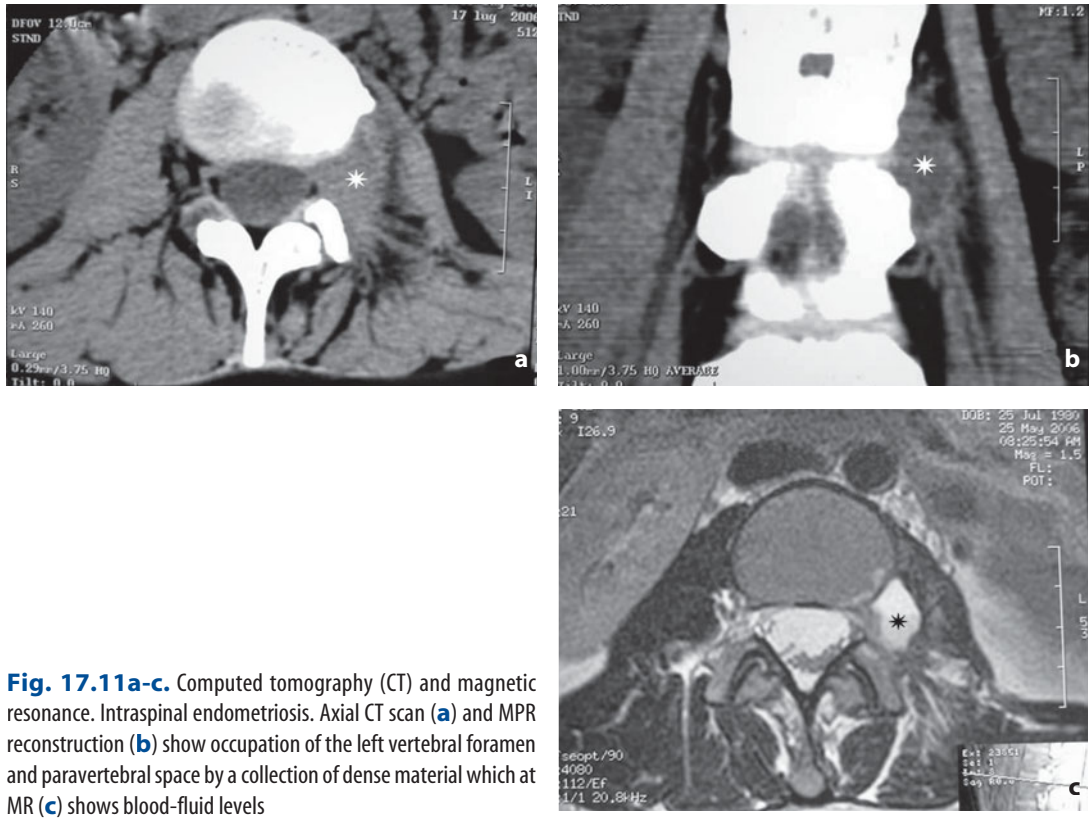

Fig. 17.11a-c. Computed tomography (CT) and magnetic resonance. Intraspinal endometriosis. Axial CT scan (**a**) and MPR reconstruction (**b**) show occupation of the left vertebral foramen and paravertebral space by a collection of dense material which at MR (**c**) shows blood-fluid levels

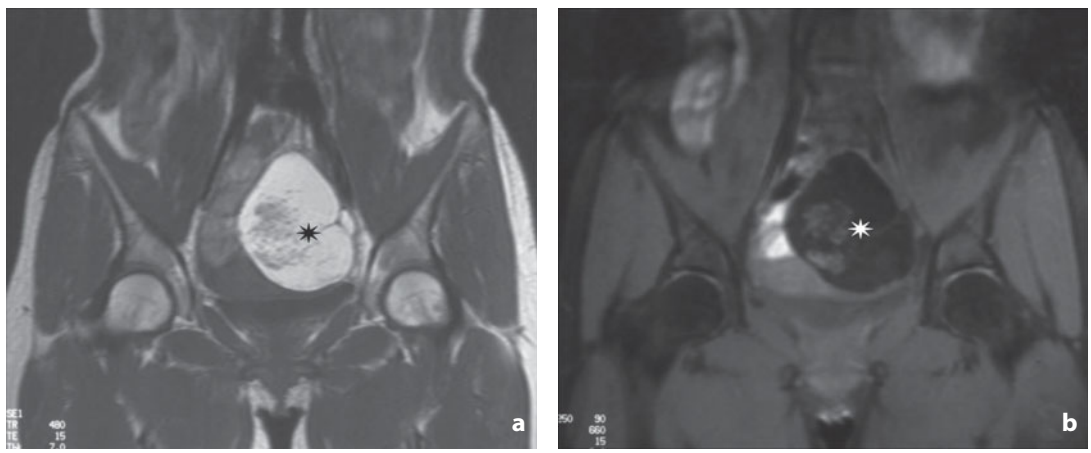

Fig. 17.12a,b. Magnetic resonance. Cystic teratoma. In the left parauterine space a mass (*asterisk*) can be visualized with prevalently hyperintense signal in the T1-weighted sequence (**a**). The loss of signal after fat signal saturation (**b**) confirms the adipose structure of the lesion

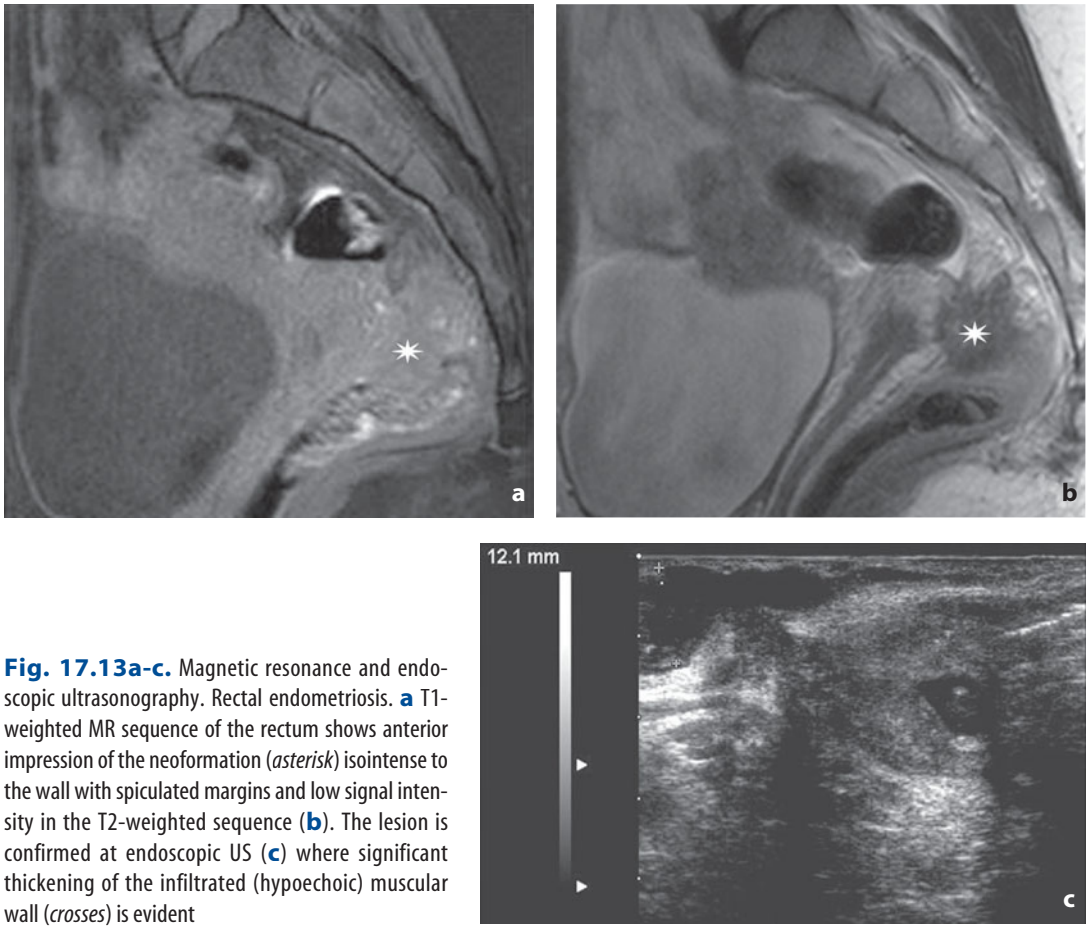

Fig. 17.13a-c. Magnetic resonance and endoscopic ultrasonography. Rectal endometriosis. **a** T1-weighted MR sequence of the rectum shows anterior impression of the neoformation (*asterisk*) isointense to the wall with spiculated margins and low signal intensity in the T2-weighted sequence (**b**). The lesion is confirmed at endoscopic US (**c**) where significant thickening of the infiltrated (hypoechoic) muscular wall (*crosses*) is evident

Bazot M, Detchev R, Cortez A et al (2003) Transvaginal sonography and rectal endoscopic sonography for assessment of pelvic endometriosis: a preliminary comparison. Hum Reprod 18:1686-1692

Bazot M, Darai E, Hourani R et al (2004) Deep pelvic endometriosis: MR imaging for diagnosis and prediction of extension of disease. Radiology 232:379-389

Carbognin G, Girardi V, Pinali L et al (2006) Assessment of pelvic endometriosis: correlation of US and MRI with laparoscopic findings. Radiol Med 111:687-701

Chapron C, Dumontier I, Dousset B et al (1998) Results and role of rectal endoscopic ultrasonography for patients with deep pelvic endometriosis. Hum Reprod 13:2266-2270

Zanardi R, Del Frate C, Zuiani C et al (2003) Staging of pelvic endometriosis based on MRI findings versus laparoscopic classification according to the American Fertility Society. Abdom Imaging 28:733-742

Endoscopic Ultrasonography

According to a number of authors, endoscopic ultrasonography (EUS) is the most sensitive and specific (100% and 67%) technique for identifying the site, extent and depth of intestinal involvement (**Fig. 17.13c**), because of its greater panoramic views of the intestinal tract. Rectal EUS is a simple and noninvasive examination which is performed with an 11.4 mm diameter instrument using 7.5 and 12 MHz frequencies,

and is able to evaluate the five layers of the rectocolonic wall. In the rectosigmoid, involvement of the muscularis propria, which appears hypoechoic and thin (<3 mm), is distinct from the hyperechoic submucosa and mucosa. In the preoperative assessment of patients with suspected endometriosis of the posterior compartment, rectal EUS – the reference standard in the diagnosis of the rectosigmoid – is mandatory. In addition to evaluating the extent of lesion and the degree of infiltration of the intestinal wall (**Fig. 17.13c**), the technique can assess the diameter of the lesion, the distance from the anal margin and the infiltration of adjacent pelvic organs, thus providing information which can radically influence the surgical approach to resection of the lesions. EUS findings can be classified into three groups: normal examination with no evidence of lesions, retroperitoneal endometrial infiltration without involvement of the intestinal wall, and endometrial infiltration of the intestinal wall which reaches at least the muscularis propria. Should the examination not be available, double, contrast barium enema is nonetheless an accurate technique given its ability to recognize the classic signs of external involvement of the intestinal wall (**Fig. 17.14**).

Magnetic Resonance Urography

With regard to endometrial implants in the urinary tract, TVUS and MR are useful in defining the dimensions of the lesion, the degree of infiltration of the bladder wall, and continuity with possible extravesical lesions. Excretory urography instead has low specificity in the identification of bladder endometriosis. Currently the most accurate and least invasive technique for the identification of ureteric endometriosis is MR urography (**Fig. 17.10a**), possibly in combination with retrograde endoscopic or radiographic studies. MR urography is useful in the diagnosis of extrinsic ureteric endometriosis (i.e. characterized by glandular and stromal endometrial tissue within the submucosa and the adventitia of the ureter), and in defining the extent, depth and level of obstruction. The technique still has several limitations in the evaluation of intrinsic endometriosis (i.e. involving the urothelium and the submucosa in the absence of an extrinsic component). Therefore integrating the examination with intraluminal US is advisable, not only for the identification of exclusively intrinsic lesions, but also to help determine the extent of periureteric disease in the form of retroperitoneal fibrosis and fluid collections within the ureter. Since asymptomatic ureteric obstruction is the rule and not the exception, patients with conventional symptoms of pelvic endometriosis without urologic manifestations should nonetheless undergo routine renal US for the early identification of changes to the upper urinary tract, thus avoiding a deterioration in renal function.

Intraluminal US and MR have excellent sensitivity in the identification of endometriosis. These techniques are, however, limited in relation to superficial lesions, which is why laparoscopy remains the reference standard in the diagnostic protocol.

In conclusion, US is therefore the first-choice technique in the clinical suspicion of endometriosis. The continuation of diagnostic examinations is influenced by the US findings. In the event of a single or multiple documented lesions with evident endometrial characteristics, the use of MR appears unnecessary given the need to directly proceed with laparoscopy. However, in cases where there is diagnostic doubt regarding the effective nature of the lesion identified, MR is preferable given its more

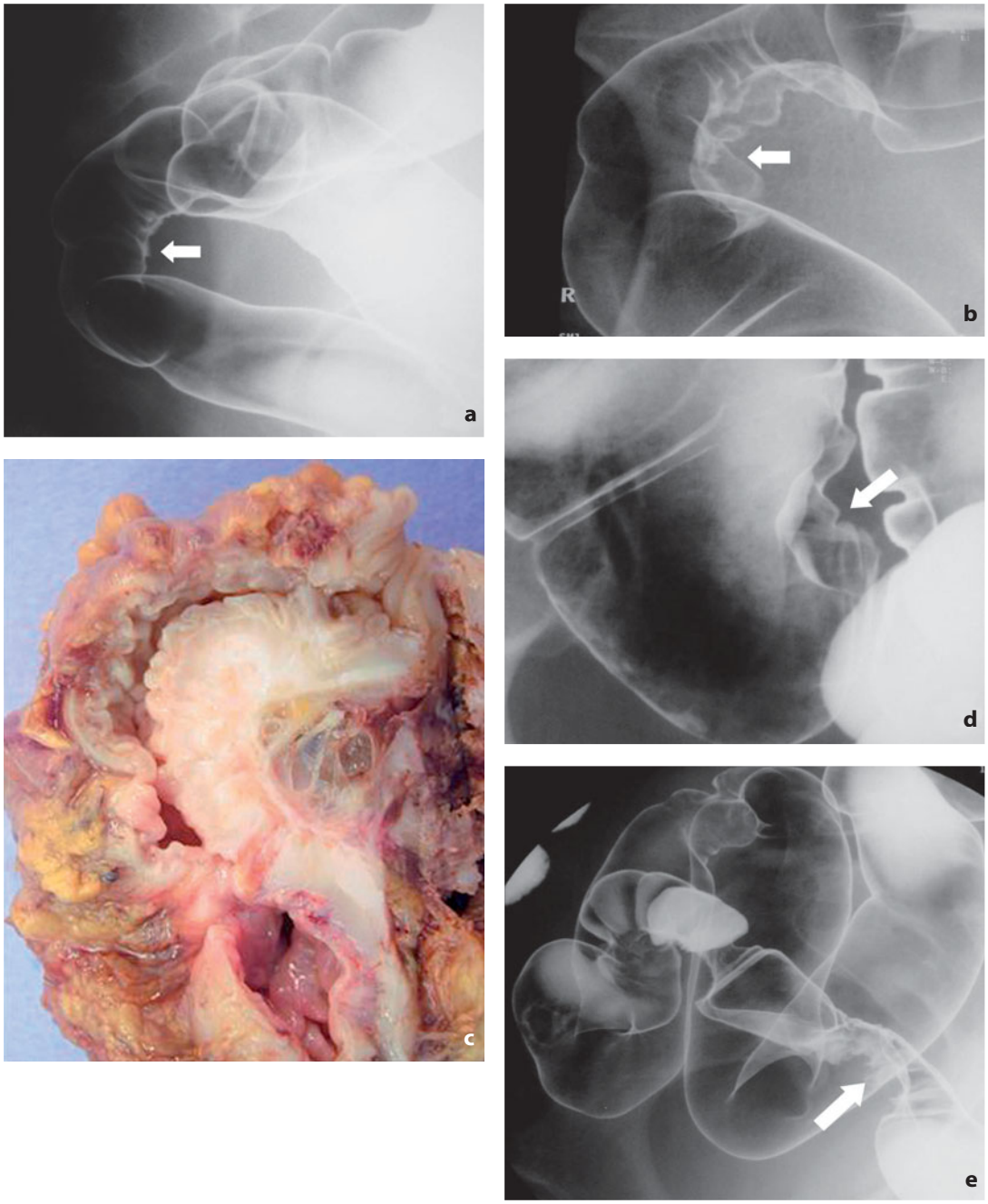

Fig. 17.14a-e. Barium enema. Intestinal endometriosis. **a** External compression on the anterior wall of the mid third of the rectum (*arrow*) with fine marginal spicules on the surface of the serosa. **b** Follow-up at two years shows recurrence of symptoms with more evident scalloped submucosal impression (*arrow*) on the anterior wall of the rectum and mild narrowing. **c** Gross specimen shows infiltration of the wall by a fibrous lesion. Different patient: external impression (*arrow*) at the cecum (**d**) and multiple impressions on the sigmoid colon (**e**) found to be endometrial implants causing narrowing of the lumen to varying degrees

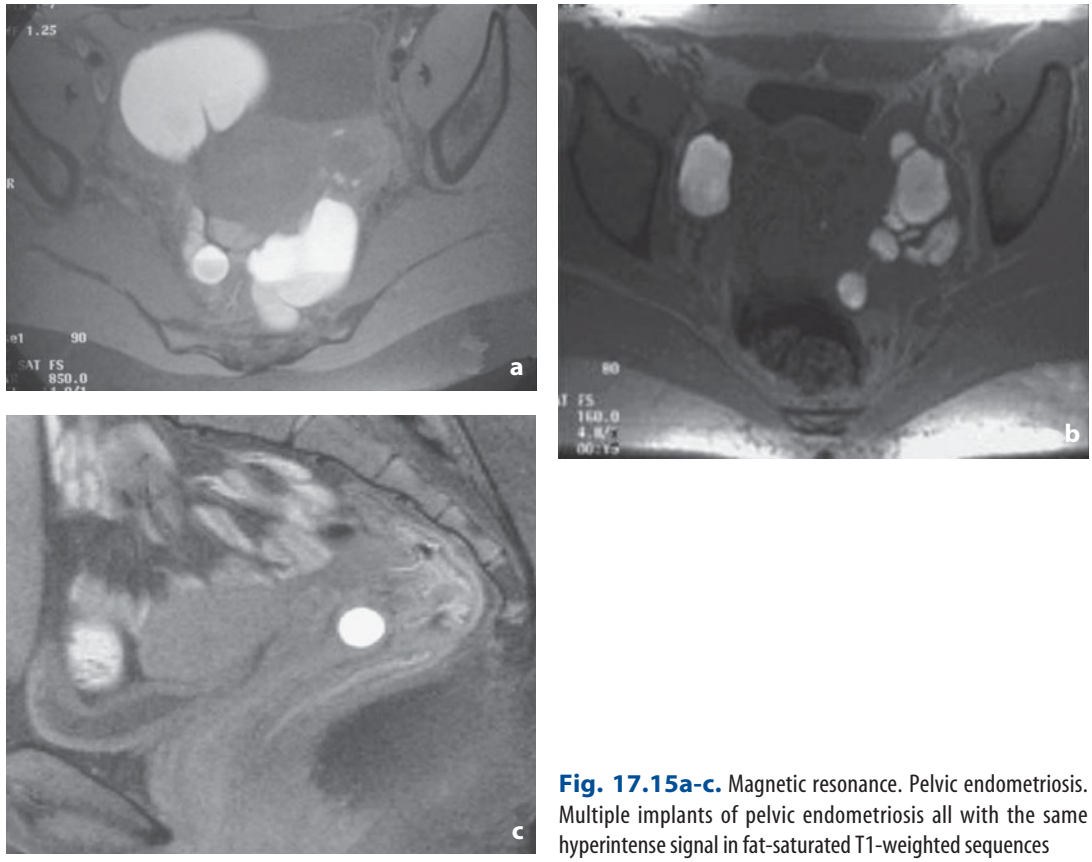

Fig. 17.15a-c. Magnetic resonance. Pelvic endometriosis. Multiple implants of pelvic endometriosis all with the same hyperintense signal in fat-saturated T1-weighted sequences

accurate structural analysis due largely to fat-saturated T1-weighted sequences (**Fig. 17.15**). MR is indispensable in all cases where clinical symptoms suggest the presence of extrapelvic implants and in evaluation of the response to hormone therapy. MR is also useful for the preoperative assessment of disease in patients with adherences in which the diagnostic validity of laparoscopy may be limited.

Balleyguier C, Chapron C, Dubuisson JB et al (2002) Comparison of magnetic resonance imaging and transvaginal ultrasonography in diagnosing bladder endometriosis. J Am Assoc Gynecol Laparosc 9:15-23

Fedele L, Bianchi S, Raffaelli R et al (1997) Pre-operative assessment of bladder endometriosis. Hum Reprod 12:2519-2522

Grasso M, Li S, Liu JB et al (1999) Examining the obstructed ureter with intraluminal sonography. J Urol 162:1286-1290

Sugimura K, Okizuka H, Kaji Y et al (1996) MRI in predicting the response of ovarian endometriomas to hormone therapy. J Comput Assist Tomogr 20:145-150

Pelvic Inflammatory Disease: Clinics and Imaging

18

L. Grazioli, L. Olivetti, A. Ranza

Pathology

Pelvic inflammatory disease (PID) involves the uterine tube (salpingitis), but may extend to the ovary (adnexitis or salpingo-oophoritis), the parametrium (parametritis) and the pelvic peritoneum (pelvic peritonitis). It may involve all of the these structures either simultaneously or subsequently.

The uterine tube is the site most commonly affected by inflammation. Possible outcomes include sterility (due to scarring and occlusion of the uterine tube) ectopic pregnancy (correlated with altered canalization of the tube) and chronic pelvic pain.

The World Health Organization defines sterility as the inability of a couple to produce offspring after two years of nonprotected intercourse. In 15-20% of cases, the history of a sterile couple includes an episode of PID. Tubal pregnancy accounts for 90% of ectopic pregnancies, with the most important risk factor for this condition being postinfection and/or postoperative damage. Between 30% and 60% of women who undergo surgery for ectopic pregnancy have a positive history for PID. Lastly, in 17% of cases PID is responsible for chronic pelvic pain persisting for more than 6 months which worsens during the periovulatory and perimenstrual phase and is not always correctly interpreted.

PID is a relatively common condition among sexually active women and therefore has a high social impact considering the difficulty in prevention, diagnosis, treatment and monitoring.

The peak incidence is in women aged 20-25 years. The incidence in Europe is around 1% and even higher among women using an intrauterine device (IUD) or with chronic infections such as cervicovaginitis.

Several obstetric conditions favoring infection are correlated with childbirth and abortion, when the uterus is more vulnerable to infections. The persistence of blood, placental residues or amniochorionic membranes in the uterine cavity, cervical incompetence and lacerations during delivery are all risk factors for inflammatory processes.

The etiopathogenesis is infective and the most common pathogens are *Chlamydia trachomatis*, anaerobic Gram, positive and, negative bacteria and common pyogens (*Streptococcus* and *Staphylococcus* species, *Escherichia coli*). *Mycobacterium tuberculosis* is a common cause of infection with an incidence of around 10-15% of cases in developing countries. In 30-40% of subjects the etiology is polymicrobial. In women using an IUD the main pathogen is *Actinomyces israelii*, which with greater frequency causes chronic suppurative infection.

The pelvic infection pathway can be:

- direct ascending spread (endometrial, endosalpingeal, intraperitoneal), as frequently occurs in gonococcal infections;
- from the parametrium with lymphatic spread, as with infections associated with the use of an IUD;
- hematogenous spread, as frequently occurs in tubercular infection.

L. Olivetti, L. Grazioli (eds.), *Imaging of Urogenital Diseases*,

PID is less commonly found in women who use oral contraceptives. One possible explanation is that the pill is thought to induce changes in the composition of the cervical mucosa, rendering it less penetrable to ascending infections.

The clinical presentation of PID can be acute, subacute or chronic.

In its most simple form, acute PID consists of hyperemic salpingitis, in which tubal congestion prevails. In a more advanced phase, the tubal lumen may be occupied by seromucous secretions (mucopurulent salpingitis) or purulent secretions (purulent salpingitis). The acute form can involve the muscular layers of the uterine tube, extending to the serous surface with the formation of adherences with adjacent organs. It may also be characterized by stenosis of both the tubal and abdominal ostium with the accumulation of intraluminal exudate and formation of a serous, blood-filled or purulent saccular collection.

Chronic tubal inflammation (salpingitis) essentially consists of two forms: the hypertrophic form characterized by tubal wall thickening and consequent reduction and/or distortion of the tubal lumen, and the atrophic form whereby the tubal walls and mucosa are thinned.

In general the acute forms are characterized by diffuse pain which may be sharp in the pelvis and radiating to the sacrum and the thigh with marked hyperthermia, foul-smelling mucopurulent vaginal discharge and moderate intermenstrual flow (sign of endometrial inflammation). Their clinical course may lead to cure or become chronic. They may become complicated with saccular collections, parametritis, abscesses in the rectouterine pouch, pelvic peritonitis and dramatic presentations of diffuse inflammation and generalized peritonitis.

The subacute and chronic forms manifest with much more aspecific symptoms: aching or heavy sensation in the lower quadrants and the sacral region, exacerbated by intercourse and associated with intermenstrual flow and dysmenorrhea.

Clinical Diagnosis

The clinical diagnosis of PID is often not easy, because symptoms may be aspecific. Pain of gastrointestinal origin, lower urinary tract infections or other diseases of gynecologic origin, such as rupture of a follicle or torsion of a uterine tube, can mimic PID.

The clinical approach is based on:

- general physical examination in the search for signs of acute abdomen and/or lymphadenopathy;
- clinical examination with a speculum to ascertain the appearance of the genital secretions;
- bimanual pelvic examination to verify the typical pain of the PID at palpation of the adnexae and the movement of the cervix.

Instrumental Diagnosis

Culdocentesis, i.e. an infrequently performed procedure consisting of transvaginal puncture of the rectouterine pouch, enables the collection of liquid for biochemical and microbiologic analysis.

Endometrial biopsy verifies the histopathologic state of the endometritis which is associated in 90% of cases of salpingitis.

The reference standard for the diagnosis of PID is direct inspection via laparoscopy. This enables not only direct visualization of the pelvic cavity and the superior abdominal quadrants, but also collection of intraperitoneal exudate and tubal cells for the purposes of an etiologic diagnosis. However, due to its invasiveness laparoscopy is especially reserved for cases of difficult diagnosis (**Fig. 18.1**).

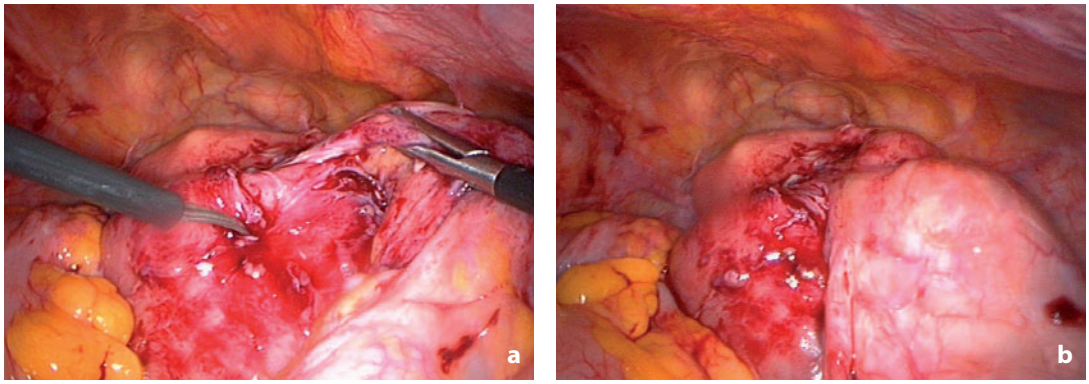

Fig. 18.1a,b. Laparoscopy. Pelvic inflammatory disease. Evident signs of hyperemic inflammation with voluminous distension of the uterine tube

Haggerty CL, Ness RB (2008) Diagnosis and treatment of pelvic inflammatory disease. Womens Health (Lond Engl) 4:383-397

Lareau SM, Beigi RH (2008) Pelvic inflammatory disease and tubo-ovarian abscess. Infect Dis Clin North Am 22:693-708, vii

Simms I, Warburton F, Weström L (2003) Diagnosis of pelvic inflammatory disease: time for a rethink. Sex Transm Infect 79:491-494

Westrom L (1980) Incidence, prevalence, and trends of acute pelvic inflammatory disease and its consequences in industrialized countries. Am J Obstet Gynecol 138:880-892

Diagnostic Imaging

Imaging techniques can provide useful information for orienting diagnosis, especially in documenting and quantifying inflammation. In addition, they are clearly less invasive and less expensive than laparoscopy.

Hysterosalpingography

Hysterosalpingography has no role to play in the diagnosis of PID and is in fact contraindicated in the acute phase. Its sole use is for identifying the possible late sequelae of a previous infection such as dilatation, distortion and tubal stenosis, as well as the presence of uterine cavity filling defects caused by adhesions (**Fig. 18.2**).

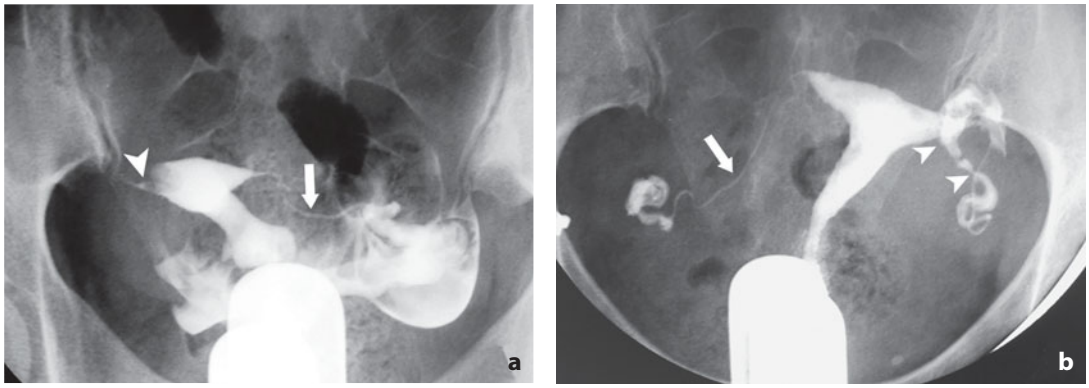

Fig. 18.2a,b. Hysterosalpingography. Pelvic inflammatory disease. **a** Stenosis of the right uterine tube at the origin (*arrowhead*). **b** Irregularity of the left uterine tube due to stenosis alternating with circumscribed dilations (*arrowheads*). The *arrow* in both images indicates the normal contralateral tube

Ultrasonography

Ultrasonography (US) is the imaging modality of first choice. It provides good diagnostic accuracy, is relatively inexpensive and does not involve the use of ionizing radiation. The latter feature is of particular importance given the prevalence of PID in women of fertile age.

The US approach can be transabdominal or transvaginal. The former offers panoramic views with the possibility of evaluating the superior abdominal quadrants and assessing the involvement of other pelvic organs. The latter provides greater detail with regard to the uterus and the adnexae.

In the early stages of PID, US can nonetheless be negative or provide aspecific findings consisting solely of the presence of free liquid in the rectouterine pouch (a finding which is also seen in other physiologic and pathologic conditions). The free liquid may appear homogeneously anechoic. However, with the progression of infection it becomes more abundant and changes its characteristics, appearing corpuscular due to the presence of blood or pus and at the same time heterogeneous due to the presence of septations. A hyperechoic ring may also be seen bounding the collection which has in the meantime become saccular (**Fig. 18.3**).

US study can also evaluate the imbibition of pelvic fibroadipose tissue and the involvement of the uterus, the uterine tubes and the ovaries, which appear swollen with heterogeneous echotexture. In particular, the tubes often appear lengthened and tortuous, distended by the fluid which influences the echotexture: anechoic (hydrosalpinx) or echogenic if pus (pyosalpinx) or blood (hematosalpinx) are present (**Figs. 18.4, 18.5**).

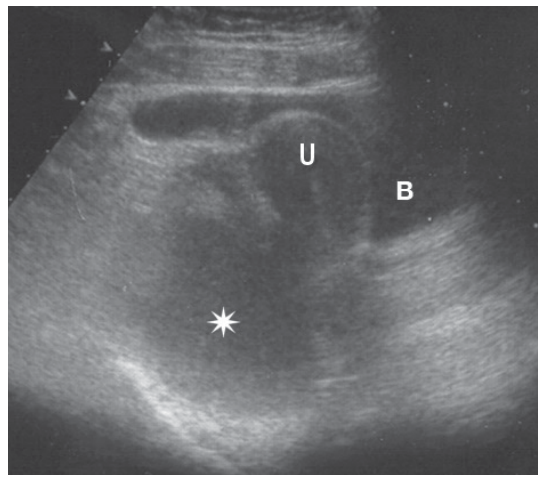

Fig. 18.3. Ultrasonography. Transabdominal approach. A moderate amount of corpuscular liquid can be seen in the rectouterine pouch. *U*, uterus. *B*, urinary bladder

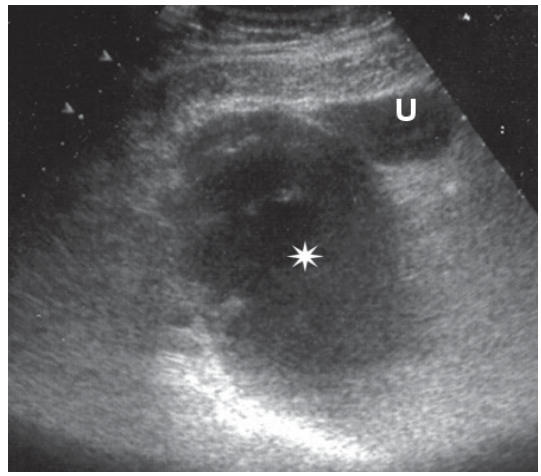

Fig. 18.4. Ultrasonography. Transabdominal approach. Pyosalpinx. The uterine tube (*asterisk*) is distended with corpuscular liquid. *U*, uterus

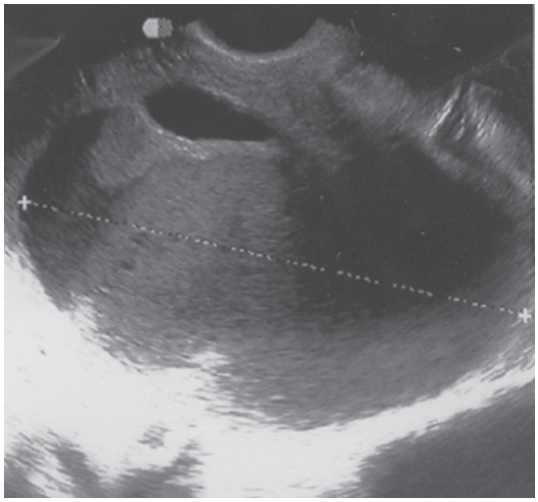

Fig. 18.5. Ultrasonography. Transabdominal approach. Same case as Fig. 18.1. Large distended heterogeneous mass of the uterine tube prevalently containing corpuscular material

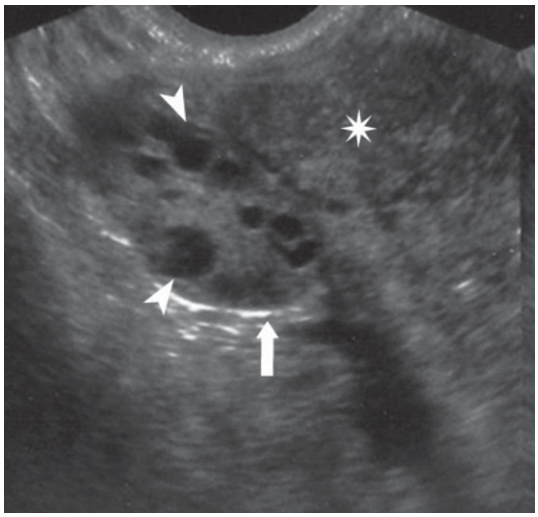

Fig. 18.6. Ultrasonography. Transvaginal approach. Abscessed oophoritis. The right ovary (*arrow*) appears swollen, heterogeneous with liquefied necrosis (*arrowheads*). The adjacent uterine tube (*asterisk*) is distended by corpuscular liquid

Involvement of the ovaries can be identified by their enlargement and the loss of corticomedullary differentiation and the presence of adjacent edema or fluid (Fig. 18.6).

Ghiatas AA (2004) The spectrum of pelvic inflammatory disease. Eur Radiol 14:E184-192

Timor-Tritsch IE, Lerner JP, Monteagudo A et al (1998) Transvaginal sonographic markers of tubal inflammatory disease. Ultrasound Obstet Gynecol 12:56-66

Computed Tomography

Computed tomography (CT) is usually less used than US and magnetic resonance (MR) in the diagnosis of PID. Factors limiting its use are ionizing radiation and the relatively low contrast resolution, which nonetheless can be improved with contrast media.

In cases of acute salpingitis, show CT findings may be normal or possibly with the sole presence of free liquid in the rectouterine pouch. However, in complicated cases

the uterine tubes may appear as a uni- or multiloculated cystic mass. After injection of contrast medium a ring of intense enhancement may be seen bounding the dilated portion of the tube (**Fig. 18.7**).

Tubo-ovarian abscess appears as a mass with liquid or near-liquid density with intraluminal septations and/or bubbles of gas (nonetheless an infrequent finding) bounded by a markedly enhancing wall (**Fig. 18.8**).

Adenopathies are often associated with cases of PID and situated in pelvic paraaortic sites and at the level of the renal hilum (ovarian lymphatic drainage is parallel to the ovarian vessels).

Other associated signs detected on CT images include: multiple fluid collections, fascial and peritoneal thickening, with clear or ill-defined margins, both lateral pelvic and central (pubic/vesical/uterine/rectal/sacral ligaments), increased attenuation and heterogeneity of prevesical, perirectal and presacral adipose tissue, and hydronephrosis due to involvement of the ureters (**Fig. 18.9**).

Like MR, CT is also able to study the extension of the inflammatory process to adjacent organs such as the appendix, cecum and greater omentum. The loss of definition of the uterine margins is suggestive of adnexal origin of the inflammatory process and can help distinguish a tubo-ovarian abscess from other causes of acute abdominal pain, e.g. diverticulitis (**Fig. 18.10**).

To improve typing, the collections can be drained under CT or US guidance.

Bennett GL, Slywotzky CM, Giovanniello G (2002) Gynecologic causes of acute pelvic pain: spectrum of CT findings. RadioGraphics 22:785-801

Sam JW, Jacobs JE, Birnbaum BA (2002) Spectrum of CT findings in acute pyogenic pelvic inflammatory disease. RadioGraphics 22:1327-1334

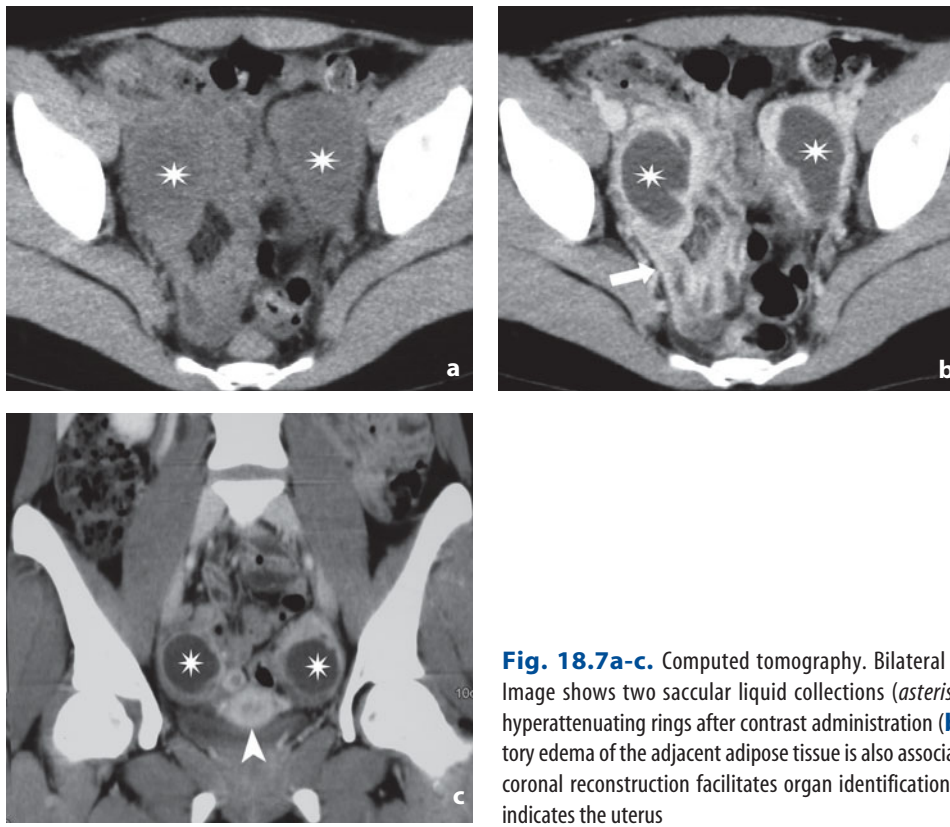

Fig. 18.7a-c. Computed tomography. Bilateral hydrosalpinx. **a** Image shows two saccular liquid collections (*asterisks*) bounded by hyperattenuating rings after contrast administration (**b, c**). Inflammatory edema of the adjacent adipose tissue is also associated (*arrow*). The coronal reconstruction facilitates organ identification. The *arrowhead* indicates the uterus

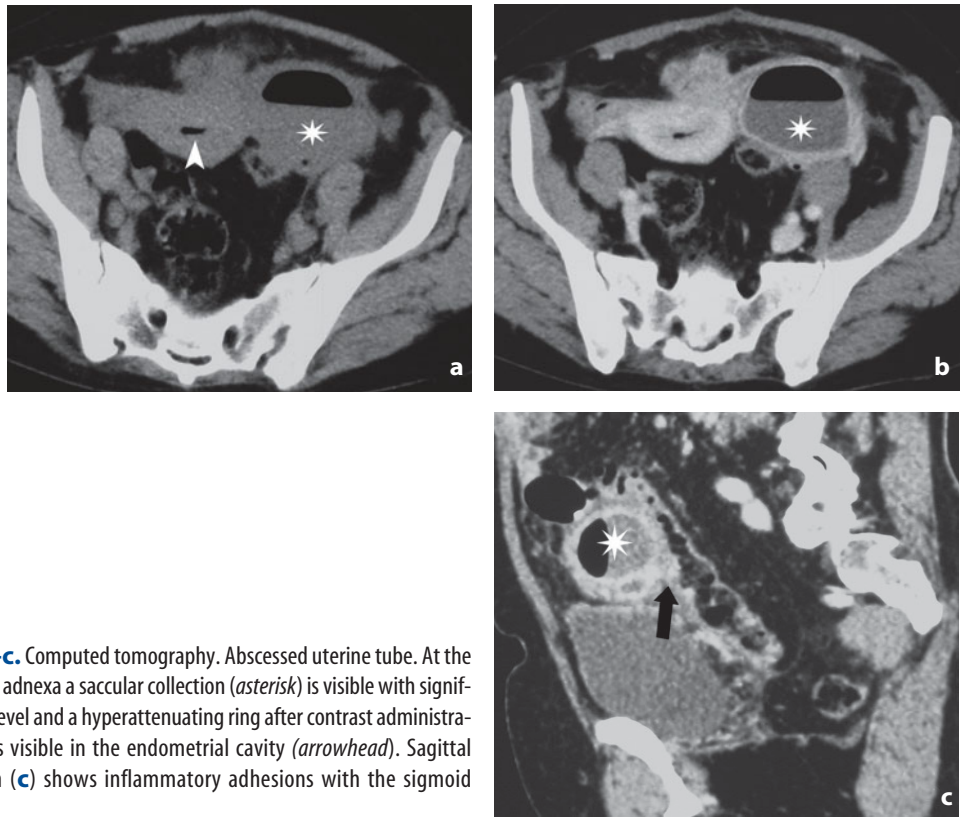

Fig. 18.8a-c. Computed tomography. Abscessed uterine tube. At the level of the left adnexa a saccular collection (*asterisk*) is visible with significant air-fluid level and a hyperattenuating ring after contrast administration (**b**). Air is visible in the endometrial cavity *(arrowhead*). Sagittal reconstruction (**c**) shows inflammatory adhesions with the sigmoid (*arrow*)

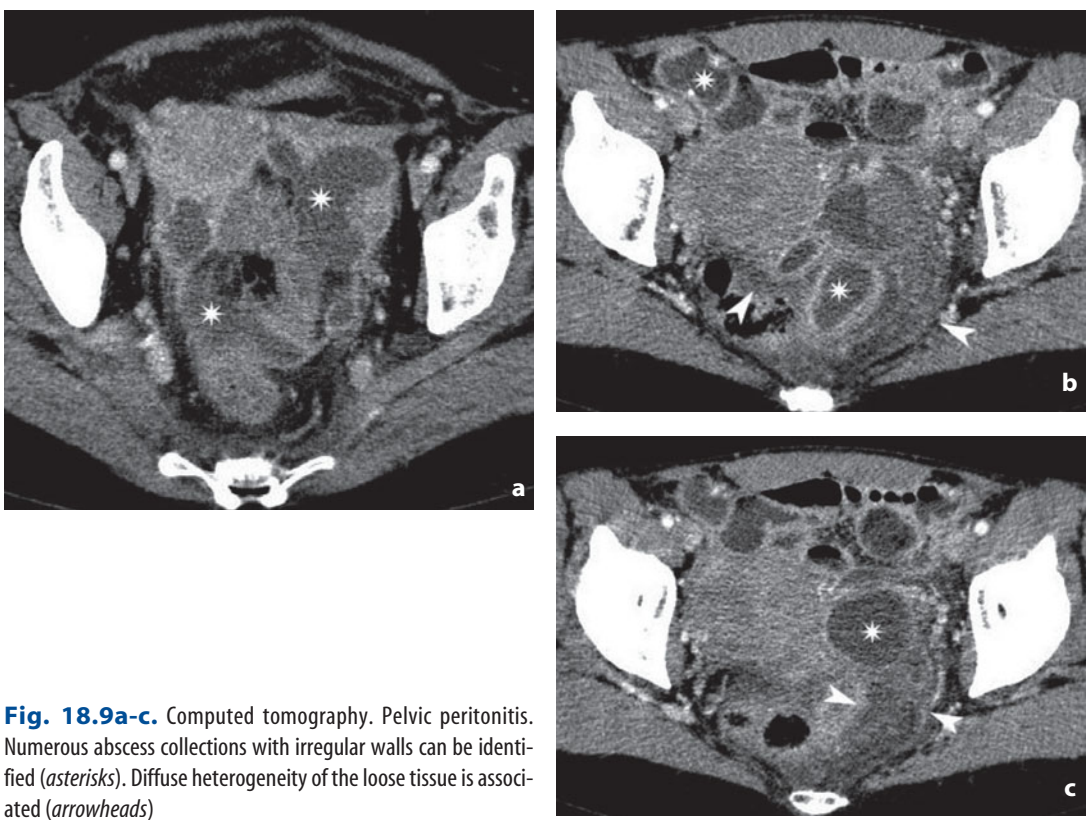

Fig. 18.9a-c. Computed tomography. Pelvic peritonitis. Numerous abscess collections with irregular walls can be identified (*asterisks*). Diffuse heterogeneity of the loose tissue is associated (*arrowheads*)

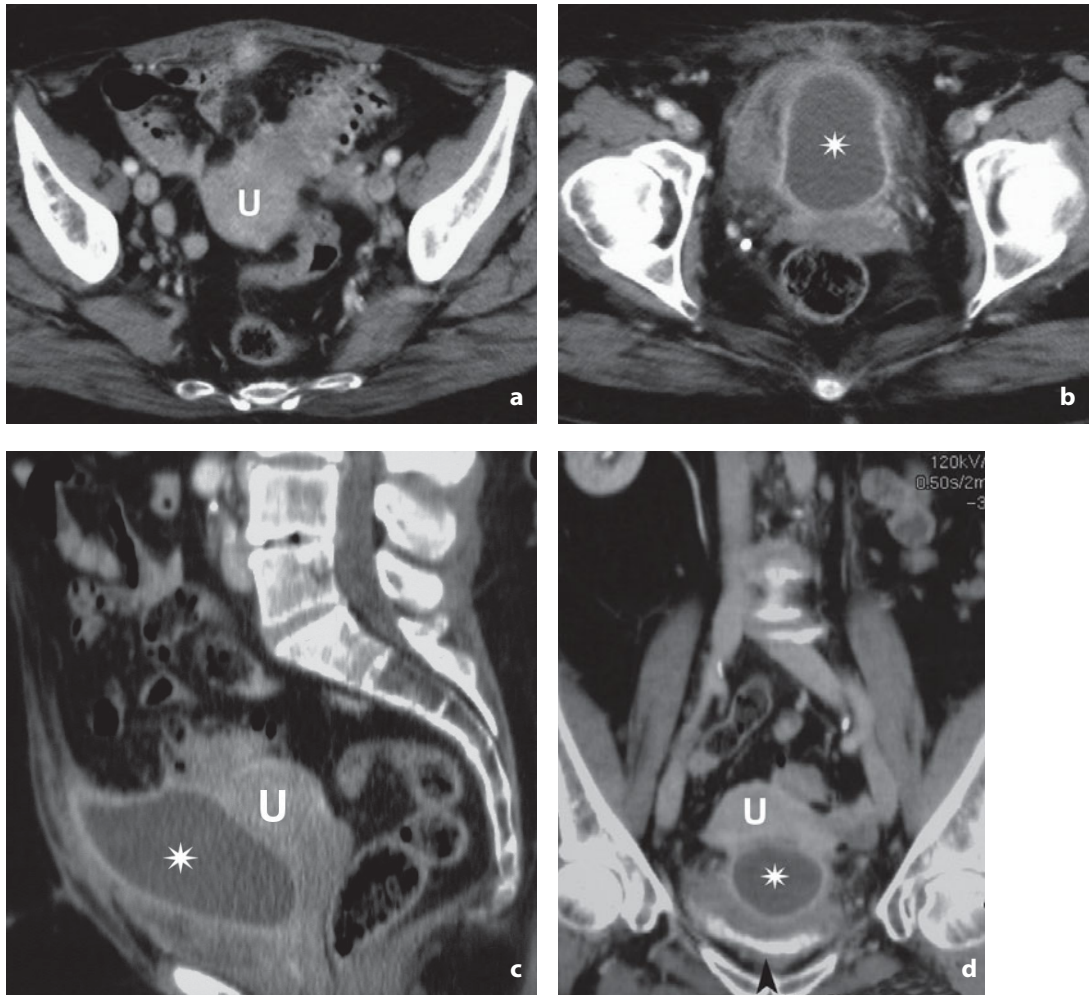

Fig. 18.10a-d. Computed tomography. Diverticulitis. **a,b** Axial scans show abscess collection bounded by a hyperattenuating ring (*asterisk*) beginning from the sigmoid, which presents numerous diverticula and edematous and thickened walls. The sagittal (**c**) and coronal (**d**) images show the abscess between the uterus (*U*) and the contrast-enhanced bladder (*arrowhead*)

Magnetic Resonance

MR is used in the more severe form and in cases where the clinical and US findings are aspecific or inconclusive. The technique produces multiplanar images without the use of ionizing radiation. MR is useful in identifying the inflammatory process, differentiating it from other diseases and quantifying its extension.

The diagnosis of PID can be made with the use of major criteria (presence of tubo-ovarian abscess, pyosalpinx, hydrosalpinx) or minor criteria (polycystic-like ovaries, presence of free liquid).

Tortuous and dilated uterine tubes are easily identifiable with the multiplanar study, especially in T2-weighted sequences, which show and characterize the intraluminal liquid (hydrosalpinx, pyosalpinx, hematosalpinx) (**Figs. 18.11, 18.12**). The tubo-ovarian abscess can have cystic-like, solid or mixed characteristics with low signal intensity in T1 and heterogeneously high signal in T2. There may be associated wall thickening, septations and pelvic adenopathies (**Fig. 18.13**).

If the uterus is involved, it appears swollen with a more intense signal than normally seen in T2-weighted images. This is accompanied by a partial loss of differentiation between the junctional zone and the myometrium, heterogeneity and endometrial thickening.

The free liquid in the pelvic cavity is best visualized in T2-weighted sequences. The signal is homogeneous and hyperintense when it is not corpuscular. In contrast, it appears less hyperintense in the presence of a serous-blood or corpuscular component.

The use of paramagnetic contrast media can increase the diagnostic accuracy since the inflamed tissues display significant enhancement.

MR is superior to US in the diagnosis of PID, with sensitivity of 95% versus 81%, specificity of 89% versus 78% and diagnostic accuracy of 93% versus 80% (**Figs. 18.14, 18.15**).

Tukeva TA, Aronen HJ, Karjalainen PT et al (1999) MR imaging in pelvic inflammatory disease: comparison with laparoscopy and US. Radiology 209:210-216

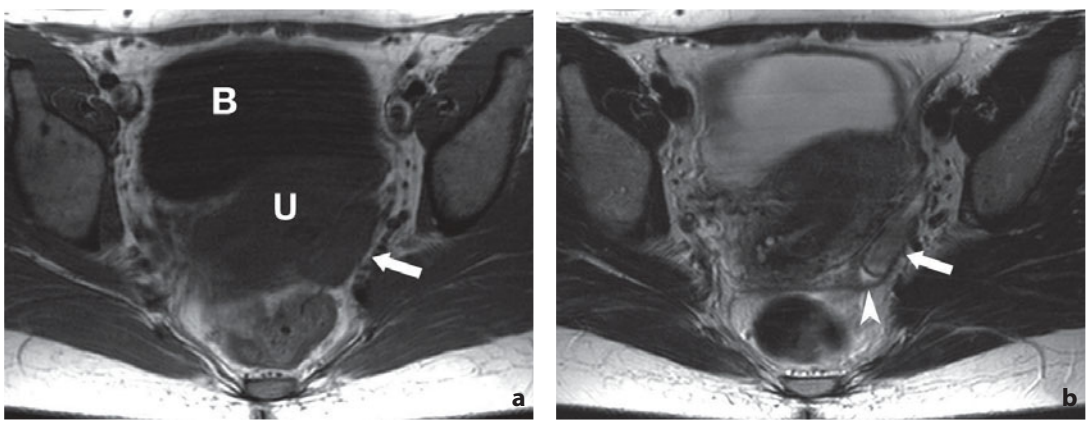

Fig. 18.11a,b. Magnetic resonance. Pyosalpinx. Axial T1- (**a**) and T2-weighted (**b**) images show mild swelling of the left uterine tube (*arrow*), adjacent to which is a small amount of inflammatory liquid (*arrowhead*). *U*, uterus; *B*, urinary bladder

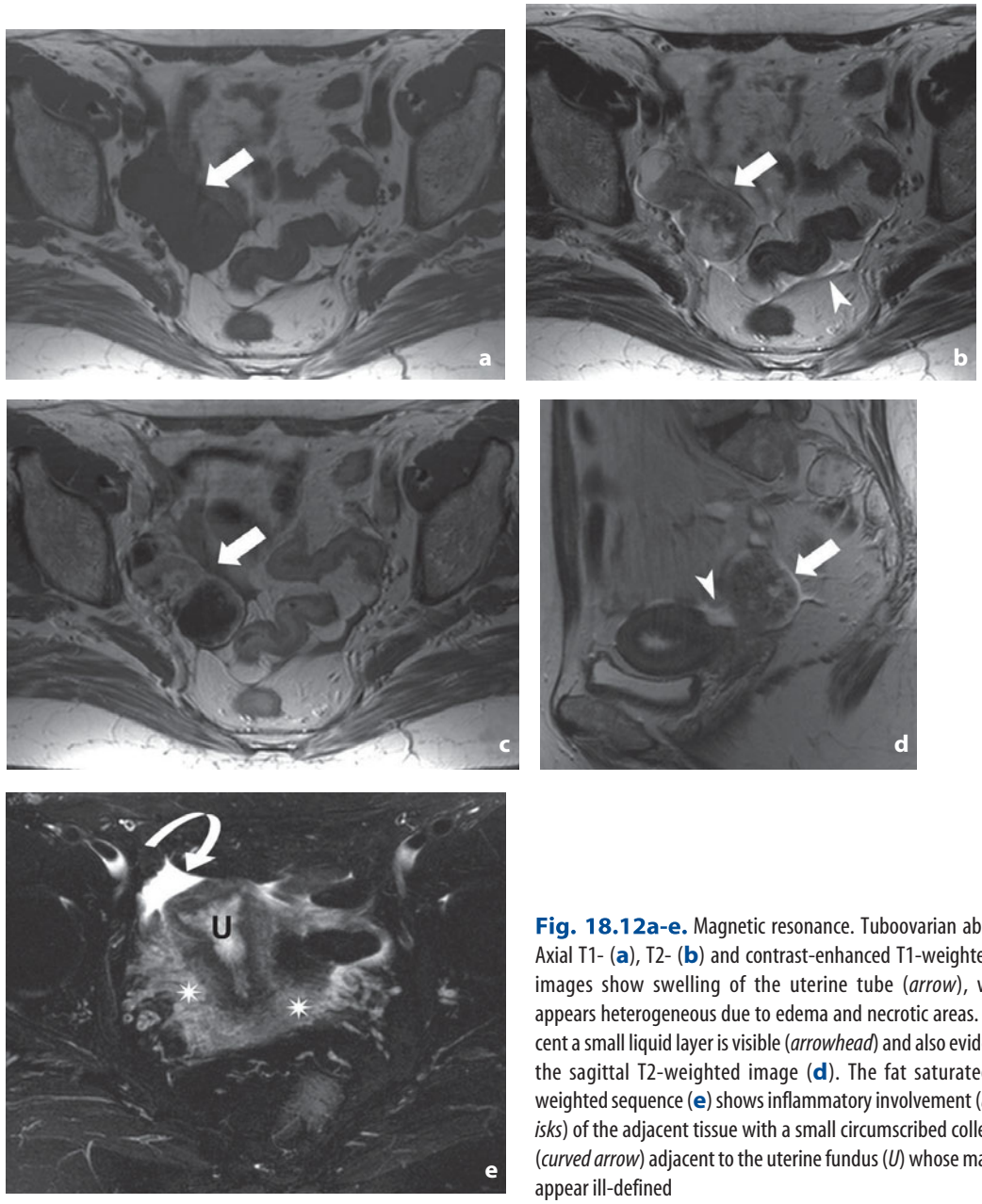

Fig. 18.12a-e. Magnetic resonance. Tuboovarian abscess. Axial T1- (**a**), T2- (**b**) and contrast-enhanced T1-weighted (**c**) images show swelling of the uterine tube (*arrow*), which appears heterogeneous due to edema and necrotic areas. Adjacent a small liquid layer is visible (*arrowhead*) and also evident in the sagittal T2-weighted image (**d**). The fat saturated T2-weighted sequence (**e**) shows inflammatory involvement (*asterisks*) of the adjacent tissue with a small circumscribed collection (*curved arrow*) adjacent to the uterine fundus (*U*) whose margins appear ill-defined

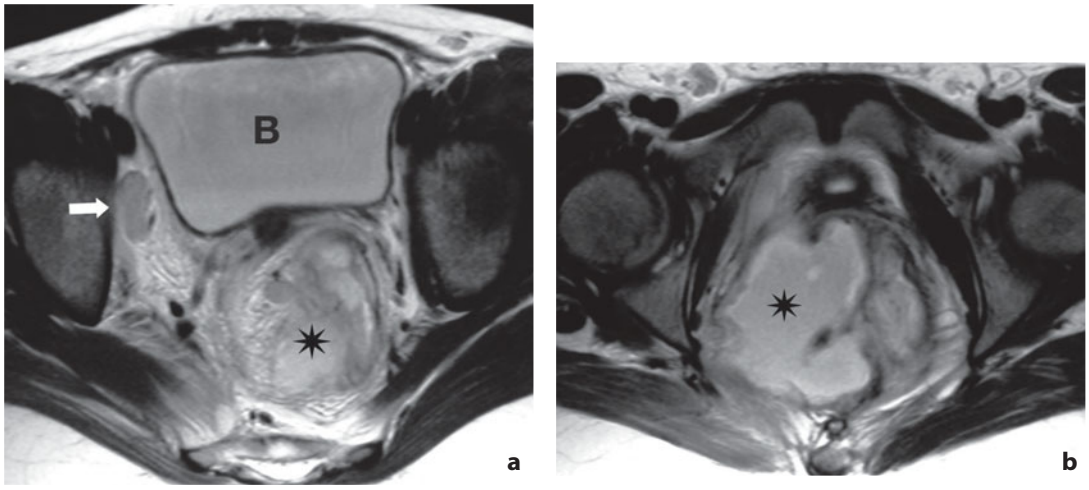

Fig. 18.13a,b. Magnetic resonance. Abscess of uterine tube. **a** Axial T2-weighted image shows a circumscribed heterogeneous collection (*asterisk*) located in the adnexae. The *arrow* indicates an enlarged right external inguinal lymph node due to inflammatory reaction. **b** More caudal plane shows saccular liquid collection also involving the right ischiorectal fossa. *B*, urinary bladder

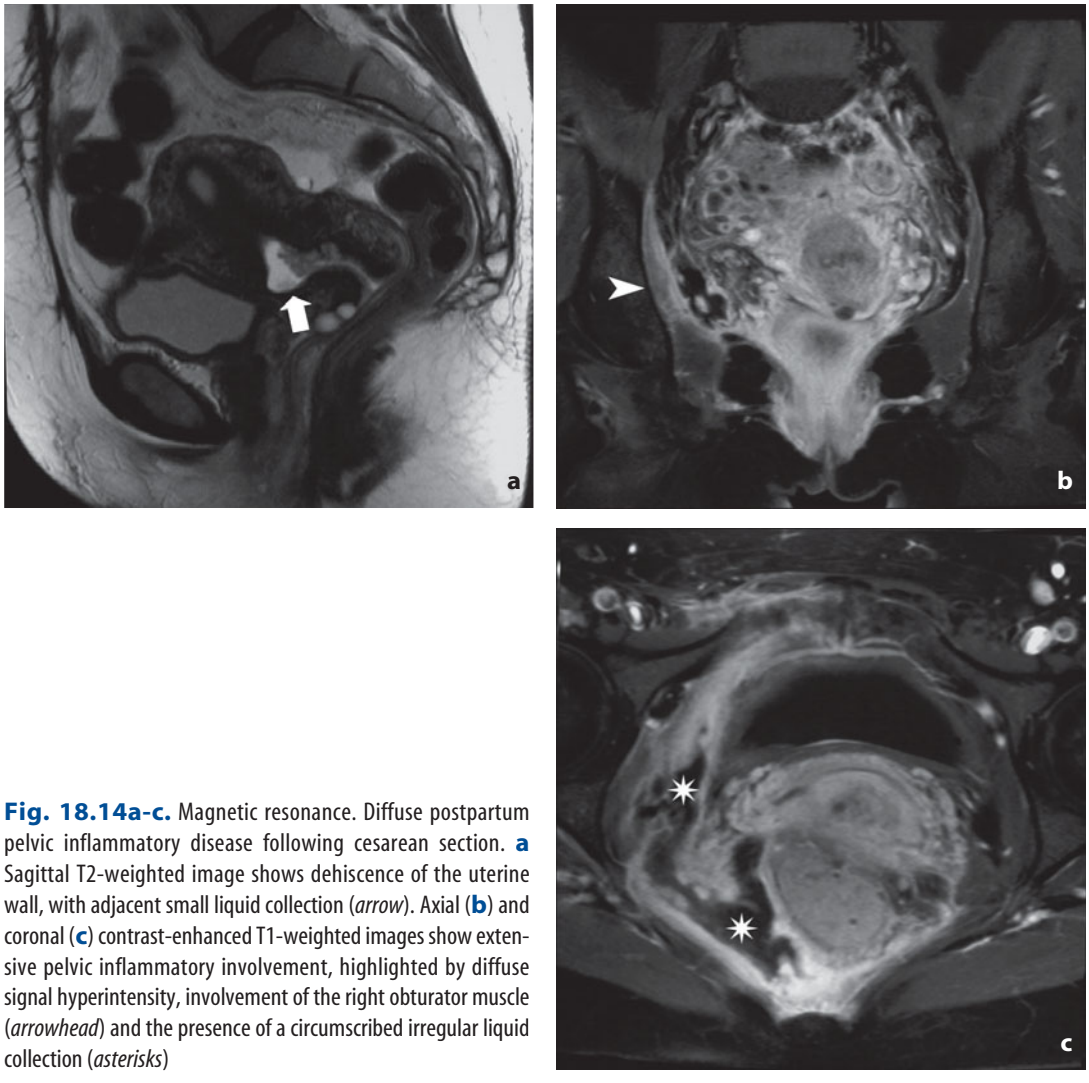

Fig. 18.14a-c. Magnetic resonance. Diffuse postpartum pelvic inflammatory disease following cesarean section. **a** Sagittal T2-weighted image shows dehiscence of the uterine wall, with adjacent small liquid collection (*arrow*). Axial (**b**) and coronal (**c**) contrast-enhanced T1-weighted images show extensive pelvic inflammatory involvement, highlighted by diffuse signal hyperintensity, involvement of the right obturator muscle (*arrowhead*) and the presence of a circumscribed irregular liquid collection (*asterisks*)

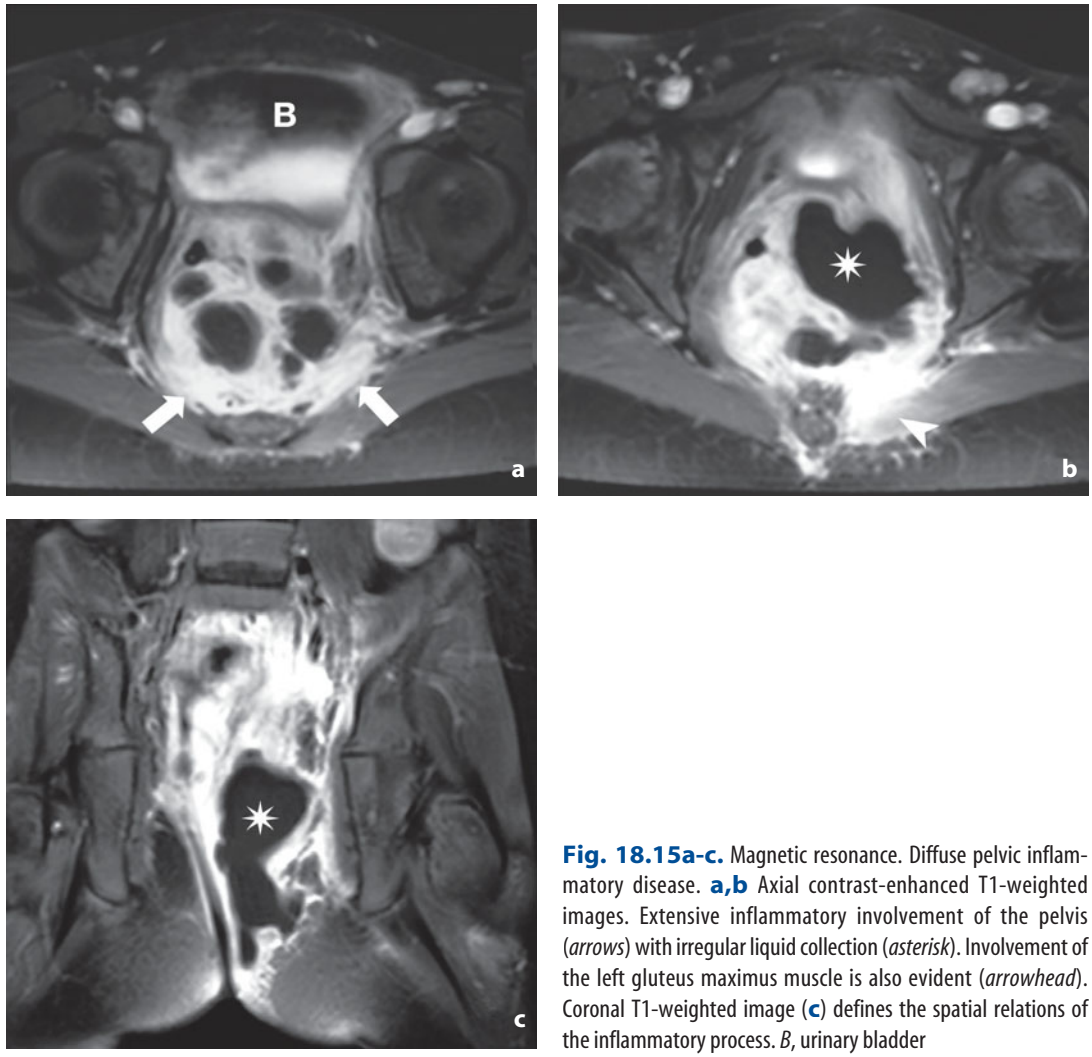

Fig. 18.15a-c. Magnetic resonance. Diffuse pelvic inflammatory disease. **a,b** Axial contrast-enhanced T1-weighted images. Extensive inflammatory involvement of the pelvis (*arrows*) with irregular liquid collection (*asterisk*). Involvement of the left gluteus maximus muscle is also evident (*arrowhead*). Coronal T1-weighted image (**c**) defines the spatial relations of the inflammatory process. *B*, urinary bladder

Clinical Approach to Uterine Disease

19

E. Sartori, D. Gatti, F. Quaglia

Uterine Fibroids

A fibroid (also known as fibroma, myoma, fibromyoma and leiomyoma) is a benign tumor of the uterus which arises from the smooth muscle cells of the myometrium. The estimated incidence between 15% and 30% is almost certainly conservative, with a peak between 35 and 50 years.

Clinical and experimental findings suggest a hormonal, especially estrogen-dependent etiopathogenesis. In fact uterine fibroids prevalently develop in reproductive age, increase in size during pregnancy and regress after menopause. Macroscopically the uterus appears altered in shape and volume by one or more nodes of a size varying from a few millimeters to over 20 cm in diameter.

Fibroids most commonly occur at the level of the uterine body (95%) in either a subserous, intramural, submucosal or intraligamentary site. In the subserous form the lesion expands towards the periphery of the wall in the form of a sessile or pedunculated projection covered by peritoneum. Intramural fibroids are located within the uterine wall, which they deform with their development. The pseudocapsule of the lesion is usually preserved intact. Submucosal fibroids develop towards the endometrial cavity, whereas the intraligamentary variety expands between the two layers of the broad ligament.

The gross appearance reveals a fascicular or vortex-like arrangement with a color varying from whitish to red. Microscopic examination reveals smooth muscle fiber cells interlaced with connective cells arranged in groups or forming vortices.

Fibroids are generally characterized by slow and progressive growth, although they occasionally grow rapidly. During menopause they undergo a gradual reduction or regression, but do not disappear completely. They can undergo degeneration (associated with poor circulation) with subsequent necrosis and inflammation. The degeneration can be differentiated into:

- hyaline: the connective tissue is replaced by acellular hyaline material;
- cystic: cavities filled with blood or a gelatinous or mucinous liquid form within the fibroid;
- fatty: the microcells are replaced by small globules of fat giving the fibroid a pale yellow color;
- calcified: common in subserous fibroids and in advanced age;
- red: this form is characterized by aseptic necrobiosis and usually occurs in large intramural lesions, especially during pregnancy, due to acute changes in blood supply.

Malignant degeneration is extremely rare (0.2-0.4%).

Occasionally atypical proliferation and/or mitotic activity can be observed, which renders the differential diagnosis with leiomyosarcoma challenging.

Uterine fibroids are symptomatic only in 20-50% of cases. Most cases are in fact diagnosed incidentally during a gynecologic examination for other reasons. When present the symptoms are correlated with the number, dimensions and above all the

L. Olivetti, L. Grazioli (eds.), *Imaging of Urogenital Diseases*,

site of the tumor. Hemorrhage is relatively frequent in the submucosal forms and is predominantly due to an increase in menstrual blood loss (hypermenorrhea, menorrhagia, menometrorrhagia). Pain is rare and can be caused by complications: necrosis, torsion, infection or expulsion of a submucous nodule. The most frequent symptom related to compression is pollakiuria. Uterine fibroids may be a cause of infertility, increased risk of miscarriage and premature birth.

Treatment is closely associated with the age and parity of the patient, presence and degree of symptoms, and the size and site of the fibroid(s).

Medical therapy is generally used to control menometrorrhagia (the most utilized agents are synthetic progestins: medroxyprogesterone acetate, norethisterone) or to correct anemia in view of surgery (gonadotrophin-releasing hormone [GnRH] agonists which inhibit the secretion of gonadotropin and block ovarian activity).

Surgical treatment can be conservative (laparotomic or laparoscopic myomectomy) or radical (laparotomic, laparoscopic or transvaginal hysterectomy).

American College of Obstetricians and Gynecologists (1994) Uterine leiomyomata. ACOG Technical Bulletin 192, Washington, DC

American Fertility Society (1992) Myomas and reproductive dysfunction: guideline for practice. The American Fertility Society, Birmingham, AL

Buttram VC Jr, Reiter RC (1981) Uterine leiomyomata: etiology, symptomatology, and management. Fertil Steril 36:433-445

Quade BJ (1995) Pathology, cytogenetics, and molecular biology of uterine leiomyomas and other smooth muscle lesions. Curr Opin Obstet Gynecol 7:35-42

Vollenhoven BJ, Lawrence AS, Healy DL (1990) Uterine fibroids: a clinical review. Br J Obstet Gynaecol 97:285-298

Endometrial Cancer

Epidemiology

Endometrial carcinoma is currently the most frequent malignant lesion of the reproductive system and second only to breast cancer among female tumors. Over the last 30 years there has seen a constant and significant increase in disease throughout the world, with an incidence of around 150,000 new cases per year. The industrialized countries are at greater risk, whereas the incidence in developing countries is lower.

Risk Factors

Eighty per cent of cases are found in women in menopause, and only 5% in women below 40 years. Hormonal factors are thought to play an important role, particularly hyperestrogenism. Risk factors also include sterility, anovulation and irregular periods, nulliparity, late menopause and unopposed estrogen. Obesity, arterial hypertension and diabetes mellitus are also certainly involved. Antiestrogens (in particular tamoxifen) taken for treatment of breast cancer have been suggested to play a role: these drugs have an estrogen-like effect on the endometrium after menopause. Lastly, the importance of genetic factors has been recognized.

Pathology

Clinically the tumor presents two forms: *circumscribed* with papillary, polypoid or plaque-like appearance or *diffuse* with extensively infiltrated endometrium and polypoid, pale and friable appearance.

Microscopically **endometrioid adenocarcinoma** is the most common subtype (75/80%) and may appear in the setting of atypical hyperplasia (even though this sequence is not compulsory for carcinogenesis). Variants of the endometrioid form are **adenocarcinoma with squamous differentiation** (or **adenocanthoma**) and **adenosquamous carcinoma**. The **mucinous** histotype accounts for 9% of endometrial carcinomas. Less frequent subtypes with poorer prognosis include **clear cell carcinoma**, **papillary serous adenocarcinoma**, **squamous carcinoma**, **undifferentiated carcinoma** and **mixed-type carcinomas**.

Spread Patterns

In most cases, in relation to its slow growth, the tumor is limited to the uterine body. The most common method of spread is to contiguous structures, with direct extension to the myometrial wall and the cervical canal and worsening of prognosis. The tumor can invade the vagina and the uterine tubes, and in 5–10% of cases ovarian metastases are present. Spread to the peritoneal cavity via free transplant through the uterine tubes is also possible. Other potential spread patterns are hematogenous, producing distant metastases, and lymphatic. In the latter case the tumor spreads to the pelvic, paracaval, para-aortic and inguinal lymph nodes via a double lymphatic drainage (one of the uterine body itself and the other of the cervix) which justifies the different involvement of the lymph nodes, even though the pelvic nodes are chiefly involved.

Prognostic Factors

The main factors considered to influence the prognosis of endometrial cancer are stage, histologic grade, myometrial invasion, histotype and lymph node metastasis. The **stage** is in relation to the extension of the tumor (Table 19.1). The **grading** presents a clear inverse correlation with survival, which varies from 80-90% for G1 to 60-70% for G3.

Myometrial invasion is an important factor when the tumor is confined to the uterus and is associated with other negative prognostic factors, such as lymph node status and degree of differentiation. Some **histotypes** (classic adenocarcinoma and with squamous differentiation, secretory carcinoma and papillary carcinoma) have a more favorable prognosis than other forms (clear cell carcinoma, mixed adenosquamous carcinoma, papillary serous carcinoma and undifferentiated carcinoma).

Lymph node metastasis is the most important prognostic factor for predicting survival. In fact some 10% of stage I patients have positive pelvic lymph nodes and 7% have involvement of the lumbar-aortic lymph nodes.

Table 19.1. International Federation of Gynecology and Obstetrics (FIGO) staging of endometrial cancer

Stage	IA	Tumor is confined to the endometrium
	IB	Tumor invades less than 50% of the myometrial thickness
	IC	Tumor invades more than 50% of the myometrial thickness
Stage	IIA	Tumor involves the cervical mucosa
	IIB	Tumor involves the cervical stroma
Stage	IIIA	Tumor involves the serosa and/or the adnexae and/or peritoneal cytology is positive
	IIIB	Presence of vaginal metastases
	IIIC	Metastases to the pelvis or to the pelvic and/or paraaortic lymph nodes
Stage	IVA	Tumor with invasion of the rectum or urinary bladder
	IVB	Distant spread or intraabdominal metastases and/or to the inguinal lymph nodes

Other minor prognostic factors include **peritoneal cytology**, **invasion of the lymphoglandular spaces**, **involvement of the tubal angles**, **tumor volume**, **the state of progesterone receptors** and **ploidy**.

Diagnosis

Clinical onset is usually characterized by irregular and abnormal blood loss. Traditionally, the diagnosis should be confirmed by histologic examination. The examination of choice is **hysteroscopy**, which enables the direct visualization of the uterine cavity with evaluation of the extent of the tumor to the cavity itself and to the cervical canal. In this way a sample of tissue that is considered pathologic can be collected for analysis by the pathologist. Once histologic confirmation has been obtained, a number of examinations are recommended to correctly evaluate the spread of the disease and to plan the best therapeutic strategy.

First of all, a **clinical examination** is performed with a thorough evaluation of the possible involvement of the cervix, vagina and the parametrium. **Transvaginal ultrasonography** can by used to measure the thickness of the endometrium and myometrium and to assess the possible invasion of the latter. Currently **magnetic resonance** is the best technique for evaluating invasion of the myometrium and the cervical stroma, in that it provides preoperative indications for modulating the radicality of surgery on the uterus and pelvic and/or lumbar-aortic lymph nodes. **Computed tomography** is able to accurately study the retroperitoneum and therefore lymph node involvement. **Chest radiography** can rule out pulmonary metastases, while **cystoscopy** and **rectosigmoidoscopy** are reserved for cases with suspected secondary involvement of the urinary bladder or colorectum.

Treatment

The optimal approach to carcinoma is surgical removal of the uterus and adnexae. The traditional **laparotomic** approach is being replaced by **laparoscopy** in centers where the operators are sufficiently experienced to perform the technique. Laparoscopy in fact guarantees similar prognostic results, less discomfort for the patient, shorter hospitalization times and faster recovery of function.

Vaginal surgery, whether laparoscopic-assisted or not, is usually reserved for patients of advanced age, particularly obese patients with associated conditions which significantly increase operative risk, and usually in the initial stages, with results similar to those obtained with laparotomy and laparoscopy. Treatment involves **preoperative lavage** of the abdominal cavity for the purposes of cytologic examination, **extrafascial hysterectomy** with **bilateral adnexectomy**, **colpectomy** of the superior third and **pelvic lymphadenectomy** possibly associated with **lumbar-aortic lymphadenectomy**. The radicality of surgery to the uterus and periuterine tissue is modulated according to the massive involvement of the uterus, neoplastic extension to the endocervix or the stroma of the uterine cervix, with possible parametrial involvement and metastasis to the various lymph node stations.

The direct positive relationship between grading, myometrial involvement and lymph node metastases has been well documented – an increase in grading or myometrial invasion is associated with an increase in the percentage of lymph node metastases. In this setting performing lymphadenectomy is of primary importance for better defining the stage of the disease and as a consequence specifying the prognosis. Lymphadenectomy includes the nodes draining the uterine body and cervix: the pelvic, lumbar-aortic and inguinal lymph nodes. The pelvic lymph nodes, and in particular the **superficial obturator** and **external iliac nodes**, are the most commonly involved, with concomitant metastasis to the lumbar-aortic lymph nodes in 40% of

cases. In the event of negative pelvic lymph nodes, the lumbar-aortic nodes are positive in only 2% of patients.

In cases considered to be at risk, the treatment of endometrial cancer also includes the possibility of performing **adjuvant therapy**, with the use of **external radiotherapy** and/or **brachytherapy** and **chemotherapy**.

Ayhan A, Tuncer R, Tuncer ZS et al (1994) Correlation between clinical and histopathologic risk factors and lymph node metastases in early endometrial cancer (a multivariate analysis of 183 cases). Int J Gynecol Cancer 4:306-309

Creasman WT, Morrow CP, Bundy BN et al (1987) Surgical pathologic spread patterns of endometrial cancer. A Gynecologic Oncology Group Study. Cancer 60:2035-2041

Frei KA, Kinkel K (2001) Staging endometrial cancer: role of magnetic resonance imaging. J Magn Reson Imaging 13:850-855

Mariani A, Maurice JW, Keeney GL et al (2003) Endometrial cancer: predictors of peritoneal failure. Gynecol Oncol 89:236-242

Sartori E, Gadducci A, Landoni F et al (2001) Clinical behavior of 203 stage II endometrial cancer cases: the impact of primary surgical approach and of adjuvant radiation therapy. Int J Gynecol Cancer 11:430-437

Trimble EL, Kosary C, Park RC (1998) Lymph node sampling and survival in endometrial cancer. Gynecol Oncol 71:340-343

Wilson TO, Podtraz KC, Gaffey TA et al (1990) Evaluation of unfavourable histologic subtypes in endometrial adenocarcinoma. Am J Obset Gynecol 162:418-426

Zaino RJ, Kurman RJ, Diana KL, Morrow CP (1996) Pathologic models to predict outcome for women with endometrial adenocarcinoma: the importance of the distinction between surgical stage and clinical stage. A Gynecologic Oncology Group Study. Cancer 77:1115-1121

Cervical Cancer

Epidemiology and Etiopathogenesis

Carcinoma of the cervix is the third gynecologic malignancy after endometrial and ovarian cancer. It is prevalent in developing countries. In Italy the incidence of cervical cancer is 10 cases per 100,000 women/year.

The mean age at diagnosis is 45, even though there is evidence of a greater frequency among younger women, probably in relation to biologic variations of the tumor induced by human papilloma virus (HPV). Almost all case of squamous carcinomas and most adenocarcinomas in fact contain DNA of HPV oncogenes. Types 6-11-16-18-31-33-35 have been shown to be associated with human gynecologic lesions. HPV 16 and 18 are the cause of 70% of cervical carcinomas.

Other risk factors include sexual promiscuity, socioeconomic conditions and exposure to carcinogens.

Clinical and Histologic Forms

There are a number of clinical presentations: *exophytic*, involving only the superficial aspect of the cervix with a polypoid or "cauliflower" appearance, friable and easily hemorrhaging; *endophytic*, or ulcerative; *endocervical*, which expands within the cervix tending to enlarge and deform it and thus conferring upon it a classic barrel-shape.

There are two fundamental histotypes:

- **squamous carcinoma**, accounting for 80% of cervical cancers. It arises from pre-

existing **squamous** dysplasia and originates from the junction between squamous and cylindrical or transformation zone epithelium;
- **adenocarcinoma**, accounting for 20% of cervical carcinomas. It arises in the pseudoglandular area of the cervical canal.

In addition to the two most common histotypes there is also **clear-cell carcinoma**, which accounts for around 5% of adenocarcinomas, and **adenosquamous carcinoma**, in which both glandular and squamous components coexist.

Spread Patterns

Carcinoma of the cervix tends to grow locally, **continuously** invading the paracervical tissues and the surrounding pelvic organs to then spread to the regional lymph nodes and in the late stage give rise to distant metastases. Direct extension occurs in different directions: longitudinal, towards the vagina; superior, involving the body of the uterus; lateral, into the parametrium and paracolpium and in advanced stages reaching the pelvic wall. Parametrial invasion can lead to uni- or bilateral ureteric obstruction. Anterior or posterior direct spread can lead to invasion of the urinary bladder and rectum, respectively.

Even lymph node metastasis is common. The paracervical and parametrial lymph nodes can be the first to be involved, even though direct involvement to the lymph nodes of the pelvic wall is more common.

The incidence of lymph node metastasis is directly proportional to the local extension of the tumor and therefore to the stage: IB=15-25%; II=25-40%; III=40-60%; IV=50-65%. Even the percentage of paracaval-para-aortic metastases increases in relation to the stage: IB=5%; II=15-30%; IV=35-40%.

Hematogenous spread of cervical cancer is decidedly uncommon, although occasionally cases of metastasis to the lungs, liver, bone and brain do occur, especially in the terminal phases of the disease.

Staging

In order to correctly plan treatment, the main aim of staging is to define the extent of the tumor at the time of diagnosis, i.e. tumor volume, stromal invasion (cervical ring), parametrial invasion, local spread, lymph node metastasis and anatomic state and course of the urinary tract.

The FIGO staging system (**Table 19.2**) is essentially based on clinical findings (gynecologic examination and colposcopy). In stage I the tumor is confined to the cervix, in stage II it has extended to the vagina or the parametrium but not to the pelvic wall, in stage III it has extended to the pelvic wall (with possible hydronephrosis or nonfunctioning kidney) and in stage IV there is invasion of the bladder or rectal mucosa or distant metastasis.

Diagnosis and Pretreatment Examinations

The clinical examination is the key to staging of cervical cancer. In particular, combined rectovaginal examination enables evaluation of the parametrium and the pelvic walls, thus identifying areas of rigidity, retraction or nodularity which may indicate neoplastic invasion.

Imaging studies integrate the clinical findings, enabling the planning of a personalized treatment program. Chest radiography, computed tomography and magnetic resonance are commonly used techniques. Urography is only occasionally used and lymphangiography has been practically abandoned. Cystoscopy and rectoscopy are

Table 19.2. FIGO staging of cervical carcinomas

Stage 0		Carcinoma in situ, intraepithelial carcinoma
Stage I		Carcinoma is confined to the cervix
	IA	Preclinical cervical carcinoma, diagnosable only under the microscope
	IA1	Microscopically evident minimal stromal invasion
	IA2	Lesions identified microscopically can be measured. Measured stromal invasion should be more than 3 mm but not more than 5 mm with a horizontal spread 7 mm or less
	IB	Lesions larger than stage IA2, identified both clinically and nonclinically. The characteristics of the invasion of the surrounding tissue should not be used to alter the staging, although they should be recorded for guiding later treatment options
Stage II		Carcinoma extends beyond the cervix, but not to the pelvic wall. Carcinoma invades the vagina, but not the inferior third
	IIA	No evidence of parametrial invasion
	IIB	Evidence of parametrial invasion
Stage III		Carcinoma extends to the pelvic wall. Rectal examination demonstrates no cancer free space between the tumor and the pelvic wall. Tumor invades the inferior third of the vagina. All cases with hydronephrosis or functional exclusion of the kidneys should be included, unless they are due to other causes
	IIIA	Invasion does not reach the pelvic wall, but does reach the inferior third of the vagina
	IIIB	Extension to the pelvic wall or hydronephrosis or functional exclusion of the kidneys
Stage IV		Carcinoma extends beyond the pelvic cavity or has clinically invaded the mucosa of the bladder or the rectum
	IVA	Tumor spread to the adjacent organs
	IVB	Distant metastasis

indicated only in advanced stages of disease with the clinical suspicion of spread to the viscera.

In clinical practice there has been a modification over time of the instrumental evaluation of the patient with cervical cancer. Instead of several examinations there is a tendency to use a single imaging technique capable of evaluating the various prognostic factors.

Prognosis and Survival

Squamous carcinoma of the uterine cervix is one of the tumors with the highest cure rate (overall rate of 50%). The prognosis is highly favorable in patients with early stage disease and extremely severe in advanced forms: 85% cure at stage I; 50-60% at stage II; 30% at stage III and 5-10% at stage IV. Tumor volume and lymph node status associated with clinical stage are the main prognostic factors. Degree of angiogenesis, involvement of the capillary-like spaces, percentage of cervical stroma invaded, extension to the uterine body, status of resection margins, patient age and comorbidities are other important prognostic factors.

Treatment

Radical hysterectomy with pelvic/lumbar-aortic lymphadenectomy is the treatment of choice in stages IA-B/IIA. The surgical approach can be integrated with pelvic radiotherapy in the event of negative prognostic factors at histology. In advanced stages the

treatment of choice is radiotherapy associated with brachytherapy and possibly chemotherapy. For patients with distant metastasis treatment generally involves systemic chemotherapy with or without pelvic radiotherapy.

Around 50% of recurrences are diagnosed during the first year of follow-up and 75% within the first two years. Central pelvic recurrences may still be treated with surgery, which may involve evisceration. Clinical follow-up is closely accompanied by imaging studies with magnetic resonance, computed tomography and positron emission tomography. The latter, and most recently introduced, modality is currently the technique of choice for systemic study of the patient.

Magrina JF, Goodrich MA, Lidner TK et al (1999) Modified radical hysterectomy in the treatment of early squamous cervical cancer. Gynecol Oncol 72:183-186

Markman M (2007) HPV vaccines to prevent cervical cancer. Lancet 369:1837-1839

Mathur SP, Mathur RS, Creasman WT et al (2005) Early non invasive diagnosis of cervical cancer. Cancer Biomark 1:183-191

Rose PG, Bundy BN, Watkins EB et al (1999) Concurrent cisplatin-based radiotherapy and chemotherapy for locally advanced cervical cancer. N Eng J Med 340:1144-1153

Zand KR, Reinhold C, Abe H et al (2007) Magnetic resonance imaging of the cervix. Cancer Imaging 7:769-776

Diagnostic Imaging of the Uterus

20

L. Olivetti, L. Grazioli, B. Frittoli

Endometritis

Pathology

Endometritis is an infection of the endometrium, often in the setting of myometritis and peri-parametritis, even though these usually are features of pelvic peritonitis.

Endometritis can be classified in **acute** and **chronic** forms. The former is characterized by purulent vaginal discharge, whereas the latter tends to be an unhealed and recurrent acute form. Chronic endometritis is a relatively rare condition, since the periodic menstrual shedding of the functional endometrium favors the healing process. The chronic form may develop into atrophy.

Endometritis arises after postabortion or postpartum infection. The most frequent agents are *Streptococcus* species, whereas gonococcal forms are less common. Today a much less common form is tubercular endometritis, which is often asymptomatic and can cause infertility. The fibrotic occlusion of the internal uterine os leads to the accumulation of caseous exudate in the endometrial cavity and enlargement of the uterus (tuberculous pyometra). The existence of syphilitic endometritis is a debatable question. Lastly, there are rare fungal, sarcoid and talc granulomatous forms.

Diagnostic Imaging

The **ultrasonography** (US) appearance can be particularly vague and aspecific, even in the presence of manifest clinical presentation. The approach may be suprapubic, although transvaginal (TVUS) is preferable for a more thorough evaluation of the organs involved and the presence of masses. The presence of liquid and occasionally air may be observed inside the endometrial cavity, which appears thickened, hypoechoic and indistinct with irregular margins (**Fig. 20.1**). If the infection occurs post-

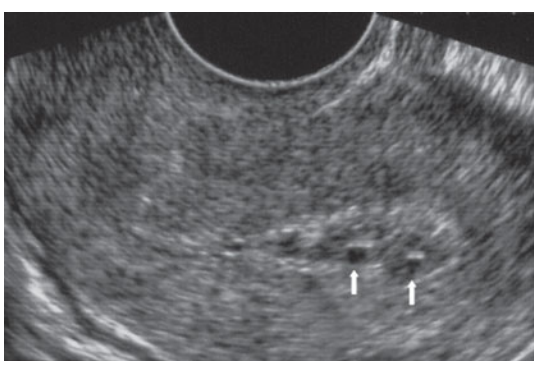

Fig. 20.1. Ultrasonography. Endometritis. Endometrial thickening following miscarriage. Central hyperechoic foci are evident with posterior shadowing produced by gas (*arrows*)

L. Olivetti, L. Grazioli (eds.), *Imaging of Urogenital Diseases*,

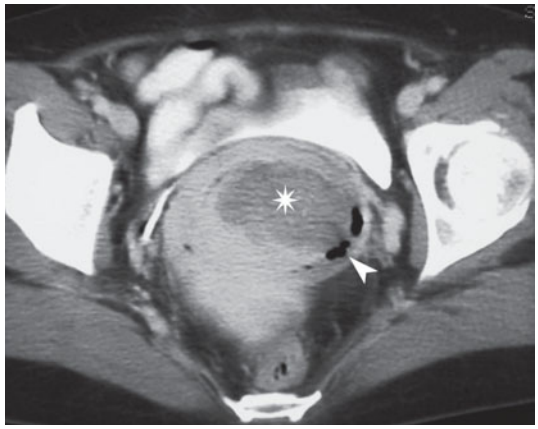

Fig. 20.2. Computed tomography. Endometritis. Axial image acquired in the venous phase. The uterus is enlarged and occupied by heterogeneous material (*asterisk*) in which small bubbles of gas are apparent (*arrowhead*)

partum, an echoic tissue component indicating the retention of placental fragments can be identified. Occasionally the findings are aspecific and include an enlarged hypoechoic uterus with thickening of the uterosacral ligaments in the more advanced forms. Often the inflammation also involves the enlarged ovary and uterine tubes, with the presence of tuboovarian abscesses. If the disease progresses, a reactive inflammation of the surrounding pelvis (pelvic peritonitis) occurs, whereas the abdominal organs appear normal. **Color Doppler** is able to evaluate vascularity and increased pulsed flow in the inflamed tissue.

Computed tomography (CT) is able to identify morphologic-structural changes of the uterus and ovaries induced by the inflammatory process when advanced, as well as even indistinct lesions of the fascial plane of the pelvic floor, thickening of the uterosacral ligaments and/or corpuscular fluid collections in the setting of pelvic peritonitis (**Fig. 20.2**).

In the acute form the uterus appears nonuniform with ill-defined borders and poor visualization of the uterine cavity. After contrast medium injection the inflamed areas usually appear hypoattenuating and well defined in the setting of a hyperperfused, and therefore hyperattenuating, uterus. In postpartum infections hemorrhagic areas/clots or placental fragments can be identified (with problems for differential diagnosis).

The finding of a superfluid liquid collection in the uterine cavity is indicative of pyometra. This is more common in postmenopausal women in case inflammation (chronic inflammation in particular) causes an obstruction of the internal uterine os. CT is unable to distinguish between a clot and placental fragments in the setting of postpartum infection.

Magnetic resonance (MR) is currently used only in the forms of pelvic peritonitis due to its high sensitivity and specificity, even though its ability to distinguish the various anatomic and structural components of the uterus is well known.

Like CT, on MR endometritis appears as an enlargement of the uterine cavity and a change in the normal signal of the endometrium, while the fluid collections have a lower signal intensity. If the inflammatory process extends to the muscle wall, heterogeneity of the myometrial junction and the myometrium itself can be observed. Associated intracavitary hemorrhage typically appears with elevated signal intensity in T1-weighted images and with low signal in T2. The presence of an air component is identifiable by an absent signal.

Mulic-Lutvica A, Axelsson O (2007) Postpartum ultrasound in women with postpartum endometritis, after cesarean section and after manual evacuation of the placenta. Acta Obstet Gynecol Scand 86:210-217

Benign Tumors

Leiomyomas

Pathology

Leiomyomas (also known as myomas, fibromas, fibromyomas or fibroleiomyomas) are benign tumors composed of smooth muscle cells interlaced in a connective tissue network and bounded by a pseudocapsule of the compressed tissue of the adjacent normal myometrium. They may arise from both the body and the neck (less common) of the uterus. On the basis of their location they are classified as submucosal, intramural or interstitial and subserous. When they are particularly large, the blood supply tends to become inadequate, with consequent tissue anoxia and frequent degenerative involution of a hyaline (63%), mucoid or myxomatous (19%), cystic (4%), fatty (3%) or hemorrhagic (3%) type. Calcifications are an expression of necrosis and are present in 8% of cases. Sarcomatous degeneration is rare and may be suspected in the event of a sudden increase in volume. Imaging is not sufficiently specific for reaching a diagnosis, unless there are clear signs of invasion or distant metastasis.

Intravenous leiomyomatosis is a rare condition characterized by growth of the mature muscle cells in the lumen of the uterine and pelvic vessels. Vessel infiltration can progress in the vessels of the broad ligament, the uterine and iliac veins and from here to the inferior vena cava and the right atrium.

Diagnostic Imaging

Plain film radiography may occasionally be diagnostic for asymptomatic uterine fibromatosis thanks to visualization of single or multiple large calcifications with variable morphologic appearance (spiraled, onion-leaf, peripheral calcified rim) (**Fig. 20.3**).

On **ultrasonography** the leiomyoma appears as a hypoechoic mass which causes attenuation of the ultrasound beam and distorts the endometrial or serous profile of the uterus. The echogenicity depends on the ratio between the muscular and fibrous components: the greater the prevalence of the latter, the greater the echogenicity, which is also correlated with the vascularity and the presence or otherwise of degenerative phenomena. Calcifications are a common and polymorphous finding. They may

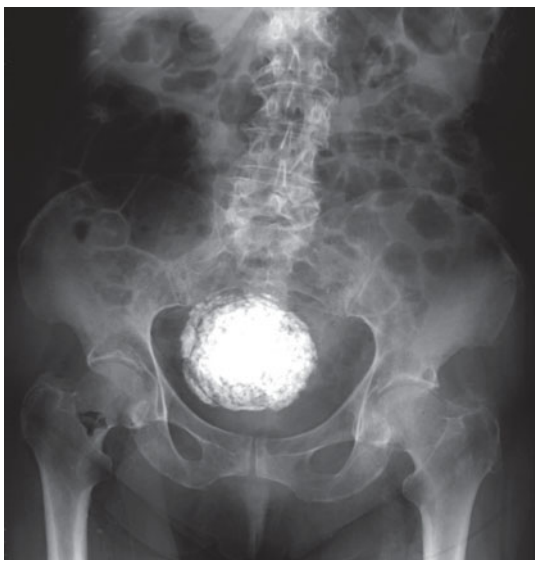

Fig. 20.3. Plain film radiography. Large centropelvic calcification attributable to the uterus

be small and only slightly limit through transmission, or they may be larger and completely absorb the ultrasound beam (Fig. 20.4).

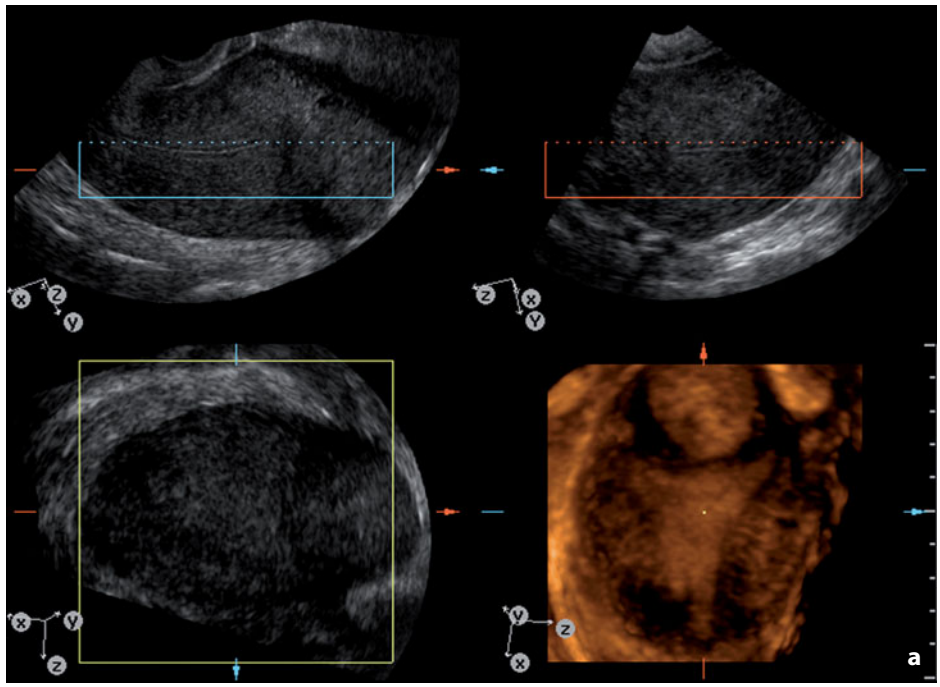

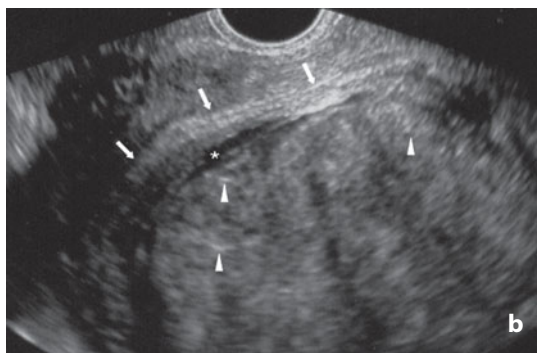

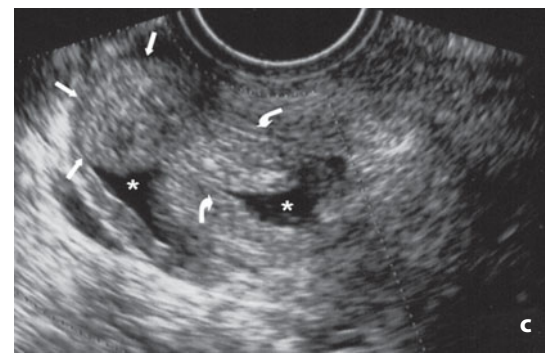

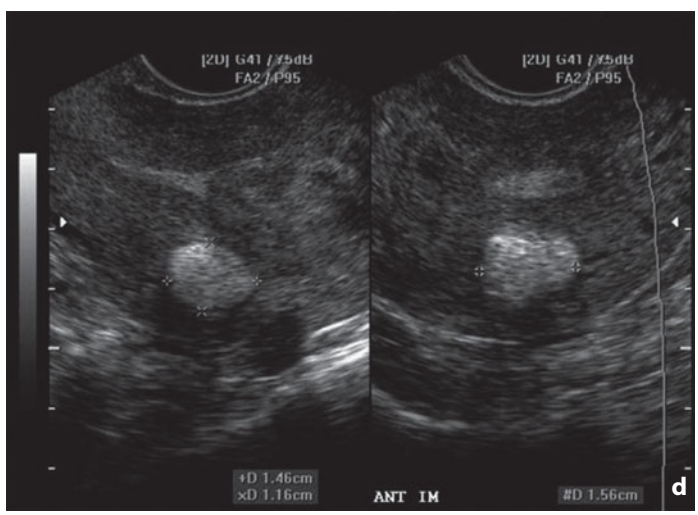

Fig. 20.4a-d. Ultrasonography. Leiomyomas. **a** Intramural leiomyoma of the uterine fundus. 3D reconstruction. **b** Large capsulated uterine leiomyoma (*arrows*). Calcified deposits (*arrowheads*) and necrotic foci (*asterisk*) can be seen. **c** Uterine myoma in expulsion. In the superior vagina a rounded mass (*arrows*) with peduncle can be distinguished between the anterior and posterior aspects of the cervix (*curved arrows*). The endocervix and the vaginal fornices are well visualized due to the interposition of blood (*asterisks*). **d** Leiomyoma (*crosses*) with focal adipose degeneration

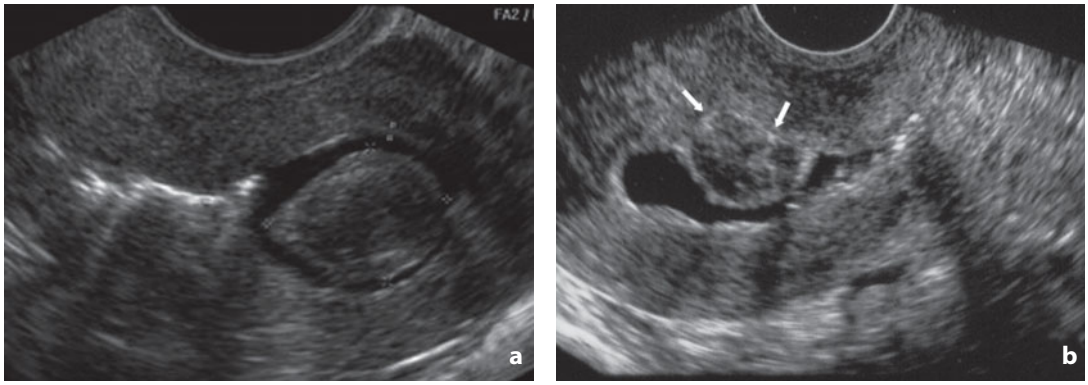

Fig. 20.5a,b. Hysterosonography. Submucosal leiomyoma. **a** The lesion bounded by crosses projects into the endometrial cavity. It appears hypoechoic with echotexture similar to the myometrium. **b** Different case. The lesion (*arrows*) projects into the uterine cavity by more than 50%

The submucosal position is evident by the distortion of the endometrial cavity, or better still, by the protrusion of 50% of the volume of the leiomyoma into the cavity. The exact location (submucosal rather than interstitial) is, however, not easy to define, particularly in postmenopausal women in whom attenuation of the ultrasound beam induced by the leiomyoma translates into poor visualization of the atrophied endometrium. These problems are easily overcome thanks to **hysterosonography**. This technique distends the endometrial cavity and highlights the endometrium, which appears intact in cases of intramural leiomyoma and interrupted by either sessile or pedunculated submucosal lesions. The latter can be differentiated from a polyp thanks to its hypoechoic appearance, its continuity with the myometrium and its vascular pattern (diffuse or peripheral) (Fig. 20.5).

Pedunculated subserous leiomyomas, which generally arise from the uterine fundus or the anterior surface of the body, are the most common cause of diagnostic error. Often the peduncle cannot be visualized, rendering identification of the uterine origin impossible. Lesions growing in the loose tissue of the broad ligament can be confused with adnexal masses. The correct diagnosis is made on the basis of the structural pattern of the lesion and the identification of the ovaries.

The morphologic US study can be integrated with **color or power Doppler**. The vascular topography generally consists of a peripheral ring and centripetal arterial branches, the appearance of which (including flowmetry) depends on many variables. The dimension of the lesion is one of the most important of these, in that in larger lesions there is a rarefaction or even an absence of the vasculature in the central necrotic portion. In these cases a generally hypo-anechoic heterogeneous liquid area is visible.

Arterial vascularization can be a predictor of growth of the leiomyoma. The absence of a vascular arterial peduncle is indicative of a stationary growth pattern, in contrast to the situation of fibromas with multiple arterial vascular foci (Fig. 20.6).

In cases of diagnosed uterine leiomyomas there is no indication for **computed tomography**. However, knowledge of the imaging characteristics is useful for differential diagnosis with other pelvic masses (Figs. 20.7, 20.8).

CT characterization requires the injection of contrast medium. Enhancement is generally late with respect to the normal myometrium, and leiomyomas may appear iso-, hypo- or hyperattenuating in relation to the different composition of the lesion: muscle fibers are more vascular than connective tissue, so when they are prevalent there is greater and longer enhancement.

When multiple and diffuse, intramural leiomyomas can lead to overall enlargement of the uterus. In contrast, when isolated they may appear as nodules with variable

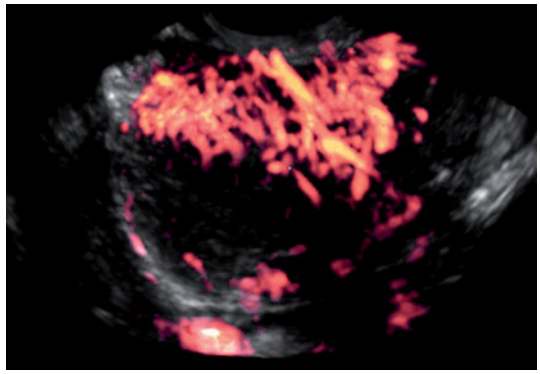

Fig. 20.6. Power Doppler. 3D reconstruction of the vasculature of a uterine myoma

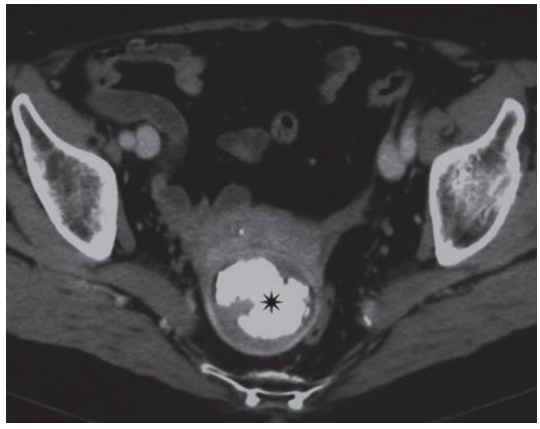

Fig. 20.7. Computed tomography. Calcified leiomyoma. Axial image acquired in the venous phase shows an upright uterus and large heterogeneous leiomyoma with extensive central calcified component (*asterisk*)

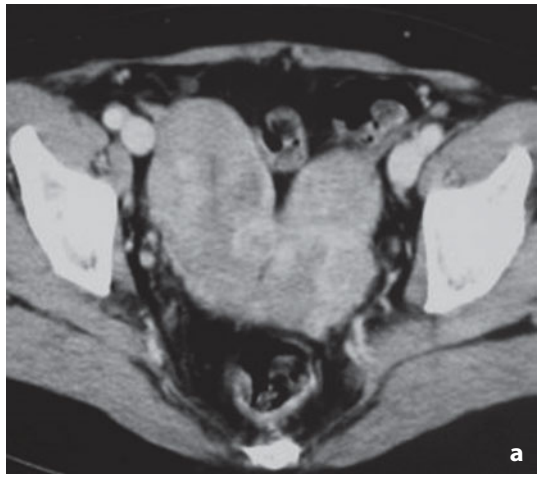

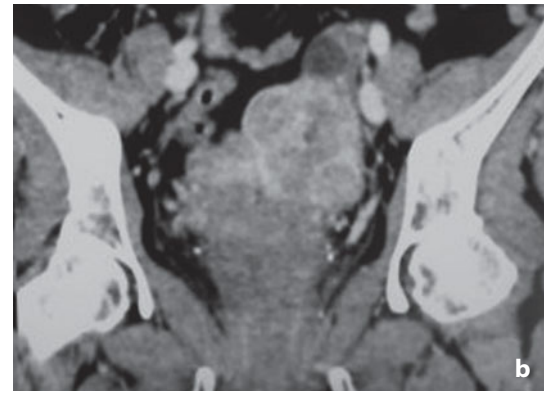

Fig. 20.8a,b. Computed tomography. Multiple intramural leiomyomas in a bicornuate uterus, the profiles of which appear deformed. Axial image (**a**) and coronal reconstruction (**b**)

morphology, dimension and density, the latter being influenced by the degenerative involution and deposition of calcium. Recognition of interstitial fibromas is facilitated by identification of the endometrial cavity (often appearing compressed and displaced). This is an important element for diagnostic purposes in that it enables an endometrial origin of the mass to be ruled out.

More challenging is the characterization of submucosal and pedunculated subserous leiomyomas.

In the context of fibrous tissue there may be heterogeneous areas with hypoattenuating irregular shape indicative of hyaline or cystic degeneration. This appearance may facilitate but also complicate the diagnosis of leiomyoma, especially in cases of complex liquid-like cystic formations with solid intraluminal components which need to be differentiated from complex cystic adnexal masses.

Areas of adipose tissue may be found within fibromas. This is the case in fibromyolipomas and lipoleiomyomas, rare lesions which are nonetheless easily identifiable on CT images.

Torsion of a pedunculated fibroma is an acute pelvic emergent condition. Ischemic necrosis may be associated with inflammation, a situation which is identifiable by the presence of gas or an intralesion purulent collection.

The limitations of CT are essentially related to differential diagnosis with solid adnexal masses such as ovarian thecomas and/or fibromas. The differential diagnosis may be assisted by the identification of normal adnexae the peduncle, or the presence of ascites, which are often associated with ovarian fibromas (Meigs syndrome) but not with uterine fibromas.

Magnetic resonance is the most precise technique for the identification, localization and characterization of leiomyomas. However, it is generally used as a problem-solving modality when TVUS and hysterosonography are nondiagnostic.

Small homogeneous intramural leiomyomas are not easily identifiable in T1-weighted images. In T2 they appear as well-defined lesions with sharp borders. The signal intensity may be iso- or more commonly hypointense to the adjacent myometrium, from which the lesion may be separated by a hyperintense rim composed of congested venous and lymphatic vessels. Leiomyomas with a markedly cellular component and little collagen appear hyperintense in T2.

The signal of leiomyomas varies in accordance with the cellular composition and areas of degeneration present in the tumor, the latter being identifiable by foci or areas of diffuse hyperintensity. In contrast, calcifications appear as areas of signal loss in both T1- and T2-weighted sequences.

The study of uterine fibromas does not usually require the injection of paramagnetic contrast material, which fails to provide significant information. Nonetheless, at 30-90 seconds after contrast medium injection there is a variable increase in signal intensity in relation to the cellularity of the lesion. In general, however, the signal is hypointense to the adjacent myometrium. Oral contrast media may instead be useful to disassociate the fibromas from adjacent bowel loops.

The MR diagnosis of submucosal and intramural fibromas is rather easy, in part thanks to the areas of degeneration. Submucosal fibromas can be readily differentiated from endometrial polyps, which typically appear hyperintense in T2-weighted images (**Figs. 20.9, 20.10**).

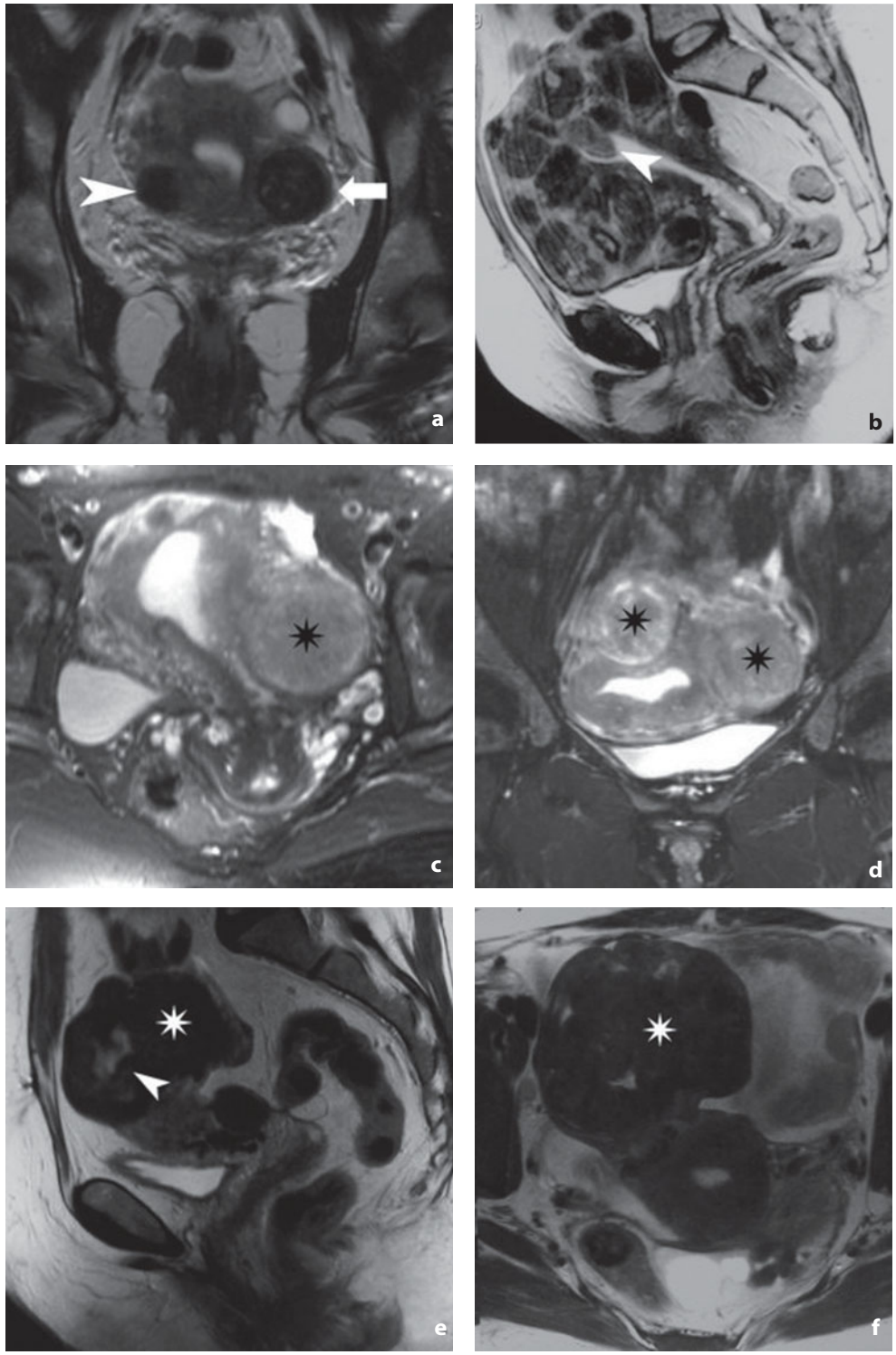

Fig. 20.9a-f. Magnetic resonance. Leiomyomas. **a** Coronal T2-weighted image. Intramural (*arrowhead*) and subserous (*arrow*) leiomyoma. **b** Sagittal T2-weighted image. Multiple intramural leiomyomas cause a change in morphology and volume of the uterus. A small submucosal leiomyoma (*arrowhead*) can be seen protruding into the endometrial canal. **c,d** Axial (**c**) and coronal (**d**) T2-weighted fat saturation images. The *asterisks* indicate two subserous exophytic leiomyomas. **e,f** Sagittal (**e**) and coronal (**f**) T2-weighted images. Large subserous leiomyoma (*asterisk*) with evidence of a small area of cystic degeneration (*arrowhead*)

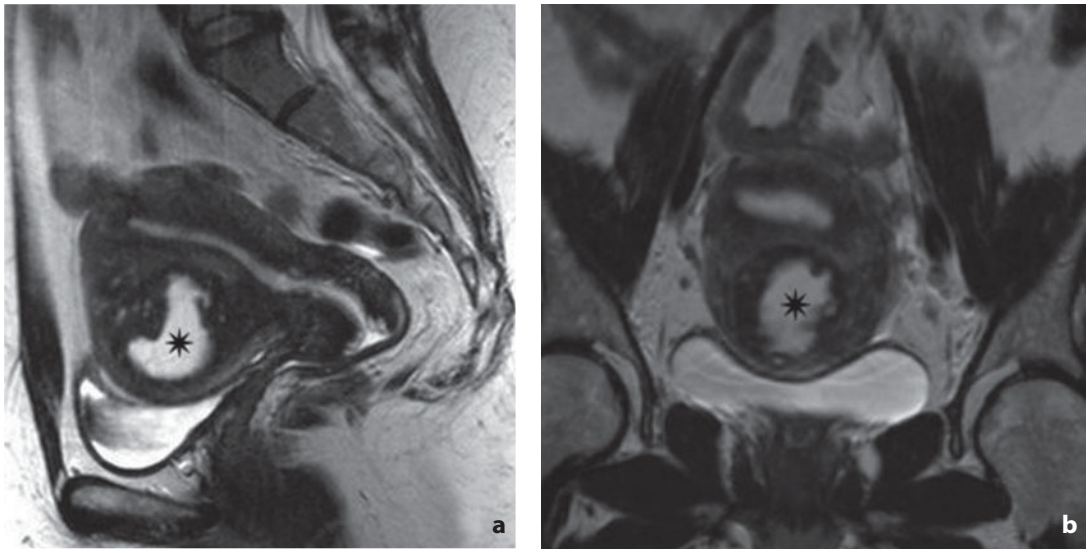

Fig. 20.10a,b. Magnetic resonance. Leiomyoma. Sagittal (**a**) and coronal (**b**) T2-weighted images. Lesion with area of cystic degeneration (*asterisk*)

Dueholm M, Lundorf E, Hansen ES et al (2002) Accuracy of magnetic resonance imaging and transvaginal ultrasonography in the diagnosis, mapping, and measurement of uterine myomas. Am J Obstet Gynecol 186:409-415

Murase E, Siegelman ES, Eric K et al (1999) Uterine leiomyomas: histopathologic features, MR imaging findings, differential diagnosis, and treatment. RadioGraphics 19:1179-1197

Williams PL, Laifer-Narin SL, Ragavendra N (2003) US of abnormal uterine bleeding. RadioGraphics 23:703-718

Adenomyosis and adenomyoma

Adenomyosis is defined as the diffuse presence of ectopic endometrial glands in the myometrium. The condition affects pluriparous women, women aged 35-50 years and women with dysmenorrhea. Prevalence varies from 5% to 70% in relation to the broad range of histologic criteria used to reach the diagnosis. In 25% of cases there is associated presence of leiomyomas: the differential diagnosis is essential because leiomyomas can be removed with myomectomy, whereas hysterectomy is the treatment of choice in symptomatic adenomyosis.

Transvaginal ultrasonography (sensitivity 80-86%, specificity 50-96%, diagnostic accuracy 68-86%) utilizes the following criteria to define the presence of adenomyosis:

- ill-defined hypoechoic myometrium indicative of hyperplasia of the smooth muscle tissue;
- heterogeneous echotexture of the myometrium indicative of echogenic hypertrophy of the ectopic endometrial glands;
- poor definition of the interface between the endometrium and myometrium due to ectopic extension of the endometrium itself;
- scattered small cysts (<5 mm) within the myometrium due to dilatation of the endometrial glands or small hemorrhagic foci.

Additional findings useful for the diagnosis include globular appearance of the uterus, preferential involvement of the posterior myometrium, areas of acoustic shadowing as with leiomyomas although unaccompanied by a mass effect (**Figs. 20.11, 20.12**).

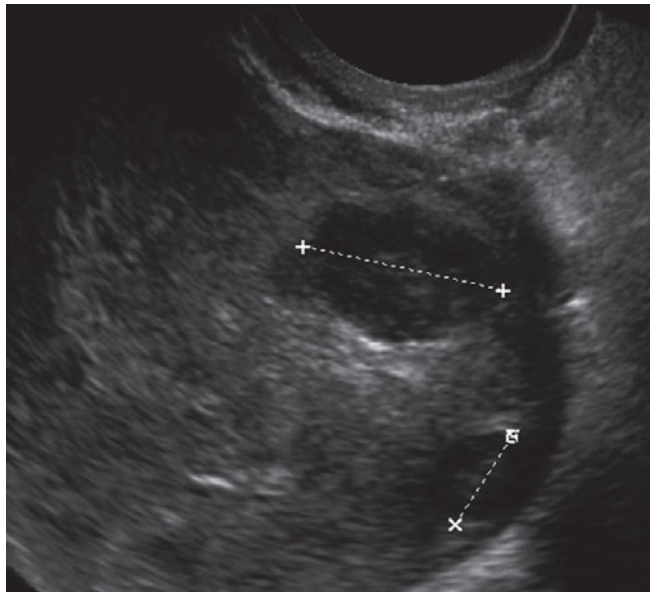

Fig. 20.11. Ultrasonography. Adenomyosis, focal form. Two-dimensional sonogram in the sagittal plane shows two hypoechoic nodules (*crosses*) and absence of pseudocapsule

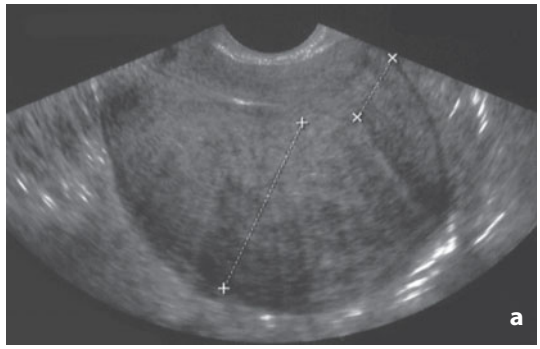

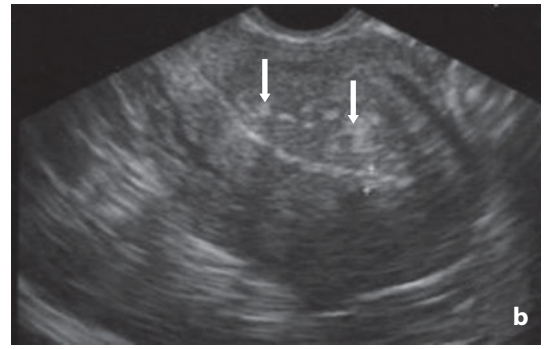

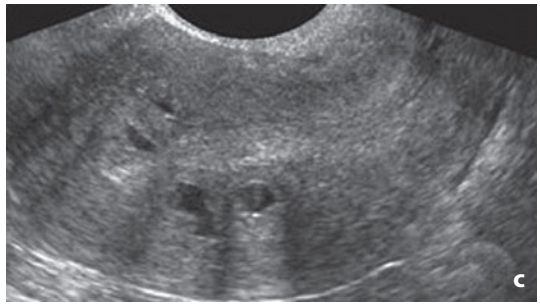

Fig. 20.12a-c. Ultrasonography. Adenomyosis, diffuse form. **a** A "comb-like" image can be visualized at the level of the posterior wall. Of special note is the asymmetrical thickness between the anterior and posterior walls (*crosses*). **b** Diffuse form. Hyperechoic foci (*arrows*) can be seen within the myometrium, and poor delineation of the junctional zone. **c** Diffuse form. Small cystic areas are visible within the myometrium

Despite the moderate diagnostic accuracy mentioned above, TVUS has a number of limitations. These include operator experience, a slow learning curve and persistent difficulty in differential diagnosis with leiomyomas.

Magnetic resonance (not necessarily performed with contrast medium injection) uses T2-weighted sequences for the diagnosis of adenomyosis. Images demonstrate a thickening of the junctional line (>12 mm; the previous cutoff of 5 mm has been abandoned due to frequent false positives) and structural heterogeneity of the myometrium, in which hyperintense spots attributable to aberrant glandular tissue may be visualized. If these spots are also evident in T1-weighted images, they likely indicate small hemorrhagic foci (**Figs. 20.13, 20.14**).

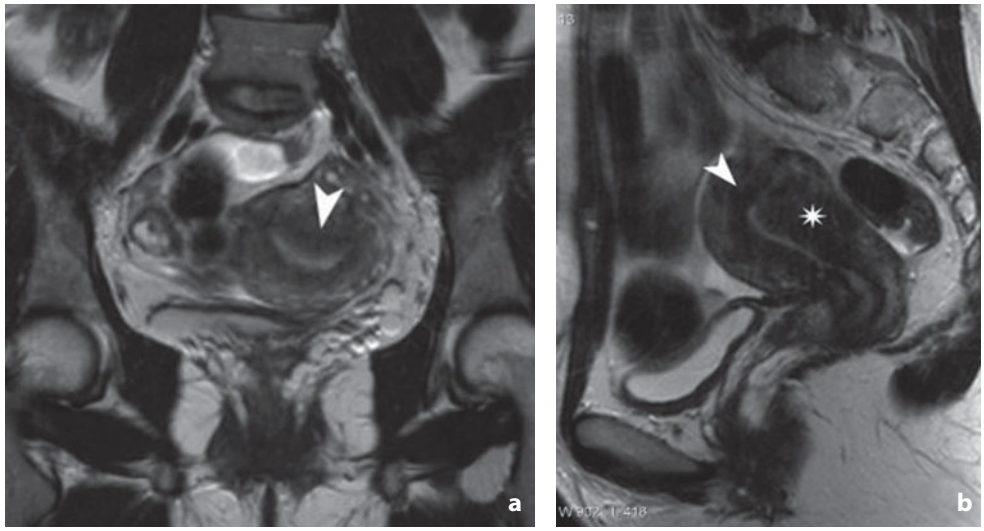

Fig. 20.13a,b. Magnetic resonance. Adenomyosis, focal form. Coronal (**a**) and sagittal (**b**) T2-weighted images. Diffuse thickening of the junctional line (*arrowhead*) with focal alteration of the signal of the myometrium (*asterisk*)

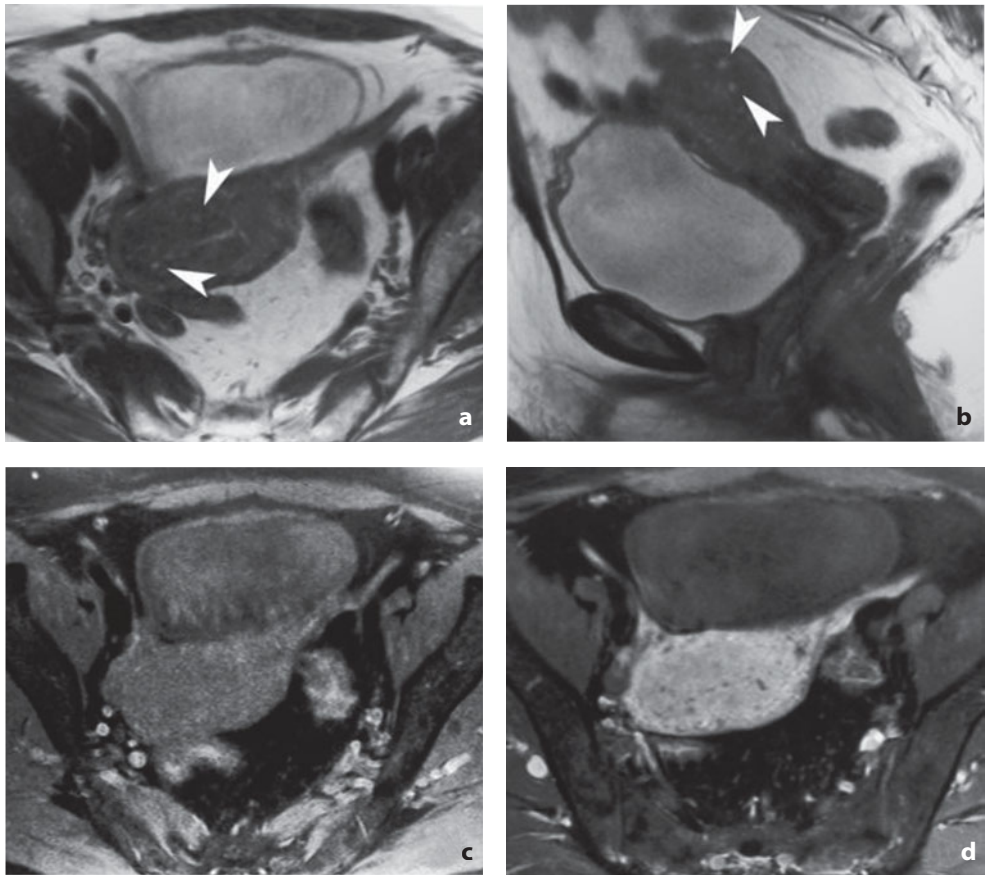

Fig. 20.14a-d. Magnetic resonance. Adenomyosis, diffuse form. Axial (**a**) and sagittal (**b**) T2-weighted images fail to identify the junctional line. Several hyperintense spots are visible within the myometrium and are referable to ectopic foci of endometrium (*arrowheads*). **c,d** Different case. In the axial fat saturated T1-weighted image before contrast medium injection (**c**) the hyperintense spots appear to be hemorrhagic foci. After contrast medium injection (**d**) the diffuse heterogeneity of the structure of the myometrium is confirmed

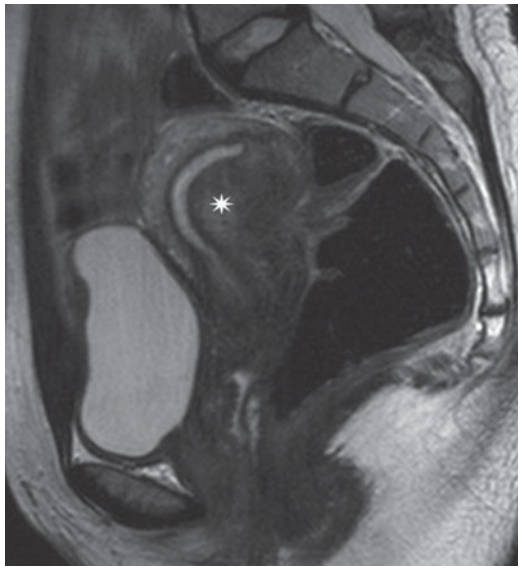

Fig. 20.15. Magnetic resonance. Adenomyoma. Sagittal T2-weighted image. Retroverted uterus. A rounded lesion (*asterisk*) with ill-defined margins can be seen at the level of the posterior wall distorting the endometrial cavity

Adenomyoma may be considered the focal, nodular form of adenomyosis. On **transvaginal ultrasonography** (sensitivity 80-82%, specificity 88-94%, positive and negative predictive values 86-91%) two main findings are required for diagnosis: ill-defined margins and the presence of hypoechoic lacunae. In the absence of these two features the diagnosis of leiomyoma may be made in 91-97% of cases.

Magnetic resonance is considered the reference standard. Diagnosis is based on the finding of a mass with ill-defined margins with hypointense signal in T2-weighted images. However, cases have been reported where the differential diagnosis between adenomyoma and leiomyoma was not possible due to a perfectly overlapping pattern of presentation (**Fig. 20.15**).

Byun JY, Kim SF, Choi BG (1999) Diffuse and focal adenomyosis: MR imaging findings. RadioGraphics 19:161-170

Dueholm M, Lundorf E, Hansen ES et al (2001) Magnetic resonance imaging and transvaginal ultrasonography for the diagnosis of adenomyosis. Fertil Steril 76:588-594

Dueholm M (2006) Transvaginal ultrasound for diagnosis of adenomyosis: a review. Best Pract Res Clin Obstet Gynaecol 20:569-582

Hyperplasia and Endometrial Polyps

Simple Benign Hyperplasia

Simple benign hyperplasia is a common cause of vaginal bleeding. In postmenopausal women the condition is frequently caused by estrogen hormone replacement therapy. Histologically, simple benign hyperplasia is characterized by excessive proliferation of the endometrial glands, with an increase in the ratio between the glands and the stromal component of the endometrium. Hyperplasia can be with or without cytologic atypia. In the presence of atypia (25% of cases), there may be associated foci of carcinoma, and since there is significant risk of malignant disease the usual treatment option is hysterectomy.

Diagnostic imaging of hyperplasia, as well as endometrial polyps, is almost the sole domain of **transvaginal ultrasonography** (since the limits of transabdominal US are well known).

Numerous studies have suggested using the thickness of the endometrium as a predictor of disease in postmenopausal patients with vaginal bleeding. These studies have attempted to establish a cutoff below and above which there is respectively either the certainty of the absence of disease or the need for endometrial sampling prompted by two reasons: (1) elevated post-test probability of endometrial disease; and (2) the lack of specificity of TVUS in the differential diagnosis between benign and malignant disease.

The anteroposterior thickness of the endometrium is the sum of the endometrium of the anterior and posterior walls, measured at the central region of the uterus, but not including the hypoechoic periendometrial rim which histologically belongs to the internal muscle fibers of the myometrium. The cutoff suggested by the Society of Radiologists in Ultrasound Consensus Panel in 2001 is 5 mm, even though others have obtained excellent results with a 4 mm upper limit of normality. Raising the value to 8 mm in postmenopausal women undergoing hormone replacement therapy is advisable.

A large meta-analysis conducted on postmenopausal women with vaginal bleeding demonstrated that the 5 mm cutoff not only identified 96% of women with endometrial carcinoma, but also 92% of women with less severe endometrial alterations. The specificity in the two cohorts was 61% and 81%, respectively. The 8% of false negatives in the US study of women with endometrial disease is acceptable when compared with the percentage findings of endometrial biopsy.

In simple benign hyperplasia TVUS shows homogeneous thickening of the endometrium with well-defined margins and an appearance very similar to that of carcinoma (stage IA).

When morphologic parameters are considered in addition to the increase in volume, several authors suggest disease predictivity increases and therefore so too does overall diagnostic accuracy. Others refute this claim, arguing that the addition of morphologic findings increases specificity to the detriment of sensitivity, which is preferable in relation to the not insignificant risk of classifying a malignant lesion as benign.

Benign cystic hyperplasia is well visualized on **transvaginal ultrasonography**. The hyperechoic endometrium is thickened and heterogeneous due to the presence of numerous very small anechoic cystic formations (**Fig. 20.16**).

Numerous studies have shown that **hysterosonography** is superior to TVUS (sensitivity 98%, specificity 88%, positive predictive value 94%, negative predictive value 97%) not only in definition of the presence of endometrial disease, but also in localization of the site and characterization of the nature of the disease. This information enables the patient to be correctly oriented towards hysteroscopy in the case of an endometrial polyp or submucosal leiomyoma.

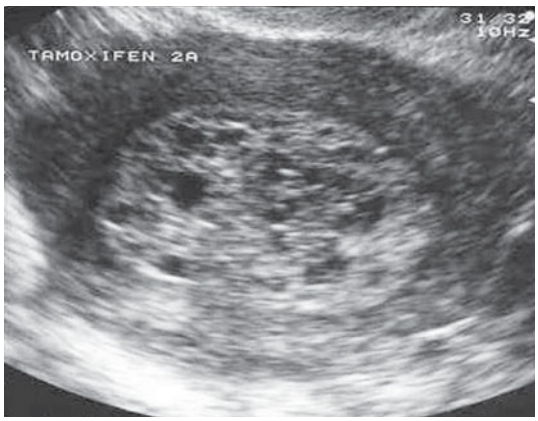

Fig. 20.16. Ultrasonography. Benign cystic endometrial hyperplasia. Increased thickness of the endometrium with heterogeneous echotexture in a woman undergoing tamoxifen therapy

At hysterosonography the endometrial cavity can be well distended. Endometrial thickening can be diffuse or focal, in which case the differential diagnosis with endometrial polyp is challenging.

There are no precise guidelines for the use of hysterosonography, which may be indicated in the following circumstances:

- patients with endometrial thickening on TVUS and negative endometrial biopsy;
- patients with inconclusive findings on TVUS;
- patients with persistent vaginal bleeding and negative findings both on TVUS and at endometrial biopsy.

Various studies have evaluated the possible use of **color Doppler** in the differential diagnosis between benign and malignant endometrial disease. The threshold values for the resistance index vary from 0.70 to 0.40 (the latter generally being preferable) and the pulsatility index from 1.00 to 2.00. Values lower than the cutoff indicate a malignant lesion. Indeed, neoplastic vessels of the endometrium are characterized by alterations to the smooth muscle component of the intima as well as numerous arteriovenous fistulae which justify the low resistance and high diastolic flow.

Flowmetry findings are nonetheless less reliable than endometrial thickness and are not recommended for daily clinical practice. The moderate overlap of values between benign and malignant disease undermines sensitivity and specificity of the individual finding. The use of color Doppler is not resolutive: the resistance of the endometrial vessels is inversely proportional to the thickness of the endometrium, such that marked hyperplasia shows low-resistance flows similar to those observed in adenocarcinoma.

Nonetheless, color Doppler can still provide important information. The presence of the color signal can be useful in differential diagnosis between a mass and an intraluminal clot. A solid lesion supplied by a single small vessel is likely to be a polyp, whereas a formation with a broad attachment supplied by several vessels is probably carcinoma of the endometrium.

Magnetic resonance currently does not have a practical role to play in the study of benign hyperplasia of the endometrium. Niche indications may include patients for whom TVUS and hysterosonography have not provided reliable results due to vertical orientation of the lesion or significantly increased volume of the uterus, or who have diffuse adenomyosis or multiple leiomyomas. On MR, however, hyperplasia appears with a thickened endometrium and isointense or mildly hypointense signal in T2-weighted sequences compared with normal tissue. In the early phases of dynamic contrast-enhanced study, hyperplasia appears hypointense to the myometrium, becoming iso- or hyperintense in the late phases (in which small hypointense foci may be attributed to cystic glandular dilatations). The appearances described are nonetheless aspecific and do not allow differential diagnosis with carcinoma of the endometrium (stage IA) (**Fig. 20.17**).

Endometrial Polyps

Endometrial polyps are usually asymptomatic but in peri- or postmenopausal women they may be the cause of vaginal bleeding in the presence of necrosis or ulceration. The polyps may have a broad attachment or be pedunculated. They may be the expression of isolated endometrial disease or associated with hyperplasia or carcinoma of the endometrium. In 20% of cases they are multiple. Endometrial polyps are composed of a glandular and a stromal component supported by a fibrovascular peduncle. Their excision is advised to resolve vaginal bleeding and to identify possible foci of hyperplasia with atypia or carcinoma.

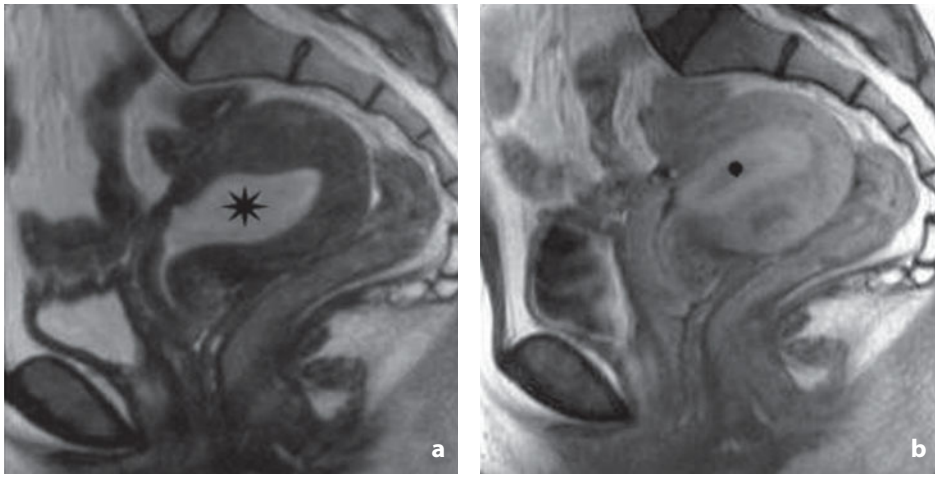

Fig. 20.17a,b. Magnetic resonance. Endometrial hyperplasia. Sagittal T2-weighted image (**a**) shows widening of the cavity (*asterisk*) due to thickening of the endometrium, which in the post-contrast T1-weighted sequence (**b**) appears enhanced with the exception of a central component consisting of secretion (*dot*)

On **transvaginal ultrasonography** the polyps may appear as focal (rounded mass, localized deviation of the hyperechoic central line) or diffuse thickening of the endometrium (Fig. 20.18). Problems for differential diagnosis with hyperplasia can be resolved with **hysterosonography**, which is particularly accurate especially when the lesion, protruding into the endometrial cavity, appears with an evident and more-or-less angulated peduncle (Fig. 20.19). **Color Doppler** can be used to study the afferent artery to the peduncle, which is characterized by high speed flow and low resistance. On **magnetic resonance** the polyp appears with intermediate signal intensity in T1-weighted sequences, whereas in T2 it appears mildly hypointense but occasionally also isointense to the adjacent endometrium, which is locally or diffusely thickened. Larger lesions show a heterogeneous structure produced by small cysts and a central hypointense component due to the central fibrous structure. After the injection of paramagnetic contrast medium (which markedly increases the ability to identify the lesion), the enhancement characteristics vary on the basis of the dimensions of the lesion. Small polyps show early enhancement which differentiates them from the normal endometrium thanks to the demonstration of the vascular peduncle. In contrast, larger formations are characterized by a heterogeneous enhancement pattern (Fig. 20.20).

Reinhold C, Khalili I (2002) Postmenopausal bleeding: value of imaging. Radiol Clin North Am 40:527-562

Smith-Bindman R, Kerlikowske K, Feldstein VA et al (1998) Endovaginal ultrasound to exclude endometrial cancer and other endometrial abnormalities. JAMA 280:1510-1517

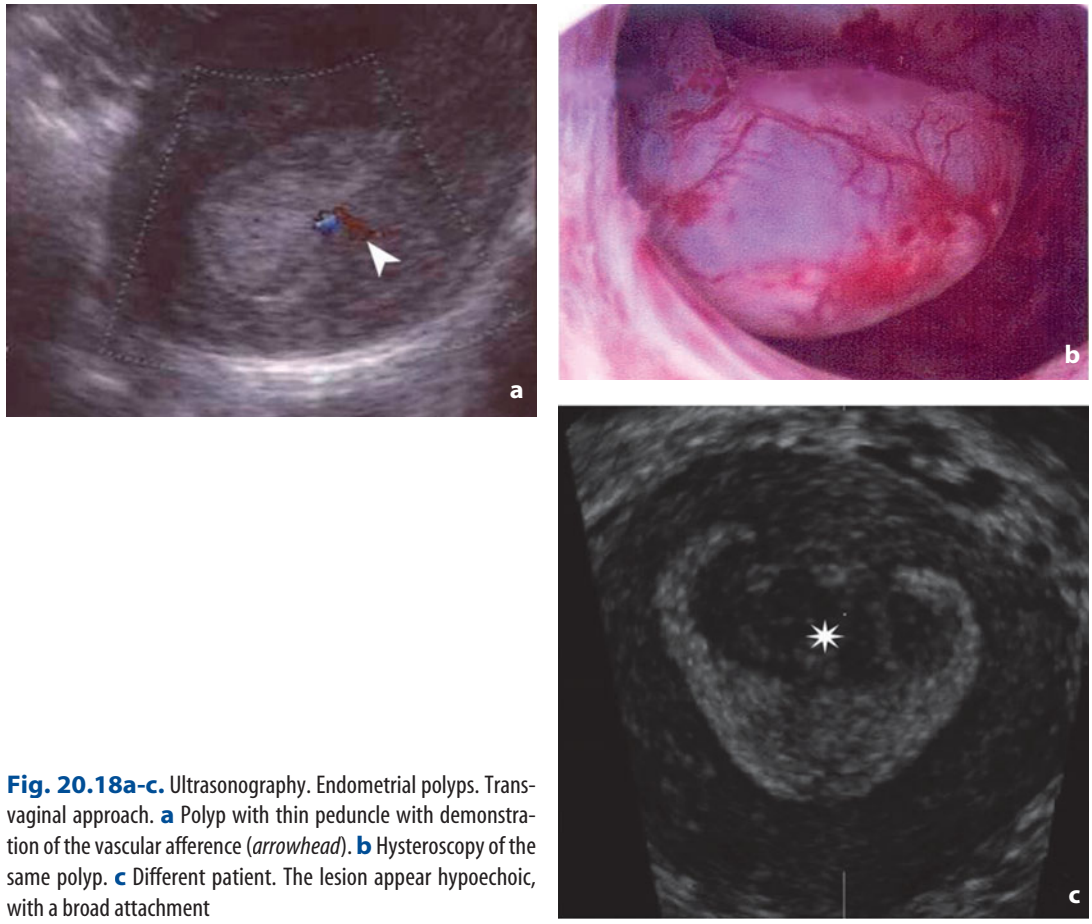

Fig. 20.18a-c. Ultrasonography. Endometrial polyps. Transvaginal approach. **a** Polyp with thin peduncle with demonstration of the vascular afference (*arrowhead*). **b** Hysteroscopy of the same polyp. **c** Different patient. The lesion appear hypoechoic, with a broad attachment

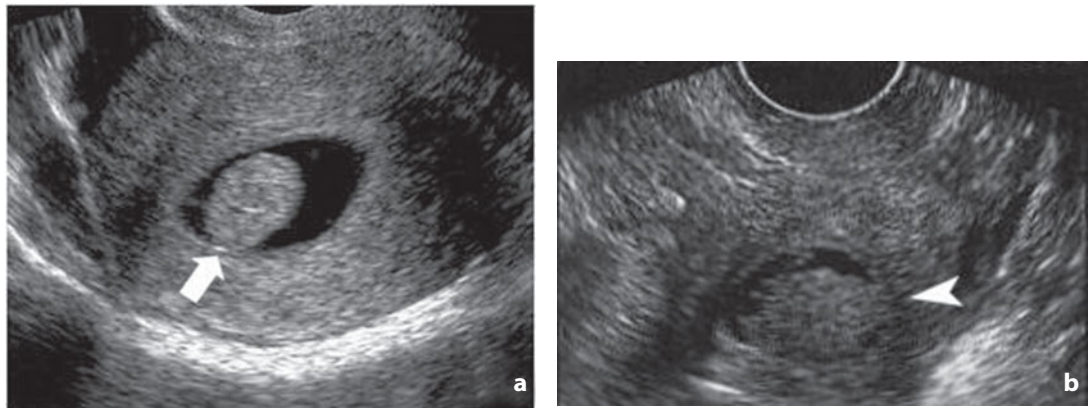

Fig. 20.19a,b. Hysterosonography. Endometrial polyp. **a** The lesion (*arrow)* projects into the lumen of the endometrial cavity which appears distended by fluid. **b** Another, larger, pedunculated lesion (*arrowhead*) with irregular margins occupying almost the entire endometrial cavity

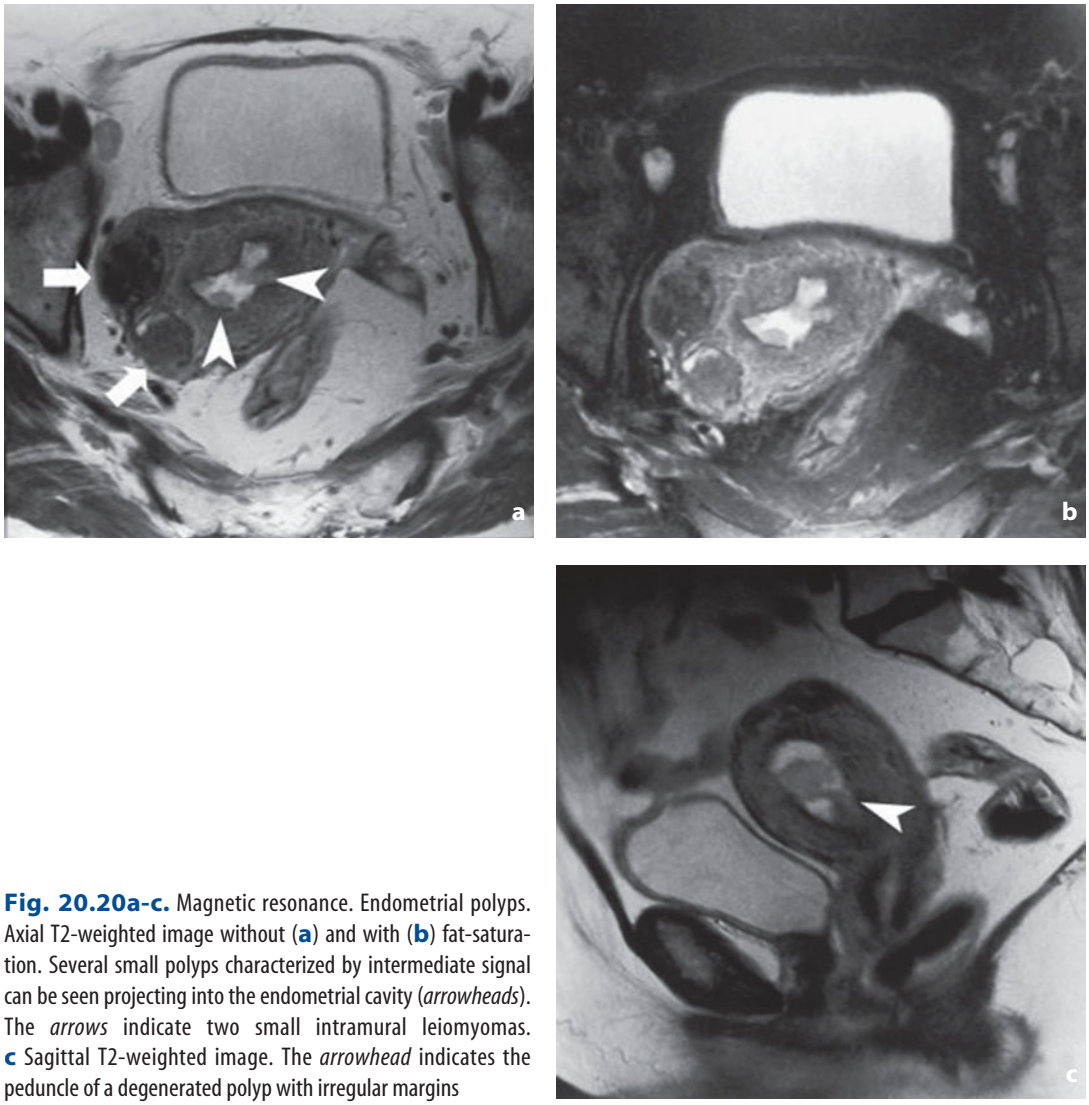

Fig. 20.20a-c. Magnetic resonance. Endometrial polyps. Axial T2-weighted image without (**a**) and with (**b**) fat-saturation. Several small polyps characterized by intermediate signal can be seen projecting into the endometrial cavity (*arrowheads*). The *arrows* indicate two small intramural leiomyomas. **c** Sagittal T2-weighted image. The *arrowhead* indicates the peduncle of a degenerated polyp with irregular margins

Malignant Tumors of the Endometrium

Pathology

The most common histotype (90%) is adenocarcinoma, characterized by an abnormal glandular proliferation to the detriment of the stroma. The differentiation in grades (G1 well differentiated, G2 moderately differentiated, G3 undifferentiated) influences prognosis. Other histotypes include:

- adenocanthoma and squamous cell adenocarcinoma, which have a similar prognosis to adenocarcinoma;
- clear cell carcinoma and papillary serous carcinoma, which are poorly differentiated with clinical and metastatic behavior similar to ovarian carcinoma and worse prognosis.

Carcinoma of the endometrium originates in situ. Later it develops isolated foci of endometrial thickening in any portion of the uterine cavity. Some tumors present as more solid polypoid nodules, while others grow with a tendency to infiltration. Over the long term both forms take on a polypoid appearance and project into the cavity,

while at the same time invading the uterine walls. In the end the entire endometrial cavity appears filled with partially necrotic friable neoplastic tissue.

Once the myometrium has been invaded, endometrial carcinoma follows four spread patterns: direct (the most common), lymphatic, peritoneal and hematogenous (usually to the lungs). The site of the tumor determines the localization of lymph node metastasis: parametrial, paracervical and obturator lymph nodes (middle and lower third of the uterine body); common iliac and paraaortic lymph nodes (upper third and uterine fundus); and inguinal lymph nodes in the case of diffusion along the round ligament.

Diagnostic Imaging

Identification

There is no noninvasive technique for the screening of carcinoma of the endometrium which is advisable for the general population or justifiable from a cost/benefit perspective. **Vaginal cytology** is only occasionally able to diagnose endometrial cancer: the incidence of false negatives exceeds 50%. **Endometrial cytology**, which is obtained with abrasive instrumentation, has a diagnostic accuracy of 88-97% and its acceptability and ease of performance could suggest it is implemented as a screening test. However, the technique is unable to diagnose tumor precursors (hyperplasia with atypia). The more precise technique for identification and diagnosis of carcinoma of the endometrium is **operative hysteroscopy**. Nonetheless, even this examination cannot be implemented on a large scale due to costs, time, the need for specialized medical personnel and patient discomfort. The diagnosis is therefore usually made at histologic examination, which in 75% of cases is performed with abrasion or aspiration without cervical dilatation. Sensitivity and specificity of dilatation and curettage (reference standard) have not been proven in large patient populations, with the term of comparison being the immediate hysterectomy thereafter. One such study carried out on 512 patients found that nonidentified lesions accounted for 10% of all cases. In the diagnosis of hyperplasia and carcinoma the incidence of false negatives has been reported at 2-6%.

Transvaginal ultrasonography is able to suggest the presence of disease. Some authors have suggested a diagnosis of alterations and endometrial cancer even when endometrial biopsy and hysteroscopy are negative. This is undoubtedly the correct approach in postmenopausal women with vaginal bleeding, the symptom being the first manifestation of endometrial carcinoma. Moreover, there is no evidence of a real benefit of US screening even in women with elevated risk, e.g. women on tamoxifen for the treatment of breast cancer (the drug is correlated with a 7.5% increased risk of endometrial cancer). Furthermore, in the absence of blood loss, US screening offers no real prognostic advantage in women with hereditary nonpolypoid cancer of the colon, who during their lifetime are at a 40-60% risk of being affected by endometrial cancer as well.

Adenocarcinoma appears as a thickening of the endometrium >15 mm in premenopausal women, >5 mm in postmenopausal women and >8 mm in postmenopausal women undergoing hormone replacement therapy. The finding of a postmenopausal endometrium with a thickness greater than the normal values is nonetheless not pathognomonic of malignant disease, as this may also occur in hyperplasia and endometrial polyps. Some authors have reported that the thickness of the endometrium in the case of malignancy is generally greater than in hyperplasia. However, there is sufficient overlap of the figures to invalidate the definitive diagnostic significance of the parameter.

The morphology of endometrial echoes can be indicative of malignancy. The presence of hypoechoic foci is in fact suggestive of a neoplasm. In general, the greater the

heterogeneity of the endometrial echotexture, the higher the likelihood of the presence of a malignant lesion. The carcinoma is also more likely to undergo bleeding than other endometrial disease, which explains the greater frequency of intrauterine anechoic layers of liquid (Fig. 20.21).

Hysterosonography with saline solution improves the diagnosis: sensitivity 89%, specificity 46%, positive predictive value 16% and negative predictive value 97%. The risk of malignant cell dissemination/tumor seeding induced by the procedure is low, estimated at around 7%.

The morphologic examination can also be integrated with **color Doppler**. Hypervascularity prevails in carcinoma with multiple small vessels in contrast with the single vessel of the peduncle of the endometrial polyp. The flow characteristics of the intraendometrial vessels enables differentiation between malignant and benign thickening, on the condition that if the endometrium is thin (<5 mm), the endometrial rim is generally avascular. The data in the literature are, however, limited and contradictory, in part due to the significant overlap of values recorded in benign and malignant lesions.

Computed tomography has no substantial role to play in the identification of carcinoma of the endometrium, although the disease may be encountered as an incidental finding.

In baseline conditions without contrast enhancement the endometrium cannot be distinguished from the myometrium. The uterus appears homogeneous with oval and triangular shape and parenchymal tissue density. In some cases an irregular central uterine hypoattenuation may be indentifiable indicating the endometrium.

The study of the uterus with injection of iodinated contrast medium involves two phases: the acquisition of scans in the arterial and venous phases at around 120 s after the beginning of administration. The healthy myometrium appears markedly vascular and therefore shows greater enhancement than the adjacent pelvic organs. Given the significant enhancement of the myometrium, the endometrial tumor appears as a central uterine heterogeneous hypoattenuating lacuna characterized by mild late enhancement (Fig. 20.22). Another possible (indirect) sign of carcinoma of the endometrium is the finding of hypoattenuating material in the uterine cavity. This occurs when the tumor obstructs the cervical canal in a similar fashion to what occurs in cervical cancer. However, it should be noted that pyometra or hydrometra are not pathognomonic of malignancy, but only of obstruction of the cervical canal.

On **magnetic resonance** images, the appearance of endometrial cancer is aspecific and variable.

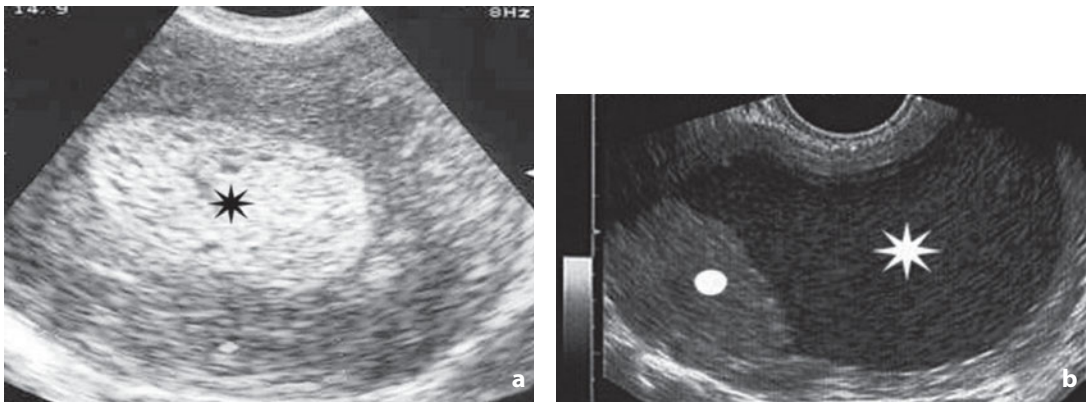

Fig. 20.21a,b. Ultrasonography. Carcinoma of the endometrium, stage IA. Transvaginal approach. **a** Evident widening of the endometrial cavity obstructed by hyperechoic tissue with a mildly heterogeneous structure (*asterisk*). **b** Different patient. The cavity is distended (*asterisk*) by corpuscular liquid (hematometra). A solid mass can be seen projecting into the lumen situated eccentrically

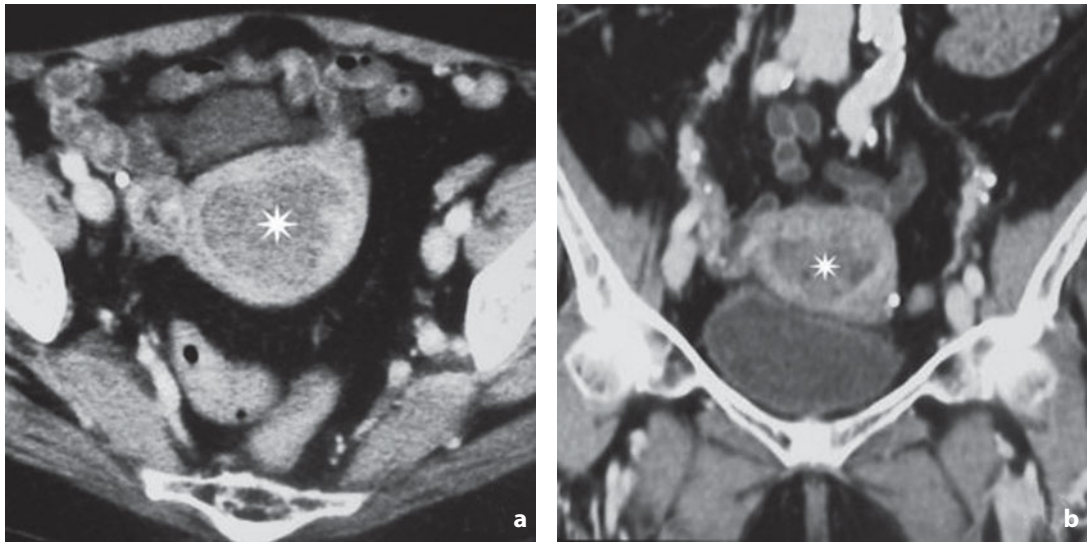

Fig. 20.22a,b. Computed tomography. Carcinoma of the endometrium. Axial image acquired in the venous phase (**a**) and relative coronal reconstruction (**b**). The endometrial cavity is enlarged and occupied by hypoattenuating tumor tissue

The study is usually performed after the patient has undergone dilatation and curettage of the endometrial cavity. This procedure has no negative effects on MR imaging, particularly in terms of staging. There are no precise guidelines regarding the most suitable time interval prior to performing the MR study. Waiting until the termination of postbiopsy vaginal bleeding appears reasonable.

In T1-weighted images the lesion appears iso- or hypointense to the myometrium in most cases and therefore cannot be differentiated from it. The only distinctive feature may be the presence of an intratumoral hemorrhagic component. In T2-weighted images the endometrial tumor is correctly identifiable as one or more nodules and/or invasive plaques with a heterogeneous signal intermediate between the normal endometrium and the myometrium (and therefore higher than the latter). In the presence of small lesions with an exclusively superficial development, the signal intensity is similar to that of normal endometrium. In other cases the intraluminal tumor has a nodular appearance with low signal intensity compared with normal endometrium (**Fig. 20.23**).

Possible indirect signs of the tumor include an increase in the width of the cavity, with a heterogeneous appearance due to a prevalent component of low signal intensity in T2. These MR findings are nonetheless aspecific, since they are also encountered in the presence of endometrial polyps, blood clots and adenomatous hyperplasia. Therefore, only histology can be diagnostic.

In the early images acquired during a dynamic post-gadolinium DTPA study, the carcinoma enhances less than the normal myometrium. The appearance can nonetheless be variable: some tumors show early enhancement while others enhance in the late phase. Hematometra and intracavitary blood collections are nonenhancing, thus making possible their differentiation from the tumor.

Staging

The most important prognostic factors in carcinoma of the endometrium are the stage of the disease and in particular, the degree of invasion of the myometrium, and the histologic grade of the tumor. These parameters are closely correlated with lymph node metastasis and 5-year survival. The latter in particular is significantly modified in stage I by invasion of the myometrium: 40-60% in deep invasion; 90-100% in the

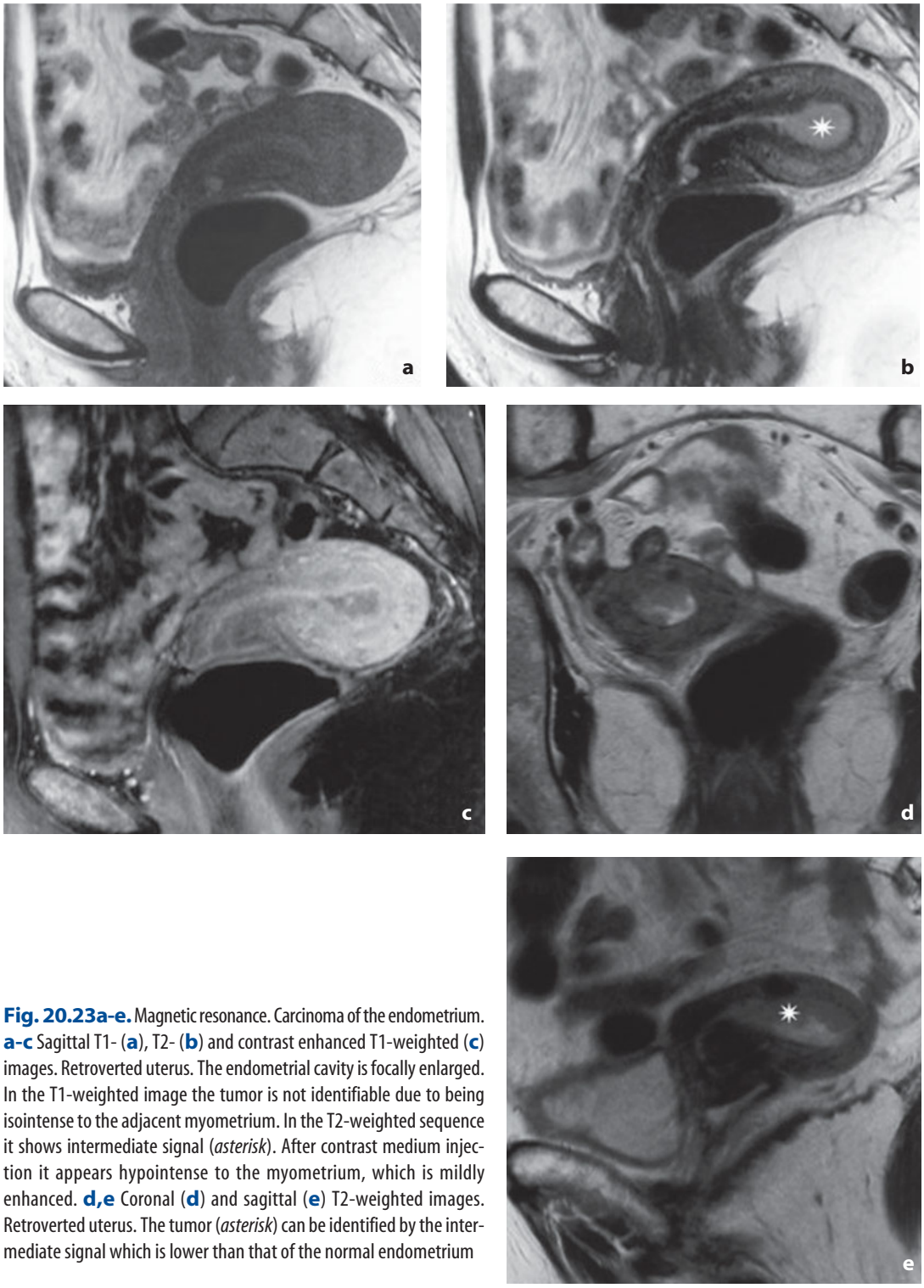

Fig. 20.23a-e. Magnetic resonance. Carcinoma of the endometrium. **a-c** Sagittal T1- (**a**), T2- (**b**) and contrast enhanced T1-weighted (**c**) images. Retroverted uterus. The endometrial cavity is focally enlarged. In the T1-weighted image the tumor is not identifiable due to being isointense to the adjacent myometrium. In the T2-weighted sequence it shows intermediate signal (*asterisk*). After contrast medium injection it appears hypointense to the myometrium, which is mildly enhanced. **d,e** Coronal (**d**) and sagittal (**e**) T2-weighted images. Retroverted uterus. The tumor (*asterisk*) can be identified by the intermediate signal which is lower than that of the normal endometrium

absence of invasion or only minimal superficial invasion. Women with a tumor confined to the uterine body (stage I) and only superficial involvement of the myometrium have 3% prevalence of paraaortic lymph adenopathy. This percentage rises to 46% in deep invasion.

The staging system generally used is the FIGO classification of the International Federation of Gynecology and Obstetrics (**Table 20.1, Fig. 20.24**). The TNM classification follows the same surgical-histologic criteria as the FIGO system, based on the findings of explorative laparotomy, total laparotomic hysterectomy with bilateral adnexectomy, peritoneal lavage and lymphadenectomy. Surgical staging, however, is clearly not possible in patients unable to undergo surgery. In such cases diagnostic imaging is indispensable in evaluating the degree of myometrial invasion, the extent of the tumor and the presence of lymph node involvement. More generally, staging with imaging becomes complementary to surgical staging and may assist the surgeon and radiotherapist in the treatment choice (to perform or not perform lymphadenectomy; to define the width of the field of irradiation).

Many studies in the past have shown that MR, being more accurate than both TVUS and CT, is the most reliable imaging modality in the staging of endometrial cancer. A meta-analysis performed in 1999, nonetheless, failed to show significant differences between the overall diagnostic accuracy of the different imaging modalities. However, in terms of invasion of the myometrium contrast enhanced MR is significantly ($p<0.002$) better than nonenhanced MR and TVUS and shows a tendency towards better results than CT. In the same meta-analysis, the absence of CT and US data made it impossible to compare of the MR findings regarding the evaluation of invasion of the cervix.

Table 20.1. Carcinoma of the endometrium. TNM and FIGO (International Federation of Gynecology and Obstetrics) classification systems

TNM	FIGO	Definition
Tx		Primary tumor cannot be assessed
T0	0	No evidence of primary tumor
Tis	0	Carcinoma in situ
T1	I	Tumor confined to uterine body
T1a	IA	Tumor limited to endometrium
T1b	IB	Tumor invades the myometrium by less than 50% of its thickness
T1c	IC	Tumor invades the myometrium by more than 50% of its thickness
T2	II	Tumor invades the cervix but does not extend beyond the uterus
T2a	IIA	Invasion of the cervical glands alone
T2b	IIB	Invasion of the cervical stroma
T3 and/or N1	III	Local and/or regional spread as specified in T3a,b and/or N1 and FIGO IIIA, B and C below
T3a	IIIA	Invasion of the peritoneal serosa and/or the adnexa (direct extension or metastasis) and/or cancer cells in ascites or peritoneal
T3b	IIIB	Invasion of the vagina (direct extension or metastasis)
N1	IIIC	Metastasis to the pelvic and/or para-aortic lymph nodes
T4	IVA	Tumor invades bladder and/or bowel mucosa (bullous edema is not sufficient for classifying a tumor as T4)
Nx		Regional lymph nodes cannot be assessed
N0		No metastasis to regional lymph nodes
N1		Metastasis to regional lymph nodes
Mx		Metastasis cannot be assessed
M0		No distant metastasis
M1	IVB	Distant metastasis (includes metastasis to the intra-abdominal lymph nodes beyond the para-aortic and/or inguinal lymph nodes; excludes metastasis to the vagina, the pelvic serosa and the adnexa)

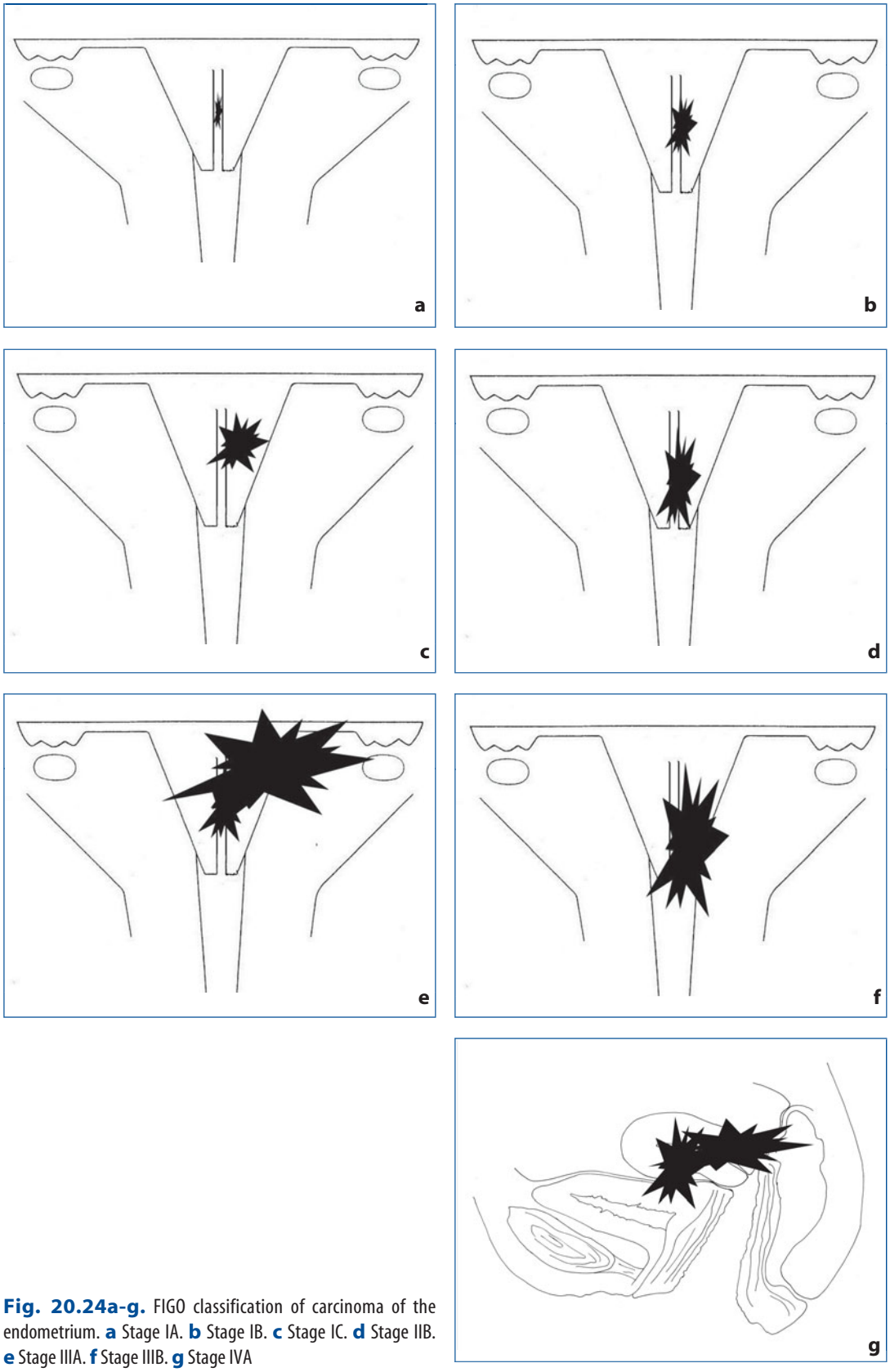

Fig. 20.24a-g. FIGO classification of carcinoma of the endometrium. **a** Stage IA. **b** Stage IB. **c** Stage IC. **d** Stage IIB. **e** Stage IIIA. **f** Stage IIIB. **g** Stage IVA

Transvaginal ultrasonography is able to accurately evaluate invasion of the endometrial tumor into the myometrium. The TVUS appearance is relatively simple. In stage IA the endometrium thickened by the tumor appears as a generally hyperechoic central uterine linear band with regular margins and generally homogeneous echotexture – the appearance is similar to the normal endometrium during the secretion phase. The endometrium appears bounded by a thin hypoechoic halo which differentiates it from the myometrium. The disappearance of the halo is frequently associated with invasion of the myometrium, which may be divided into superficial and deep layers. In this setting the diagnostic accuracy of TVUS varies from 73% to 93%. A proposal to simplify this evaluation involves only calculating the thickness of the residual myometrium: when less than 5 mm, invasion may be considered deep, whereas if it is greater than 5 mm invasion is in contrast superficial (**Fig. 20.25**).

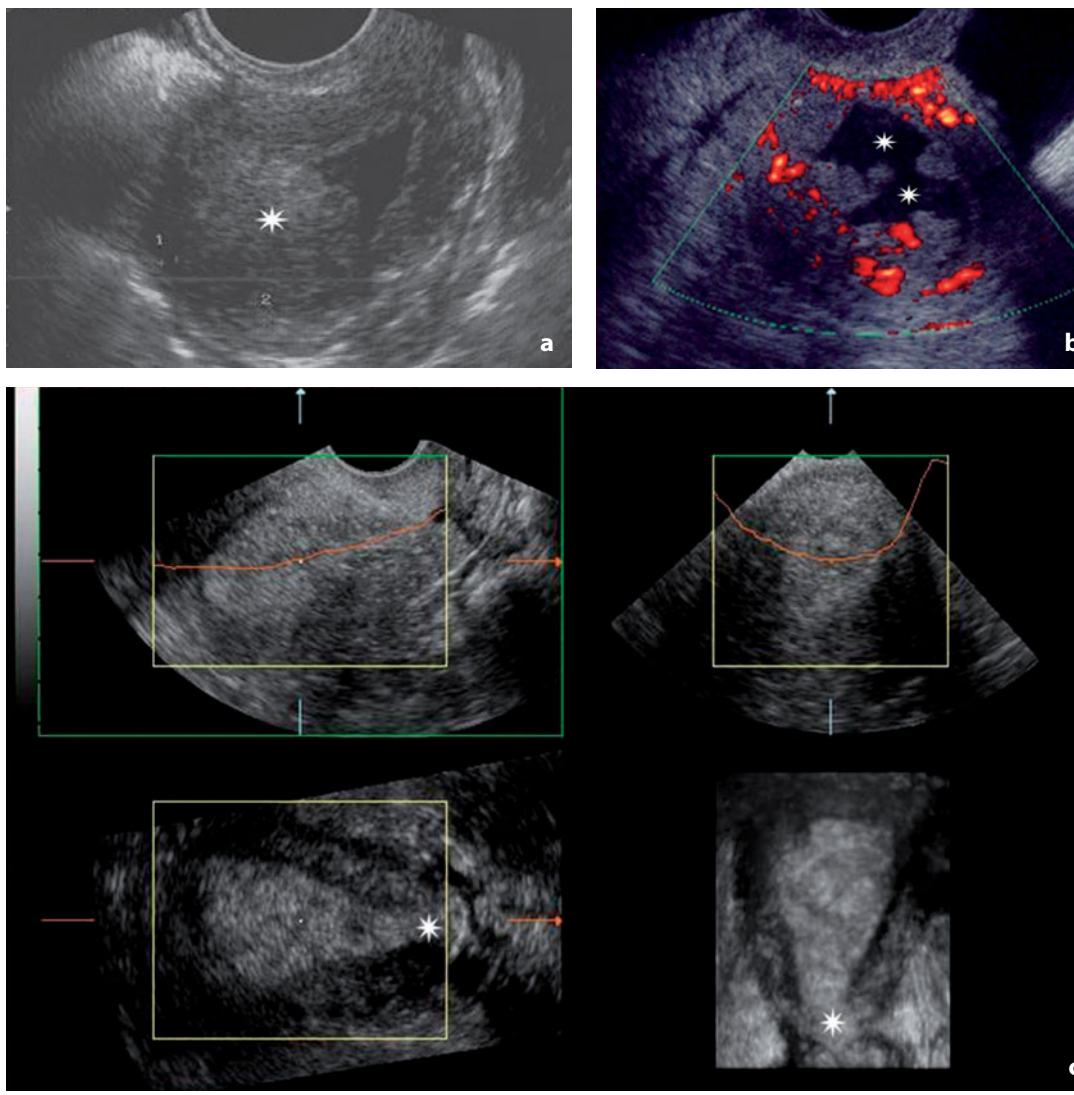

Fig. 20.25a-c. Ultrasonography. Carcinoma of the endometrium. **a** Stage IC. The tumor (*asterisk*) focally invades the external half of the myometrium. **b** Stage IC. Different patient. Invasion of the entire thickness of the myometrium. The endometrial cavity (*asterisks*) has irregular and fimbriated margins. **c** Stage II. The tumor extends to the cervical canal (*asterisk*), with invasion of the cervical stroma. The findings are well documented in the 3D reconstruction

There are, however, anatomic situations regarding carcinoma of the endometrium as well as certain features of the US technique which can lead to error. Tumors with massive intraluminal development may compress the myometrium without actually invading it, thus simulating an advanced substage (IC). In other cases, especially in elderly patients, distinguishing the hypoechoic halo separating the endometrium and myometrium can be challenging. In still other situations the low echogenicity of the adenocarcinoma hinders visualization of its border with the myometrium, thus not enabling a correct evaluation of the invasion. Lastly, in the senile uterus the generally very thin myometrial walls lead to an overestimation of the malignant invasion.

Other factors limiting US staging include: limited field of view which hampers the evaluation of the parametrium, the cervix and the lymph nodes; limited contrast resolution of the soft tissues; and the anatomy of the subject being examined, where obesity and an upright uterus can limit the diagnostic value of the examination.

Computed tomography is not used in standard clinical practice for the evaluation of invasion of the myometrium. Some authors, however, have reported that CT is also able to evaluate invasion of the myometrium, thanks to an invasion index given by the ratio of the minimum/maximum thickness of the normal myometrium. The diagnostic accuracy varies in the studies performed with conventional CT from 84% to 88%. More recent studies with spiral CT scanners have reported sensitivity 83% and specificity 42%. Therefore, even with CT evaluation, errors are evidently possible, some being dependent on the macroscopic appearance of the tumor and others on the nature of the findings themselves. As with TVUS, the polypoid appearance of the tumor contributes to the overestimation of myometrial invasion, because it distends the uterine cavity and thins the myometrium. The finding of thinned uterine walls is also a cause of overstaging. Lastly, highly vascular uterine tumors which deeply invade the wall are difficult to distinguish from intramural myomas and cause frequent errors in staging.

CT has a sensitivity of 25% and specificity of 75% in the evaluation of invasion of the cervix.

In essence CT has clear limitations in defining stages I and II. The accuracy is better in the more advanced forms, i.e. in evaluation of invasion of the bladder and the rectum. In evaluation of peritoneal implants and lymph node metastases (for the latter the only valid criterion is size), CT suffers from the same limitations as other imaging techniques (**Fig. 20.26**).

Magnetic resonance has for some time been the imaging modality of choice in the staging of histologically diagnosed carcinoma of the endometrium. It is particularly indicated in the definition of myometrial invasion, which is a critical parameter for planning the extension of lymphadenectomy. Patients with >50% invasion have an increased probability of extrauterine spread of the disease and a 6-7 times higher incidence of pelvic or lumbar aortic lymph node metastasis.

A stage IA tumor appears contained within the endometrial cavity, which may be normal or enlarged in appearance. The junctional zone, with low signal intensity in T2-weighted images, the subendometrial enhancement in the dynamic sequence and the zone of reduced signal of the most internal layer of the myometrium are all preserved and intact. The tumor-myometrium interface is clear and regular, regardless of the sequence used.

A stage IB tumor shows focal or diffuse interruption of the junctional line, of the subendometrial enhancement and the of low zone signal of the innermost layer of the myometrium. In the absence of these findings the diagnosis is made on the basis of the irregularity of the interface between the endometrium and myometrium (otherwise smooth and regular), or direct documentation of the tumor in the internal half of the myometrial wall.

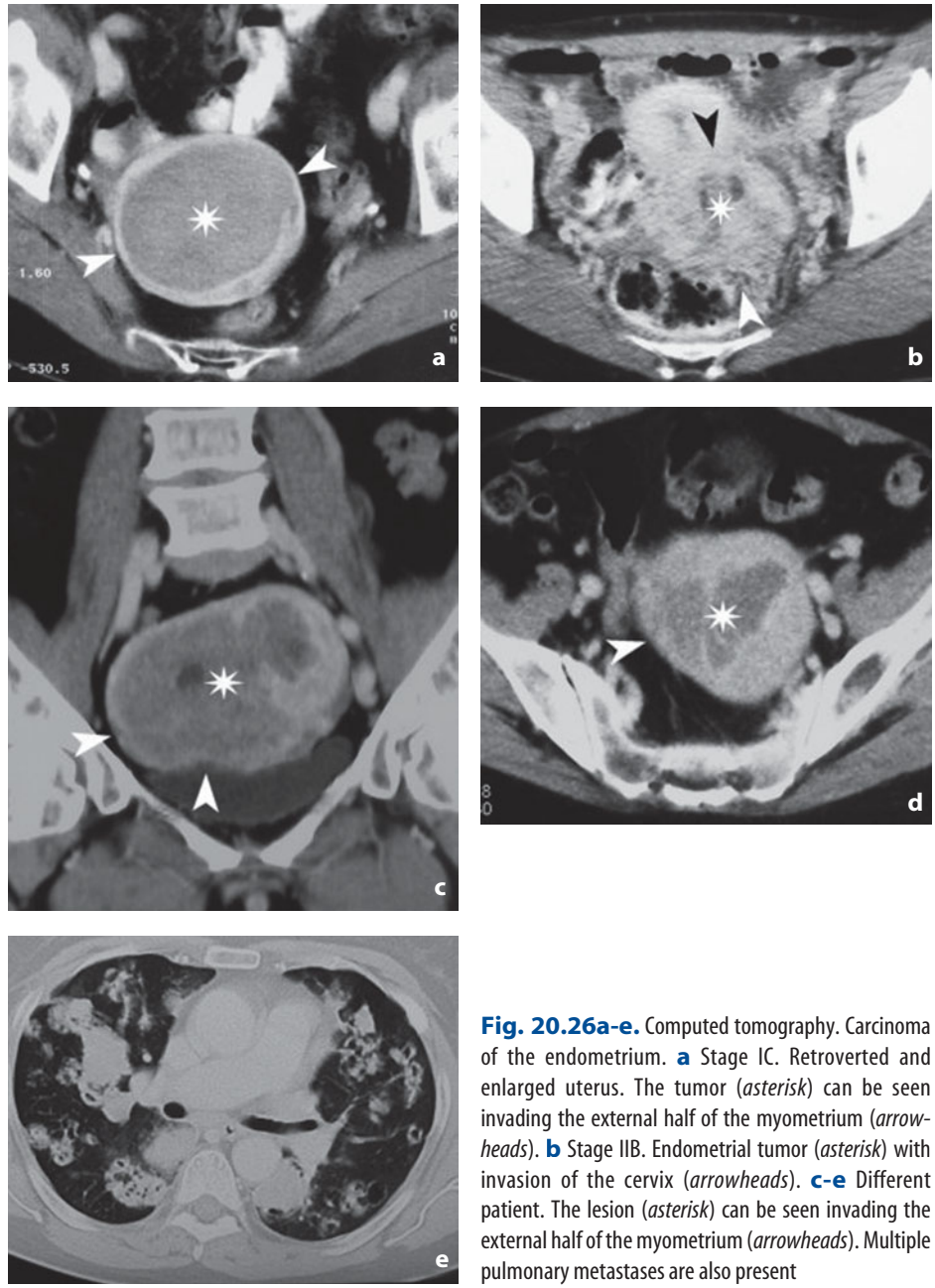

Fig. 20.26a-e. Computed tomography. Carcinoma of the endometrium. **a** Stage IC. Retroverted and enlarged uterus. The tumor (*asterisk*) can be seen invading the external half of the myometrium (*arrowheads*). **b** Stage IIB. Endometrial tumor (*asterisk*) with invasion of the cervix (*arrowheads*). **c-e** Different patient. The lesion (*asterisk*) can be seen invading the external half of the myometrium (*arrowheads*). Multiple pulmonary metastases are also present

A stage IC tumor is diagnosed when the lesion invades the external half of the myometrium. Deep invasion (as well as superficial invasion) should be confirmed in planes that are orthogonal to each other (Fig. 20.27).

Particular attention needs to be paid to patients with adenomyosis. In this disease, the endometrium-myometrium interface is in itself irregular, such that in the absence of other findings this irregularity is not enough to diagnose superficial invasion. In contrast, the complete interruption of the junctional line with deep myometrial invasion may not be evident.

The injection of gadolinium increases the diagnostic accuracy of MR in the evaluation of myometrial invasion (the endometrium enhances less than the myometrium),

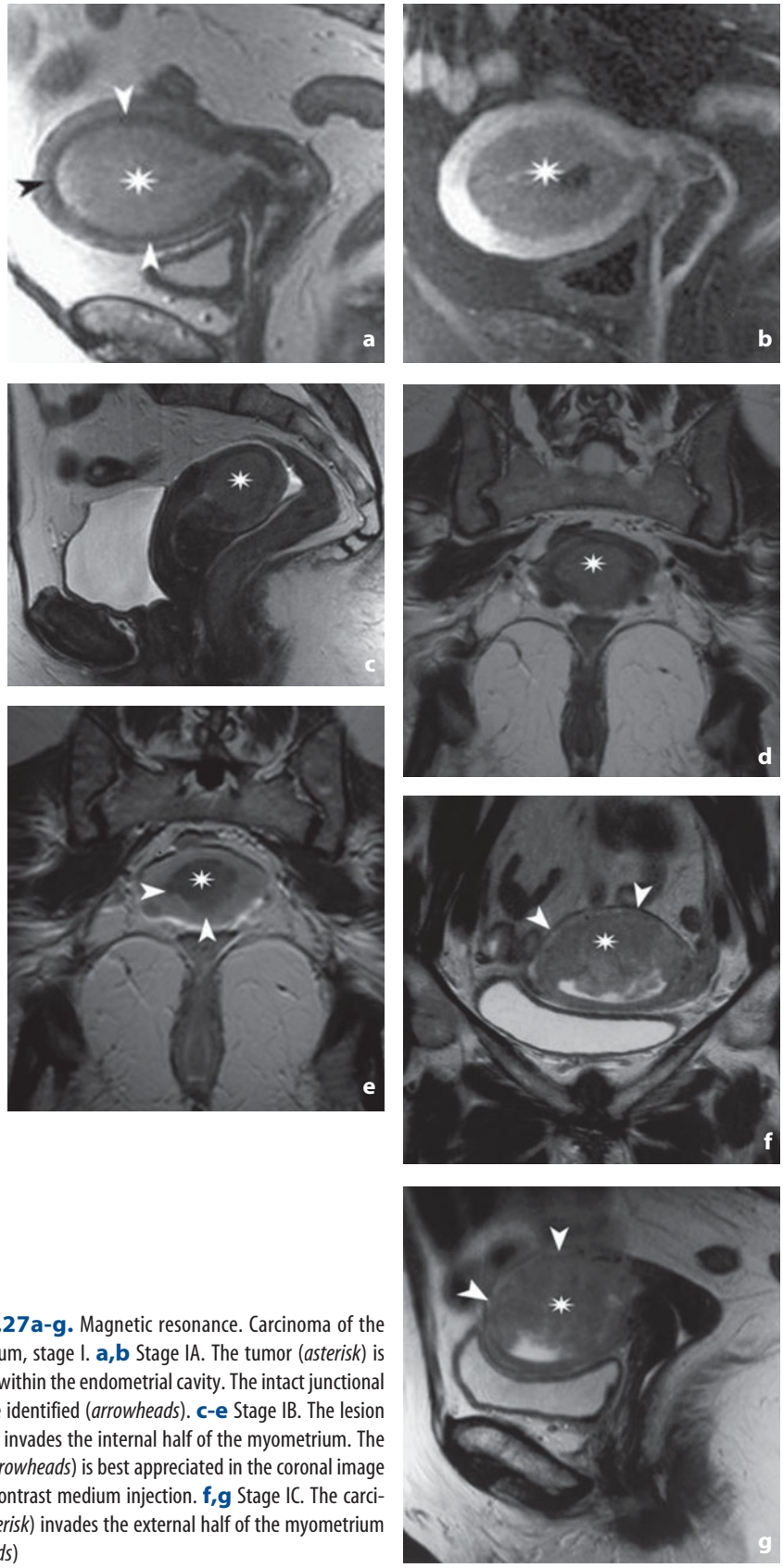

Fig. 20.27a-g. Magnetic resonance. Carcinoma of the endometrium, stage I. **a,b** Stage IA. The tumor (*asterisk*) is contained within the endometrial cavity. The intact junctional line can be identified (*arrowheads*). **c-e** Stage IB. The lesion marginally invades the internal half of the myometrium. The finding (*arrowheads*) is best appreciated in the coronal image (**e**) after contrast medium injection. **f,g** Stage IC. The carcinoma (*asterisk*) invades the external half of the myometrium (*arrowheads*)

eliminating reliance on visualization of the junctional line which is often absent in postmenopausal women (who in fact make up the age group most frequently affected by malignant lesions of the uterine body). The pretest probability of real myometrial invasion in grade 1, 2, and 3 tumors is 13%, 35% and 54%, respectively. If MR findings are positive the probability rises to 60%, 84% and 92%, whereas if negative, i.e. in the absence of myometrial invasion at imaging, the probability falls to 1%, 5% and 10%. In essence, in patients with grade 1 and 2 tumors invasion can be ruled out if not identified on MR images. Therefore, on the basis of these findings there is no need for intraoperative frozen section acquisition, or lymph node sampling. In grade 3 tumors the absence of MR evidence of invasion of the myometrium reduces the probability of lymph node metastasis, thus deferring lymphadenectomy. However, for the sake of correctness, it should be noted that many authors do not agree with this therapeutic strategy.

The evaluation of invasion of the myometrium can become particularly challenging in certain conditions. These include the presence of an indistinct junctional line, thinning of the myometrium (as mentioned above), a small uterus, irregular thickening of the junctional line due to adenomyosis, and distortion of the myometrium by a bulky leiomyoma.

Stage II tumors are characterized by extension from the uterine body to the cervix (diagnostic accuracy of MR >92%). Stage IIA is given by an enlargement of the uterine os and the cervical canal with preservation of the fibrocervical stroma. False positives may be caused by polypoid extension of the endometrial carcinoma, pooling of secretions or the coexistence of a cervical polyp. Contrast-enhanced study can help to resolve diagnostic uncertainty. Stage IIB is given by interruption of the cervical stroma (**Fig. 20.28**).

MR is able to stage advanced tumors (stage III and IV) with a high degree of accuracy.

In stage IIIA tumors the external margin of the uterus is irregular and/or interrupted. Invasion of the parametrium is shown by tumor extension beyond the uterine serosa into the parametrial adipose tissue. The adnexae are involved by direct extension or metastasis. According to some authors, peritoneal localizations are better demonstrated with MR than with CT, even though nodules <1cm cannot be visualized regardless of the imaging technique used. Involvement of the superior third of the vagina (stage IIIB) is shown by focal loss of the low signal of the vaginal wall. The diagnosis of stage IIIC is made (better in T1-weighted sequences without and with contrast enhancement and possibly fat saturation) in the presence of pelvic or paraaortic lymph nodes with a short axis >1 cm (**Fig. 20.29**).

Focal interruption of the regular low signal of the walls of the urinary bladder and/or rectum is indicative of invasion of those organs (stage IVA). Findings indicating stage IVB include distant metastases, intra-abdominal and/or inguinal lymphadenopathies (in addition to the paraaortic lymphadenopathies). In the early part of the 1990s the diagnostic accuracy of MR in staging carcinoma of the endometrium was reported to be 83-92%. More recent studies have confirmed these results, reporting a sensitivity of 87% and specificity of 91% in the diagnosis of myometrial invasion, a sensitivity of 80% and specificity of 96% in invasion of the cervix, and a sensitivity of 50% and specificity of 95% in the diagnosis of lymph node metastasis (encumbered by the well known difficulty in differential diagnosis between metastatic and reactive lymph nodes). There is significant agreement ($p<0.001$) between MR imaging and anatomic-surgical findings in the evaluation of myometrial invasion.

In the light of the above, the following guidelines can be proposed for the staging of carcinoma of the endometrium:

- no imaging technique is required in patients with grade I tumor and a nonenlarged uterus at gynecologic examination, since the pretest probability of myometrial and cervical invasion as well as lymph node involvement is low. If the findings of the physical examination are inconclusive or there is a pelvic comorbidity, US, CT or

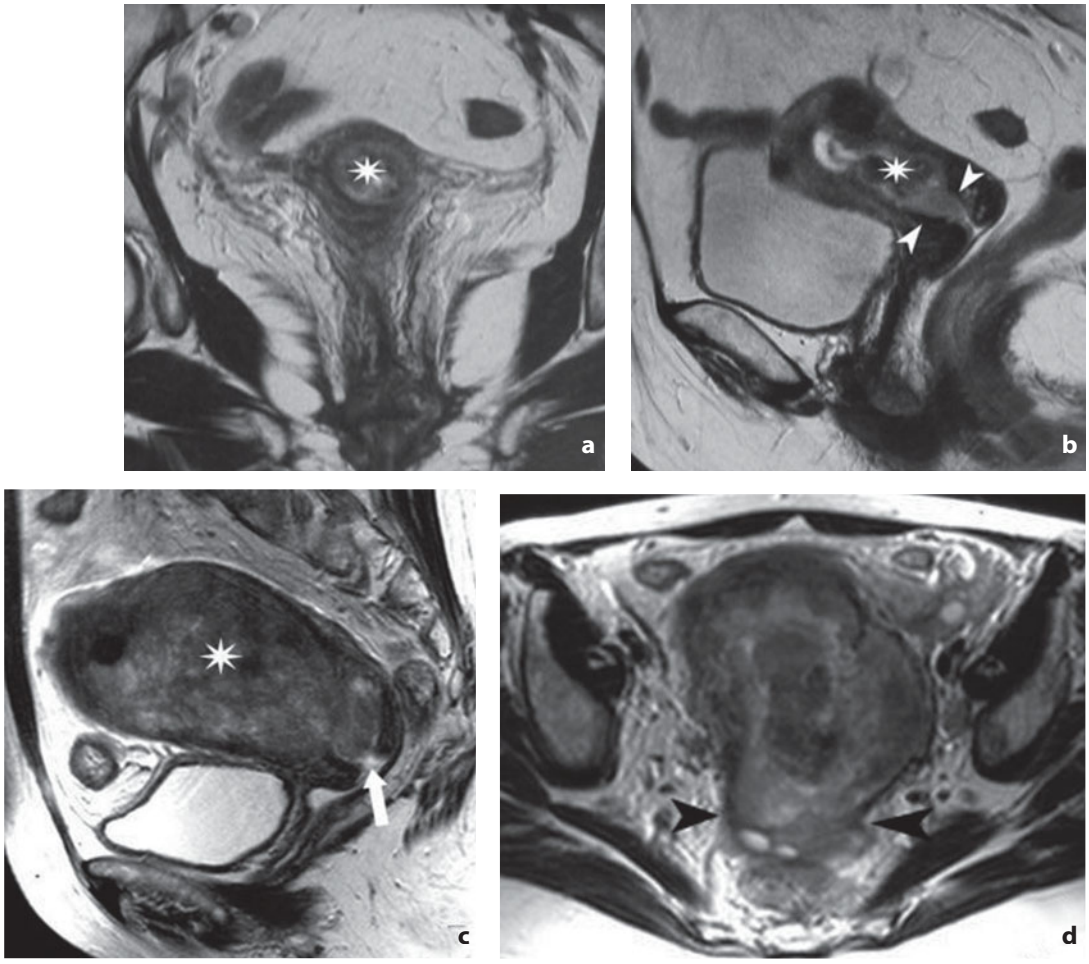

Fig. 20.28a-d. Magnetic resonance. Carcinoma of the endometrium, stage II. **a,b** The tumor (*asterisk*) extends to the cervix, enlarging and occupying the internal uterine os (*arrowheads*). There are no evident signs of invasion of the cervical stroma. **c,d** Stage IIB. Large tumor (*asterisk*) extending to the cervical canal (*arrow*) and invading the cervical stroma (*arrowheads*)

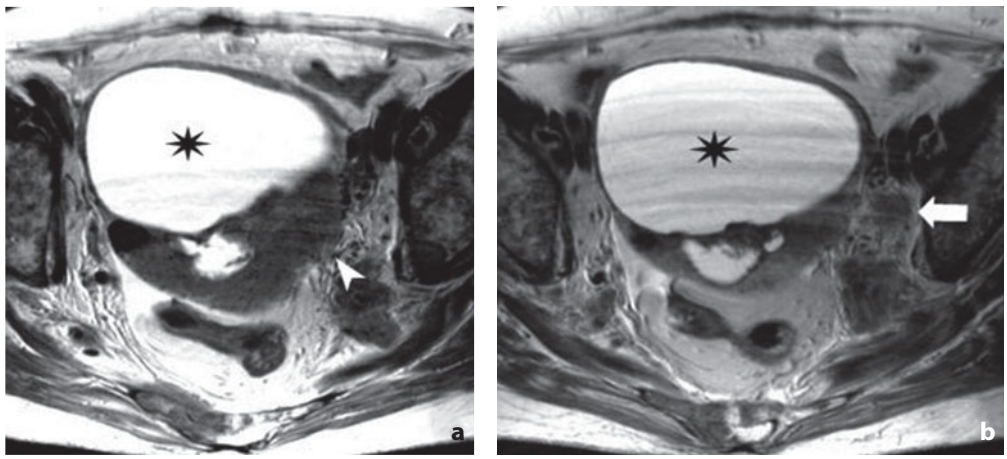

Fig. 20.29a,b. Magnetic resonance. Carcinoma of the endometrium, stage IIIC. **a** The lesion invades the peritoneal serosa (*arrowhead*) and metastasizes to a lymph node of the left obturator chain (*arrow* in **b**). Note the marked pooling of secretions (*asterisk*) in the endometrial cavity due to obstruction of the internal uterine os

MR are indicated for initial radiologic evaluation;
- patients with high grade papillary or clear cell carcinoma should undergo a CT or MR study given the high pretest probability of lymph node metastasis;
- patients with possible invasion of the cervix at gynecologic examination and with a positive or inconclusive result from dilatation and curettage should undergo MR, because this is the only imaging modality that has proven reliable in making a diagnosis in these conditions;
- patients requiring a panoramic evaluation of the abdomen and pelvis should undergo contrast enhanced MR since this is the only technique able to simultaneously study the myometrium, cervix and lymph nodes.

Akin O, Mironov S, Pandit-Taskar N et al (2007) Imaging of cancer of uterine cancer. Radiol Clin North Am 45:167-182

Arko D, Takac I (2000) High frequency transvaginal ultrasonography in preoperative assessment of myometrial invasion in endometrial cancer. J Ultrasound Med 19:639-643

Ascher SM, Reinhold C (2002) Imaging of cancer of the endometrium. Radiol Clin North Am 40:563-576

Frei KA, Kinkel K, Bonél HM et al (2000) Prediction of deep myometrial invasion in patients with endometrial cancer: clinical utility of contrast-enhanced MR imaging – a meta-analysis and Bayesian analysis. Radiology 216:444-449

Kinkel K, Kaji Y, Yu KK et al (1999) Radiologic staging in patients with endometrial cancer: a meta-analysis. Radiology 212:711-718

Cervical cancer

Pathology

Cervical cancer is one of the most common female tumors, especially in women below 50 years. Even in postmenopausal women it is the third most common gynecologic neoplasm. There is an initial peak in incidence among women aged 35-45, with a second peak in the 60-65 age range.

The incidence is on the whole in decline, thanks to cytologic screening (Papanicolaou or Pap test). When performed in the event of a positive finding at colposcopy, the Pap test is able to identify precancerous alterations and tumors at a very early stage, thus enabling their eradication prior to invasion. Currently there is also a trend towards a reduction in age due to the higher frequency of young patients affected by infections of the cervical epithelium from human papilloma virus (HPV).

The types of potentially more oncogenic HPV are strains 16 and 18. If they persist in the cell after clinical recovery, there is an increased risk of degeneration, particularly in the presence of risk cofactors such as promiscuity in young subjects, poor personal hygiene, frequent genital infections, multiple pregnancies, immunosuppression in HIV-positive subjects or prolonged use of oral contraceptives. Other possible risk factors include smoking, vitamin deficiency and a genetic predisposition.

In 80-90% of cases the tumor of the cervix is a squamous cell carcinoma which most commonly arises from the pavement epithelium of the exocervix. A less common site of onset is the transition zone with endocervical epithelium.

The tumor can be assessed as:
- preinvasive cancer or cervical intraepithelial neoplasia (CIN), when the lesion has not spread beyond the basement membrane separating the epithelium from the underlying stroma;

- invasive cancer, when the cancerous cells of the epithelium have more-or-less extensively invaded the underlying connective tissue, reaching the vessels and the lymph ducts;

The preinvasive form cannot be identified with gynecologic examination alone. Lesion grading at cytology is as follows:

- grade I CIN: mild dysplasia involving less than 1/3 of the epithelium;
- grade II CIN: moderate dysplasia involving 1/3-2/3 of the epithelium;
- grade III CIN: severe dysplasia involving more than 2/3 of the epithelium, carcinoma in situ.

In the presence of a positive Pap test, a biopsy should be performed to define the degree of invasion.

In the early phases the tumor is totally asymptomatic. Aspecific symptoms appearing only in the invasive phase include intermenstrual vaginal bleeding, vaginal secretion and dyspareunia. Pelvic pain radiating to the back and lower limbs (with unilateral lymphedema), hematuria and ascites are suggestive of larger lesions with spread to adjacent structures.

Diagnostic Imaging

Identification

In standard clinical practice diagnostic imaging has no role to play in the identification of the lesion, if not correlated to the role of staging.

Ultrasonography can evaluate the uterine cervix with both the suprapubic and transvaginal and/or transrectal approach, with the images of the latter two being markedly more detailed.

The suprapubic approach is able to visualize the tumor only in advanced stages when it has caused an increase in size, irregular margins and heterogeneous echotexture of the uterine cervix with concomitant distortion of the cervical canal. TVUS and TRUS are able to more accurately evaluate the diameters of the cervix.

The tumor rarely appears as a well-defined hypoechoic mass. More often, due to its invasive characteristics, it appears with diffusely heterogeneous echotexture and air trapped in the fornices and the cervical canal (**Fig. 20.30**).

On **computed tomography** images the normal cervix has a highly varied enhancement pattern in relation to the different degrees of vascularity and structural composition, correlated with age. However, hypoattenuation with respect to the uterine body and fundus prevails. Due to the poor contrast resolution of CT, visualization of the tumor is limited, even after the injection of contrast medium when the cervical carcinoma may appear iso- or hypoattenuated to the normal stroma. The hypoattenuation is justified by the presence of necrosis, ulceration or reduced vascularity (**Fig. 20.31**). In the event of a prior biopsy or prevalent tissue necrosis air bubbles may be identified within the mass. The cervix generally has smooth and well defined-margins if the tumor is confined. In the more advanced forms, the cervix appears enlarged with irregular margins. The involvement of the cervical canal and the uterine body make differential diagnosis between carcinoma arising from the cervix or uterine body difficult. The obstruction of the cervical canal leads to pooling of blood, serous secretions or pus within the endometrial cavity, which consequently appears enlarged.

Magnetic resonance is the imaging modality which provides the best definition of the tumor. In T2-weighted images the tumor is characterized by intermediate signal intensity which replaces the hypointensity of the cervical stroma. The sensitivity of the technique enables the detection of even small lesions, although with problems of differential diagnosis with cervicitis and conization outcomes. MR is unable to identify lesions that develop superficially. Dynamic study with contrast medium, despite

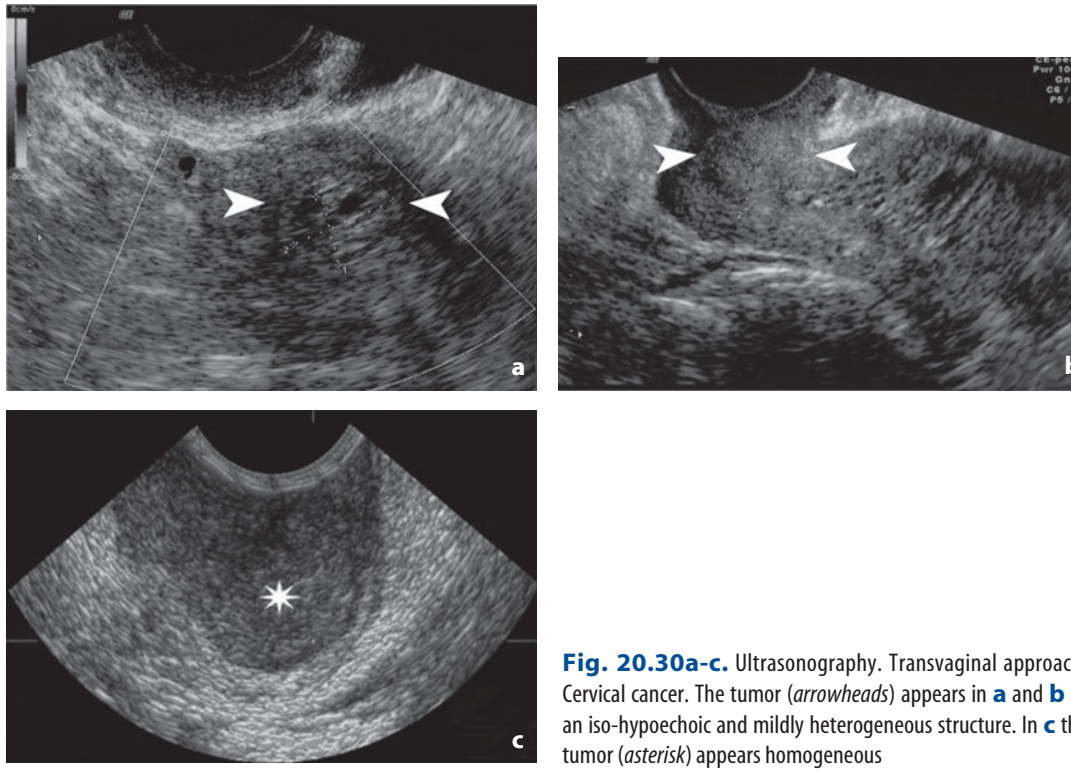

Fig. 20.30a-c. Ultrasonography. Transvaginal approach. Cervical cancer. The tumor (*arrowheads*) appears in **a** and **b** as an iso-hypoechoic and mildly heterogeneous structure. In **c** the tumor (*asterisk*) appears homogeneous

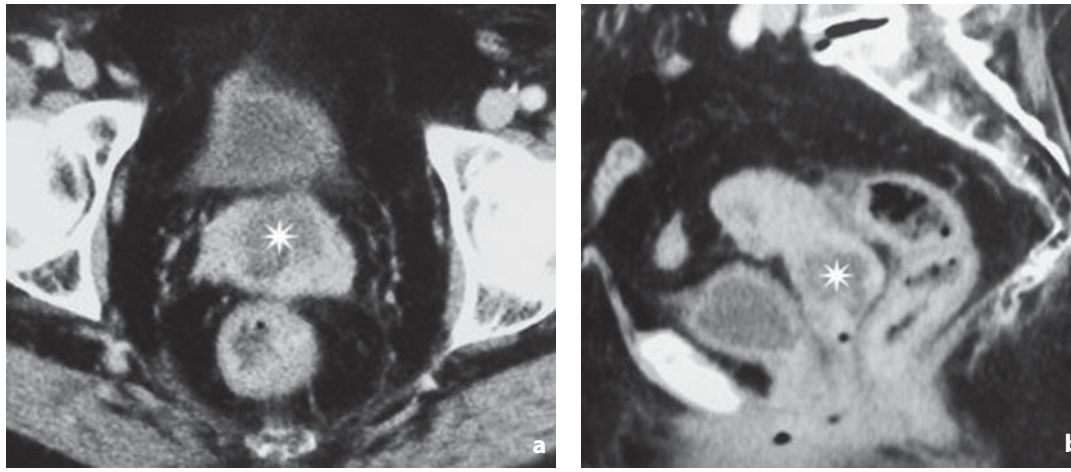

Fig. 20.31a,b. Computed tomography. Cervical cancer in a patient already operated on for colon cancer. Current metrorrhagia. Axial (**a**) and sagittal (**b**) images depict carcinoma of the cervix, which appears as a solid hypoattenuating lesion with irregular margins (*asterisk*)

not being used on a routine basis by many, is able to visualize the vascularity of the lesion (generally lower than stroma) and becomes a predictor of the radiosensitivity of the tumor (Fig. 20.32).

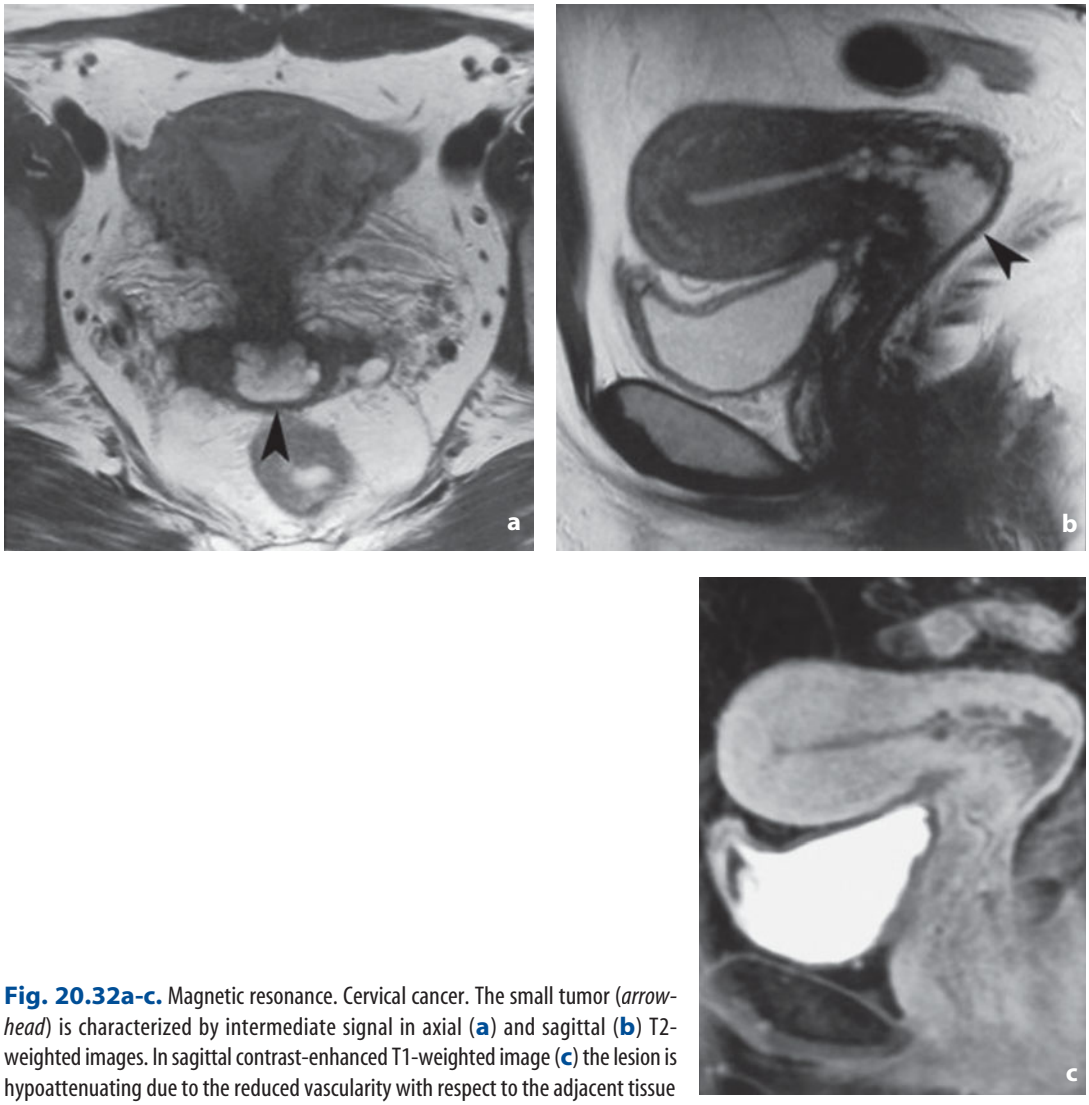

Fig. 20.32a-c. Magnetic resonance. Cervical cancer. The small tumor (*arrowhead*) is characterized by intermediate signal in axial (**a**) and sagittal (**b**) T2-weighted images. In sagittal contrast-enhanced T1-weighted image (**c**) the lesion is hypoattenuating due to the reduced vascularity with respect to the adjacent tissue

Staging

Prognosis depends on the primary tumor volume and the clinical stage.

The clinical staging system proposed by the International Federation of Gynecology and Obstetrics (FIGO) is the most utilized. The therapeutic approach is established according to the tumor stage: radical hysterectomy or radiotherapy may be proposed for stages IIA or lower; in the more advanced stages the only treatment is radiotherapy with or without chemotherapy. A crucial determinant in the therapeutic approach, therefore, is involvement of the parametrium.

FIGO recommends a clinical staging system based on gynecologic examination with colposcopy and lesion biopsy, chest radiograph, cystoscopy, sigmoidoscopy, urography and barium enema to evaluate the regional and distant spread of disease. The main difficulty with clinical examination lies in the evaluation of invasion of the parametrium and the lateral pelvic wall, as well as estimation of the size of the tumor. Lymph node involvement is not included in the FIGO classification, but it is a very important parameter in the TNM staging system (**Table 20.2, Fig. 20.33**). The above-

mentioned aspects justify the use of diagnostic imaging in clinical practice.

Ultrasonography is unable to provide a reliable evaluation of the invasion of the parametrium or the pelvic wall or the involvement of the regional lymph nodes. It can, however, diagnose ureterohydronephrosis resulting from ureteric stricture secondary to neoplastic invasion of the parametrium. US, therefore, does not appear to be a satisfactory technique for regional staging.

Although not considered in the FIGO classification, **computed tomography** is often used in tumor staging given the difficulty gynecologists have in evaluating both endocervical and exocervical tumor spread (uterine body, parametrium, lateral pelvic wall) and the impossibility of evaluating intra- and extrapelvic lymph node involvement. In particular, high resolution multislice examination with its multiplanar reconstructions in the sagittal or coronal planes increases the utility of the technique.

A crucial feature for staging purposes, as noted above, is the evaluation of involvement of the parametrium. On CT images this appears as a thin hypoattenuating layer of connective tissue, smooth muscle fibers and fat extending laterally from the uterus to the pelvic wall between the layers of the broad ligament. Invasion, which is most likely in tumors >2 cm, is identifiable by loss of definition of the margins of the cervix and increase in density of the parametrial adipose tissue. This finding, however, may also be due to inflammation associated with the cervical tumor (**Fig. 20.34**). A more certain albeit indirect sign of advanced involvement of the parametrium is ureterohydronephrosis due to ureteric stricture in the portion running in the parametrium. The presence of tumor in the adipose tissue of the parametrium and involvement of the ureter causing hydronephrosis, which is well demonstrated on CT images, classifies the patient as stage IIIB. Perivascular invasion and increase in the thickness of the uterosacral ligaments may be considered signs of parametrial invasion, although they are aspecific, since they may be due to ulceration and infection of the tumor or the result of prior surgery. Pelvic nodules produced by endometriosis may also create interpretation problems. Diagnostic errors (false positives of invasion of the parametrium) may be the result of an inadequate consideration of the normal parauterine and paracervical ligaments, which appear as thin hyperattenuating bands with a diameter no greater than 3-4 mm. Upon digital rectal examination, invasion of the pelvic wall is diagnosed when the pelvic wall can no longer be separated from the tumor. On CT this is suspected when the tumor is less than 3 mm from the bone and muscle planes. In the event of massive invasion, solid enhancing tissue may be visual-

Table 20.2. Carcinoma of the cervix. TNM and FIGO (International Federation of Gynecology and Obstetrics) classification systems

TNM	FIGO	Definition
Tis	0	Tumor in situ
T1	I	Tumor confined to uterus
T1a	IA	Diagnosis is only microscopic
T1a1	IA1	Depth ≤3 mm, horizontal spread ≤7 mm
T1a2	IA2	Depth >3-5 mm, horizontal spread ≤7 mm
T1b	IB	Clinically visible or microscopic lesion larger than IA2
T2	II	Extension beyond the uterus, not to the pelvic wall or the lower third of the vagina
T2a	IIA	Absence of evident parametrial involvement
T2b	IIB	Evident parametrial involvement
T3	III	Extension up to the pelvic wall and/or the lower third of the vagina
T3a	IIIA	Invasion of the lower third of the vagina without extension to the pelvic wall
T3b	IIIB	Extension to the pelvic wall and/or hydronephrosis or excluded kidney
T4	IVA	Invasion of the bladder or rectal mucosa and/or extension beyond the pelvic cavity
M1	IVB	Distant metastasis

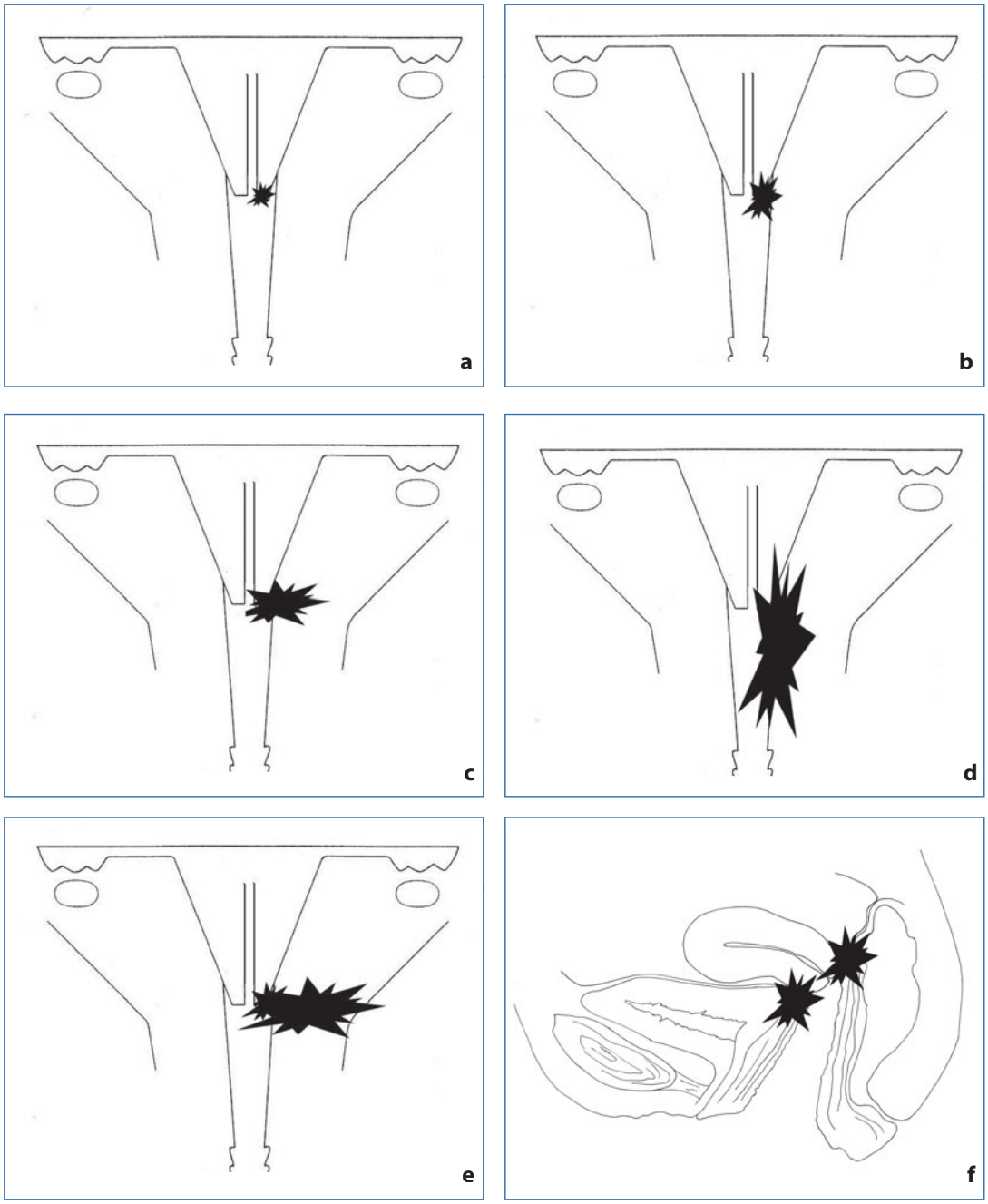

Fig. 20.33a-f. FIGO classification of carcinoma of the cervix. **a** Stage IB. **b** Stage IIA. **c** Stage IIB. **d** Stage IIIA. **e** Stage IIIB. **f** Stage IVA

ized surrounding the iliac vessels, invading the pyriform and internal obturator muscles, and eroding the pelvic bones.

Involvement of the urinary bladder and rectum (stage IVA) is defined by cytoscopy and rectoscopy with biopsy collection. On CT it is hypothesized in the presence of obliteration of the perivesical and perirectal fat, asymmetric nodular thickening of the bladder or rectal wall, and in the more advanced cases intraluminal polyps and/or the formation of fistulae. The sensitivity of CT for the invasion of the bladder mucus is very low.

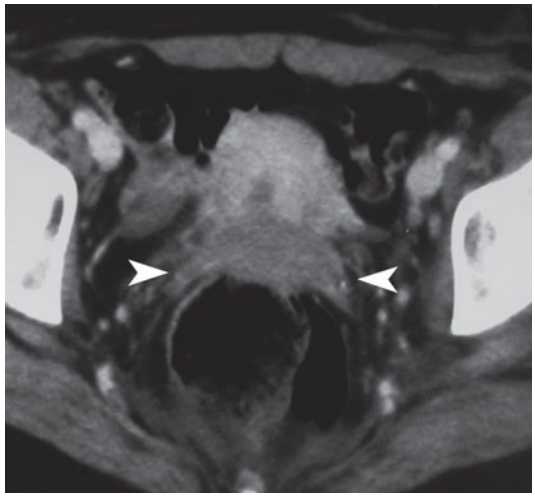

Fig. 20.34. Computed tomography. Cervical cancer, stage IIB with bilateral invasion of the parametrium identifiable by the solid tissue with irregular margins in the pericervical adipose tissue (*arrowheads*)

The CT finding of enlarged pelvic lymph nodes is considered equivalent to stage IIIB (extension to the pelvic wall). If the para-aortic or inguinal lymph nodes are involved, the tumor is deemed to be stage IVB (distant metastasis). The probability of lymph node metastasis in stage IIB is slightly lower than, if not the same as, the higher stages.

The definition of metastatic involvement is based on size. Lymph nodes greater than 1 cm in the short axis are considered pathologic. In reality, this criterion should take into consideration the anatomic site of the node. In this case the normal limit for external iliac nodes is 10 mm, but falls to 9 mm for common iliac nodes and 7 mm for internal iliac nodes. Patients with cervical cancer can have secondary infection resulting in adenopathy. Therefore, neoplastic and hyperplastic lymph nodes cannot be distinguished solely on the basis of size on CT images. Micrometastases may be present in lymph nodes of normal size, and the use of contrast medium provides little useful additional information. On the other hand, a revision of findings reveals that the normal size reduces the probability of metastases, whereas an increase in size increases the probability only marginally. No better information can be obtained with MR or lymphography. A definite sign of metastasis, however, is central lymph node necrosis.

While it is understood that the lymph nodes of the parametrium are the first to become involved, there are three possible drainage routes from the uterine cervix: lateral, along the external iliac vessels; hypogastric or medial, along the internal iliac vessels; and presacral, along the uterosacral ligament. All of these routes lead to the common iliac lymph nodes, with subsequent involvement of the para-aortic nodes.

In the case of lateral spread involving the external iliac chain, the tumor first metastasizes to the medial group, which receives lymph from the inguinal lymph nodes and is situated posterior to the vein. Then it spreads to the middle group between the artery and the vein and the group lateral to the artery. Lastly, metastasis reaches the common iliac chain. The lymph nodes of the common iliac chain are medial, middle and lateral. The medial nodes are located between the common iliac arteries and include the lymph nodes anterior to the sacral promontory. The middle nodes lie between the common iliac vessels anteriorly, the psoas muscle laterally and the vertebral column medially. The lateral nodes are external to the common iliac artery.

In the hypogastric route, the tumor spreads along the branches of the internal iliac artery and then involve the lymph nodes which lie between the internal and external iliac vessels. In a later stage the tumor spreads to the common iliac lymph nodes.

Tumor spread along the presacral route involves the lymphatic plexus anterior to the sacrum and coccyx.

CT can be used as a guide for the biopsy of enlarged lymph nodes and as a support for radiotherapy planning, as well as for monitoring patients with recurrences. Recurrences, which are treated in a separate chapter, are defined as a lesion with onset a minimum of six months after primary tumor regression. CT has high specificity and sensitivity in the evaluation of recurrences and is commonly used in follow-up. Distant metastases are more frequently observed in the presence of recurrences.

Although microinvasive carcinoma (FIGO IA) is not identifiable, **magnetic resonance** is currently the best technique for staging cervical cancer, given its elevated contrast and spatial resolution provided by surface coils.

In stage IB disease (clinically invasive tumor confined to the cervix) the hyperintense lesion in T2-weighted sequences is completely surrounded by the hypointense cervical stroma. The identification of an intact stromal ring enables invasion of the parametrium to be ruled out with a high degree of accuracy (**Fig. 20.35**).

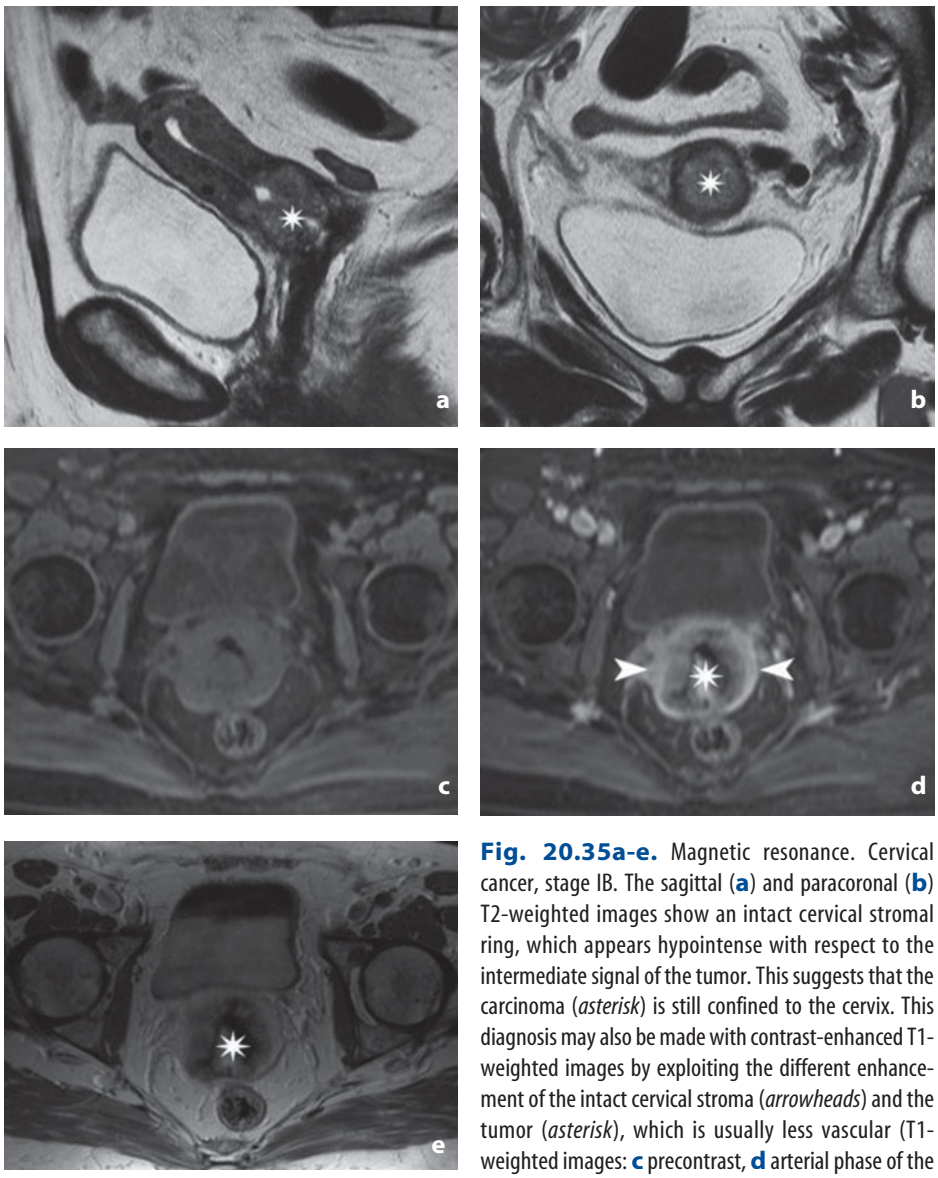

Fig. 20.35a-e. Magnetic resonance. Cervical cancer, stage IB. The sagittal (**a**) and paracoronal (**b**) T2-weighted images show an intact cervical stromal ring, which appears hypointense with respect to the intermediate signal of the tumor. This suggests that the carcinoma (*asterisk*) is still confined to the cervix. This diagnosis may also be made with contrast-enhanced T1-weighted images by exploiting the different enhancement of the intact cervical stroma (*arrowheads*) and the tumor (*asterisk*), which is usually less vascular (T1-weighted images: **c** precontrast, **d** arterial phase of the dynamic study, **e** late phase)

Stage IIA (tumor invading the upper two thirds of the vagina without invasion of the parametrium) is usually diagnosed clinically. On T2-weighted MR images, invasion is visualized by the elevated signal intensity of the lesion which replaces the low signal of the vagina (**Fig. 20.36**). This evaluation can be challenging, with the risk of overstaging, if a large exophytic tumor causes distension of the fornices.

On MR images certain signs of extension to the parametrium (stage IIB) are anomalous irregular signal intensity of the tumor in the parametrium itself and obliteration of the periureteric fat space (**Fig. 20.37**). Dynamic study may be useful, although in general nonenhanced axial and coronal T1- and T2-weighted sequences are sufficient for evaluation of invasion of the parametrium.

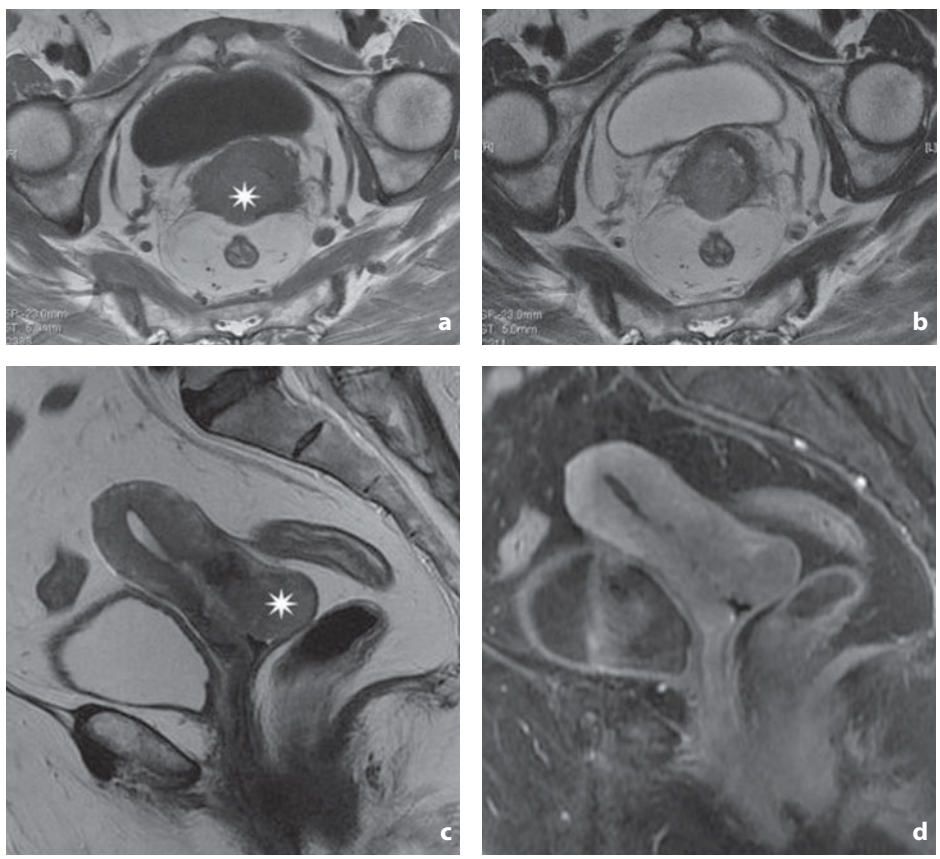

Fig. 20.36a-d. Magnetic resonance. Cervical cancer, stage IIA. Axial T1- (**a**) and T2-weighted (**b**) images. Sagittal images weighted in T2 (**c**) and T1 after contrast medium administration with fat saturation (**d**). The tumor can be identified invading the posterior vaginal fornix (*asterisk*)

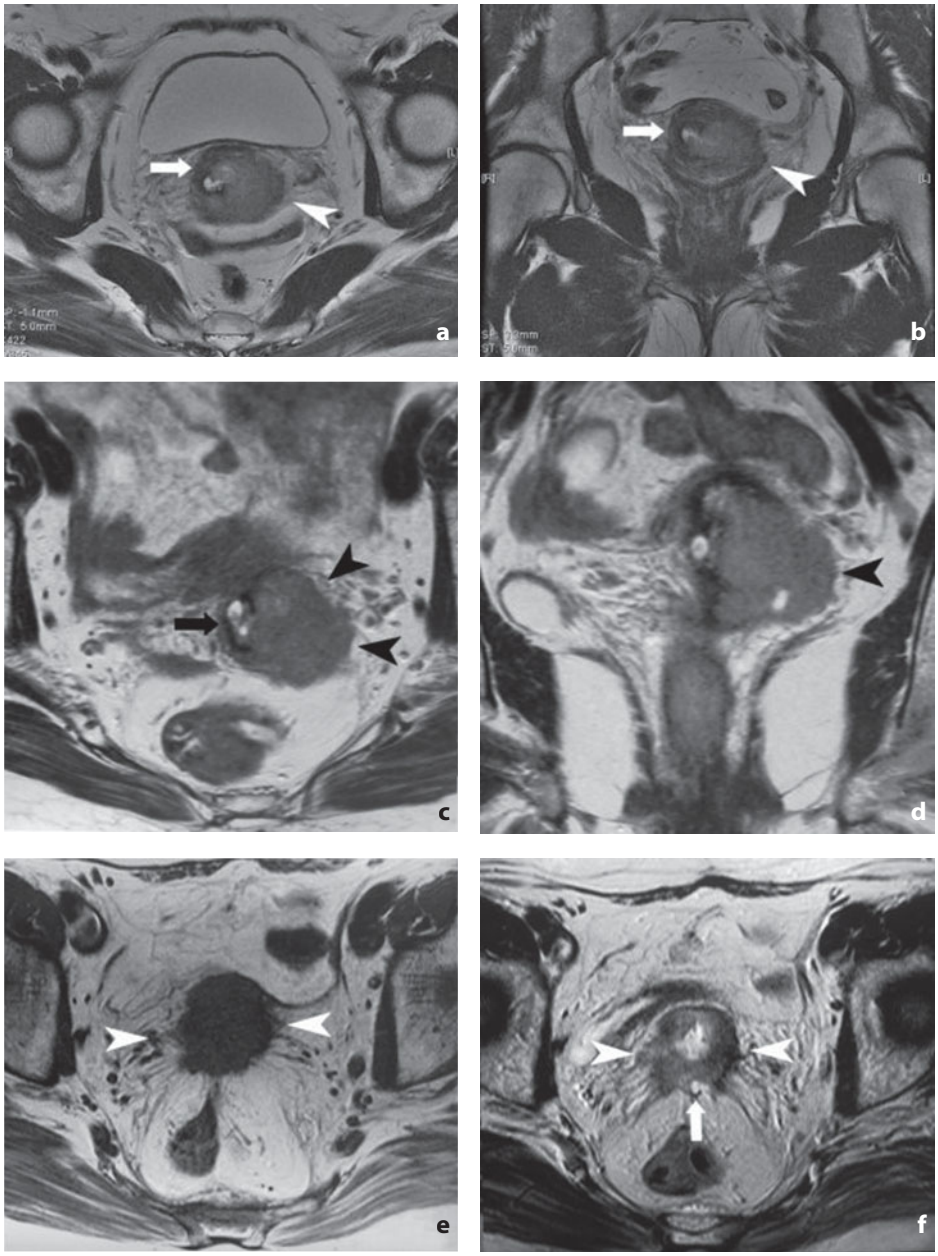

Fig. 20.37a-f. Magnetic resonance. Cervical cancer, stage IIB. Axial (**a**) and coronal (**b**) T2-weighted images show initial invasion of the left parametrium (*arrowhead*) subsequent to neoplastic invasion of the cervical stroma which appears partially conserved on the right (*arrow*). **c,d** Images show a case where invasion of the left parametrium (*arrowhead*) is more evident. Note the intact cervical stromal ring and the right parametrium (*arrow*). **e,f** Images show carcinoma invading both left and right parametrium. Diagnosis is possible on the basis of the spiculated tissue (*arrowheads*) penetrating the pericervical adipose tissue. Involvement of the mesorectal fascia is also evident (*arrow*)

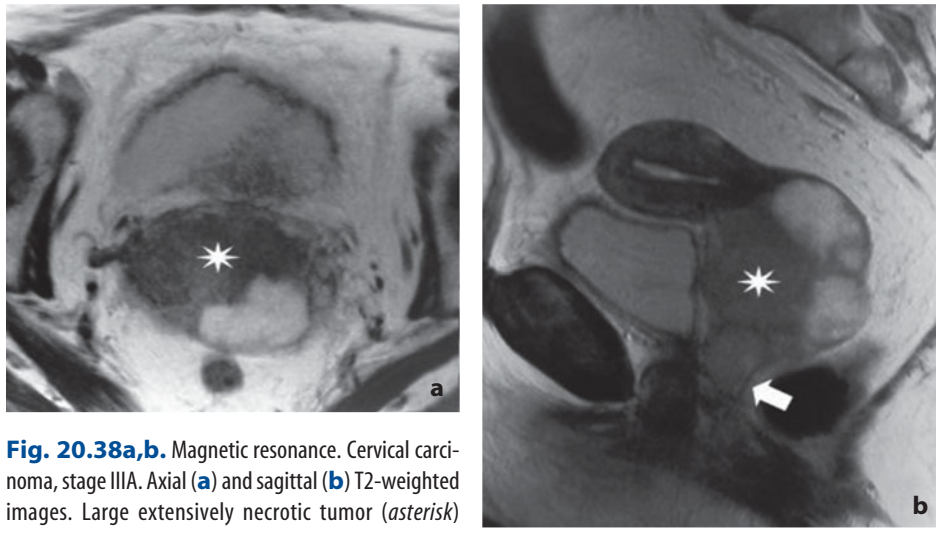

Fig. 20.38a,b. Magnetic resonance. Cervical carcinoma, stage IIIA. Axial (**a**) and sagittal (**b**) T2-weighted images. Large extensively necrotic tumor (*asterisk*) invading the vagina up to the inferior third (*arrow*)

In stage IIIA (clinical diagnosis) the tumor involves the inferior third of the vagina, without extension to the pelvic wall (**Fig. 20.38**).

A tumor extending to the pelvic wall or causing hydronephrosis is classified IIIB. The evaluation of possible hydronephrosis can be performed with MR urography (**Fig. 20.39**). Neoplastic involvement of the internal obturator, pyriform and levator ani muscles is identified by an increase in signal intensity of these structures in T2-weighted images.

The focal interruption of the hypointense signal of the bladder and rectal wall or the segmental increase in thickness of the rectal wall can make the diagnosis of stage IVA challenging (**Fig. 20.40**). A number of signs can be helpful: the presence of a fatty hyperintense cleavage plane between the tumor and the hypointense bladder or rectal wall rules out involvement of those organs; hyperintensity of the mucosa in T2-weighted images is not in itself an expression of neoplastic invasion since this may also be found in the presence of edema.

The presence of distant metastases (stage IVB) is best defined with CT. With regard to lymph node metastases the observations made above are valid (**Fig. 20.41**).

Akin O, Mironov S, Pandit-Taskar N et al (2007) Imaging of cancer of uterine cancer. Radiol Clin North Am 45:167-182

Nicolet V, Carignan L, Bourdon F et al (2000) MR Imaging of cervical carcinoma: a practical staging approach. RadioGraphics 20:1539-1549

Okamoto Y, Tanaka YO, Nishida M (2003) MR imaging of the uterine cervix: imaging-pathologic correlation. RadioGraphics 23:425-445

Pannu HK, Corl FM, Fishman EK (2001) CT evaluation of cervical cancer: spectrum of disease. RadioGraphics 21:1155-1168

Sahdev A, Reznek R (2006) Imaging in endometrial and cervical cancer: why, when and how. RSNA Categorical course in diagnostic radiology: Genitourinary Radiology, pp 11-22

Scheidler J, Heuck AF, Reinhold C (2002) Imaging of cancer of the cervix. Radiol Clin North Am 45:577-590

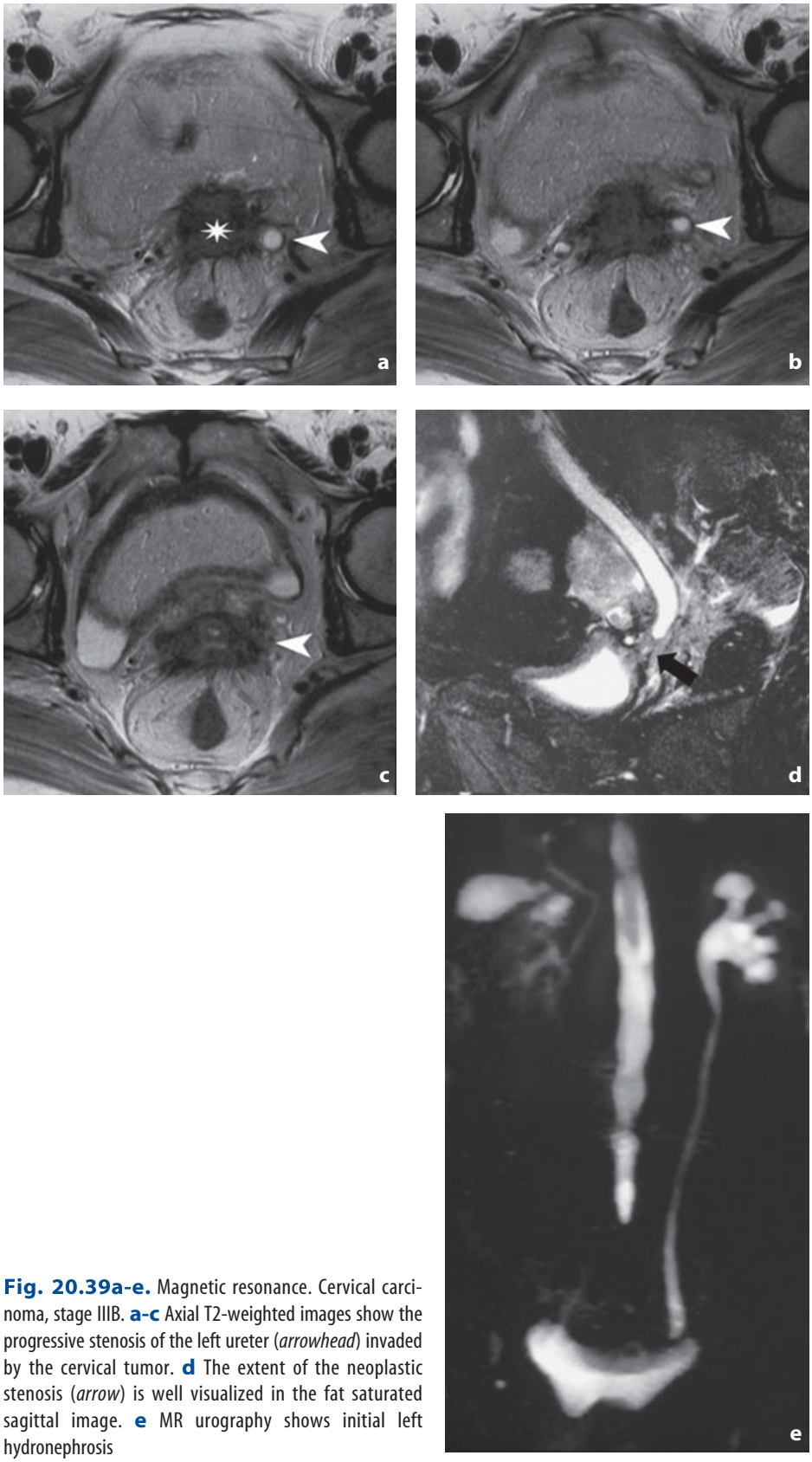

Fig. 20.39a-e. Magnetic resonance. Cervical carcinoma, stage IIIB. **a-c** Axial T2-weighted images show the progressive stenosis of the left ureter (*arrowhead*) invaded by the cervical tumor. **d** The extent of the neoplastic stenosis (*arrow*) is well visualized in the fat saturated sagittal image. **e** MR urography shows initial left hydronephrosis

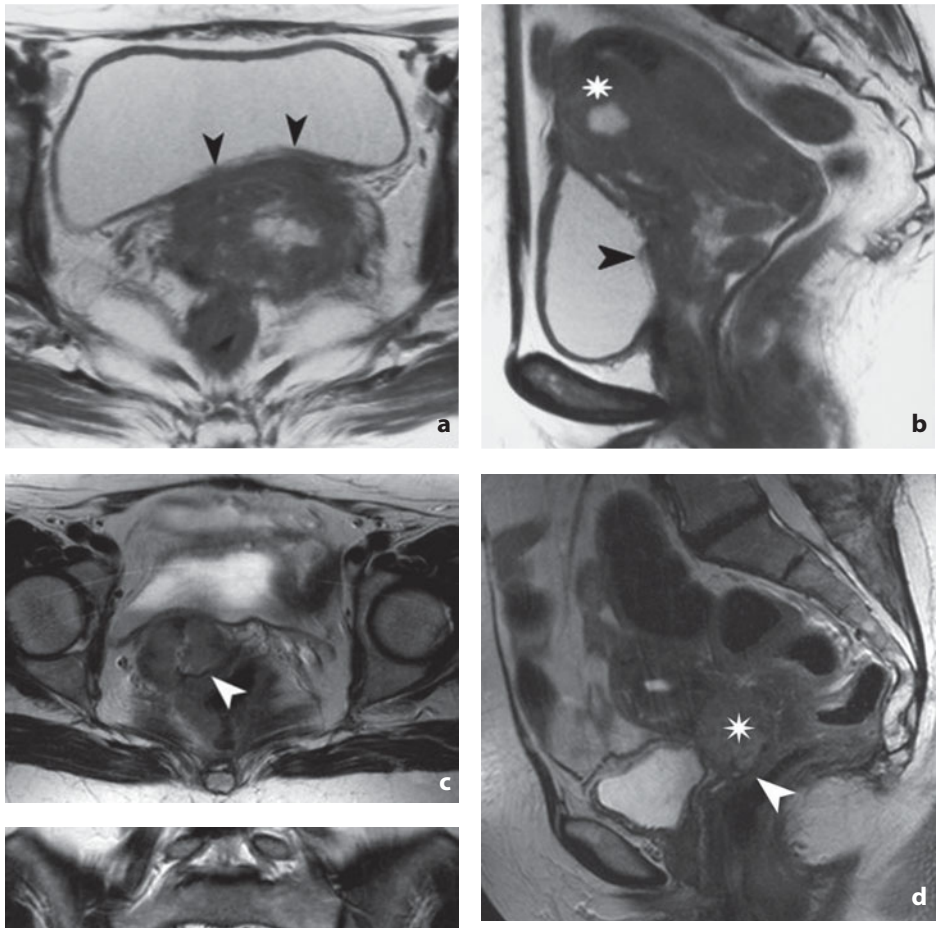

Fig. 20.40a-e. Magnetic resonance. Cervical carcinoma, stage IVA. **a,b** Axial (**a**) and sagittal (**b**) T2-weighted images. The tumor can be seen invading the anterior aspect of the vagina and focally invading the bladder wall, which appears thickened with a heterogeneous signal (*arrowhead*). A leiomyoma with cystic degeneration can also be identified (*asterisk*). **c-e** Axial (**c**), sagittal (**d**) and coronal (**e**) T2-weighted images. The tumor (*asterisk*) can be seen invading the anterior aspect of the rectal wall (*arrowhead*)

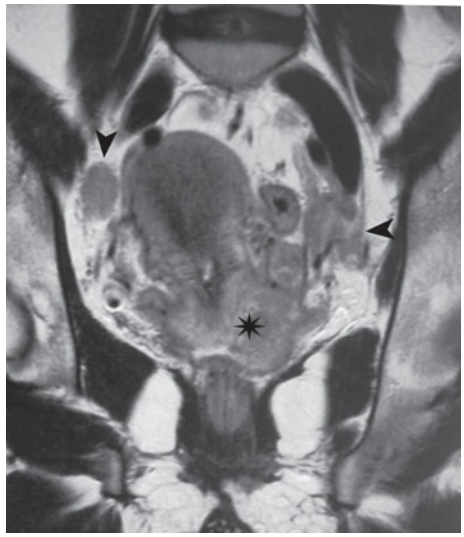

Fig. 20.41. Magnetic resonance. Lymph node metastasis in cervical cancer. The coronal T2-weighted image shows the cervical tumor (*asterisk*). Enlarged lymph nodes indicating metastasis can be appreciated at the level of both internal iliac chains

Clinical Approach to Adnexal Disease

21

S. Pecorelli, F. Odicino, G. Tisi

The diagnostic-instrumental finding of an alteration to the adnexal region occurs in 1.5-2% of females over 40 years of age and poses a complex problem of differential diagnosis. Correct identification of the condition is crucial for the appropriate clinical management of the disease.

Adnexal lesions are divided into ovarian and tubal.

1. Ovarian lesions can be non-neoplastic (**Fig. 21.1**) or neoplastic (**Fig. 21.2**) in origin. The non-neoplastic lesions include congenital lesions, infectious lesions of bacterial, viral or mycotic origin, noninfectious inflammatory lesions, inclusion cysts and glands, functional and nonfunctional lesions derived from follicular and stromal elements, and vascular lesions. Neoplastic ovarian lesions are histologically classified as epithelial and nonepithelial.

2. Tubal lesions include uterine tube cysts (hydatid of Morgagni and peritubal cysts), paraovarian cysts (which are generally benign and asymptomatic, developing between the layers of broad ligament from embryonic rests), ectopic pregnancies, benign connective and epithelial tumors (tubal polyps and papillomas, fibromyomas, adenomatoid tumors) and malignant tumors (epithelial, connective and metastatic).

Campbell S, Bhan V, Royston P et al (1989) Transabdominal ultrasound screening for early ovarian cancer. BMJ 299:1363-1367

Malformations

Ovarian malformations are rare. The unilateral absence of an ovary is generally secondary to complete agenesis of the urogenital folds and is for the most part associated with the nondevelopment of the uterine tube, half of the uterus, and the homolateral

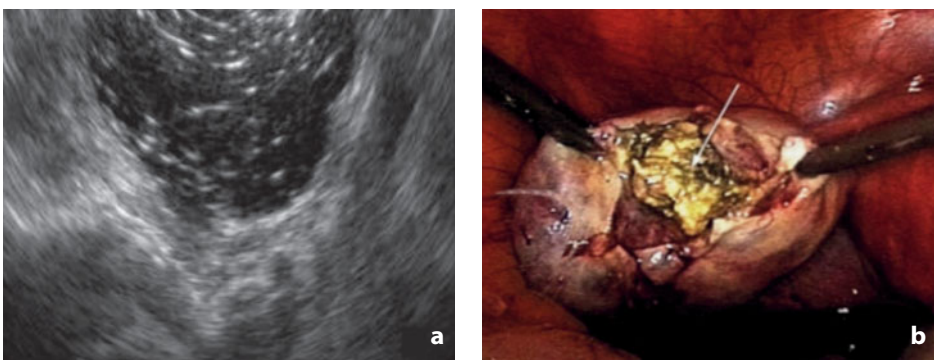

Fig. 21.1a,b. Mature cystic teratoma. Sonogram (**a**) and intraoperative image (**b**)

L. Olivetti, L. Grazioli (eds.), *Imaging of Urogenital Diseases*,

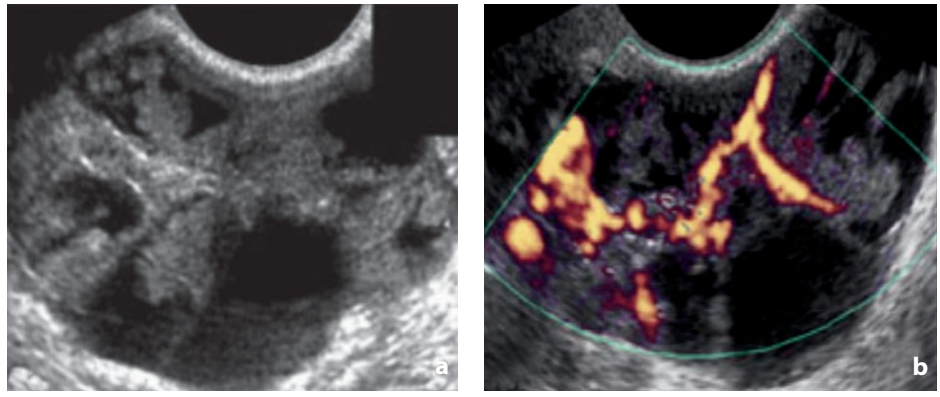

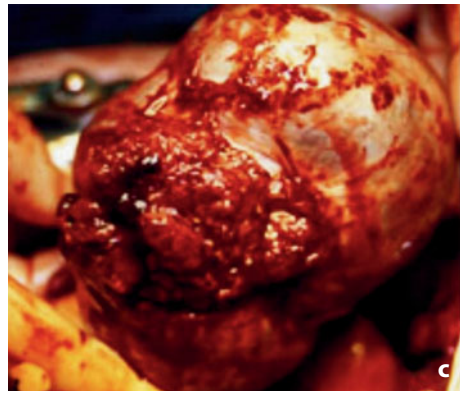

Fig. 21.2a-c. Ovarian cancer. Sonograms (**a,b**) and intraoperative image (**c**)

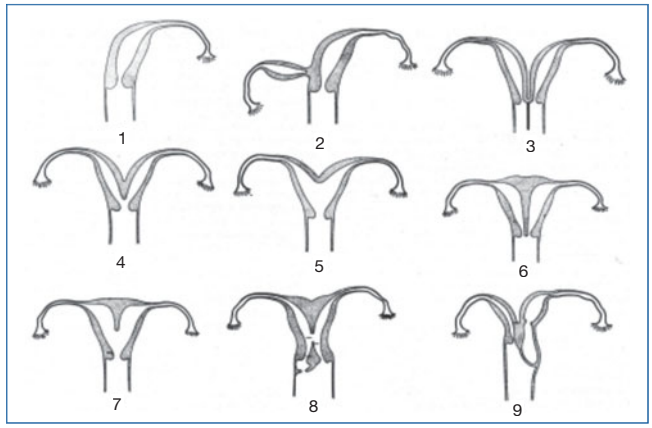

Fig. 21.3. Malformations of the female reproductive system. (*1*) Unicornuate uterus. (*2*) Unicornuate uterus with rudimentary horn having endometrial cavity but non-communicating. (*3*) Didelphys uterus with duplex vagina. (*4*) Bicornuate uterus. (*5*) Arcuate uterus. (*6*) Septate uterus. (*7*) Partial septate uterus. (*8*) Uterus with communicating septum and arcuate fundus, vagina with septum and unilateral atresia, vagino-vaginal fistula. (*9*) Bicornuate uterus with noncommunicating vaginal septum

ureter and kidney (Fig. 21.3). The presence of a supernumerary ovary is rare and presumably derives from separate primordium.

Several chromosomal diseases, of which Turner's syndrome is the most common, can alter ovarian morphology (rudimentary ovaries).

Tubal malformations often pass unobserved since they are difficult to identify on physical examination. They may arise from embryogenic alteration of the most cranial portion of the Müllerian ducts, or from accidental lesions such as torsion or inflammation.

The most common congenital lesions include hypoplasia of the uterine tube, the presence of accessory tubal orifices and the existence of accessory or supernumerary tubes.

A frequent finding on the surface of tubes is multiple minute serous cysts (peritubal cysts) originating from an invagination of the tubal epithelium which are in no way pathologic.

Jacobs IJ et al (1990) A risk of malignancy index incorporating CA125, ultrasound and menopausal status for the accurate preoperative diagnosis of ovarian cancer. Br J Obstet Gynecol 97:922-29

Schneider VL et al (1993) Comparison of Doppler with two-dimensional sonography and CA125 for predictionof malignancy of pelvic masses. Obstet Gynecol 81:983-88

Inflammation

The uterine tubes are the tract of the female reproductive system where infection occurs relatively frequently, often with long-term consequence: sterility (due to closure of the tubal lumen), increased incidence of ectopic pregnancy or formation of collections within the tubal lumen (hydro-sactosalpinx/pyosalpinx) (**Fig. 21.4**).

The anatomic-pathologic classification of adnexitis (pathologic infection of the adnexa) is summarized in **Table 21.1**.

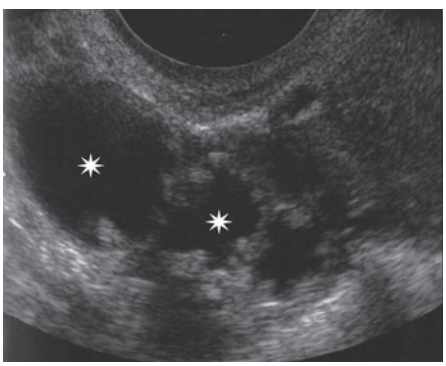

Fig. 21.4. Pyosalpinx, sactosalpinx. Oval-shaped adnexal enlargement with irregular anechoic areas (*asterisks*)

Table 21.1. Classification of infectious adnexitis

I. Acute adnexitis
1. Tubal lesions
   - Catarrhal salpingitis (endosalpingitis)
   - Interstitial salpingitis
   - Perisalpingitis
   - Purulent salpingitis (sactosalpinx)
2. Ovarian lesions (rarely isolated)
   - Interstitial exudative ovaritis
   - Parenchymatous ovaritis
   - Suppurative ovaritis
   - Periovaritis
   - Ovarian abscess

II. Chronic adnexitis
1. Tubal lesions
   - Hydrosalpinx
   - Chronic pyosalpinx
   - Hematosalpinx (ectopic pregnancy, endometriosis, fibroids)
2. Ovarian lesions
   - Tubo-ovarian cyst
   - Tubo-ovarian abscess

The symptoms of inflammatory disease of the adnexa are rather variable. Bilateral pain located in the inferior abdominal quadrants and radiating towards the lumbar-sacral region is a commonly reported symptom in acute adnexitis. This may be substituted by a sense of heaviness or burning in the presence of a chronic condition. Other symptoms include purulent discharge, menstrual irregularity and tenderness upon palpation of the adnexal region. Elevated temperature (38-40 °C) is always present in the acute form and is generally associated with neutrophil leukocytosis. Chronic forms may manifest with slight persistent fever.

Tumors

Ovarian tumors are subdivided into benign and malignant lesions. Both types can be classified on the basis of the tissue from which they arise as epithelial and nonepithelial lesions (**Table 21.2**).

Malignant ovarian tumors of epithelial origin account for one-sixth of malignant lesions in women. The probability of becoming ill with ovarian cancer during a lifetime is 1 in 70 (with an estimated incidence of 22,430 new cases in the United States in 2007). Ovarian cancer accounts for one-quarter of deaths from cancer, and is the

Table 21.2. Classification of ovarian neoplastic lesions

Epithelial lesions

1. Serous tumors
   - benign
   - with atypia or borderline
   - malignant
2. Mucinous tumors
   - benign
   - with atypia or borderline
   – intestinal
   – cervical-like
   – Müllerian
   - malignant
3. Endometrioid tumors
   - benign
   - with atypia
   - malignant
4. Clear cell tumors
   - benign
   - with atypia
   - malignant
5. Transition cell tumors (Brenner)
   - benign
   - borderline
   - malignant
6. Mixed epithelial tumors
7. Undifferentiated carcinomas
8. Malignant mixed mesodermal tumors (MMMT)
9. Sarcomas

Nonepithelial lesions

- Sex cord-stromal tumors
  – granulosa and theca cell tumors
  – Sertoli-Leydig tumors
  – gynandroblastoma
  – sex cord tumor with annular tubules
  – nonclassified tumors
- Germ cell tumors

Metastatic lesions

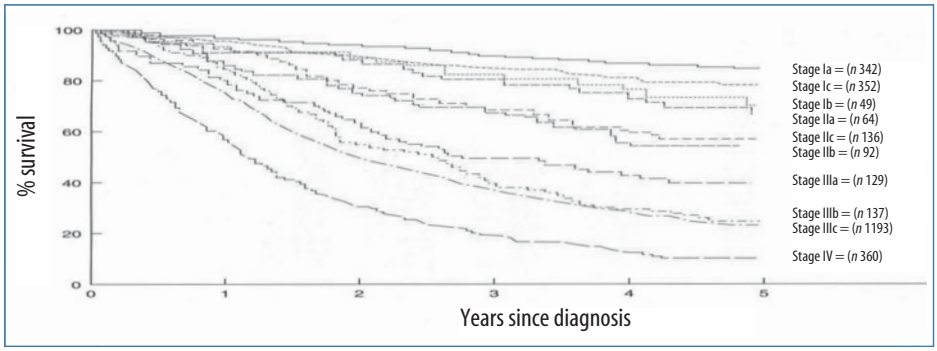

Fig. 21.5. Malignant ovarian tumors. Survival in relation to stage. 24th FIGO Annual Report

leading cause of death from gynecologic tumors. The high mortality is mainly linked to the fact that the diagnosis is generally made in an advanced stage of disease (**Fig. 21.5**). The most common nonepithelial lesion is the germ cell tumor, which mainly affects women below 20 years of age, whereas the peak incidence of epithelial tumors occurs in peri- or postmenopausal women (>50 years).

The etiology of epithelial tumors is to date unknown, with numerous factors being implicated: environmental, dietary, reproductive, endocrine, viral and hereditary. Factors thought to be protective include multiparity, early age of first pregnancy and the use of oral contraceptives.

Ovarian cancer does not produce specific signs or symptoms for most of its natural history. The symptoms, often with late onset, include enlargement of the abdomen (due to ascites or increased volume of the tumor) and dull abdominal-pelvic pain. On rare occasions the tumor may manifest with acute abdomen related to torsion or rupture of the lesion. Only 15% of patients report atypical vaginal bleeding. A swelling of the pelvis may also be occasionally found. In these cases a pelvic US study associated with various tumor serum markers (CA125, CA19-9, CA15-3, alpha-fetoprotein, beta-HCG and others) can provide useful information.

There is no evidence that screening is able to significantly reduce mortality for ovarian cancer, either in the general population or in subjects at risk due to family history. Therefore, on the basis of the state of the art, i.e. in the absence of proof of the effectiveness of such a program, screening for ovarian cancer is not indicated as a part of public health policy.

The management of a US-identified adnexal mass depends on a combination of a number of predictors, the most important being age and state of menopause, size of the mass, US characteristics with regard to morphology and vascularity, presence of symptoms, level of serum CA125 (or other markers) and unilaterality or bilaterality of the lesion.

Figure 21.6 shows a flowchart summarizing tumor management proposed in 2004 in the setting of the Italian National Guidelines Project (PNLG).

Staging is performed intraoperatively according to the guidelines drawn up by the international scientific associations (**Table 21.3**).

The most common procedure for ovarian cancer therapy is radical cytoreductive surgery on the reproductive and adjacent structures, except in highly selected cases. Chemotherapeutic agents (principally platinum-containing compounds and taxanes) may be introduced in the treatment plan prior to surgery to reduce the extent of the disease and render it easier to attack surgically. This may be done after primary debulking for complementary purposes in the case of residual disease or adjuvant purposes in patients with high risk of recurrence, or for treatment of recurrence.

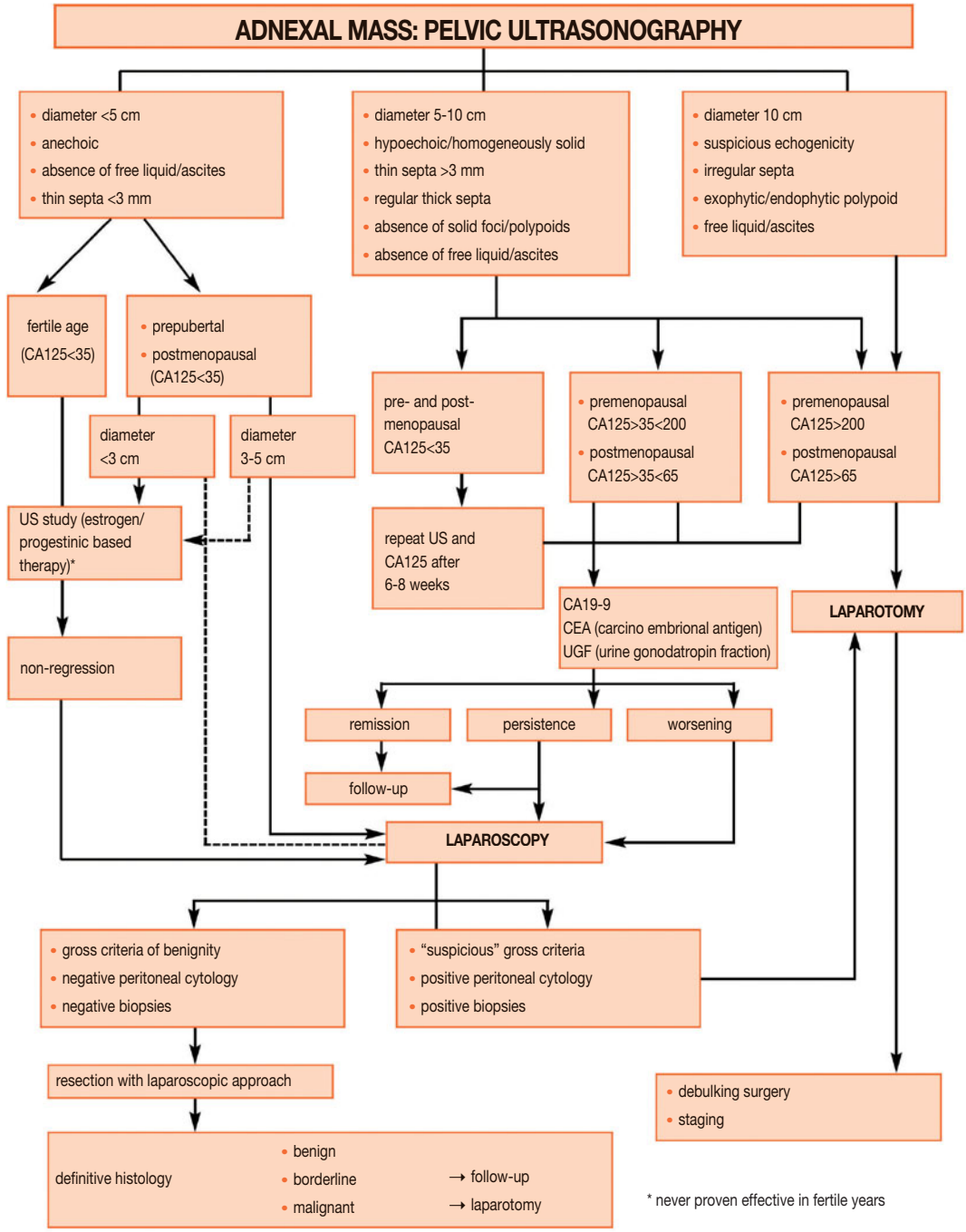

Fig. 21.6. Management of a pelvic mass (PNLG, 2004)

Follow-up of patients treated for ovarian cancer has the dual purpose of verifying the state of the disease and evaluating the presence of treatment complications. Recurrence of disease generally involves the peritoneal and retroperitoneal serosa. The site and symptoms, which are generally late onset, make an early diagnosis challenging. There are no controlled clinical trials which define standard conduct in this setting.

Table 21.3. FIGO/TNM staging of ovarian cancer

TNM	FIGO	Definition
T1	**I**	**Confined to the ovaries**
T1a	**IA**	One ovary, intact capsule
T1b	**IB**	Both ovaries, intact capsule
T1c	**IC**	Capsular rupture, tumor on the surface, neoplastic cells in the ascites or the peritoneal lavage
T2	**II**	**Extension to the pelvis**
T2a	**IIA**	Uterus, tube(s)
T2b	**IIB**	Other pelvic tissues
T2c	**IIC**	Neoplastic cells in the ascites or peritoneal lavage
T3 and/or N1	**III**	**Extrapelvic peritoneal metastasis and/or metastasis in the regional lymph nodes**
T3a	**IIIA**	Microscopic peritoneal metastases
T3b	**IIIB**	Gross peritoneal metastases <2 cm
T3c and/or N1	**IIIC**	Gross peritoneal metastases >2 cm and/or metastases in the regional lymph nodes
M1	**IV**	**Distant metastasis (excluding peritoneal metastases)**

Einhorn N, Bast R, Knapp R et al (2000) Long-term follow-up of the Stockholm screening study on ovarian cancer. Gynecol Oncol 79:466-470

Jemal A, Siegel R, Ward E et al (2007) Cancer statistics 2007. CA Cancer J Clin 57:43-66

Kazerouni N, Greene MH, Lacey JV Jr et al (2006) Family history of breast cancer as a risk factor for ovarian cancer in a prospective study. Cancer 107:1075-1083

Markman M (1994) Follow-up of the asymptomatic patient with ovarian cancer. Gynecol Oncol 55:S134-137

Pecorelli S, Sartori E, Santin A (1994) Follow-up after primary therapy: management of the symptomatic patient - surgery. Gynecol Oncol 55:S138-142

Progetto Nazionale Linee Guida, Diagnosi e terapia del carcinoma ovarico. Chapter 5, Il trattamento chirurgico. In: www.pnlg.it/lgn_carcinoma_ovarico

Reed NS, Sadozye AH (2005) Role of chemotherapy in the management of epithelial ovarian cancer. Expert Rev Anticancer Ther 5(1):139-147

The ICON and AGO Collaborators (2003) Paclitaxel plus platinum-based chemotherapy versus conventional platinum-based chemotherapy in women with relapsed ovarian cancer: the ICON 4/AGO_OVAR-2.2 trial. Lancet 1361:2099-2106

Diagnostic Imaging of the Adnexa

22

K. Menni, D. Turilli

Introduction

The correct pretreatment diagnostic approach to ovarian lesions is fundamental. Establishing the probability-risk of malignancy is an especially important feature in terms of the choice of surgical approach – laparoscopy or laparotomy. Diagnostic imaging is particularly useful in identifying the lesion, defining its exact origin, differentiating between physiologic and pathologic findings and predicting the risk of malignancy in the neoplastic forms.

The therapeutic strategy is of course based not only on imaging findings, but also on clinical findings and the age of the patient. Indeed, in young patients, unless there is a proven malignancy, the main aim is conservative surgery in order to preserve fertility.

Below nine years of age 80% of ovarian masses are malignant. In particular, all solid lesions should be considered as such until there is proof to the contrary. In girls older than nine, adolescents and young women only 5% of lesions are malignant, even though in this age group some 35% of all malignant lesions are found. Above 45 years of age the percentage of malignant lesions rises to 1/3 of the total. During pregnancy the diagnosis of ovarian lesions is common (0.15-1%) due to the increased ultrasonography (US) examinations. Most of these are asymptomatic cysts which tend to spontaneously resolve. In the event of malignant lesions the therapeutic strategy depends on the size and morphology of the lesion and the gestational age.

Most ovarian lesions are asymptomatic at diagnosis and their identification is an incidental finding at US performed for other indications (most commonly during a periodic gynecologic examination).

US is a diagnostic imaging modality capable of providing useful information regarding the site and nature of the lesion, especially with the use of transvaginal transducers. The technique can also be used to orient a possible second-level study, represented by magnetic resonance (MR). Thanks to the use of high-resolution sequences in the various planes in space and the injection of contrast medium, MR can better characterize the lesion and enable differentiation between adnexal and extra-adnexal lesions (intra- and extraperitoneal). Indeed, both have similar sites and structure.

Knowledge of some of the imaging characteristics is useful for their differentiation.

The finding of a pelvic mass well distinct from the ovary enables the diagnosis of nonovarian lesion. Often, however, pelvic masses may be large and the ovary may not be visible, either included in or compressed by the mass itself.

The following features are suggestive of ovarian origin of the mass:

- identification in small lesions of healthy ovarian parenchyma with follicles;
- an acute angle between the ovary and the lesion;
- posterior or posterolateral displacement of the uterus (aspecific finding);
- lateral displacement of the iliac vessels (typical finding);
- identification of vessels which supply or emerge from the adnexal mass;
- identification and adjacency of the suspensory ligament of the ovary to the mass.

L. Olivetti, L. Grazioli (eds.), *Imaging of Urogenital Diseases*,

Once ovarian origin has been established, MR is better than US or computed tomography (CT) in discriminating between benign and malignant disease, whilst using common criteria:

- dimension;
- structure;
- ancillary findings such as lymphadenopathies, ascites, peritoneal carcinosis.

Particularly indicative of benignity are:

- dimensions less than 4 cm;
- entirely cystic structure;
- thick walls (greater than 3 mm);
- absence of internal septations or mural nodules;
- absence of ascites, lymphadenopathies and peritoneal carcinosis.

In contrast, signs especially suggestive of malignancy include:

- dimensions greater than 4 cm;
- thick walls (greater than 3 mm);
- septations;
- solid lobulated mass;
- mixed structure (cystic and solid);
- intralesional circles;
- psammomatous calcifications;

and especially:

- mural nodules or solid components in cystic lesions;
- necrosis within solid components (most predictive element);
- peritoneal carcinosis;
- lymphadenopathies;
- ascites (particularly if abundant and/or sparing of the rectouterine pouch).

None of these signs taken individually are however sufficiently reliable for a diagnosis.

MR is the most precise technique for local staging in the case of malignancy. In contrast, CT plays a crucial role in the localization of distant metastases.

Ovarian lesions, which may be classified as functioning or nonfunctioning on the basis of the production or otherwise of hormones (estrogens, androgens or thyroid hormones) are here divided into non-neoplastic and neoplastic, with the latter being further subdivided into benign and malignant.

Non-neoplastic Lesions

Functional Ovarian Cysts

Ovarian cysts smaller than 3 cm are considered functional or physiologic. They make up most adnexal cystic lesions and include follicles in various stages of development, corpus luteum cysts and inclusion cysts. Although typical in reproductive years, they may also be found in postmenopausal women. On average they measure 1 cm and should not exceed 5 cm, although they may occasionally reach up to 8-10 cm (**Fig. 22.1**). Corpus luteum cysts generally regress spontaneously over period that is usually greater than three months.

Follicular cysts present as rounded or oval formations. On **US** they appear anechoic with smooth walls. If complicated by hemorrhage they are heterogeneously hypo- or hyperechoic with thickened walls, ill-defined margins and occasionally with fluid-fluid levels. On **color Doppler** they appear with no intracystic vasculature.

In the preovulatory phase the wall may be richly vascular. **Transvaginal US** (TVUS) is the reference standard for the diagnosis and follow-up of lesions larger than 3 cm and atypical cysts. On **CT** the density is fluid and the walls appear thin (<3 mm). If complicated by hemorrhage, the cysts have a higher density and thicker walls.

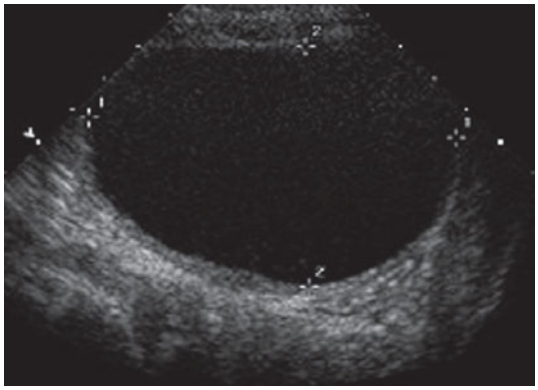

Fig. 22.1. Transabdominal ultrasonography. Ovarian cyst. Sonogram shows left adnexal mass almost 6 cm in size, oval in shape, anechoic with thin walls. The compressed ovarian parenchyma is identifiable dorsally in the periphery as a solid crescent. The lesion was no longer identifiable at 30 days follow-up

On **MR** they appear with thin walls (<3 mm) and a fluid signal which is low in T1-weighted images and intermediate-high in T2. If complicated by hemorrhage, they often appear with fluid-fluid levels, thicker walls and variable signal.

Corpus luteum cysts present as rounded or oval with thicker and ill-defined walls (Fig. 22.5d, see page 425). They may mimic solid lesions if they collapse.

TVUS is the reference standard for the diagnosis and follow-up of lesions larger than 4 cm and atypical cysts. On US they appear as simple unilocular cysts with anechoic content. If the cysts are complicated by hemorrhage, the content is heterogeneous and often with fluid-fluid level. On **color Doppler** the wall of the cyst appears vascular and the contiguous ovarian parenchyma shows elevated vascularity. There is no evidence of vasculature in the intracystic content. On **CT** the walls appear enhanced, and in the case of rupture a hyperattenuating liquid (>30-50 HU) may be seen in the pelvis indicating hemorrhage. On **MR** the walls appear hypointense in T1-weighted sequences and hyperintense in T2, while the cystic content has a varying signal according to whether it is fluid or hemorrhagic.

Para-ovarian and Peritubal Cysts

These arise from rests of the mesonephric duct and are usually an incidental finding. They are more common in middle-aged women and account for 10-20% of adnexal masses. They are round or oval formations, and unilocular with thin walls and size between 1 and 12 cm.

Their **imaging** characteristics are similar to those of functional cysts, from which they may be differentiated only if they are clearly separate from the homolateral ovary.

Peritoneal Inclusion Cysts or Pseudocysts or Benign Cystic Mesotheliomas

These are fluid collections produced by the ovaries which remain trapped in peritoneal adhesions. They are found in patients with pelvic inflammatory disease, endometriosis or prior surgery. They appear almost exclusively in premenopausal years. They vary in size and have ill-defined margins since they have no wall of their own.

At **imaging** they tend to take on the morphology of the space they occupy and may displace the surrounding structure. The ovary or the uterine tube, which are typically trapped within the pseudo-wall or the internal part of the cyst itself by thick and irregular adhesions, can mimic a solid nodule. Occasionally the cysts appear oblong in

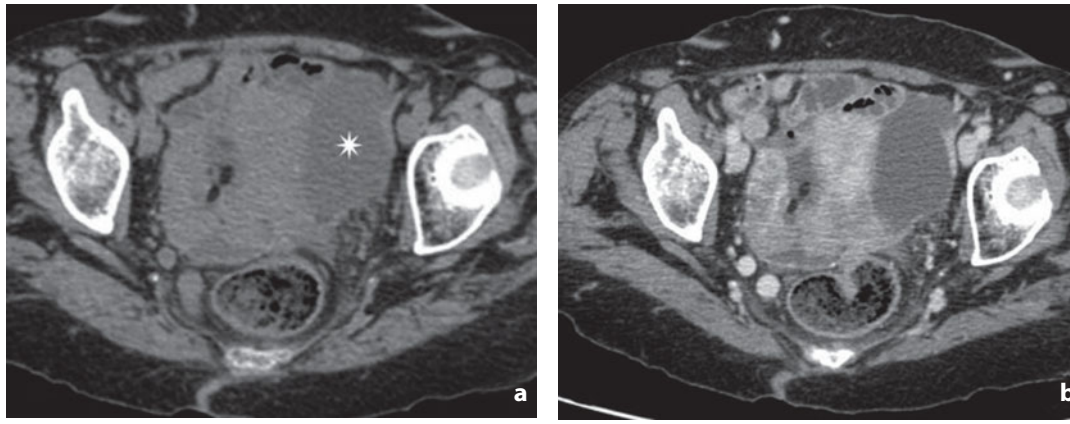

Fig. 22.2a,b. Computed tomography. Peritoneal inclusion cysts. **a** Image shows an oblong para-uterine mass (*asterisk*) with fluid content and thin walls. After contrast medium administration (**b**) the lesion displays no wall enhancement and neither septations nor solid nodular components are identifiable

shape with a parauterine location (Fig. 22.2). The internal structure depends on the content, which in most cases is fluid-like and therefore anechoic on US, with density below 20 HU on CT and low signal on MR T1-weighted images and high signal in T2. If hemorrhagic, the intracystic liquid has high density on CT, elevated signal on MR T1-weighted images and low signal in T2. The finding of internal septa is relatively common.

Theca Lutein Cysts

These develop in patients with elevated serum levels of human chorionic gonadotropin. They are less common than other cysts and are associated with multiple gestations, trophoblastic disease, and pregnancy complicated by fetal hydrops or ovarian hyperstimulation syndrome.

They appear as simple multilocular cysts with thin walls. They are typically bilateral and larger than physiologic cysts (on average 6-12 cm, but occasionally even 20 cm).

On **US** they have fluid content, and are anechoic with thin internal septations. The walls appear smooth without solid nodularities. **Color Doppler** reveals vasculature only in the surrounding parenchyma. On **CT** they have low density. On **MR** the signal intensity is that of a simply cyst. If complicated by hemorrhage, they appear heterogeneous in all imaging modalities.

Polycystic Ovary Syndrome

This is a complex endocrinologic disorder characterized by inadequate secretion of gonadotropin with consequent amenorrhea. It affects 5-10% of women of reproductive age and is found in 50% of women with fertility problems. The syndrome is associated with an increased risk of endometrial carcinoma in patients below 40 years of age due to chronic estrogenic hyperstimulation. It may be associated with congestion of the pelvic venous vessels in patients suffering from chronic pelvic pain. The diagnosis is based on alterations to clinical features and biochemical markers as well as imaging findings.

The imaging modality of choice is **TVUS**, while **MR** is a complementary technique to rule out virilizing tumors. The ovaries appear moderately enlarged (around 5 cm) and

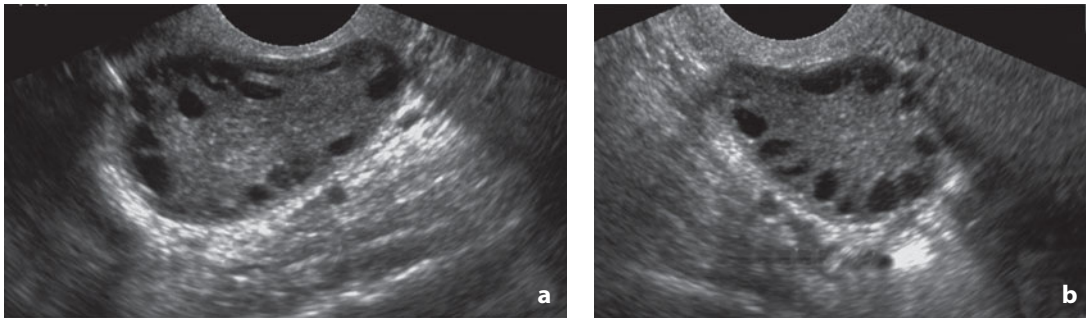

Fig. 22.3a,b. Transabdominal ultrasonography. Polycystic ovary. Both ovaries appear enlarged with multiple small anechoic cystic formations situated on the ovarian surface

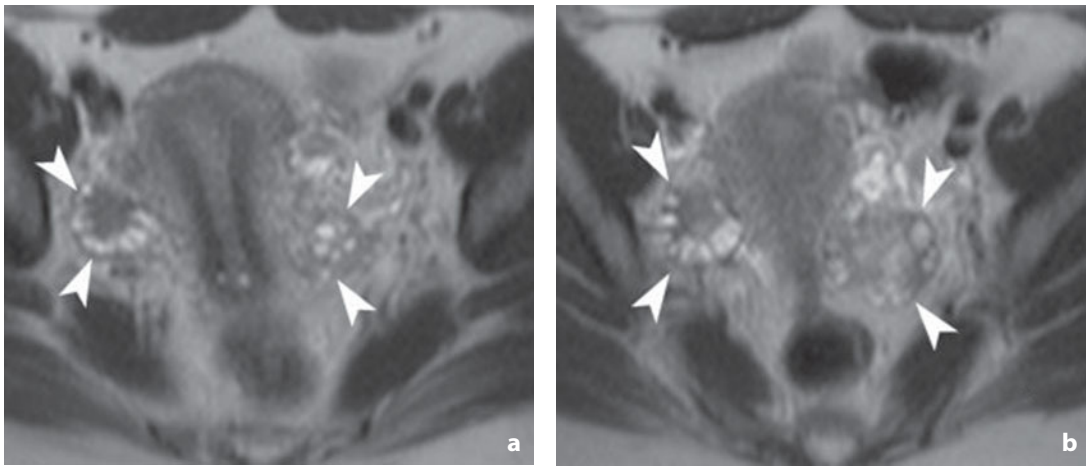

Fig. 22.4a,b. Magnetic resonance. Polycystic ovary. Axial T2-weighted images. Multiple follicles are identifiable on the surface of the ovaries (*arrowheads*). The stroma in the central portion of the right ovary is more hypointense than normal

spheroid in shape with an abnormally large number of follicles situated peripherally (Fig. 22.3). On MR around 10 follicles between 2 and 8 mm can be seen surrounding a central stromal component appearing more hypointense than normal in both T1- and T2-weighted sequences in the absence of a dominant follicle. On rare occasions one ovary may appear normal (Fig. 22.4).

Benign Neoplastic Lesions

These account for around 80% of all ovarian tumors. Although there is a wide variety, the most frequent histologic types account for most benign ovarian tumors.

Cystadenoma

Cystadenoma accounts for around 37% of benign tumors and 37-50% of benign lesions in women of reproductive age. Its frequency increases with age and in postmenopause it accounts for some 80% of benign ovarian tumors. It appears as a uni- or multilocular cystic lesion with thin walls and serous, mucinous and occasionally hemorrhagic content. Mural nodulations are rare and suggestive of malignant degeneration.

The two types, *serous* and *mucinous*, differ in their pathologic appearance, prognosis and clinical course. Serous cystadenomas account for around 40% of benign ovarian lesions; their peak incidence is between 40 and 50 years and they are bilateral in 20% of cases. Mucinous cystadenomas account for 20-25% of benign ovarian tumors and are bilateral in only 2-3% of cases. Calcifications are typical of serous lesions. The intracystic content is gelatinous and the lesions tend to be larger at presentation (on average 10 cm, although they can reach 30 cm). In contrast to serous lesions, the mucinous variety is typically multilocular, with the content varying in composition in the various loculations, which are usually small and separated by thin septations.

Although they have common characteristics, imaging can help to differentiate the two forms. Both present as well bounded cysts with weakly enhancing walls. When present, the internal septations appear thin and regular (<3 mm).

Serous forms appear on **US** as cysts with a diameter usually >6 cm, anechoic with enhanced through transmission and thin walls. **Color Doppler** demonstrates the absence of parietal flow.

On **CT** they appear hypoattenuating on nonenhanced images. After contrast administration they show no enhancement and appear as simple cystic lesions often large in size with thin or nonvisible walls without septations or solid chips (**Fig. 22.5**).

On **MR** they are characterized by low signal in T1-weighted images and high signal in T2.

The initial evaluation of the lesion is performed with US, although MR is needed for their characterization. CT can prove useful for planning surgical treatment.

Mucinous forms appear on **US** generally as large multilocular cysts with variable echogenicity. Often both a transvaginal approach with **color Doppler** and a transabdominal approach is required to evaluate the entire lesion when they are particularly large.

Precontrast **CT** images are able to identify calcifications. After contrast administration multilocular cystic lesions can be identified with thin walls and septations. The various loculations contain fluid with differing degrees of attenuation.

On **MR** mucinous cysts display variable signal intensity in relation to the different fluid content (fluid, hemorrhage or protein) present in the loculations. The gelatinous liquid has a weakly hyperintense signal in T1-weighted images and therefore it is higher than water. In T2-weighted sequences the signal is lower with respect to serous fluid. The blood material contained within the loculations can be readily identified on MR images. After contrast medium administration, enhancement of the septations and the wall can be seen without evidence of solid nodularities.

Cystadenofibroma

These account for 1.7% of ovarian tumors. Their presentation at diagnosis is usually a large mass with smooth and regular margins, consisting of serous lesions mixed with varying quantities of fibrous stroma. Cystadenofibromas can have a cystic form with only microscopic foci of stromal tissue, a prevalently cystic form or a complex form with alternating cystic and solid components. The tumor shows no endocrine activity.

On **US** it can mimic a malignancy and appear as a complex cyst with thin walls and thin, although occasionally thick, septations and solid mural nodulations which reveal significant vascularity on **color Doppler**. On **CT** images the tumor appears heterogeneous with solid nodules. After contrast medium administration it appears as a uni- or multilocular mass with septations and mural nodularities or solid components which appear markedly enhanced. On **MR** in T2-weighted sequences the cystic component shows high signal, whereas the solid components have a low signal with enhancement in the postcontrast T1-weighted images.

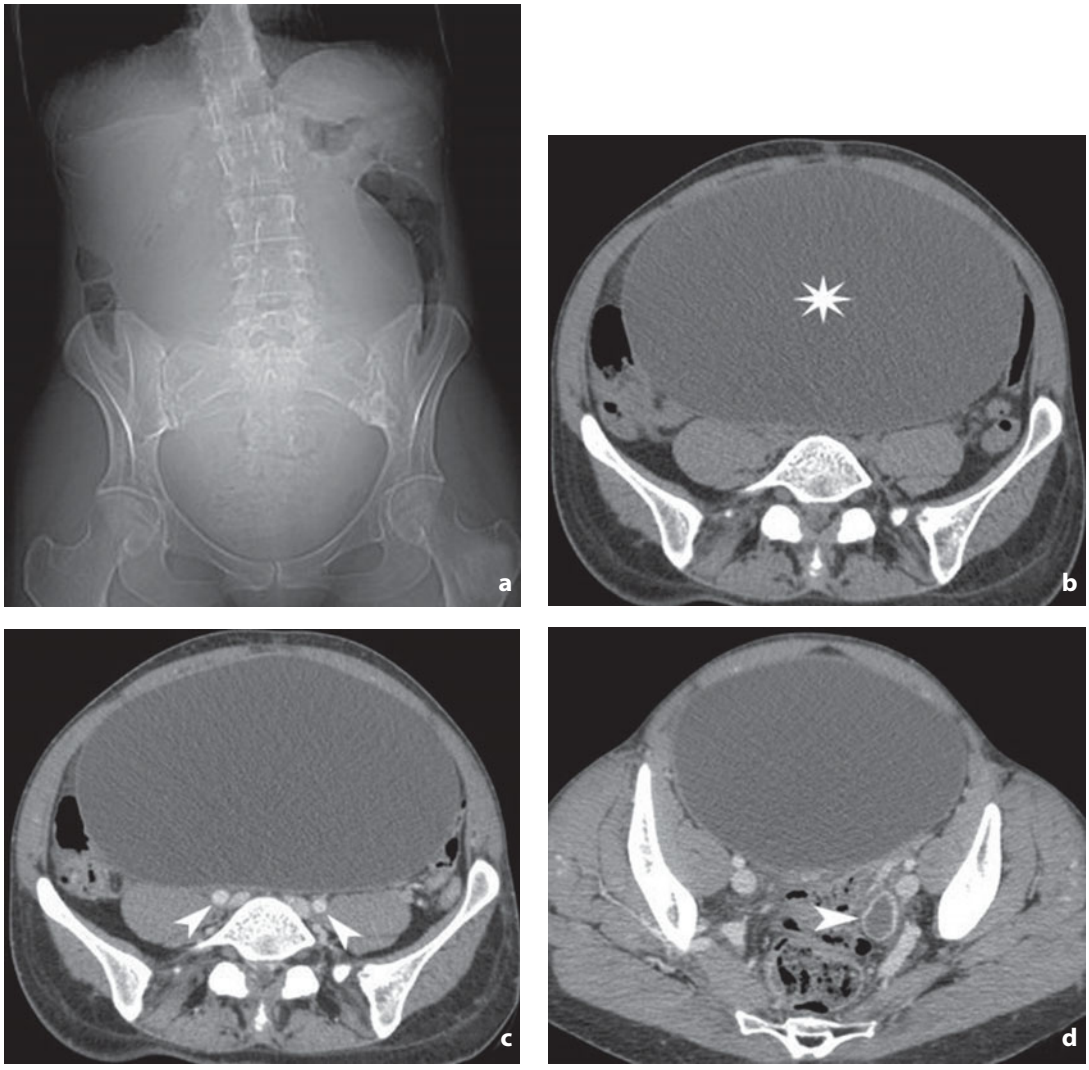

Fig. 22.5a-d. Plain film radiography and computed tomography. Right serous cystadenoma and left corpus luteum cyst. **a** The anteroposterior view of the plain abdominal film shows poorly represented bowel loops with greater opacity in the central abdominal quadrants and imprint and lateral displacement of the visible tracts of the large intestine. **b** Nonenhanced CT shows large oval expansive abdominal-pelvic lesion (*asterisk*) with sharp regular margins, thin walls and fluid-density content compressing and displacing the adjacent structures. **c** After contrast medium administration the image shows no areas of abnormal enhancement, nodules or septa and better demonstrates the relations with the iliac vessels (*arrowheads*). **d** A more caudal scan of the same mass shows the left ovary, in which an oval-shaped lesion (*arrowhead*) is visualized with fluid content and intensely enhancing walls: corpus luteum cyst

Benign Teratoma

Benign teratoma is the most common ovarian tumor in patients over 45 years and accounts for more than 70% of tumors in women less than 19 years of age. The tumor arises from the primordial germ cells and can grow not only at the level of the ovaries, but also in any organ or tissue along the course taken by the primordial germ cells during embryonal organogenesis to arrive in the gonads. Benign teratoma is made up of a large variety of well-differentiated tissues: ectodermic, mesodermic and endodermic.

The most common variety (99%) is the mature cystic teratoma or dermoid cyst, which typically has a content consisting of sebaceous liquid mixed with hair, skin, bone, cartilage, nerve tissue, and fragments of mucus similar to gastric or intestinal mucus. More rare is the monodermal teratoma, which is typically solid and is subdivided into struma ovarii and carcinoid tumor.

Mature Cystic Teratoma or Dermoid Cysts

This is a prevalently unilateral lesion (10-15% bilateral). In most cases (88%) it is a unilocular cyst containing sebaceous material with nodulations (Rokitansky nodules or dermoid plug) (**Fig. 22.6**) containing fat and calcifications, teeth and bone fragments (**Fig. 22.7a**). There is also a form with thin and regular internal septations (**Fig. 22.8**). Fat is present in more than 90% of lesions, teeth in 31% and parietal calcifications in 56%. Only in a minority of cases (15%) is the fat absent or present only in minimal quantities.

Dermoid cysts are usually asymptomatic and grow slowly. Some gynecologists are in favor of surgery for lesions >6cm. Complications include: rupture (acute abdomen and granulomatous peritonitis caused by the fat content), torsion (in more than 16% of cases), malignant degeneration (extremely rare: usually arising from the "dermoid plug", in large lesions >10 cm and most commonly in postmenopausal women, in the sixth and seventh decade of life, where some 2% of the lesions occur).

On **US** the diagnosis is not always easy in relation to the different tissues contained in the lesion. There are three typical presentations:

- cystic lesion with more echogenic intracystic nodules (Rokitansky nodules or dermoid plugs);
- "tip of the iceberg" appearance: diffusely or partially echogenic mass with diminished through transmission caused by the sebaceous material or hair contained within the lesion;
- "dermoid mesh" appearance: thin multiple lines and hyperechoic dots caused by hair in the cyst.

Calcifications (bone and teeth) and fluid-fluid levels can also be identified.

On **CT** and **MR** the finding of fat in the cystic mass is pathognomonic of mature cystic teratoma. The fat has a density between -20 and -120 HU. Another typical CT finding is the presence of parietal calcification or the dermoid plug.

On **MR** (**Fig. 22.7b-e**) the lesion appears oval or round with well defined margins and elevated signal in T1-weighted sequences and low signal in fat saturated T1-weighted images. In T2-weighted images the signal may be variable, although it tends

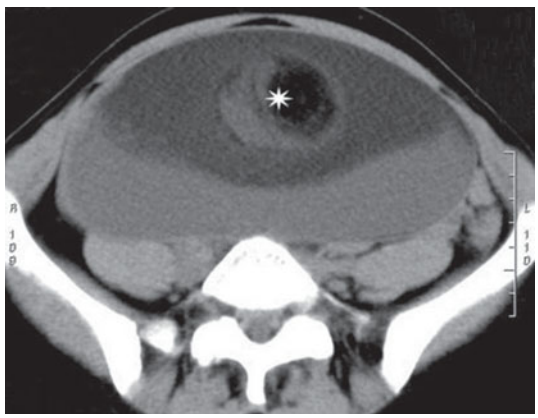

Fig. 22.6. Computed tomography. Benign cystic teratoma. Contrast-enhanced examination. Large oval-shaped unilocular mass with smooth and moderately thick walls and fluid-fat level. In the superior portion an adipose nodule (*asterisk*) of around 5 cm can be visualized (dermoid plug)

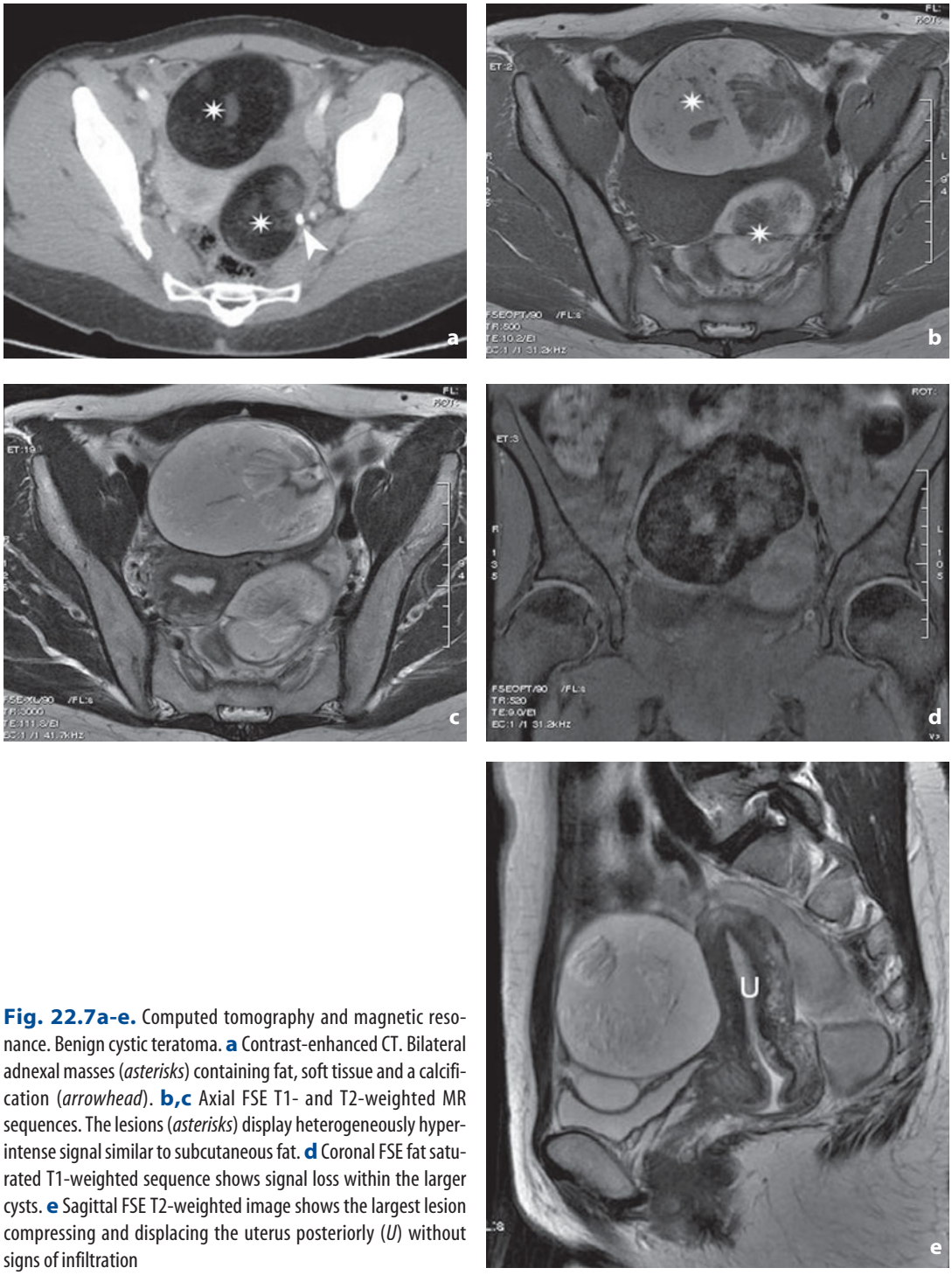

Fig. 22.7a-e. Computed tomography and magnetic resonance. Benign cystic teratoma. **a** Contrast-enhanced CT. Bilateral adnexal masses (*asterisks*) containing fat, soft tissue and a calcification (*arrowhead*). **b,c** Axial FSE T1- and T2-weighted MR sequences. The lesions (*asterisks*) display heterogeneously hyperintense signal similar to subcutaneous fat. **d** Coronal FSE fat saturated T1-weighted sequence shows signal loss within the larger cysts. **e** Sagittal FSE T2-weighted image shows the largest lesion compressing and displacing the uterus posteriorly (*U*) without signs of infiltration

to be similar to that of subcutaneous adipose tissue. The calcifications may not be visible on MR images or may be identifiable as areas of low signal intensity.

In a patient with acute abdomen and the presence of dermoid cyst, the finding of sebaceous fluid in the peritoneal cavity is suggestive of rupture.

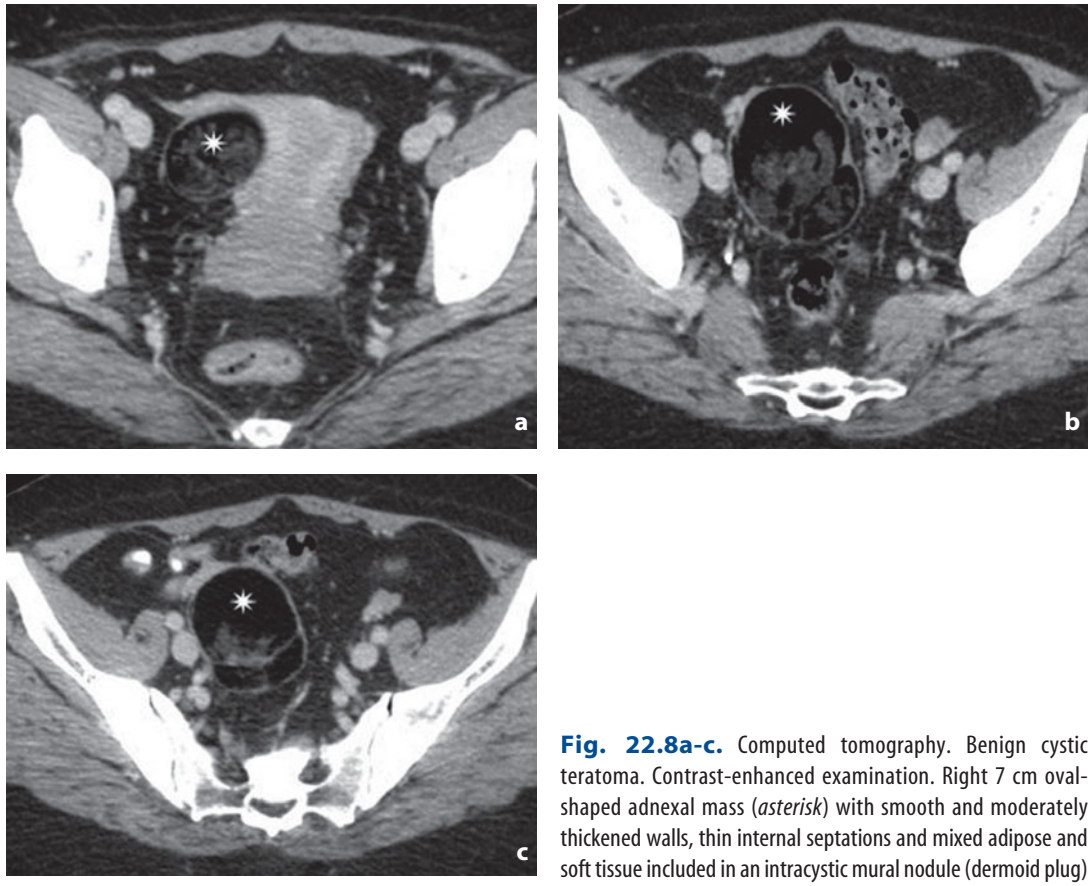

Fig. 22.8a-c. Computed tomography. Benign cystic teratoma. Contrast-enhanced examination. Right 7 cm oval-shaped adnexal mass (*asterisk*) with smooth and moderately thickened walls, thin internal septations and mixed adipose and soft tissue included in an intracystic mural nodule (dermoid plug)

Monodermal Teratoma

Monodermal teratoma consists mainly or exclusively of a single type of tissue and includes:

- *struma ovarii*: rare form (3%) composed prevalently of thyroid tissue, histologically represented by thyroid follicles in varying degrees of colloid regression. Macroscopically the lesion is unilateral with a diameter usually not exceeding 10 cm and with a smooth surface. In 30% of cases the teratoma causes hyperthyroidism. Excision of the lesion leads to a regression of related symptoms;
- *carcinoid tumor* is frequently associated with mature cystic teratoma or mucinous ovarian tumor. It typically appears in the postmenopausal period and is rarely associated with carcinoid syndrome.

Brenner Tumor

This is a rare tumor accounting for 1-3% of ovarian tumors with onset on average at around 50 years. It is generally benign, presenting as borderline or malignant in less than 2% of cases. The tumor is typically a small solid unilateral mass and may present calcifications. In 60% of cases its size is >2 cm. The diagnosis is often incidental and only rarely does it produce estrogens. In more than 20% of cases it is associated with mucinous cystadenomas or other epithelial tumors.

Differential diagnosis with other adnexal lesions is challenging on **US**. The tumor

presents as a solid hypoechoic mass with calcification causing posterior shadowing. In the borderline or malignant form it may appear as a hypoechoic cystic mass with solid components. On **CT** it appears as a small solid mass with large amorphous calcifications, and on **MR** as an entirely solid mass with low signal intensity in both T1- and T2-weighted sequences. The calcifications may be difficult to identify. After contrast medium administration, the enhancement is intense and homogeneous.

Sex Cord-Stromal Tumors

These account for 8% of all ovarian tumors and include granulosa cell tumor, Sertoli-Leydig tumors and the subgroup of thecoma-fibroma. They are diagnosed in all age ranges, although the incidence is greater in peri- and postmenopausal women. Differential diagnosis is based on the hormone activity of the tumor: granulosa cell tumors tend to secrete estrogens, whereas Sertoli-Leydig tumors may produce androgens. Most lesions are confined to the ovary at the time of diagnosis.

Granulosa Cell Tumor

This is a tumor with low grade malignancy, typically unilateral and with variable size (on average 12 cm). In 5-25% of cases it is associated with endometrial cancer. The lesion may be entirely cystic or completely solid – in the latter case it displays homogeneous enhancement and high signal intensity on T2-weighted **MR** sequences. It may also appear in a mixed solid and cystic form with hemorrhagic content.

Sertoli-Leydig Tumor

This is usually unilateral with size varying from 5 to 15 cm, even though it can be so small as to be unidentifiable at imaging. The lesion presents as a solid homogeneous mass which may be lobular, or as a solid mass with peripheral cysts or as a cystic lesion with solid mural nodules. The cysts may display moderately high signal on T1-weighted **MR** images, whereas the solid components have an intermediate signal in T2 and are mildly enhancing on both **CT** and **MR**.

Tumors of the Thecoma-Fibroma Group

These are solid ovarian tumors accounting for 3-4% of the total and 10% of solid adnexal masses. The tumors are typically unilateral (90%) and are found in peri- and postmenopausal women.

Fibroma is a connective tissue tumor composed of fibroblasts immersed in collagen. It has a smooth surface, hard consistency and size varying from a few millimeters up to 30-40 cm. Usually it does not produce hormones. The most significant clinical feature is the possibility that ascites (varying from a few mL to many liters) are associated with ovarian fibroma and pleural effusion (Meigs syndrome), which may be bilateral but often right unilateral may also be associated. The reason for the frequent finding of ascites and pleural effusion is still debatable, since it is unclear whether it is due to a disturbance of the lymphatic or venous circulation.

Fibrothecoma is composed of thecal cells and abundant fibrous tissue (**Fig. 22.9**). Unlike fibroma, in 60% of cases the tumor produces estrogen accompanied by uterine bleeding. In more than 20% of cases it is associated with carcinoma of the endometrium.

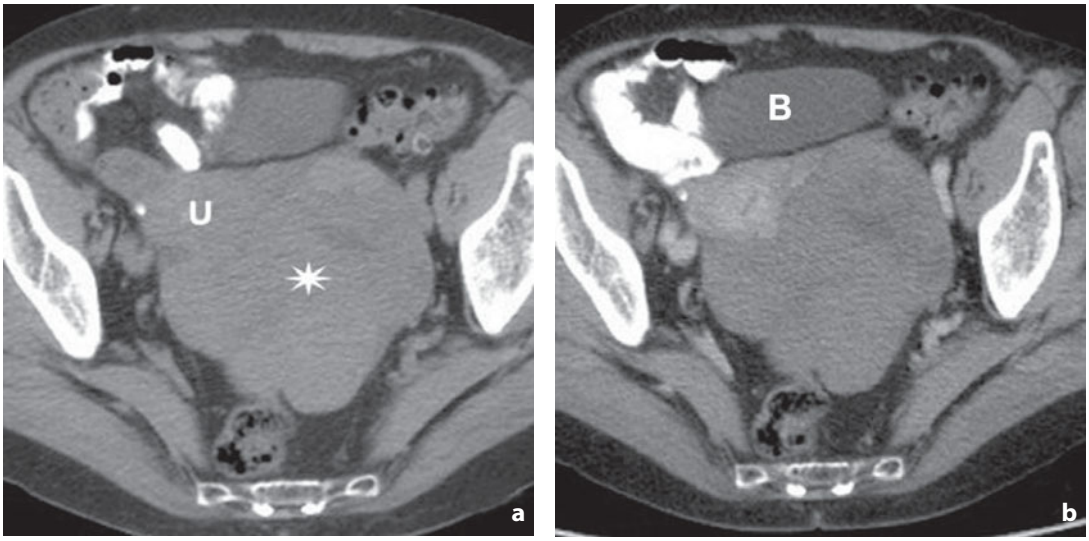

Fig. 22.9a,b. Computed tomography. Fibrothecoma. **a** Nonenhanced examination. Multilobular left adnexal mass (*asterisk*) with sharp smooth margins appearing hypoattenuating to the uterus (*U*). **b** After contrast medium administration mild heterogeneous enhancement is apparent inferior to the uterus, the fundus of which is shifted anterolaterally to the right. *B*, urinary bladder

On both **CT** and **MR** images fibroma and fibrothecoma when small appear similar to leiomyomas (on MR - intermediate or low signal on T2-weighted images and very low or low-intermediate in T2). Larger tumors may have a heterogeneous structure with patches of elevated signal intensity within the areas of low MR signal, indicating the presence of edema or cystic degeneration. The lesions may also present amorphous calcification which can be identified on CT images.

Sclerosing Stromal Tumor

This is a rare subtype which affects young women aged below 30 years. Microscopically it presents a capsule with edema of the peripheral ovarian stroma surrounding the highly vascular nodule. The lesion may produce estrogen and, more rarely, androgen and be the cause of menstrual irregularity.

On **US** the lesion appears solid with heterogeneous echotexture and a central hypoechoic area. **Color Doppler** displays the tumor surrounded by large vessels.

On **CT** sclerosing stromal tumor appears as a heterogeneous solid lesion with a more hypoattenuating central portion. After contrast medium administration the enhancement is intense at the periphery with centripetal progression. On **MR** the capsule appears as a thin ring of low signal intensity in both T1- and T2-weighted sequences. In the latter an irregular area of low signal may be apparent surrounding the central component with a nodular appearance and very high signal. Like on CT, in dynamic study the lesions display initial peripheral enhancement with centripetal progression.

Buy JN, Ghossain MA, Moss AA et al (1989) Cystic teratoma of the ovary: CT detection. Radiology 171:670-697

Ghossain MA, Buy JN, Lignères C et al (1991) Epithelial tumors of the ovary: comparison of MR and CT findings. Radiology 181:863-870

Hricak H, Chen M, Coakley FV et al (2000) Complex adnexal masses: detection and characterization with MRI: multivariate analysis. Radiology 214:39-46

Kinkel K, Hricak H, Lu Y et al (2000) US characterization of ovarian masses: a meta-analysis. Radiology 217:803-811

Outwater EK, Siegelman ES, Junt JL (2001) Ovarian teratomas: tumor types and imaging characteristics. RadioGraphics 21:475-490

Saksoud FA, Johnson SC (2004) Recognition of the ovarian origin of pelvic masses with CT. RadioGraphics 24:S133-S146

Yamashita Y, Hatanaka Y, Torashima M et al (1994) Mature cystic teratomas of the ovary without fat in the cystic cavity: MR features in 12 cases. AJR Am J Roentgenol 163:613-616

Malignant Neoplastic Lesions

Malignant lesions and borderline tumors of the ovary account for 21% and 4% of the total, respectively. Some 85-90% of malignant lesions which appear after 40 years of age are epithelial forms arising from celomic (Müllerian) epithelium. Malignancies arising from germ cells are, in contrast, much more rare and have a peak incidence below 25 years.

Epithelial ovarian cancer accounts for 4% of all malignant tumors in females and is responsible for 5% of cancer deaths. The incidence and mortality have increased in the last decade by 30% and 18%, respectively. The lesion is usually silent and therefore only diagnosed in an advanced stage in around 75% of cases.

In most cases the onset of epithelial ovarian cancer is between 50 and 60 years with a prevalence of the serous form (49%) over the mucinous form (36%). At diagnosis the dimensions of the lesions of both forms typically exceed 4-5 cm. On both **CT** and **MR** they appear as complex multilocular cystic lesions and are indistinguishable from each other. The most significant risk factor is familial, while others include nulliparity with age above 40 years or first pregnancy above 35 years, late menopause, delayed menarche (>14 years), infertility, prior pelvic irradiation and breast cancer.

Clinical evaluations, **TVUS** and serum **CA125** assay have been proposed as screening tests. Unfortunately they are not recommended on a large scale in the general population because they have not led to significant decreases in mortality in large clinical screening studies.

US is highly sensitive and specific in identification of the ovarian mass (90-96% and 98-99%, respectively), although the positive predictive value is only around 70%. CA125 is the glycoprotein antigen most commonly used as a tumor marker in ovarian cancer. However, values above 35 U/mL are not specific, since they can be found in other epithelial malignancies (pancreas, lung, breast and colon) as well as non-Hodgkin's lymphoma. Even benign conditions may be associated with elevated CA125 levels: cirrhosis, pancreatitis, peritonitis, endometritis, pregnancy, benign ovarian cysts, pelvic inflammatory disease and ascites.

The CA125 level is influenced by the menstrual cycle and women of fertile age may return false-positive tests. As a result, the marker is more specific in postmenopausal women, where CA125 also helps to discriminate between benign and malignant forms: values >65 U/mL are in fact predictive of malignancy in the presence of a pelvic mass. More than 80% of women with advanced epithelial ovarian cancer have high CA125 levels. Nonetheless, in the early stages of the disease the sensitivity of the marker is only 25%. CA125 does, however, play a key role in monitoring the effectiveness of treatment in patients with known tumor.

Serum levels of alpha-fetoprotein and human chorionic gonadotropin may be helpful in the preoperative diagnosis of endodermic breast cancer, embryonic carcinoma, choriocarcinoma or mixed germ cell tumor.

Table 22.1. International Federation of Gynecology and Obstetrics (FIGO) staging for ovarian cancer

Stage	
I	Growth limited to the ovaries
IA	Growth limited to a single ovary, no ascites, no tumor on external surface, capsule intact
IB	Growth limited to both ovaries, no ascites, no tumor on external surface, capsule intact
IC	Tumor either stage IA or IB but with tumor on surface of one or both ovaries, ruptured capsule or ascites positive for malignancy
II	Growth involving one or both ovaries, with pelvic extension
IIA	Extension and/or metastases to the uterus or tubes
IIB	Extension to other pelvic tissues (including the peritoneum)
IIC	Stage IIA or IIB but with tumor on surface of one or both ovaries, ruptured capsule, ascites with malignant cells or positive peritoneal lavage
III	Tumor involving one or both ovaries, with peritoneal implants outside the pelvis, omentum and/or positive retroperitoneal or inguinal nodes. Superficial metastases on the hepatic capsule classify the tumor stage III. Growth is limited only to the pelvis with extension to the small intestine and pelvic omentum
IIIA	Tumor grossly limited to pelvis, negative lymph nodes but histologic proof of microscopic disease on abdominal peritoneal surfaces
IIIB	Confirmed implants outside of pelvis in the abdominal peritoneal surface; no implant exceeds 2 cm in diameter and lymph nodes are negative
IIIC	Abdominal implants larger than 2 cm in diameter and/or positive retroperitoneal or inguinal lymph nodes
IV	Growth involves one or both ovaries with distant metastases. Pleural effusion with positive cytology

Even though the reference standard in staging (**Table 22.1**) is laparotomic surgery (preferable to the laparoscopic approach which tends to understage in 20-40% of cases), CT and MR are fundamental for preoperative evaluation and can influence the treatment choice. The two techniques have similar sensitivity, specificity and diagnostic accuracy in staging (63-69%, 100% and 70-90%, respectively). The choice of one or the other modalities, therefore, depends on factors such as cost, availability, possible contraindications and experience of the radiologist. CT is more commonly used both for its wider availability and its shorter examination times.

Epithelial Forms

Serous Adenocarcinoma

This is the most common malignancy, accounting for over half of the epithelial forms. In two thirds of cases it is bilateral. The clinical presentation is a multilocular cystic mass with serous, hemorrhagic or turbid content with intracystic solid components.

US, **CT** and **MR** can be used for both the identification and characterization of the mass.

The most common first approach is US. The malignancy appears as a cystic mass with heterogeneous content, thin walls, septations, nodules and intracystic solid components (**Fig. 22.10**). On **color Doppler** the solid component displays marked vascularity. Nonenhanced CT is able to identify a low attenuating mass with solid components. In around 30% of cases at histology, but only 12% on CT, psammomatous bodies can be visualized which appear as small calcifications. After contrast medium administration the fluid component of the cyst is nonenhancing, whereas the solid component displays marked enhancement (**Fig. 22.11**). CT is used in the advanced forms to evaluate the possible presence of peritoneal carcinosis or distant metastasis. On MR the cystic component has low or intermediate signal in T1-

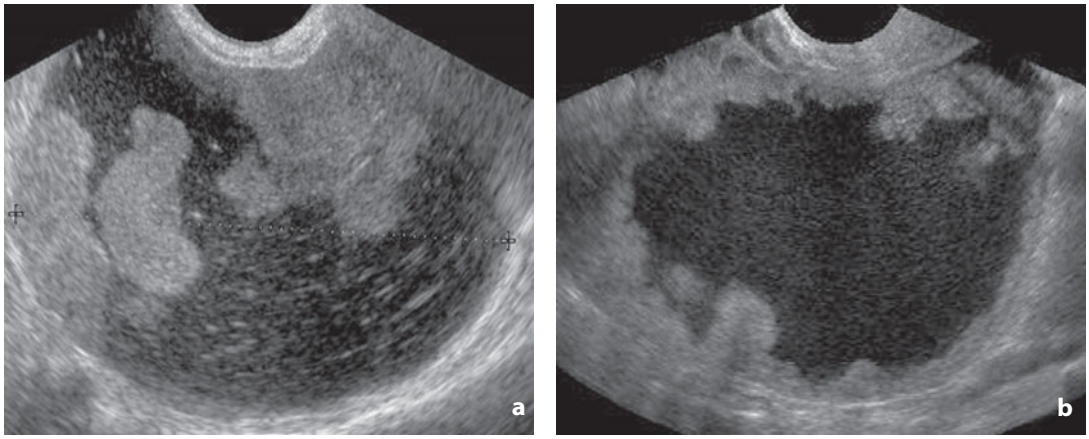

Fig. 22.10a,b. Transvaginal ultrasonography. Serous adenocarcinoma. **a** Large cystic lesion with thin walls containing corpuscular blood material and large solid components. **b** Different mass with cystic appearance and mildly thicker walls displays multiple solid mural components within the lumen

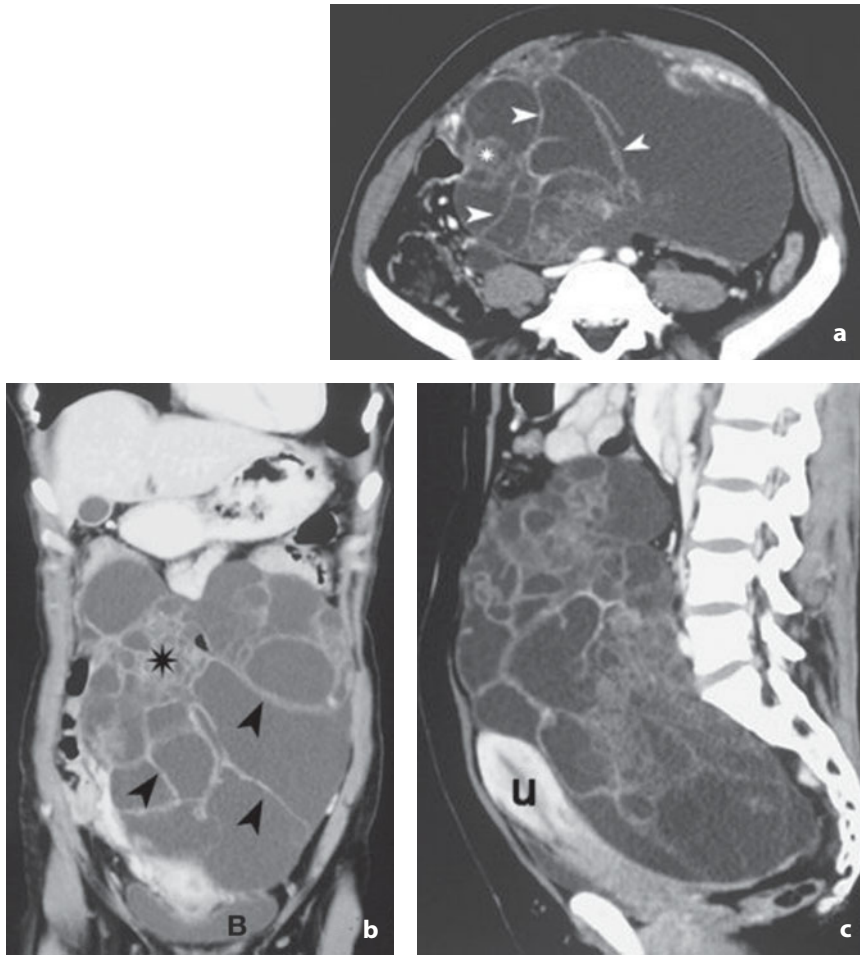

Fig. 22.11a-c. Computed tomography. Serous adenocarcinoma. **a** Contrast-enhanced examination. Large mixed-composition lesion with fluid component containing irregular septa (*arrowheads*) and enhancing solid component (*asterisk*). The coronal (**b**) and sagittal (**c**) reconstructions show the mass extensively occupying the abdomen. *U*, uterus; *B*, urinary bladder

weighted images and high signal in T2. The solid components, in contrast, have intermediate signal intensity in T1-weighted sequences and variable intensity in T2. The solid components show enhancement after contrast medium administration.

Mucinous Adenocarcinoma

This accounts for one-third of all epithelial forms. Clinical presentation at diagnosis is generally of a large multilocular cystic lesion with hemorrhagic or protein content and solid areas or intracystic nodules. Only rarely is the lesion prevalently solid. Around two-thirds of cases are diagnosed at stage I of the FIGO classification. Mucinous adenocarcinoma is bilateral in only 5-10% of cases and may be associated with pseudomyxoma peritonei (peritoneal implants of the mucin content of the lesion).

On **US** it appears as a multilocular cystic mass (**Fig. 22.12**) with content of varying echogenicity in relation to the quantity of mucin and other solid vascular components on **color Doppler**.

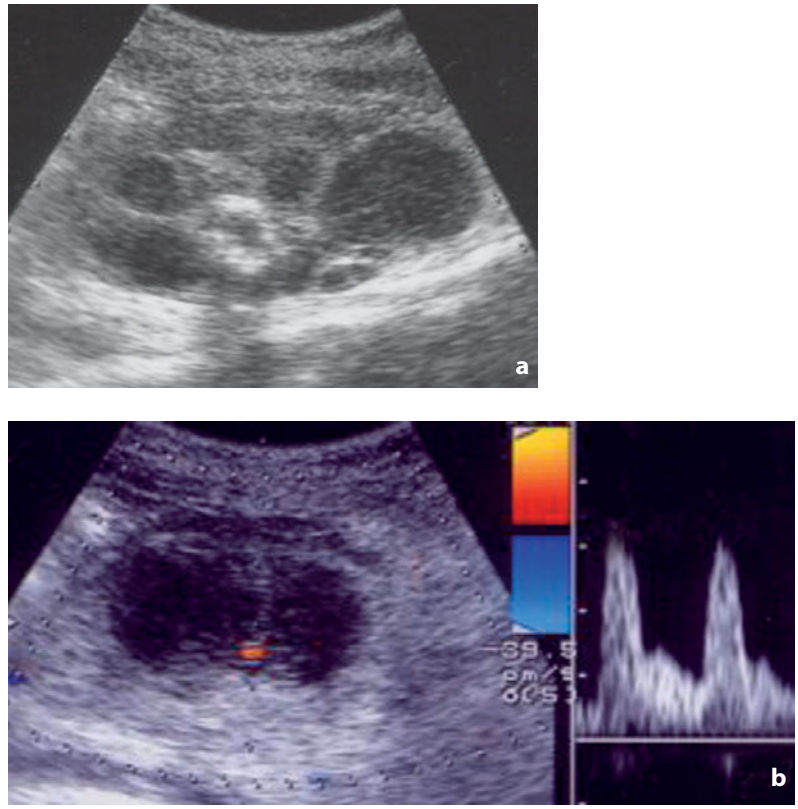

Fig. 22.12a,b. Transabdominal ultrasonography. Mucinous adenocarcinoma. **a** Large and multilocular left adnexal mass with cystic components separated by thin septations and highly vascular solid components at color Doppler (**b**)

On nonenhanced **CT** images low density multilocular masses can be identified with hyperattenuating components due to solid tissue or the high protein content of the mucin. After contrast medium administration the fluid component is nonenhancing, whereas the thick septa and solid components show marked enhancement.

Also on **MR** the signal intensity is linked to the quantity of mucin, and is therefore higher and lower than water in T1- and T2-weighted sequences, respectively. In the latter the solid components display intermediate signal intensity. After contrast medium administration the thick septa and the solid components show enhancement.

Endometrioid Carcinoma

This accounts for 8% of epithelial forms and in one third of cases at diagnosis is associated with the presence of endometrial hyperplasia or carcinoma. An association with both breast cancer and, more rarely, endometriosis has been reported (the finding in an endometrioma of an enhancing mural nodule is highly suggestive of ovarian malignancy) (**Fig. 22.13**). The tumor is bilateral in 30% of cases and appears as a solid and cystic lesion containing mucin or a greenish fluid. A rarer presentation is a solid mass with an extensive hemorrhagic or necrotic component. Endometrioid carcinoma has no specific imaging characteristics (**Fig. 22.14**).

Clear-cell Carcinoma

This accounts for 2-7% of epithelial malignancies. In three quarters of cases the tumor is diagnosed in stage I, although the prognosis tends to be worse than other histologic subtypes of the same stage. It is the malignant lesion most commonly associated with endometriosis, hypercalcemia (paraneoplastic syndrome) and thromboembolic complications. It appears as a unilocular cyst with thick walls and multiple intracystic nodules or as a multilocular cystic mass (**Fig. 22.15**).

Borderline Forms

These have low malignant potential and a markedly better prognosis and account for 4-14% of the total. The mean age of incidence is 40 years. The lesion is commonly bilateral and on average measures 7-20 cm. There are both serous and mucinous forms, the latter tending to be larger and possibly associated with pseudomyxoma peritonei. On **CT** and **MR** they cannot be differentiated from other epithelial forms.

Nonepithelial Forms

Germ Cell Tumors

These account for 2-3% of all ovarian malignancies, although in women below 20 years they make up more than two-thirds of the total. Their presentation is a solid rapidly growing and prevalently unilateral mass which often metastasizes to the peritoneum and retroperitoneal lymph nodes. In contrast to epithelial forms germ cell tumors often metastasize with hematogenous spread, especially to the liver and lung which often show involvement at diagnosis. Ascites are present only in 20% of cases. Elevated levels of serum HCG and alpha-fetoprotein may help in orienting the diagnosis.

Subtypes include, in decreasing order of incidence, dysgerminoma, immature teratoma, endodermal sinus tumor, and embryonic and nongestational choriocarcinomas.

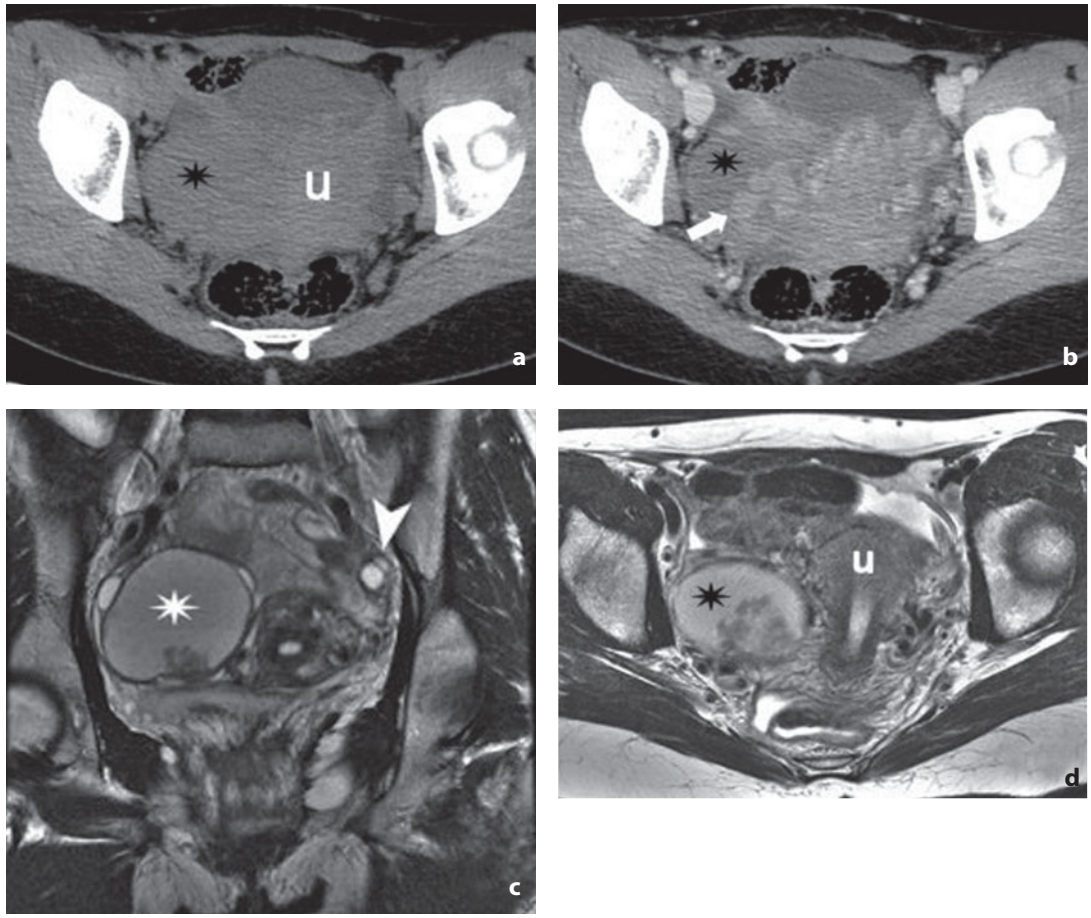

Fig. 22.13a-h. Computed tomography and magnetic resonance. Borderline endometrioid adenocarcinoma in endometrial cyst. **a** Nonenhanced CT. Expansive and weakly hyperattenuating right adnexal mass (*asterisk*). **b** After contrast medium administration a nonenhancing cystic component (*asterisk*) can be identified associated with intensely enhancing mural nodules (*arrow*). **c** Coronal T2-weighted MR image shows the right adnexal origin of the lesion (*asterisk*) with healthy ovarian parenchyma compressed in the periphery. The contralateral ovary (*arrowhead*) can also be identified without lesions. *(cont.* ⟶*)*

Dysgerminoma arises prior to reproductive age in 75% of cases and during pregnancy or postpartum in 15-20% of cases. The tumor is usually diagnosed in an early stage and is often bilateral. At imaging it appears as a solid, multilocular and well-defined lesion. **CT** is able to visualize punctate calcifications and areas of attenuation due to necrosis or hemorrhage. After contrast medium administration, the malignancy shows marked enhancement, especially in the fibrovascular septa. On **MR** dysgerminoma appears with low signal intensity in T1-weighted images and intermediate in T2 where the septa appear hypointense and the areas of necrosis hyperintense. Similar to CT, the septations may show marked contrast enhancement.

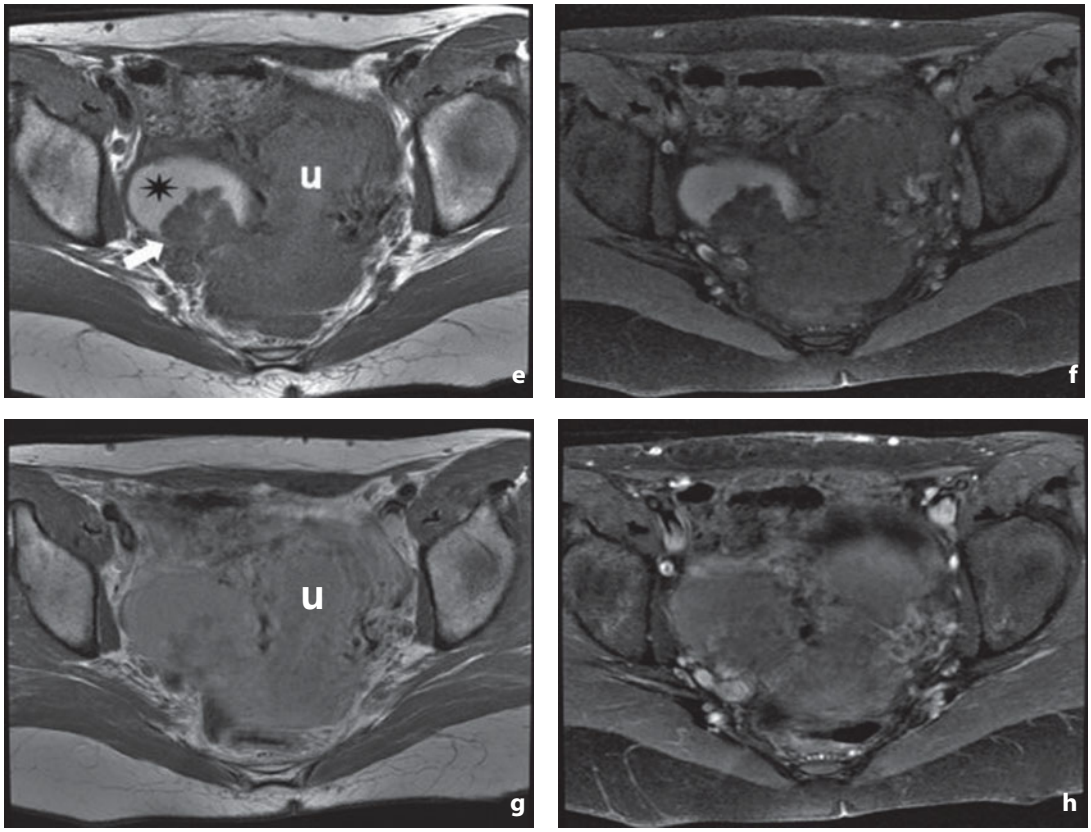

Fig. 22.13a-h. *(cont.)* **d** In the axial T2-weighted image the fluid component (*asterisk*) appears hyperintense, whereas the solid components are hypointense. In the axial T1-weighted images without (**e**) and with (**f**) fat saturation, the fluid component (*asterisk*) maintains its hyperintense signal and the solid components (*arrow*) remain hypointense. In the axial T1-weighted images without (**g**) and with fat saturation after contrast medium administration (**h**) minimal enhancement can be seen prevalently in the peripheral portion of the solid components. *U*, uterus

Immature teratoma typically arises in subjects between 10 and 20 years of age much like dermoid cysts, in comparison to which it is much rarer (less than 1%). In addition, the malignancy is associated with dermoid cysts in 26% of cases. Unlike the benign forms (prevalently cystic) it is usually large at diagnosis and appears as a solid mass or prevalently solid mass with cystic components, areas of fat and calcifications. In the absence of adipose tissue the differential diagnosis with carcinoma cannot be made. The lesion may produce steroids and cause precocious puberty. On **CT** images punctate foci of fat and scattered calcifications are indicative of teratoma. The cystic components contain serous fluid or more rarely sebaceous or adipose material. On **MR** the small foci of fat have elevated signal intensity in T1-weighted images which falls in fat saturated sequences.

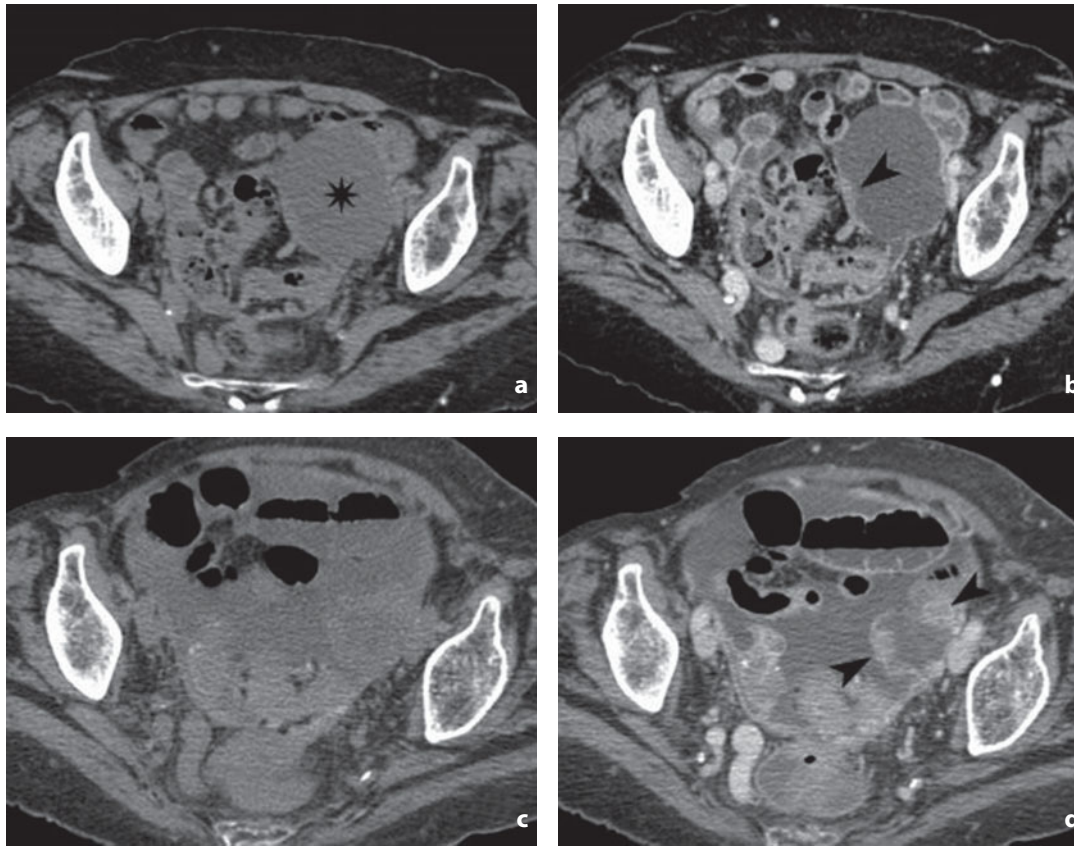

Fig. 22.14a-d. Computed tomography. Endometrioid adenocarcinoma. **a** Nonenhanced CT. Oval-shaped left adnexal mass (*asterisk*) with fluid content and wall thickening medially. **b** After contrast medium administration mild enhancement of the thickened wall can be identified (*arrowhead*). The patient did not undergo surgery due to severe heart disease. **c** At CT follow-up the nonenhanced image shows the lesion with diffusely irregular and thickened walls and the appearance of ascites. **d** Contrast-enhanced image shows marked enhancement of the walls with intracystic and exophytic nodulations (*arrowheads*). The malignancy is better visualized due to the presence of ascites

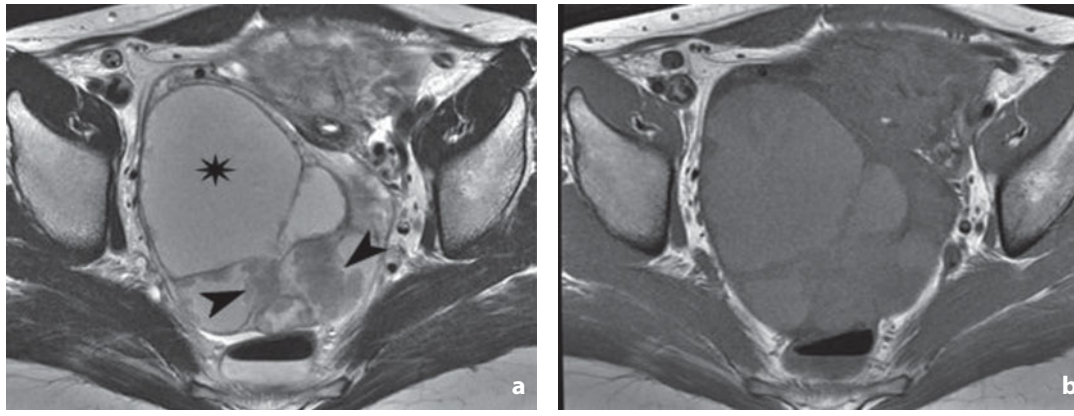

Fig. 22.15a-h. Magnetic resonance. Clear cell adenocarcinoma. **a** Axial T2-weighted MR sequence. Expansive 12 cm multilobular right adnexal mass with intermediate-high signal intensity fluid content (*asterisk*), irregular internal septations and hypointense intracystic solid nodulations (*arrowheads*). The residual ovarian parenchyma is compressed anteromedially with small follicles visible. The uterus is displaced to the left and anteriorly. **b** Axial T1-weighted image. The cystic component shows weakly hyperintense signal similar to elevated protein concentration while the septa and nodules are hypointense. *(cont.* ⟶*)*

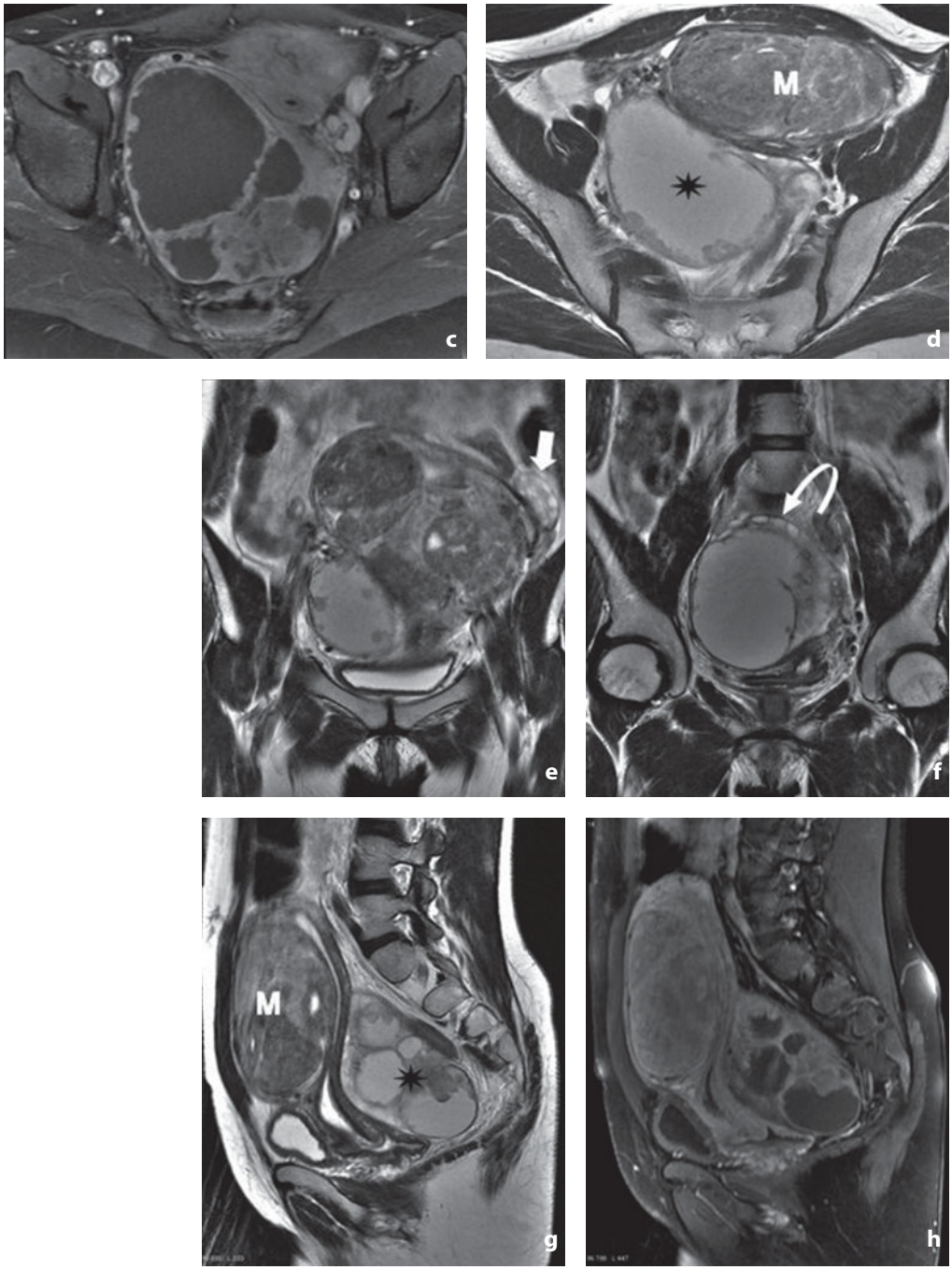

Fig. 22.15a-h. *(cont.)* **c** Axial fat saturated contrast-enhanced T1-weighted image shows marked enhancement of the septations and the solid nodules. **d** Axial T2-weighted image more cranial than the previous images. In front of the ovarian malignancy (*asterisk*) two large oval-shaped solid and heterogeneous expansive lesions can be identified attributable to uterine myomas (*M*). **e** Coronal T2-weighted image shows the left ovary (*arrow*) shifted cranially and laterally. **f** Coronal T2-weighted image better depicts the residual right ovarian parenchyma with several follicles pushed to the periphery (*curved arrow*). **g** Sagittal T2- and **h** T1-weighted images with fat saturation after contrast medium administration. The uterus is deformed and compressed by both the leiomyomas (*M*) and the ovarian malignancy (*asterisk*)

Spread Patterns of Ovarian Malignancies

The main spread pattern in ovarian cancer is direct extension via exfoliation of the neoplastic cells in the peritoneal cavity, with involvement of the peritoneal, visceral and parietal layers, especially at the level of the diaphragm, the right subphrenic space, the hepatic surface and Morrison's pouch. The intraperitoneal spread of neoplastic cells depends on the anatomy of the peritoneal spaces, the effect of gravity and the pressure changes induced by respiration. Therefore the most frequent anatomic sites of such metastases often coincide with those of the collection of ascitic liquid, such as the rectouterine pouch, the mesentery proximal to the ileocecal junction, the sigmoid mesocolon and the right paracolic gutter, as well as the mesentery proper and the greater omentum. The peritoneal implants may be solitary or, more commonly, multiple varying in size and appearance (linear pattern, cystic-like or nodular) (**Figs. 22.16, 22.17**). They may coalesce and surround the viscera or diaphragm. Occasionally they may present calcifications, particularly in serous malignancies.

Both **CT** and **MR** have elevated sensitivity (80-90%) and specificity (80-95%) in the identification of peritoneal neoplastic implants provided the lesions are larger than 2 cm (**Fig. 18**). Nodules smaller than 1 cm are difficult to recognize and the sensitivity of both techniques in these cases is <50%. In addition to small lesions, another limitation is the site; the techniques have particular difficulty identifying lesions on the intestinal surface, the mesentery and the bladder dome. In this setting **CT-PET** does not seem to offer any better results, with overall sensitivity 60-80%. Therefore, **laparoscopy** is still the most reliable approach for both the identification and characterization of the lesions (sensitivity 98-100%, specificity 95-100% in the various study populations) (**Fig. 22.19**). CT, MR and laparoscopy are used for defining the peritoneal cancer index, which is given by the size of the nodules and the spread of peritoneal carcinosis. It is therefore an expression of the stage of disease and an essential element for the planning of treatment and evaluation of prognosis.

In contrast to peritoneal metastasis, lymphatic and hematogenous spread are less common. Lymphatic spread occurs along three pathways: the first and most important involves the external iliac and obturator lymph nodes via the uterine-ovarian ligaments and the parametrium; the second leads to the superior common iliac and para-aortic lymph nodes between the renal hilum and the aortic bifurcation along the ovarian vessels; the third and least common is spread to the external iliac and inguinal lymph nodes via the round ligament. In stages I and II around 14% of lymph nodes are positive for metastasis. This percentage rises to 64% in stages III and IV. Hematogenous spread is the latest and most commonly leads to involvement of the liver, lung, pleura and kidneys (**Fig. 22.20**).

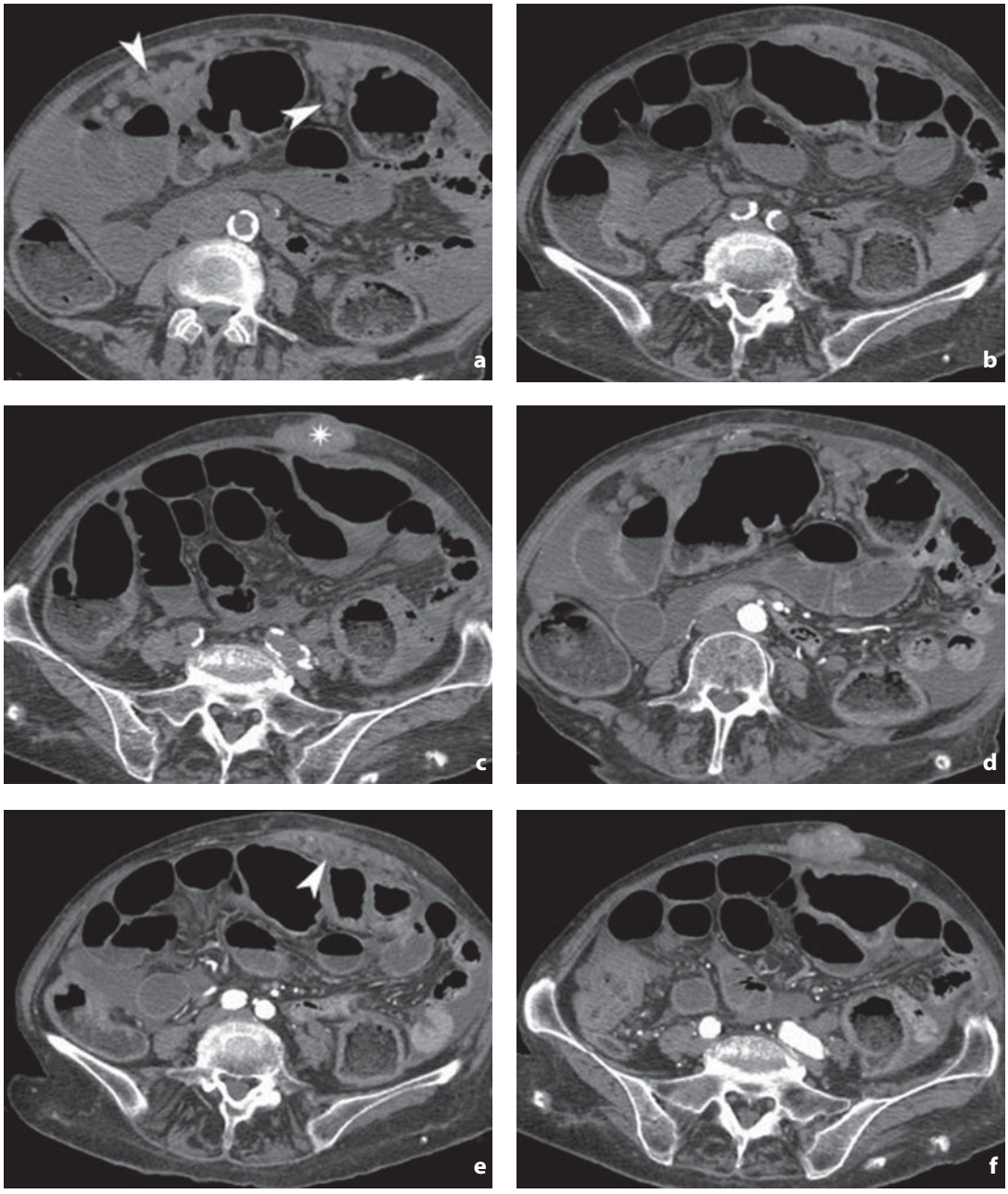

Fig. 22.16a-f. Computed tomography. Peritoneal carcinosis. **a-c** Nonenhanced CT shows multiple solid nodules (*arrowheads*) in the greater omentum and a Sister Mary Joseph nodule at the umbilicus (*asterisk*). **d-f** After contrast medium administration the nodules show marked enhancement and associated ascites is apparent

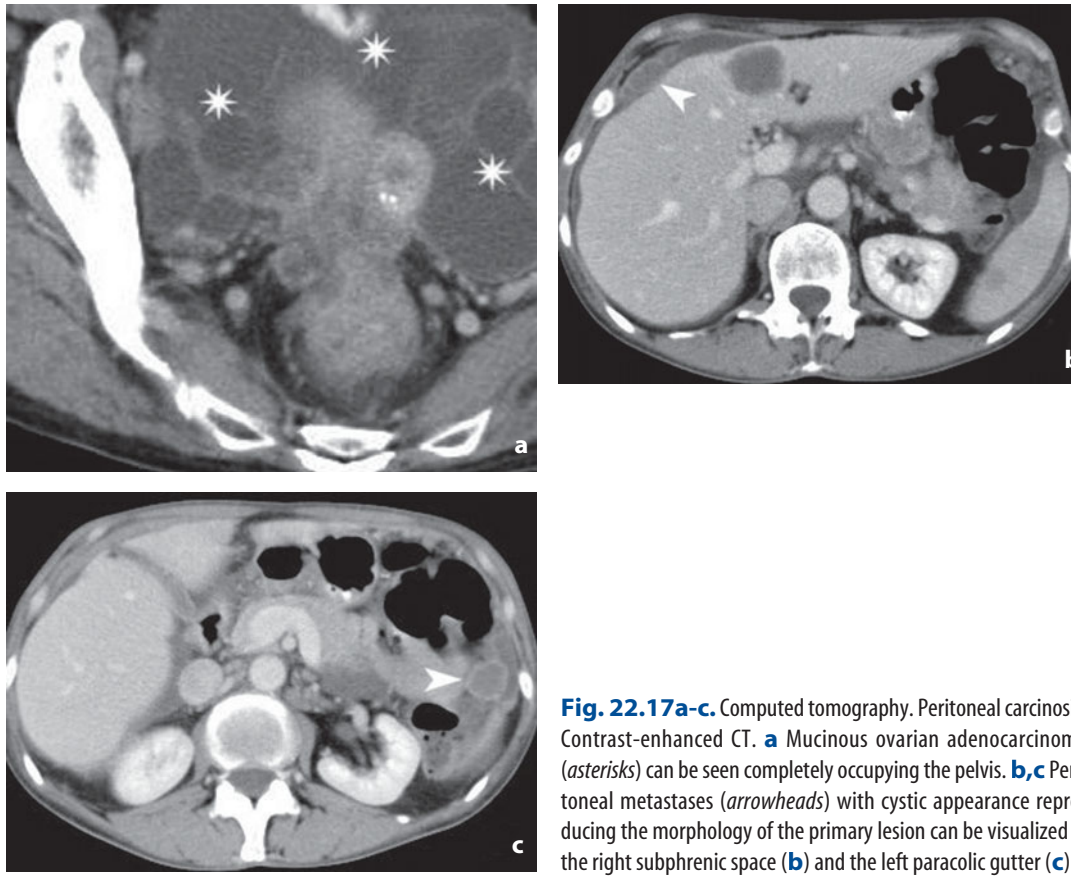

Fig. 22.17a-c. Computed tomography. Peritoneal carcinosis. Contrast-enhanced CT. **a** Mucinous ovarian adenocarcinoma (*asterisks*) can be seen completely occupying the pelvis. **b,c** Peritoneal metastases (*arrowheads*) with cystic appearance reproducing the morphology of the primary lesion can be visualized in the right subphrenic space (**b**) and the left paracolic gutter (**c**)

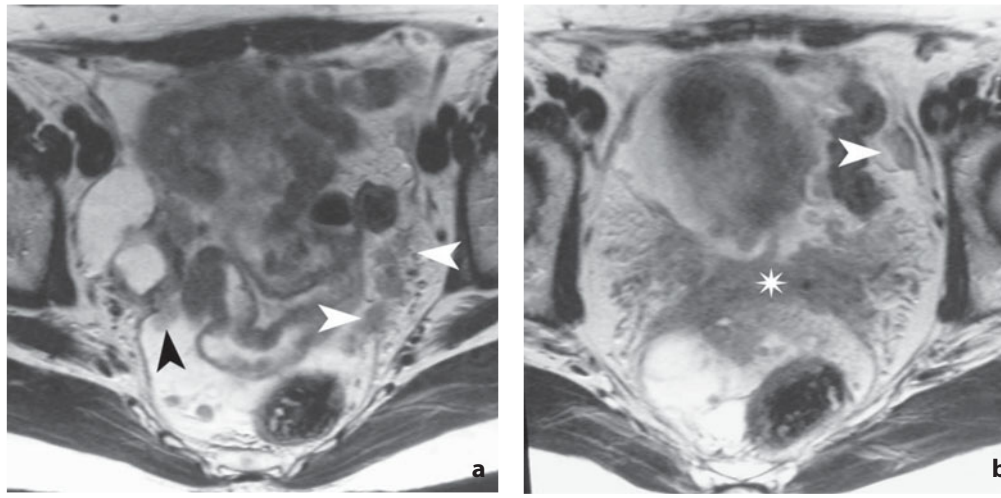

Fig. 22.18a-e. Magnetic resonance. Patient already having undergone surgery for ovarian carcinoma. **a** Multiple nodules (*arrowheads*) adhering to the pelvic parietal peritoneum with associated extensive solid plaque (*asterisk* in **b**). *(cont.* ⟶*)*

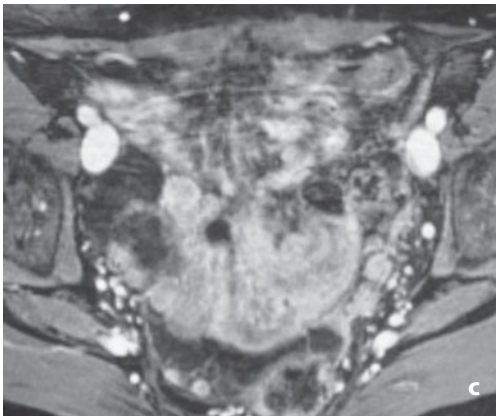

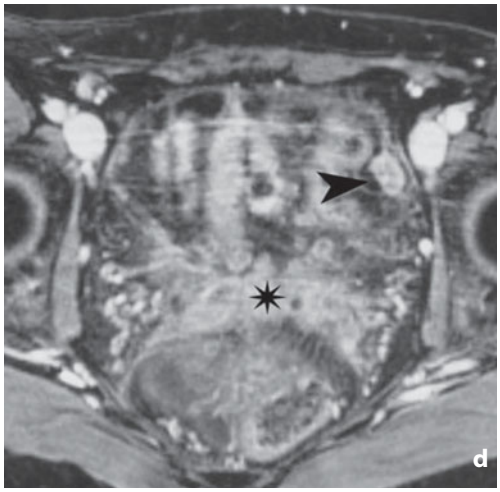

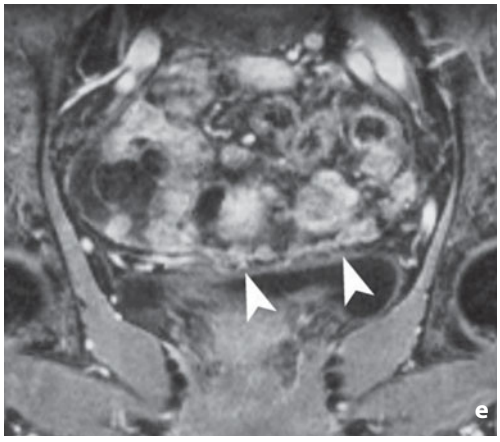

Fig. 22.18a-e. *(cont.)* **c-e** Peritoneal implants (*asterisk* and *arrowheads*) show marked enhancement after administration of paramagnetic contrast medium. Ascites can also be identified

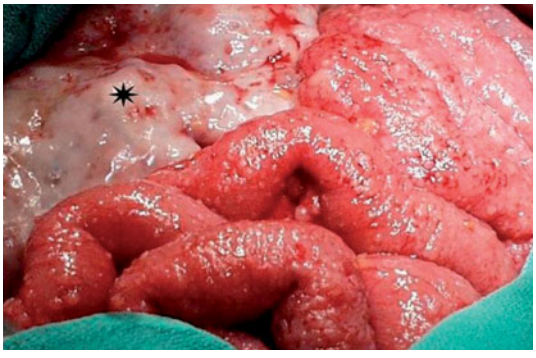

Fig. 22.19. Laparoscopy. Intraoperative image shows multiple nodules adhering to the visceral peritoneum of the jejunoileal loops. Neoplastic involvement of the greater omentum is also evident (*asterisk*)

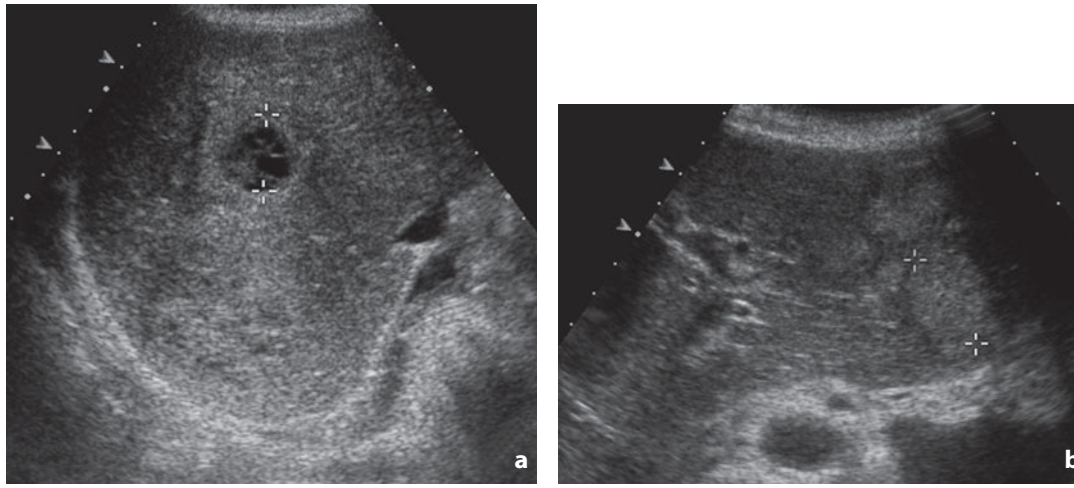

Fig. 22.20a,b. Ultrasonography. Hepatic metastases from ovarian adenocarcinoma. Cystic lesions (**a**) and hyperechoic solid lesions (**b**) can be seen coexisting

Metastases

Around 5-15% of ovarian malignancies are metastases from lymphomas, carcinomas of the colon (Fig. 22.21), stomach (Fig. 22.22) and breast and less frequently from melanomas, carcinoids and carcinomas of the endometrium, pancreas and gallbladder. They are more common in premenopausal women because in this stage of life the ovaries are much more highly vascular. Rarely are metastases unilateral, especially in endometrial cancer.

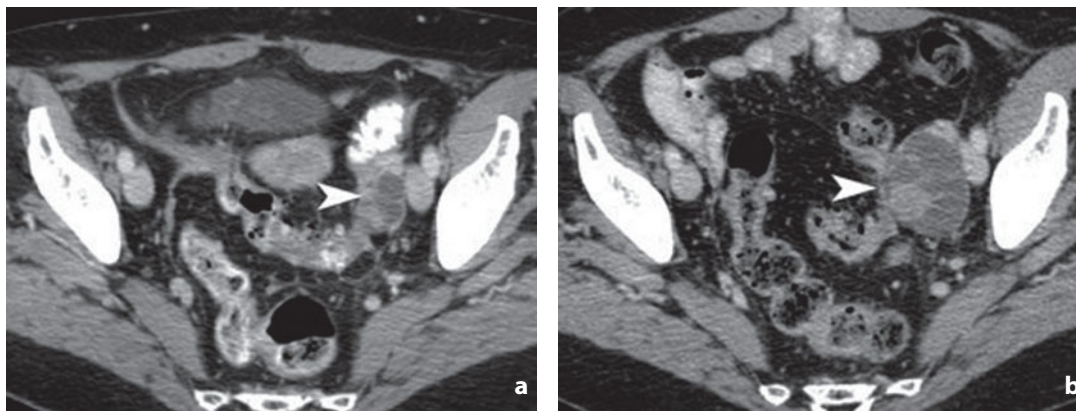

Fig. 22.21a,b. Computed tomography. Ovarian metastases from colon cancer. **a** Contrast-enhanced CT shows expansive left adnexal lesion with mixed structure (*arrowhead*). Subsequent contrast-enhanced CT follow-up (**b**) shows increased size of both the cystic and solid components

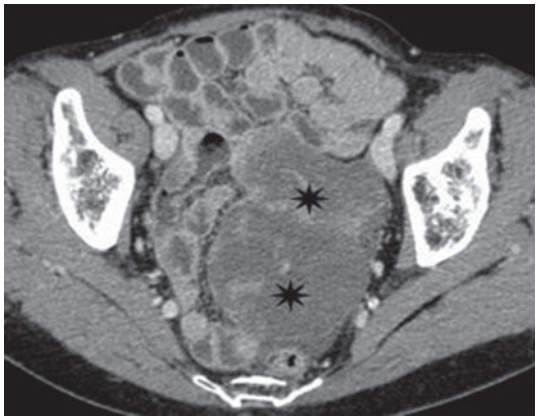

Fig. 22.22. Computed tomography. Ovarian metastasis from stomach cancer. Contrast-enhanced CT shows large expansive adnexal lesion (*asterisks*) with marked heterogeneous enhancement due to diffuse necrotic-cystic components

Uterine Tube Carcinoma

Primary uterine tube carcinoma is extremely rare, accounting for only 0.3-1.1% of all gynecologic malignancies. It is often serous and has a peritoneal spread pattern similar to epithelial ovarian cancer, although with a greater tendency for distant metastasis. Following the onset of pain due to tubal distension or anomalous uterine bleeding, the tumor is diagnosed in an early stage. However, it can mimic hydrosalpinx, a condition with which it is frequently associated. A signal higher than fluid in T1- and T2-weighted **MR** sequences is suggestive of hematosalpinx. The tumor appears as a solid or cystic mass, much like ovarian cancer (**Fig. 22.23**). A spindle-shaped cystic structure with interdigitating septa adjacent to the mass represents the dilated tube. Distension of the uterine cavity and ascites are common findings.

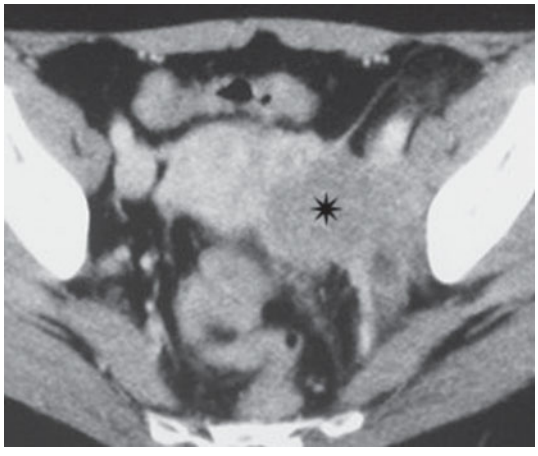

Fig. 22.23. Computed tomography. Uterine tube carcinoma. Contrast-enhanced CT shows solid expansive left adnexal lesion (*asterisk*) with smooth margins and heterogeneous enhancement

Brown DL, Zou KH, Tempany CM et al (2001) Primary versus secondary ovarian malignancy: imaging findings of adnexal masses in the Radiology Diagnostic Oncology Group Study. Radiology 219:213-218

Coakley FV, Choi PH, Gougoutas CA et al (2002) Peritoneal metastases: detection with spiral CT in patients with ovarian cancer. Radiology 223:495-499

Jung SE, Lee JM, Rha SE et al (2002) CT and MR imaging of ovarian tumors with emphasis on differential diagnosis. RadioGraphics 22:1305-1325

Jeong YY, Outwater EK, Kang HK (2000) Imaging evaluation of ovarian masses. RadioGraphics 20:1445-1470

Kishimoto K, Awaya H, Matsunaga N et al (2002) Paraovarian cyst: MR imaging features. Abdom Imaging 27:685-689

Low RN, Chen SC, Barone R (2003) Distinguishing benign from malignant bowel obstruction in patients with malignancy: findings at MRI. Radiology 228:157-165

Mironov S, Akin O, Pandit-Taskar N et al (2007) Ovarian cancer. Radiol Clin North Am 45:149-166

Outwater EK, Wagner BJ, Mannion C et al (1998) Sex cord-stromal and steroid cell tumors of the ovary. RadioGraphics 18:1523-1546

Sironi S, Messa C, Mangili G et al (2004) Integrated FDG PET/CT in patients with persistent ovarian cancer: correlation with histologic findings. Radiology 233:433-440

Tanaka YO, Yoshizako T, Nishida M et al (2000) Ovarian carcinoma in patients with endometriosis: MR imaging findings. AJR Am J Roentgenol 175:1423-1430

Part VIII
Oncologic Recurrences of the Female Reproductive System

Clinical Approach 23

E. Sartori, L. Carrara, B. Pasinetti

The follow-up procedures subsequent to the primary treatment of a gynecologic malignancy can be assimilated with a screening test performed on the general population. Here the aim of monitoring is the early diagnosis and subsequent treatment of disease recurrence to improve survival of the individual and the population in question.

The main aims of a follow-up program include assessment of the results of treatment, detection of iatrogenic damage and early diagnosis of disease recurrence or a second malignancy or precancerous lesions having the same etiopathogenesis as the treated tumor.

Ovary

Ovarian cancer is still today a disease with a severe prognosis. Indeed, despite the initial positive response to treatment, 75% of women with stage III or stage IV disease present a recurrence or progression of the disease.

The use of aggressive surgical debulking and platinum-based chemotherapy has led to a growing number of patients with malignant ovarian epithelial tumors going into both clinical and instrumental remission. The close clinical monitoring of previously treated patients makes early diagnosis of recurrence possible; this prevalently occurs in the abdominal-pelvic cavity or on the surface of the hepatic capsule, the pelvic and/or lumbar-aortic lymph nodes, the hepatic parenchyma, the lung/pleura, spleen and brain. The average time interval to recurrence depends on the stage of the disease: around 24 months for advanced stages and over 60 months for the initial stages.

The most common follow-up programs include a clinical-instrumental evaluation with a general examination of the physical condition of the patient, evaluation of symptoms of recurrence, serial measurement of serum CA125 levels and periodic abdominal-pelvic US examinations. CT and/or PET are performed in select cases, e.g. increased CA125 in the absence of clinical evidence of disease. Clinical-instrumental monitoring programs should continue for more than five years after the termination of primary treatment, with progressively wider intervals: every three months in the first year, every four months in the second and third year, every six months until the fifth year and annually thereafter. Accurate identification with imaging of the location and spread of malignant recurrence should contribute to the selection of a small number of patients able to undergo surgery for isolated tumor recurrence.

The cure of recurrence is still a difficult goal to achieve. The rate of complete response to treatment is directly proportional to the interval free from disease. This finding is supported by the observation that most patients, after having undergone repeated antiblastic therapy subsequent to the first course, associated with surgical treatment when susceptible to secondary debulking, have increasingly shorter

L. Olivetti, L. Grazioli (eds.), *Imaging of Urogenital Diseases*,

disease-free periods until death. Currently the median survival after recurrence varies between 12 and 24 months.

Armstrong DK (2002) Relapsed ovarian cancer: challenges and management strategies for chronic disease. Oncologist 7:20-28

Jemal A, Siegel R, Ward E et al (2007) Cancer statistics, 2007. CA Cancer J Clin 57:43-66

NIH consensus conference. Ovarian cancer. Screening, treatment, and follow-up. NIH Consensus Development Panel on Ovarian Cancer (1995). JAMA 8:491-497

Endometrium

The main factors influencing the course of disease in patients with carcinoma of the endometrium are histotype, grade, myometrial invasion, invasion of the lymphovascular spaces, peritoneal cytology and the presence of lymph node metastases. The probability of a recurrence of endometrial cancer is between 8% and 19%.

The site of recurrence may be extrapelvic or local-regional, including isolated vaginal, central and regional pelvic (walls, lymph nodes) recurrences.

The type of primary treatment and adjuvant therapies influence the possibility of recovery from recurrences, whether regional or distant. Adjuvant radiotherapy in fact reduces the frequency of pelvic recurrences, but not distant recurrences, which constitute the major problem of high risk endometrial carcinomas.

Around 33% of recurrences arise at the local level, while distant metastases account for 57%. In 10% of cases recurrence is both local and distant.

Follow-up protocols include an examination every three months in the first year, every four months in the second year, every six months until the fifth year and annually thereafter. The examinations include patient history, clinical evaluation and rectovaginal examination.

There is no broad consensus regarding the diagnostic procedures to use in the follow-up program: Pap test, US and abdominal-pelvic CT are advisable every 12 months. Plain chest film is indicated at 12 and 24 months.

Despite being operator dependent, the general physical and pelvic examination is the least costly and least invasive technique available for the monitoring of endometrial malignancy. It leads to a diagnosis of recurrence varying from 11% to 83% (mean 28%), with 82% of asymptomatic recurrences being diagnosed with this technique.

The most common symptoms of recurrence are both pelvic and abdominal pain, followed by weight loss, asthenia and vaginal bleeding. Retrospective studies have shown that more than 80% of recurrences are diagnosed on the basis of either the gynecologic physical examination alone or the symptoms reported by the patient. Overall, only 2.5% of all recurrences are diagnosed by vaginal vault cytology.

Follow-up is also useful for the diagnosis of possible metachronous tumors, which are not uncommon in patients with endometrial cancer. Indeed, around 6.5% of patients treated for endometrial carcinoma develop breast cancer, and some 4% develop another primary tumor, especially colon cancer in patients with a family history of Lynch II syndrome.

The five-year survival rate from recurrences varies in the literature from 10% to 38%, with a better prognosis for isolated vaginal recurrences which may benefit from surgery or radiotherapy. The survival from recurrences is influenced not only by the site but also by the time to appearance: early onset recurrences are in fact associated with reduced mean survival.

Agboola OO, Grunfeld E, Coyle D et al (1997) Costs and benefits of routine follow-up after curative treatment for endometrial cancer. CMAJ 157:879-886

Berchuck A, Anspach C, Evans AC et al (1995) Postsurgical surveillance of patients with FIGO stage I/II endometrial adenocarcinoma. Gynecol Oncol 59:20-24

Kew FM, Roberts AP, Cruickshank DJ (2005) The role of routine follow-up after gynecological malignancy. Int J Gynecol Cancer 15:413-419

Podczaski E, Kaminski P, Gurski K et al (1993) Detection and patterns of treatment failure in 300 consecutive cases of 'early' endometrial cancer after primary surgery. Gynecol Oncol 47:323-327

Salvesen HB, Akslen LA, Iversen T et al (1997) Recurrence of endometrial carcinoma and the value of routine follow up. Br J Obstet Gynaecol 104:1302-1307

Shumsky AG, Stuart GC, Brasher PM et al (1994) An evaluation of routine follow-up of patients treated for endometrial carcinoma. Gynecol Oncol 55:229-233

Tjalma WA, van Dam PA, Makar AP et al (2004) The clinical value and the cost-effectiveness of follow-up in endometrial cancer patients. Int J Gynecol Cancer 14:931-937

Cervix

The natural history of cervical cancer is influenced by a variety of prognostic factors, the most accredited of which are useful for the purposes of correct treatment planning. These include: stage of the disease, diameter of the primary tumor, depth of stromal invasion, involvement of the lymphovascular spaces, positive resection margins, lymph node metastases and others of debatable interpretation, including the histotype and degree of differentiation. It has been widely demonstrated that the association of several risk factors leads to a reduction in the local control of disease, relative increase in the risk of recurrence and lower survival in both global and disease-free terms.

Recurrences of cervical cancer appear in over 70% of cases within 24 months from the termination of primary treatment. The peak incidence occurs between 18 and 36 months from treatment, even though recurrences at over 60 months have been described, although in lower percentages.

Early diagnosis of recurrence or the persistence of disease is among the aims of an appropriate follow-up program. Therefore, at the termination of primary treatment, the patient should undergo periodic clinical and instrumental examinations with the aim of identifying disease recurrence as early as possible in order to improve survival and reduce morbidity.

Follow-up examinations every 3 months are advisable during the first 2 years from primary treatment. In the third year examinations may be held every six months and then annually from the fifth year for a lengthy period of time, since cases of very late recurrences have been described. Each scheduled visit should include an accurate evaluation of any symptoms reported by the patient which may be a help in the early recognition of a latent state of disease. Lumbar radiculopathy or pelvic pain is the dominant symptom (20-50%), along with vaginal bleeding (6-15%). More rare events are weight loss and anorexia (1-5%), edema of the lower limbs (5-12%) and dyspnea with cough and hemoptysis (1-5%). It should, however, be borne in mind that 10-40% of recurrences are asymptomatic.

Pelvic examination is performed with gynecologic vaginal and rectal examination, Pap test, colposcopy and biopsy of any suspicious lesion.

In terms of classification, recurrences can be subdivided into pelvic (central and lateral), regional (to regional lymph nodes), abdominal and distant (aortic lymph nodes or superior stations, lung, bone, liver). The site of recurrence is linked to the

stage of disease, primary therapy performed and the presence of a number of decisive prognostic factors. In particular the presence of lymph node metastases is the prognostic factor with the greatest weight in determining the risk of recurrence and influencing the site. Recurrence in patients with positive lymph nodes occurs for the most part in the pelvic wall or distantly. In contrast, the site tends to be central pelvic in patients with negative lymph nodes. Overall the percentage of recurrence in patients with disease at stage IB/IIA, N- is 15%, which rises to 40% with positive pelvic lymph nodes and 70% if both pelvic and lumbar-aortic lymph nodes are involved.

Patients with vaginal or pelvic recurrences who are eligible for surgery or radiotherapy benefit the most from the treatment of recurrences. Metastatic localizations are usually treated with cisplatin-based chemotherapy which has shown a percentage of response between 20% and 30%.

Averette HE, Ngoyen HN, Donato DN et al (1993) Radical hysterectomy for invasive cervical cancer. Cancer 71:1422-1437

Duyn A, Van Eijkeren M, Kenter G et al (2002) Recurrent cervical cancer: detection and prognosis. Acta Obstet Gynecol Scand 81:351-355

Sugiyama T, Yakushiji M, Noda K et al (2000) Phase II study of irinotecan and cisplatin as first-line chemotherapy in advanced or recurrent cervical cancer. Oncology 58:31-37

The clinical management of recurrences requires personalized follow-up in terms of the performance status of the patient or the need to control the side-effects of treatment. Bearing in mind the burden of indispensable examinations required to reach a diagnosis of asymptomatic recurrence, it is worthwhile investigating the patient's point of view, given the obvious time commitment and stress induced by performing systematic imaging procedures. During the clinical interview in the follow-up examinations the use of a questionnaire would be desirable to investigate the psychological problems caused by periodic check-ups and the impact these can have on the quality of life of the patient.

Diagnostic Imaging

24

L. Grazioli, C. Stanga, S. Gambarini

The main aims of imaging in the follow-up of patients treated for malignancies of the reproductive system (uterine cervix, endometrium, ovary or vulva) are evaluation of the effectiveness of the therapy itself and early recognition of the onset of tumor recurrence. Around 30% of patients with cervical cancer die due to persistence or recurrence of disease within the first two years of treatment. In carcinoma of the endometrium a varying percentage between 3% and 15% of patients with low risk (stage IA/IB) and between 20% and 45% with high risk (stage IC or above) develop a recurrence after treatment. In approximately 2/3 of ovarian cancers extrapelvic implants are present at the time of staging with a consequent elevated risk of recurrence.

In order to be able to intervene in the best possible way with additional treatment – whether surgical, medical or radiotherapeutic – to improve the duration and quality of survival, the study of tumor recurrence of the female reproductive system utilizes various imaging modalities: conventional radiology (plain chest film and in some cases urography), ultrasonography (US) (transabdominal and/or transvaginal), computed tomography (CT), magnetic resonance (MR) and CT-PET.

The **plain chest film** has the aim of identifying secondary pulmonary lesions, but it has been almost completely replaced by the more sensitive and specific chest CT.

Intravenous urography is used for the study of postoperative and/or postradiotherapy sequelae, especially in cases in which the recurrence involves organs of the urinary tract, causing displacement, compression or invasion (**Fig. 24.1**). This technique, too, is being increasingly replaced by study with multidetector-row CT. Indeed, acquisitions in the late phase of contrast-enhanced study enable high-quality multiplanar reconstructions there are very similar to urographic images, while at the same time providing the possibility of the wide field of view typical in CT images.

While **US** is indispensable for the identification, characterization and staging of many malignancies of the female reproductive system (especially carcinoma of the endometrium), it plays a secondary role in the follow-up of these diseases and is even more marginal in the study of recurrences. In the case of cervical and endometrial cancers, for example, US study (performed with the transvaginal approach) is often limited by poor specificity in differentiating the postradiotherapy and/or postoperative appearance from possible disease recurrence. In the case of ovarian malignancies, transvaginal US can be useful in the identification of regional recurrence, but even when associated with the transabdominal approach the technique has tremendous difficulty in recognizing and describing the presence of small peritoneal implants. In vulvar malignancies, transabdominal US may play a role in follow-up and restaging (search for synchronous metastases and local recurrences).

The use of more panoramic modalities such as **CT** and **MR** has become common practice including in evaluation of prior therapy.

L. Olivetti, L. Grazioli (eds.), *Imaging of Urogenital Diseases*,

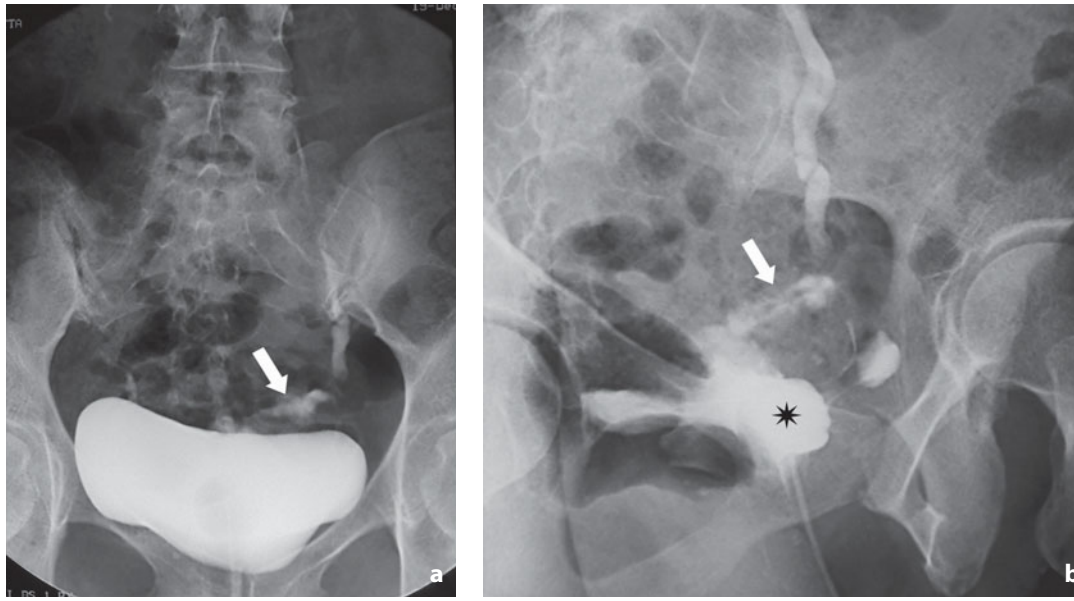

Fig. 24.1a,b. Urography. Ureterovaginal fistula. Appearance after radical hysterectomy due to cervical cancer. **a** Urographic image shows the leakage of iodinated urine (*arrow*) with opacification of the vagina (*asterisk)* shown in the detailed radiograph (**b**)

Recurrences of Ovarian Malignancies

Patients with ovarian cancer almost always undergo debulking surgery, since this approach, which may be followed by adjuvant chemotherapy, improves survival. However, the number of women with extrapelvic lesions at the time of diagnosis or in whom optimal debulking cannot be achieved due to local extension of the disease at staging (residual neoplastic tissue with a maximum diameter of less than 1 cm) is relatively large. These conditions raise the risk of tumor recurrence, which is defined as the resumption of disease after complete response to initial treatment, after negative findings at "second look" surgery when performed, or a disease-free interval of at least 6 months after the primary intervention.

The most common manifestation of the recurrence of ovarian cancer is the presence of neoplastic tissue at the level of the pelvic cavity, near to the surgical bed or the adjacent organs (**Fig. 24.2**). Recurrence can also manifest via intraperitoneal spread, which is the typical spread pattern of ovarian tumors, followed by lymphatic and hematogenous spread. The spread of neoplastic cells within the peritoneal cavity is supported by the normal flow of peritoneal liquid from the pelvis towards the hemidiaphragms along the colonic gutter, especially on the right up to the hepatic margin, and by the collection of that liquid in a number of recesses (rectouterine pouch, paravesical spaces, Morrison's pouch, right colonic gutter, omentum). In these sites, in addition to the omentum, metastatic implants can already be identified at the time of staging, and they should be sought in suspicion of recurrences (**Fig. 24.3**).

The main lymphatic pathway of metastasis is the one accompanying the ovarian veins up to the retroperitoneal lymph nodes at the level of the renal hila. Other pathways follow the lymphatic vessels coursing laterally to the broad ligaments up to the internal iliac and obturator lymph nodes, or along the round ligament up to the external iliac and inguinal lymph node stations.

Hematogenous spread is characteristic of advanced disease and is identified with increasing frequency in relation to the lengthening of survival, thanks to repeated

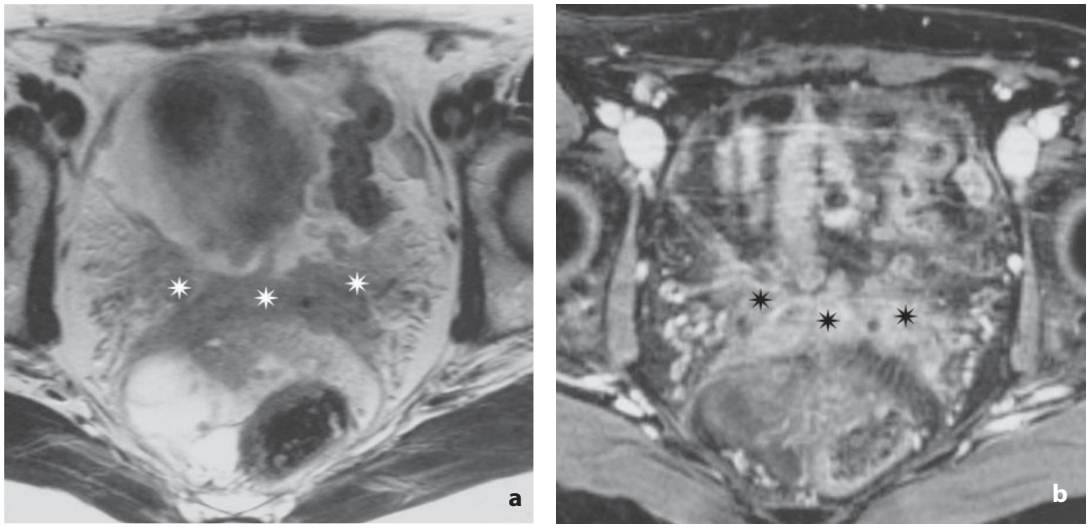

Fig. 24.2a,b. Magnetic resonance. Pelvic recurrence of ovarian cancer. T1-weighted image (**a**) shows a solid plaque (*asterisks*) with irregular margins and significant enhancement after injection of paramagnetic contrast medium (**b**)

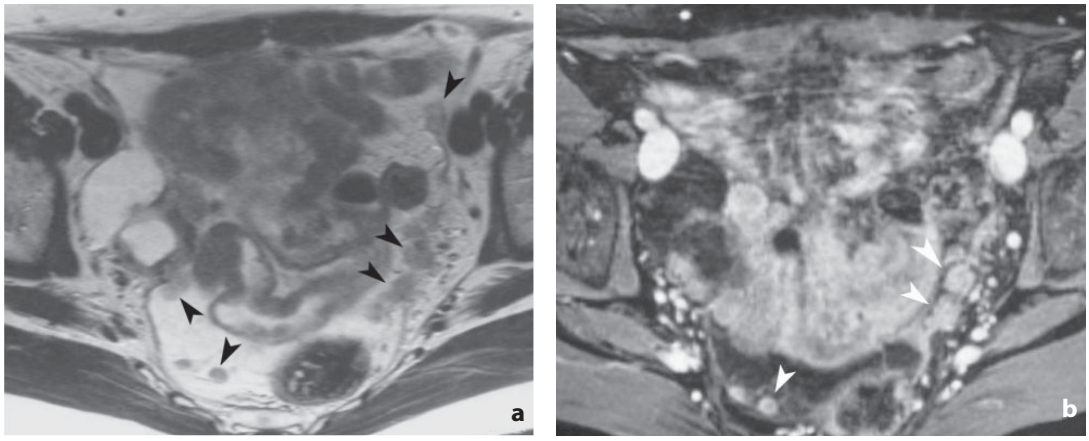

Fig. 24.3a,b. Magnetic resonance. Pelvic recurrence of ovarian cancer. Same case as previous figure. **a** Numerous peritoneal tumor implants can be identified in the rectouterine pouch adhering to the peritoneal layer of the left wall (*arrowheads*), with nodular appearance and showing enhancement after contrast medium administration (**b**)

cycles of adjuvant chemotherapy. The most commonly involved sites are the pleura and lung, liver and bone, as well as the brain, spleen, pancreas, suprarenal gland and subcutaneous tissue.

The follow-up of patients who undergo surgery for ovarian cancer is rather rigorous (3-4 months) and is performed after second look surgery, essentially with clinical examination, assay of the tumor marker CA125 and pelvic US. CT and MR are usually reserved for cases where clinical suspicion requires an in-depth diagnostic study due to increased CA125, onset of symptoms or suspicious findings at the physical examination or US study. However, with the advent of multislice technology and the possibility of acquiring thin-sliced images and obtaining multiplanar reconstructions, second look surgery performed at the termination of adjuvant chemotherapy has begun to be replaced by abdominal CT. The imaging technique is able to evaluate the response to treatment and to visualize possible foci of residual disease, even with a diameter less than 1 cm.

In the event of suspected recurrence, CT is generally preferred to MR, in that it is more available, faster and less expensive and has elevated sensitivity (70-90%). MR is more susceptible to motion artifacts and less sensitive in identifying initial abdominal peritoneal implants, although it is more accurate in identifying small pelvic peritoneal implants and bone metastases.

The CT examination, performed after administration of contrast medium and opacification of the bowel loops via the oral administration of water, involves the acquisition of images in the venous phase (at around 100 s) and, where necessary, in the excretory phase (5-10 min). Reconstructions in the sagittal and coronal planes enables an improved evaluation of the curved structures (diaphragm and pelvic organs), paracolic gutters and the peritoneal recesses, in which metastatic implants are frequently found. Regional recurrences manifest as solid lesions with attenuation values similar to soft tissue, or cystic lesions with thickened walls and/or intralesional septations. Ascites suggest the presence of peritoneal carcinomatosis, which manifests in the form of plaque-like thickening or single or multiple nodules in the peritoneal layers and recesses, the omentum (if they are large and extensive the involvement of the omentum is defined "omental cake"), hemidiaphragms (especially the right hemidiaphragm) and bowel loops. These nodules may present characteristics similar to those of the primary lesion and have a solid or cystic appearance, possibly even multilocular (**Fig. 24.4**). They may also involve the capsule of parenchymal organs such as the liver or spleen, and in this case they should be differentiated from secondary implants arising from hematogenous spread (**Fig. 24.5**). Implants with a calcified appearance in relation to the primary malignancy are also common. Some 20% of serous papillary tumors, for example, which are rich in psammomatous bodies, may present calcifications in both the primary mass and the metastatic implants.

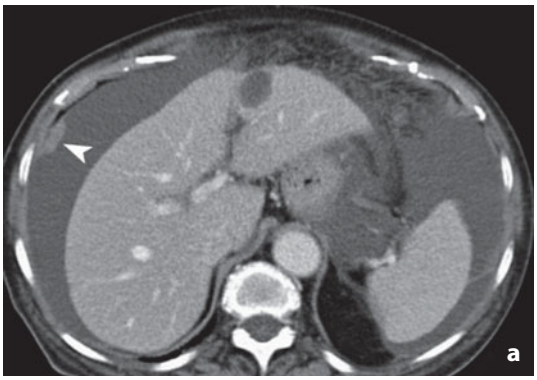

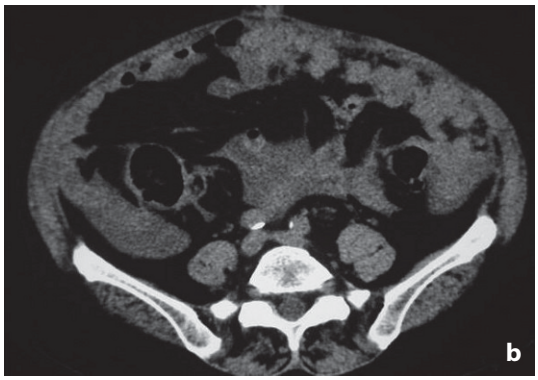

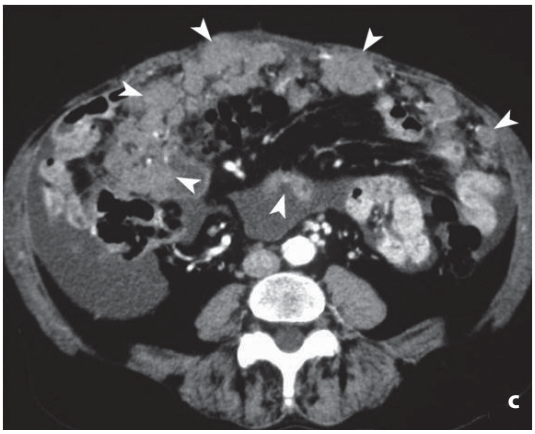

Fig. 24.4a-c. Computed tomography. Peritoneal metastases. **a** Small plaque-like implant in the right subphrenic space (*arrowhead*) with concomitant ascites. **b,c** Different case. Nonenhanced (**b**) and contrast-enhanced (**c**) images show numerous moderately vascular nodules involving the greater omentum and visceral peritoneum (*arrowheads*)

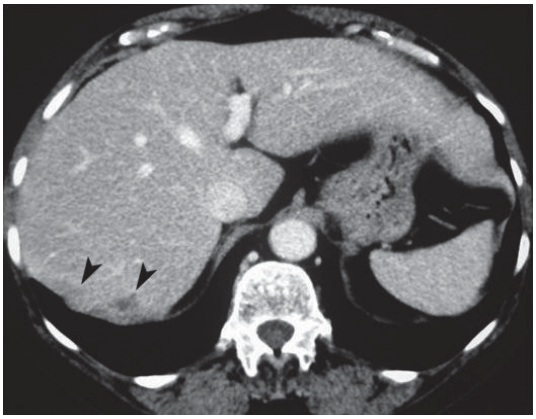

Fig. 24.5. Computed tomography. Neoplastic implants of the hepatic capsule (*arrowheads*) causing retraction and irregularity of the hepatic margin

CT is also indicated in the search for lymph node recurrences (pelvic or lumbar-aortic) and distant metastases with extrapelvic or extra-abdominal location. Liver metastases in particular are characterized by hypoattenuating lesions with poor contrast enhancement and possible "target" appearance given by a ring of tissue which is mildly hyperattenuating with respect to the lesion in the venous phase. The presence of an acute angle with the hepatic margin confirms an intraparenchymal site of the nodule and therefore hematogenous spread, with a worse prognosis than a capsular implant. The presence of pleural effusion is suggestive of a pleural implant, which manifests as enhancing plaque-like thickening or nodularity of the pleural wall. An increasing finding is secondary implants at the level of soft tissue (with a nodular or pseudocystic appearance and attenuation values which increase after contrast medium administration), the suprarenal glands (which appear swollen with attenuation values >20 HU in nonenhanced images) and the spleen (with characteristics similar to those of hepatic lesions).

Recently the use of CT-PET has been proposed for the early identification of recurrence of ovarian cancer. However, studies performed on larger populations than those currently available are required for a real confirmation of the potential role of this imaging modality.

Funt SA, Hricak H, Abu-Rustum N et al (2004) Role of CT in the management of recurrent ovarian cancer. AJR Am J Roentgenol 182:393-398

Kwek JW, Iyer RB (2006) Recurrent ovarian cancer: spectrum of imaging findings. AJR Am J Roentgenol 187:99-104

Pannu HK, Bristow RE, Montz FJ et al (2003) Multidetector CT of peritoneal carcinomatosis from ovarian cancer. RadioGraphics 23: 687-701

Pannu HK, Bristow RE, Cohade C et al (2004) PET-CT in recurrent ovarian cancer: initial observations. RadioGraphics 24:209-223

Recurrences of Uterine Malignancies

The follow-up of uterine cancer is particularly influenced by the alterations induced by radiation and/or surgical therapy, which modify the anatomy of the pelvic structures. This makes more difficult the recognition, characterization and staging of local recurrence or postoperative and/or postradiotherapy complications. In addition, there has been an increase in the incidence of recurrence in atypical sites, which is probably related to the increasingly common irradiation of the entire pelvic cavity. This finding, which has also been encountered in ovarian cancer, is further evidence of the need for extensive evaluation of the entire abdomen and chest of these patients.

In International Federation of Gynecology and Obstetrics (FIGO) stage I and II malignancies of the endometrium and cervix, the treatment of choice is surgery, followed, where necessary, by radiotherapy. The latter is the treatment of choice in advanced tumors.

In postoperative patients CT is often the first-choice technique given its availability, speed, low cost and ability to provide an evaluation of the entire abdomen, thus enabling the identification of residual neoplastic tissue or recurrences, with good sensitivity (90%). The examination is performed after the administration of contrast media, which are generally water administered orally to opacify the gastrointestinal tract, and nonionic contrast medium administered intravenously. The scans are acquired with thin slices (to obtain sagittal and coronal reconstructions) in the venous phase (at around 100 s) and in the late phase in the event of urinary tract involvement (5-10 min).

The most frequent recurrence sites in cervical cancer are the vaginal vault, the wall and the lymph nodes of the pelvic cavity if the patient underwent surgery alone. In the case of radiotherapy, recurrence sites are frequently extrapelvic: the liver, retroperitoneal lymph nodes and lungs.

Tumor recurrences in cervical cancer appear as a solid mass with attenuation values in the range of soft tissue. They are identifiable on the basis of morphology and shape, as well as enhancement characteristics. In some cases the solid tissue may be characterized by the presence of a central area with increased hypoattenuation due to necrotic phenomena or it may have a cystic-like appearance. There may be concomitant uni- or bilateral hydronephrosis if the recurrences obstruct the ureters. Extrapelvic recurrences may manifest as adenopathies, hypoattenuating hepatic nodules, peritoneal implants, pulmonary or lytic bone lesions. In the case of endometrial cancer the endopelvic recurrences appear as moderately enhancing solid masses located in the central area of the pelvis related to the vaginal vault or contiguous to other pelvic organs (bladder, rectum) (**Fig. 24.6**). Alternatively, recurrences appear in the form of pelvic or extrapelvic adenopathies, ascites (in relation to the presence of peritoneal implants) and hypoattenuating hepatic lesions.

CT is unable to differentiate between solid tissue arising from tumor recurrences and fibrotic scar tissue originating from surgery and/or radiotherapy. In contrast, MR is able to more precisely define the post-treatment pelvic anatomy (**Figs. 24.7, 24.8**), although with slightly reduced diagnostic accuracy in the first six months, due to inflammation or edema.

Numerous studies have demonstrated the superiority of magnetic resonance in identifying residual tumor tissue or the onset of recurrences, thanks to its greater contrast resolution. MR is therefore the imaging modality of choice in the follow-up of cancer treated with radiotherapy alone, where the recurrences appear with the same characteristics as the primary lesion (**Fig. 24.9**). Furthermore, in these patients MR is able to identify postradiotherapy complications such as vaginal fistulas, which have a hyperintense signal in T2-weighted sequences and show enhancement after the administration of contrast medium due to the inflammation. In postoperative patients MR can identify fibrotic thickening of the round ligament or the peritoneum (which show no enhancement after contrast medium administration), lymphocele

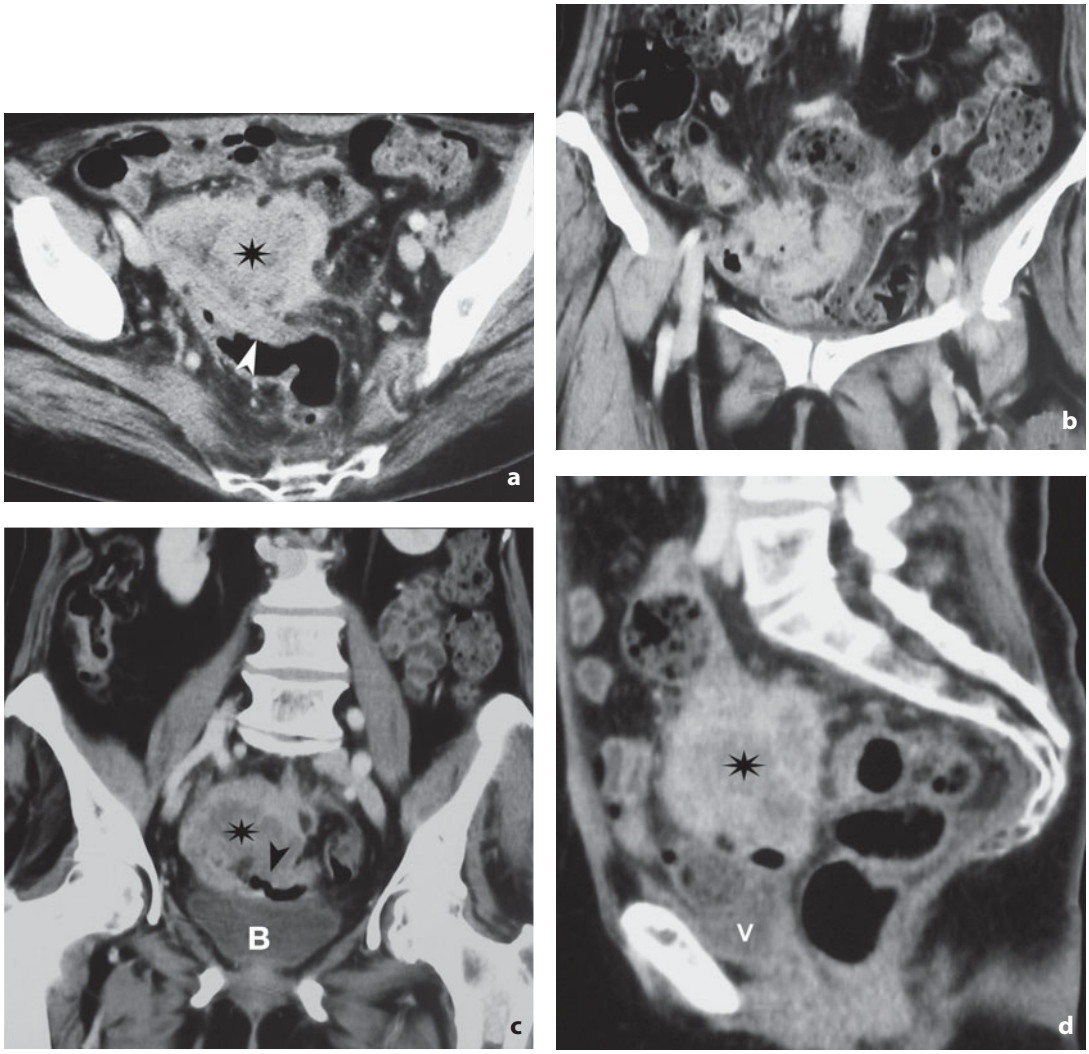

Fig. 24.6a-d. Computed tomography. Recurrence of endometrial cancer. Appearance after radical hysterectomy. Axial image (**a**), coronal (**b, c**) and sagittal reconstructions (**d**). Large solid and heterogeneous mass with irregular margins (*asterisk*) can be identified in the centre of the pelvis above the rectouterine pouch infiltrating the sigmoid colon (*arrowhead*). B, urinary bladder

(hyperintense in T2-weighted sequences) or postradiotherapy sequelae. Lastly, MR is able to evaluate the presence of residual neoplastic tissue or recurrences not only when larger than 1 cm, but also when smaller, thanks to the elevated signal intensity in T2-weighted sequences and the more-or-less marked enhancement in T1-weighted images, particularly in fat-saturated sequences after the administration of gadolinium-based contrast medium (Fig. 24.10). This broad range of parameters enables the MR study to even evaluate the possible involvement of adjacent structures, such as the parametrium and ovaries (if not removed), bladder and ureters and rectum and the muscular structures of the pelvic cavity, with greater sensitivity and specificity than CT.

The identification of regional lymph node metastases is essentially based on the criterion of size for both modalities (lymph node probably metastatic if short axis >1 cm). However, several preliminary studies using superparamagnetic iron oxide

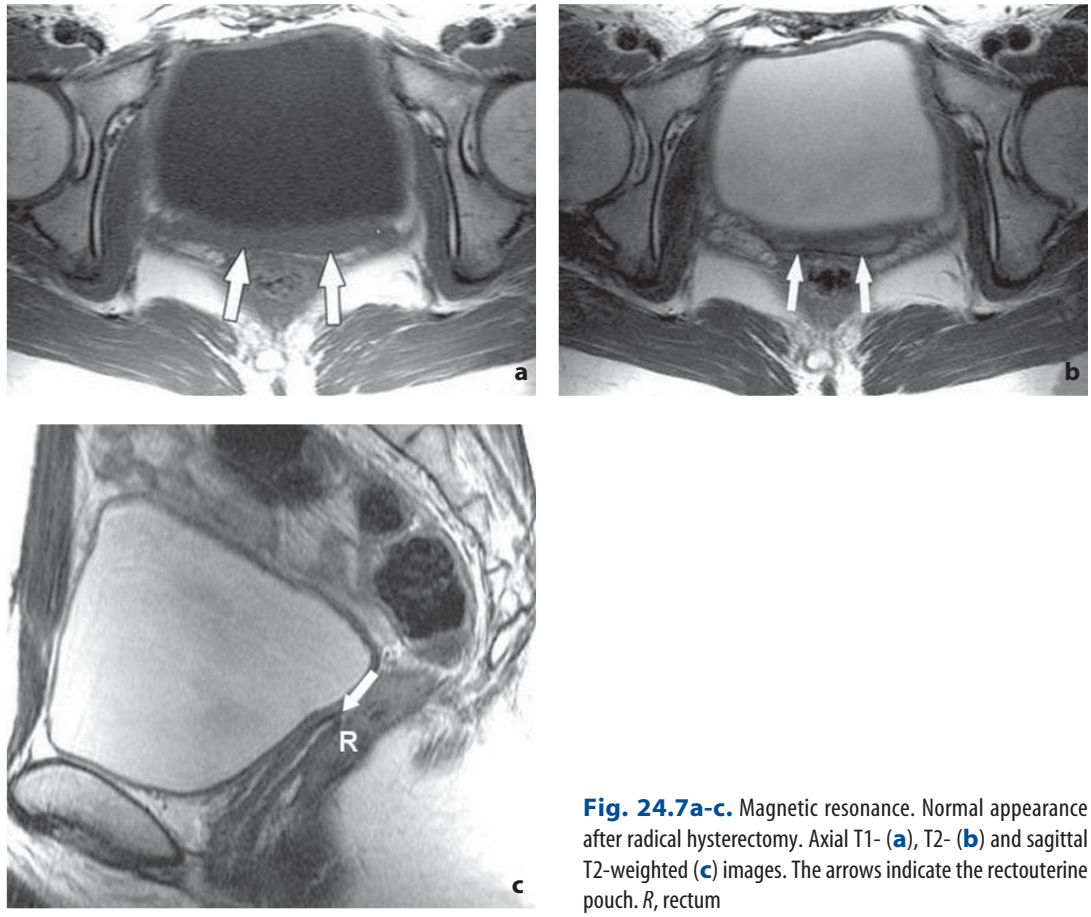

Fig. 24.7a-c. Magnetic resonance. Normal appearance after radical hysterectomy. Axial T1- (**a**), T2- (**b**) and sagittal T2-weighted (**c**) images. The arrows indicate the rectouterine pouch. *R*, rectum

(SPIO) nanoparticles indicate MR may be able to distinguish normal lymph nodes from those affected by tumor recurrence (**Fig. 24.11**). An important distinction which needs to be made in recurrences of endometrial or cervical cancer is whether lymph node involvement includes the primary stations (paracervical, parametrial, external iliac, hypogastric or obturator lymph nodes) or the secondary stations (common iliac, presacral, inguinal or para-aortic lymph nodes). This is because involvement of the latter has a significantly less favorable prognosis.

Fulcher AS, O'Sullivan SG, Segreti EM et al (1999) Recurrent cervical carcinoma: typical and atypical manifestations. RadioGraphics 19:S103-S116

Jeong YY, Kang HK, Chung TW et al (2003) Uterine cervical carcinoma after therapy: CT and MR imaging findings. RadioGraphics 23:969-981

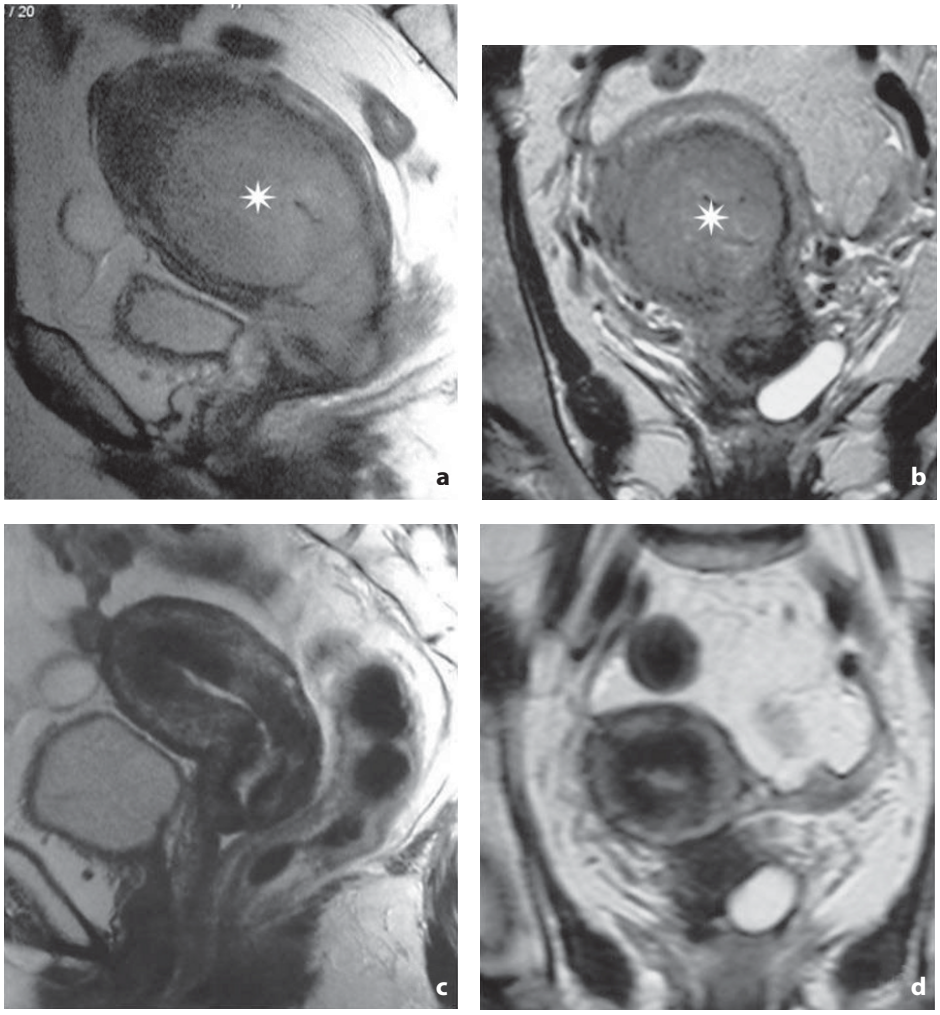

Fig. 24.8a-d. Magnetic resonance. Appearance after radiotherapy. Primary tumor (**a,b**) and after radiotherapy (**c,d**). The sagittal (**a**) and coronal (**b**) images show a large mass (asterisk) which extends from the endometrial cavity to the cervical canal. In the corresponding post-treatment images no signs of gross residual disease are identifiable

Reznek RH, Shadev A (2005) MR imaging in cervical cancer: seeing is believing. The 2004 Mackenzie Davidson Memorial Lecture, Br J Radiol 78:S73-S85

Sugimura K, Okizuka H (2002) Post-surgical pelvis: treatment follow-up. Radiol Clin N Am 40:659-680

Weber TM, Sostman HD, Spritzer CE et al (1995) Cervical carcinoma: determination of recurrent tumor extent versus radiation changes with MR imaging. Radiology 194:135-139

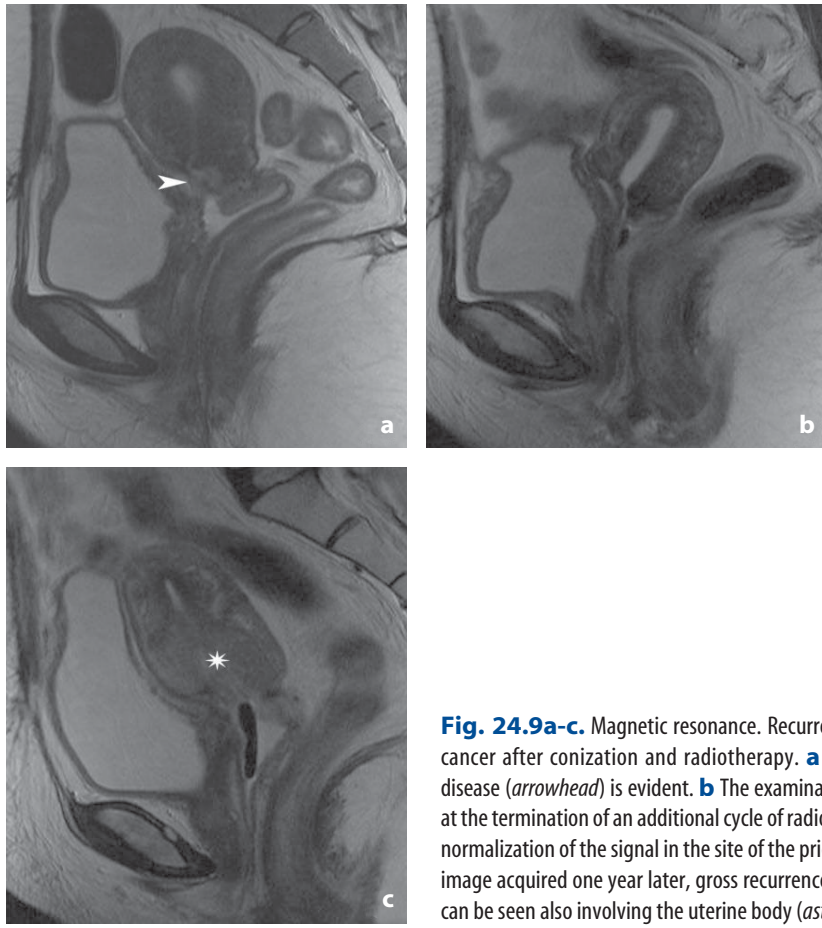

Fig. 24.9a-c. Magnetic resonance. Recurrence of cervical cancer after conization and radiotherapy. **a** Persistence of disease (*arrowhead*) is evident. **b** The examination performed at the termination of an additional cycle of radiotherapy shows normalization of the signal in the site of the prior lesion. In the image acquired one year later, gross recurrence of the disease can be seen also involving the uterine body (*asterisk* in **c**)

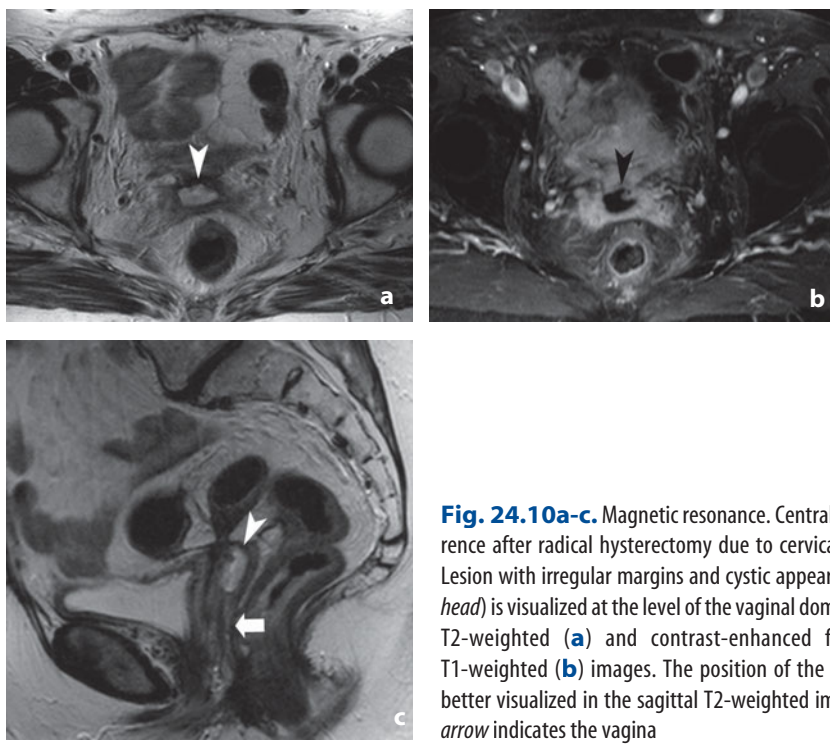

Fig. 24.10a-c. Magnetic resonance. Central pelvic recurrence after radical hysterectomy due to cervical carcinoma. Lesion with irregular margins and cystic appearance (*arrowhead*) is visualized at the level of the vaginal dome in the axial T2-weighted (**a**) and contrast-enhanced fat-saturated T1-weighted (**b**) images. The position of the recurrence is better visualized in the sagittal T2-weighted image (**c**). The *arrow* indicates the vagina

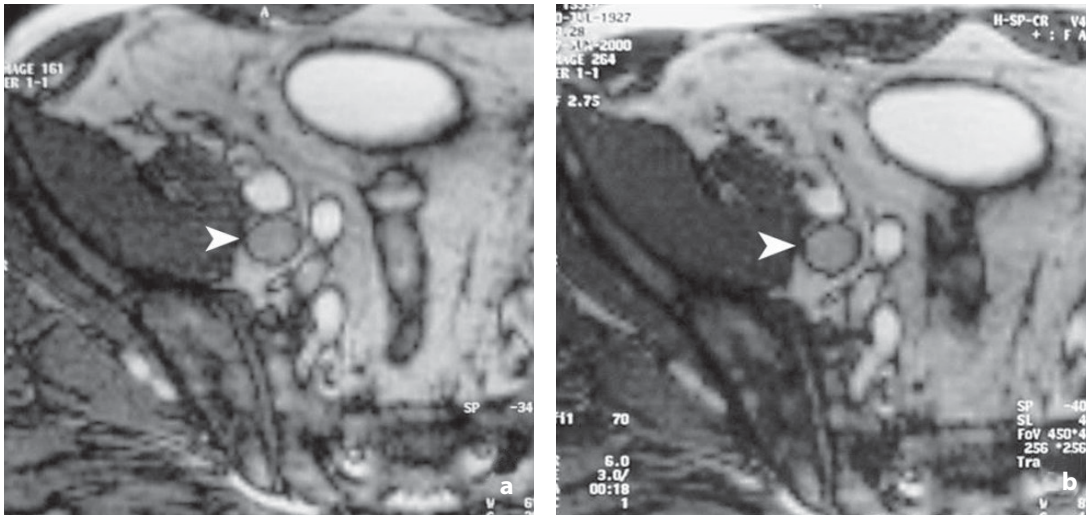

Fig. 24.11a,b. Magnetic resonance. Lymph node recurrence in patient operated on due to cervical cancer. At the level of the obturator chain a round lymph node (arrowhead) with borderline size and suspicious of metastasis can be identified in the image acquired prior to administration of USPIO (**a**). The contrast-enhanced image (**b**) shows no signal loss in the lymph node, indicating the complete replacement of healthy tissue with neoplastic growth

Recurrences of Vulvovaginal Malignancies

Recurrences of vulvovaginal malignancies is defined as the regional or distant reappearance of disease after a 6-month disease-free period. The frequency reported in the literature varies from 25% to 40%, partly due to the histology of the primary tumor (90-95% of cases are squamous cell carcinomas) and the stage of disease at diagnosis.

The most common sites of recurrence are the perineum and the inguinal and pelvic lymph nodes. Some 20% of recurrences manifest as distant and/or multiple implants, especially in patients with advanced disease at diagnosis.

In the case of exclusively perineal location, the treatment of choice is surgical excision, with reasonable prospects of survival (50% at 5 years). In the case of other sites, treatment (surgery or chemotherapy-radiotherapy) is palliative.

The techniques used in the identification and study of recurrences of vulvovaginal malignancies are CT and MR. The former is more commonly indicated in the study of distant lesions (lungs, liver), while the latter is better able to study local and regional recurrences thanks to its elevated contrast resolution (**Fig. 24.12**). Evaluation of the extent of the recurrences, in relation to adjacent organs is indispensable for correct preoperative planning. In this setting, contrast medium may be used to distinguish neoplastic tissue (characterized by postcontrast enhancement) from surgical and/or radiotherapeutic outcomes.

Maggino T, Landoni F, Sartori E et al (2000) Patterns of recurrence in patients with squamous cell carcinoma of the vulva. A multicenter CTF study. Cancer 89:116-122

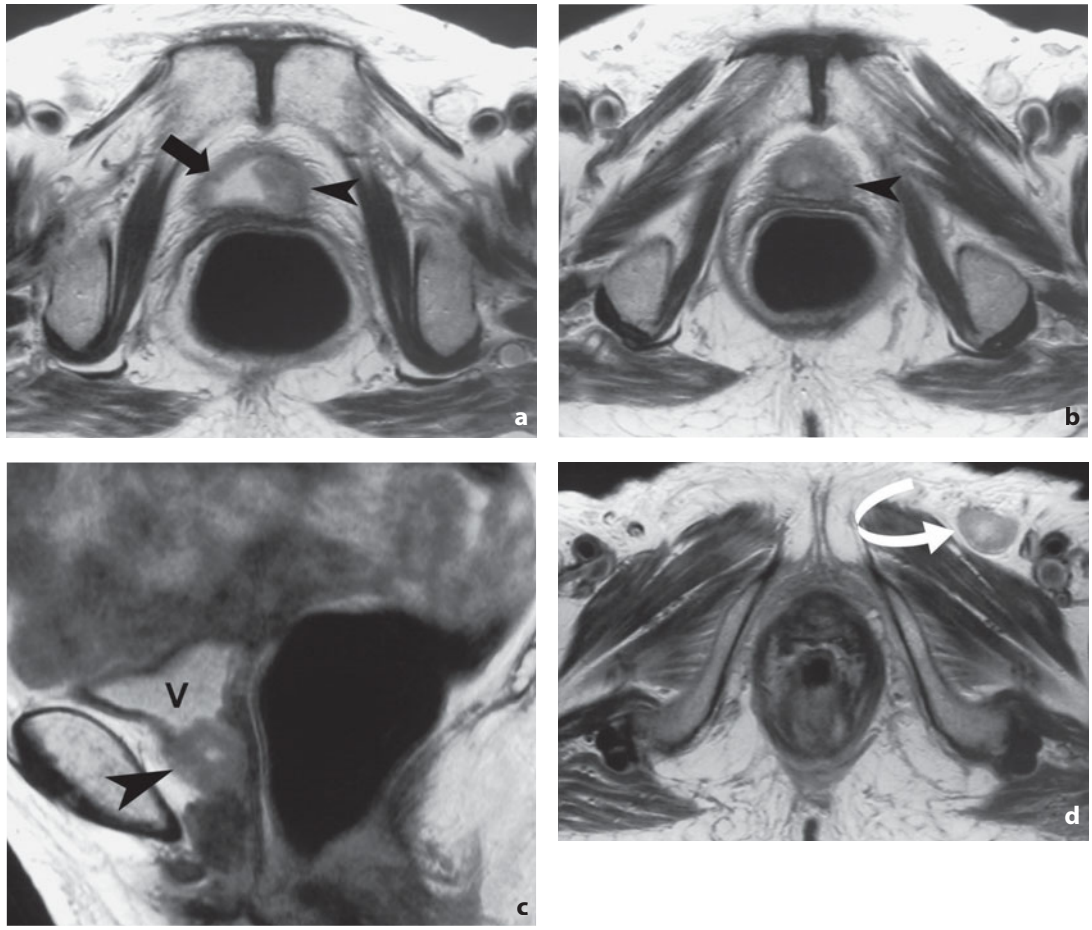

Fig. 24.12a-d. Magnetic resonance. Pelvic recurrence of vulvar cancer. The axial T2-weighted images (**a,b**) show a solid mass (*arrowhead*) invading the fundus and neck of the bladder (*arrow*). The finding is confirmed in the sagittal T2-weighted image (**c**). **d** Contrast-enhanced axial image acquired more caudally than the previous images shows left inguinal metastatic lymph nodes (*curved arrow*)

Part IX
Interventional Radiology

Prostate Biopsy

25

S. Cosciani Cunico, A. Moroni, G. Mirabella, C. Simeone

The clinical suspicion of prostate cancer requires histologic confirmation. In addition to the diagnosis, the biopsy correlated with other clinical parameters should also provide information on the local extent of disease to improve the clinical approach and facilitate the choice of the most appropriate treatment.

Prostate biopsy may also be required to better define the diagnosis of carcinoma encountered incidentally during transurethral resection of the prostate (TURP), or to identify local recurrence of disease following radical prostatectomy or radiotherapy.

Indications

The indications for performing a prostate biopsy may arise from abnormalities detected during digital rectal examination (DRE) of the prostate or transrectal ultrasonography (TRUS), or on the basis of serum levels of prostate specific antigen (PSA) and its derivatives.

The existence of a tumor may be suspected given DRE finding of increased consistency, asymmetry or loss of definition of the prostate margins. However, particularly in initial intracapsular states, many cases of malignant lesions produce no alterations in the consistency of the gland.

The typical US finding of a tumor consists of a hypoechoic area in the most peripheral portion of the gland. The possibility of prostatic carcinoma isoechoic to the surrounding parenchyma should not be underestimated.

An increase in PSA is currently the most objective parameter for indicating prostate biopsy. A value above 10 ng/mL is correlated with an incidence of prostate cancer between 40% and 60%. Even in the presence of a positive DRE and normal TRUS, patients with PSA >10 ng/mL are candidates for US-guided prostate biopsy whether symptomatic or not. One area which is still controversial is the indication for biopsy in the presence of a lower level of serum PSA. The extensive implementation of prostate biopsies in patients with PSA between 4 and 10 ng/mL (known as the gray zone) implies elevated costs given the large number of patients in this category, while returning only 10–25% of cases positive for carcinoma. To improve specificity a number of additional parameters have been proposed (PSA density, PSA velocity, PSA ratio, PSA transition zone, PSA doubling time). Of these the most reliable index for the early detection of prostate cancer in patients with PSA in the gray zone appears to be the PSA ratio, i.e. the ratio between free PSA and total PSA. Therefore, subjects with a PSA ratio >20% and serum PSA >4 ng/mL are also candidates for prostate biopsy.

It should also be borne in mind that there are factors which reduce the suspicion of prostate cancer, such as non-elevated PSA in relation to age (PSA age), a “stable” PSA over time (PSA velocity <0.75 ng/mL), total PSA between 4 and 10 ng/mL in patients with a large prostate. There are also a number of conditions which induce a chronic increase in PSA (e.g. indwelling catheter, chronic prostatitis).

L. Olivetti, L. Grazioli (eds.), *Imaging of Urogenital Diseases*,

Catalona WJ, Partin AW, Slawin KM et al (1998) Use of the percentage of free prostate-specific antigen to enhance differentiation of prostate cancer from benign prostatic disease: a prospective multicenter clinical trial. JAMA 20, 279:1542–1547

Catalona WJ, Smith DS, Ornstein DK (1997) Prostate cancer detection in men with serum PSA concentrations of 2.6 to 4.0 ng/mL and benign prostate examination. Enhancement of specificity with free PSA measurements. JAMA 277:1452–1455

Luboldt HJ, Swoboda A, Borgermann C et al (2001) Early Detection Project Group of the German Society of Urology. Clinical usefulness of free PSA in early detection of prostate cancer. Onkologie 24:33–37

Oesterling JE, Jacobsen SJ, Chute CG et al (1993) Serum prostate-specific antigen in a community-based population of healthy men. Establishment of age-specific reference ranges. JAMA 270:860–864

Sershon PD, Barry MJ, Oesterling JE (1994) Serum prostate-specific antigen discriminates weakly between men with benign prostatic hyperplasia and patients with organ-confined prostate cancer. Eur Urol 25:281–287

Smith DS, Catalona WJ (1994) Rate of change in serum prostate specific antigen levels as a method for prostate cancer detection. J Urol 152:1163–1167

Patient Preparation

Prostate biopsy is an invasive technique not without complications, which can nonetheless be prevented by observing the following precautions. It is crucial that patients stop antiplatelet therapy at least seven days prior to biopsy. Antiplatelet therapy should be replaced by subcutaneous injection of heparin. Antibiotic prophylaxis beginning from the day prior to the procedure is advisable. The biopsy is performed with local anesthesia is usually associated with or preceded by premedication with benzodiazepine and atropine.

Technique

Prostate biopsy can be performed with either a transrectal or transperineal approach.

The transrectal approach is generally performed with the patient in the left lateral decubitus position. Using longitudinal scans, samples are taken for each lobe in the parasagittal plane, at the level of the apex, the median line, the base and possibly also the transition zone, with an angle of 45°. The transrectal approach can be rapidly performed, is normally well tolerated by the patient and requires no local anesthesia. However, it does carry the risk of prostate infections and lesions to the rectum.

The transperineal approach is performed with the patient in the lithotomy position. Shaving and disinfection of the perineal region is required. The needle is inserted anterior to the anal margin at the height of the tendinous centre of the perineum (a poorly vascular and innervated area) until it reaches the posterior portion of the prostatic apex and passes through the gland towards the base, parallel to the rectal wall, according to a perpendicular plane with respect to the samples taken with the transrectal approach (**Figs. 25.1, 25.2**).

Regardless of the approach adopted, prostate biopsy requires US guidance. A transrectal transducer with needle guide is required, or alternatively a coaxial guide mounted on the US transducer can be used (**Fig. 25.3**). The biopsy gun (**Fig. 25.4**) consists of a spring-loaded needle (usually 18 gauge) with a side notch in the distal region and an external sheath which slides over the needle. When the gun is fired, the

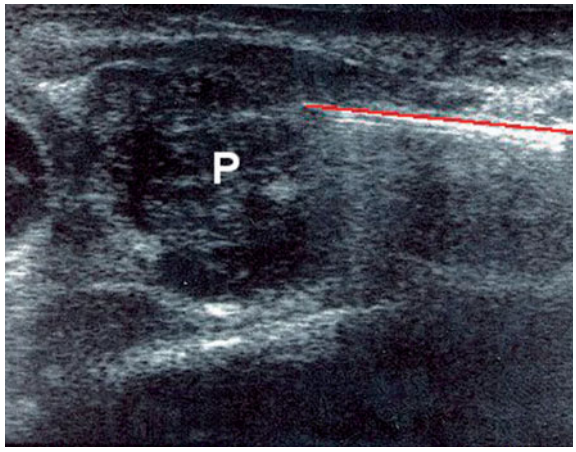

Fig. 25.1. Transperineal biopsy. The biopsy needle is shown in red. *P*, prostate

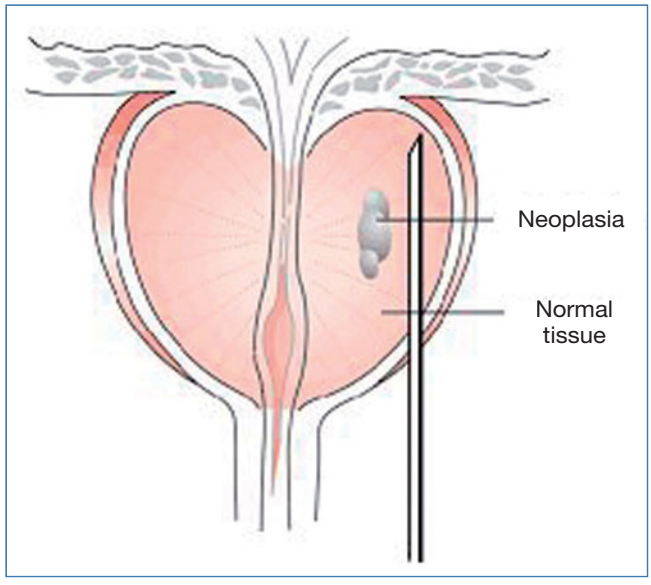

Fig. 25.2. Transperineal biopsy. Depiction of the approach to histologic verification of prostate cancer

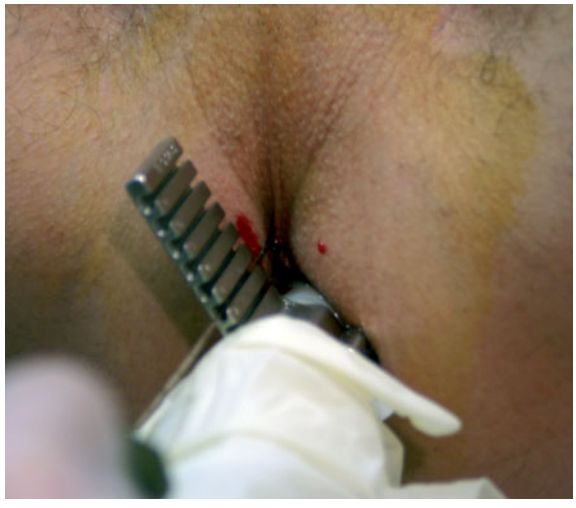

Fig. 25.3. Transperineal biopsy. Patient in the lithotomy position with sonographic transducer in the rectum

Fig. 25.4. Biopsy gun and needle

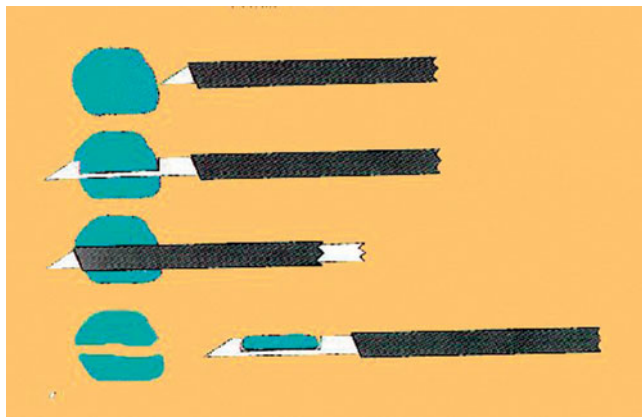

Fig. 25.5. Biopsy needle illustrating the mechanism of obtaining the needle core

sliding sheath opens once the needle enters the prostate and closes onto a sample of tissue then the needle is withdrawn. In this way a core of prostatic parenchyma remains in the side notch of the needle (**Fig. 25.5**). The biopsy cores obtained have a length of around 12–15 mm according to the type of needle used. The integrity, length and quality of the core should be evaluated, and if necessary the maneuver repeated. The cores are classified by site, fixed in formalin or pre-embedded in a tissue cassette or "sandwich", and sent to the pathology department for analysis.

The need to obtain multiple cores arises from the characteristics of the prostatic tumor, which often cannot be identified with digital rectal examination (DRE) or transrectal ultrasonography (TRUS).

Over the years a number of different biopsy schemes have been proposed. In 1989 Hodge proposed six cores (standard sextant biopsies) (**Fig. 25.6**). This approach was modified in 1995 by Stamey, who suggested more lateral cores than those indicated by Hodge (**Fig. 25.7**). The subsequent schemes have all involved more than six cores (**Figs. 25.8–25.11**). However, it is still not clear what the optimal number is. Even though simply doubling the number of cores –using the transrectal approach – is not enough to increase diagnostic accuracy, 10–12 cores are currently advised. This provides relatively good diagnostic accuracy, is well tolerated by the patient and enables a better definition of the histologic grade. The biopsy of several zones (apex,

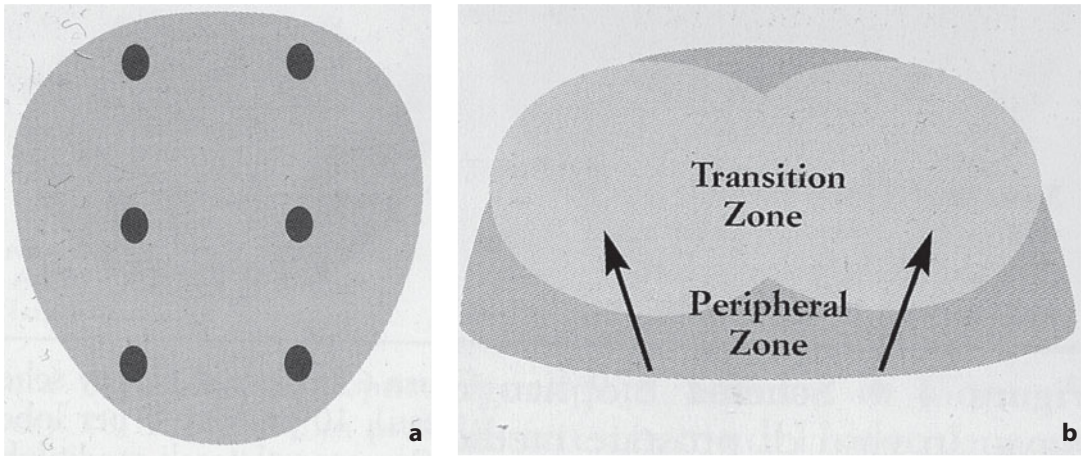

Fig. 25.6a,b. Biopsy scheme according to Hodge (Gruppo Italiano per la Redazione delle Linee Guida per la Biopsia Prostatica. Foreword to the prostate biopsy guidelines. EDIMES 2005)

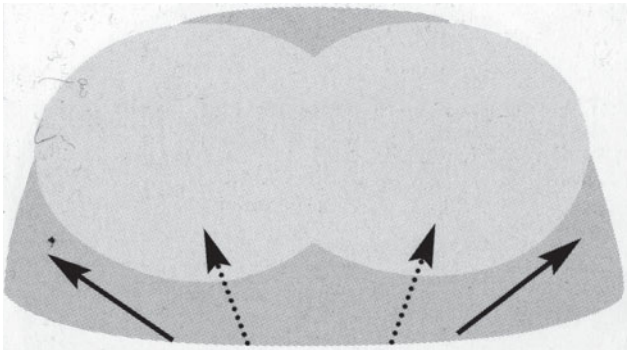

Fig. 25.7. Biopsy scheme according to Stamey (Gruppo Italiano per la Redazione delle Linee Guida per la Biopsia Prostatica. Foreword to the prostate biopsy guidelines. EDIMES 2005)

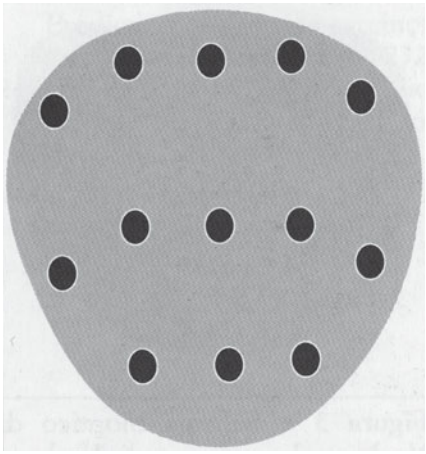

Fig. 25.8. Biopsy scheme according to Eschew, "five regions" (Gruppo Italiano per la Redazione delle Linee Guida per la Biopsia Prostatica. Foreword to the prostate biopsy guidelines. EDIMES 2005)

transition zone and seminal vesicles) can be particularly important in planning the most appropriate therapy.

There is a certain amount of scientific evidence to suggest performing biopsies targeted at hypoechoic areas of the peripheral zone in addition to the traditional sextant biopsies. In contrast, biopsies targeted at hypoechoic areas in addition to extensive mapping with ten or more cores do not appear to increase diagnostic

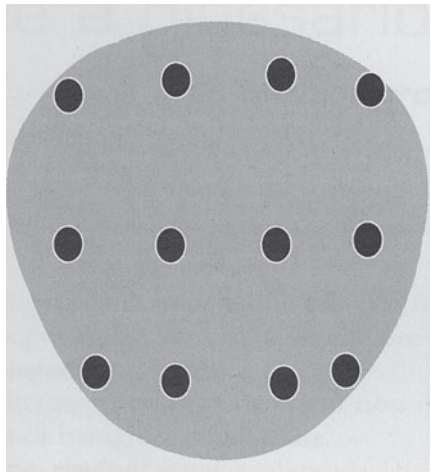

Fig. 25.9. Biopsy scheme according to Gore (Gruppo Italiano per la Redazione delle Linee Guida per la Biopsia Prostatica. Foreword to the prostate biopsy guidelines. EDIMES 2005)

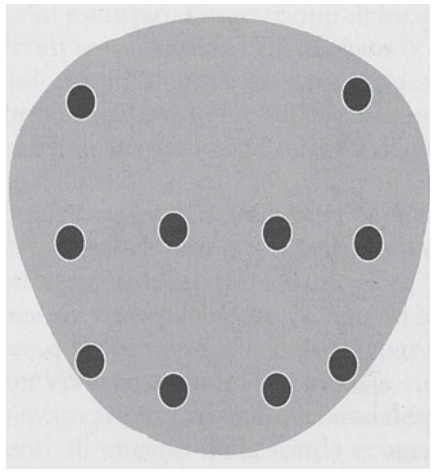

Fig. 25.10. Biopsy scheme according to Presti (Gruppo Italiano per la Redazione delle Linee Guida per la Biopsia Prostatica. Foreword to the prostate biopsy guidelines. EDIMES 2005)

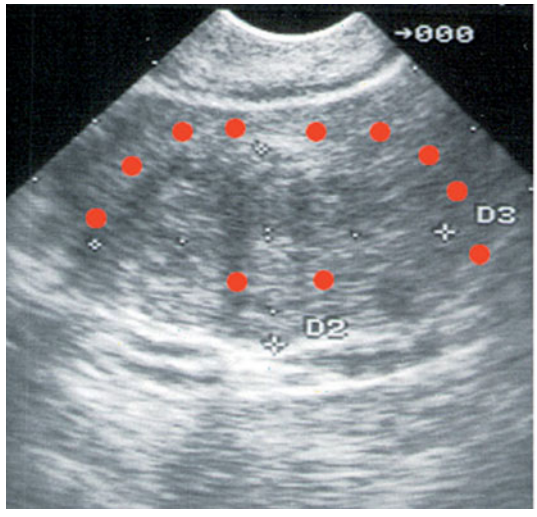

Fig. 25.11. Transperineal biopsy scheme

accuracy. There is little evidence in favor of additional biopsies targeted at suspicious zones from color Doppler.

There is evidence in favor of biopsy schemes which involve performing a number of cores in relation to prostate volume. The risk of a biopsy error is significantly correlated with volume, although the advantage of further increasing (>12) the number of cores in the case of large prostates has still not been defined by appropriate studies.

Biopsy of the transition zone should not be performed in the first instance, but rather reserved especially for patients with previous negative biopsies and high serum PSA levels.

Hodge KK, McNeal JE, Terris MK et al (1989) Random systematic versus directed ultrasound guided transrectal core biopsies of the prostate. J Urol 142:71–74; discussion 74–75

Lemaître L, Villers A, Mouton D et al (2006) Echographie et biopsies de prostate. J Radiol 87 (2 Pt 2):201–209

Rifkin MD, Kurtz AB, Goldberg BB (1983) Sonographically guided transperineal prostatic biopsy: preliminary experience with a longitudinal linear-array transducer. AJR Am J Roentgenol 140:745–747

Stamey TA (1995) Making the most out of six systematic sextant biopsies. Urology 45:2–12

Takenaka A, Hara R, Hyodo Y et al (2006) Transperineal extended biopsy improves the clinically significant prostate cancer detection rate: a comparative study of 6 and 12 biopsy cores. Int J Urol 13:10–14

Vis AN, Boerma MO, Ciatto S et al (2000) Detection of prostate cancer: a comparative study of the diagnostic efficacy of sextant transrectal versus sextant transperineal biopsy. Urology 56:617–621

Complications

Prostate biopsy with multiple cores is a safe procedure which is well tolerated by most patients. Nonetheless there are associated minor complications (pain, mild blood loss from the urethra or rectum, hemospermia, or hematuria) in 17–40% of cases, and major complications (hyperpyrexia, sepsis, massive hematuria, acute urinary retention, prostatitis) in 2–3% of cases.

The minor complications rarely have clinical importance and often clear up in several days. Infectious complications are more common with the transrectal approach, although thanks to antibiotic prophylaxis they are relatively low.

Inflammatory complications with edema of the gland and acute urinary retention (which involves the placement of a bladder catheter) increases with the number of cores, particularly those in the transition zone.

Treatment of Varicocele 26

G.P. Cornalba, G. Giordano

Introduction

Dilatation of the pampiniform plexus, commonly defined varicocele, is a relatively frequent condition in the male population, which is often associated with infertility and dyspermia (30-45%). It is caused by an inversion in flow in the internal spermatic vein which empties on the left into the renal vein and on the right directly into the inferior vena cava. In 85% of cases the varicocele involves the left spermatic vein, for anatomic reasons: venous reflux occurs more commonly through the internal spermatic vein or through the dilated collateral branches which anastomose with the renal vein, and more rarely from tributary venous branches of the lumbar veins, the inferior vena cava or the iliac veins.

The association between male infertility and varicocele has been well documented in the literature. Varicocele is in fact found in 20-40% of infertile males.

In the case of infertility only a correction of the varicocele can lead to improvement in the quality of the seminal fluid.

Diagnostic imaging appears indispensable in the study of varicocele and is carried out with color Doppler and venography, the latter having both diagnostic and interventional capabilities.

Chakraborty J, Hikim AP, Jhunijhunwala JS (1985) Stagnation of blood in the microcirculatory vessels in the testes of men with varicocele. J Androl 6:117–126

Cohen MS, Plaine L, Brown JS (1975) The role of internal spermatic vein plasma catecholamine determination in subfertile men with varicocele. Fertil Steril 26:1243–1249

Laven JS, Haans LC, Mali WP et al (1992) Effects of varicocele treatment in adolescents: a randomized study. Fertil Steril 58:756–762

Ultrasonography

Ultrasonography (US) examination associated with color Doppler enables precise measurement of the size of the pampiniform plexus and evaluation of the flow of the spermatic vein.

The evaluation should be performed with the patient both supine and upright, before and after the Valsalva maneuver.

Five types of varicocele have been classified according to their anatomic variants (**Table 26.1**). In the past the diagnosis of varicocele was made with the B-mode US examination by evaluating only the diameter of the pampiniform plexus, which needs to be greater than 3 mm. Today the use of color Doppler is indicated to correctly quantify the venous reflux, which needs to be prolonged for more than 2 s.

The color Doppler classification of the grades of varicocele by Sarteschi takes into account the characteristics of the reflux, its duration and the changes it undergoes during the Valsalva maneuver (**Table 26.2**).

L. Olivetti, L. Grazioli (eds.), *Imaging of Urogenital Diseases*,

Table 26.1. Anatomic variants of left varicocele

I	Solitary testicular vein without valves
II	Retroperitoneal collateral branches to the ascending lumbar vein and/or retroaortic vessels contiguous to the lumbar vein which empty into the inferior vena cava
III	Subdivision of the internal spermatic vein in to two main parallel branches with collateral vessels in between
IV	Collateral circulation afferent to the renal and/or perirenal veins
V	Bifurcated renal vein passing anterior and posterior to the aorta

Table 26.2. Color Doppler classification of varicocele

Grade 1	Prolonged reflux in the vessels of the inguinal canal only during the Valsalva maneuver
Grade 2	Small posterior varicosities reach the upper pole of the testicle and increase in diameter during the Valsalva maneuver. Color Doppler shows evident venous reflux in the supratesticular region only during the Valsalva maneuver
Grade 3	Vessels appear dilated up to the lower pole of the testicle when the patient is standing, whereas no dilatation is evident with the patient in the supine position. Color Doppler shows evident reflux only during the Valsalva maneuver
Grade 4	Venous dilatation identifiable with the patient both standing and supine. The dilatation increases with the patient standing and during the Valsalva maneuver
Grade 5	Presence of patent venous dilatation in both the prone and supine position. Color Doppler shows significant baseline venous reflux which does not increase after the Valsalva maneuver

Liguori G, Trombetta C, Garaffa G et al (2004) Color Doppler ultrasound investigation of varicocele. World J Urol 22:378–381

Sarteschi LM, Paoli R, Bianchini M et al (1993) Lo studio del varicocele con eco-color-Doppler. Giornale Italiano di Ultrasonologia 4:43-49

Endovascular Procedure

Although venography has been sidelined in terms of its diagnostic role, which today is brilliantly performed by US, the technique has been proposed as one of the possible therapeutic options for the treatment of varicocele. In fact, not only is venography minimally invasive, but it is also highly effective and comparable to surgery.

Prior to the procedure analysis of the seminal liquid needs to be performed (concentration, percentage of motility and normal morphology) as well as clinical evaluation possibly associated with color Doppler study (**Fig. 26.1**).

The percutaneous technique can be performed as an outpatient procedure in all cases of varicocele types I and III, and in types II and IV if the catheter can be inserted up to the inguinal ligament proximal to the collateral branches. However, given the difficulty of catheterization in type V varicocele, the percutaneous procedure is reserved only for select cases.

The technique is carried out with puncture of the right femoral vein, brachial vein or jugular vein in conditions of local anesthesia.

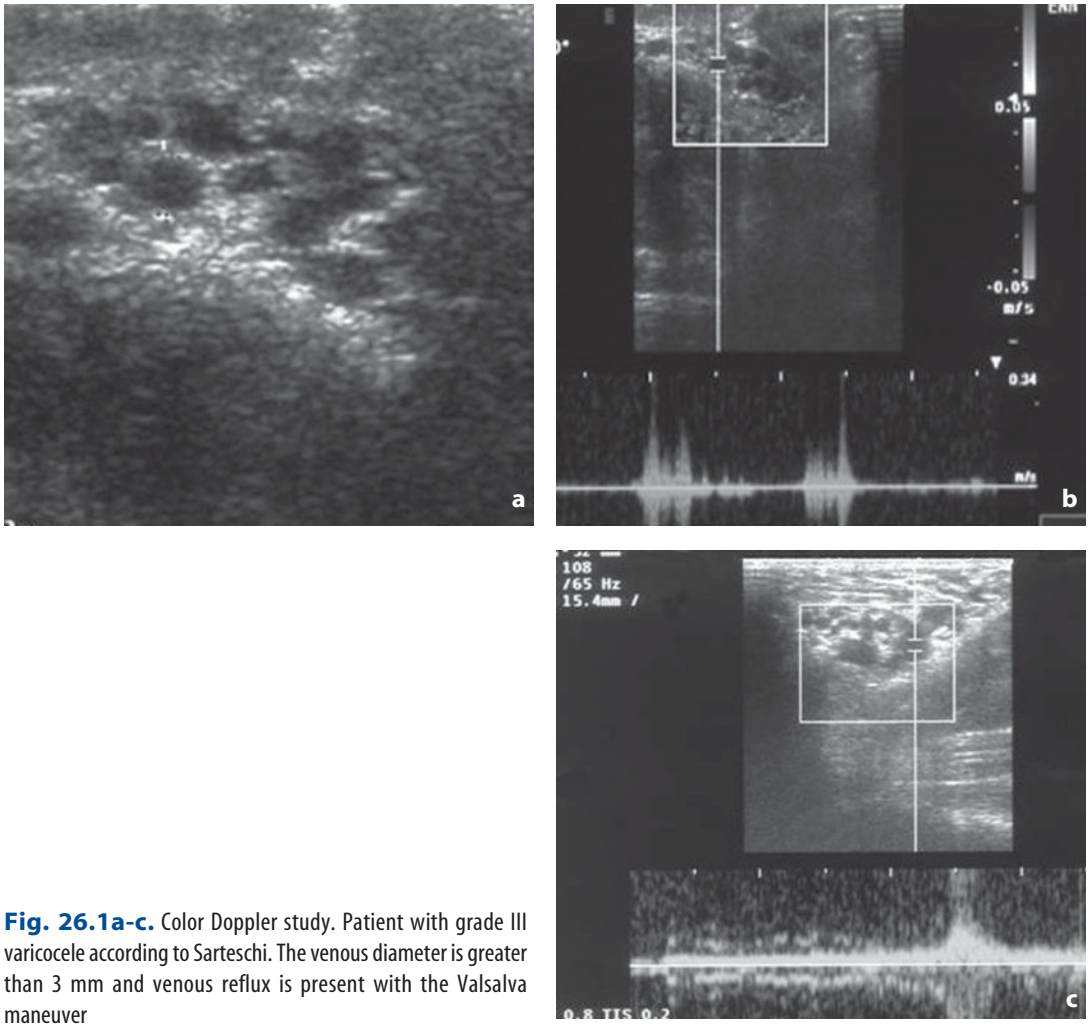

Fig. 26.1a-c. Color Doppler study. Patient with grade III varicocele according to Sarteschi. The venous diameter is greater than 3 mm and venous reflux is present with the Valsalva maneuver

The left internal spermatic vein is selectively catheterized. The preferred catheters are the Cobra type, whereas in the event of treatment of the right spermatic vein a Simmons catheter is preferred when the access is transfemoral. If instead the approach is transjugular or transbrachial, a multipurpose catheter can be successfully used.

Venography is done by having the patient carry out the Valsalva maneuver and performing views at 30°, using 7–15 mL of contrast medium at 5 mL/s. The treatment to be adopted is decided based on the type of varicocele found. The most commonly used methods in the percutaneous treatment of varicocele are mechanical occlusion with Gianturco spirals, detachable balloons or the use of sclerosing agents. The most widely used sclerosing agent is polydocanol (Atossisclerol) (**Fig. 26.2**). The others include sodium tetradecyl sulfate and hypertonic glucose solution (70–80%) with monoethanolamine and absolute ethanol. The use of glues (NBCA) has also been described, which have the advantage of reducing the risk of phlebitis of the pampiniform plexus in the event of overly distal embolization.

During administration of the sclerosing agent and contrast medium, it is advisable to have the patient perform a compression with their hands at the level of the inguinal ring to prevent possible flow of the sclerosing agent into the pampiniform plexus itself.

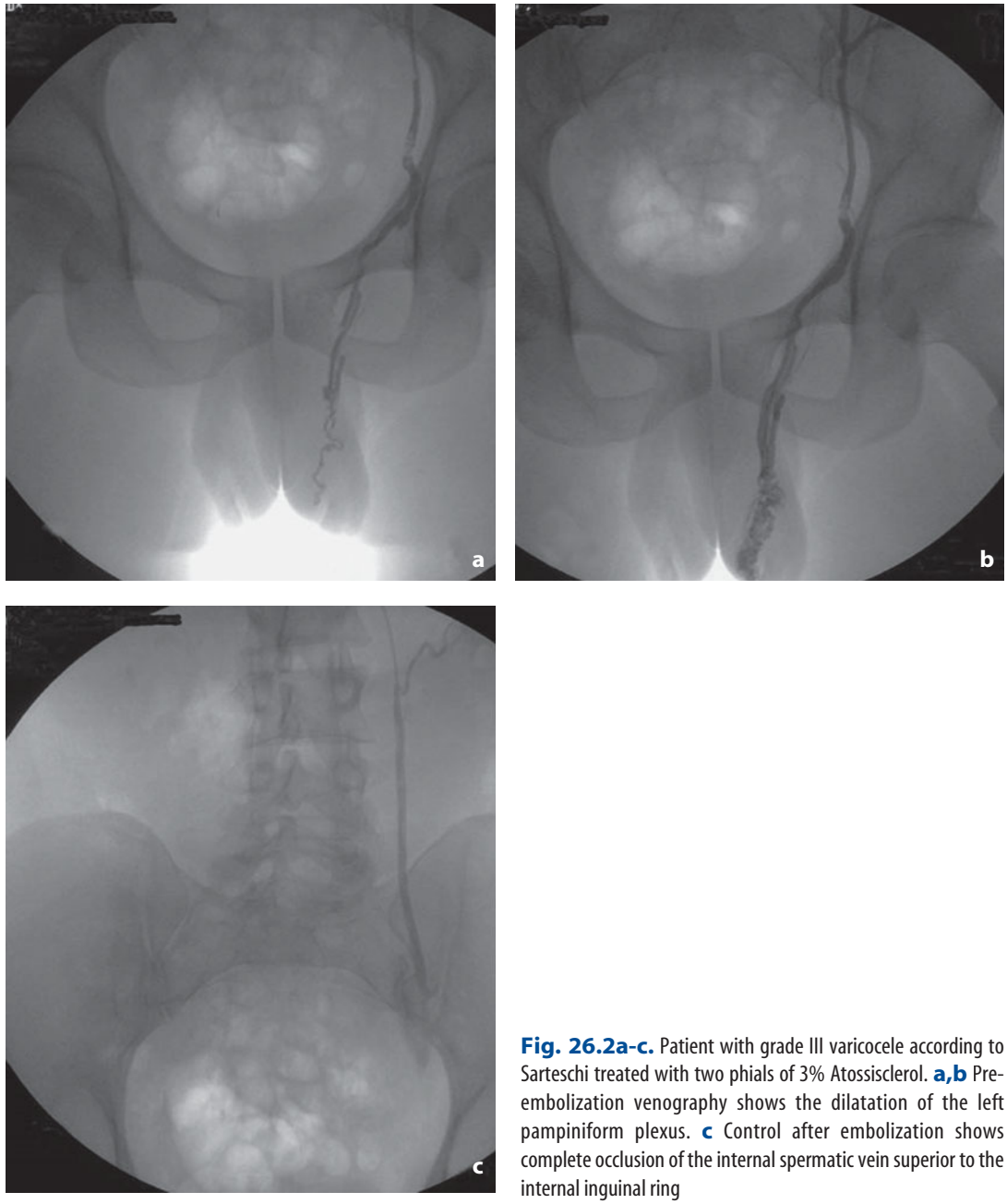

Fig. 26.2a-c. Patient with grade III varicocele according to Sarteschi treated with two phials of 3% Atossisclerol. **a,b** Pre-embolization venography shows the dilatation of the left pampiniform plexus. **c** Control after embolization shows complete occlusion of the internal spermatic vein superior to the internal inguinal ring

The use of spirals or detachable balloons reduces embolization times. However, they are not indicated when a rich collateral network is present due to the risk of early recurrence. In these cases the use of sclerosing agents is required.

The combined use of spirals and sclerosing agents in the same procedure is also possible in select cases (Fig. 26.3).

Complications of endovascular embolization of varicocele are relatively infrequent. The most severe include very rare phlebothrombosis of the pampiniform plexus and the venous districts anastomosing with the internal spermatic vein, and possible migration of the sclerosing agent into the systemic circulation. The rate of recurrence reported in the literature is between 10% and 15%.

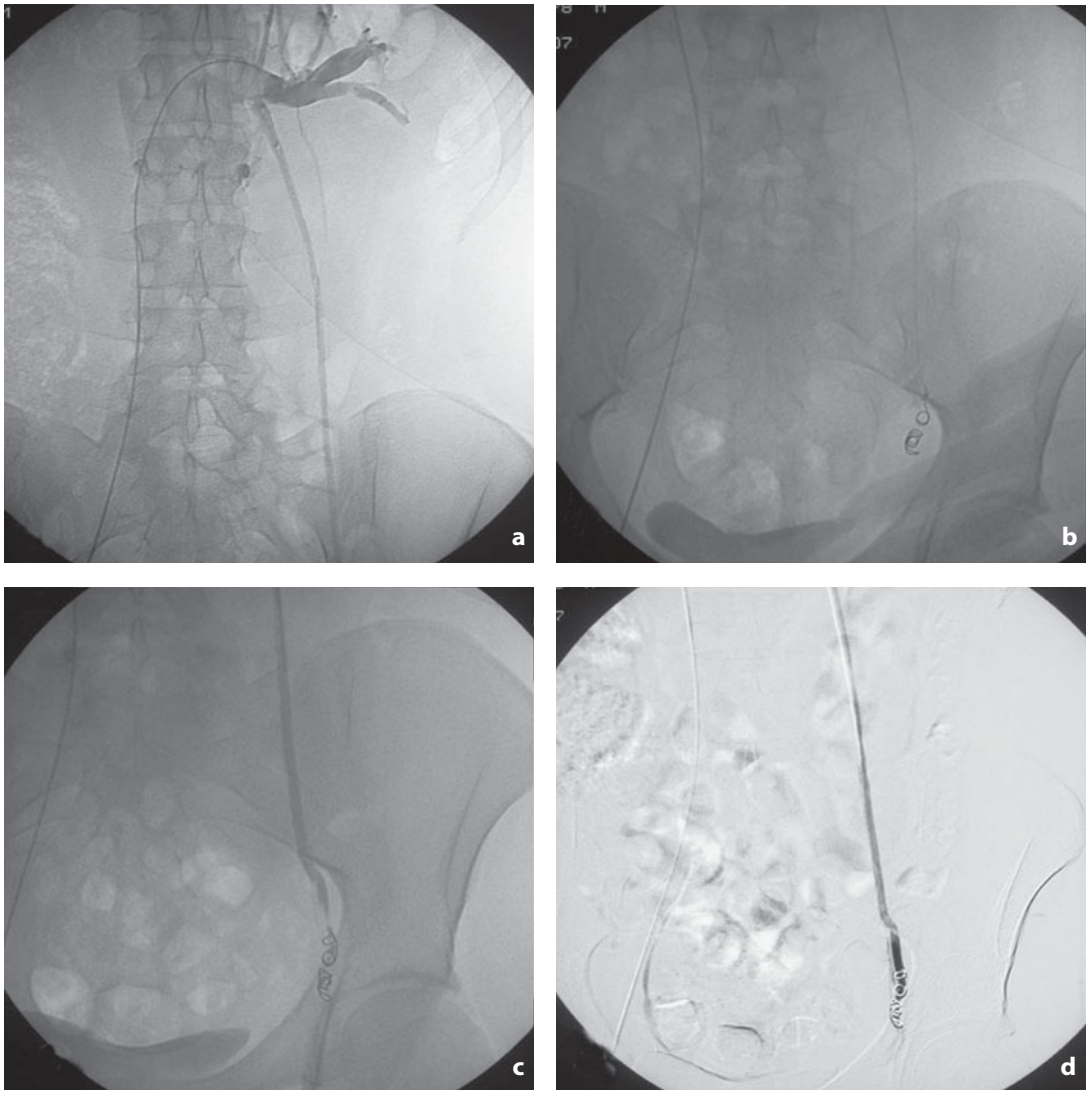

Fig. 26.3a-d. Combined endovascular therapy of varicocele. **a** Venography shows the regular origin of the internal spermatic vein from the left renal vein. **b** Embolization with metal spirals 3 mm in diameter and 20 mm in length. **c** Administration of 3% Atossisclerol with contrast medium. **d** Final control shows the complete occlusion of the internal spermatic vein superior to the inguinal ring

Careful attention needs to be paid to fluoroscopy times to reduce to a minimum the exposure of the gonads to ionizing radiation. Collimation should also be adjusted to limit the field to the anatomic region of interest.

Once the embolization procedure has been completed, there are no special instructions for the patient: bed rest for 48 h and abstention from physically demanding activities for 15–20 days is advisable. In addition, prophylactic antibiotic therapy is prescribed for five days and analgesics when required.

Follow-up generally involves a simple color Doppler study one month after the procedure to assess the complete embolization of the pampiniform plexus or the presence of collateral vessels in a possible recurrence, and an analysis of the seminal liquid at 3 months.

Bach D, Bahren W, Gall H et al (1988) Late results after sclerotherapy of varicocele. Eur Urol 14:115–119

Belgrano E, Puppo P, Quattrini S et al (1984) The role of venography and sclerotherapy in the management of varicocele. Eur Urol 10:124–129

Di Bisceglie C, Fornendo R, Grosso M et al (2003) Follow up of varicocele treated with percutaneous retrograde sclerotherapy: technical, clinical and seminal aspects. J Endocrinol Invest 26:1059–1064

Pisco JM, Basto I, Batista AM et al (1992) Percutaneous sclerotherapy of varicocele. Acta Med Port 5:477–481

Drainage and Embolization Techniques

27

G.P. Cornalba, G. Giordano

Introduction

The first step in urinary interventional procedures was made by Goodwin when in 1955 he developed the procedure of percutaneous nephrostomy. Since then interventional procedures for the urinary tract have multiplied such that today, with the contribution made by new technology, they range from percutaneous nephrostomy to ureteric stenting, from ureteroplasty to the treatment of renal and/or vesical bleeding caused by trauma or inoperable neoplasm.

Goodwin WE, Casey WC, Woolf W (1955) Percutaneous trocar (needle) nephrostomy in hydronephrosis. JAMA 157:891-894

Percutaneous Nephrostomy

Percutaneous nephrostomy is a procedure that is done in the presence of hydronephrosis with supravesical obstruction causing anuria, to avoid acute kidney failure with irreversible damage to the nephrons. It can be performed to guarantee access to the renal collecting system during diagnostic and therapeutic procedures (e.g. the treatment of renal or ureteric calculi) or during the waiting period prior to surgery for ureteric stricture or fistula or with palliative purposes in inoperable patients.

This outpatient procedure has a percentage of technical success, reported in the literature at around 95% when dilatation of the pelvicaliceal system is present. It may also be performed with the pelvicaliceal cavity non-dilated, with a percentage of technical success of 90% for an expert operator.

A number of preliminary blood tests are indispensable, such as hematocrit, coagulation profile and kidney function. If the patient is undergoing antiplatelet therapy, this should be interrupted at least one week prior to the procedure. Percutaneous nephrostomy is usually performed with local anesthesia (20 mL of lidocaine) and disinfection of the skin at the site of the puncture. Anxiolytic agents such as diazepam (5-10 mg) may be administered.

The patient should be in the prone or prone-oblique position with the ipsilateral side inclined by 20-30 degrees.

Puncture of the pelvicaliceal cavity may be performed normally with fluoroscopic guidance. Ultrasonography (US) may be used to precisely monitor the trajectory of the needle in real time. Rarely and in select cases, computed tomography (CT) guidance may also be used.

The puncture should be aimed at a calix of the lower pole along the posterolateral half of the kidney to avoid the hilar vessels.

When performing the procedure the renal anatomy, and in particular the vasculature, should be borne in mind. Indeed the diameter of the arterial vessels decreases in proximity to the cortex, and at about 1-2 cm from the lateral renal margin there is a line,

L. Olivetti, L. Grazioli (eds.), *Imaging of Urogenital Diseases*,

known as the Brodel line, which bounds an area of reduced parenchymal vascularity.

Puncture towards the lower pole avoids the transpleural passage. Occasionally, however, higher access can be useful, as in cases of the removal of calculi. Nonetheless, the point of access should not be above the 12th rib.

In the case of puncture of a transplanted kidney the approach is anterior, oblique caudocranially and lateromedially, with the patient supine. Special attention needs to be paid to the adjacent hollow organs.

The puncture may be done with either a Chiba or trocar needle.

Using the former – a thin 21/22 gauge needle – the kidney is punctured by directing the needle towards the pelvicaliceal cavity of the lower pole. The stylet is removed and, maintaining aspiration, the sheath is withdrawn and urine should flow from the needle. Then with the opacification of the upper urinary tract by contrast medium a 0.018" guidewire is passed over the needle, the needle is removed and a coaxial kit consisting of three pieces (an external sheath and two internal supports, one plastic and the other metallic) is placed over the guidewire. Only the external plastic sheath of the kit is left in place and a 0.035" or 0.038" guidewire is inserted, upon which the drainage tube is positioned.

Puncture with a trocar needle is performed with a 5-8 French needle catheter consisting of a catheter mounted on a rigid support with stylet.

The 7-8 French nephrostomy drainage catheter is usually a pigtail catheter if positioned in the pelvis (**Fig. 27.1**) or a straight-end catheter if positioned in the ureter.

It is advisable to make repeated passages with fascial dilators of increasing diameter in the event of particular resistance to the introduction of the drainage catheter. If it needs to remain in place for a lengthy period, it is best replaced with catheters of a greater diameter. In this case a nephrostomy tube up to 10-12 French can be used, which should be substituted every 3-6 months to avoid encrustation.

Hemorrhagic complications are relatively infrequent, although a small amount of bleeding manifesting as hematuria in the first 48 h after the procedure is not uncommon. The hematuria generally resolves spontaneously; in case should it not then there are a number of steps which can be taken, e.g. washing with cold physiologic solution and substituting the drain with a larger-diameter catheter.

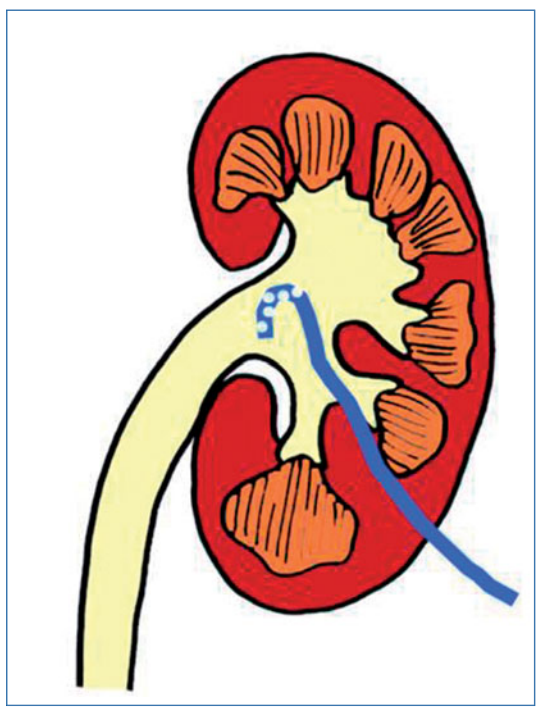

Fig. 27.1. Diagram of percutaneous nephrostomy. The drainage catheter is introduced via an inferior caliceal group

Should the hemorrhagic complication persist with a fall in hematocrit, a possible vascular cause should be suspected, such as laceration of a vessel with subcapsular hematoma, or formation of a pseudoaneurysm or an iatrogenic arteriovenous fistula. The US or CT demonstration of such lesions requires a subsequent angiography be performed to proceed with the necessary embolization.

Sepsis occurs in 1.4-21% of cases and is by far more common in patients with pyonephrosis, for whom antibiotic prophylaxis is advisable.

Less frequent complications include pneumothorax, puncture of the bile ducts, formation of urinomas and lesions of the intercostal arteries.

Barbaric ZL (1984) Percutaneous nephrostomy for urinary tract obstruction. AJR Am J Roentgenol 143:803-809

Barbaric ZL, Hall T, Cochran ST et al (1997) Percutaneous nephrostomy: placement under CT and fluoroscopy guidance. AJR Am J Roentgenol 169:151-155

Dyer RB, Regan JD, Kavanagh PV et al (2002) Percutaneous nephrostomy with extensions of technique: step by step. RadioGraphics 22:503-525

Farrel TA, Hicks MS (1997) A review of radiologically guided percutaneous nephrostomies in 303 patients. J Vasc Interv Radiol 8:769-774

Ureteric Stenting

Ureteric stenting is performed in the treatment of both benign and malignant constrictive-obstructive disease to re-establish the patency of the ureter itself.

Benign disease includes stricture due to postinflammatory fibrosis, removal of calculi and trauma, as well as disease secondary to retroperitoneal fibrosis, where the stent is able to delay surgery in the wait for the results of medical therapy.

In the setting of malignant disease, which today is the most common indication, the stent may be used in the wait for surgery or during radiotherapy or chemotherapy to safeguard renal function. In the case of patients with no likelihood of undergoing radical surgery, the procedure may be considered palliative and replaces more invasive treatment such as ureterocutaneostomy or ureteroileostomy.

Special indications include iatrogenic fistula subsequent to gynecologic or urologic procedures or procedures on the colon. Stent placement makes closure of the fistula possible in most cases.

The success rate reported for the procedure is 75% in the case of malignant lesions and 60% in the case of a damaged ureter.

Most ureteric stents are placed in a retrograde fashion. Antegrade stent implantation is preferable when percutaneous manipulation is already required, such as in lithiasis (**Fig. 27.2**), or when the retrograde approach fails.

When electively performed, ureteric stenting is preferably done around one week after nephrostomy. The nephrostomy catheter is replaced by an angiographic introducer, possibly with a reinforced sheath, and a cobra 5 F angiographic catheter is passed over it. A guidewire – usually a 3 mm J-tipped wire – is inserted into the catheter and used to negotiate the stricture or obstruction.

Today hydrophilic guides are indicated in place of metal ones since they involve less trauma and are better able to push through tight strictures.

Once the stricture or obstruction has been passed, the catheter is advanced into the urinary bladder. At this stage the first guide is replaced with a second more rigid guide, e.g. Amplatz stiff/superstiff. The stent is then placed over this and advanced by an appropriate pushing catheter.

The most commonly used ureteric stent is the double-J type, the proximal and distal ends of which are coiled with multiple holes (**Fig. 27.3**). The proximal end is placed in the renal pelvis and the distal end in the bladder. At this point the guidewire is removed.

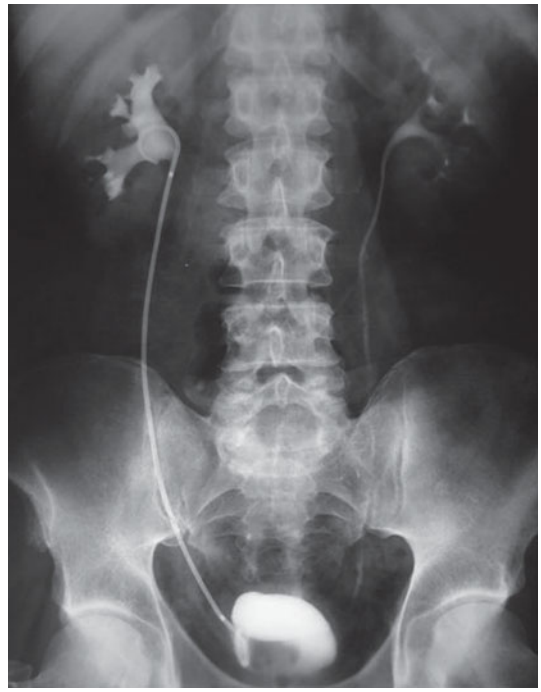

Fig. 27.2. Urography. Control of the position of right ureteric stent in benign disease. The stent appears patent and the renal pelvis is not dilated

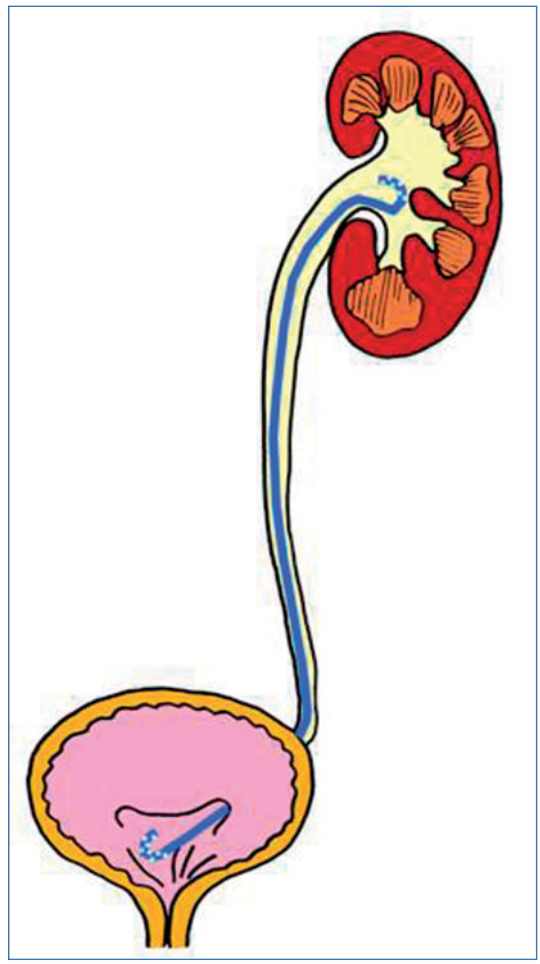

Fig. 27.3. Diagram of ureteric stenting. The stent is positioned normally with its ends placed in the inferior caliceal group and the urinary bladder

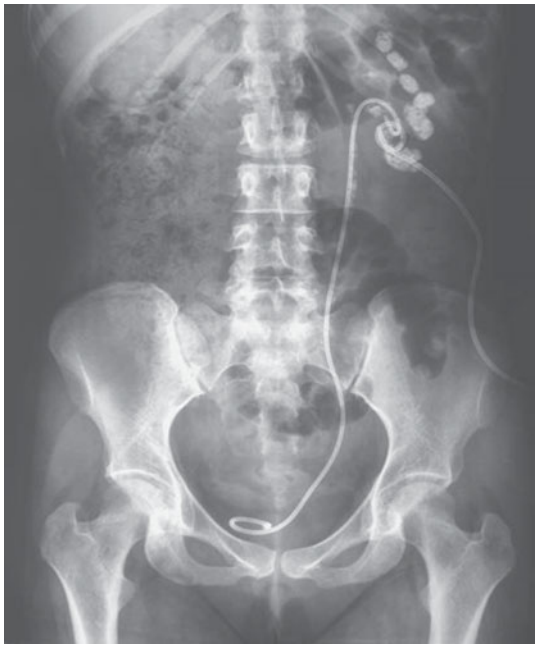

Fig. 27.4. Plain abdominal film. Patient with left renal and ureteric calculosis. Control after the placement of ureteric stent and percutaneous nephrostomy

Initially an external catheter is always left in the renal pelvis, usually the same one used as a pushing catheter, for the purpose of performing a pyelography to assess the patency of the stent and to maintain an access if should blood or other material cause obstruction of the stent (**Fig. 27.4**). The catheter is kept open for 12 h and subsequently closed.

If there are no complications the external catheter may be removed 6–12 h later. In contrast, if the presence of blood is observed, the external catheter is left in place to perform lavage until the problem is resolved.

Ureteric stents commercially available today maintain patency (12 months on average) better than in the past. Their substitution can therefore be put off over time.

US follow-up performed every 2–3 months is advisable. In the case of suspected occlusion, dynamic scintigraphy should be performed or the stent directly replaced. This is nonetheless advisable every 6–8 months and obviously in all cases of dislocation or unresolved obstruction (**Fig. 27.5**).

The procedure is encumbered by the risk of infection, for which prophylactic antibiotic therapy may be advisable. Complications include injury to the ureter due to stent maneuvering and the creation of fistulas.

Occlusion of the stent in the first 48–72 h is likely due to clots. After this period other causes are more likely, such as the presence of calculi.

Haleblian G, Kijvikai K, de la Rosette J et al (2008) Ureteral stenting and urinary stone management: a systematic review. J Urol 179:424-430

Hausegger KA, Portugaller HR (2006) Percutaneous nephrostomy and antegrade ureteral stenting: technique-indications-complications. Eur Radiol 16:2016-2030

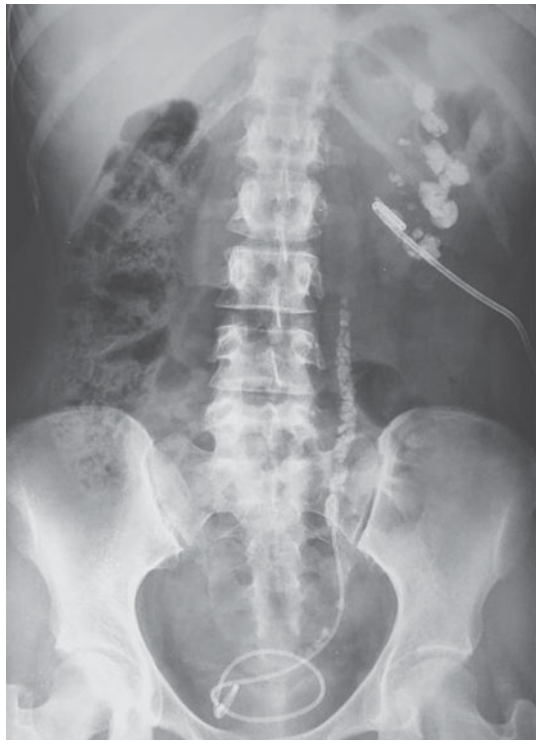

Fig. 27.5. Plain abdominal film. Patient with left renal and ureteric calculosis and ureteric stent incorrectly positioned

Ureteroplasty

Ureteroplasty is the dilatation of the ureter with a balloon-tipped catheter.

The indications for this type of procedure are undergoing progressive evolution. Benign stricture is currently the condition which benefits most from the technique. The procedure is an alternative to surgery and ureteric stent placement with the problems related to their substitution.

Since the strictures which best respond to this technique are recent ones – not more than 3 months old – the lesions which are most frequently treated successfully are iatrogenic or post-traumatic, followed by conditions of scarring secondary to treatment for lithiasis.

The procedure may also be applied to tubercular or postradiotherapy-induced stricture. Another possible application is setting of the transplanted kidney, where there may be associated ischemic damage to the ureter.

Ureteroplasty is usually performed after having left the nephrostomy catheter in place for around one week. This is substituted and the balloon, whose extremities are identifiable by the presence of two radio-paque markers, is positioned with the aid of a guidewire at the level of the stricture. The balloon is then inflated to 6-12 atmospheres for 30-60 s. In the event of tight stricture, balloons with larger diameters may be used, which are inflated to 18 atmospheres. This is often required with anastomotic strictures with the bladder or neobladder. Repeated insufflations are required and are performed with a manometric syringe. However, during the inflation procedure, attention must be paid to never exceeding the nominal pressure of balloon rupture.

The types of balloon catheters most commonly used are Gruntzig, usually 5 French, with a length of 4 cm and a diameter of 6-8 mm for the intermediate portion of the ureter and 8-10 mm for the ureteropelvic junction. In the event of tight stricture, larger, diameter catheters may be used, which allow higher inflation pressure.

After the dilatation has been performed a 10 French double-J stent is placed, which may be removed endoscopically within 2 months.

The dilatation procedure may cause laceration of the ureteric epithelium, especially in the event of balloon rupture, but this tends to resolve spontaneously. However, stenting is advisable to facilitate the process of re-epithelization.

de la Taille A, Ravery V, Hoffmann P (1997) Le traitement des stenoses de l'uretere par cathe-ters de dilatation a haute pression. Prog Urol 7:408-414

Ravery V, de la Taille A, Hoffmann P et al (1998) Balloon catheter dilatation in the treatment of ureteral and ureteroenteric stricture. J Endourol 12:335-340

Arterial Embolization

Interventional radiology today plays a frontline role in the treatment of urinary tract bleeding. The first indications for embolization of the renal artery were made in 1970. They were limited to symptomatic hematuria and the palliative treatment of inoperable or metastatic primary renal cancer.

With the development of new techniques and the growing experience of operators, there has been a broadening of indications. Today these include vascular malformations, angiomyolipomas, the control of traumatic or iatrogenic bleeding and the preoperative devascularization of malignant lesions to reduce the risk of hemorrhage. However, the role of preoperative renal embolization is still controversial. In fact there is little agreement among various studies regarding the real benefits of the procedure prior to nephrectomy. It is nonetheless certain that the technique enables the surgeon to work on an organ with a markedly reduced blood supply.

The introduction of small-diameter catheters and more appropriate embolizing agents has led to a drastic reduction in the morbidity associated with the procedure.

Patient preparation is the same as for diagnostic angiography: a number of blood tests are indispensable (hematocrit, coagulation profile, creatininemia and azotemia) and peripheral venous access is made available.

Selective catheterization of the renal artery is performed, usually with a cobra catheter and transfemoral access. After the diagnostic phase the embolization is performed, which may be done with permanent embolizing agents such as metal spirals, microparticles of polyvinyl alcohol (PVA) or microspheres, or with temporary agents such as Gelfoam (**Fig. 27.6**).

More than one type of embolizing agent may be used in the same procedure to obtain satisfactory results. When possible, superselective embolization is mandatory to preserve residual renal parenchyma.

The complications associated with the procedure and typical of postembolization syndrome (nausea, vomiting, fever and pain) can be cleared up with appropriate pharmacologic treatment. Other more operator-dependent complications include incomplete devascularization and the migration of embolizing material to other regions.

Endovascular embolization is today also indicated in the palliative treatment of nonoperable hemorrhaging bladder malignancies, with the procedure being able to reduce the often massive hematuria. Complete control of hematuria has been reported in 69% of cases.

The mini-invasiveness of arterial embolization and the markedly lower rate of complications than with surgical techniques (which these patients are often unable to undergo given their poor general conditions) have led to the success of the procedure, making it an indispensable option in the treatment of these hemorrhagic lesions.

As with all embolization procedures, being as selective as possible is crucial for reducing ischemic complications to a minimum.

After performing diagnostic pelvic angiography, the technique involves cannulation

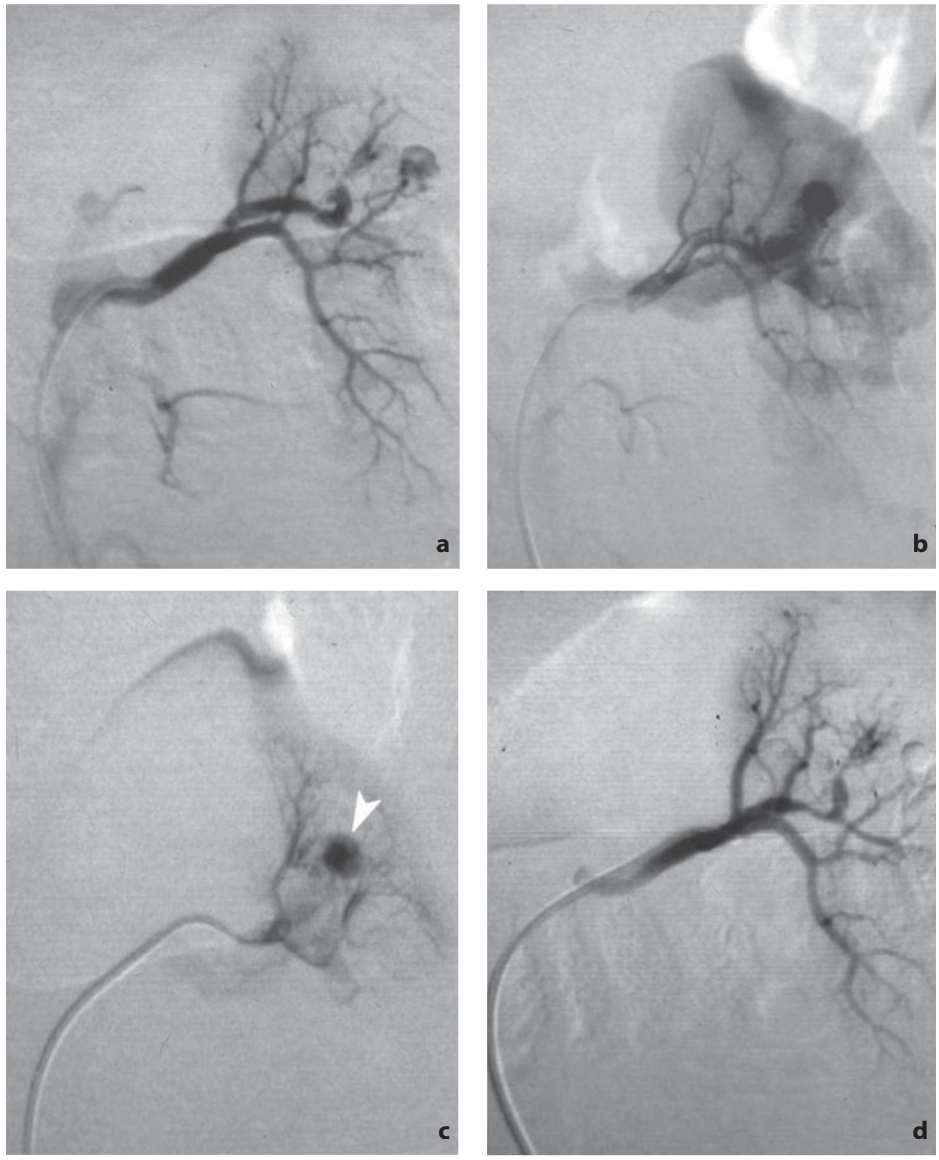

Fig. 27.6a-d. Renal angiography. **a-c** Extravascular leakage of contrast medium at the level of an interlobar artery (*arrowhead*). Superselective catheterization and subsequent embolization with PVA (**d**)

of the internal iliac artery with a cobra, Simmons or pig-tail catheter. The anterior branch of the vessel is catheterized and embolization is done (Fig. 27.7). Special attention must be paid to whether the lesion is supplied by contralateral arterial branches. In this case these branches also need to be embolized. Some authors also perform preventative embolization of the contralateral iliac artery to impede future collateral circulation.

The embolizing agents are those indicated earlier in the description of renal embolization.

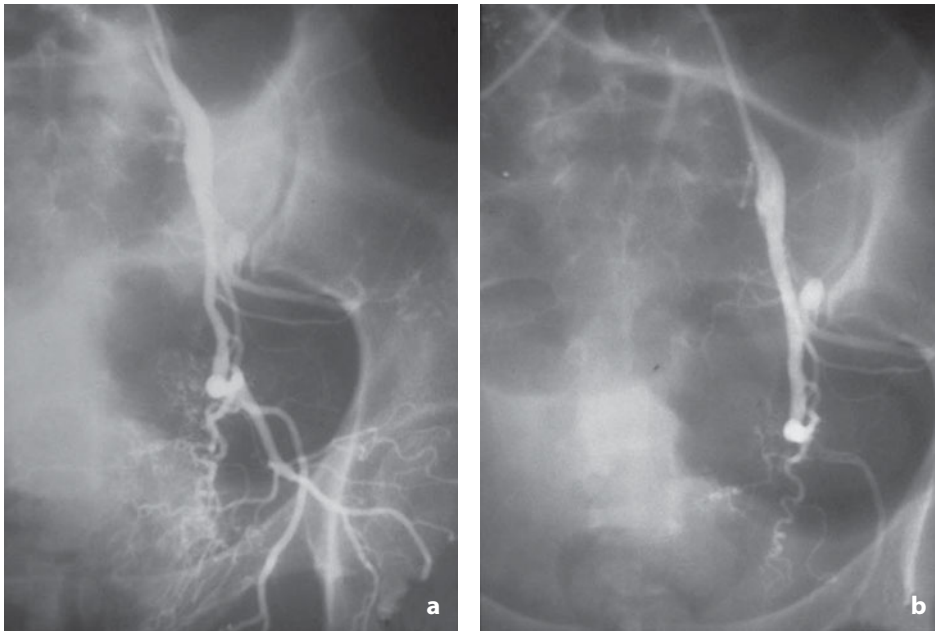

Fig. 27.7a,b. Patient with inoperable bladder cancer. **a** Hypervascularity corresponding to the lesion. **b** Subsequent embolization with microparticles of PVA at the level of the left internal iliac artery. Complete exclusion of the newly formed arterial circulation

Kadir S, Marshall FF, White RI Jr et al (1983) Therapeutic embolization of the kidney with detachable silicone balloons. J Urol 129:11-13

Pisco JM, Martin JM, Correia GM (1989) Internal iliac artery: Embolisation to control haemorrhage from pelvic neoplasms. Radiology 172:337–339

Turini D, Nicita G, Fiorelli C et al (1976) Selective transcatheter arterial embolization of renal carcinoma: an original technique. J Urol 116:419-421

Subject Index

O

P

R

S

T

U

V

W

Z